The Miocene volcanism of the Sulcis area (SW Sardinia, Italy): Petrology, petrogenesis and geodynamic significance

Guillem Gisbert Pinto

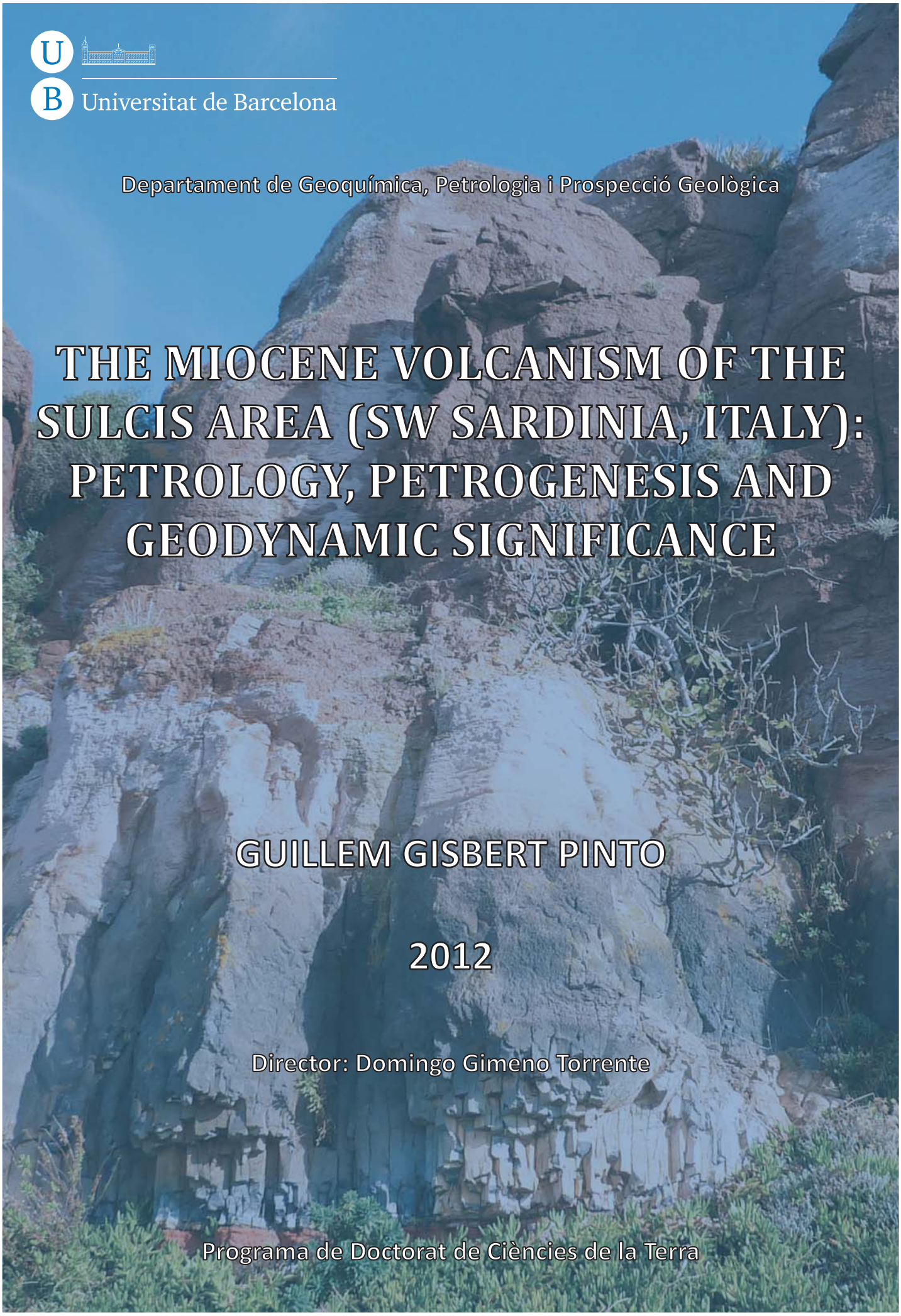

Universitat de Barcelona

Departament de Geoquímica, Petrologia i Prospecció Geològica

THE MIOCENE VOLCANISM OF THE SULCIS AREA (SW SARDINIA, ITALY): PETROLOGY, PETROGENESIS AND GEODYNAMIC SIGNIFICANCE

GUILLEM GISBERT PINTO

2012

Director: Domingo Gimeno Torrente

Programa de Doctorat de Ciències de la Terra

Universitat de Barcelona

Departament de Geoquímica, Petrologia i Prospecció Geològica

Grup de Petrologia i Geoquímica Fonamental i Aplicada (PEGEFA)

THE MIOCENE VOLCANISM OF THE SULCIS AREA (SW SARDINIA, ITALY): PETROLOGY, PETROGENESIS AND GEODYNAMIC SIGNIFICANCE

Doctorand

Guillem Gisbert Pinto

Director

Dr. Domingo Gimeno Torrente

Barcelona, Maig de 2012

AGRAÏMENTS

Tot i que a vegades sembli que no hagi de callar ni sota l'aigua, aquells que em coneixen saben que en el fons sóc persona de poques paraules. Així que seré breu. Fer aquesta tesi ha estat un procés llarg; gairebé quatre anys donen per moltes i variades situacions i experiències, i moltes sou les persones que en un moment o altre m'heu donat el vostre consell, suport i ajuda tant a nivell científic com tècnic, burocràtic o personal, o que, simplement, m'heu acompanyat i m'heu fet passar grans moments durant aquest temps, ajudant-me tots vosaltres a continuar endavant fent que la tesi arribés finalment a bon port i que jo pogués conservar la salut mental. Sense entrar a donar noms, perquè la llista seria molt llarga i segur que em deixaria algú, us vull agrair a tots haver estat al meu costat: moltes gràcies.

A nivell personal voldria fer una menció especial al meu director de tesi, en Domingo Gimeno, per haver-me donat la oportunitat de fer aquesta tesi, a la Meritxell Aulinas, per ser un exemple a seguir i gran font de consell i suport (a més de per acollir-me al seu despatx durant els últims mesos de feina), i als meus pares per haver-me donat sempre suport. A nivell institucional estic agraït a la Università degli Studi di Cagliari per haver-me acollit durant l'estada breu de tres mesos i mig que vaig realitzar, i a la minera Carbosulcis SpA per haver-me donat accés a les seves instal·lacions i documentació.

Finalment no puc oblidar el tema econòmic, ja que he pogut dedicar quatre anys a temps complet a fer aquesta tesi gràcies a haver gaudit de les beques FI de la Generalitat de Catalunya i FPU del Govern d'Espanya. A més, he pogut realitzar tot el treball de camp i laboratori gràcies als fons del projecte de recerca CGL2007-63727/BTE del Ministeri d'Educació i Ciència. Per acabar, mencionar que aquest treball ha estat realitzat en el marc del Grup Consolidat d'Investigació PEGEFA (SGR 2005-795 i SGR 2009-972, Generalitat de Catalunya).

CONTENTS

ABSTRACT

During the Cenozoic the western Mediterranean area underwent a complex geodynamic evolution driven by the interaction between African and Eurasian plates, which brought it to its current configuration. Geodynamics were complex due to the presence of several microplates, oceanic and continental crust, and changes in stresses caused by its own evolution. In this recent evolution of the western Mediterranean, the Corsica-Sardinia microplate played a central role, which was recorded by its tectonic evolution and volcanism. During Oligo-Miocene the roll-back of the NW-wards subducting Apulian subduction zone caused the Corsica-Sardinia microplate to detach, drift and rotate from the European continental margin to its present position, opening the Liguro-Provençal Basin and generating abundant subduction-related orogenic volcanism. After a pause in retreat, subsequent evolution of the roll-back since Pliocene left Sardinia in its current position as the trench retreated SE-ward opening the southern Tyrrhenian basin. Extensional tectonics related to the opening of the southern Tyrrhenian produced in Sardinia the generation of abundant anorogenic alkaline volcanism.

The Oligo-Miocene volcanism in Sardinia provides key information on the initial processes of this geological evolution. In particular, the study area, the Sulcis, corresponds to the crustal part of the Corsica-Sardinia block that underwent most displacement and extension during drifting and rotation of this microplate. In this area, a special volcanic suite was produced which began sharing the same calc-alkaline characteristics as the rest of the subduction-related volcanism throughout Sardinia but that later migrated to different compositions, mildly alkaline, including the rarely occurring peralkaline volcanism. In spite of the marked differences of the Sulcis magmatism with respect to that in other regions of Sardinia, and of its great interest and importance as a source of information for the correct interpretation of the recent geodynamic evolution of central and western Mediterranean and the volcanism associated with it, this sector prior to this study could

be regarded as probably the poorliest known Oligo-Miocene volcanic area in Sardinia from a geochemical, petrological and volcanological point of view. This special volcanic suite was considered to be only one more manifestation of the widespread subduction-generated orogenic volcanism of Sardinia. The present work has, at least partially, solved this situation.

Oligo-Miocene volcanic rocks in the Sulcis are found in the mainland and in two minor islands (Santo Antioco and San Pietro) and consists of a lower sequence more than 400 m thick of andesitic (basaltic andesite and andesite) domes and lava flows, over which lies an upper sequence also more than 400 m thick formed by a piling of ignimbritic sheets which in previous studies had been subdivided into 17 units. The upper sequence is formed by transitional to mildly alkaline magmas with trachytitic and dominant rhyolitic compositions, including comendites.

A thorough and detailed study of the Sulcis Oligo-Miocene volcanic suite has been carried out in this study involving the revision of the available data on volcanostratigraphy and cartography and the characterization of the geochemistry, petrography and mineral chemistry of the several units present in this suite, which has allowed us to obtain significant information on the petrogenesis of this suite and its geodynamic significance.

Several field campaigns have been conducted in which the existing cartography and the volcanostratigraphy described in literature have been revised. A thorough sampling has been done in which all units and most facies of each unit have been systematically sampled, putting special emphasis in the ignimbritic sequence and its less studied areas in the Sulcis. Samples collected in this research, and some samples available from previous work in the study area by the host research group, have been prepared for petrologic study including petrography, mineral chemistry and whole rock geochemistry. Mineral chemistry has been analysed using an electron microprobe on a selection of 47 thin sections. Whole rock geochemical analysis has included major and trace element determination by X-Ray Fluorescence (XRF), Inductively Coupled Plasma with Optical Emission Spectrometry (ICP-OES) and Inductively Coupled Plasma with Mass Spectrometry (ICP-MS) (new whole rock geochemical data of a total of 281 samples are provided), and Sr, Nd and Pb isotope ratios analysis using Thermal Ionisation Mass Spectrometry (TIMS) (26 samples). A comprehensive geochemical database for the Sulcis has been built by using own data and by revising and incorporating data collected from literature.

As a result of the field and laboratory work all units have been characterised from the volcanostratigraphic, petrographic and geochemical point of view, and several volcanostratigraphy and mapping problems have been solved.

Revision of the volcanostratigraphy of the Sulcis ignimbritic suite has resulted in the definition of a new unit, Carloforte, located between Monte Ulmus and Parigianu units, and peralkaline in composition. This unit, previously considered to be part of Monte Ulmus, crops out in San Pietro Island and northern mainland and is characterised by bearing large highly porphyritic black pumices.

Most of the doubts during the field work in the Suclis area arise from the macroscopic, and sometimes even microscopic, similarity between two or more of the ignimbrites present in the area. The systematic sampling and analysis of the whole rock geochemistry of all the described ignimbritic units in the Sulcis has allowed us to characterise its chemistry and to develop a methodology for unit recognition based on whole rock geochemistry. Although this methodology has been developed for fresh samples, it has been observed that it also works for most of the available data from slightly altered rocks. Geochemistry-based unit recognition has been a fundamental tool for solving volcanostratigraphic and mapping doubts during the development of this work, and remains a powerful tool for future studies.

The study of the whole rock geochemistry data has also allowed us to obtain significant information on the generation of the magmas that formed the Sulcis volcanic suite and its geodynamic significance, and combination with petrographic observations has provided valuable information on the evolution of these magmas from its formation to its eruption.

Isotope and trace element data have revealed that the mantle beneath Sardinia presented in pre-Late Cretaceous times an EMI signature which was subsequently modified by the CAP event in Late Cretaceous and by subduction-released fluids from Oligocene to Miocene. The CAP event metasomatised the existing mantle by introducing a HIMU signature which produced the change in composition of the mantle from EMI to EAR-like. Metasomatism was not complete and left a diffusely stratified mantle with an upper part with an EMI signature and a lower more EAR-like region, both of them having an OIB mantle source-like composition. Subduction released into the mantle wedge hydrous fluids and partial melts carrying sediment and MORB isotope and trace element compositions, which introduced mostly into the more EAR-like mantle a subduction signature.

Oligo-Miocene orogenic magmas in Sardinia, including the andesitic lower sequence in the Sulcis, were produced in the subduction-modified more EAR-like mantle portion by lowering of the melting temperature due to the input of subduction fluids. Magmas from the ignimbritic sequence in the Sulcis, though, are interpreted to have had a different origin. Unlike all the previous petrogenetic theories, which considered it as part of the regular orogenic magmatism, it

is proposed that it represents a transition from orogenic to anorogenic magmatism. It is suggested that the transition was due to a change in the melting mechanism from fluid- to extension-controlled, related to the cessation in the subduction influence below the Sulcis. Despite the change in melting mechanism, the magma source continued to be the subduction-modified more EAR-like mantle. The mechanism proposed to explain the contemporaneous occurrence of both orogenic and anorogenic magmatisms in Sardinia during the emplacement of the Sulcis ignimbritic suite is the formation of a slab break-off which started south of Sardinia and progressed northward opening a slab window. Slab break-off not only explains the occurrence of anorogenic magmas, but also the strong slowdown in subduction and roll back of the trench, which produced the 6 Ma-long pause in magmatic and tectonic activity between the end of the Corsica-Sardinia rotation and the opening of the southern Tyrrhenian basin.

The ignimbritic sequence in the Sulcis was formed by arrival and differentiation of several magma batches with slightly different initial compositions, apparently at least one for each unit except for Lenzu and Seruci units, which formed by evolution of the magma that generated the immediately preceding units. Magma differentiation was dominated by crystal fractionation processes, which produced similar evolutionary trends, assimilation having a very small effect only appreciable in Pb isotopes. Fractionating assemblage in the more primitive magmas was dominated by pyroxenes, plagioclase and spinel, although amphibole and biotite may occasionally have significantly contributed to magma evolution. In more evolved magmas sanidine appeared in the fractionating assemblage, while pyroxene presence decreased. The most differentiated magmas presented a fractionating assemblage largely dominated by sanidine, with occurrence of quartz in the peralkaline magmas which buffered SiO_2 content. Peralkaline magmas are interpreted to have formed by evolution by simple crystal fractionation of magmas slightly more alkaline than those found in the Sulcis, which were not sampled by any of the studied eruptions. The possibility of the more alkaline regular magmas in the Sulcis being the parental magmas of peralkaline ones, which was suggested in previous studies of this suite, has been tested using numerical modelling. Although further work is needed, it has been found that no relation by simple crystal fractionation is possible, and that the only way in which these two magmas could be related is by a mechanism of crystal fractionation plus assimilation of previously precipitated amphibole.

The study of feldspar petrography and mineral chemistry has shown that feldspar crystallisation conditions changed along the sequence, with variations induced by magma composition differences, magma mixing/mingling processes, assimilation of wall rock, or different water activity. Regular feldspar crystallisation involved the apparition of plagioclase as the first crystallising feldspar. As magmas evolution progressed, these reached a cotectic in the feldspar

ternary system, simultaneously crystallising two feldspars (plagioclase and sanidine) whose compositions progressively converged toward the feldspar system minimum composition. Further magma evolution caused magmas to reach a reaction zone in which plagioclase was reabsorbed as it changed in composition. At this point sanidine mantles could grow over plagioclase. In the most extreme case, that of peralkaline magmas, these crystallised a single alkali feldspar (sanidine), and both the liquid and feldspar reached the minimum composition in the Ab-Or system. Magma mingling produced the occurrence of different feldspar populations in a single unit and the destabilization of these. Higher water pressure delayed the crystallisation of sanidine. Finally, wall rock assimilation produced compositional zoning in sanidines in one of the units.

RESUM

1 INTRODUCCIÓ I OBJECTIUS

1.1 Motivació de l'estudi

El Mediterrani central i occidental és una de les àrees geològicament més complexes i controvertides del món. Aquesta àrea està formada per un nombre relativament alt de microplaques que s'han mogut i col·lisionat d'una manera particularment activa durant els últims 30 Ma. El resultat d'aquests moviments és un mosaic de plaques on les unitats volcàniques marquen els events geodinàmics soferts per aquesta àrea i proporcionen evidències no només de l'evolució cortical sinó també de les característiques del mantell situat sota aquesta regió.

Durant aquests últims 30 Ma alguns dels events més rellevants que han tingut lloc al Mediterrani occidental han estat la subducció de placa oceànica sota Sardenya i el sud de Còrsega marcada per la generació de magmatisme d'arc; el desplaçament i rotació antihorària de Còrsega i Sardenya (degut al funcionament en *roll-back* de la subducció) i formació associada a aquest de l'espai oceànic Liguro-Provençal en posició de rere-arc; i la formació en context de rere-arc del Tirrè per continuació del desplaçament de la subducció cap a SE, amb la formació d'arcs volcànics associats, incloent l'actiu actualment a les Eòlies. El vulcanisme oligo-miocè de Sardenya ocupa una posició central dins d'aquest marc geodinàmic i proporciona informació clau sobre els processos inicials d'aquesta evolució geològica. En particular, el sud-oest de Sardenya, on es troba l'àrea estudiada, correspon a la part del bloc Sard-Cors que va patir més desplaçament i extensió durant la rotació d'aquesta microplaca, produint-s'hi una associació volcànica especial que inicialment va compartir les mateixes característiques amb la resta del vulcanisme oligo-miocè de Sardenya, però que posteriorment va migrar cap a composicions diferents, més alcalines, incloent el poc freqüent vulcanisme peralcalí.

Malgrat els esforços fets per a la caracterització del vulcanisme orogènic oligo-miocè de Sardenya, i del gran interès i importància que té la seqüència volcànica del Sulcis com a font d'informació per a la correcta interpretació de l'evolució geodinàmica recent del Mediterrani oriental i del vulcanisme associat, el sector del Sulcis romania encara com una de les àrees de vulcanisme orogènic menys conegudes de Sardenya des del punt de vista petrològic i vulcanològic. Per tal de resoldre, com a mínim en part, aquest dèficit de coneixement, es va escollir el Sulcis com a àrea de treball per aquest estudi.

1.2 Objectius

El primer objectiu plantejat per aquest estudi ha estat la caracterització petrològica i geoquímica de la successió volcànica oligo-miocena del Sulcis, particularment de la seqüència piroclàstica, i especialment de la part superior d'aquesta, la que inclou les unitats làviques i piroclàstiques peralcalines. Aquesta caracterització sistemàtica ha permès acomplir altres objectius que inclouen: el desenvolupament una metodologia per identificar unitats ignimbrítiques en base a la geoquímica de roca total, sovint clau donada la gran semblança macroscòpica (i fins i tot microscòpica) entre unitats, especialment en el cas de les més soldades i reomòrfiques; la revisió de la cartografia existent amb l'ajut de la petrografia i la geoquímica, que tot i que no era un objectiu principal de l'estudi ha estat necessària per tal de poder-lo desenvolupar correctament, així com la correlació de les unitats volcàniques aflorants a les diferents àrees del Sulcis; i la interpretació petrogenètica de l'associació magmàtica del Sulcis en el context de l'evolució recent del Mediterrani occidental. Un altre dels objectius plantejats, la datació radiomètrica de les unitats estudiades, ha quedat finalment fora de l'abast d'aquest estudi. Ara bé, els resultats aquí exposats proporcionen les eines i coneixements necessaris per tal de poder realitzar aquestes datacions amb èxit en un futur immediat.

2 CONTEXT GEOLÒGIC

2.1 Situació de l'àrea d'estudi

L'illa de Sardenya es troba al centre del Mediterrani occidental, entre 38°51' i 41°15' de latitud N i 8°8' i 9°50' de longitud E. L'àrea d'estudi d'aquesta treball, la regió del Sulcis, es troba al sud-oest de Sardenya, entre 38°56' i 39°17' de latitud N i 8°13' i 8°45' de longitud E (Fig. 1).

2.2 Context geodinàmic

Abans de l'Oligocè Còrsega i Sardenya es trobaven formant part del marge continental europeu a l'occident mediterrani. Tot i que no hi ha acord sobre la posició exacta d'aquest bloc, un dels últims treballs apunta a que aquest es trobaria entre els Pirineus i els Alps (Schettino and Turco,

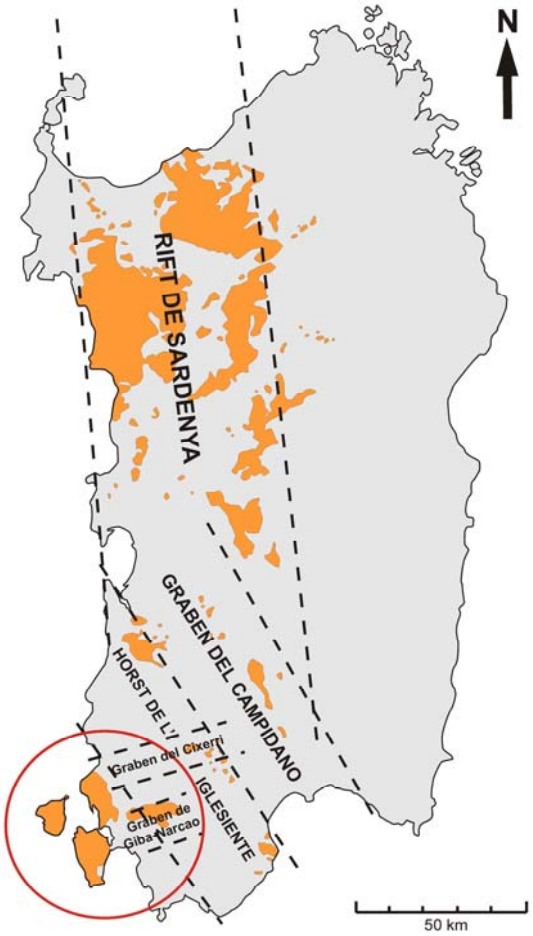

Figura 1: Situació de l'àrea d'estudi i del vulcanisme oligo-miocè a l'illa de Sardenya

2006). La progressiva convergència entre les plaques Africana i Euroasiàtica, amb el continu creixement dels Pirineus, finalment va provocar una reorganització de plaques en què a començaments del Rupelià (33,1 Ma) la zona on tenia lloc la deformació deguda al moviment convergent es va desplaçar dels Pirineus als marges sud i est d'Ibèria. A l'inici la deformació va ser acomodada als marges d'Ibèria amb la formació d'estructures compressives. A continuació, l'antiga escorça oceànica que limitava amb aquest marge va començar a subduir cap a N i NO (Coulon, 1977; Beccaluva et al., 1989), formant una fossa de SO a NE i posteriorment detonant l'evolució extensional del Mediterrani occidental en començar a migrar cap a SE amb un mecanisme de *roll-back*. La migració de la subducció va produir el desenganxament, migració i rotació antihorària de la placa Sard-Corsa des del marge continental europeu fins a la seva posició actual (Cherchi and Montadert, 1982), obrint la conca Liguro-Provençal en situació de rere-arc, i generant abundant magmatisme orogènic associat (Coulon, 1977). Sardenya va rotar 45° respecte l'Europa continental a partir de 20,5 Ma, i la rotació va acabar al voltant dels 15 Ma. La major part de la rotació, més de 30°, va tenir lloc entre els 20,5 i 18 Ma, coincidint amb el període de màxima activitat volcànica a Sardenya (Gattacceca et al., 2007). Amb l'inici del *roll-back*, la situació

tectònica local va canviar de compressiva a extensional, generant a Sardenya estructures en horst i graben controlades per falles normals, blocs basculats i estructures transverses, essent la principal estructura el Rift de Sardenya, un graben de 200 km de llarg que creua l'illa de N a S, i on es troba la major part del vulcanisme orogènic de l'illa (Fig. 1). Finalitzat el desplaçament de l'illa, els últims indicis de tectònica extensional corresponen al Burdigalià inferior (Casula et al., 2001). Després d'uns milions d'anys de pausa en l'activitat tectònica, l'evolució del *roll-back* va continuar a partir del Pliocè, deixant Sardenya enrere en la seva posició actual a mesura que la subducció es desplaçava cap a SE obrint el Tirrè sud com a conca de rere-arc. La tectònica extensional relacionada amb l'obertura del Tirrè va produir a Sardenya la reactivació de les estructures extensives, formant al sud de l'illa el graben del Campidano, i la generació d'abundant magmatisme anorogènic alcalí durant el Plio-Pleistocè (Beccaluva et al., 1989; Sartori et al., 1989).

2.3 Geologia de Sardenya

A l'actualitat Sardenya és una porció de continent amb una escorça d'uns 30 km i una litosfera d'uns 80 km de gruix situada entre dues zones d'escorça continental aprimada i escorça oceànica, les conques Liguro-Provençal i Tirrènica. El registre geològic pre-Oligocè és molt semblant al que es troba al NE de la península Ibèrica i SE de França. El basament de l'illa està format per roques hercíniques, dominantment plutòniques al sector NE, amb roques metamòrfiques d'origen principalment sedimentari aflorant al centre i SE. El grau de metamorfisme decreix cap al SO des d'alt grau al contacte amb els plutons fins a quasi absent al Sulcis i Sarrabus (Egger et al., 1988), de les zones internes a les externes de l'orogen hercínic. Per sobre del basament hercínic es poden trobar roques sedimentàries mesozoiques a l'E i NO de l'illa, encara que la seva extensió areal és petita, i la seva potència i seqüència estratigràfica estan reduïdes respecte el NE d'Ibèria i sud de França. Els materials eocens i post-eocens (marins a continentals) reomplen les estructures de graben formades durant les fases extensionals, com ara el Rift Sard o el graben del Campidano. Les roques volcàniques dels cicles oligo-miocè i plio-pleistocè cobreixen i s'intercalen amb aquestes roques sedimentàries més joves.

2.4 El vulcanisme oligo-miocè de Sardenya

Un dels primers estudis sistemàtics de les roques volcàniques calco-alcalines formades durant la migració i rotació de la microplaca Sard-Corsa va ser el de Coulon (1977), que va establir la seqüència vulcanoestratigràfica per l'àrea del Logudoro-Bosano, al NO de Sardenya. Coulon va subdividir la seqüència en tres parts: la sèrie andesítica inferior, la superior i la terminal. Més tard, en un estudi global sobre aquest vulcanisme, Assorgia et al. (1997), inspirats en el treball de Coulon, van reconèixer una successió volcànica comuna a tota l'illa, formada per quatre sèries

principals. També van observar que les roques volcàniques oligo-miocenes afloraven sobretot al NO de Sardenya, on la seqüència estava quasi sempre completa, i en menor mesura a diversos sectors de l'O de l'illa, on aquesta no ho estava. Les quatre sèries principals d'Assorgia et al. (1997) són: *Lower Basic-Intermediate Lavic Series* (LBLS) (33/28-23 Ma; Savelli, 1975; Beccaluva et al., 1985), *Lower Acid-intermediate Explosive Series* (LAES) (23-20 Ma; Savelli et al., 1979; Assorgia et al., 1995), *Upper Basic-Intermediate Lavic Series (UBLS)* (19-16 Ma; Coulon, 1977; Maccioni et al., 1990) i *Upper Acid-Intermediate Explosive Series (UAES)* (17-13 Ma; Araña et al., 1974; Savelli et al., 1979; Maccioni et al., 1990; Morra et al., 1994; Assorgia et al., 1995). A aquesta última pertany la seqüència ignimbrítica del Sulcis, objecte d'estudi d'aquest treball.

2.5 El Sulcis

L'àrea del Sulcis és una zona baixa topogràficament limitada al NNE pel horst de l'Iglesiente, que és tallat per dos petits grabens E-O (Cixerri i Giba-Narcao). Aquesta estructura ja era present durant l'emplaçament de la seqüència volcànica estudiada. A l'actualitat l'àrea emergida del Sulcis està limitada al SO pel mar, que divideix la regió en una porció a terra ferma i dues illes principals (Santo Antioco i San Pietro). El Sulcis, com la major part de les àrees costaneres de Sardenya, presenta una escorça aprimada de 26-28 km de gruix (Chamot-Rooke et al., 1999).

El substrat pels materials volcànics oligo-miocens està format pel basament metamòrfic paleozoic (que aflora al horst de l'Iglesiente i és dominat per una seqüència carbonatada i siliciclàstica), cobert per roques sedimentàries mesozoiques (a l'E de l'illa de Santo Antioco afloren calcàries cretàciques) i dipòsits sedimentaris detrítics eocens a miocens (Formacions Cixerri i Ussana (Pecorini and Pomesano Cherchi, 1969)).

La seqüència volcànica oligo-miocena del Sulcis consisteix en una part inferior formada per un apilament de doms i colades de composició andesítica de vora 400 m de gruix, recoberta per un apilament d'unitats piroclàstiques de caràcter predominantment ignimbrític de més de 400 m de potència.

3 RECERCA PRÈVIA AL SULCIS

La presència de roques volcàniques al Sulcis es coneix des de mitjans del segle XIX (La Marmora, 1857). L'estudi d'aquestes roques va començar amb els treballs de Bertolio (1895), que va definir les comendites a l'illa de San Pietro, i Johnsen (1912). A començaments del segle XX es va dur a terme la primera cartografia d'aquesta àrea (Novarese and Pullè, 1920, 1926; Taricco, 1932; Novarese et al., 1933), en la qual es van fer les primeres subdivisions de la seqüència volcànica en 5 unitats. La seqüència vulcanoestratigràfica establerta es va acceptar durant 50 anys fins que es

van dur a terme nous estudis de més detall. Durant aquest període hi va haver diverses contribucions al coneixement dels materials volcànics del Sulcis, especialment de l'illa de San Pietro (Chayes and Zies, 1964; Garbarino and Maccioni, 1968, 1969, 1970a, 1970b; Noble and Haffty, 1969; Araña et al., 1974). A finals dels 80 es va fer un nou esforç per tal d'obtenir mapes geològics més detallats del Sulcis. Com a resultat es van publicar nous mapes per les illes de San Pietro (Garbarino et al., 1985; Garbarino et al., 1990) i Santo Antioco (Maccioni et al., 1990). A la vegada, l'observació dels sondejos de prospecció realitzats per la minera Carbosulcis SpA a la part nord de la terra ferma del Sulcis, els quals creuaven tota la seqüència ignimbrítica, va permetre dur a terme un estudi detallat d'aquesta per part d'Assorgia i col·laboradors. Com a resultat van veure la llum diverses publicacions (Assorgia et al., 1990a, 1990b, 1992a, 1992b), en les que es definien un total de 10 unitats ignimbrítiques, i un nou mapa de la terra ferma (Assorgia et al., 1992c). En un treball posterior Assorgia et al. (1994) van reconèixer dues noves unitats, assolint les 12 acceptades fins que en un treball recent a l'Isola de San Pietro Mundula et al. (2009) van definir algunes unitats menors més. Una última unitat ha estat definida en un mapa encara no publicat però recentment disponible a internet (Pasci and Orrù, pendent de publicació). Els treballs d'Assorgia i col·laboradors dels anys 90 van proporcionar el primer joc extens de dades petrogràfiques i geoquímiques de la regió, que va permetre fer les primeres classificacions geoquímiques i interpretacions petrogenètiques. Aquest joc de dades va ser ampliat per Morra et al. (1994) en un estudi que es va centrar en la petrogènesi de l'associació magmàtica del Sulcis, i en especial de les comendites. A partir de la publicació de Morra et al. (1994), els treballs realitzats a la zona van ser més específics, centrant-se principalment en una unitat o composició. Una atenció especial s'ha dedicat a l'estudi d'una de les unitats, la Nuraxi, que ha estat objecte d'estudi de diversos treballs (Gimeno et al., 1996, 2002, 2003; Pioli, 2003; Pioli and Rosi, 2005; Pioli et al., 2008). Brotzu et al. (1997a) van estudiar la seqüència andesítica de Narcao, Cioni and Funedda (2005) les laves comendítiques de San Pietro des del punt de vista estructural, i Conte et al. (2010) van abordar la petrogènesi de la seqüència andesítica del sud de l'illa de Santo Antioco.

Pel que fa al treball previ del grup de recerca a la zona, el director del grup, Domingo Gimeno, va participar en els treball d'Assorgia i col·laboradors. Fruit d'això es disposa d'un extens joc de mostres provinents dels sondejos de la minera. Posteriorment es van realitzar dues campanyes de camp, una al 1996 que es va centrar a l'illa de Santo Antioco, i una altra al 2006, centrada al nord de l'illa de San Pietro. Com a resultat d'aquestes es va obtenir un altre joc de mostres que complementava l'anterior. Finalment, al 2005 es va desenvolupar un treball de final de carrera

centrat en la caracterització vulcanoestratigràfica i geoquímica d'una de les últimes unitats de la seqüència, la de Serra di Paringianu (Roselló, 2005).

Durant la realització del present estudi s'han portat a terme dos treballs de final de carrera més, centrats al SO de l'illa de Santo Antioco (Rodríguez, 2009; Ramon, 2009).

4 METODOLOGIA

Per assolir els objectius plantejats per aquest treball la recerca desenvolupada ha seguit els passos clàssics d'un estudi petrològic, és a dir: treball de camp i mostreig, selecció de mostres i preparació d'aquestes per a estudi petrogràfic, anàlisi de la química mineral i anàlisi de la geoquímica de roca total.

4.1 Treball de camp i mostreig

Realitzar un mostreig sistemàtic dels materials oligo-miocens del Sulcis s'ha considerat un dels punts claus per a l'èxit d'aquest estudi. Per aquesta raó un dels objectius principals del treball de camp ha estat la revisió de la vulcanoestratigrafia establerta a la literatura i dels mapes disponibles per tal de garantir que les mostres recollides fossin atribuïdes a la unitat correcta i que totes les unitats fossin mostrejades, incloent tantes fàcies com fos possible de cadascuna. Aquesta tasca s'ha desenvolupat durant diverses campanyes de camp dutes a terme entre març de 2008 i març de 2010. Tot i que tota l'àrea d'estudi ha estat coberta durant el treball de camp, s'ha posat especial atenció en les illes de San Pietro i Santo Antioco perquè aquestes eren les àrees menys estudiades dins de la zona d'estudi. A l'hora de mostrejar s'ha tingut en compte la col·lecció de mostres del Sulcis de la que ja es disposava a la facultat fruit dels treballs previs del grup de recerca a la zona d'estudi. En total s'han recollit 371 noves mostres.

4.2 Selecció i preparació de mostres

Al moment de començar aquest estudi es disposava a la Facultat de Geologia d'unes 400 làmines primes elaborades durant treballs anteriors, i de dades de al voltant de 100 anàlisis de roca total. Contemplant el material ja disponible s'ha fet una selecció de mostres (tant de noves com de ja mostrejades anteriorment) per al seu estudi petrogràfic i geoquímic. S'han preparat làmines primes per la majoria de les noves mostres i per algunes de les antigues al Servei de làmina prima de la Facultat de Geologia de la Universitat de Barcelona. Un joc més petit de mostres (242 en total) s'ha preparat per dur a terme anàlisis geoquímiques de roca total. Per a això s'han molturat fraccions representatives d'aquestes en un molí d'anelles de carbur de wolframi després d'haver extret els cossos externs (enclavaments, clasts accidentals, etc.) i les parts alterades. Les mostres

que havien estat recollides a prop de la costa (menys de 200 m) han estat dessalades amb aigua destil·lada abans de la seva molturació.

4.3 Química mineral

La química mineral de fenocristalls, microfenocristalls i xenocristalls ha estat analitzada quantitativament sobre una selecció de 47 làmines primes representant totes les unitats usant la microsonda electrònica Cameca SX 50 dels Serveis Científico-Tècnics de la Universitat de Barcelona (SCT-UB).

4.4 Geoquímica de roca total

Un punt clau d'aquest estudi ha estat la construcció d'una extensa base de dades de geoquímica de roca total. S'ha parat molta atenció en la selecció de les mostres i dels mètodes d'anàlisi. De totes les mostres seleccionades per a analitzar s'ha realitzat una caracterització bàsica determinant els elements majors i alguns traces mitjançant Fluorescència de raigs X, així com la pèrdua al foc (Loss on ignition, LOI) als SCT-UB. A continuació s'ha realitzat una segona selecció de les mostres més fresques i representatives, de les quals s'ha dut a terme una caracterització més detallada mitjançant l'anàlisi de més elements traça per Espectrometria de masses de plasma acoblat inductivament (ICP-MS) i Espectroscòpia d'emissió òptica de plasma acoblat inductivament (ICP-OES), també als SCT-UB. Finalment, un últim i més reduït joc de 26 mostres ha estat analitzat per obtenir dades d'isotopia. Les anàlisis d'isòtops s'han dut a terme per Espectrometria de masses amb ionització tèrmica (TIMS) al Centro de Apoyo a la Investigación de Geocronología y Geoquímica Isotópica de la Universidad Complutense de Madrid (CAI), on s'ha determinat la isotopia d'Sr i Nd, i al Department of Earth Sciences de la Carleton University (Canadà), on s'ha determinat la isotopia de Pb.

5 RESULTATS DE LA VULCANOESTRATIGRAFIA

Tot i l'esforç dedicat a la revisió de la vulcanoestratigrafia i cartografia existents, no és l'objectiu d'aquest estudi proporcionar una descripció vulcanoestratigràfica detallada de cada unitat o un nou mapa; això es deixa per futurs estudis on s'abordarà, a més, la interpretació dels mecanismes eruptius i d'emplaçament de les unitats estudiades.

Com s'ha explicat anteriorment, fruit del treball realitzat al Sulcis al llarg dels anys la seqüència volcànica existent es va subdividir en una unitat andesítica basal sobre la qual es troben un conjunt d'unitats predominantment ignimbrítiques.

Pel que fa a les unitats ignimbrítiques, Assorgia et al. (1990b) van reconèixer una estructura comuna per a la majoria d'elles. Segons els autors l'estructura de les ignimbrites es caracteritza per la presència dels següents nivells:

a) Nivell basal de gra fi no cohesiu amb un gruix de centimètric a decimètric, color blanquinós, i ric en cristalls lliures i pumites.
b) Nivell obsidianaci (vitròfir) de gruix variable (típicament de pocs decímetres a mig metre), de color negre i baixa porfiricitat, format pel soldatge de lentícules de vidre calent no vesiculat. Les porcions superiors poden adquirir tonalitats com les del cos central.
c) Cos central, en la majoria d'unitats format per fàcies eutaxítiques, mostrant diversos graus de soldatge i una fàbrica que varia de massiva a fluïdal.
d) Part superior (normalment faltant a les unitats menys soldades) rica en pumites en una matriu cinerítica.

El principal, i sovint únic, constituent de totes les ignimbrites és el cos central, que forma la major part del seu gruix. Els altres tres nivells es poden o no haver format, i a) i d) fins i tot si s'han format poden no haver-se conservat degut a la seva escassa resistència a l'erosió. Aquesta estructura està millor desenvolupada i conservada a les unitats soldades.

Fruit de la revisió de la vulcanoestratigrafia, així com de la petrografia i geoquímica de la seqüència volcànica dels Sulcis, s'ha optat per subdividir una de les unitats peralcalines existents, la Monte Ulmus, en dues unitats, de manera que es defineix en aquest treball una nova unitat ignimbrítica, la Carloforte, anteriorment considerada la part superior de la Monte Ulmus. Aquesta unitat, fortament soldada i eutaxítica, es caracteritza per la presència d'abundants pumites negres centimètriques a decimètriques riques en cristalls de sanidina de fins a un centímetre de llargada. Aquesta unitat es troba a la part central de la porció en terra ferma del Sulcis, i a l'illa de San Pietro, on té la màxima expressió. A partir de la observació de la distribució areal de les fàcies presents es creu que aquesta ignimbrita tindria el seu origen un punt molt a prop a l'E del sector conegut com La Piramide, a l'E de l'illa de San Pietro.

A la Taula 1 es presenten les àrees d'aflorament i principals característiques vulcanoestratigràfiques de les unitats en què se subdivideix el vulcanisme oligo-miocè del Sulcis. Aquestes característiques es complementen amb les descrites referents a la petrografia. La Figura 2 és un mapa del Sulcis on es mostra la distribució de les unitats.

Unitat	Àrea d'afloramen t	Principals característiques
CL/PG	S de l'illa de San Pietro	Colonne/Punta Genniò: ignimbrita cinerítica moderadament soldada.
PM	S de l'illa de San Pietro	Punta Mingosa: ignimbrita cinerítica afírica moderadament soldada
SP	Extensa, centre de la terra ferma i a les dues illes	Serra di Paringianu: ignimbrita extremadament soldada i eutaxítica amb abundants pumites gris clar i gris fosc extremadament aplanades. Vitròfir basal. Fàcies no soldades al nord de les illes de San Pietro i Santo Antioco.
PA	Centre de la terra ferma i a les dues illes	Paringianu: unitat ignimbrítica complexa escassa a moderadament soldada. Majoritàriament cinerítica. Baixa porfiricitat i contingut de pumites.
CF	Illa de San Pietro i centre de la terra ferma	Carloforte: ignimbrita fortament soldada i eutaxítica amb abundants pumites negres riques en sanidina. També conté pumites grises i blanques.
MU	Centre i S de la terra ferma i a les dues illes	Monte Ulmus: unitat ignimbrítica afírica fortament soldada i eutaxítica, ocasionalment amb escasses pumites negres aplanades. Vitròfir basal.
CO	Centre de la terra ferma i a les dues illes, màxima expressió a San Pietro	Comendites: unitat complexa. Colades de lava i ignimbrites variablement soldades amb o sense vitròfir basal. Pot contenir fenocristalls de quars.
MZ	Centre de la terra ferma i a les dues illes	Matzaccara: unitat ignimbrítica complexa variablement soldada. Presenta biotita de color bronze.
MCR	O de l'illa de San Pietro	Montagna di Capo Rosso: colades de lava i ignimbrites moderadament soldades riques en lítics.
PC	O de l'illa de San Pietro	Punta dei Cannoni: unitat ignimbrítica moderada a fortament soldada, eutaxítica i porfírica. Abundants grans (diversos dm) pumites.
NU	Extensa, es troba a tota l'àrea estudiada	Nuraxi: ignimbrita extremadament soldada i eutaxítica. Escasses pumites grises extremadament aplanades. Reomòrfica. Vitròfir basal.
CA	N de terra ferma, i escassament al N de l'illa de Santo Antioco	Conca is Angius: unitat ignimbrítica complexa escassament soldada amb abundants pumites i lítics accidentals. Presenta estructures de desgasificació.
MC	Tot el S i E de terra ferma (Carbonia, Narcao) i illa de Santo Antico	Monte Crobu: ignimbrita moderada a extremadament soldada i eutaxítica amb abundants a molt abundants pumites grises i ocasionalment negres molt aplanades. Reomòrfica. Vitròfir basal.
MLN	E de l'illa de Santo Antioco	Monte la Noce: colades de lava, cinerites i ignimbrites moderada a extremadament soldades amb vitròfir basal. Afírica.
SE	Terra ferma N i central	Seruci: ignimbrita fortament soldada i eutaxítica amb pumites decimètriques. Vitròfir basal.
AC	Extensa, del N de terra ferma fins al graben de Giba-Narcao	Acqua sa Canna: ignimbrita pobrament soldada formada per diverses unitats de flux amb gradació normal de pumites
LE	Terra ferma N	Lenzu: ignimbrita fortament soldada i eutaxítica amb abundants grans pumites decimètriques. Vitròfir basal.
CM	Terra ferma N i central	Corona Maria: ignimbrita escassa a moderadament soldada i eutaxítica amb abundants pumites i fragments lítics. Té vitròfir basal.
AND	S de l'illa de Santo Antioco i graben de Giba-Narcao	Andesites: colades i doms de lava amb bretxes associades

Taula 1: Àrea d'afloramen t i principals característiques de les unitats volcàniques oligo-miocenes del Sulcis

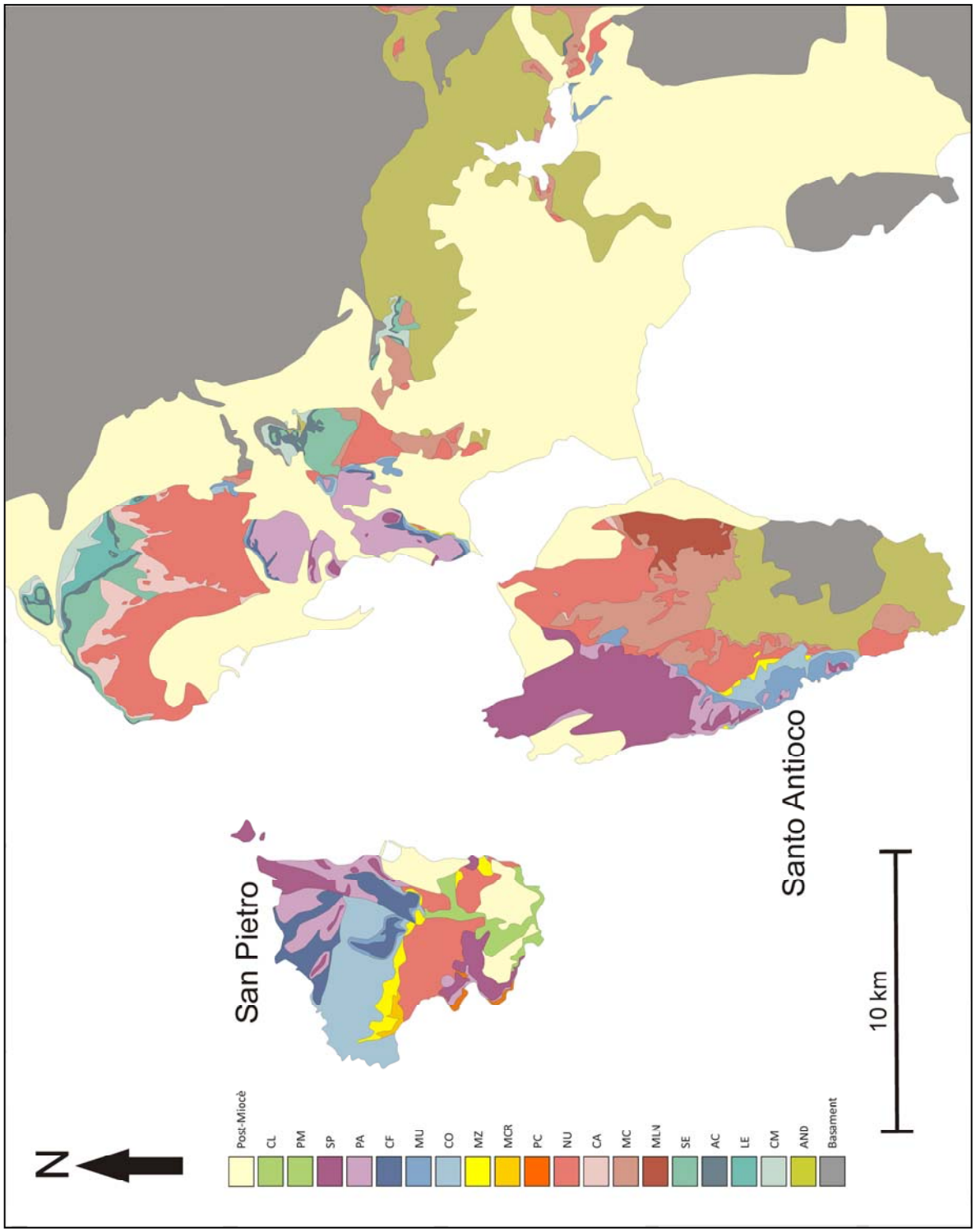

Figura 2: Cartografia simplificada del vulcanisme oligo-miocè del Sulcis

6 RESULTATS DE PETROGRAFIA I QUÍMICA MINERAL

L'observació petrogràfica de les roques volcàniques del Sulcis ha mostrat abundant variabilitat textural dins de la seqüència fruit de la presència de doms i colades de lava i de roques piroclàstiques, i dins d'aquestes últimes de dipòsits ignimbrítics amb diferents graus de compactació i soldatge.

Els doms i colades de lava són típicament porfírics (amb l'excepció de les colades de la unitat MLN) formats per un conjunt de fenocristalls en una matriu vítria o parcialment cristal·litzada que pot presentar diferents graus de desvitrificació. A més, poden contenir cossos externs al magma, anomenats genèricament enclavaments. Pel que fa a les ignimbrites, aquestes són roques fragmentàries formades per un conjunt de piroclastos que inclouen els *shards* (fragments fins de vidre), pumites, cristalls i fragments de cristalls, i enclavaments (tant xenòlits com lítics accidentals). La compactació i soldatge fan variar la textura dels dipòsits originals generant roques més cohesives amb textura eutaxítica evidenciada per l'estirament i aplanament dels *shards* i pumites. Graus molt alts de soldatge i reomorfisme associat poden arribar a esborrar la textura piroclàstica original d'una ignimbrita. En funció del grau de soldatge les ignimbrites es troben més o menys afectades per processos de desvitrificació, que afecten tant el vidre dels *shards* com el de les pumites.

Pel que fa al contingut mineral, amb l'excepció de les andesites, que mostren una paragènesi dominada per plagiòclasi i piroxens, l'associació típica està dominada per feldspats (un o dos), que estan acompanyats per minerals opacs (òxids de Fe i Ti) i màfics accessoris. Aquests són sobretot piroxens, amb la presència en algunes unitats d'amfíbol o biotita. A les comendites, acompanyant els feldspats també es pot trobar quars. Ocasionalment s'ha trobat zircó i apatita. Cal destacar la presència en algunes unitats de cristalls d'amfíbol de fase vapor cristal·litzats com a clapes poiquilítiques a la matriu (a les comendites) o com a cristalls hipidiomòrfics en vesícules (textura miarolítica).

A la Taula 2 es resumeixen les principals característiques de les unitats estudiades observades a partir de l'estudi petrogràfic. La química mineral de les diferents fases trobades es mostra gràficament als diagrames de les Figures 3 a 6. La llegenda de la Figura 3 és la mateixa que s'utilitzarà per la química de roca total.

7 RESULTATS DE LA GEOQUÍMICA DE ROCA TOTAL

Les dades obtingudes a partir de l'anàlisi de la geoquímica de roca total no han estat incorporades directament a la base de dades de geoquímica. Només s'han aprofitat aquelles anàlisis que

Unitat	Porfiricitat	Fases minerals	Característiques destacables
CL/PG	10	sa+pl+opq±zrn	
PM	<1	sa+ano+pl+opq+m.a.±zrn	Afírica. No domina cap dels tres feldspats
SP	1-20	pl+ano+opq+px+amp	Dues poblacions de pumites molt aixafades
PA	<10	sa+pl+opq±bt±zrn	Generalment baix contingut en lítics i pumites. Pl accessòria amb mantell de sa
CF	10-20	sa+opq+ano	Pumites negres riques en sa amb una composició amb més An que les sa de la matriu, i signes de reabsorció. Ano com a possibles xenocristalls
MU	<3	sa+qz+opq+zrn+amp(v)	Afírica. Amp sòdic en fase vapor
CO	5-30 fins a 50	sa+qz+amp+opq+amp(v)	Amp sòdic (fenocristalls i fase vapor) i sòdic-càlcic (fase vapor i fenocristalls parcialment reabsorbits)
MZ	3-20	pl+bt+opq	Caracteritzada pel relativament alt contingut en bt.
MCR	5-20	sa+pl+opq±zrn	En ignimbrita és rica en lítics. Domina la sa, que forma mantells sobre la pl
PC	fins a 50	ano+pl+opq+cpx+opx	Elevada porfiricitat. Domina l'ano, que està corroïda, excepte en les fàcies negres, on només hi ha pl. Els px només estan sans en fàcies negres
NU	20-30	sa+pl+opq+cpx±amp(v)	Elevada porfiricitat, pobra en lítics. Els feldspats poden formar glomèruls de fins a 8 mm
CA	10	sa+pl+opq	Lítics abundants.
MC	10-20	sa+pl+opq+amp(v)	Clar domini de sa sobre pl. En les pumites negres la sa està corroïda i la pl té més Or que la de la matriu
MLN	<5	pl+opq±bt	Molt afírica. A la base de les ignimbrites es pot trobar bt molt escassa
SE	10-20	pl+opq+m.a.±opx±cpx +amp(v)	Conté màfics alterats i els piroxens sans només es troben en una fàcies concreta
AC	10-20	pl+bt+opq±amp	
LE	10-20	pl+sa+opq+opx±zrn	Lítics escassos
CM	10-30	pl+cpx+opq±bt±amp	Lítics abundants. Domini de pl
AND		pl+opx+cpx+opq±ol	Holocristal·lines porfíriques

Taula 2: Resum de les característiques petrogràfiques de les unitats volcàniques del Sulcis. Abreviacions minerals: amp: amfíbol; ano: anortòclasi; bt: biotita; cpx: clinopiroxè; ol: olivina; opq: mineral opac; opx: ortopiroxè; pl: plagiòclasi; px: piroxè; qz: quars; sa: sanidina; zrn: zircó; m.a.: màfic alterat; (v): fase vapor

presentaven una bona qualitat i que a més pertanyien a roques no alterades. Els primers criteris emprats han estat que les anàlisis havien de mostrar un LOI per sota de 2,5% en pes (quantitat màxima indicada a Le Maitre et al. (1989) per poder considerar una roca com a fresca), i la suma de majors havia d'estar per sobre de 98% en pes. Una excepció han estat les anàlisis corresponents als vitròfirs, ja que aquests nivells poden contenir grans quantitats d'aigua en solució al vidre, fins a un 7% (Smith et al., 2001). Així mateix, la projecció de les dades obtingudes en diagrames binaris ha permès detectar aquelles mostres que presentaven signes d'alteració (per exemple continguts anòmals de Na_2O o K_2O) i silicificació, que és un procés recurrent en ignimbrites d'aquestes composicions. La norma CIPW s'ha calculat mitjançant el software integrat al programa IGPET (Carr, 2005), que segueix el mètode d'Irvine and Baragar (1971). En total en aquest treball es proporcionen 281 noves anàlisis de roca total.

Figura 3: Llegenda per la química mineral i química de roca total

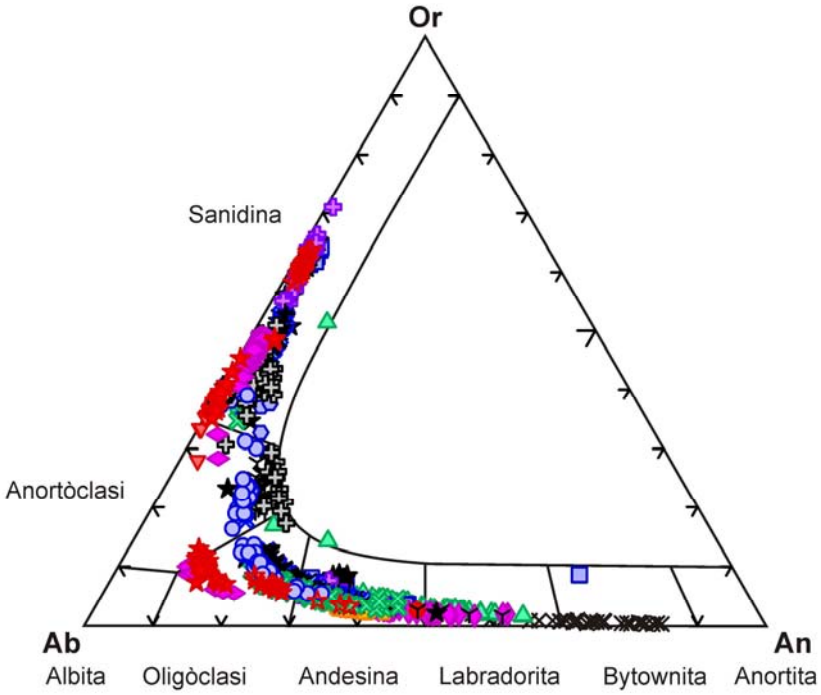

Figura 4: Composicions dels feldspats estudiats

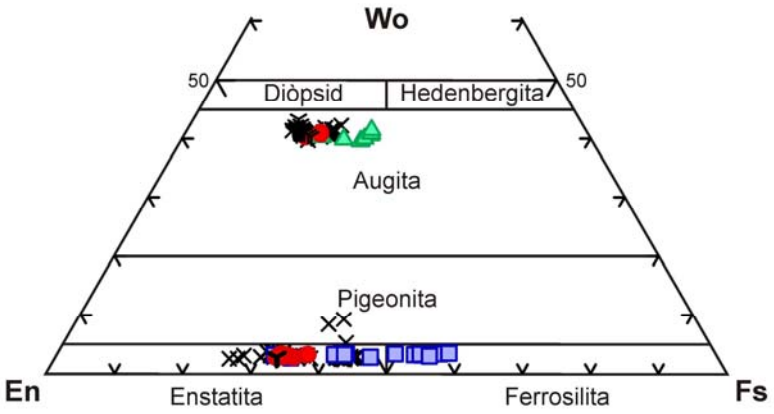

Figura 5: Composicions dels piroxens estudiats

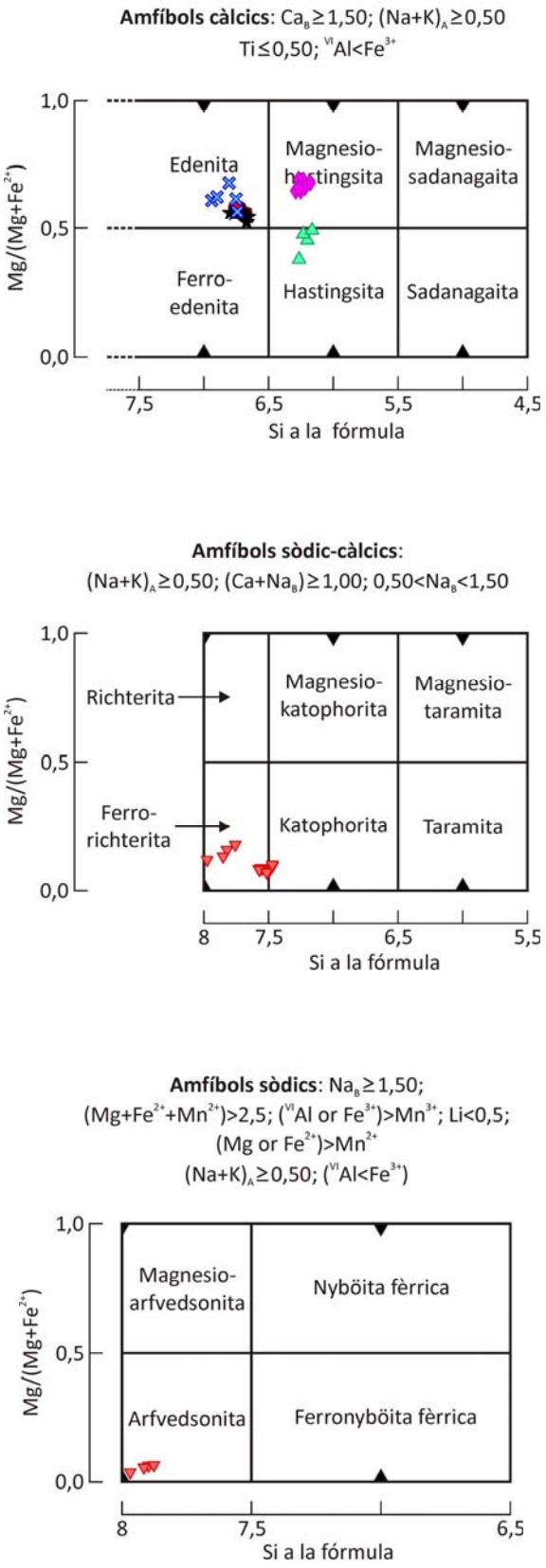

Figura 6: Composicions dels amfíbols estudiats

Les dades pròpies obtingudes han servit a la vegada per poder revisar les dades publicades anteriorment a la bibliografia i seleccionar aquelles que mostraven bona qualitat i que per tant han pogut ser incorporades a la base de dades de geoquímica de roca total. S'han revisat els treballs d'Araña et al. (1974), Assorgia et al. (1994), Morra et al. (1994), Cioni and Funedda (2005), i Conte et al. (2010). També s'han revisat les dades de Rosselló (2005) i Ramon (2009).

Les roques analitzades han estat classificades seguint el sistema proposat a Le Maitre et al. (1989), que utilitza el diagrama TAS (Total Alkalis versus Silica) definit per Le Bas et al. (1986). Les roques de la seqüència andesítica es representen en els camps de l'andesita basàltica i andesita, mentre que les roques de la seqüència ignimbrítica es troben majoritàriament en el camp de les riolites, amb només algunes unitats (CM, AC, PC, i mostres de MZ i CF) situades al camp de les traquites (Fig. 7). Les roques peralcalines (CO, MU, CF) han estat classificades segons MacDonald (1974a), obtenint composicions comendítiques excepte per tres mostres que entren lleugerament al camp de les pantellerites. En el diagrama TAS es pot observar que les unitats no es troben alineades en una sola tendència, sinó que se'n poden reconèixer vàries. Pel que fa a la resta d'elements majors, els diagrames Harker mostren tendències que indiquen el fraccionament de fenocristalls (Fig. 8). També es poden observar tendències de fraccionament en comparar el contingut d'alguns traces respecte la sílice.

Pel que fa als elements traça la projecció del contingut d'aquests en diagrames multielementals normalitzats respecte el mantell primitiu (Sun and McDonough, 1989) dóna perfils similars als de magmatisme orogènic de subducció, amb enriquiment de LILE respecte HFSE (Fig. 9). Les anomalies creixents amb el grau de diferenciació de Ba, Sr, P, Eu i Ti indiquen el fraccionament de feldspats, apatita i òxids amb Ti.

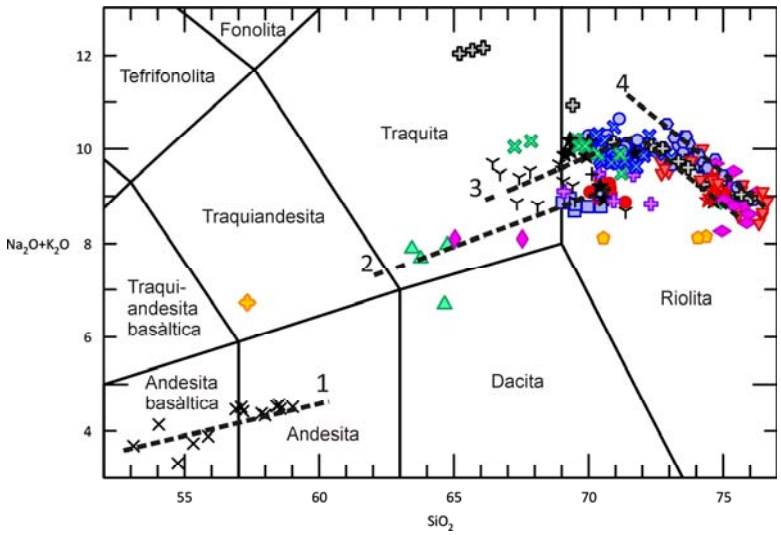

Figura 7: Ampliació del sector del diagrama TAS que conté les roques estudiades. Es poden observar diverses tendències evolutives. Concentracions en % en pes

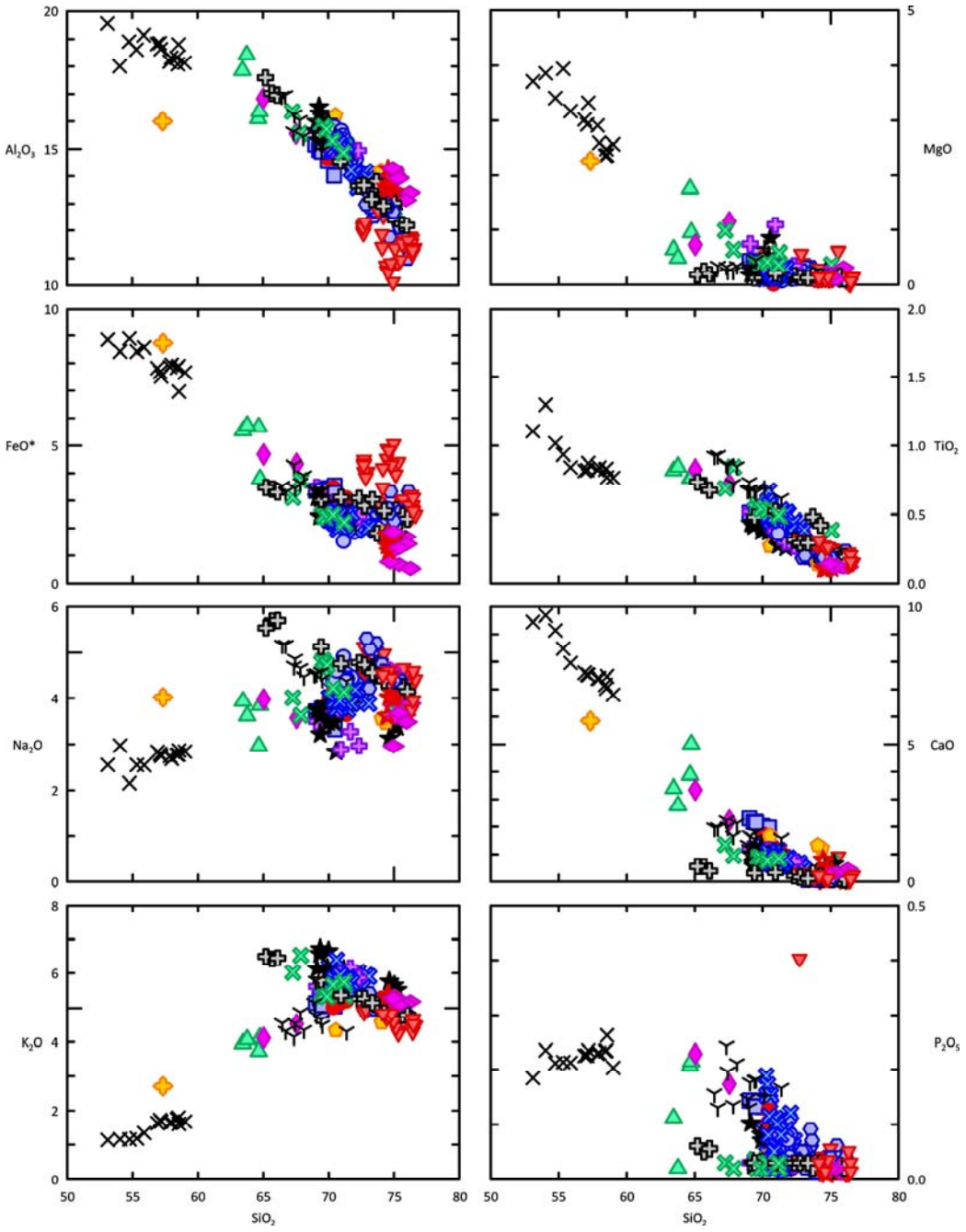

Figura 8: Diagrames Harker per les roques estudiades. Concentracions en % en pes

Les dades isotòpiques disponibles actualment pel vulcanisme oligo-miocè del Sulcis es mostren a la Figura 10. Els isòtops d'Sr, Nd i $^{206}Pb/^{204}Pb$ mostren unes tendències lineals ascendents, indicant una variació gradual al llarg de la seqüència ignimbrítica de la isotopia dels magmes que la generen. La isotopia de $^{207}Pb/^{204}Pb$ (i també la de $^{208}Pb/^{204}Pb$, que mostra una tendència similar però una mica menys marcada) mostra, dins de la tendència general, tres sub-tendències descendents.

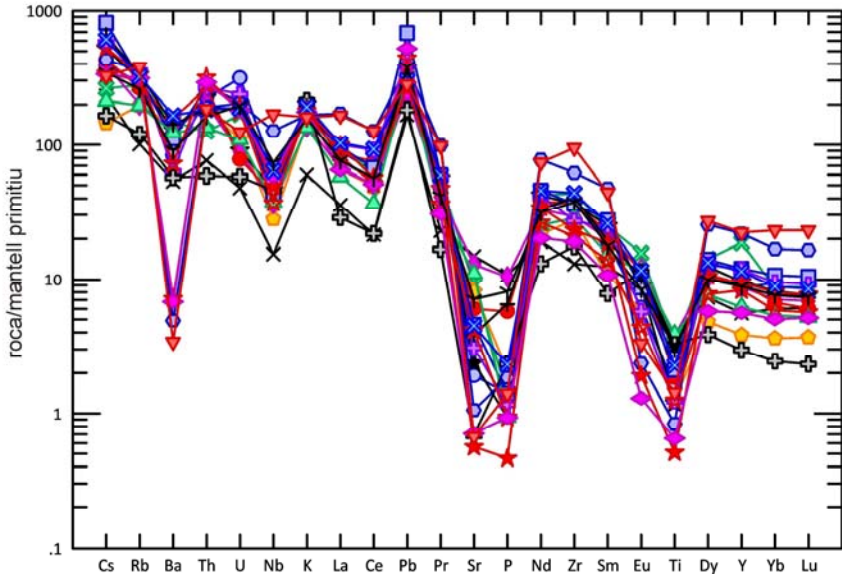

Figura 9: Elements traça normalitzats respecte el mantell primitiu (Sun and McDonough, 1989)

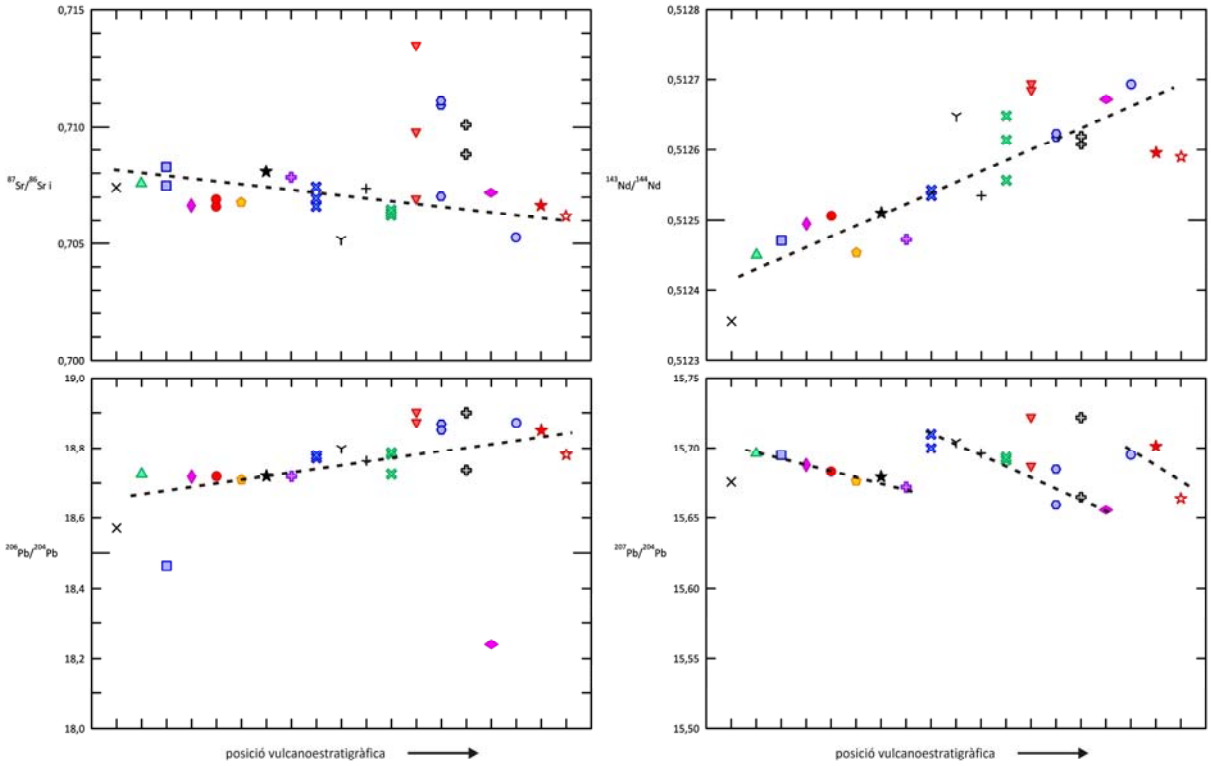

Figura 10: Isotopia d'Sr, Nd i Pb de les mostres del Sulcis. Falta $^{208}Pb/^{204}Pb$, que té un comportament similar a $^{207}Pb/^{204}Pb$

8 DISCUSSIONS I CONCLUSIONS

En aquest últim apartat del resum es discuteixen breument els principals assumptes tractats durant aquest estudi, aportant les principals conclusions obtingudes. L'elaboració i discussió dels resultats obtinguts durant aquest estudi s'ha centrat en dos aspectes principals: en el desenvolupament d'una metodologia que permeti reconèixer les unitats ignimbrítiques en base a la geoquímica de roca total, i en la discussió de la petrogènesi d'aquesta associació magmàtica i les seves implicacions geodinàmiques en el marc de l'evolució del Mediterrani occidental.

8.1 Reconeixement d'unitats basat en la geoquímica de roca total

En fer treball de camp al Sulcis, la majoria de les vegades les característiques macroscòpiques de les ignimbrites (components, color, estratigrafia, etc.) són suficients per reconèixer la unitat que es té davant. A més, en cas de necessitat es pot obtenir informació addicional de l'estudi petrogràfic. Ara bé, en alguns casos la manca d'afloraments junt amb la semblança entre algunes unitats (tant macroscòpica com, en molts casos, microscòpica), o la presència de fàcies molt diferents d'unitats conegudes, fan que sigui més difícil reconèixer a quina unitat pertany una mostra o aflorament. En aquest casos la geoquímica de roca total pot representar una eina molt eficaç. En aquest estudi s'ha desenvolupat una metodologia per resoldre els dubtes de reconeixement d'unitats en base a la geoquímica de roca total. Aquesta metodologia es basa en l'ús de diagrames binaris que comparen el contingut en elements traça de les roques del Sulcis. Els elements escollits per construir els diagrames han estat aquells que mostren més resistència a l'alteració, és a dir, els immòbils, dels quals s'han usat Ti, Zr, Y i Nb. Ocasionalment també s'han utilitzat Th, Rb, Sr i Zn, que, tot i ser més mòbils que els elements anteriors, s'han mostrat com a útils en alguns casos.

Normalment, durant el treball de camp es pot arribar a una identificació aproximada de la unitat amb la que es tracta o de la seva posició estratigràfica, de manera que en la majoria de casos els dubtes d'identificació es restringeixen a haver de diferenciar entre dues unitats concretes que presentin gran similitud. Per aquest motiu s'ha generat un primer joc de diagrames per resoldre els dubtes generats pels principals parells d'unitats que típicament poden causar problemes. Ara bé, en alguns casos ni tan sols es pot arribar ni a una identificació aproximada de la unitat amb la que es tracta. Això es pot deure a la presència d'afloraments petits i/o aïllats, o a la presència d'una fàcies desconeguda. Per aquests casos s'ha desenvolupat una metodologia més exhaustiva basada en la combinació de diversos diagrames binaris que permet, per la majoria d'unitats, reconèixer a quina unitat pertany una mostra gràcies només a la geoquímica. La Figura 11 mostra un dels primer diagrames a utilitzar per a la identificació d'una mostra.

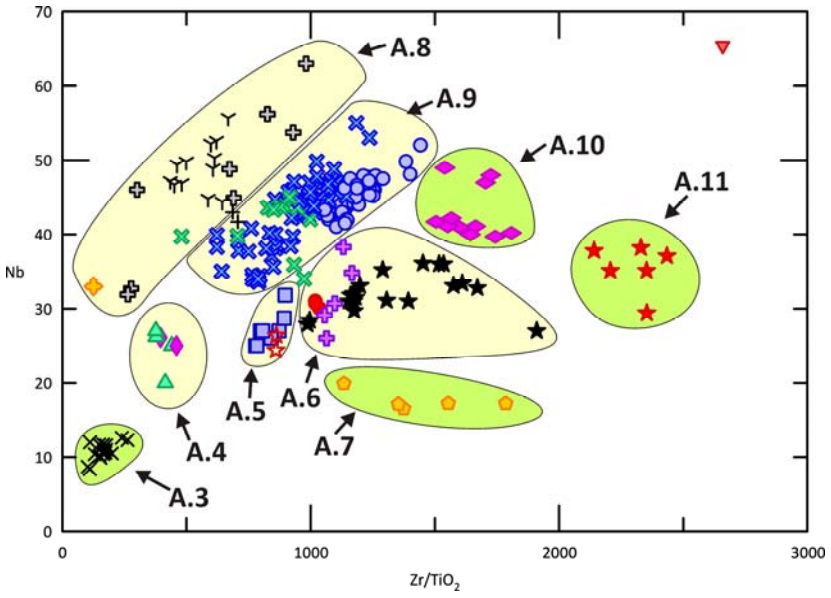

Figura 11: Diagrama usat pel reconeixement d'unitats. S'observa com les unitats es distribueixen en diferents àrees que permeten identificar-les. Per les àrees on hi ha més d'una unitat s'utilitza posteriorment un altre diagrama. Concentracions en ppm

Aquesta metodologia ha estat elaborada a partir de l'estudi de mostres de roca fresca, sense alterar ni silicificar, i per tant en principi només hauria de ser emprada per roques en aquestes condicions. Sovint, però, hi ha la necessitat d'identificar mostres concretes que no es troben en les millors condicions. Per això s'ha investigat l'aplicabilitat d'aquesta metodologia per la identificació de roques moderadament alterades i silicificades usant les dades de geoquímica de roca total descartades prèviament. Cal tenir present que no s'ha fet un mostreig específic de roques alterades, de manera que les mostres alterades estudiades segurament no són representatives de tota la variabilitat química que pot provocar l'alteració, i per tant els resultats són merament orientatius. Tot i això, s'ha vist que la majoria de diagrames mantenen la seva utilitat en tractar amb roques alterades.

La metodologia desenvolupada ha estat de gran utilitat durant la realització d'aquest treball, permetent resoldre dubtes cartogràfics i vulcanoestratigràfics. A més ha permès correlacionar les diverses fàcies presents en algunes de les unitats estudiades, així com identificar la unitat a la que pertanyen enclavaments trobats dins d'algunes unitats com la SP. Alhora també ha servit per comprovar si les dades de geoquímica disponibles a la bibliografia havien estat atribuïdes a la unitat correcta. Un dels exemples més clars de la utilitat d'aquest mètode va tenir lloc quan es va poder reconèixer correctament una mostra aïllada recuperada d'un sondeig en curs de la minera Carbosulcis SpA, identificant immediatament la posició estratigràfica del front del sondeig. Tots aquests fets demostren que el reconeixement d'unitats ignimbrítiques en base a la química de

roca total, que tradicionalment no s'ha contemplat com a útil per l'heterogeneïtat que solen presentar aquest dipòsits, és possible i que pot ser usat tant en l'àmbit acadèmic com comercial, no només al Sulcis sinó segurament també en altres àrees d'estudi.

8.2 Formació dels magmes i implicacions geodinàmiques

Des del treball de Coulon (1977) es considera que el vulcanisme oligo-miocè de Sardenya correspon a un magmatisme calcoalcalí d'afinitat orogènica format per fusió parcial d'una font mantèl·lica provocada per la subducció. Al Sulcis, tot i l'evident diferència composicional del magmatisme ignimbrític present respecte la part andesítica de la seqüència i la resta del magmatisme de Sardenya, es va considerar que l'origen dels magmes era el mateix ja des dels primers estudis geoquímics (Assorgia et al., 1990b). Morra et al. (1994) va fer la primera modelització petrogenètica del Sulcis, centrada en la seqüència ignimbrítica, i lligant genèticament aquesta part de la seqüència amb la part inferior andesítica.

Font magmàtica

Els elements traça i les relacions isotòpiques de les roques volcàniques del Sulcis evidencien que els magmes estudiats es van originar a partir d'una font mantèl·lica. Els perfils d'elements traça en els diagrames multielementals normalitzats respecte la composició del mantell primitiu mostren morfologies típiques de magmatisme de zona de subducció, amb enriquiment de LILE respecte HFSE causat per l'aport de fluids enriquits en elements mòbils alliberats per la placa subduïda al mantell sobre aquesta. Els perfils es mantenen aproximadament paral·lels al llarg de la seqüència, tant andesítica com ignimbrítica, mostrant que tots els magmes es van originar en una font de composició similar. Aquest perfil és compartit amb la resta del magmatisme oligo-miocè de Sardenya.

Els diagrames normalitzats respecte la composició de les condrites aporten dades sobre la composició mineralògica de l'àrea font. Els perfils normalitzats mostren un enriquiment relatiu de LREE, amb un pendent més elevat de La a Sm, i un tram pla a les HREE. El pendent pla de les HREE mostra que no hi havia granat com a fase residual de fusió, i que per tant segurament aquest mineral no hi era. L'enriquiment de LREE respecte HREE indica que les fases principals de l'àrea font eren olivina i piroxè. Tot i que no s'evidencia en aquests diagrames, la presència de flogopita i amfíbol es corrent en mantells metasomatitzats per subducció i per tant es pot esperar que també hi fossin sota Sardenya.

L'estudi de les relacions isotòpiques del Sulcis, comparant aquestes amb diferents reservoris isotòpics, incloent tant reservoris mantèl·lics com possibles fonts de contaminació (com ara sediments subduïts o escorça continental), i amb la resta del magmatisme de Sardenya (tant

oligo-miocè com plio-pleistocè) ha proporcionat informació sobre la composició i origen de les fonts magmàtiques mantèl·liques presents sota l'illa de Sardenya. Les dades disponibles indiquen que el mantell sota Sardenya tenia abans del Cretaci superior una composició com la de les fonts dels magmes tipus OIB, amb una signatura isotòpica EMI. A partir del Cretaci superior l'ascens de la Central Atlantic Plume (CAP, Harangi et al., 2006; Piromallo et al., 2008) va causar un metasomatisme que va introduir al mantell una signatura isotòpica tipus HIMU. Aquesta ploma tenia també una composició de font de magmes tipus OIB, típica de les plomes mantèl·liques. Aquest metasomatisme no va ser complet, deixant un mantell amb una estratificació difosa amb una porció superior amb composicions encara tipus EMI feblement contaminada pel HIMU, i una porció inferior més rica en HIMU. Aquest mantell metasomatitzat per HIMU es pot trobar arreu de la regió Euro-Mediterrània, constituint un reservori comú per la regió que ha rebut diversos noms al llarg dels anys, i que en aquest treball s'anomena tipus EAR (EAR, Cebria and Wilson, 1995). Posteriorment, amb l'inici de la subducció oligocena els fluids alliberats per la placa subduïda (que eren tan fluids aquosos expulsats pel sediment i per la porció superior de l'escorça oceànica com fosos parcials de sediment) van metasomatitzar el mantell, introduint una signatura de subducció tan pel que fa als elements traça com als isòtops, afectant principalment la porció tipus EAR d'aquest. Els magmes orogènics oligo-miocens, incloent els magmes del Sulcis, van ser originats en el mantell tipus EAR metasomatitzat per la subducció i presenten una composició isotòpica que traça una línia de barreja entre un mantell pròxim a EAR i una component de sediment més escorça oceànica (Fig. 12). Els magmes anorogènics plio-pleistocens, en canvi, van ser generats en la porció superior del mantell i per tant mostren composicions tipus EMI, marcant l'inici d'una tendència de barreja cap a les composicions tipus EAR. El fet de que el magmatisme de Sardenya aparentment no mostrés la component tipus EAR (ja que el magmatisme anorogènic presenta composicions EMI, mentre que al magmatisme orogènic la composició tipus EAR està camuflada pel metasomatisme de subducció) havia fet pensar que el component tipus EAR omnipresent al Mediterrani no es trobava sota Sardenya, on només unes poques mostres (RPV, Lustrino et al., 2000) presenten composicions similars a aquest. La revisió de les dades ha mostrat que l'aparent manca de mantell tipus EAR a Sardenya no es deu a una variació lateral de la composició del mantell, sinó a una variació en profunditat, de manera que el magmatisme anorogènic sard, generat a menys profunditat que l'orogènic, no va arribar a mostrejar el reservori tipus EAR excepte en escasses ocasions.

Els diagrames de relacions isotòpiques respecte la posició estratigràfica mostrats a la Figura 10 mostren tendències lineals excepte per la relació $^{207}Pb/^{204}Pb$. Aquestes tendències s'expliquen millor per un canvi progressiu de la composició isotòpica de la font mantèl·lica, més que no pas

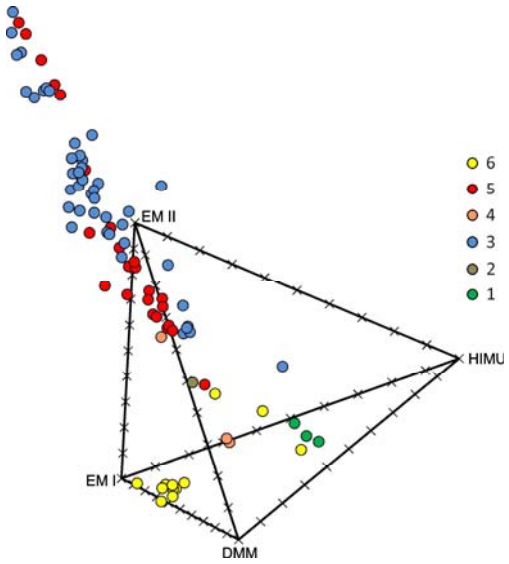

Figura 12: Diagrama tetraèdric on s'observen les tendències descrites. 1: mantell tipus EAR; 2: MORB alterat; 3: sediments; 4: magmatisme oligo-miocè de Sardenya; 5: magmatisme del Sulcis; 6: magmatisme plio-pleistocè

per processos de contaminació de magmes amb una composició isotòpica inicial igual, ja que els valors d'isotopia depenen de la posició estratigràfica i no del grau de diferenciació del magma. L'excepció de $^{207}Pb/^{204}Pb$ es deu a que aquest isòtop és el més susceptible a la contaminació. Així, es considera que els processos d'assimilació van jugar un paper menor en l'evolució d'aquests magmes. Aquestes tendències lineals marquen una disminució progressiva de la signatura de subducció en les relacions isotòpiques, i per tant de la influència dels fluids de subducció en la generació dels magmes del Sulcis.

Formació dels magmes del Sulcis

En el diagrama TAS la seqüència ignimbrítica del Sulcis es troba clarament separada de la resta del magmatisme oligo-miocè de Sardenya. Mentre que aquest últim es troba en posicions subalcalines típiques de magmes orogènics, les ignimbrites del Sulcis es troben a la zona transicional a feblement alcalina del diagrama. Atès que per la pròpia construcció del diagrama TAS les sèries comagmàtiques es projecten en aquest seguint traces subparal·leles a les línies d'igual saturació de sílice, és difícil justificar que tot el magmatisme del Sulcis pertanyi a una mateixa sèrie magmàtica com van proposar Morra et al. (1994). Alhora s'evidencia que el mecanisme de formació dels magmes que van generar la seqüència ignimbrítica devia ser diferent del que va formar la resta del magmatisme orogènic.

La majoria del magmatisme orogènic oligo-miocè de Sardenya, incloent el del Sulcis, es va emplaçar en un context tectònic local extensiu. Tot i que es considera que variacions en la intensitat de l'extensió poden provocar variacions en l'alcalinitat dels magmes generats en

contextos extensius, tots els magmes orogènics de Sardenya, des del emplaçats sense extensió fins als formats sota les condicions de màxima extensió generades durant la màxima velocitat de rotació del bloc Sard-Cors, presenten les mateixes condicions de subalcalinitat, mantenint-se en el sector inferior del diagrama TAS. Així, malgrat les variacions en el grau d'extensió la formació dels magmes orogènics estava en tot moment dominada per la subducció. Per tant es considera que l'únic mecanisme capaç de causar un augment en l'alcalinitat dels magmes devia ser una disminució en la influència de la subducció que provoqués un canvi en el mecanisme de fusió dels magmes del Sulcis de fusió dominada pels fluids de subducció a fusió dominada per l'extensió, és a dir, un trànsit de magmatisme orogènic de subducció a magmatisme anorogènic. Aquesta disminució en la influència dels fluids de subducció s'evidencia, com s'ha vist anteriorment, en les relacions isotòpiques dels magmes estudiats. Per tant, es podrien considerar els magmes que van generar la seqüència ignimbrítica com a transicionals cap a anorogènics o fins i tot purament anorogènics, ja que ja no estaven influïts per la subducció. Aquest caràcter transicional a anorogènic dels magmes de la seqüència superior del Sulcis es confirma en projectar les dades en el diagrama Nb vs. Zr, que pel magmatisme de Sardenya separa clarament els magmatismes orogènic i anorogènic (Fig. 13).

Així, al Sulcis es va donar inicialment un magmatisme orogènic com el de la resta de Sardenya que va donar lloc a la formació de la seqüència andesítica. A partir d'un cert moment, però, per un

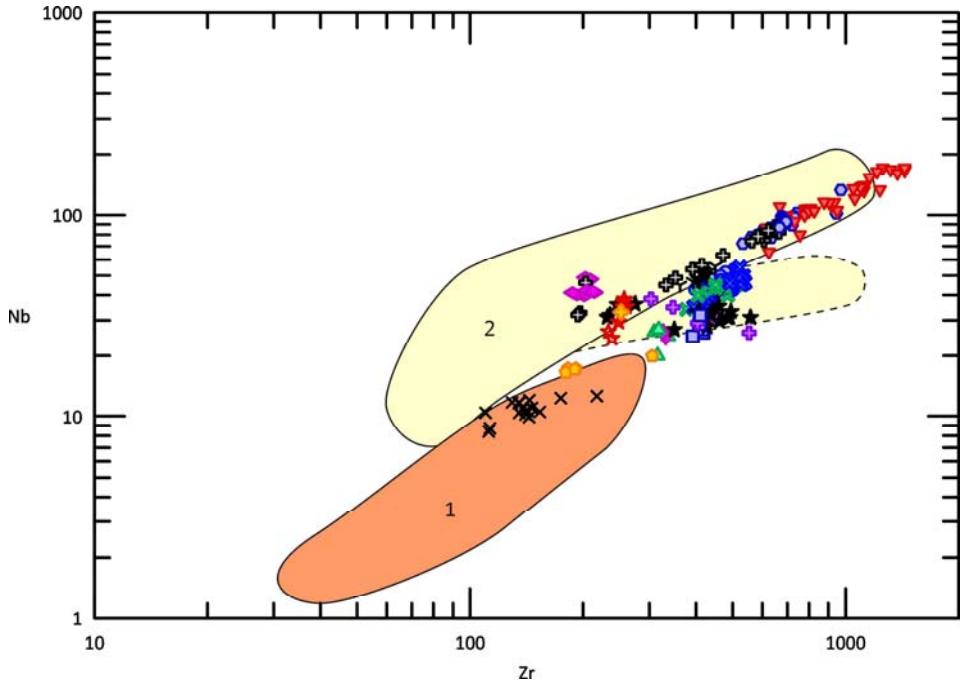

Figura 13: Separació entre el magmatisme orogènic (1) i anorogènic (2) de Sardenya, amb projecció de les dades del Sulcis. Concentracions en ppm

motiu que es comentarà més endavant, la influència de la subducció a la porció de mantell sota el Sulcis va disminuir fortament o fins i tot parar. En una subducció compressiva això hagués significat el final del vulcanisme. Però al Sulcis el context extensiu va provocar que continués la fusió del mantell. Al començament el mantell encara era ric en fluids de subducció, generant, per tant, magmes quasi orogènics. A mesura que continuava la fusió, però, cada cop hi havia menys aigua, generant magmes que tendien progressivament cap a més clarament anorogènics. En aquest punt el menor grau de fusió respecte el magmatisme orogènic va causar l'augment en l'alcalinitat observable al TAS, alhora que el grau d'extensió i la presència residual de fluids controlaven el grau d'alcalinitat, cosa que explica la presència de magmes de diversa alcalinitat dins de la seqüència ignimbrítica, només alguns dels quals arriben a la peralcalinitat.

Aquesta hipòtesi descarta la proposada per Morra et al. (1994), alhora que el trànsit proposat pel magmatisme del Sulcis d'orogènic a anorogènic és coherent amb la presència de les comendites, ja que excepte per les comendites del Sulcis no s'ha descrit mai cap roca peralcalina formada en context orogènic de subducció. Si bé és cert que hi ha comendites associades a zones de subducció actives, aquestes es troben sempre en posicions de rere-arc, mai en associació amb els magmes orogènics.

Implicacions geodinàmiques

Hi ha diverses observacions que han permès perfilar un model evolutiu per Sardenya que permeti justificar el trànsit del magmatisme del Sulcis d'orogènic a anorogènic a finals del cicle volcànic oligo-miocè de Sardenya. El magmatisme anorogènic del Sulcis és contemporani amb magmatisme orogènic a altres regions de Sardenya situades més al nord, encara que aquest ja es trobava en una fase de molt poca activitat, de manera que el procés causant d'aquest trànsit no va poder ser generalitzat. Alhora, no hi ha magmatisme orogènic contemporani ni posterior al del Sulcis a l'E d'aquesta regió. Finalment, les datacions disponibles indiquen que entre el final del desplaçament de Sardenya, amb la tectònica i vulcanisme associats, i l'obertura del sud del Tirrè, que va comportar la reactivació de la tectònica extensional i la formació del vulcanisme anorogènic plio-pleistocè de Sardenya, hi ha una interrupció de quasi 6 Ma en l'activitat tectònica i magmàtica. El model que es proposa i que permet justificar la formació simultània dels magmatismes orogènic i anorogènic oligo-miocens i la llarga pausa en l'activitat tectònica i magmàtica és la formació d'un trencament en la placa subduïda.

Es proposa que a mesura que la microplaca Sard-Corsa s'aproximava a la seva situació actual, al sud de l'illa de Sardenya la placa subduïda va cedir, iniciant-se un trencament progressiu que va avançar cap al N (Fig. 14). L'origen del trencament al S de Sardenya és fàcil de justificar, ja que en

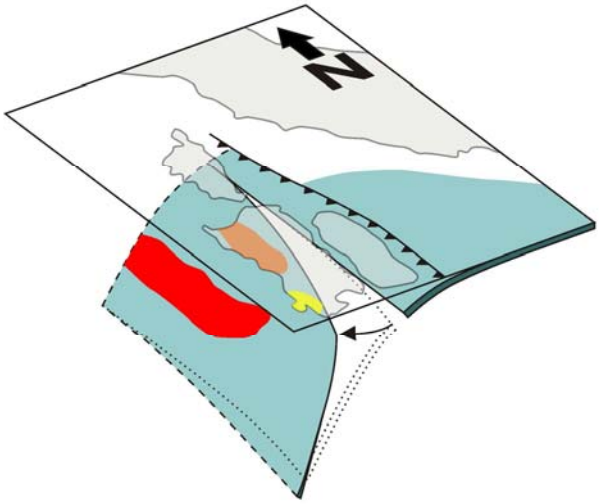

Figura 14: Diagrama esquemàtic del model proposat per l'evolució de la subducció. L'àrea en vermell representa la zona d'alliberament de fluids de subducció i de formació de magmatisme orogènic. La zona taronja és on es donen els últims events de magmatisme orogènic de Sardenya, contemporanis al vulcanisme anorogènic del Sulcis, que està marcat en groc

aquest punt es trobava la zona de la subducció que contenia més placa subduïda, alhora que representava el límit entre dues porcions de la subducció que es movien en direccions diferents (al sector nord amb rotació antihorària i al sector sud amb horària). Fins i tot alguns autors, com ara Séranne (1999), han proposat la presència en aquest punt d'una zona transformant (North Balearic Transform Zone). A mesura que el trencament avançava cap al N, la zona ja trencada s'enfonsava ràpidament a causa de l'*slab pull*, generant una finestra a la placa subduïda. Alhora, això provocaria una disminució en l'*slab pull* i per tant en la velocitat de subducció, de retrocés del *roll-back* i de rotació de la microplaca. Si es considera que el trencament va tenir lloc per sobre del punt d'alliberament de fluids de subducció, a aquelles regions on arribava la finestra de subducció s'aturava l'aport de fluids, mentre que més al nord encara n'hi hauria producció. En els punts on ja no hi havia aport de fluids de subducció la tectònica extensional present va permetre continuar amb la fusió, generant els magmes transicionals a anorogènics del Sulcis. Això explica la presència simultània de magmatisme orogènic i anorogènic. A més, la disminució en la velocitat de subducció va provocar la disminució observada en la producció de magmatisme orogènic. És probable que el final del magmatisme i quasi absència de tectonisme després del cicle oligo-miocè es degués al trencament complet de la placa subduïda, o com a mínim d'una porció significativa d'aquesta. Només al cap d'alguns milions d'anys l'*slab pull* va ser capaç de reactivar el *roll-back*, que finalment va generar la conca de rere-arc que és el Tirrè, deixant Sardenya a la seva posició actual. L'absència de vulcanisme orogènic plio-pleistocè a Sardenya concorda amb aquest model, ja que quan la subducció va aconseguir tornar a funcionar normalment va caldre un temps per a

que la placa subduïda tornés a assolir profunditats d'alliberament de fluids i per tant de formació de magmatisme orogènic, el qual va ser suficient per desplaçar la zona d'erupció dels nous magmes orogènics més enllà de l'illa de Sardenya.

8.3 Evolució dels magmes des de la formació fins a l'erupció

L'estudi combinat de la química de roca total, de la petrografia i de la química mineral ha permès interpretar com va ser l'evolució dels magmes del Sulcis des de la seva formació al mantell fins a la seva emissió a la superfície. Les dades disponibles evidencien que les unitats presents al Sulcis es van formar a partir de l'evolució de diferents bossades de magma amb composicions inicials lleugerament diferents que van evolucionar en cambres magmàtiques corticals predominantment per processos de cristal·lització fraccionada, amb només un paper menor per part de l'assimilació.

Aports de magma al sistema

La presència de vàries tendències evolutives pels magmes del Sulcis s'observa al diagrama TAS, però també en altres diagrames binaris com ara el Nb vs. Rb. A més, al llarg de la seqüència no hi ha un augment progressiu del grau de diferenciació dels magmes, sinó que sovint hi ha retorns cap a composicions més primitives. Tot plegat posa de manifest que la seqüència present al Sulcis es va originar a partir de diferents bossades de magma. De fet s'ha vist que excepte les unitats LE i SE, que es poden considerar com a formades per evolució dels magmes que van generar les unitats immediatament precedents, totes les unitats ignimbrítiques representen l'arribada d'una nova bossada de magma al sistema.

Evolució genèrica dels magmes del Sulcis

Les tendències observades als diagrames binaris d'elements majors i alguns traces indiquen que l'evolució dels magmes estudiats va estar dominada per processos de cristal·lització fraccionada. Tot i que s'ha dit que el magmatisme del Sulcis presenta diverses tendències evolutives, aquestes són el producte de l'evolució de magmes amb composicions inicials només lleugerament diferents, que van produir petites variacions en les associacions minerals fraccionants i per tant en les tendències evolutives. Tenint això present, les tendències són prou semblants com per poder estudiar tot el magmatisme en conjunt per tal de poder interpretar quines van ser les fases fraccionants.

L'evolució dels magmes més bàsics va estar dominada pel fraccionament d'olivina, piroxens i plagiòclasi. A partir de composicions andesítiques o similars en grau d'evolució l'associació mineral passava a estar dominada per plagiòclasi, amb piroxens com a fases màfiques principals, tot i que ocasionalment l'amfíbol i la biotita també podien jugar un paper important en aquells

magmes amb més aigua. El piroxè es troba com a fenocristalls fins a continguts en SiO_2 al voltant del 70% en pes al magma. En arribar al camp riolític la sanidina apareixia a l'associació fraccionant, tot i que no esdevenia la fase fraccionant principal fins a continguts en SiO_2 de al voltant del 72% en pes, punt a partir del qual la inflexió en el diagrama binari K_2O vs. SiO_2 indica la importància del fraccionament d'aquesta fase en l'evolució dels magmes. En els magmes peralcalins, que representen uns dels més evolucionats de la seqüència, el quars s'afegia a la sanidina com a fase fraccionant, fet que limitava el posterior augment del contingut en SiO_2 dels magmes. Durant tota l'evolució dels magmes precipitaven òxids de Fe i Ti, que influïen sobretot en el contingut en TiO_2 del magma, i en menor mesura en el de FeO, tot i que la seva importància com a fases fraccionants disminuïa progressivament amb l'evolució magmàtica fins al punt que són quasi inexistents en les unitats més evolucionades. Tot i que només s'ha observat apatita en les andesites, el contingut en P_2O_5 dels magmes indica que aquest element s'enriquia amb la diferenciació en els magmes andesítics, mentre que en els magmes més diferenciats el fraccionament era més eficient produint-ne un empobriment progressiu. També s'ha observat la presència de zircó en els magmes estudiats, tot i que només es va produir un fraccionament suficient d'aquest mineral com per empobrir els magmes en Zr en el cas de les unitats més diferenciades no peralcalines (PA i PM principalment). En els magmes peralcalins l'excés d'àlcalis i els continguts elevats en halògens mantenien una elevada solubilitat del zircó, fet que causava un enriquiment constant en Zr més enllà del que és esperable en magmes no peralcalins.

Malgrat que s'ha discutit anteriorment que la isotopia i els elements traça descarten una contribució significativa dels processos d'assimilació en la modificació del quimisme dels magmes estudiats, les tres tendències menors, de traça comparable entre sí, observables en la isotopia de $^{207}Pb/^{204}Pb$ i $^{208}Pb/^{204}Pb$ s'han interpretat com a producte de contaminació dels magmes durant la seva permanència a la cambra magmàtica. Els tres magmes d'inici de les tendències s'interpreten com a episodis més importants de contaminació per assimilació deguts a una permanència més llarga a la cambra, mentre que les tendències descendents serien degudes a l'arribada de nous magmes sense contaminar que progressivament diluirien aquesta contaminació en els magmes resultants.

Cristal·lització dels feldspats

Els feldspats són les fases dominants en les associacions minerals fraccionants en totes les roques estudiades al Sulcis. En les roques menys evolucionades la plagiòclasi és l'únic feldspat fraccionant, mentre que en els magmes més diferenciats només s'observa sanidina. Les roques de composicions intermèdies presenten una associació amb dos feldspats, contenint simultàniament plagiòclasi i sanidina.

L'estudi de la petrografia i de la química mineral dels feldspats ha mostrat que la cristal·lització d'aquests minerals va variar al llarg de la seqüència, sent aquestes variacions produïdes per diferències en les composicions dels magmes, per processos de *mixing* i *mingling* de magmes, per assimilació de roca encaixant, o per diferents activitats d'aigua. En la cristal·lització normal dels magmes, la més freqüent, aquella fora de l'equilibri per intervenció de la cristal·lització fraccionada, el primer feldspat a aparèixer és la plagiòclasi. A mesura que l'evolució del magma progressa, la composició del fos d'aquest s'aproxima al cotèctic del sistema ternari dels feldspats, començant a cristal·litzar, quan hi arriba, dos feldspats simultàniament (plagiòclasi i sanidina), la composició dels quals varia amb la cristal·lització al llarg de la intersecció del liquidus i el solvus del sistema, convergint cap a la composició del mínim del sistema. A mesura que la cristal·lització progressa, el líquid es mou al llarg del cotèctic i els feldspats es van apropant en composició fins que arriba un punt en què la plagiòclasi comença a ser reabsorbida alhora que va canviant de composició. En alguns casos en aquest punt es produeix el creixement de sanidina sobre la plagiòclasi (observable al Sulcis en les unitats MCR i PA). En cas de la continuar la cristal·lització, en els casos més extrems (com ara el de les roques peralcalines), s'arriba a la cristal·lització d'un sol feldspat, sanidina, i tant les composicions del feldspat com del líquid assoleixen la composició del mínim del sistema Ab-Or. Les unitats estudiades representen magmes en diferents punts d'aquesta història evolutiva. Els processos de *magma mingling*, com el que va afectar les unitats MC o PC per exemple, van produir la presència de diverses poblacions de feldspats en una sola unitat, i la desestabilització d'algunes d'aquestes per canvis de composició del fos en el que es trobaven els cristalls i/o per variacions de temperatura. En els magmes que presentaven una major activitat d'aigua aquesta va retardar la formació de sanidina, provocant una major cristal·lització de plagiòclasi i, en el cas de la SP, formant una associació de plagiòclasi amb anortòclasi en comptes de plagiòclasi amb sanidina. Finalment, la modificació local de la composició original del magma per difusió de components de la roca encaixant va provocar a la unitat MU l'aparició de zonació química a les seves sanidines.

<u>Magmes peralcalins</u>

L'últim punt que es tracta en aquest resum és l'aparició de magmes peralcalins al magmatisme del Sulcis. Anteriorment s'ha vist que la presència de magmes peralcalins al Sulcis és coherent amb la interpretació del seu magmatisme ignimbrític com a magmatisme anorogènic amb formació de magmes transicionals a lleugerament alcalins, que típicament són els que acaben donant els magmes peralcalins arreu del món. Falta interpretar com va ser l'evolució d'aquests magmes, que va permetre que arribessin a la peralcalinitat.

En base a l'estudi de les tendències observables als diagrames binaris de química de roca total, i a la comparació d'aquestes amb les d'altres associacions magmàtiques amb presència de roques peralcalines, s'interpreta que els magmes peralcalins es van formar per evolució per simple cristal·lització fraccionada de magmes lleugerament més alcalins que els que es poden observar a la seqüència ignimbrítica del Sulcis no peralcalina (la que forma la tendència 3 a la Figura 7). Tot i això, s'ha estudiat la possibilitat de que els magmes peralcalins del Sulcis es poguessin generar a partir dels magmes més alcalins trobats a l'àrea, com ara el de la unitat NU, tal com van proposar Morra et al. (1994), mitjançant modelització numèrica de contingut d'elements majors. Malgrat que encara cal millorar la modelització, s'ha trobat que no hi ha relació possible entre la NU i els magmes peralcalins a través de simple cristal·lització fraccionada, i que l'única manera de passar d'una composició a l'altra es assumint un mecanisme de cristal·lització fraccionada amb assimilació d'amfíbol cristal·litzat prèviament.

LIST OF ABBREVIATIONS

Ab: albite

AC: Acqua sa Canna

Acm: acmite

AFC: Assimilation and Fractional Crystallisation

AI: Agpaicity Index

Amp: amphibole

An: anorthite

AND: Andesites

Ano: anorthoclase

Ap: apatite

Bt: biotite

CA: Conca is Angius

CAI: Centro de Apoyo a la Investigación de Geocronología y Geoquímica Isotópica (Universidad Complutense de Madrid)

CAP: Central Atlantic Plume

CF: Carloforte

CHUR: Chondritic Uniform Reservoir

CL: Colonne

CM: Corona Maria

CMR: Common sublithospheric Mantle Reservoir

CO: Comendites

Cpx: clinopyroxene

Crn: corundum

D: Distribution Coefficient

Di: diopside

DL: Detection Limit

DMM: Depleted MORB Mantle

EAR: European Asthenospheric Reservoir

EMI: Enriched Mantle I

EMII: Enriched Mantle II

EMP: Electron Micro-Probe

En: enstatite

FOZO: Focal Zone

Fs: ferrosilite

HFSE: High Field Strength Elements

HIMU: High-μ

HREE: Heavy Rare Earth Elements

Hyp: hypersthene

ICP-MS: Inductively Coupled Plasma with Mass Spectrometry

ICP-OES: Inductively Coupled Plasma with Optical Emission Spectrometry

Ilm: ilmenite

LE: Lenzu

LILE: Large Ion Lithophile Elements

LL: lower limit of the calibration range

LOI: Loss on Ignition

LREE: Light Rare Earth Elements

LVC: Low Velocity Component

Mag: magnetite

MC: Monte Crobu

MCR: Montagna di Capo Rosso

MLN: Monte la Noce

MORB: Mid-Ocean Ridge Basalts

MU: Monte Ulmus

MZ: Matzaccara

NBTZ: North Balearic Transform Zone

NU: Nuraxi

OIB: Ocean Island Basalts

Ol: olivine

Opq: opaque mineral

Opx: orthopyroxene

Or: orthoclase

PA: Paringianu

PC: Punta dei Cannoni

PDC: Pyroclastic Density Current

PG: Punta Genniò

Pl: plagioclase

PM: Punta Mingosa

ppm: parts per million

Qz: quartz

REE: Rare Earth Elements

RPV: Radiogenic Pb Volcanics

Rt: rutile

Sa: sanidine

SCT-UB: Serveis Científico-Tècnics de la Universitat de Barcelona

SE: Seruci

SP: Serra di Paringianu

TAS: Total Alkalis versus Silica

TIMS: Thermal Ionisation Mass Spectrometry

Ttn: titanite

UL: upper limit of the calibration range

UPV: Unradiogenic Pb Volcanics

Vol: volume

Wo: wollastonite

Wt: weight

XRF: X-Ray Fluorescence

Zrn: zircon

THE MIOCENE VOLCANISM OF THE SULCIS AREA (SW SARDINIA, ITALY): PETROLOGY, PETROGENESIS AND GEODYNAMIC SIGNIFICANCE

INTRODUCTION

MOTIVATION OF THIS STUDY

The Central and Western Mediterranean area is one of the most complex and controversial geological regions over the world. Between the Eurasian and African plates, it is constituted in fact by a relatively high number of microplates that moved and collided in a particularly active way during the last 30 Ma. The result of these movements is a kind of microplate patchwork where the volcanic units mark the geodynamic events underwent in this area and provide evidence not only of the crustal evolution but also of the characteristics of the mantle placed beneath these microplates. This geological puzzle has started to be deciphered just in the course of the last 40 years, and the process is still ongoing.

During the last 30 Ma several geological events of major relevance in the evolution of this area have been: the subduction of oceanic plate under Sardinia and Southern Corsica marked by the generation of arc volcanism; the Miocene anticlockwise displacement of Corsica and Sardinia and the associated creation of the Liguro-Provençal oceanic space in a back-arc position due to subduction roll-back; the back-arc generation of the Tyrrhenian oceanic space by further eastward migration of subduction; the formation of an active volcanic arc in eastern Tyrrhenian area; and finally the formation of Etna and the peri-Thyrrenian Pleistocene to present volcanoes in Italy, including the currently active Aeolian area arc. In this context, Sardinian Miocene volcanism occupies a central situation in this geodynamic framework and provides key information on all the initial processes of this geological evolution. In particular, southwestern Sardinia corresponds to the crustal part of the Corsica-Sardinia block that underwent most displacement and extension during drifting and rotation of this microplate, producing a special volcanic suite which began sharing the same characteristics as the rest of the subduction-related volcanism throughout

Sardinia but that later migrated to different compositions including the rarely occurring peralkaline volcanism.

Considering the history of the petrology and volcanology knowledge, the central and western Mediterranean area concentrates a large number of the seminal studies that deeply influenced knowledge for at least two centuries. Activity at Etna and Vesuvius volcanoes attracted the attention of early scientists during the Illustration epoch, and, even before, the 79 AD eruption of Vesuvius was the first one to be described from the point of view of eruptive mechanisms. Sardinia was also a key place of this discovery process. La Marmora (Voyage en Sardaigne, 1857) described (and illustrated with geological sketches) for the first time a large number of extinct volcanoes and volcanic units in Sardinia. By the end of 19th century peralkaline rhyolitic rocks (comendites) were for the first time described in San Pietro Island (Bertolio, 1895). In the absence of a systematic geological mapping of Sardinia Island provided by the Servizio Geologico d'Italia (published sheets were mainly focused on the rich mining districts of the island), during the first half of the 20th century the references on Miocene Sardinian volcanism were generic (undifferentiated rocks in the mapping of the Sulcis area close to the Carbonia lignite beds), sparse, and mainly associated to descriptive notes of mines (i.e. the Mn and Cu mines in the Bosano area), most of them produced in the autarchic fascist period. After World War II the volcanic districts of the island were studied by university schools, singularly the University of Parma under the direction of Prof. Deriu, providing as a result a large number of thematic maps on the volcanic districts of the island and a number of publications on this subject in the 50's to 70's period.

These thematic maps provided a base for the increase of knowledge produced in the last 40 years. The first milestone in the evolution of knowledge in Sardinia was the work by Christian Coulon, mainly focused in northwestern Sardinia and developed during the 70's, that lead to the petrological characterization of the volcanic cycles of Miocene volcanism with orogenic affinity, which were related to the north-westernwards (relative to the present geography) subduction of an oceanic plate under the Sardinia continental microplate. In parallel, a second milestone was the geochronological and paleomagnetic data that provided evidence of the anticlockwise movement of the Corsica-Sardinia block from the European continental margin to its present position. In the Sulcis region, Garbarino studied again San Pietro Island comendites and provided the first modern volcanological map of the island. The second half of the 80's gave up to 107 Logs of the Ocean Drilling Project (ODP) scientific perforation on the Tyrrhenian sea bottom and the subsequent interpretation of the two-phased back-arc opening of this oceanic space and the

study of the associated volcanism, a new milestone that produced an enormous increase of knowledge on the geodynamic and petrological features of central Mediterranean.

In the area of study, the parallel work of Carbosulcis SpA geologic staff (in mainland Sulcis) and the Cagliari University researchers produced three volcanological maps of the Sulcis mainland and San Pietro and Santo Antioco islands, the cartographic base for the present study, with an irregular quality (excellent, good and poor respectively), and a great handicap: the absence of correlation of the several volcanic units between the three maps. Also, the scientific team formed around Prof. Assorgia (Cagliari University) provided in collaboration with the Carbosulcis SpA geologic staff the first attempt at a volcanostratigraphic description of this area and the first petrochemical characterization with modern analytical techniques of these rocks. Later, Morra et al. (1994) did the first petrogenetic interpretation of the volcanic succession, and in particular of the comenditic end of it, as a product of volcanism in an orogenic geodynamic environment, implicitly considering the whole succession as the product of a single magma evolutionary trend produced by fractional crystallization. Two Italian PhD Thesis (Del Vecchio, 1989; Pioli, 2003) were conducted on particular aspects of the Sulcis volcanic district. During the development of this work, a new cartographic synthesis of southern Sulcis mainland and Santo Antioco Island has been conducted by the Servizio Geologico d'Italia; this map is still not published but we had limited access to the data and it has been extremely useful to contrast it with our own maps.

Given this context, the Sulcis sector was regarded as probably the poorliest known orogenic volcanic area in Sardinia from a petrological and volcanological point of view, in spite of its great interest and importance as a source of information for the correct interpretation of the recent geodynamic evolution of central and western Mediterranean and the volcanism associated with it. To solve this, at least partially, this area was chosen for the development of the present PhD Thesis.

OBJECTIVES

The first objective of this study was the petrological and geochemical characterization of the Oligo-Miocene volcanic succession of the Sulcis area, in particular of the pyroclastic succession, and especially of the upper part of the sequence containing the peralkaline lavic and pyroclastic units. This careful and systematic characterization allowed the accomplishment of other objectives which were: the development of a methodology for ignimbritic unit identification based on whole rock geochemistry, sometimes key given the great macroscopic (and even petrographic) similarities between units, especially in the case of the highly welded and rheomorphic ones; a cartographic revision, assisted with petrography and geochemistry, which

although it was not a main objective of the Thesis it was necessary in order to correctly conduct it, as well as the correlation between volcanic units cropping out at the Sulcis Mainland and the minor islands of Santo Antioco and San Pietro; and the petrogenetic interpretation of the Sulcis suite in the framework of western Mediterranean evolution. The petrogenetic study including Sr-Nd-Pb isotopic geochemistry carried out in the present study is the first one done for this volcanic district, and can be considered a core part of the work, since it provided important geodynamic and petrological results. Another of the initially projected objectives, the obtaining of a new radiometric chronostratigraphic set of data, finally resulted beyond of the possibilities of the study. But the results exposed here provide the required tools and knowledge in order to correctly choose the samples to be dated, and dating is in course of execution by the research team.

THESIS STRUCTURE

This Thesis is divided into four parts containing a total of ten chapters, and six appendixes. The first part has an introductory character and provides an overview of some theoretical concepts dealt with during the Thesis (Chapter 1), an introduction to the geological context of the study (Chapter 2), and a revision of the previous work carried out in the study area (Chapter 3). Part two is focused on the methodology followed for the development of the present study. It contains one single chapter (Chapter 4), but is complemented by two appendixes providing information on precision and accuracy of the analytical techniques used (Appendix 2) and detailed description of lab protocols (Appendix 3). Part three presents the main results obtained from the study of the volcanic succession, relating to volcanostratigraphy (Chapter 5), petrography and mineral chemistry (Chapter 6) and whole rock geochemistry (Chapter 7). The last part of this Thesis contains the discussion on whole rock geochemistry-based unit characterization and recognition (Chapter 8) and petrogenesis of the volcanic suite, regarding magma generation and its relationship with the geodynamic context (Chapter 9) and magma evolution and crystallization (Chapter 10). Finally, a summary of the main conclusions obtained in the present study is presented. To help following the presentation of results and the discussions, a reference chart is provided in Appendix 1 containing a brief description of the units present in the studied sequence, abbreviations of their names used in the text, and the legends used in geochemistry and mineral chemistry diagrams and in maps, which are the same throughout the whole volume.

PART I: INTRODUCTION

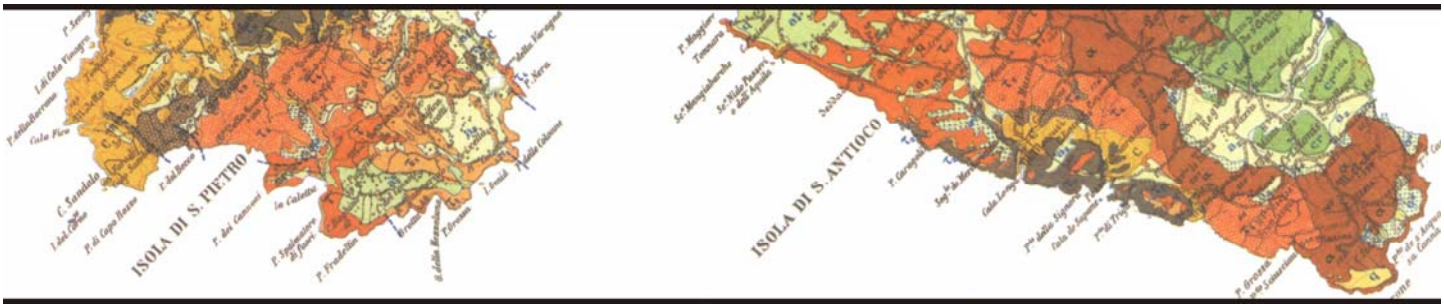

CHAPTER 1: SUBJECT INTRODUCTION

1.1 MAGMA GENERATION MECHANISMS

Rocks are formed by a mixture of different minerals with various melting temperatures. As a result of the different melting points, as well as of the interaction between chemical components which modifies these temperatures, rocks melt over a range of temperature rather than at a specific one. The temperature at which melting first starts in a rock is known as the solidus temperature. The temperature at which the last bit of rock melts and the whole rock becomes a liquid is known as the liquidus temperature. Melting is a process requiring a lot of energy, so in natural systems liquidus is almost never reached. Instead, only a fraction of the original rock is melted generating a batch of melt which will have a composition different from that of the original rock. This process is known as partial melting. Most of the magmas generated in the Earth are formed by partial melting.

Three mechanisms have been recognised for a rock to reach the solidus temperature and start melting: increasing temperature, reducing pressure, and lowering the solidus temperature by changing rock composition (Fig. 1.1). The first mechanism consists in heating the rock until the solidus is crossed. Heating may be caused by burial of the rock into deeper and hotter zones (e.g. by orogen building or subduction), or by heat transfer from a hotter body (e.g. basic magma underplating lower continental crust).

Solidus and liquidus temperatures increase with pressure. Reducing confining pressure while keeping the temperature nearly constant may cause the rock to reach the solidus. This kind of melting is known as decompression melting or pressure-release melting. It is the typical melting process occurring in extensional settings and hot spots. If decompression is faster than cooling, melting occurs (e.g. in hot spots, where mantle plumes undergo an adiabatic ascent).

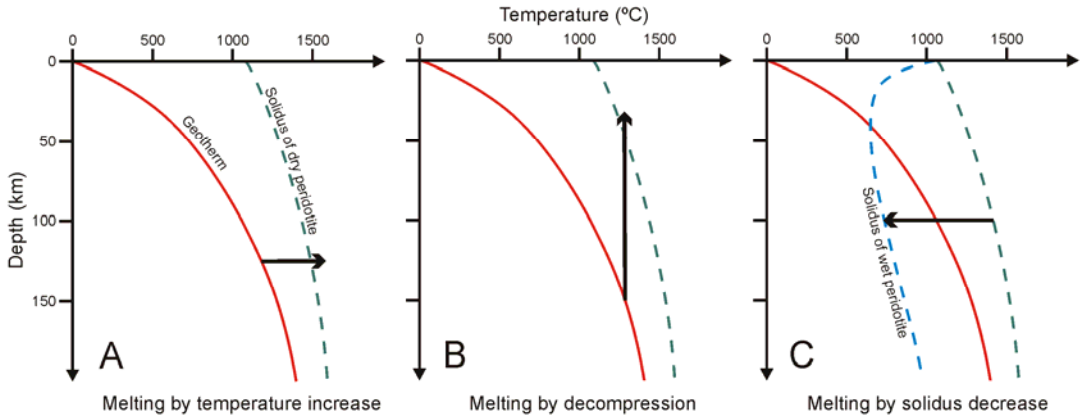

Figure 1.1: The three main melting mechanisms

The last mechanism consists in changing the composition of the rock to a new one with a lower solidus temperature. This is usually done by the addition of water. The melting temperature of a water-poor rock is considerably higher than that of a rock containing abundant water. Water has a strong effect on lowering melting temperature of rocks. If initial temperature of a "dry" rock is sufficiently high, addition of even small amounts of water will reduce its solidus temperature enough to begin melting. This mechanism is typical of subduction zones, where the slab releases water from subducted sediments and hydrothermally altered upper regions of the crust on burial. Water is released into the mantle wedge or lithospheric mantle producing melting and generating the magma which will form the volcanic arcs observable over subduction zones.

Chemical composition of the generated magma will be strongly controlled by the original mineralogical and chemical composition of the source area and by the melting mechanism. Due to the heterogeneous geochemical behaviour of chemical elements, the mineral phases being melted, as well as the amount of partial melting, condition the concentration of the different elements in the final melt by releasing them in varying proportions. Major elements are mainly controlled by the composition of the main mineral phases being melted, but trace elements behave in a much more complex way.

1.2 GEOCHEMICAL BEHAVIOUR OF TRACE ELEMENTS IN MAGMATIC SYSTEMS

Trace elements are usually defined as those present in a rock in concentrations of less than 0.1 wt %, that is less than 1000 µg/g (ppm). Some trace elements may form mineral phases on their own, but most commonly they substitute major elements in rock-forming minerals. Trace elements are usually grouped according to their properties. Variations observed when comparing separated groups or elements within a group are used as indicators of petrological processes.

Trace elements are mainly classified according to their behaviour in magmatic systems. When a rock is partially melted, elements display a preference either for the melt phase or the solid phase (mineral phase). If a mineral is in chemical equilibrium with a liquid, elements are partitioned between the two phases according to their chemical activity in each. For elements whose concentration is low (less than 1 wt %) a constant partition (or distribution) coefficient can be defined for the given crystal-liquid equilibrium as

$$K_D = \frac{\text{concentration in mineral}}{\text{concentration in liquid}}$$

Rocks are formed by several minerals; to properly characterise how an element will distribute between the solid and liquid phase a bulk distribution coefficient (D) must be defined. D is calculated from the K_D for each mineral phase, and the weight proportion of each mineral phase within the rock. It is obvious that for a given element D will strongly depend on liquid composition and mineral assemblage. Two types of behaviour may be recognised. Elements with a $D << 1$ are termed incompatible; they will be preferentially concentrated in the liquid phase during melting and crystallisation. In contrast, those with $D > 1$ are called compatible and these will be preferentially retained or extracted in the residual or crystallising solid phases respectively. During the course of magma evolution mineral assemblage may vary, with the total consumption of some phases and appearance of others; as a result elements may change in behaviour from compatible to incompatible and vice versa. An example for this is P, which behaves as incompatible in basic magmas until due to magma evolution apatite appears as a crystallising phase. When apatite starts to precipitate P is heavily extracted from the liquid into the new phase, thus behaving as a compatible element.

It is sometimes useful to subdivide elements on the basis of their charge/size ratio. This property is described as field strength. Small highly charged cations are known as high field strength elements (HFSE), and large cations with a small charge are known as low field strength elements or large ion lithophile elements (LILE). HFSE include lanthanides, Sc, Y, Th, U, Pb, Zr, Hf, Ti, Nb and Ta. LILE include CS, Rb, K and Ba. To these may be added Sr, divalent Eu and divalent Pb. In the presence of an aqueous solution HFSE generally behave as immobile, while LILE are mobile.

Elements with the same ionic charge and size are expected to show very similar geochemical behaviour. Example of this may be element pairs such as Hf and Zr or Nb and Ta, but also element groups as is the case for rare earth elements (REE), which include lanthanides. REE usually form trivalent cations, with ionic radius slightly decreasing from La to Lu. The slight ionic radius variation determines that, even having very similar behaviour, light REE are slightly more incompatible than heavy REE.

Oxygen activity may play an important role in the control of element behaviour. Oxygen activity determines the ionic state of a given element, thus controlling its compatibility. One of the most widely used examples is Eu and its partition between plagioclase and basaltic melts. Under high oxygen activities Eu^{3+} is formed, which behaves like the rest of REE as an incompatible element. However, under low oxygen activities Eu^{3+} turns to Eu^{2+}, which can partition into plagioclase more easily. There is an order of magnitude difference in the partition coefficient between Eu^{2+} and Eu^{3+}.

1.3 SUBDUCTION-RELATED MAGMATISM

Subduction of an oceanic plate may occur beneath another oceanic plate or beneath a continental plate. In both cases magmatism generates a volcanic chain on the upper plate, parallel to the subduction trench. When subduction is beneath an oceanic plate volcanism generates an island arc. If it is a continental one, a continental arc is formed (also known as active continental margin).

Magma is generated in subduction zones primarily by water addition to the mantle wedge and lithospheric mantle, causing the peridotite to melt and produce basaltic magmas. During ascent of magma towards the surface ponding may occur at several levels below and inside the crust. Assimilation and fractional crystallisation (AFC) processes progressively modify magma composition during its ascent. In island arcs lithosphere is thin and denser compared to continental one, opportunities for magma evolution are few and primitive magmas dominate. In continental settings, though, lithosphere is thick and formed by less dense materials, with presence of physical discontinuities, making magma ascent difficult and favouring magma stagnation and therefore AFC processes. Therefore, more evolved (silicic) magmas dominate in active continental margins.

Island arcs show a wide range of magma types, from basalts through basaltic andesites and andesites to dacites and rhyolites. Although there is a considerable variation between island arcs, dominant rock type is andesite, with basalts and basaltic andesites being fairly common, and the more evolved types (dacites and rhyolites) being rare. Continental arcs present an even wider diversity of magmas, and typically produce a greater proportion of evolved magmas than island arcs. Although andesites are still common, there are more dacites and rhyolites, and basalts and basaltic andesites are rare.

Magmas generated in subduction settings share common chemical characteristics. Most of the volcanic rocks in volcanic arcs are calc-alkaline in composition. In addition, low-K tholeiitic and potassic magmas can also be associated with an active subduction. These magmas have trace

element and isotopic fingerprints that are usually interpreted as reflecting the fluid effect in their genesis, which does not restrict to water addition. Aqueous fluids and silicate melts released from the subducted slab produce a metasomatism of the mantle wedge, changing its chemical composition. Generated magmas have higher ratios of large ion lithophile elements (such as Cs, Rb, Ba, K, Sr) and Pb to high field strength elements (e.g. Nb, Ta, Zr, Hf and Ti). LILE are soluble in aqueous fluids, so they are carried by released fluids from the slab to the mantle wedge, which becomes enriched in these elements in comparison to immobile elements like the HFSE and REE. Metasomatism is thus reflected by negative anomalies in HFSE and relative enrichment of LILE in patterns of primitive mantle-normalised multielemental diagrams (Figure 1.2 is an example of the Aeolian Islands, considered a typical subduction zone).

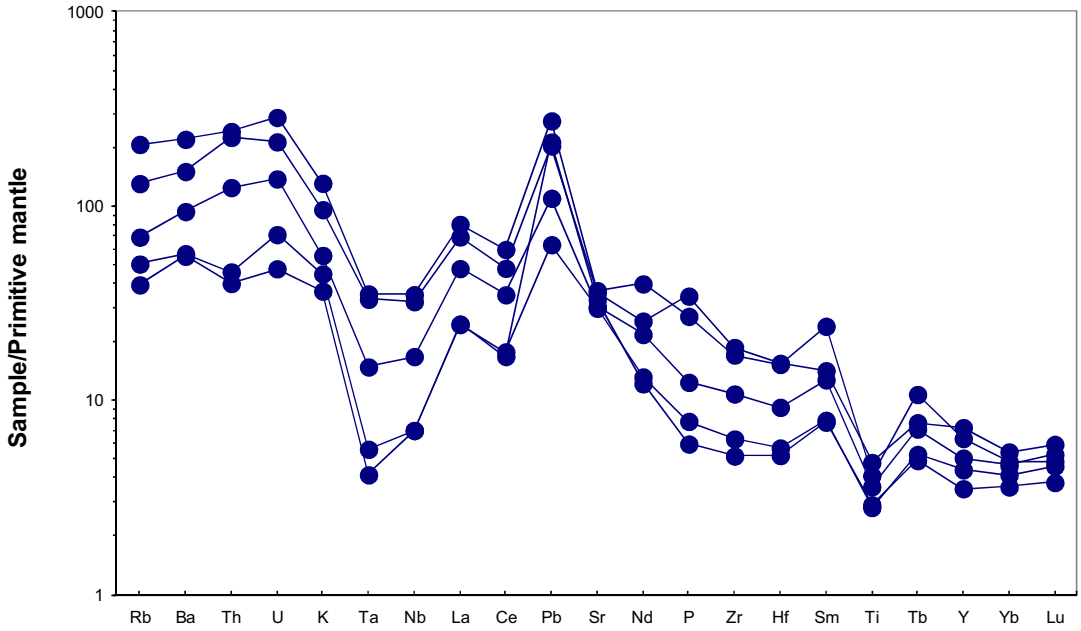

Figure 1.2: Multielemental diagram for samples from the Aeolian Islands (Ellam et al., 1989) showing contents normalised to primitive mantle (normalizing values of Hofmann (1988))

1.4 SILICIC VOLCANISM

Volcanic eruptions present a wide variety of styles, products and scales: effusive or explosive, from quiet small scale Hawaiian to very violent plinian or ultraplinian eruptions. Properties determining eruptive dynamics are mainly two: magma viscosity and gas content.

Magma viscosity is controlled by various factors: silica content, water content, temperature, and crystal and gas bubble content (Fig. 1.3). These factors are not independent; for a given temperature, the higher the silica content the more viscous magma is. In addition, Si-rich magmas form at lower temperatures than mafic ones, and for a given composition lower temperature

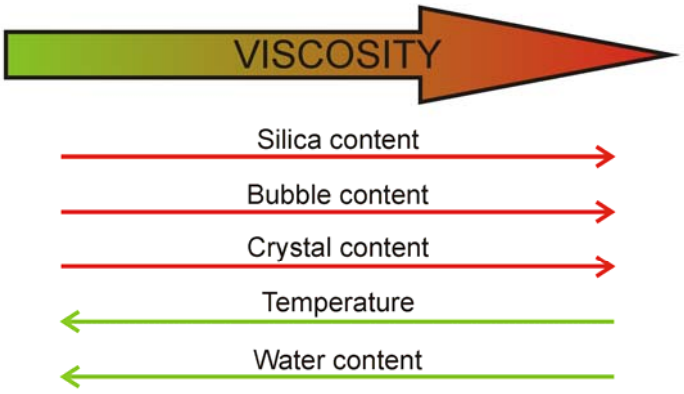

Figure 1.3: Factors controlling viscosity

implies higher viscosity, so the two factors sum up to make Si-rich magmas more viscous. The presence of crystals and gas bubbles also increases magma viscosity. Water content, on the other hand, prevents silica polymerisation, thus reducing magma viscosity. Its solubility increases with silica content; typical water contents in magmas are from 0.1-1.5 wt % in basaltic magmas, to 3-7 wt % in rhyolitic ones (Parfitt and Wilson, 2008). Despite the strong effect of water on viscosity, it is not enough to counteract the silica and temperature effect. Instead, when exsolution of volatiles (mainly water and CO_2) takes place, decrease in water content in melt causes a dramatic increase in viscosity, at the same time that the higher water amount produces higher bubble presence and so higher viscosity. For comparison, a rhyolite can be 10^9 times as viscous as basalts (Parfitt and Wilson, 2008).

In absence of interaction of the magma with external water, gas content of magma on reaching the surface ultimately determines whether an eruption is explosive or effusive. Gas poor lavas erupt effusively, while bubble growth in gas-rich lavas causes magma acceleration and disruption producing explosive emission. Gas content in the lava is conditioned by the original volatile content of magma, and by the capacity of gas bubbles to escape the magma, which in turn is conditioned by magma viscosity and the amount of time available for the bubbles to move through the magma (determined by ascent rate of magma).

Mafic magmas, with a lower intrinsic viscosity and volatile content, tend to produce eruptions with higher proportion of effusive activity. Silica-rich magmas, on the other hand, tend to produce mainly explosive activity because volatile content is higher and viscosity prevents gas bubbles to escape the magma.

1.4.1 Products of effusive silicic volcanism

Effusive emission of silicic lavas produces, depending on viscosity, a gradation from relatively short and thick lava flows to lava domes. Lava flows are formed by less viscous and gas poor lavas, while domes are formed by much more viscous lavas (usually cooler than the ones forming lava flows) which may still contain an important amount of gas bubbles that have not expanded violently due to the confining pressure. Dome collapse releases confining pressure, which may trigger an explosive disruption of the structure.

1.4.2 Products of explosive silicic volcanism

Explosive silicic volcanic activity produces the fragmentation of lava, releasing a jet of pyroclasts and gas into the atmosphere. Emitted pyroclasts can fall ballistically to the ground, become entrained in a convective hot air current forming an eruptive column and plume, or be transported laterally within a pyroclastic density current (Fig. 1.4).

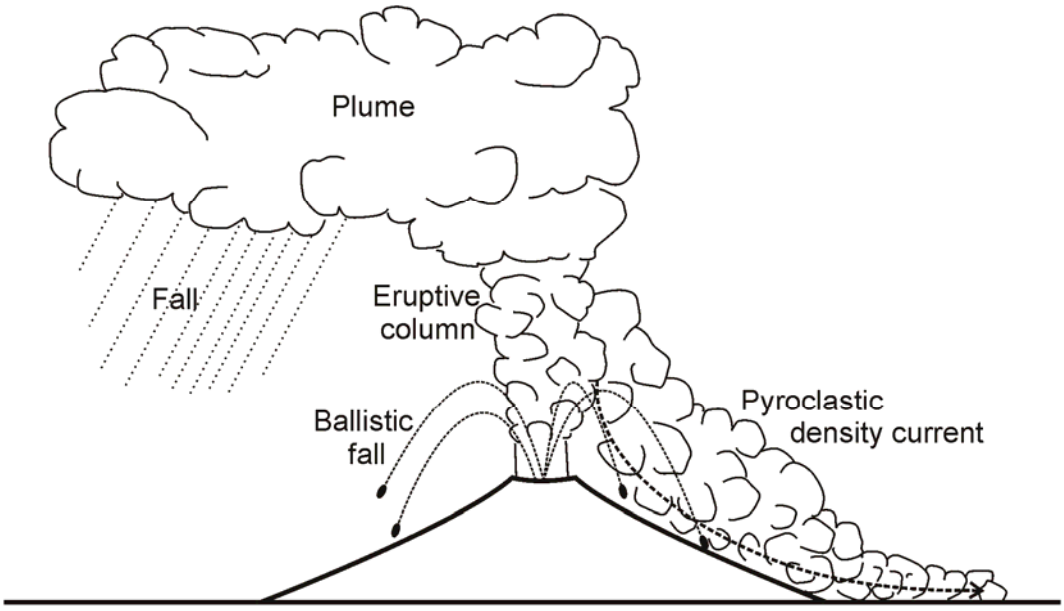

Figure 1.4: Transport mechanisms of pyroclasts

Pyroclastic fall

Pyroclasts entrained in a plume travel suspended in hot air away from the emission centre until they are gravitatively separated and fall to the ground. This process effectively separates pyroclasts by size and density, so the resulting deposits typically show good sorting. Pyroclastic fall from a plume deposits like snow, which homogeneously mantles the ground, with thicknesses gradually decreasing radially from the emission centre.

Pyroclastic density currents

Sulpizio and Dellino (2008) define pyroclastic density currents (PDCs) as moving mixtures of particles and gas that flow across the ground, and originate in different ways and from various sources, during explosive eruptions or gravity-driven collapse of domes. They may be short-lived (highly unsteady) or relatively long-lived (sustained unsteady to quasi-steady) phenomena, driven by both magmatic or phreatomagmatic melt fragmentation. Either if they are concentrated or diluted suspensions of gas and particles, PDCs consist of two essential and intergradational counterparts: an underflow and a coignimbrite plume. The underflow is denser than the atmosphere and flows in direct contact with the ground. It usually comprises a basal part dominated by particle-particle interaction overlaid by a turbulent part dominated by traction processes. The coignimbrite plume is less dense than the atmosphere and lofts convectively. Mass transfer occurs between the two parts during flow due to changing conditions, as for example caused by slope variation.

PDC deposits record processes and physical conditions in a generically defined flow-boundary zone that includes the lowermost part of the current, the flow-deposit boundary, and the uppermost part of the deposit (Branney and Kokelaar, 2002). The flow boundary zone is that lower part of the current where particle-particle interaction dominates the transport mechanisms and promotes deposition.

There are two end-members of PDC: pyroclastic flows and pyroclastic surges. Pyroclastic flows are highly concentrated mixtures in which particle-particle interactions dominate the pyroclast motion, and generate massive deposits. On the other hand, pyroclastic surges are thought to be diluted suspensions in which particles are carried mainly in turbulent suspension and in a thin flow-boundary, generating stratified deposits. Between these two end-members a continuous spectrum exists whose sedimentological characteristics mainly depend on the interplay between particle concentration, shear rate and depositional rate over space and time (Sulpizio and Dellino, 2008). An excellent reference publication on PDC is that of Branney and Kokelaar (2002), in which further information on transport and emplacement mechanisms of PDC can be consulted.

Depending on energy and particle concentration, a PDC can be more or less influenced by topography. PDCs are generally affected by topography to some degree, tending to concentrate in valleys, although high energy and diluted PDCs can surmount barriers up to several hundred meters high. As a result of the topographic influence, deposition preferentially occurs in low zones, tending to smooth the surface (differently from pyroclastic falls, which homogeneously mantle the ground), and to produce flat tops.

1.4.3 Ignimbrites

An ignimbrite is the deposit of a PDC, and is made of juvenile pyroclasts (from fine ash to meter-sized bombs) and crystal fragments, commonly with scattered lithic fragments. Depending on the nature of the eruption and PDC that originated the deposit, ignimbrites can vary from small topographically strongly conditioned finger-like deposits some hundreds of meters long, to large volume mantles that can cover areas up to several thousand square kilometers radially from the eruptive centre, capable even of surpassing obstacles several hundred meters high. Some of the biggest known single ignimbrites are those of Toba and Yellowstone, which exceed the 3,000 km^3 (Wilson, 1993). Aspect ratio is used to quantify the expansion of an ignimbrite, comparing the mean deposit thickness with the diameter of a circle with an area equal to that of the deposit (Walker et al., 1980). Aspect ratio can vary from 1:100 to 1:100,000 or more. Small aspect ratios represent thin deposits that cover wide areas. Eruption of large volume ignimbrites from shallow magma chambers may produce caldera collapse events.

On a smaller scale, single ignimbrites can be formed by a single or by several flow units, each one recording variations in the PDC dynamics such as lateral movement or waxing and wanning phases. Deposits may also record variations on the supply of pyroclastic materials and on its composition.

Post-depositional evolution of ignimbrites:

Ignimbrites are deposited in a period of time several orders of magnitude smaller than the time needed for their cooling. On deposition and during cooling several processes take place such as compaction, degassing, jointing, welding or devitrification. When two or more ignimbrites are deposited in close succession they may share a cooling history, forming a single cooling unit. When some time has passed and an older ignimbrite has significantly cooled before a new one is deposited, they will undergo separate histories and will form a complex cooling unit. Cooling history conditions the processes occurring, and therefore the final characteristics of the deposit.

When pyroclasts are finally deposited, and as more material is added on top, compaction begins. Compaction tends to expel intersticial and intragranular air and gas, which may concentrate and form degassing structures such as pipes, or become trapped in vesicles or vesiculation planes. Compaction can lead to a thickness reduction of pyroclastic deposits of up to 30 % or more. If pyroclasts are viscous enough, compaction may deform them, flattening them and making them adapt to each other, reducing porosity and enhancing gas expel. Pyroclast flattening and stretching can take place also during deposition as a response to shear stresses acting on particles. Either due to compaction or shear stresses, flattening of pyroclasts produces what is

known as eutaxitic texture and its typical macroscopic indicator, fiamme. If deposit temperature is still higher pyroclasts may weld to each other. Welding of ignimbrites varies from non-existent in the ones formed by "cooler" PDCs to extremely welded, in which case the pyroclastic nature of the deposit can have been completely obliterated forming a uniform mass resembling a lava. During cooling, deposits in the process of welding can be capable of flowing due to shear stresses applied on the deposit by the overriding PDC or caused by slope; this is known as rheomorphism.

The welding degree of an ignimbrite depends on several factors. Chemical composition of juvenile particles conditions its viscosity for a given temperature, thus controlling the capability of welding. Apart from silica content, alkalis and volatiles reduce melt viscosity and liquidus temperature, enhancing welding. For a given composition welding degree mostly depends on local temperature and load conditions within the ignimbrite. The higher these are the more welding occurs. Temperature within an ignimbrite is not homogeneous, not only by heat loss through its perimeter, which is more efficient through its top, but also due to deposition of cooler regions such as cooler flow units or, at a smaller scale, foreign cooler clasts captured during pyroclastic density current flow, such as lithic fragments. Cooler regions at the perimeter and within the unit prevent or reduce welding in those zones. Finally, load favours welding promoting clast deformation and compaction. In an originally homogeneous deposit, the highest welding degree will be at the lower parts, which combine higher temperature and load.

High-temperature devitrification of ignimbrites may occur, transforming the glassy matrix of the deposit into crystalline aggregates, which are generally formed by alkali feldspars and silica polymorphs. If devitrification is severe, the pyroclastic nature of the deposit may be obliterated (Streck and Grunder, 1995).

Last but not least, the cooling and degassing process of ignimbrite deposits involves migration upwards of expelled gas through the deposits, which can produce redistribution of some chemical elements, typically involving a loss of alkalis, especially Na (Noble, 1970). This fact must be borne in mind when attempting to classify these rocks using geochemical data (e.g. TAS diagram and Shand's index).

CHAPTER 2: GEOLOGICAL SETTING

2.1 LOCATION OF THE STUDY AREA

Sardinia Island is located in the middle of the western Mediterranean Sea, between 38° 51' and 41° 15' latitude N and 8° 8' and 9° 50' longitude E. The study area of this thesis is in the Sulcis region, in SW Sardinia, between 38° 56' and 39° 17' latitude N and 8° 13' and 8° 45' longitude E (Fig. 2.1).

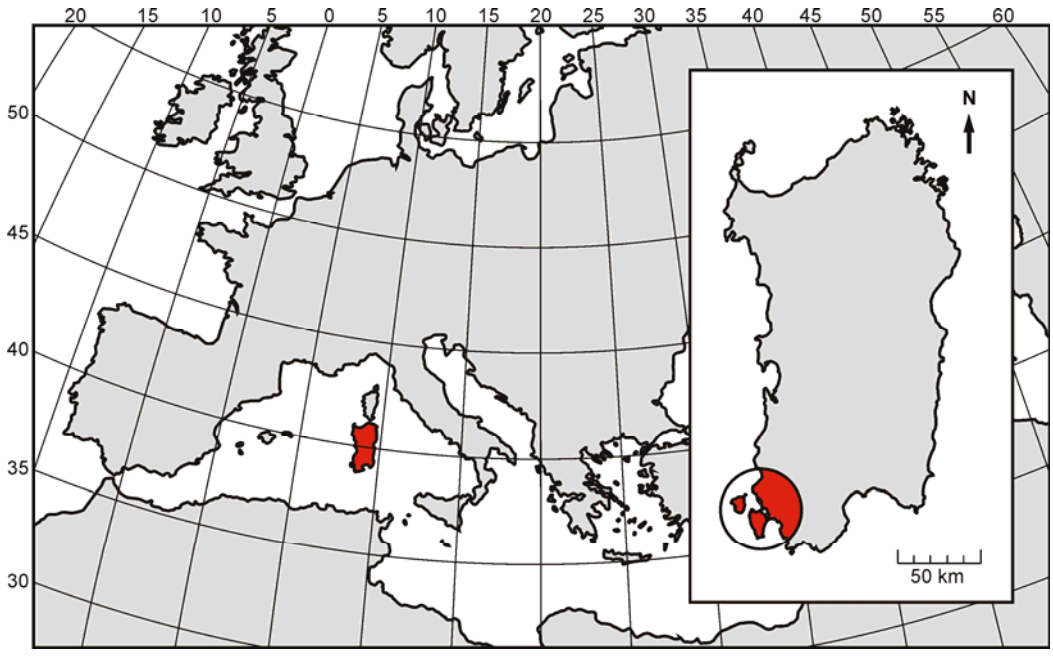

Figure 2.1: Location of the study area

2.2 GEODYNAMIC SETTING

The geological evolution of Sardinia during the Cenozoic was influenced by one of the major geodynamic events affecting western Mediterranean during this period, the drift and

counterclockwise rotation of the Corsica-Sardinia microplate from the European margin to its current position (Cherchi and Montadert, 1982) and the opening of the Liguro-Provençal Basin in Oligocene-Miocene times. The movement was caused by the roll-back of the NW-wards subducting Apulian subduction zone (Rollet et al., 2002). Abundant calc-alkaline magmatism of orogenic affinity (Coulon, 1977) was generated by this subduction, causing arc volcanism to take place throughout western Sardinia.

Geodynamics of Western Mediterranean during Tertiary were driven by the interaction between African and Eurasian Plates, which was complex due to the presence of some microplates, oceanic crust, and changes in stresses caused by its own evolution. The Corsica-Sardinia microplate, as a piece playing an important role in this evolution, registered in its geological record important information of this period. The study of the geologic evolution of Sardinia has been a key point for the understanding of geodynamics in western Mediterranean during this period.

Since the first paleomagnetic studies of Sardinian volcanic materials it was evidenced that the Corsica-Sardinia microplate had undergone a counterclockwise rotation during the Tertiary. Many paleomagnetic and geochronological works have been devoted to quantify and place in time this movement (Nairn and Westphal, 1968; De Jong et al., 1969, 1973; Bobier and Coulon 1970; Coulon et al., 1974; Manzoni, 1974, 1975; Westphal et al., 1976; Bellon et al., 1977; Edel and Lörtscher, 1977; Edel, 1979; Savelli et al., 1979; Montigny et al., 1981; Cherchi and Montadert, 1982; Vigliotti and Langenheim, 1995). Most of these studies were carried out on the calc-alkaline Oligocene and Miocene volcanic rocks of Sardinia. More recently there have been several studies dealing with this subject which have combined existing data with new ones including paleomagnetism, geochronology, geophysical survey and revision of stratigraphic and structural information (Casula et al., 2001; Edel et al., 2001; Faccenna et al., 2002; Speranza et al., 2002; Schettino and Turco, 2006; Gattacceca et al., 2007). As a result, we now have a picture of the geodynamic and geologic evolution of Western Mediterranean in general and of Sardinia in particular.

Although it is clear to most authors that the Corsica-Sardinia microplate was part of the southern European continental margin until Late Oligocene, there is still no agreement on the exact location occupied by this plate. One of the most recent studies dealing with this problem (Schettino and Turco, 2006) places the plate between the Pyrenees and the Alps. According to these authors, Corsica and Sardinia were part of the north-eastern margin of Iberia. The ongoing convergence between Africa and Eurasia, with the growing of the Pyrenees, finally caused a plate reorganization which shifted, during Early Rupelian (33.1 Ma), the zone where deformation due to convergent motion occurred. The convergent boundary between Africa and Eurasia moved from

the Pyrenees belt, which ceased to represent a major plate boundary, to along the southern and eastern margins of Iberia. At the beginning deformation was accommodated at the Iberian margins with the formation of fold and thrust structures. Afterwards, the old oceanic crust limiting with this continental margin started to subduct towards N and NW (Coulon, 1977; Beccaluva et al., 1989), forming a SW-NE trench and later triggering the extensional evolution of western Mediterranean as it started to migrate south-eastwards with a roll-back mechanism (Fig. 2.2, a). Timing of this subduction has been established from the study of the widespread calc-alkaline magmatism of orogenic affinity associated with it (Coulon, 1977; Beccaluva et al., 1989, and references therein), which is very well exposed in Sardinia. On this island, subduction-related volcanic activity occurred during a protracted time span from 32.1 to 11.6 Ma (Araña et al., 1974; Savelli et al., 1979; Montigny et al., 1981; Beccaluva et al., 1985).

With the starting of the retreat of the subduction, the tectonic setting changed from compressive to extensional, affecting a broad area of the European Mediterranean margin from SW Spain to southern France - there it superimposed with the Rhine-Rhone rifts (European Rift System, which started forming in late Eocene (Casula et al., 2001) by reactivation of previous structures) generating a rift system all along (Fig. 2.2, b). This rifting created in Sardinia horst and graben structures controlled by major normal faults, tilted blocks, and by transverse structures, the main structure being the Sardinia Trough, a 200 km long graben which crosses the island from N to S. The formation of main extensional structures was ended by lower Burdigalian (Casula et al., 2001). This graben system still dominates the topography of Sardinia. Retreating of the subduction by roll-back caused a progressive crustal thinning in a back-arc position, and finally the opening of the Valencia Trough and the Liguro-Provençal basin (Fig. 2.2, c to f). The rifting of the Liguro-Provençal basin started between 30 and 28 Ma ago (Cravatte et al., 1974; Cherchi and Montadert, 1982; Séranne, 1999).

Concerning the Corsica-Sardinia microplate, it first drifted SE-wards pulled by the trench as it was retreating, and afterwards rotated counterclockwise as the retreating direction of the subduction shifted from SE to ESE (Schettino and Turco, 2006, and references therein). According to the latest study, Sardinia rotated 45° counterclockwise with respect to stable Europe after 20.5 Ma (Aquitanian), and the rotation was essentially complete by 15 Ma. About 30° rotation occurred between 20.5 and 18 Ma, corresponding to the period of maximum volcanic activity in Sardinia (Gattacceca et al., 2007, and references therein).

The end of the subduction under Sardinia, and therefore the end of the calc-alkaline volcanism, occurred at the end of the Burdigalian/beginning of the Langhian, when an eastward movement

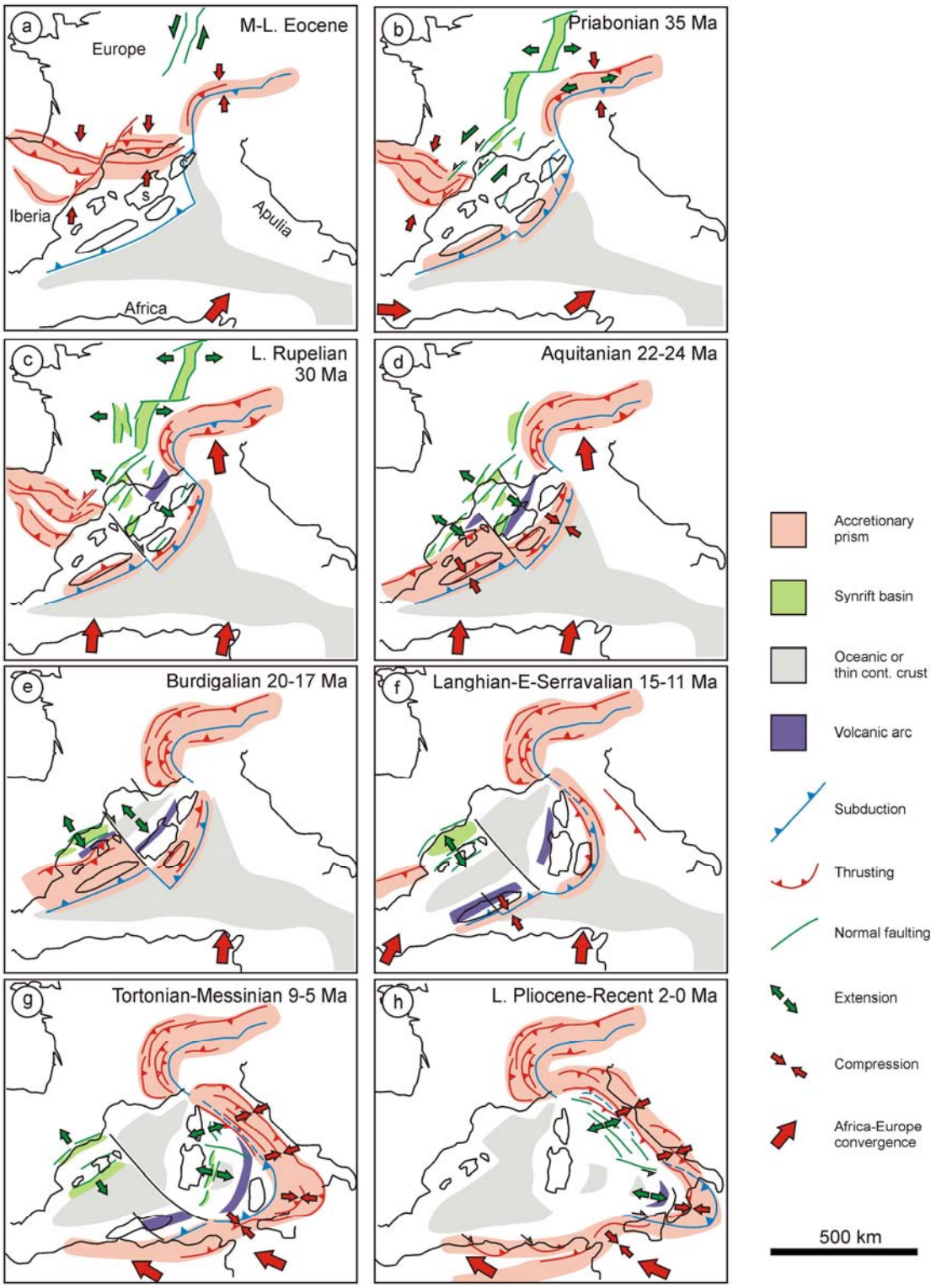

Figure 2.2: Geodynamic evolution of Western Mediterranean from Middle Eocene to present. Modified from Séranne (1999)

towards the Apennines of the eastern part of the subduction occurred (Casula et al., 2001) and Sardinia was left back in its present day position whereas the Calabrian block was carried along with the retreating trench to the SE (Faccenna et al., 2002), opening the southern Tyrrhenian sea (Fig. 2.2., g and h). A small NE-SW compressive phase has been detected in Sardinia at lower-middle Burdigalian, corresponding to the end of rotation of the microplate (Cherchi and Montadert, 1982).

Sardinia underwent a sharp restart of extensional tectonics during Pliocene-Pleistocene with further development of the NNW-SSE Campidano graben in central-south-western Sardinia, overprinting the main Sardinia Trough (Guerrera et al., 2004). This new extensional phase, to which a widespread prevalent alkaline basaltic volcanism is associated, is to be connected with the opening of southern Tyrrhenian Basin (Beccaluva et al., 1989; Sartori et al., 1989).

2.3 GEOLOGY OF SARDINIA

At present Sardinia is a piece of continent with a crust about 30 km thick and a lithosphere of ca. 80 km in between two oceanic to thinned continental crust zones, the Liguro-Provençal and Tyrrhenian basins (Lustrino et al., 2009). Pre-Oligocene geological record in Sardinia is very close to that found in north-eastern Spain and south-eastern France. The basement of the island is formed by Hercynian rocks, dominantly plutonic igneous rocks at the north-eastern sector, and with metamorphic rocks of sedimentary origin outcropping in the centre and southeast (Fig. 2.3). Grade of metamorphism decreases towards SW from high grade by the plutons to almost no metamorphism at the Sulcis and Sarrabus (Egger et al., 1988), from internal to external zones of the Hercynian orogen. Mesozoic sedimentary rocks are found mantling this basement in the E and NW, although their areal extension is small, and its thickness and stratigraphic succession is very reduced if compared to north-eastern Spain and southern France. Eocene and post-Eocene sedimentary materials (marine to continental) fill the graben structures formed during extensional phases, such as the Sardinia Trough and Campidano graben, which divide the island in two. Volcanic rocks of the Oligo-Miocene and Plio-Pleistocene cycles cover and intercalate with these younger sedimentary rocks.

2.4 THE OLIGO-MIOCENE VOLCANISM OF SARDINIA

One of the first systematic studies of the calc-alkaline volcanic rocks formed during the migration and rotation of the Corsica-Sardinia microplate was that by Coulon (1977), who established the volcanostratigraphic sequence for the Logudoro-Bosano area in north-western Sardinia. He subdivided the sequence in three parts: Lower andesitic series (Série andésitique inferieure),

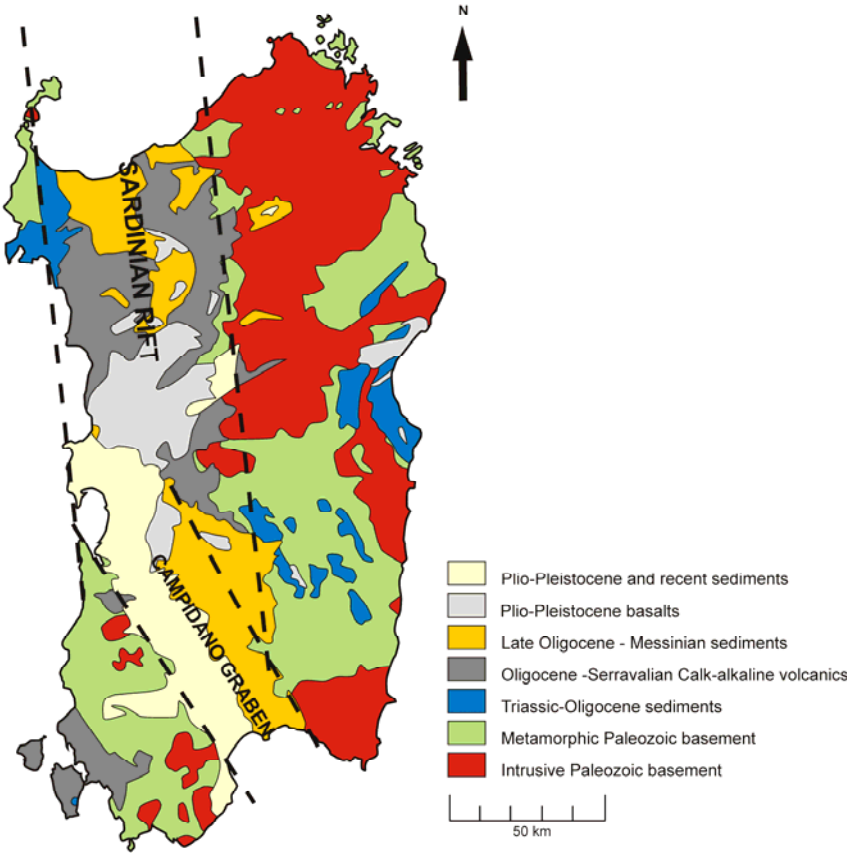

Figure 2.3: Simplified map of the geology of Sardinia. Modified from Carmignani et al. (1994) and Speranza et al. (2002)

Upper andesitic series (S.A. supérieure) and Terminal andesitic series (S.A. terminale). Later on, in a global study by Assorgia et al. (1997) inspired in the work by Coulon (1977), the authors recognised a common succession for all the volcanic zones on the island, formed by four main series. Oligo-Miocene volcanic rocks were observed to crop out mainly in north-western Sardinia, where the succession is mostly complete, and in various western sectors of the island, where it is not (Fig. 2.4).

Assorgia et al. (1997) defined the following four main series, from oldest to youngest:

Lower Basic-Intermediate Lavic Series (LBLS) (33/28-23 Ma; Savelli, 1975; Beccaluva et al., 1985): it crops out in Bosano, Sulcis and southern Campidano. It has a basic to intermediate composition (dacites, andesites and subordinate basalts) and affinity changing from tholeiitic to calc-alkaline. It is mainly formed by lavic materials such as domes and small lava flows, with subordinate pyroclastites (falls, small pyroclastic flows and surges).

Lower Acid-intermediate Explosive Series (LAES) (23-20 Ma; Savelli et al., 1979; Assorgia et al., 1995): it crops out in central-western (Bosano) and central (Fordongianus) Sardinia. It is formed

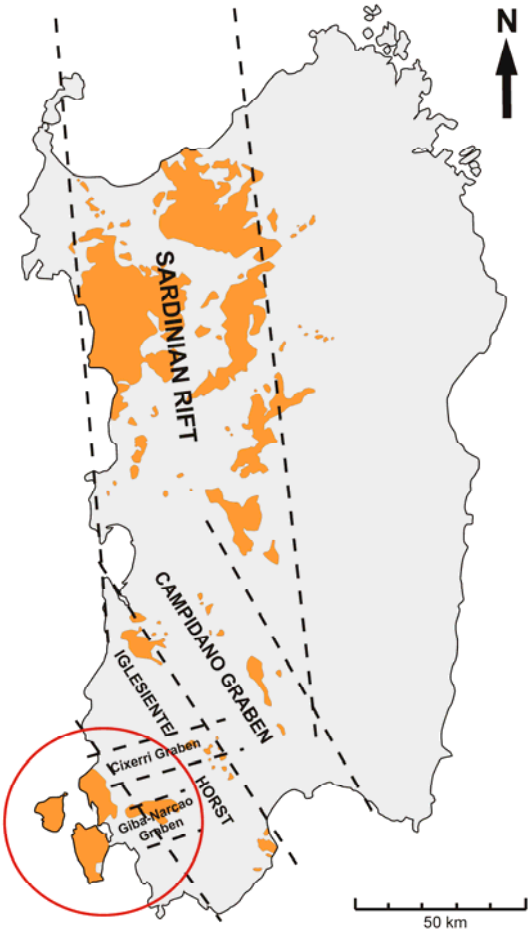

Figure 2.4: Products of the Oligo-Miocene volcanism in Sardinia. Modified from Gattacceca et al. (2007)

by large volume rhyodacitic pyroclastic flows and essentially dacitic lava flows or lava-like ignimbrites.

Upper Basic-Intermediate Lavic Series (UBLS) (19-16 Ma; Coulon, 1977; Maccioni et al., 1990): it crops out mainly in western Sardinia (Bosano, Mte. Arcuentu) and in southern Sardinia (Sulcis). It is formed by andesitic to basaltic materials as subaerial lava flows and submarine lava flows and pyroclastites (pillow lavas and hyalocastites of Marmilla; Maccioni, 1969, 1974), as well as rare lava domes, sills and dykes. Explosive activity was subordinate and related to phreatomagmatism, being characterized by pyroclastic surges and rare pyroclastic falls.

Upper Acid-Intermediate Explosive Series (UAES) (17-13 Ma; Araña et al., 1974; Savelli et al., 1979; Maccioni et al., 1990; Morra et al., 1994; Assorgia et al., 1995): it crops out in the south-western (Sulcis) and north-western (Logudoro-Bosano) Sardinia. It is formed by dacitic to rhyolitic materials (up to comenditic in the Sulcis) in mainly pyroclastic density current deposits (ignimbrites, of low and high temperature), and subordinate lava flows (in the Sulcis region made of comenditic lava).

2.5 THE SULCIS AREA

The Sulcis area is a topographically low zone limited to the NNE by the horst region of the Iglesiente, which is crosscut by two minor transverse (E-W) grabens (Cixerri and Narcao) (Fig. 2.4). This structure was already present at the time the Miocene volcanic materials were erupted (Assorgia et al., 1992a). Nowadays the outcropping emerged area is limited to the SW by the sea, which divides the region in a mainland and two major islands (San Pietro and Santo Antioco). The Sulcis, like most coastal regions of Sardinia, presents a thinned crust 26-28 km thick (Chamot-Rooke et al., 1999).

The substrate for the Oligocene-Miocene volcanic materials is formed by a metamorphic Paleozoic basement (outcropping at the Iglesiente horst, mainly carbonate and siliciclastic sequences (Garbarino et al., 2005)) mantled by Mesozoic sedimentary rocks (Cretaceous limestones crop out in Santo Antioco Island) and Eocene to Miocene clastic sedimentary deposits (Cixerri and Ussana formations (Pecorini and Pomesano Cherchi, 1969)).

The Oligocene-Miocene volcanic succession in the Sulcis area consists of basaltic and andesitic domes at the bottom and a thick pile (up to 400m according to Assorgia et al. (1992a)) of pyroclastic products of evolved composition and dominantly ignimbritic character in the upper part of the succession (Assorgia et al., 1990a, 1990b), corresponding to the Upper Acid-Intermediate Explosive Series of Assorgia et al. (1997).

CHAPTER 3: PREVIOUS WORK

3.1 HISTORY OF RESEARCH IN THE SULCIS AREA

The presence of volcanic rocks in the Sulcis region was recognised in middle 19th century (La Marmora, 1857). Since then, many studies have been devoted to the investigation of these rocks, starting with the ones by Bertolio (1895), who defined comendites in San Pietro Island, and Johnsen (1912). In the early 20th century the mapping of the Sulcis area was carried out (Novarese and Pullè, 1920, 1926; Taricco, 1932; Novarese et al., 1933). First, two units were recognised in the volcanic succession in the Sulcis mainland in the first two maps: a lower unit formed by "liparitic tuffs" and an upper one described as "liparitic vitrophyres". With the stratigraphic study carried out during the mapping by Novarese et al. (1933), which included the mainland and the two minor islands (Fig. 3.1), more units were defined. The authors offered a more comprehensive stratigraphy of volcanic units, based mainly on observations performed at Santo Antioco and San Pietro islands. The sequence established, described in detail by Taricco (1934) was made of a lower andesite formation, covered by two rhyolitic formations mainly consisting of ignimbrites and tuff liparites (τ_4 and τ_3 on the sheets 232 and 232bis of the Geological Map of Italy), of comendites and, finally, again of rhyolitic products (lava, tuffs and ignimbrites) (τ_2, τ_1, τ). This volcanostratigraphic sequence was accepted with minor modifications for 50 years until new detailed studies were carried out. During this time some contributions were made to the knowledge of Sulcis volcanics, mainly in San Pietro Island (Chayes and Zies, 1964; Garbarino and Maccioni, 1968, 1969, 1970a, 1970b; Noble and Haffty, 1969; Araña et al., 1974 (being the latter a geochronologic work)).

In the late 80's a new effort was made to obtain a more detailed geological mapping of the Sulcis region. As a result new sheets for San Pietro (Garbarino et al., 1985; Garbarino et al., 1990) and Santo Antioco (Maccioni et al., 1990) islands were published. In these sheets the

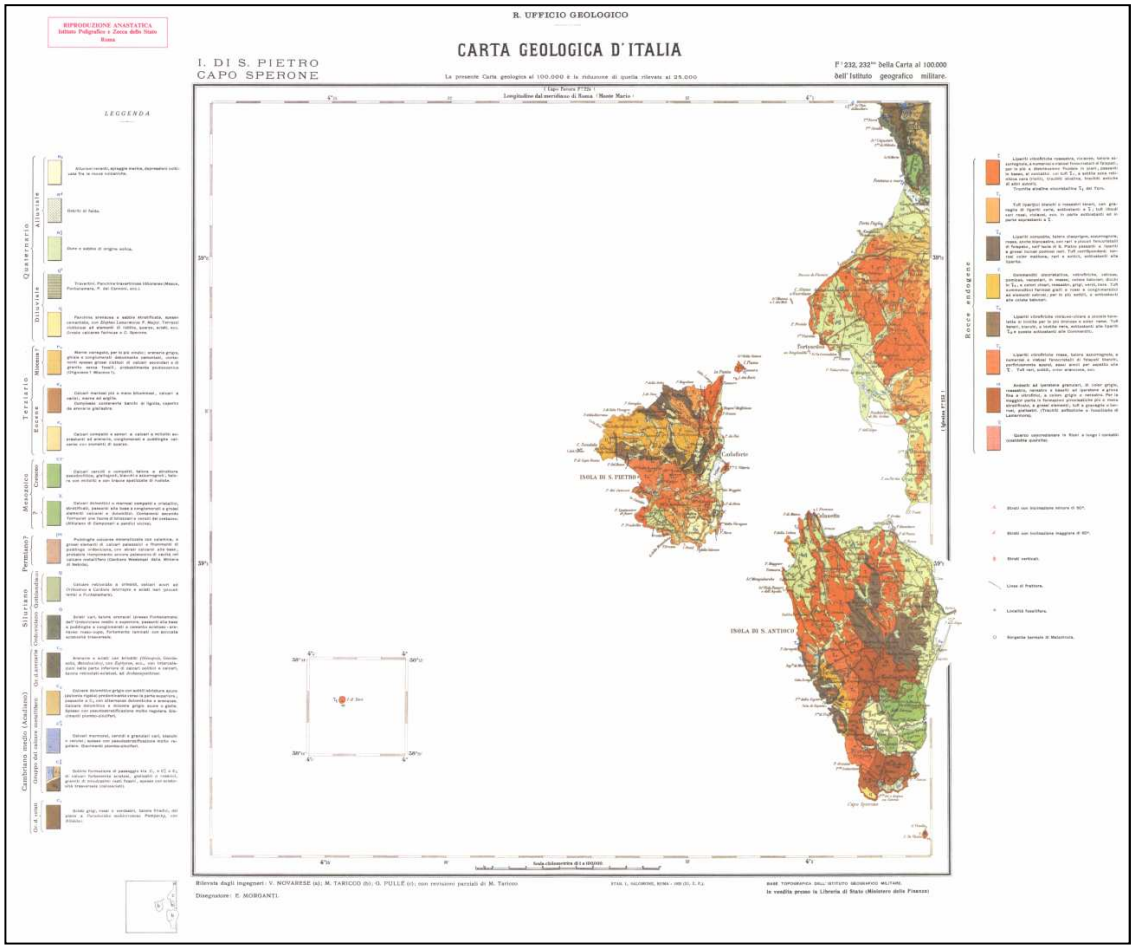

Figure 3.1: One of the first geological maps of the Sulcis area, Novarese et al. (1933)

volcanostratigraphic sequence was further subdivided into 12 acid units in San Pietro and 8 units in Santo Antioco (7 acid ignimbrites plus base andesites). Unfortunately this cartographic study was not associated to a geochemical one; due to this fact and to the macroscopic similarity between some units, cartographic errors occurred by unit misidentification, especially at Santo Antioco. At the same time, the study of the prospective boreholes net made by Carbosulcis SpA mining company at the coal-bearing basin of northern Sulcis mainland allowed a detailed study of the acid ignimbritic sequence, carried out by Assorgia and collaborators. In this sector coal layers exist below the volcanic succession, so boreholes crossed the whole volcanic sequence. Several publications resulted from this study (Assorgia et al., 1990a, 1990b, 1992a, 1992b), in which 10 ignimbritic units were recognised and described for the mainland, which could be correlated to those outcropping in the minor islands, as well as a new map of the mainland (Assorgia et al., 1992c). Boni et al. (1990) shortly described the four upper units outcropping at San Pietro Island, correlating them with those described by Assorgia et al. which could be observed at northern Santo Antioco and Portoscuso area in the mainland. In a later study of comendites, Assorgia et al. (1994) distinguished two new units, increasing to 12 the number of ignimbritic units described

until the moment. Some minor units were introduced for San Pietro Island in the study by Mundula et al. (2009). The last cartographic study in the Sulcis is an unpublished map of the Servizio Geologico d'Italia (Pasci and Orrù, unpublished) which contains southern mainland and Santo Antioco Island. This map correlates for the first time all the defined units between these two areas. In this map a new minor unit is introduced cropping out south of Santo Antioco town.

The studies by Assorgia and collaborators in the 90's provided the first extensive set of petrographic and geochemical data involving all the main ignimbritic units present in the Sulcis mainland, which allowed a whole rock geochemical classification of the defined units, as well as the first petrogenetic interpretations. The geochemical dataset was expanded by the research by Morra et al. (1994), a study which dealt with the petrogenesis of the magmatic suite present at Sulcis, paying special attention to comendites.

From this publication by Morra et al. (1994), new studies on Miocene volcanic rocks of the Sulcis region were more specific, mostly focussing on one unit or composition. Special attention has been paid to the study of the formation mechanisms and emplacement behavior of one of the units (Nuraxi unit), being this object of study in several investigations: Gimeno et al. (1996, 2002, 2003), study on the unit's vitrophyric level; Pioli (2003); Pioli and Rosi (2005), study on rheomorphism; Pioli et al. (2008), study on magnetic fabric, welding texture and deformation fabric. Brotzu et al. (1997a) studied the basalt-andesite suite in Narcao. Cioni and Funedda (2005) studied the comenditic lava flows in San Pietro from a structural point of view. Finally, Conte et al. (2010) dealt with the petrogenesis of the basalt-andesite suite of southern Santo Antioco Island.

3.2 VOLCANOSTRATIGRAPHIC SEQUENCE

As a result of the research mentioned above, the Oligocene-Miocene volcanism of the Sulcis region was characterised. It represents an orogenic calc-alkaline magmatic sequence constituted by an early succession (lower sequence) of basaltic andesites, andesites and minor basalts with low-medium K tholeiitic affinity (Assorgia et al., 1992a) cropping out in the Giba-Narcao area and in southern Santo Antioco Island, and a younger succession (upper sequence) of dacitic to rhyolitic (up to peralkaline) ignimbrites (though locally effusive volcanism occurred), covering San Pietro Island and northern sectors of Santo Antioco Island and Sulcis mainland. This younger succession corresponds to the Upper Acid-Intermediate Explosive Series of Assorgia et al. (1997).

The andesitic sequence is formed by a thick (up to 400 m, Assorgia et al. (1992a)) succession of small lava flows, domes (and associated dykes) and minor pyroclastic to epiclastic breccias. This lower sequence was emplaced between 28.5 ± 0.5 and 17.8 ± 0.5 Ma (Bellon, 1976).

The upper sequence, a thick (at least 400 m) succession formed by several ignimbritic bodies and minor lava flows and domes (comendites in Northern San Pietro), lies over the terrigenous continental materials of Cixerri (Middle Eocene-Middle Oligocene) and Ussana (Middle Oligocene-Lower Miocene) formations (Pecorini and Pomesano Cherchi, 1969), as well as over the basic to intermediate lower sequence. As described before, the upper sequence has been subdivided into 12 main units, which may be separated by reworked material and paleosoils. Most of these units are represented by single pyroclastic flows and interpreted as single cooling units, whereas other units are clearly constituted by several pyroclastic flows (e.g. Acqua sa Canna and Comendites) (Assorgia et al., 1992a). The age of the upper sequence ranges from 17.6 ± 0.8 to 15.1 ± 0.2 Ma (Beccaluva et al., 1985; Maccioni et al., 1990; Pasci et al., 2001).

The 12 main units of the upper sequence described in literature are, from base to top: Corona Maria (CM), Lenzu (LE), Acqua sa Canna (AC), Seruci (SE), Monte Crobu (MC), Conca is Angius (CA), Nuraxi (NU), Matzaccara (MZ), Comendites (CO), Monte Ulmus (MU), Parigianu (PA) and Serra di Paringianu (SP). Figure 3.2, reproduced from Morra et al. (1994), presents the main characteristics of these units. A description of the volcanostratigraphy of the ignimbritic upper sequence, including minor and new units, is given in the corresponding chapter of the results part of this Thesis.

The Sulcis sector apparently lacks an ignimbritic sequence with an age of between 23 and 18 Ma (Bellon, 1976; Coulon, 1977; Savelli et al., 1979; Beccaluva et al., 1985), which is present and widespread in other sectors of the island (Assorgia et al., 1992b) as the Logudoro and Bosano (Deriu, 1962; Coulon, 1977; Assorgia, 1990a, 1990b), the western sector of Arcuentu (Assorgia et al., 1986a, 1986b) and the middle valley of the Tirso river (Porcu, 1972).

3.3 GEOCHRONOLOGY

Special attention has been paid during the past years in obtaining radiometric ages for volcanic rocks in Sardinia related to the orogenic magmatism originated during the drift and rotation of the Corsica-Sardinia microplate in order to chronologically constrain this event. As part of this magmatism, volcanics in the Sulcis region have also been the object of these studies; nearly 40 datings involving both lower and upper sequence are available. Next, data collected from previous studies are provided, sorted by unit.

Andesites:

- **28.5 ± 1.0 Ma** (whole rock, K/Ar). Andesite, Monte Narcao, mainland Sulcis. Coulon (1977).

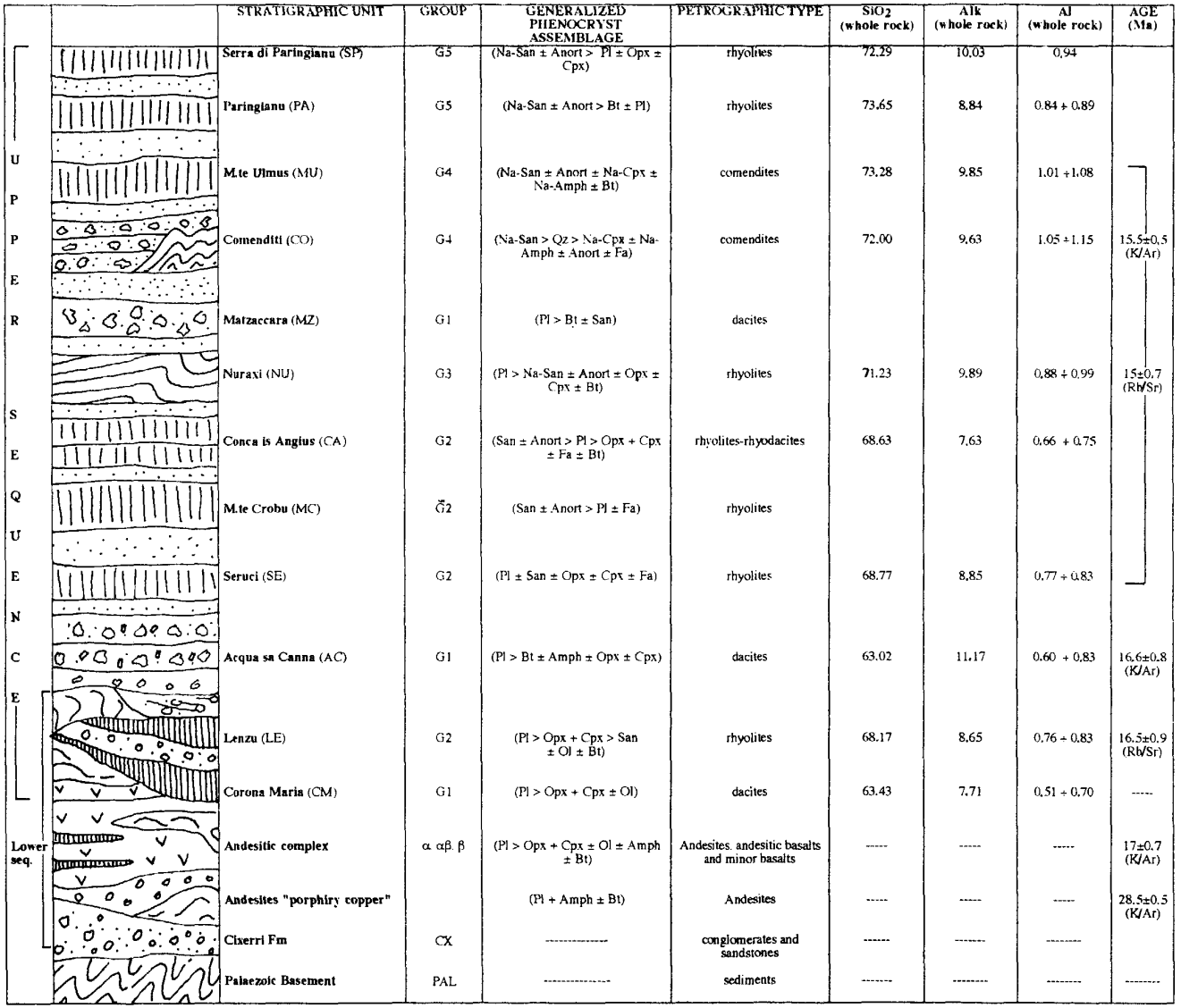

	STRATIGRAPHIC UNIT	GROUP	GENERALIZED PHENOCRYST ASSEMBLAGE	PETROGRAPHIC TYPE	SiO_2 (whole rock)	Alk (whole rock)	Al (whole rock)	AGE (Ma)
UPPER SEQUENCE	Serra di Paringianu (SP)	G5	(Na-San ± Anort > Pl ± Opx ± Cpx)	rhyolites	72.29	10.03	0.94	
	Paringianu (PA)	G5	(Na-San ± Anort > Bt ± Pl)	rhyolites	73.65	8.84	0.84 ÷ 0.89	
	M.te Ulmus (MU)	G4	(Na-San ± Anort ± Na-Cpx ± Na-Amph ± Bt)	comendites	73.28	9.85	1.01 ÷ 1.08	
	Comenditi (CO)	G4	(Na-San > Qz > Na-Cpx ± Na-Amph ± Anort ± Fa)	comendites	72.00	9.63	1.05 ÷ 1.15	15.5±0.5 (K/Ar)
	Matzaccara (MZ)	G1	(Pl > Bt ± San)	dacites				
	Nuraxi (NU)	G3	(Pl > Na-San ± Anort ± Opx ± Cpx ± Bt)	rhyolites	71.23	9.89	0.88 ÷ 0.99	15±0.7 (Rb/Sr)
	Conca is Angius (CA)	G2	(San ± Anort > Pl > Opx + Cpx ± Fa ± Bt)	rhyolites-rhyodacites	68.63	7.63	0.66 ÷ 0.75	
	M.te Crobu (MC)	G2	(San ± Anort > Pl ± Fa)	rhyolites				
	Seruci (SE)	G2	(Pl ± San ± Opx ± Cpx ± Fa)	rhyolites	68.77	8.85	0.77 ÷ 0.83	
	Acqua sa Canna (AC)	G1	(Pl > Bt ± Amph ± Opx ± Cpx)	dacites	63.02	11.17	0.60 ÷ 0.83	16.6±0.8 (K/Ar)
	Lenzu (LE)	G2	(Pl > Opx + Cpx > San ± Ol ± Bt)	rhyolites	68.17	8.65	0.76 ÷ 0.83	16.5±0.9 (Rb/Sr)
	Corona Maria (CM)	G1	(Pl > Opx + Cpx ± Ol)	dacites	63.43	7.71	0.51 ÷ 0.70	-----
Lower seq.	Andesitic complex	α αβ β	(Pl > Opx + Cpx ± Ol ± Amph ± Bt)	Andesites, andesitic basalts and minor basalts	-----	-----	-----	17±0.7 (K/Ar)
	Andesites "porphiry copper"		(Pl + Amph ± Bt)	Andesites	-----	-----	-----	28.5±0.5 (K/Ar)
	Cixerri Fm	CX	----------	conglomerates and sandstones	------	-------	--------	
	Palaezoic Basement	PAL	----------	sediments	-------	--------	--------	--------

Figure 3.2: Main characteristics of the main volcanostratigraphic units described before and at Morra et al. (1994). Reproduced from Morra et al. (1994)

- **25.6 ± 0.9** / **26.3 ± 0.9 Ma** (plagioclase, K/Ar). Montigny et al. (1981).
- **23.2 ± 0.9 / 23.8 ± 0.9 Ma** (hornblende, K/Ar). Perdaxius, Sulcis mainland. Montigny et al. (1981).
- **22.8 ± 0.8 / 23.4 ± 0.8 Ma** (hornblende, K/Ar). Montigny et al. (1981).
- **18.6 ± 0.7** / **19.0 ± 0.7 Ma** (plagioclase, K/Ar). Perdaxius, Sulcis mainland. Montigny et al. (1981).
- **18.3 ± 1.1 Ma** (whole rock, K/Ar). Porto di Torre Cannai, Santo Antioco. Maccioni et al. (1990).
- **18.0 ± 1.3** / **16.7 ± 1.0 Ma** (whole rock, K/Ar). Poligenic breccias, Monte Arbus and Montarveddu, Santo Antioco. Maccioni et al. (1990).
- **17.6 ± 0.4 Ma** (whole rock, K/Ar). Andesite, Capo Sperone, Santo Antioco. Coulon (1977).
- **17.3 ± 0.9 Ma** (whole rock, K/Ar). Scaralettus, Santo Antioco. Maccioni et al. (1990).
- **14.0 ± 0.4 Ma** (whole rock K/Ar). Hypersthene andesite, Monte Arbus, Santo Antioco. Araña et al. (1974).

Lenzu:

- **16.5 ± 0.9 Ma** (whole rock, Rb/Sr). Morra et al. (1994).

Acqua sa Canna:

- **16.6 ± 0.8 Ma** (plagioclase, K/Ar). Morra et al. (1994).

Nuraxi:

- **17.6 ± 0.8 Ma** (whole rock, K/Ar). Corungiu Murvonis, Santo Antioco. Maccioni et al. (1990).
- **16.6 ± 0.7 Ma** (whole rock, K/Ar). Sa Scrocchita, Santo Antioco. Maccioni et al. (1990).
- **15.79 ± 0.16 Ma** ($^{40}Ar/^{39}Ar$). Pasci et al. (2001); Pioli (2003).
- **15 ± 0.7 Ma** (whole rock, Rb/Sr). Morra et al. (1994).

Punta dei Cannoni: (minor unit in San Pietro Island)

- **18.2 ± 0.8 Ma** (K/Ar). Punta dei Cannoni, San Pietro. Garbarino et al. (1990).

Comendites:

- **18.1 ± 0.8 Ma** (K/Ar). Cala Fico, San Pietro. Garbarino et al. (1990).
- **17.7 ± 0.8 Ma** (whole rock, K/Ar). Near Monte Mercuri, Santo Antioco. Maccioni et al. (1990).

- **16.5 ± 0.8 Ma** (K/Ar). Unit 11 in Volcanological map of San Pietro, Montagna di Capo Rosso, San Pietro. Garbarino et al. (1990).
- **15.5 ± 0.5** (plagioclase, K/Ar). Morra et al. (1994).
- **14.8 ± 0.4 Ma** (Glass, K/Ar). Comenditic perlite, Cala Fico, San Pietro. Araña et al. (1974).
- **14.6 ± 0.4 Ma** (Alkali Feldspar with minor quartz K/Ar). Comenditic perlite, Le Commende, San Pietro. Araña et al. (1974).
- **13.8 ± 0.4 Ma** (Alkali Feldspar with minor quartz K/Ar). Comenditic perlite, Cala Fico, San Pietro. Araña et al. (1974).

Carloforte: (this unit will be defined in the results section)

- **16.0 ± 0.7 Ma** (K/Ar). La Piramide, San Pietro. Garbarino et al. (1990).

Paringianu:

- **17.0 ± 0.8 Ma** (sanidine, K/Ar). Ignimbrite, Monte Genere, Portoscuso area. Boni et al. (1990).
- **15.1 ± 0.7 Ma** (K/Ar). Punta delle Oche, San Pietro. Garbarino et al. (1990).

Serra di Paringianu:

- **17.6 ± 0.8 Ma** (whole rock, K/Ar). Rhyolitic vitrophyre, Rio Sturulliu, Portoscuso area. Boni et al. (1990).
- **17.3 ± 0.8 Ma** (whole rock, K/Ar). Rhyolitic vitrophyre, Su Medadeddu, Portoscuso area. Boni et al. (1990).
- **16.9 ± 0.8 Ma** (whole rock, K/Ar). Rhyolitic vitrophyre, Punta del Castello, San Pietro. Boni et al. (1990).
- **16.7 ± 0.7** / **16.0 ± 0.7 Ma** (whole rock, K/Ar). Calasetta, Santo Antioco. Maccioni et al. (1990).
- **16.2 ± 0.7 Ma** (whole rock, K/Ar). Rhyolitic vitrophyre, Calasetta, Santo Antioco. Boni et al. (1990).
- **15.1 ± 0.2 Ma** ($^{40}Ar/^{39}Ar$). Pasci et al. (2001), reference in Gattacceca et al. (2007).

Punta Mingosa: (minor unit in San Pietro Island, top of the ignimbritic sequence)

- **15.8 ± 0.7 Ma** (whole rock K/Ar). Rhyolitic ignimbrite, Paringianu, Portoscuso area. Boni et al. (1990).

- **15.0 ± 0.7** (whole rock, K/Ar). Rhyolitic ignimbrite, Le Colonne, San Pietro. Boni et al. (1990).

Other datings of unidentified units:

- **15.5 ± 0.5 Ma** (Alkali Feldspar with minor quartz K/Ar). Alkali-rhyolitic perlite near Genarbi, San Pietro. Araña et al. (1974).
- **15 Ma** (K/Ar). Ignimbrite in western San Pietro. Bellon et al. (1977).
- **13.0 ± 0.6 Ma** (whole rock, K/Ar). Isola del Toro, S of Santo Antioco Island. Maccioni et al. (1990).

Figure 3.3 summarizes the available data. As can be seen in this figure, little information can be obtained from them. Scattering of data and error range make impossible to clearly attribute a specific age to each unit. Except for the $^{40}Ar/^{39}Ar$ datings by Pasci et al. (2001) the rest of the data corresponds to K/Ar datings and Rb isochrones, which can be deeply affected by alteration processes. Datings by Pasci et al. (2001) are considered the most reliable ones and allow to restrict the age of the upper half of the ignimbritic sequence (between Nuraxi and Serra di Paringianu units) at 15.95 to 14.9 Ma.

3.4 WORK OF THE RESEARCH GROUP IN THE SULCIS AREA

The research group in which this study has been conducted has worked in the Sulcis area since the middle 80's, when the director of the group, Domingo Gimeno, collaborated in the first studies by Assorgia et al. (Fig. 3.4). As a result of this collaboration, a group of samples was collected from the borehole cores prior to their partial destruction by Carbosulcis SpA, and kept at the Universitat de Barcelona (1989-1993). Two additional small field campaigns were carried out in 1996 (mainly focused on western and northern Santo Antioco Island) and 2006 (centred in northern San Pietro Island). Samples from the 1996 campaign were used in a study about vitrophyres (Gimeno et al., 1996, 2003). Finally, in 2005 a degree's minor thesis project was carried out by an undergrad student supported by the group. This study focused on the volcanostratigraphic and geochemical characterisation of one of the last ignimbrites (Serra di Paringianu unit) in northern San Pietro Island (Roselló, 2005).

During the realisation of this Thesis, another two small studies have been carried out, corresponding also to degree's minor thesis. These studies have focused on the mapping of the southwestern coast of Santo Antico Island, with minor geochemical characterisation of the volcanic materials (Rodríguez, 2009; Ramon, 2009).

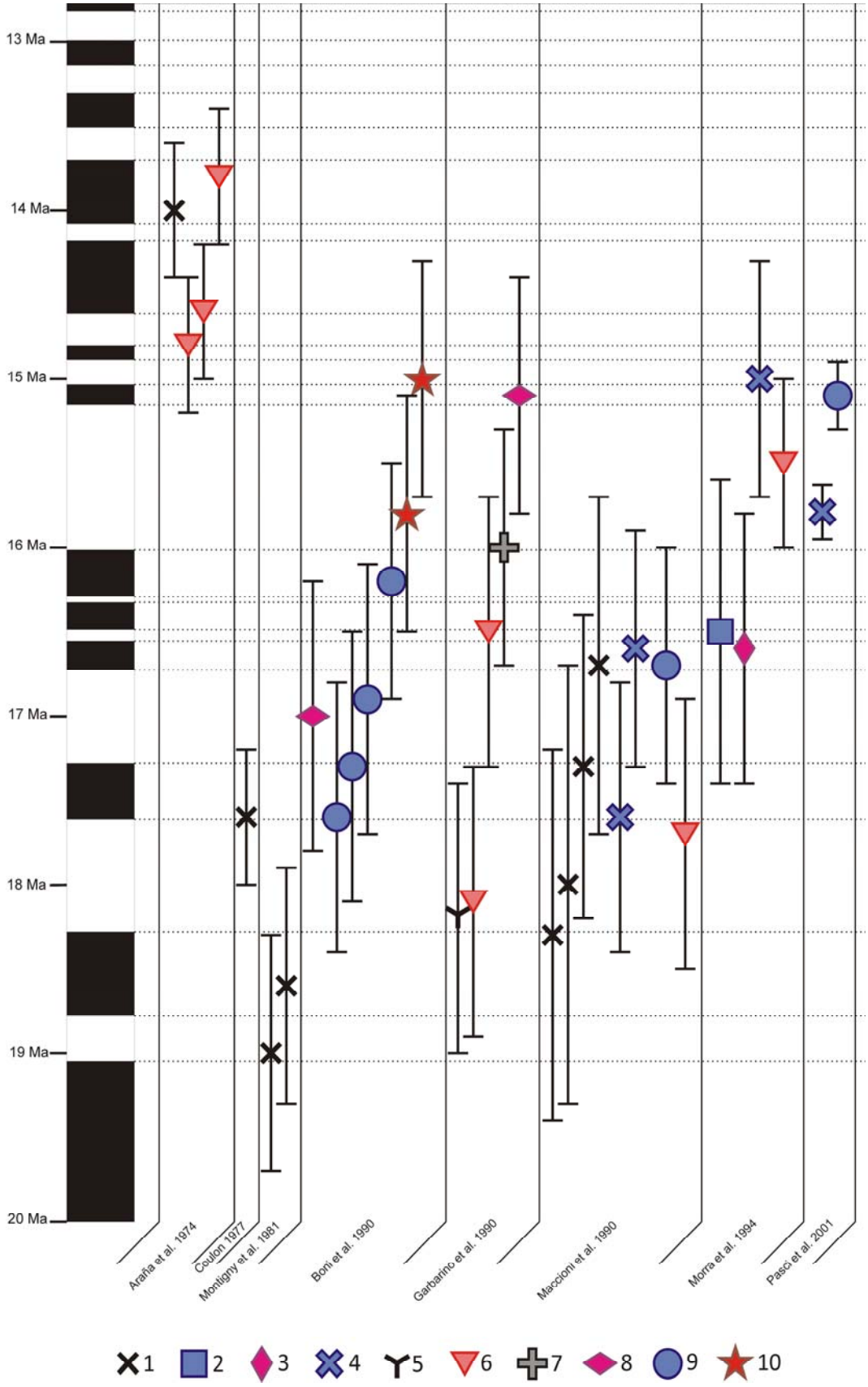

Figure 3.3: Geochronological ages from the Sulcis area available in literature. 1: Andesites; 2: Lenzu; 3: Acqua sa Canna; 4: Nuraxi; 5: Punta dei Cannoni; 6: Comendite; 7: Carloforte; 8: Paringianu; 9: Serra di Paringianu; 10; Punta Mingosa. Symbols in this figure belong to a legend established for the whole Thesis, which can be consulted in Appendix 1

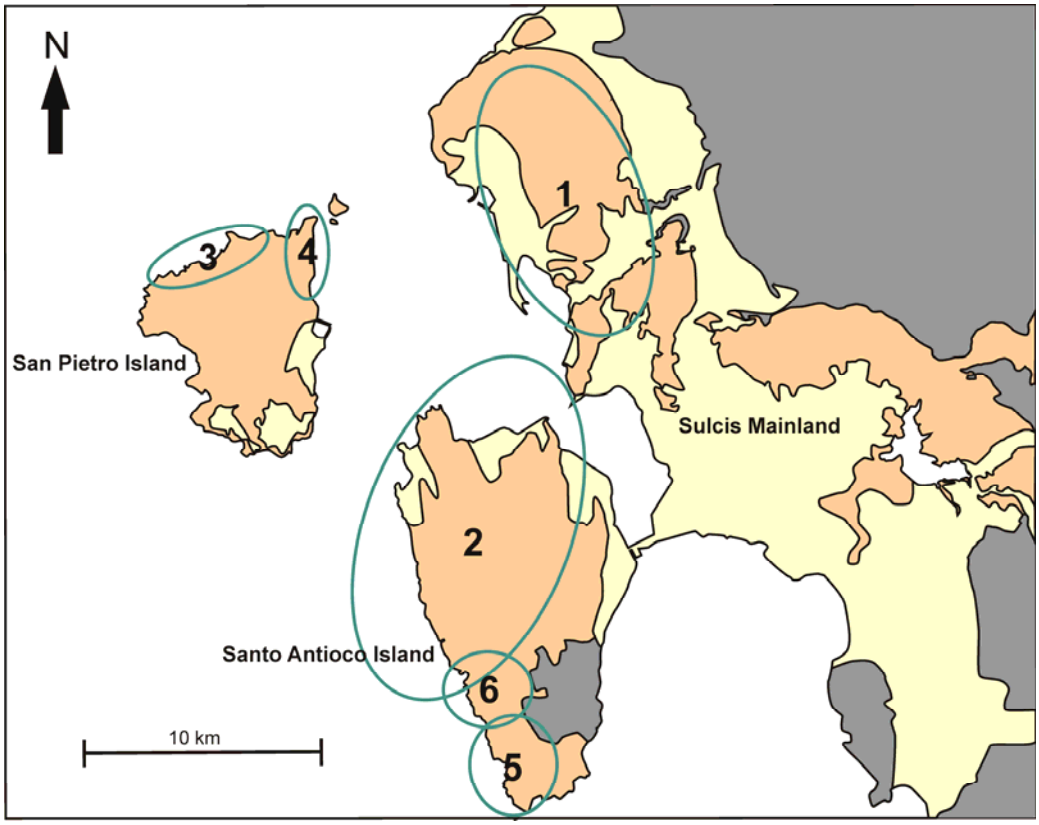

Figure 3.4: Areas studied in previous work of the research group members. 1) Domingo Gimeno in late 80's; 2) 1996 field campaign; 3) 2006 field campaign; 4) Rosselló (2005); 5) Rodríguez (2009); 6) Ramon (2009)

PART II: METHODOLOGY

CHAPTER 4: METHODOLOGY

4.1 INTRODUCTION

To fulfil the objectives set out for this Thesis research has followed the typical steps of a classical petrologic study; these are: field work and sampling, sample selection and preparation, petrographic study, mineral chemistry analysis and whole rock geochemical analysis (Fig. 4.1). In this chapter, information is given on how each one of the steps has been developed.

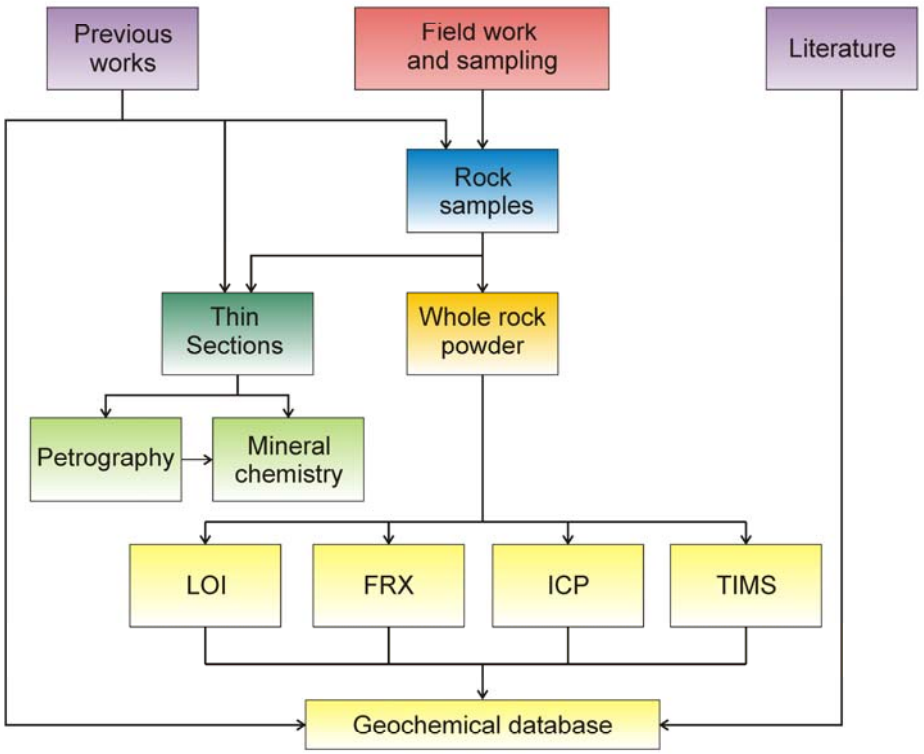

Figure 4.1: Methodology followed in this study

4.2 FIELD WORK AND SAMPLING

A thorough sampling of the Oligo-Miocene volcanic materials in the Sulcis was clearly a key point for the success of the present Thesis. For this reason, a main aim of the field work was the revision of the volcanostratigraphy established in literature and of the available geological maps in order to guarantee that collected samples were attributed to the correct unit, and that all of them were sampled including as much facies as possible of each one.

For this purpose, several field work campaigns were carried out between March 2008 and March 2010. Although the whole study area was covered during these campaigns, special attention was paid to San Pietro and Santo Antioco islands because they were the least studied areas (as seen in the previous chapter).

At the time of sample collection, previous studies and sampling were taken into account. Regarding previous research, studies carried out by Assorgia and collaborators (Assorgia et al., 1990a, 1990b, 1992a) and that of Morra et al. (1994), which were based on samples from the borehole cores from Carbosulcis SpA in the mainland, produced a complete set of data belonging to almost all the main units, but with a better coverage of the lower half of the ignimbritic sequence (units of the upper part of the sequence are thinner or lacking in the mainland). These studies provide geochemical and petrographic data which have been used for the present study.

Some sampling had already been done previous to the present study by members of the research group (see previous chapter). A set of 598 samples collected from the borehole cores from Carbosulcis SpA in the 1989-1993 period by Domingo Gimeno was available. As in the studies stated before, this set also represented better the lower half of the ignimbritic sequence. Another 127 and 40 samples were available from the 1996 and 2006 field campaigns respectively. Finally, the study by Rosselló (2005) produced 43 samples.

Considering the samples and data already available, for the present study little sampling was done on the mainland; it was considered sufficiently well characterised. Just a few samples were collected in the north to obtain data following our own methodology in order to make published and own data comparable, and in the south where volcanic materials had not been yet sampled. Most of the sampling was, hence, centred on the two minor islands, where new sampling complemented the ones previously done. In total, 371 new samples were collected (Fig. 4.2).

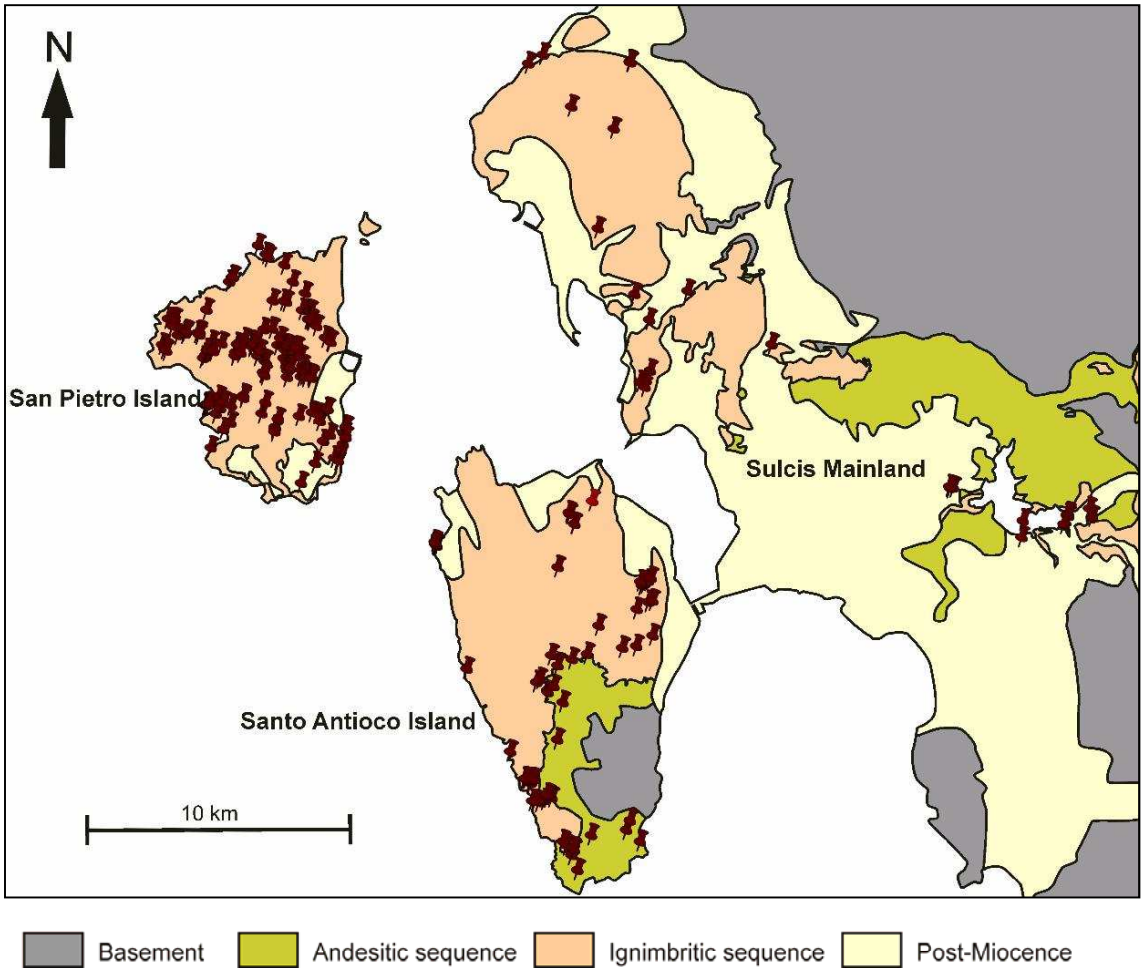

Figure 4.2: Samples collected for this study

4.3 SAMPLE SELECTION AND PREPARATION

About 400 thin sections had already been prepared from old samples by previous work of the research group, and about 100 whole rock geochemical analyses had been performed. Contemplating this, a selection of samples was done among new and unstudied old samples in order to prepare them for petrographic and geochemical study.

Preparation for petrographic study consisted in the elaboration of polished thin sections (microprobe proof) in the *Servei de làmina prima* of the *Universitat de Barcelona*. Thin sections for most of the new samples were made.

A smaller set of samples was prepared for whole rock geochemical analysis. A representative amount of each sample was ground to powder after removing external bodies (enclaves, accidental clasts, etc.) and weathered parts using a wolframium carbide rings mill. Rock samples collected at or near (less than 200 m) the coast were desalted to remove marine salts; this was done by putting rock slices into distilled water for 4 days (with 2 water changes). The same rock

powder was used for all analyses of major and trace elements, as well as for isotopes. In total, 242 samples were prepared.

4.4 PETROGRAPHIC STUDY

The petrographic study of samples was performed using a petrographic microscope in the facilities of the *Departament de Geoquímica, Petrologia i Prospecció Geològica* in the *Facultat de Geologia* of the *Universitat de Barcelona*.

4.5 MINERAL CHEMISTRY

The mineral chemistry of phenocrysts, microphenocrysts and xenocrysts was quantitatively analysed on a selection of 47 thin sections representing all units using an electron microprobe (EMP) in the *Serveis Científico-Tècnics* of the *Universitat de Barcelona* (SCT-UB).

The EMP used for the analysis was a Cameca SX 50 equipped with 4 spectrometers and an EDS. An acceleration voltage of 20 KV, a current beam of 15 nA and measuring time of 10 seconds in both peak and background were the working conditions for analysing all elements except Na. Sodium mobilization and volatilization is a recurrent problem in EMP analysis. To minimize Na loss, this element was analysed separately in first place widening the beam, reducing current to 6 nA, and compensating the lower current with a longer measuring time (20 s). All calculations were made by the program Xmas Plus of SAMx, which uses the Pouchou and Pichoir (PAP) method for matrix correction.

Analysed minerals included feldspars, pyroxenes, biotite, amphibole, titanite and minerals of the magnetite-ulvospinel series. Analysed elements were, for all of them: Si, Ti, Al, Fe, Mg, Ca, Na and K. In addition to these common elements, Ba and Rb were analysed in feldspars and biotite, Mn and Cr in pyroxene, biotite, amphibole and titanite, and Ni in biotite and titanite. All cited elements were analysed in spinels.

Internal reference samples were analysed at the beginning of each session to calibrate the equipment (Table A.2.1 in Appendix 2). Figure A.2.1 in Appendix 2 shows the precision for all the analysed elements and concentrations.

4.6 WHOLE ROCK GEOCHEMISTRY

A key part of the present study has been the building of an extensive and consistent whole rock geochemical database. Much attention was paid to sample selection and geochemical analysis methods. Of the samples selected for geochemical analysis, a basic geochemical characterisation was obtained by determining the content in major and some trace elements using X-Ray

Fluorescence (XRF) at the SCT-UB. Subsequently, a subset of the most fresh and representative samples was further characterised by analysing more trace elements (including rare earth elements) using Inductively Coupled Plasma with Optical Emission Spectrometry (ICP-OES) and Inductively Coupled Plasma with Mass Spectrometry (ICP-MS) at the SCT-UB. Finally, a last small set of the best characterised samples was selected for isotope analyses, which were performed by Thermal Ionisation Mass Spectrometry (TIMS) at the *Centro de Apoyo a la Investigación de Geocronología y Geoquímica Isotópica* of the *Universidad Complutense de Madrid* (Spain) (CAI) and the Department of Earth Sciences of Carleton University (Canada). Loss on ignition was performed for all samples undergoing geochemical analyses at the SCT-UB.

As a result of the multiple analytical methods employed, some major and trace elements were analysed by more than one technique. In the final part of this section it is discussed which value was selected for each element.

Now, a brief explanation is given about each method. Detailed sample preparation protocols for LOI, XRF and ICP analyses are provided in Appendix 3.

4.6.1 Loss on Ignition (LOI)

A LOI analysis was carried out for each sample to evaluate its content in structural volatile elements by means of calcination in a furnace at 950° C. This is necessary to know its degree of weathering and to subsequently normalize whole rock composition to anhydrous composition for its classification based on whole rock geochemistry.

4.6.2 X-Ray Fluorescence (XRF)

Analysis of major and some trace elements (Table 4.1) was done using a Philips PW2400 sequential X-Ray spectrophotometer. Equipment was periodically calibrated using 64 primary standards (shown in Table A.2.2 in Appendix 2). Analytical conditions are shown in Table A.2.3 in Appendix 2. Further control on analyses quality was done by analysing an international reference sample (JB-3 of the Geological Survey of Japan) as inner standard with each set of samples; results were used for precision and accuracy calculations (Table A.2.4 in Appendix 2). A total of 242 samples were analysed by XRF.

4.6.3 Inductively Coupled Plasma with Optical Emission Spectrometry (ICP-OES)

Major and some trace elements (listed in Table 4.1) of 92 samples were determined by ICP-OES using a Perkin Elmer Optima 3200 RL. At every session the equipment was calibrated using solutions with the concentrations shown in Table A.2.5 in Appendix 2. One blank was prepared in each set of 15 samples for control, as well as an international reference sample every two sets.

Element	FRX	ICP-MS	ICP-OES	Element	FRX	ICP-MS	ICP-OES
Si	x			La		x	
Ti	x		x	Li		x	
Al	x		x	Lu		x	
Fe	x		x	Mo	x	x	
Mn	x		x	Nb	x	x	
Mg	x		x	Nd		x	
Ca	x		x	Ni	x	x	
Na	x		x	Pb	x	x	
K	x		x	Pr		x	
P	x		x	Rb	x	x	
				Sb		x	
As		x		Sc		x	
Ba	x	x	x	Sm		x	
Be		x		Sn	x	x	
Bi		x		Sr	x		x
Ce	x	x		Ta		x	
Co	x	x		Tb		x	
Cr	x	x		Te		x	
Cs		x		Th	x	x	
Cu	x	x		Tl		x	
Dy		x		Tm		x	
Er		x		U		x	
Eu		x		V	x	x	
Ga	x	x		W	x	x	
Gd		x		Y	x	x	
Ge		x		Yb		x	
Hf		x		Zn	x	x	x
Ho		x		Zr		x	

Table 4.1: Analytical techniques used for each element

Prepared solutions were used for both ICP-OES and ICP-MS analyses. A determination of the precision and accuracy of the method had been made in a previous study of the research group (Aulinas, 2008) by repeatedly measuring two international reference samples provided by the Geological Survey of Japan (JB-1b and JB-3). Results for these calculations are given in Table A.2.6 in Appendix 2. The same methodology was followed for the ICP-MS.

4.6.4 Inductively Coupled Plasma with Mass Spectrometry (ICP-MS)

Trace elements (including rare earth elements) were analysed using a Perkin Elmer Elan 6000. In every session the equipment was calibrated using calibration solutions shown in Table A.2.7 in Appendix 2. Calculated precision and accuracy are given in Table A.2.8 in Appendix 2.

4.6.5 Thermal Ionisation Mass Spectrometry (TIMS)

Strontium and Nd isotopic ratios were determined for 26 samples in the CAI facilities using a VG-Micromass Sector 54 with 5 Faraday boxes using the multidynamic collection method. $^{87}Sr/^{86}Sr$ measures were corrected for possible ^{87}Rb interferences and normalised to $^{88}Sr/^{86}Sr = 0.1194$ to

correct possible mass fractionation during sample charging onto the filament and measuring. $^{143}Nd/^{144}Nd$ measures were corrected for possible ^{142}Ce and ^{144}Sm interferences, and normalised to $^{146}Nd/^{144}Nd = 0.7219$ for possible mass fractionation.

During the analysis of samples two isotopic reference samples (NBS-987 for Sr and La Jolla for Nd) were repeatedly analysed. Obtained mean values are shown in Table 4.2. These values were used to correct measured values for possible drift referred to the standard, using for that purpose the certified reference values of the standards shown in the same table. Analytical errors are referred to two times the standard deviation and are 0.01 % for $^{87}Sr/^{86}Sr$ and 0.006 % for $^{143}Nd/^{144}Nd$.

Lead isotopic ratios of the same 26 samples were determined at the Department of Earth Sciences, Carleton University, Canada, using a Triton TIMS. All runs were corrected for mass fractionation using international standard NBS-981 from the National Institute of Standards and Technology and following Todt et al. (1996). The average ratios measured for NBS-981 are shown in Table 4.2. The obtained data were normalised to the reference values shown in the same table.

Isotope ratios	Measured value ± 2σ	Reference value
Sr: NBS987		
$^{87}Sr/^{86}Sr$	0.710254 ± 0.00004	0.710240
Nd: La Jolla		
$^{143}Nd/^{144}Nd$	0.511850 ± 0.00005	0.511850
Pb: NBS981		
$^{206}Pb/^{204}Pb$	16.891 ± 0.0068	16.9045
$^{207}Pb/^{204}Pb$	15.4300 ± 0.0090	15.4963
$^{208}Pb/^{204}Pb$	36.5080 ± 0.0295	36.7219
$^{207}Pb/^{206}Pb$	0.913460 ± 0.000200	0.91475
$^{208}Pb/^{206}Pb$	2.16132 ± 0.00090	2.16771

Table 4.2: Measured and certified values for the analysed reference samples. 2σ is calculated for n=8 in Sr and n=6 in Nd. In the case of Pb, 2σ represents the reproducibility over the 2 months previous to these analyses

4.6.6 Data selection

XRF is the technique requiring less manipulation of the sample (reducing the preparation error), and requires no solubilisation of it (errors produced by incomplete solubilisation of hardly soluble compounds - such as zircon - are avoided). Moreover, although accuracy is slightly lower in XRF than in ICP, precision is good enough to make results from different samples fully comparable. For these reasons data from this technique have been preferred when data from ICP were also available, especially in the case of major elements, because XRF directly measures silica concentration and ICP does not. For most trace elements, data from XRF have been selected to keep geochemical data from samples analysed only by XRF and those analysed by XRF+ICP

comparable. In some cases, though, quality of XRF data is not good enough and ICP data have been selected; this is the case for Cr, Cu, Mo and Ni. A last case is that of Ba, Ce, Sn, Sr, which for the most evolved samples present values too close to or below the lower limit of the calibration range of XRF; when values are below this limit ICP data have been selected. Table 4.3 summarises which has been the selected technique for each element.

Element	Technique	Element	Technique
Si	XRF	La	ICP
Ti	XRF	Li	ICP
Al	XRF	Lu	ICP
Fe	XRF	Mo	ICP + XRF
Mn	XRF	Nb	XRF
Mg	XRF	Nd	ICP
Ca	XRF	Ni	ICP + XRF
Na	XRF	Pb	XRF
K	XRF	Pr	ICP
P	XRF	Rb	XRF
		Sb	ICP
As	ICP	Sc	ICP
Ba	XRF + ICP (if <LL)	Sm	ICP
Be	ICP	Sn	XRF + ICP (if <LL)
Bi	ICP	Sr	XRF + ICP-OES (if <LL)
Ce	XRF + ICP (if <LL)	Ta	ICP
Co	XRF	Tb	ICP
Cr	ICP + XRF	Te	ICP
Cs	ICP	Th	XRF
Cu	ICP + XRF	Tl	ICP
Dy	ICP	Tm	ICP
Er	ICP	U	ICP
Eu	ICP	V	XRF
Ga	XRF	W	XRF
Gd	ICP	Y	XRF
Ge	ICP	Yb	ICP
Hf	ICP	Zn	XRF
Ho	ICP	Zr	XRF

Table 4.3: Analytical data used for each element. ICP is ICP-MS unless otherwise stated. "If<LL" means that ICP value was chosen when XRF value was under the lower limit of the calibration range

PART III: RESULTS

CHAPTER 5: VOLCANOSTRATIGRAPHY

5.1 INTRODUCTION

An important part of the field work has been devoted to the revision of the available cartography as well as of the volcanostratigraphy established in literature to guarantee that collected samples were correctly attributed to the corresponding unit, and that all units were sampled. Despite the huge amount of information collected during field work, it is not the aim of this Thesis to produce a highly detailed volcanostratigraphic description of each unit or a new map; this is left to future studies where interpretation of eruptive and emplacement mechanisms will be attempted. Therefore, only a brief volcanostratigraphic description of the main units is given in this chapter in order to summarize the information available at the moment, coming from literature, previous research group studies, and own fieldwork, and to make the following results and discussion chapters understandable.

5.2 VOLCANOSTRATIGRAPHY OF THE OLIGO-MIOCENE VOLCANIC MATERIALS IN SULCIS

As briefly explained in introductory chapters, the Oligo-Miocene volcanic succession in the Sulcis area consists of two differentiated parts. A lower part made by a thick pile (up to 400m) of andesitic (andesite, basaltic andesite and rare basalt) domes and associated products is overlain by an upper one formed by pyroclastic materials (with the exception of some comenditic lava flows and domes and lava flows in two minor units) of evolved composition (trachyte, rhyolite and minor dacite) and dominantly ignimbritic character. This succession corresponds to the Upper Acid-Intermediate Explosive Series of Assorgia et al. (1997).

Little attention has been paid to the andesitic succession and its stratigraphy in literature due to, among other reasons, scarcity of outcrops and borehole data and the difficulty in studying a dome piling. On the other hand, many efforts have been made to subdivide the ignimbritic sequence in

several units, especially since the borehole net made by the mining company Carbosulcis SpA provided a large number of drill cores cutting the whole ignimbritic sequence. Staff from this company provided the basic volcanic stratigraphy and a good mapping of the mainland Sulcis.

Studies carried out in the Sulcis mainland, mostly based on the abovementioned borehole cores, subdivided the ignimbritic sequence into 12 main units. These were described in Assorgia et al. (1990a, 1990b, 1992a, 1992b) and Morra et al. (1994) and are from base to top:

- Corona Maria
- Lenzu
- Acqua sa Canna
- Seruci
- Monte Crobu
- Conca is Angius
- Nuraxi
- Matzaccara
- Comendites
- Monte Ulmus
- Paringianu
- Serra di Paringianu

From the study of the two islands of Santo Antioco and San Pietro, some other minor units were recognised:

- Monte la Noce, in Santo Antioco, older than Monte Crobu unit and base unit in the island (Pasci and Orrù, unpublished).
- Unit 17, in the "Carta Vulcanologica dell'Isola di San Pietro" (Garbarino et al., 1990), which lies above Nuraxi; this unit has been further subdivided into two units: Punta dei Cannoni south of the main lower units relief in San Pietro, and Montagna di Capo Rosso north of it (Mundula et al., 2009).
- Punta Mingosa, in San Pietro, lies on top of Serra di Paringianu unit (Mundula et al., 2009).
- Two minor units have been recently described (Mundula et al., 2009) on top of Punta Mingosa unit: Geniò and Colonne. These have yet to be formally characterized and mapped, so less attention has been paid to them.

To facilitate following the text in this and the next chapters there is a reference chart available in Appendix 1 in which the main characteristics and stratigraphic position of each unit are presented, and a map is provided with the names of the main towns in the Sulcis and of significant landmarks mentioned in the text (Figure A.4.2 in Appendix 4)

Before starting to describe each unit separately, it is worth mentioning that most of the ignimbritic units share a common structure which was recognised by Assorgia et al. (1990b). According to the authors most ignimbrites present the following structure:

a) Fine grained loose basal layer some centimeters to decimeters thick, whitish in colour, rich in free crystals and pumices.
b) Obsidianaceous layer (vitrophyre) of variable thickness (typically from few decimeters to half a meter), mainly constituted by sintering of non-vesiculated glass lenticles, black in colour and poorly porphyritic.
c) Central body, in most units formed by eutaxitic facies, showing variable welding degree and a massive to fluidal fabric.
d) Upper part (usually lacking in the less welded units) rich in pumices within a cinder matrix.

The main, and sometimes only, constituent of all ignimbrites is the central body, which forms most of its thickness. The other three levels may or may not have been formed, and a) and d) even when formed may have not been preserved due to its scarce resistance to erosion. Figure 5.1 presents example pictures of the mentioned parts. This structure is better developed and preserved in the welded units.

Next, a brief description of each unit is given.

5.2.1 Andesites (AND)

The andesitic succession crops out in the southern part of Santo Antioco Island and in the Giba-Narcao graben (Fig. A.4.3 in Appendix 4). It is up to 400 m thick (Assorgia et al., 1992a) and is formed by high- to low-aspect ratio lava flows and small lava domes (typically less than 1 km across), associated with minor pyroclastic deposits, locally cut by lava dykes (Conte et al., 2010). Dome emplacement was mainly subaerial but evidences of subaqueous emplacement are present (dome-related andesitic debris flows in southern Santo Antioco and peperites).

Lavas are porphyritic, with a typical phenocryst association of plagioclase and pyroxenes in mm-sized crystals (Fig. 5.2).

Figure 5.1: Examples of the different parts of an ignimbrite. a) base of the Nuraxi unit at the mainland. A 20 cm-thick basal layer is present below the vitrophyre, which is about half meter thick. Above the vitrophyre there is the lower part of the main body of the ignimbrite; b) detail of the basal layer of Nuraxi; c) detail of the vitrophyre of Nuraxi; d) detail of the central part of Serra di Paringianu unit in highly welded and eutaxitic facies at the locality of Calasetta; e) and f) correspond to the Monte Crobu unit, in welded facies (e), and at the upper part of the ignimbrite (f), which is scarcely welded and less eutaxitic

Figure 5.2: Appearance of andesites in the field and in hand specimen. a) andesite outcrop in southern Santo Antioco Island formed by lava flows, breccias and dikes; b) close up of an andesite outcrop in the mainland; c) hand specimen

5.2.2 Corona Maria (CM)

The Corona Maria unit (Assorgia et al., 1990a) is only found in the Sulcis mainland, cropping out in the northern and central sectors and being largely expressed in the Carbosulcis SpA boreholes (Fig. A.4.4). Its thickness ranges from 15 m to a maximum of 40 m.

CM is scarcely to moderately welded, and the four levels described by Assorgia et al. (1990b) have been found in it.

The vitrophyric layer is black, porphyritic, and some decimeters thick. It may present abundant lithic fragments and flattened pumices altered to reddish colours. The main body has an eutaxitic porphyritic texture with lithic fragments and big pumices (Fig. 5.3). The vitreous groundmass is reddish dark-coloured. Porphyricity in this level is given by mm-sized plagioclase and pyroxene phenocrysts. This unit is characterised by the presence of a high amount of varied lithic fragments. These represent several rock types of basic composition with different textures and colours, but are mainly formed by massive andesitic lavas. Besides the massive lithic clasts, many "basic pumices" can be found. That is, bits of vesicular basic magma isolated as pumices within

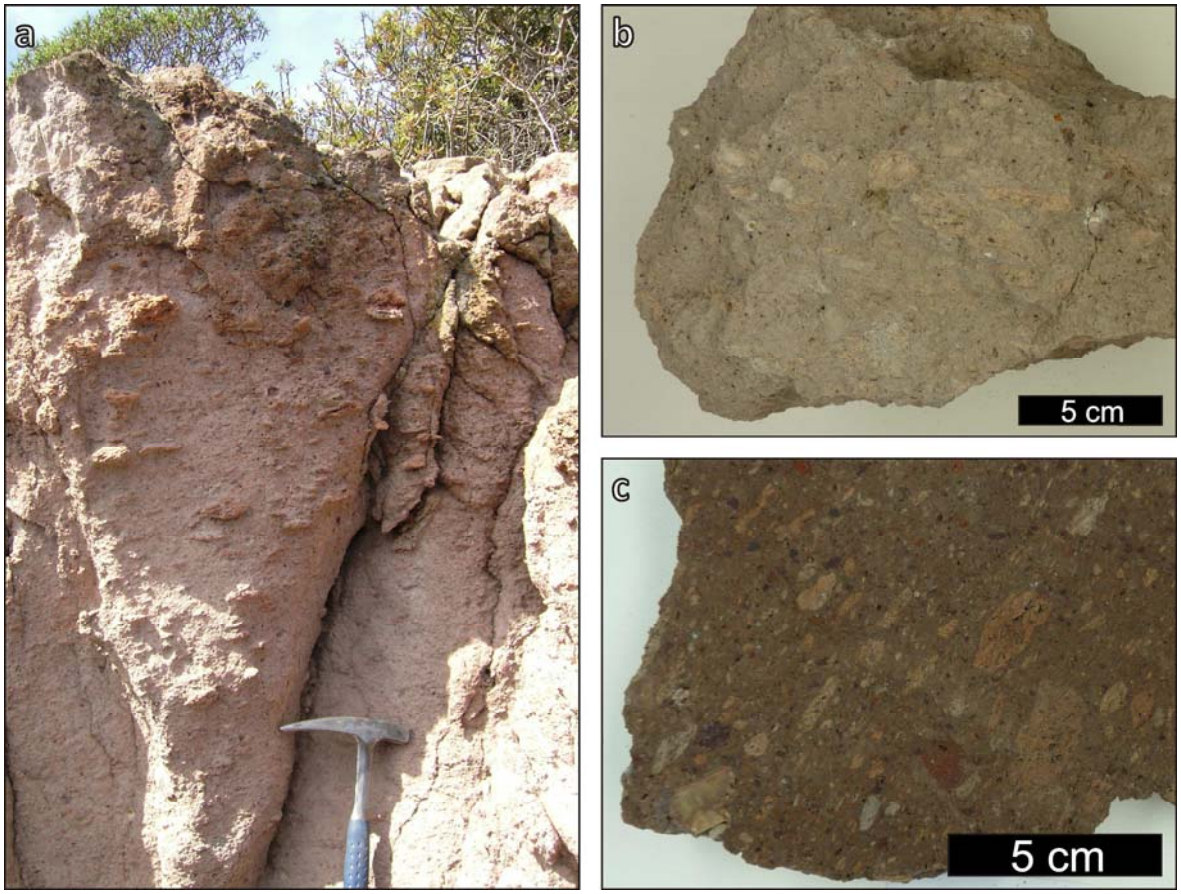

Figure 5.3: Appearance of Corona Maria unit in the field and in hand specimen. a) outcrop in the mainland; b) hand specimen; c) rock slice

the groundmass, perfectly recognisable either macroscopically or microscopically. These pumices were vesicled in origin and partially or totally collapsed upon emplacement, with shredded ends, and were usually deformed on emplacement or by rheomorphic processes. In many cases these pumices incorporated crystals from the groundmass. The CM unit presents in this main body some characteristic levels which are well individualised and allow a correct correlation between boreholes; an example of this is a level rich in extremely squeezed green pumices.

The CM unit ends with a complex upper level which includes cineritic coignimbrite-type deposits, more porous and far less welded, with a clear development of traction sedimentary structures. This upper part of the unit is usually so bentonitised that the characteristics of the original deposit cannot be discerned anymore, which caused it to be sometimes misinterpreted as sedimentary material (as in Assorgia et al., 1990b).

5.2.3 Lenzu (LE)

Lenzu unit (Assorgia et al., 1990a) may be separated from CM by a bentonitised level up to 15 m thick in average (Assorgia et al., 1992a) which belongs to the top of CM unit. Like CM, this unit has

only been found in the mainland, particularly in the northern sector (Fig. A.4.5). Its thickness is smaller than that of the previous unit, ranging from 2 to 13 m (Assorgia et al., 1990b).

It has a basal layer over which a well developed porphyritic black vitrophyric level up to 1 m thick is found (Assorgia et al., 1990b). LE unit main body is macroscopically very uniform, being highly welded (Fig. 5.4). The main body is massive, of a reddish-greyish colour, with a marked eutaxitic porphyritic texture, and presents abundant big collapsed pumices (up to 20-30 cm in diameter) strongly flattened at the base and more ellipsoidal at the top. It has subhoritzonal surfaces where vesicles are preferentially concentrated. Porphyricity is given by the presence of feldspars and, in less amount, pyroxene crystals.

5.2.4 Acqua sa Canna (AC)

Between LE and Acqua sa Canna (Assorgia et al., 1990a) units exists an interbedded level of continental origin consisting of sand and silt and/or pyroclastic-epiclastic levels, with a thickness ranging from 2 to 17 m (Assorgia et al., 1990b). Part of this deposit, originally interpreted as

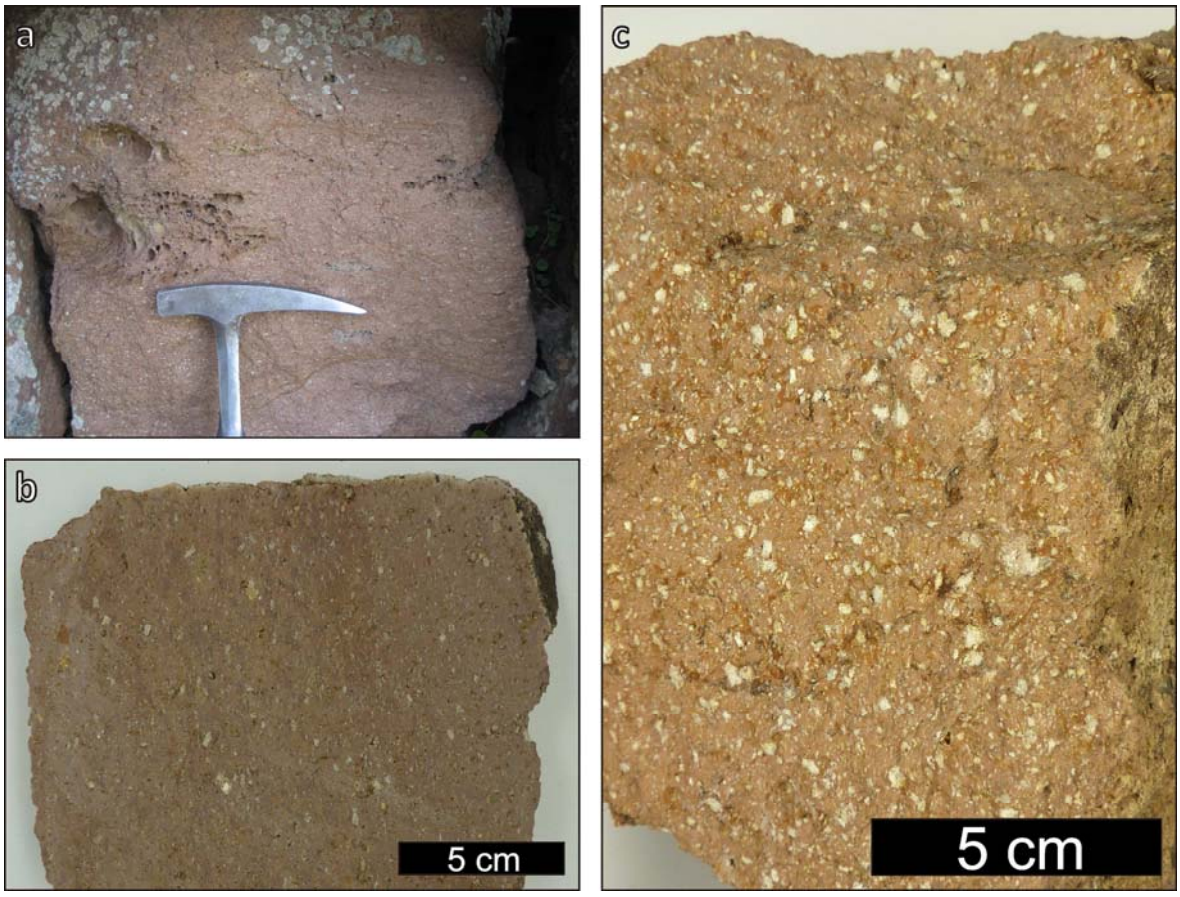

Figure 5.4: Appearance of Lenzu unit in the field and in hand specimen. a) building block of a "nuraghe" made from LE unit. Two highly vesicular pumices can be seen; b) rock slice; c) hand specimen

sedimentary, corresponds to the bentonitised top of LE unit. This unit is also only found in the mainland, although it is more widespread; it crops out from the northern parts of mainland to the Narcao graben, where it lies over the Andesites (Fig. A.4.6). It presents an average thickness of about 20 m. Cincotti et al. (1992) estimated its areal extension as some 250 km^2, and a total volume not smaller than 5 km^3 (large volume ignimbrites).

The AC unit is in fact an ignimbritic complex formed by several flows, differentiated one from the other by their varied composition and volcanological characteristics that share, however, some features including: presence of biotite (which is a mineral scarcely found in other units), high fragmentation degree, and poor welding (Fig. 5.5). Base surge deposits can be found at the base of some eruptive events, marking its beginning. According to Cincotti et al. (1992), in some places pauses in the eruptive activity can be found evidenced by sedimentary and epiclastic intercalated levels and/or weathered deposits. This unit is well individualised by its previous and following units (LE and Seruci), which are markedly different.

The typical AC pyroclastic deposit has a base surge over which the main body of the flow was deposited. This main body is a low grade ignimbrite of whitish to pinkish-greyish colour with eutaxitic texture and abundant several centimeter-sized pumices which become concentrated to the top of the deposit. Other components are phenocrysts (mainly plagioclase with minor biotite) and juvenile lithic fragments. Degassing structures may be present, mainly degassing pipes. Cincotti et al. (1992) recognised depositional trends involving lithic clasts; in proximal sectors lithic clasts become more abundant, locally forming accumulations of decimeter-sized fragments at the base of the flows (co-ignimbrite lag breccia).

Cincotti et al. (1992) claimed to have found in the sector between Giba and Monte Sirai a basaltic andesite lavic event within the AC deposits, which was interpreted by the authors as a late manifestation of the andesitic basal sequence. Revision of this sector showed that these events were in fact below the ignimbritic acid sequence, therefore belonging to the normal andesitic series.

5.2.5 Seruci (SE)

The Seruci unit (Assorgia et al., 1990a) is found at the mainland with a minimum thickness of 9 m and a maximum of 40 m (Assorgia et al., 1990b). It crops out in the same area than CM, in northern and central mainland (Fig. A.4.7).

SE is a high grade ignimbrite, highly welded, displaying porphyritic eutaxitic texture (Fig. 5.6). A basal layer is usually present at its base, overlaid by a porphyritic vitrophyre with up to 5 vol % lithic fragments and a thin zebrate pattern that grades into an eutaxitic welded level with a planar

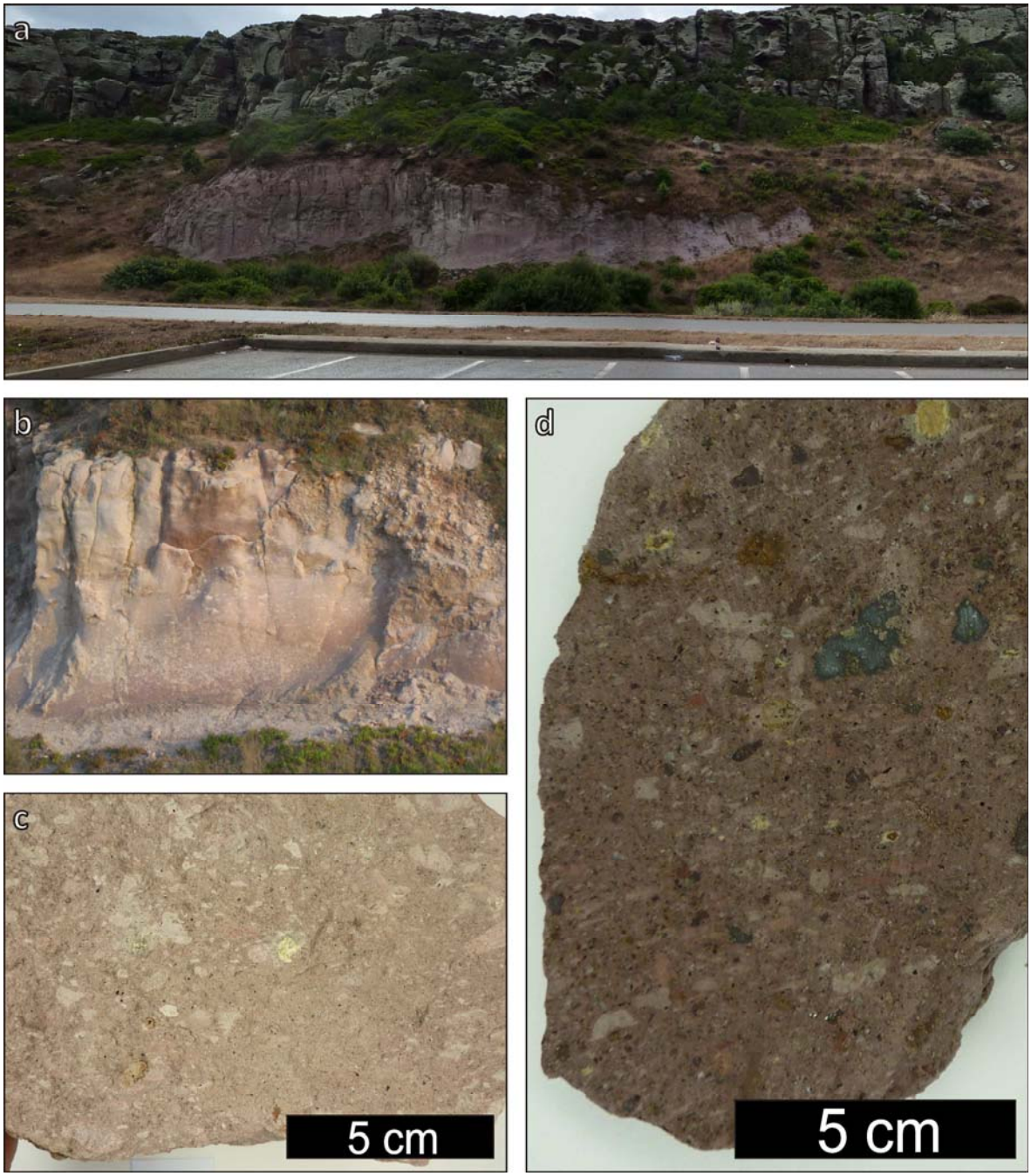

Figure 5.5: Appearance of Acqua sa Canna unit in the field and in hand specimen. a) outcrop in northern mainland (north of Portoscuso), the lower pink unit is AC, the upper one is Seruci. Outcropping thickness of AC is 5 meters; b) close-up of the AC part of the outcrop; c) hand specimen; d) rock slice

anisotropy marked by fiammes, which can be either compact or vesicular, and which may present two populations (light and slightly darker grey). The groundmass, of a brownish colour, is vitreous and shows a fluidal structure accentuated in the main body by the presence of vesiculation accumulations following surfaces roughly parallel to flows (Assorgia et al., 1990b, 1992a). Vesicles are also concentrated inside pumices by post-emplacement reinflation. Lithic fragments are

Figure 5.6: Appearance of Seruci unit in the field and in hand specimen. a) SE outcrop in northern mainland; b) SE unit vitrophyre, the black region is about 20 cm thick; c) close-up of the outcrop with a big decimeter-sized pumice; d) hand specimen

present. Porphyricity is given mainly by plagioclase crystals. In proximal sectors dark, presumably basic in composition, flattened pumices can be found at the base of the unit.

SE unit is macroscopically very similar to LE, being different from the latter by its thickness, by the zebrate pattern of the basal vitrophyre, by the higher abundance of lithic clasts in its basal part, which locally hindered the homogeneous formation of the vitrophyric texture, and by the selective concentration of the abundant vesiculation present in the deposit in pumices.

5.2.6 Monte la Noce (MLN)

Monte la Noce unit (Pasci and Orrù, unpublished) crops out exclusively in eastern Santo Antioco Island, representing the base of the ignimbritic cycle cropping out at the island (Fig. A.4.8). Outcropping thickness is of about 30 to 40 m.

It is defined in Pasci and Orrù (unpublished) as formed by lava flows with flow structures and frequently obsidianaceous autoclastic lava breccias (Fig 5.7), but it also includes pyroclastic deposits. It is aphyric to scarcely porphyritic with plagioclase and biotite mm-sized crystals. At the

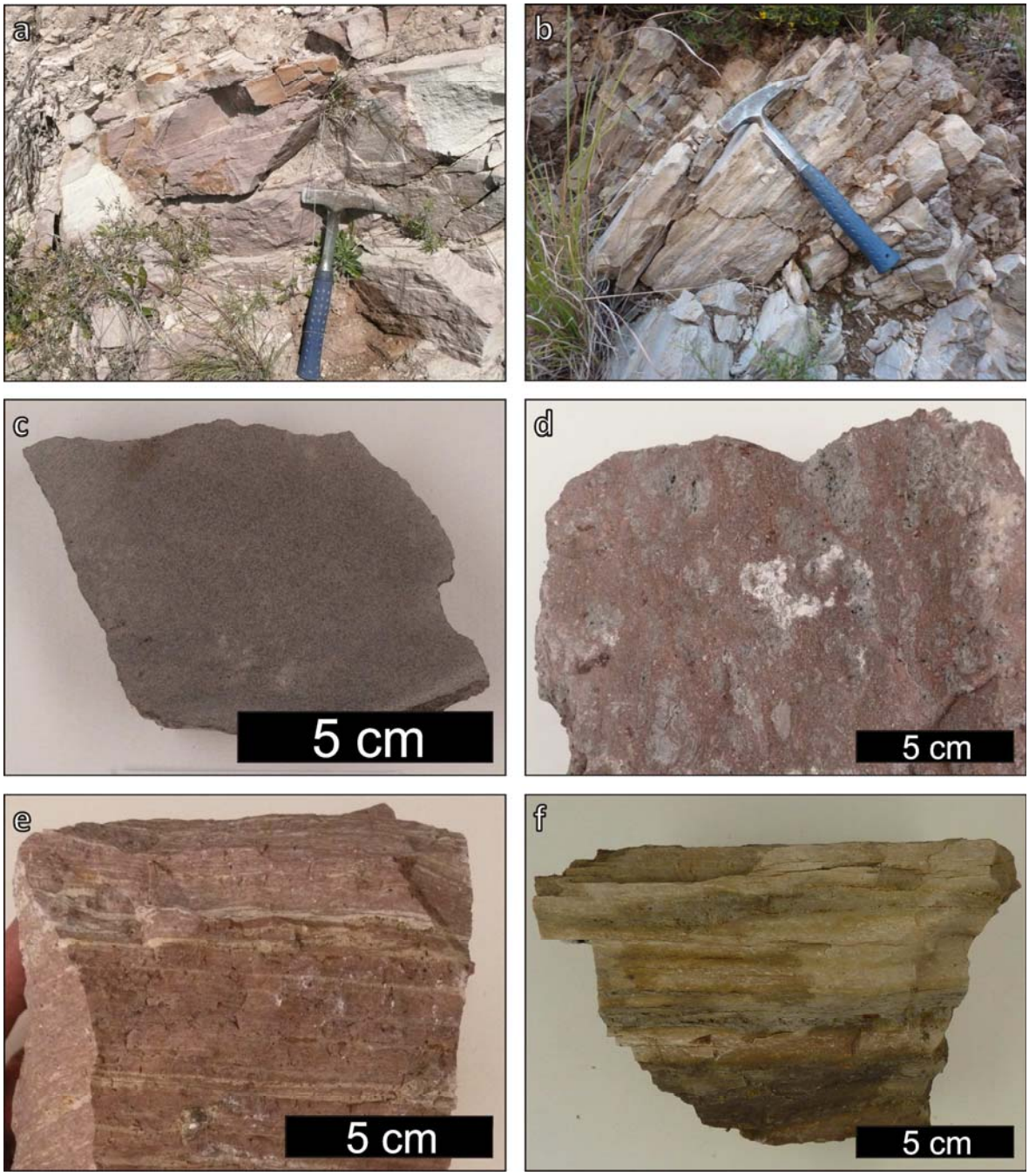

Figure 5.7: Appearance of Monte la Noce unit in the field and in hand specimen. a) outcrop of extremely welded and eutaxitic MLN ignimbrite; b) outcrop of banded lava flow; c) rock slice of cineritic MLN; d) hand specimen of moderately welded MLN ignimbrite; e) hand specimen of extremely welded and eutaxitic ignimbrite; f) hand specimen of banded lava flow

base it is intercalated with ignimbritic (tuff, lapilli-tuff and tuff breccias) and epiclastic deposits (volcaniclastic greywacke). General colour of the unit is light greyish purple. Locally, an extremely welded ignimbrite can be found, also aphyric but for very scarce and small (< 0.5 mm) plagioclase and biotite crystals, with a basal vitrophyre half a meter thick and an eutaxitic main body of

reddish brown matrix containing grey-light purple pumices. This unit is still to be better characterised.

5.2.7 Monte Crobu (MC)

The Monte Crobu unit (Assorgia et al., 1992b) is a widespread unit which can be found in whole southern and eastern mainland (Carbonia, Narcao) and in Santo Antioco Island (Fig. A.4.9). It was described as being formed by two extremely welded eutaxitic flow units, which together sum up to almost a hundred meters in thickness in the mainland (probably close to the emission centre), decreasing to the west and north.

This unit has a black aphyric basal vitrophyre less than half a meter thick. The main body of the ignimbrite is strongly welded, with an overall reddish brown colour, and is highly eutaxitic and porphyritic (Fig. 5.8). Porphyricity is given by mm-sized feldspars, which lie in a reddish-brown aphanitic groundmass as well as inside pumices. Pumices are mostly light grey (though in some zones dark grey/black pumices can be observed alone or coexisting with light grey ones) and highly vesicular. They are always strongly flattened, marking the eutaxitic texture of the rock, and can reach dimensions up to 80 cm in length. Their abundance varies from a few percent to more than 50 vol %, becoming dominant over the groundmass and modifying the overall unit colour. In some facies vesiculation may be abundant, organizing parallel to flow surfaces. Rheomorphic structures may be present.

Towards the upper part of the unit the ignimbrite turns to less welded and eutaxitic, becoming similar to the unit above, and thus difficult to differentiate from it.

5.2.8 Conca is Angius (CA)

Conca is Angius (Assorgia et al., 1990a) is mostly found in northern mainland, and in some outcrops of the northernmost Santo Antioco Island (Fig. A.4.10). Its areal extension complements that of MC unit; most of the mainland and Santo Antioco Island is covered by these two units but there is little overlap between them, only found in northernmost Santo Antioco Island. This unit is, like AC, a complex unit, showing different explosive events very close in time (it represents a cooling unit (s.l.)). Its thickness ranges from few to more than 50 m (Assorgia et al., 1990b), decreasing from northern mainland to west and south (where it partly overlaps with the MC unit).

CA is a low grade ignimbrite, always slightly- to non-welded, with a high fragmentation degree (Fig. 5.9). Its overall colour varies from whitish to light pink and is formed by ash, mm-sized feldspar phenocrysts, light-coloured cm-sized rounded pumices and abundant lithic fragments. White pumices are abundant throughout the unit, while at the upper regions some dark green

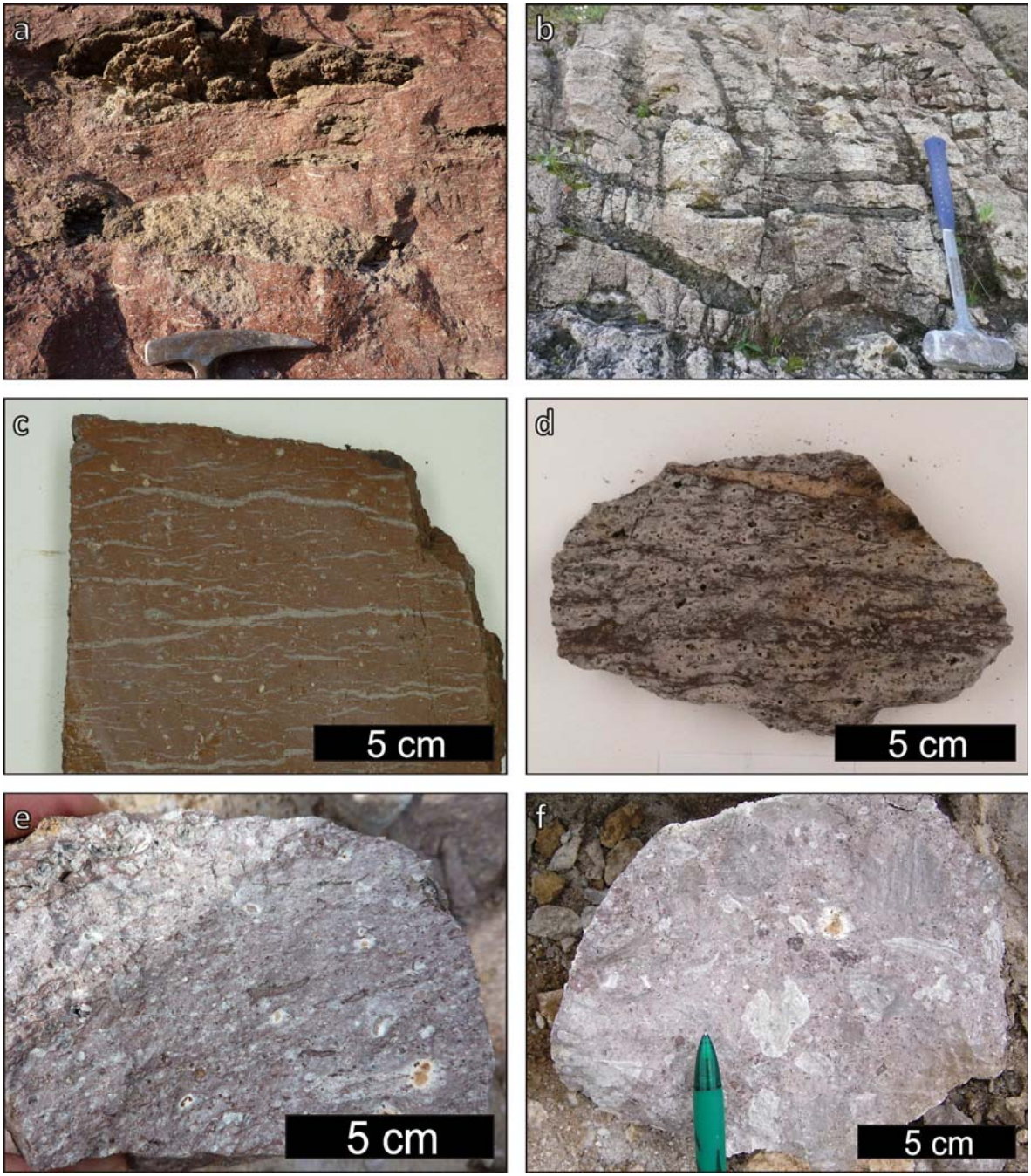

Figure 5.8: Appearance of Monte Crobu unit in the field and in hand specimen. a) outcrop detail of MC unit in reddish brown facies with decimeter-sized grey pumices; b) MC unit in facies with black decimeter-sized pumices; c) rock slice of MC in facies similar to those in picture a), grey lines are extremely flattened pumices; d) rock slice of MC in facies similar to those in picture b), the reddish brown regions are shard matrix, while grey ones are made of pumices; e) hand specimen of another welded facies; f) hand specimen of MC in scarcely welded facies found at the top of the unit

pumices may appear, which are more flattened. Degassing pipes are frequent at all levels. Due to its high porosity and low welding CA shows variable degrees of weathering, with highly bentonitized sections.

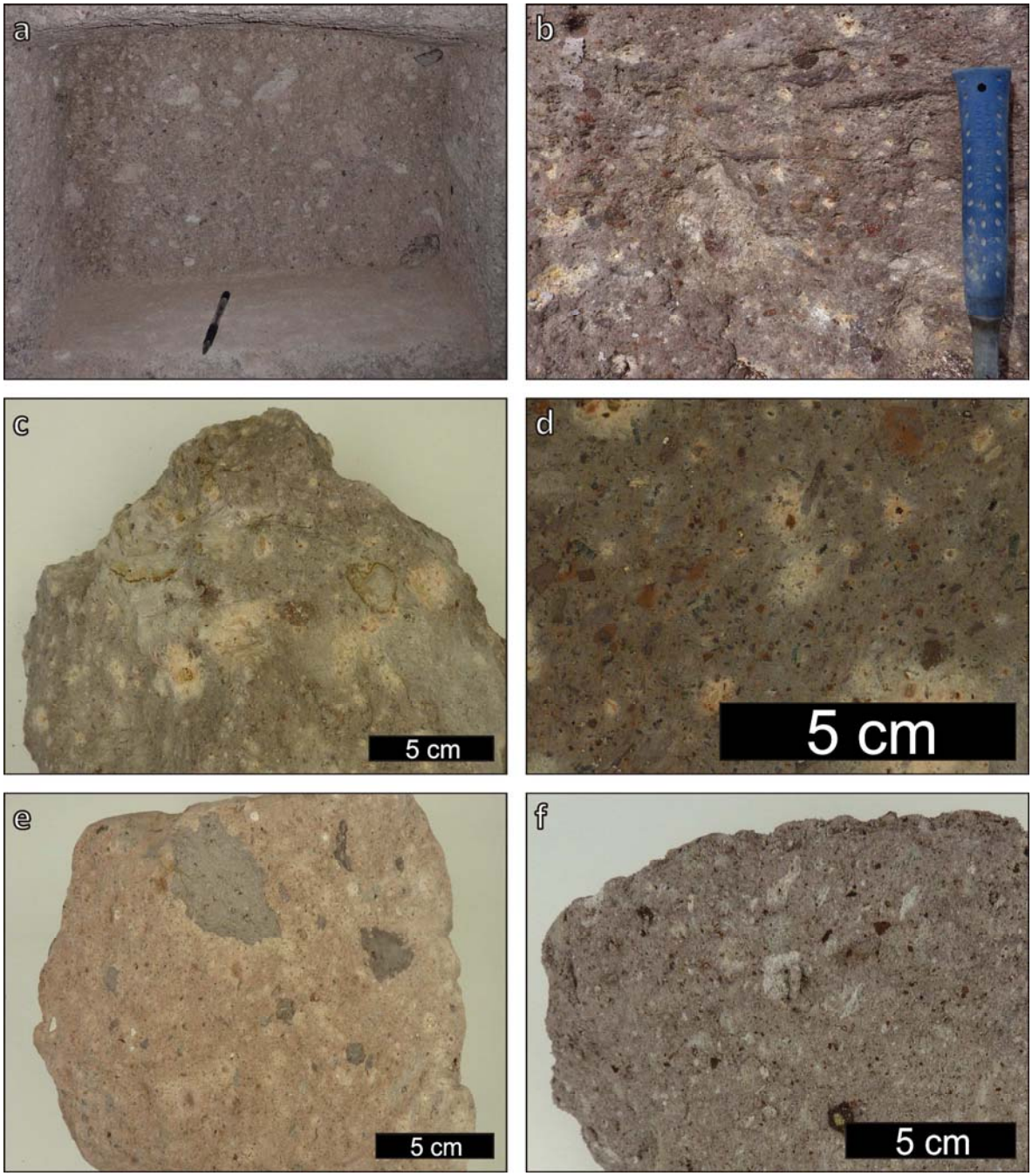

Figure 5.9: Appearance of Conca is Angius unit in the field and in hand specimen. a) niche in a Punic hypogeus in the town of Santo Antioco. The softness of this scarcely to non-welded unit made it appropriate for hypogeus excavation; b) close-up of outcrop in the mainland; c), e) and f) hand specimens; d) rock slice of the sample shown in c)

5.2.9 Nuraxi (NU)

The Nuraxi unit (Assorgia et al., 1990a) is one of the most widespread within the ignimbritic sequence. It can be found extensively in the mainland and in both minor islands, in an area more than 600 km^2 wide (Pioli and Rosi, 2005) (Fig. A.4.11). The thickness of this unit is notorious, averaging about 20 m, and varying depending on the sector from 10 to 160 m (a borehole near

Matzaccara). In average its thickness and grain-size decrease from west to east (Pioli and Rosi, 2005). NU unit is the basal unit cropping out at San Pietro Island.

In most places NU unit presents a non-consolidated feldspar-rich basal layer (pumice and ash fall bed; Pioli and Rosi, 2005) less than 40 cm thick, over which lays the high-grade Nuraxi unit ignimbrite. At the base of the welded ignimbrite a crystal-poor black basal vitrophyric level is always present, with a thickness ranging from 40 cm to 1.5 m (Pioli and Rosi, 2005), and with centimeter-sized columnar disjunction at the base (Fig. 5.10). The main body of the ignimbrite is extremely welded and massive, with a high crystal content (5 to 30 vol %) which gives the unit a marked porphyritic character. The dark reddish brown colour is a characteristic feature of this ignimbrite, although in some places may appear grey. Porphyricity is given by equidimensional to tabular white feldspar crystals less than 5 mm in size that can occur alone or in glomerules. Crystal and glomerule contents increase from the base to the top (Assorgia et al., 1992b). Lithic fragments are scarce (less than 5 vol %) and small (less than 4 cm). This unit usually shows little macroscopic evidence of fragmentation, only in the upper parts extremely flattened vesiculated light grey to reddish pumices some cm (up to a dm) wide can be observed. Therefore, this unit can sometimes be misidentified as a lava flow. In the lower, more massive regions of the ignimbrite, many subhorizonal flat gas concentration surfaces elongated with the flow direction can be found, originated by selective concentration of gases in planes during flow of the pyroclastic deposit. In the upper regions, the ignimbrite becomes more porous and far less welded. A macroscopic singular characteristic of the upper sectors of this unit is the occurrence of silica as crystals, especially inside degassing vesicles.

Pioli and Rosi (2005) subdivided the Nuraxi unit in two (Upper and Lower Ignimbrite). The upper ignimbrite corresponds to the upper crystal and pumice richer portion of the deposit.

The Nuraxi unit shows abundant evidences of rheomorphic flow in many places, both at micro- and macro-scale. At macro scale, folds with a wavelength ranging from some dm to tens of m can be observed.

In some localities (e.g. centre of San Pietro Island) this unit crops out largely autobrecciated into cm- to dm-sized angular equant clasts.

5.2.10 Punta dei Cannoni (PC)

The Punta dei Cannoni unit (Mundula et al., 2009) is only found in the western coast of San Pietro Island between NU and Matzaccara units (Fig. A.4.12). Its thickness can be up to some tens of meters.

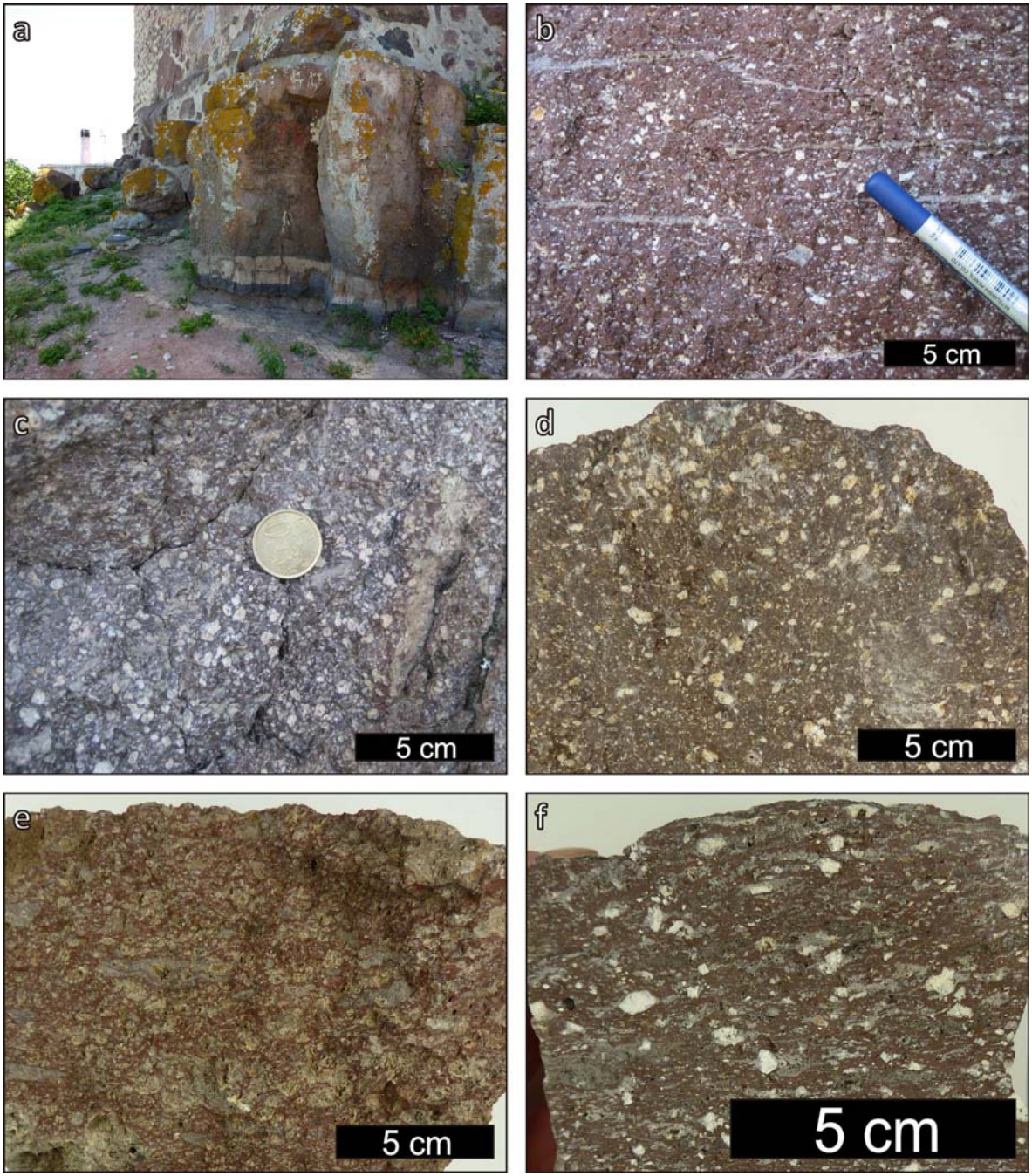

Figure 5.10: Appearance of Nuraxi unit in the field and in hand specimen. a) base of NU unit in Santo Antioco town next to the punic *Tophet*. The massive main body can be seen over the basal vitrophyre; b) c) d) e) and f) are different facies of this unit, the one shown in picture b) being the most abundant

PC unit is formed by several flow deposits of some meters thick which share similar features. This moderately to strongly welded unit is characterised by a high porphyricity (20-30 vol %) of white mm-sized feldspar phenocrysts in a brown groundmass, and by the presence of abundant big moderately flattened and vesicular light grey pumices up to a meter wide (Fig. 5.11). Decimeter-sized moderately flattened ellipsoidal bodies occur at some levels; they are porphyritic batches of

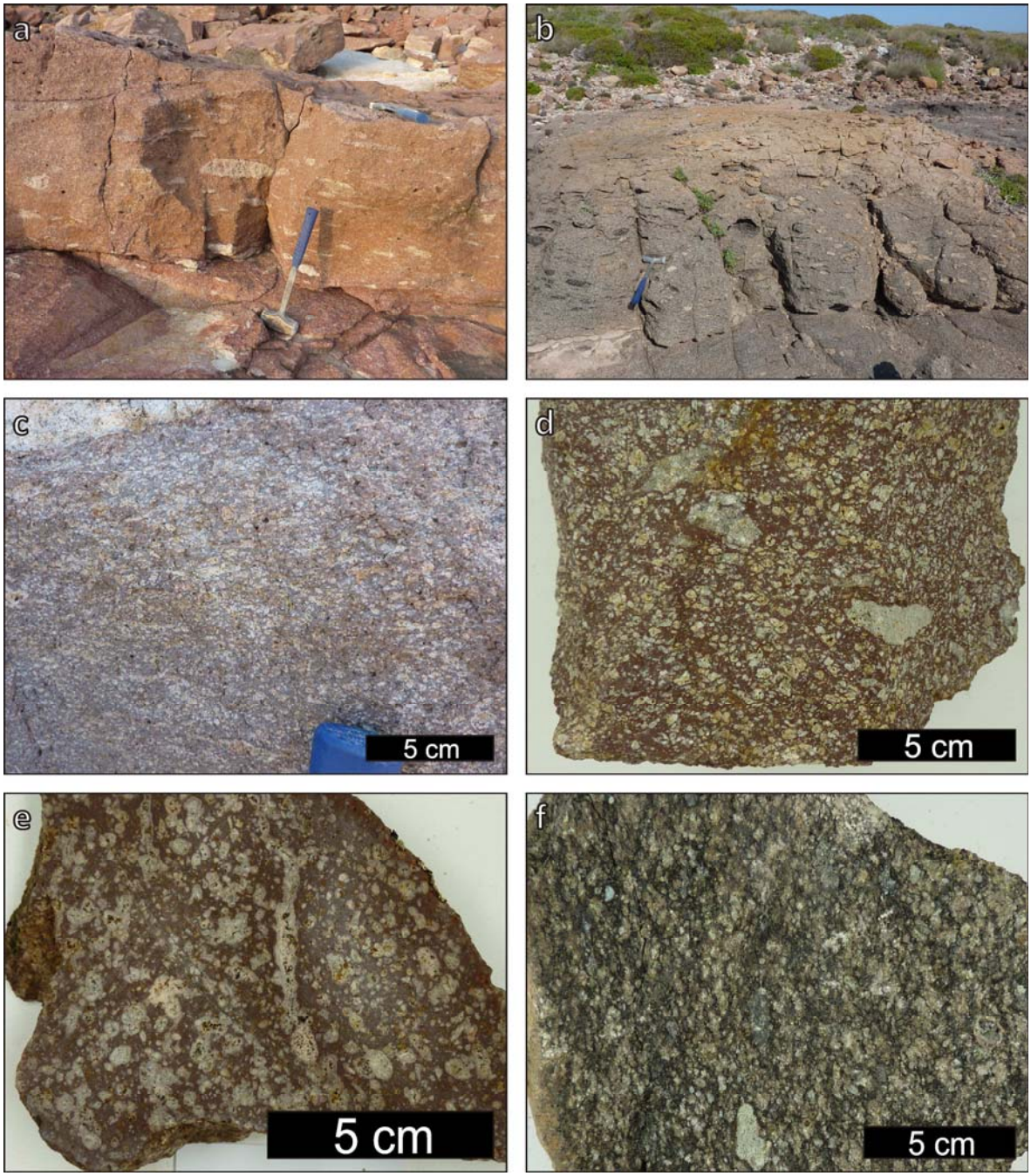

Figure 5.11: Appearance of Punta dei Cannoni unit in the field and in hand specimen. a) outcrop of the most abundant facies, with big decimeter-sized pumices; b) black groundmass level; c) close-up of an outcrop with the typical facies; d) hand specimen; e) rock slice; f) hand specimen from the level with black groundmass

a greyish groundmass colour, with a non-vesicular appearance. Lithic fragments are present. In the middle of the top region of the unit two flows less than a meter thick may appear that have the particularity of presenting the same characteristics than the rest of the unit but having black groundmass and brown and black pumices.

5.2.11 Montagna di Capo Rosso (MCR)

The Montagna di Capo Rosso unit (Mundula et al., 2009) is only found in western San Pietro Island, between NU and Matzaccara units (Fig. A.4.13). There is no areal overlap with PC unit so the relative chronology between these two units cannot be solved. It is about 80 m thick and consists of a piling of lava flows and pyroclastic density current deposits some meters thick. It has porphyritic texture given by the presence of feldspar phenocrysts (Fig. 5.12). Pyroclastic materials may present abundant cm-sized rounded pumices and angular lithic fragments.

5.2.12 Matzaccara (MZ)

The Matzaccara unit (Assorgia et al., 1990b) is, like Nuraxi, one of the most widespread units. It is found in the mainland and in the two minor islands (Fig. A.4.14). However, due to its relatively small thickness (up to 10 m (Assorgia et al., 1992b)), low or inexistent welding for most of its extension, and frequent weathering to bentonite, it barely crops out. Exceptions to this are the facies cropping out at San Pietro Island, where this unit is present as a non-welded to extremely

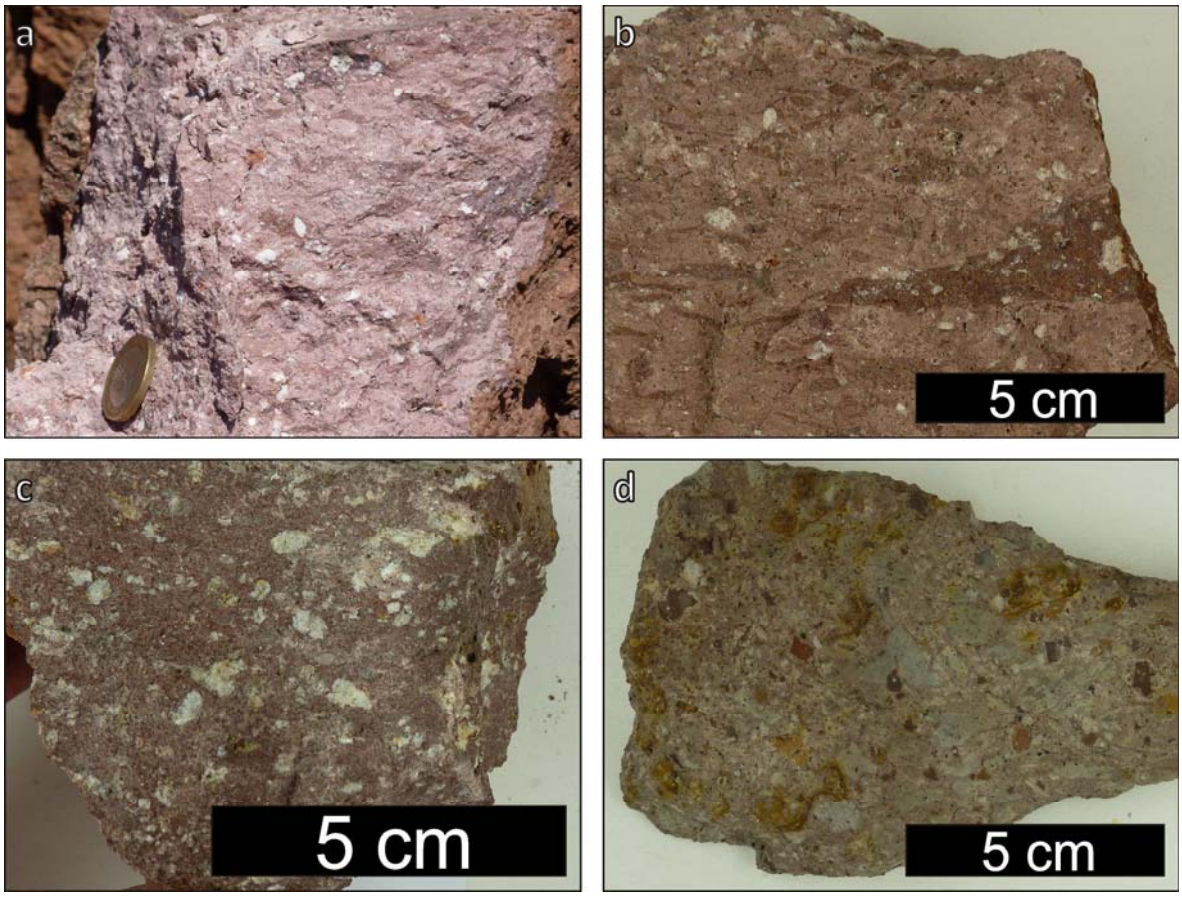

Figure 5.12: Appearance of the pyroclastic facies of Montagna di Capo Rosso unit in the field and in hand specimen. a) close-up of an outcrop; b) and c) hand specimens; d) rock slice

welded ignimbrite, in some cases very well preserved.

MZ unit is formed by some different flows and/or facies, most of which share common characteristics. This unit is mostly grey in colour and is characterised by a high fragmentation (ash) and low porphyricity (Fig. 5.13). Porphyricity is given by feldspar and bronze-coloured biotite

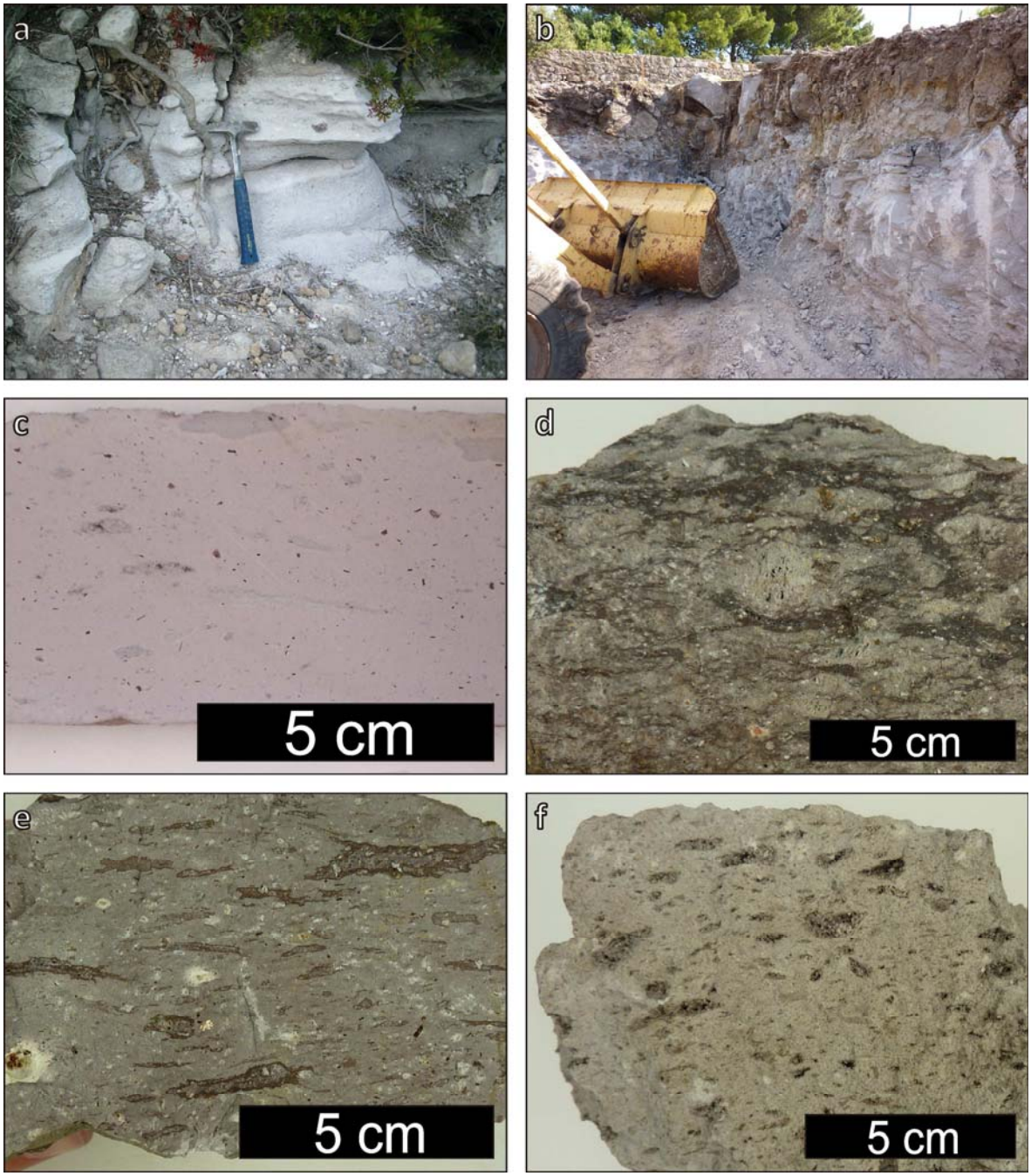

Figure 5.13: Appearance of Matzaccara unit in the field and in hand specimen. a) outcrop in western Santo Antioco Island. At this location MZ unit is a non-welded cinerite; b) outcrop in San Pietro Island. At this location MZ unit is a moderately welded ignimbrite with dark pumices; c) rock slice of a sample from Santo Antioco Island; d), e) and f) hand specimens of some of the MZ facies present in San Pietro Island

crystals, which are a diagnostic feature of this unit and are abundant compared to the occurrence of this mineral in the other units. The main macroscopic components of this unit are: scarce white or dark small pumices, free crystals and magmatic lithic fragments (usually weathered, centimeter-sized, and sometimes accumulated in degassing paths (Assorgia et al., 1992b)). Welded facies in San Pietro Island present higher pumice content, and these are bigger (up to some dm) and flattened, giving a strong eutaxitic texture to the deposit.

5.2.13 Comendites (CO)

Comendites unit (Assorgia et al., 1990a) crops out irregularly in central mainland and in the minor islands (Fig. A.4.15). At the mainland, CO occur south of the Paringianu fault, in the central sector, reaching a maximum thickness of 50 m in borehole and 10 m at surface (Assorgia et al., 1990b). In Santo Antioco Island CO outcrop along a narrow band in the western sector of the island. Both in mainland and Santo Antioco, CO are represented by pyroclastic density current deposits. San Pietro Island is where comendites are more abundant, showing diversity of deposits; they occur as lava flows and domes and as pyroclastic density current deposits, being volumetrically dominant the lavic forms, which mantle the north of the island. On this island CO were object of study of multiple studies (Bertolio, 1895; Johnsen, 1912; Taricco, 1934; Garbarino and Maccioni, 1968, 1969; Araña et al., 1974; Garbarino et al., 1985, 1990; Cioni et al., 2001; Cioni and Funedda, 2005).

Comenditic lavas are characterised by their high porphyricity (up to 50 vol %) and light colours (grey to yellowish or greenish) (Fig. 5.14). Flow banding is usually well marked. Porphyricity is given by millimeter-sized phenocrysts of clear sanidine and quartz, and minor amounts of alkaline mafic minerals (Na-Fe amphiboles). Sanidine may show a blue iridiscence. CO form thick lava flows that can reach several tens of meters in thickness, with origin in multiple eruptive centres.

The pyroclastic fraction of Comendites is very complex, being formed by several cooling units that may consist of more than a single pyroclastic density current deposit, and that have limited areal distribution. Paleosoils can be found separating different eruptive events within Comendites. Basal vitrophyres may occur. Despite being formed by several flow deposits, all the comendites share some common characters such as being light coloured (mostly yellowish or pinkish white or light grey), having a very high degree of fragmentation (they are mostly fine grained) and a relatively high porphyricity (Fig. 5.15). Porphyricity is given by sanidine and quartz crystals, with minor alkaline mafic minerals. CO may have small pumices and lithic accidental fragments, always in low amount and small size (some mm to few cm). When present, pumices are strongly flattened. Welding degree varies from low to high. Towards the upper zone of individual flow deposits, cineritic laminated facies interpreted as ash cloud surges have been preserved in some

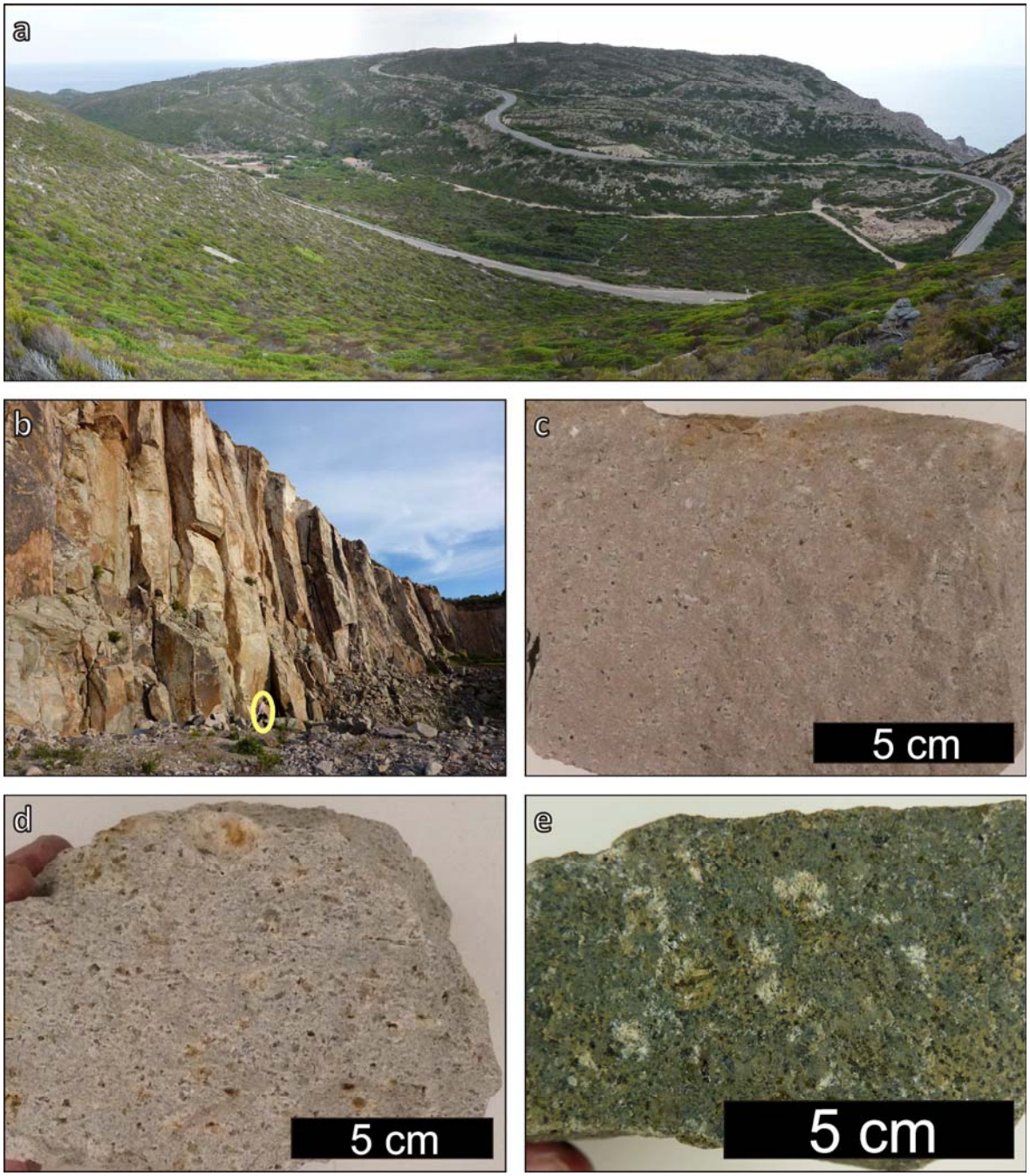

Figure 5.14: Appearance of Comendites unit lava flows in the field and in hand specimen. a) CO lava flow in northwestern San Pietro Island. Flow ribbons can be seen; b) quarry in CO lava flow with prominent columnar jointing, see person for scale; c), d) and e) different CO lava facies

locations (Assorgia et al., 1994). Levels of accretionary lapilli may be present. Parts of the less welded deposits are frequently altered to bentonitic materials.

5.2.14 Monte Ulmus (MU)

When Monte Ulmus unit was first described (Assorgia et al., 1990b, 1992a) it was considered to be formed by a basal highly welded portion very poor in macroscopic components (phenocrysts,

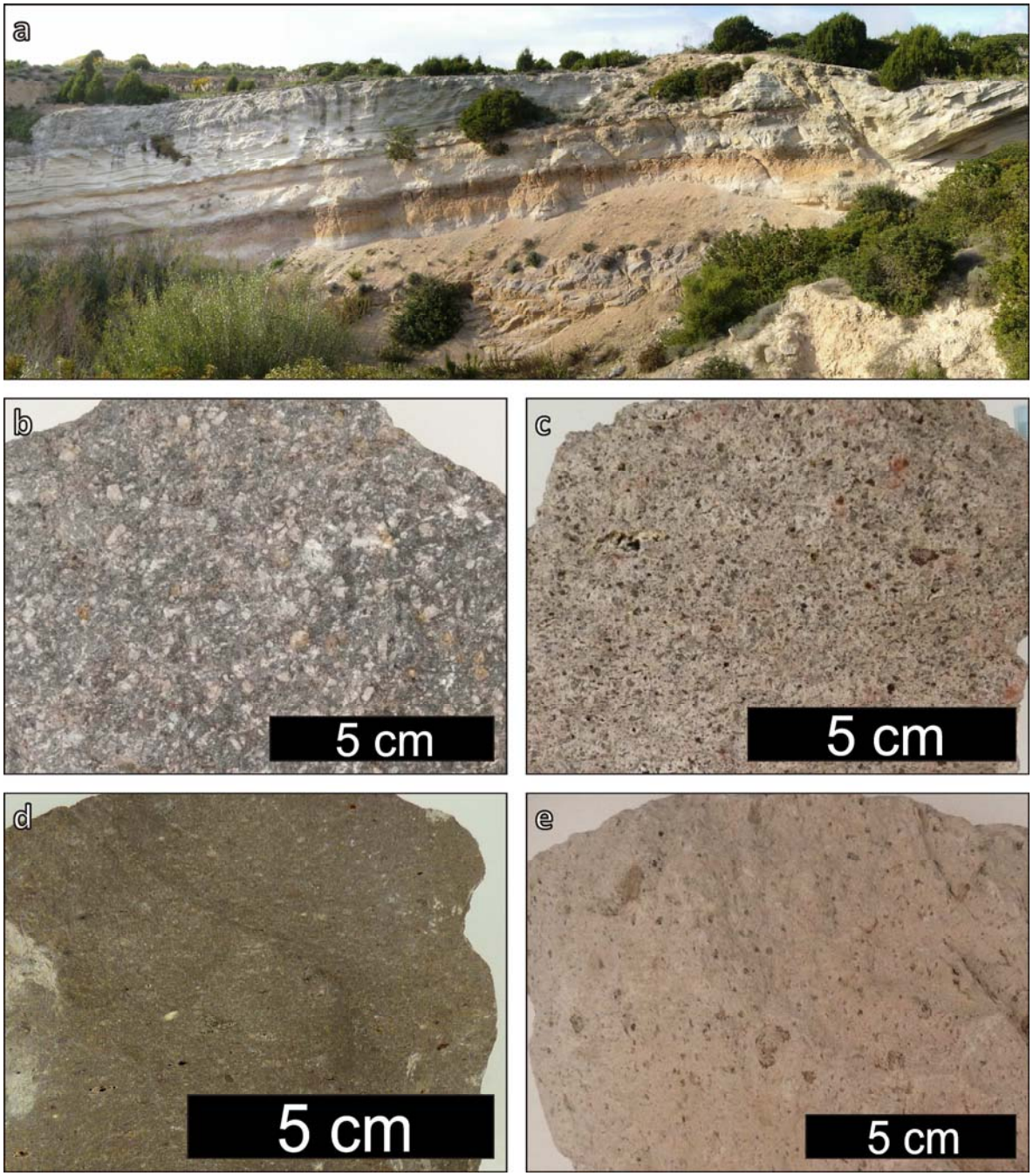

Figure 5.15: Appearance of pyroclastic Comendites unit in the field and in hand specimen. a) scarcely welded comenditic ignimbrites at Santo Antioco Island. Quarry placed east of Cala Saboni; b), c), d) and e) different CO facies

pumices, lithic fragments), and an upper part rich in black pumices. Recent fieldwork has revealed that these two portions can be considered, in fact, two separate units. The basal portion is considered by the author the original MU unit, while the upper one will be described as a new unit (Carloforte).

The Monte Ulmus is a very widespread unit, like NU, and can be found in the entire mainland south of Paringianu fault and in both minor islands (Fig. A.4.16). According to Assorgia et al.

(1992a), in the mainland it may be separated from the CO by a detritic layer up to 6 meters thick; this probably corresponds, at least in part, to bentonitized CO upper part. Its thickness ranges from less than a meter at San Pietro Island to more than 40 at the central mainland and western Santo Antioco Island.

MU unit is similar to the previous CO, but it has been described as a different unit due to its homogeneity in most of its extension and its characteristic features. It is a high grade ignimbrite (highly welded) of a greenish light grey to pink colour (Fig. 5.16). It presents a basal black to brick-red aphyric vitrophyre with a thickness of 30 cm to 1 m, which may present cm-sized lithophysae structures, and locally abundant accidental lithic clasts content. At Cala Saboni mm- to cm-sized yellowish lithic fragments can be found which consist in metasomatised limestone fragments containing garnet (previous work of the research group). As said before, this unit is very poor in macroscopic components; it is mostly formed by fine ash, showing only a light porphyricity (3 vol % sanidine crystals less than 2 mm wide), and occasionally dark highly vesiculated flattened pumices in the upper regions. These dark pumices can reach half a meter in size in western Santo Antioco Island. Other characteristic features of this unit are the intense rheomorphism and the presence of planar flow-elongated gas accumulation zones which show strong lineations due to flow (Assorgia et al., 1992a).

From Santo Antioco Island to the north, this unit thins out to show, in central San Pietro Island and western mainland, a particular condensed facies (Fig. 5.17). In San Pietro it can be observed how this unit thins from some meters showing the same characteristics as in Santo Antioco to only half a meter, becoming almost aphyric and extremely welded. In this condensed form it is formed by a 20 to 40 cm-thick black vitrophyre and a reddish-pink aphyric highly eutaxitic upper region.

5.2.15 Carloforte (CF)

The Carloforte unit (this study) was originally considered the upper part of the MU unit, but the study of San Pietro Island has revealed that it may be considered a separate unit. It is restricted to San Pietro Island, where it has large surface expression, and central mainland, with a thickness from a few to 30 meters (Fig. A.4.17). It is not present in Santo Antioco Island. There is no evidence of substantial time lapse between the deposition of MU and CF units, being possibly products of the same eruption.

The CF unit is a high grade ignimbrite, strongly welded and moderately eutaxitic, characterised by the presence of highly vesicular and porphyritic black pumices (Fig. 5.18). Pumice content and size vary considerably with distance. In what has been interpreted as proximal deposits in central San

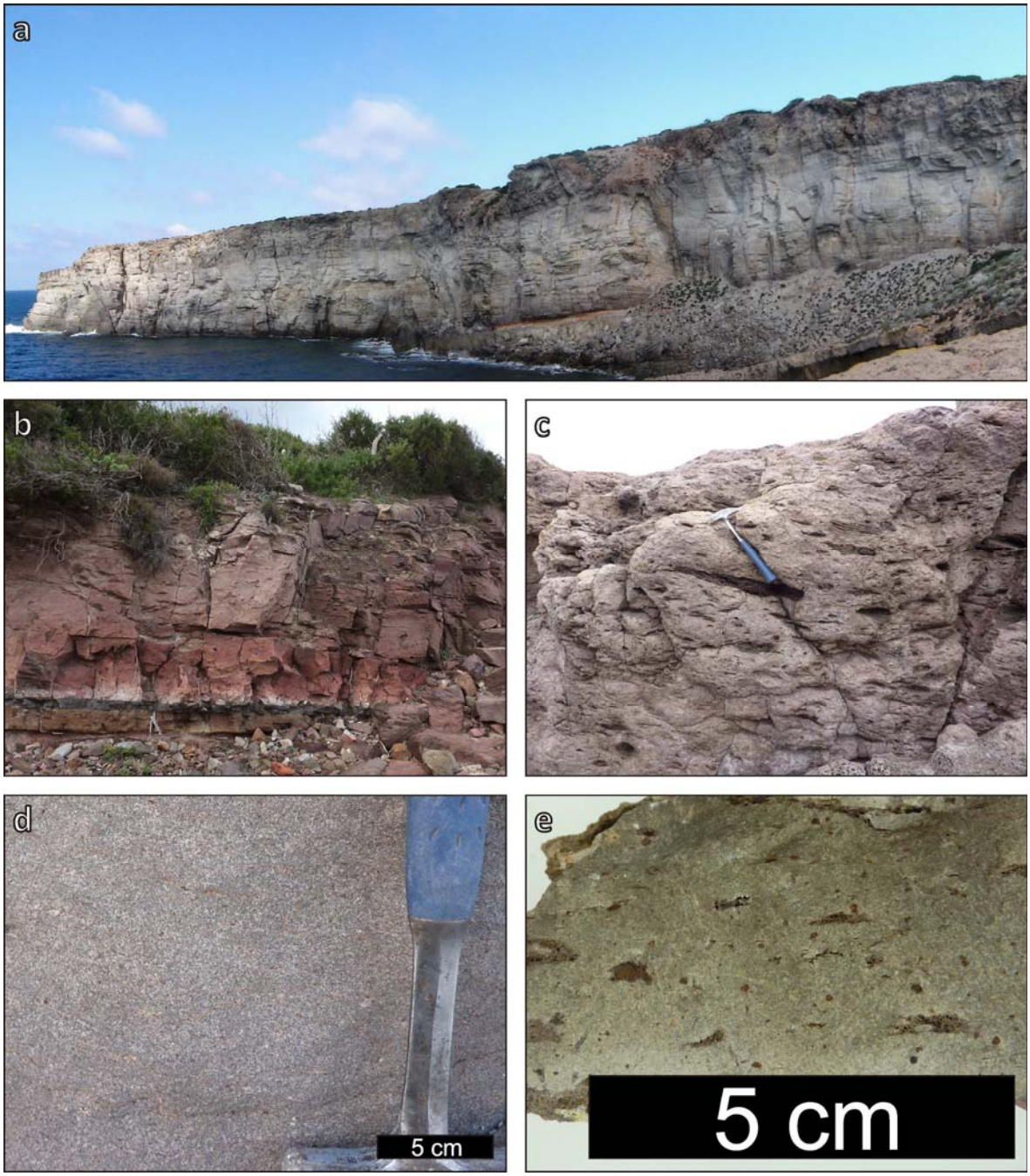

Figure 5.16: Appearance of Monte Ulmus unit at Santo Antioco Island in the field and in hand specimen. a) MU unit; b) base of MU unit with vitrophyre; c) MU facies with black decimeter-sized pumices; d) close-up of MU in highly rheomorphic facies without pumices; e) hand specimen of MU with small pumices

Pietro Island, at the sector of La Piramide, pumices are more than half a meter wide, whereas in distal facies (northern San Pietro and mainland) they barely reach one centimeter. Observations suggest that the origin of this ignimbrite probably was at a small distance east of La Piramide sector. Pumice content decreases with distance from almost 40 vol % to less than 10 vol %. Pumice porphyricity is given by abundant very clear tabular sanidine crystals up to a cm in size. White pumices, as well as lithic fragments in varying amounts, are found; both components vary

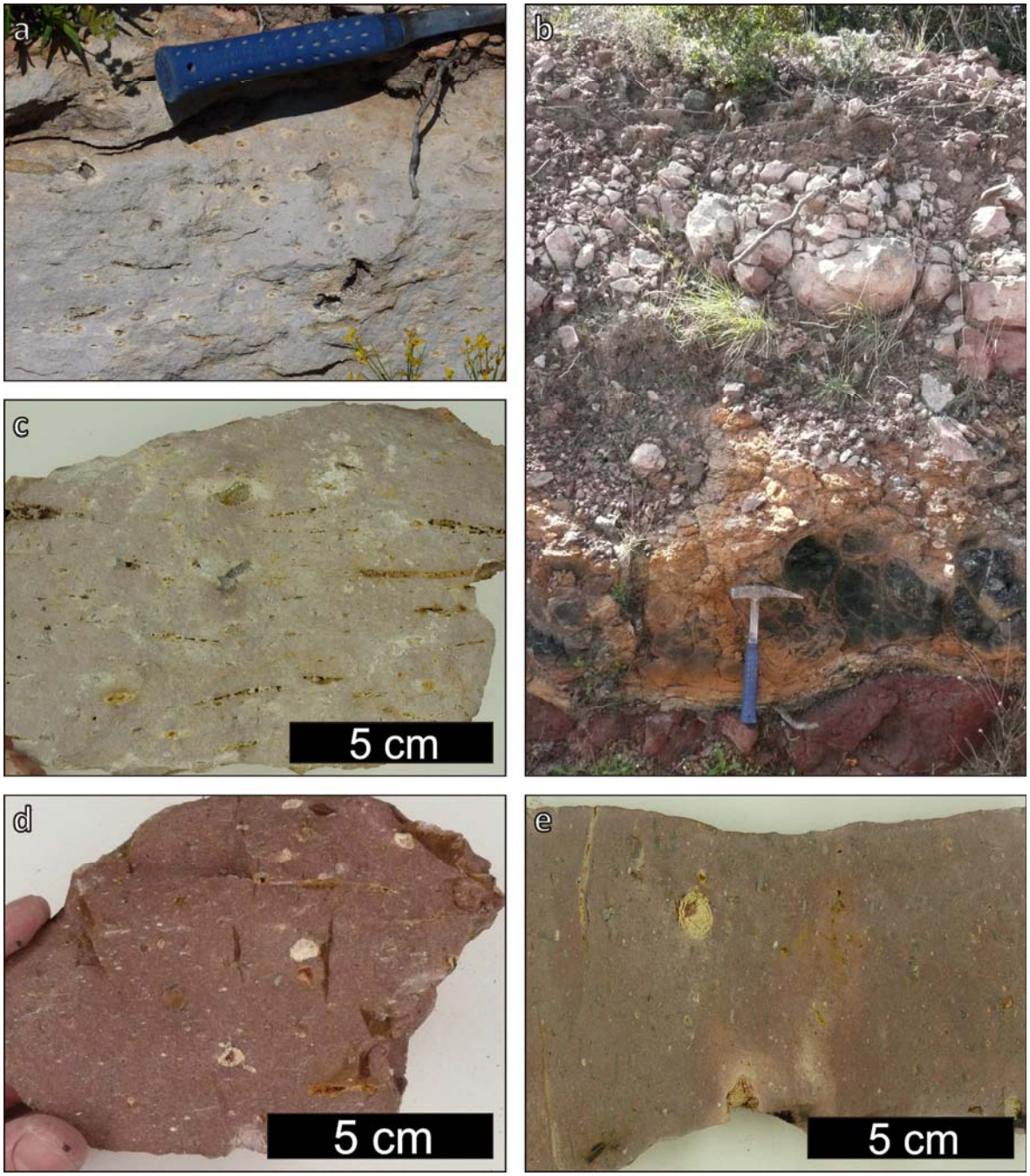

Figure 5.17: Appearance of Monte Ulmus unit at San Pietro Island in the field and in hand specimen. a) outcrop close-up of moderately condensed facies; b) condensed MU facies with partly altered basal vitrophyre; c) hand specimen of moderately condensed MU facies; d) and e) hand specimen and rock slice of condensed MU pink facies

in size in a way similar to that of black pumices. Groundmass is cineritic and its colour is light grey. It is variably porphyritic, containing mm-sized sanidine crystals.

5.2.16 Paringianu (PA)

The Paringianu unit (Assorgia et al., 1990a) is widespread and can be found in both islands and in the central mainland, with a thickness usually under 20 m (Fig. A.4.18). It is formed by several

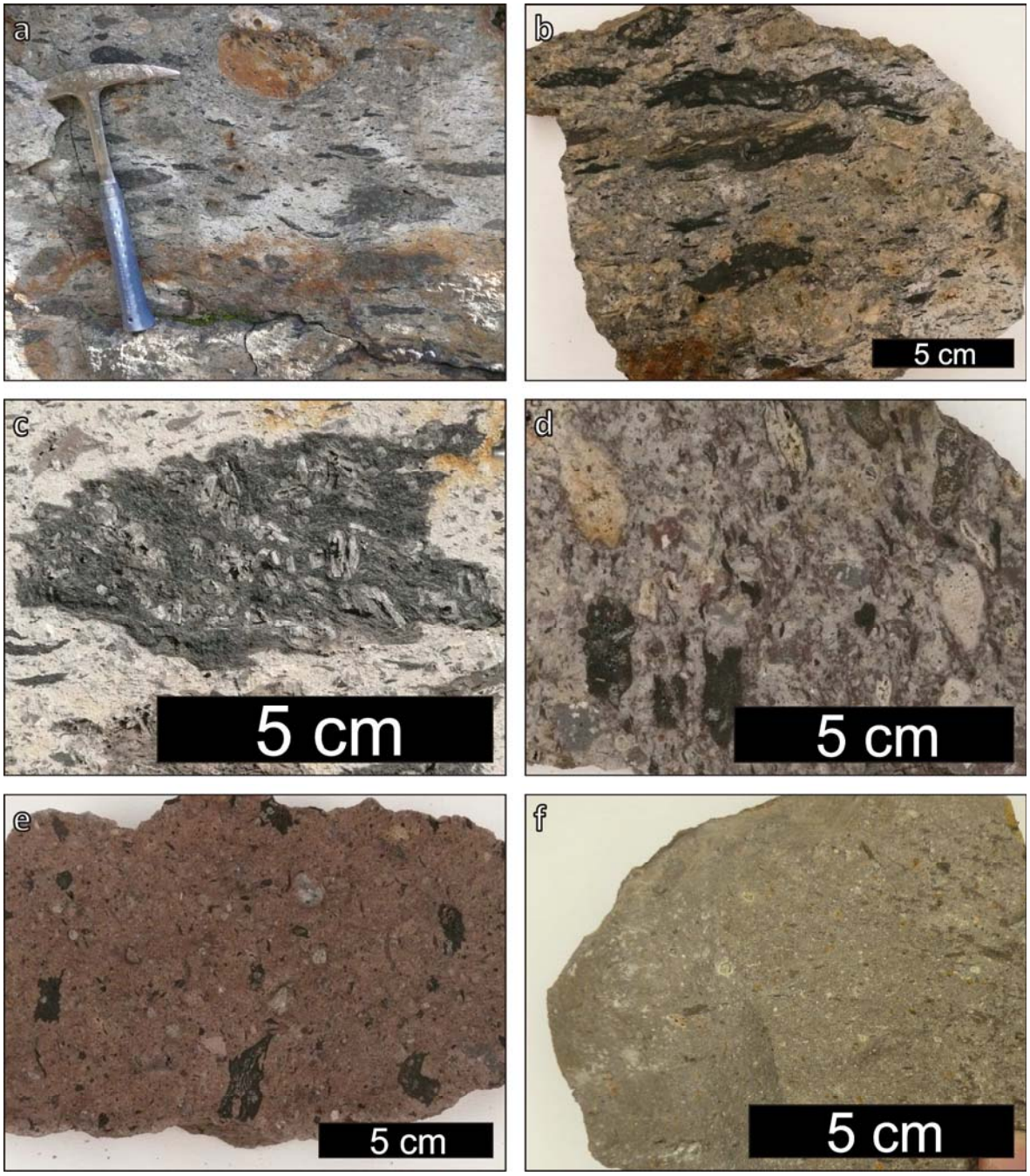

Figure 5.18: Appearance of Carloforte unit in the field and in hand specimen. a) outcrop close-up, in the main road in La Piramide site; b) hand specimen; c) detail of a crystal-rich black pumice; d) hand specimen showing the multiple components forming this unit; e) scarcely welded hand specimen; f) fine grained facies hand specimen

deposits, most of which are low-grade ignimbrites. It is usually affected by low to high degrees of weathering, making its study difficult.

PA deposits are massive, porphyroclastic, extremely fragmented, without any indication of oriented texture in most outcrops, without clast selection, and non- to slightly welded (Fig. 5.19). Their colour varies from white to light pink or yellow. Macroscopically, PA unit is formed by a

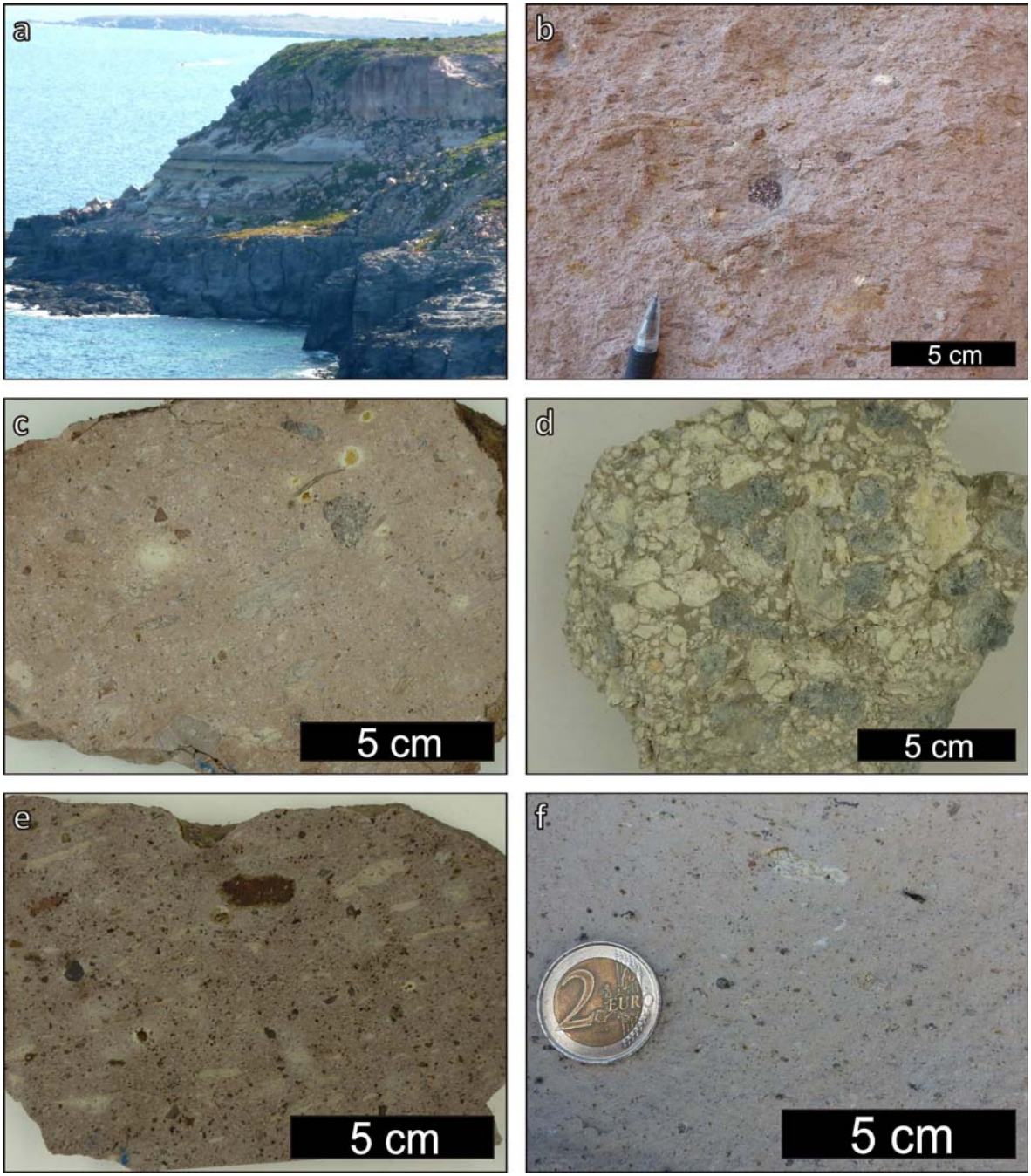

Figure 5.19: Appearance of Paringianu unit in the field and in hand specimen. a) northern coast of San Pietro Island. The basal unit is CF, over it PA presents two different facies, a white one and a pink one; b) outcrop close-up of the pink facies shown in picture a); c) and d) two different facies from San Pietro Island in rock slice and hand specimen; e) and f) two different facies from the Sulcis mainland

cineritic matrix which contains low proportions (usually less than 10 vol %) of small (less than 4 cm) lithic fragments, small pumices (less than 10 cm wide in places where they are very flattened), and few mm-sized feldspar crystals. Degassing structures such as pipes can be observed. In most places it is difficult to appreciate significant macroscopic differences in a vertical profile.

On the two islands, PA unit can contain, together with the massive ignimbritic facies described above, some layered facies which can be interpreted as fall and epiclastic deposits. Fall deposits are enriched in small round pumices, and epiclastic ones are enriched in the lithic component.

5.2.17 Serra di Paringianu (SP)

Serra di Paringianu (Assorgia et al., 1990b) is the last widespread unit in the Sulcis region, and is present in the central mainland and in the two minor islands (Fig. A.4.19). As a consequence of being at the top of the sequence, it has been eroded in many places, especially in the mainland, making the estimation of its total thickness difficult. On the two islands it has been better preserved, covering an important portion of those. Outcropping thickness varies from few to some 30 to 40 m.

The Serra di Paringianu unit is a massive high grade ignimbrite (strongly welded) characterised by the presence of a thick (40 cm to 1.5 m) crystal-poor black basal vitrophyre, overall maroon colour, porphyricity given by abundant white mm-sized feldspars, and eutaxitic texture evidenced by abundant extremely flattened dm-sized light grey pumices that may contain the same crystals as the groundmass (Fig. 5.20). Two pumice populations (light and darker grey) typically occur. The vitrophyre presents in many locations lithophysae structures, cm to dm in size. The lower meters of the unit may lack pumices, which appear progressively upwards. Rheomorphism is frequent and can develop flow foliation. In most of its extension the SP unit is very uniform, but in two places (northern San Pietro and north-western Santo Antioco), the sequence is more complex and some subunits can be recognised (Rosselló, 2005). In these two locations the SP unit begins with the black vitrophyre, which grades into a crystal-poor pumice-free maroon basal portion of the unit (few m thick). The ignimbrite becomes gradually richer in crystals (from 5 to 10 vol %) and small (mm to cm) light grey pumices start to appear. Pumices are extremely flattened. Afterwards, the second type of pumices appear, being this slightly darker, bigger (up to 20-40 cm long), less flattened, and usually containing feldspar crystals like those contained in the matrix. Over this basal strongly welded part of the ignimbrite lies a non-welded to moderately-welded deposit. This non-welded deposit is very different from the previous one in colour and composition. It has an overall grey colour and is formed by a grey ash matrix containing 1-2 vol % of feldspar crystals, grey rounded pumices (10-15 vol %), grey fiammes (15 vol %) and abundant (20-30 vol %) massive equant porphyritic maroon lithic fragments, which are angular to rounded. In some places the lithic fragments present eutaxitic texture with fiammes. The size of the lithic fragments ranges from a few mm to 20 cm. The thickness of this subunit is of about 3 meters at the northern coast of San Pietro. A second maroon eutaxitic section which ends laterally is then

Figure 5.20: Appearance of Serra di Paringianu unit in the field and in hand specimen. a) base of SP unit at the locality of Calasetta (northern Santo Antioco Island). The basal vitrophyre is 1.5 m thick; b) typical aspect of the main body of SP unit with the two pumice populations; c) transition between the high grade ignimbrite and the moderately welded grey facies; d) detail of the moderately welded grey facies with evident pumices; e) hand specimen of the maroon high grade ignimbrite with presence of phenocrysts and small light grey pumices; f) close-up of the moderately welded facies with the presence of maroon lithic fragments

present at northern San Pietro; its characteristics are similar to those of the upper portion of the basal eutaxitic subunit, although it has a slightly higher crystal content (15 vol %), and some small red-pinkish fiammes can be found. Observable thickness has a maximum of 5 m. Then, a second

unwelded to moderately welded grey unit occurs. It is similar to the former one, but slightly richer in grey pumices (10 to 20 vol %), that can also be bigger (dm). The unit ends with a final maroon eutaxitic subunit like the basal one. At northern San Pietro the top of the unit can be observed; it presents syn-depositional degassing structures such as gas blisters (half meter high, 4 to 13 m wide). The well welded sections show a strong eutaxitic texture (at all scales) and an evident rheomorphic deformation of the deposit.

5.2.18 Punta Mingosa (PM)

Punta Mingosa (Mundula et al., 2009) is the uppermost unit of the ignimbritic sequence. It has a limited areal extension; it can only be found in southern San Pietro Island (Fig. A.4.20). The thickness of Punta Mingosa unit is less than 30 m.

It is a moderately welded fine-grained massive ignimbrite with a lower part of light pink colour, and an upper grey part (Fig. 5.21). It is formed by a cineritic matrix containing few crystals (less than 3 vol %) and lithic fragments (less than 3 vol %, smaller than 1 cm, mostly smaller than 2-3 mm). Crystals are mainly feldspars, and minor mafic minerals.

5.2.19 Punta Geniò and Colonne (PG/CL)

Punta Geniò and Colonne units have been recently named (Mundula et al., 2009) and still need to be characterised. They are found in southern San Pietro Island and are mainly moderately welded cinerites (Fig. 5.22).

Figure 5.23 is a simplified provisional map showing the distribution of the studied units in the Sulcis area. Table 5.1 summarizes the most significant characteristics of each unit.

5.2.20 Unit similarities

It is appreciable from the previous descriptions and pictures of the ignimbritic units present in the Sulcis that there are strong similarities between different units, especially the porphyritic welded ones, while at the same time some units present wide facies variability (in occasions each facies resembling other units). Both factors contribute to make unit identification in the field difficult, particularly when outcrop continuity is scarce and stratigraphic position of the observed unit cannot be easily established. This has made correlation between different areas laborious, and has resulted in several mapping errors over the years. Some units present characteristic features, such as the presence of a given mineral (e.g. bronze biotite in MZ) or pumice type (e.g. porphyritic black pumices in CF unit), which allow a correct identification even in very different facies. Other units, though, are so similar macroscopically and even microscopically between them, or so different between various facies, that other resources need to be used in order to correctly

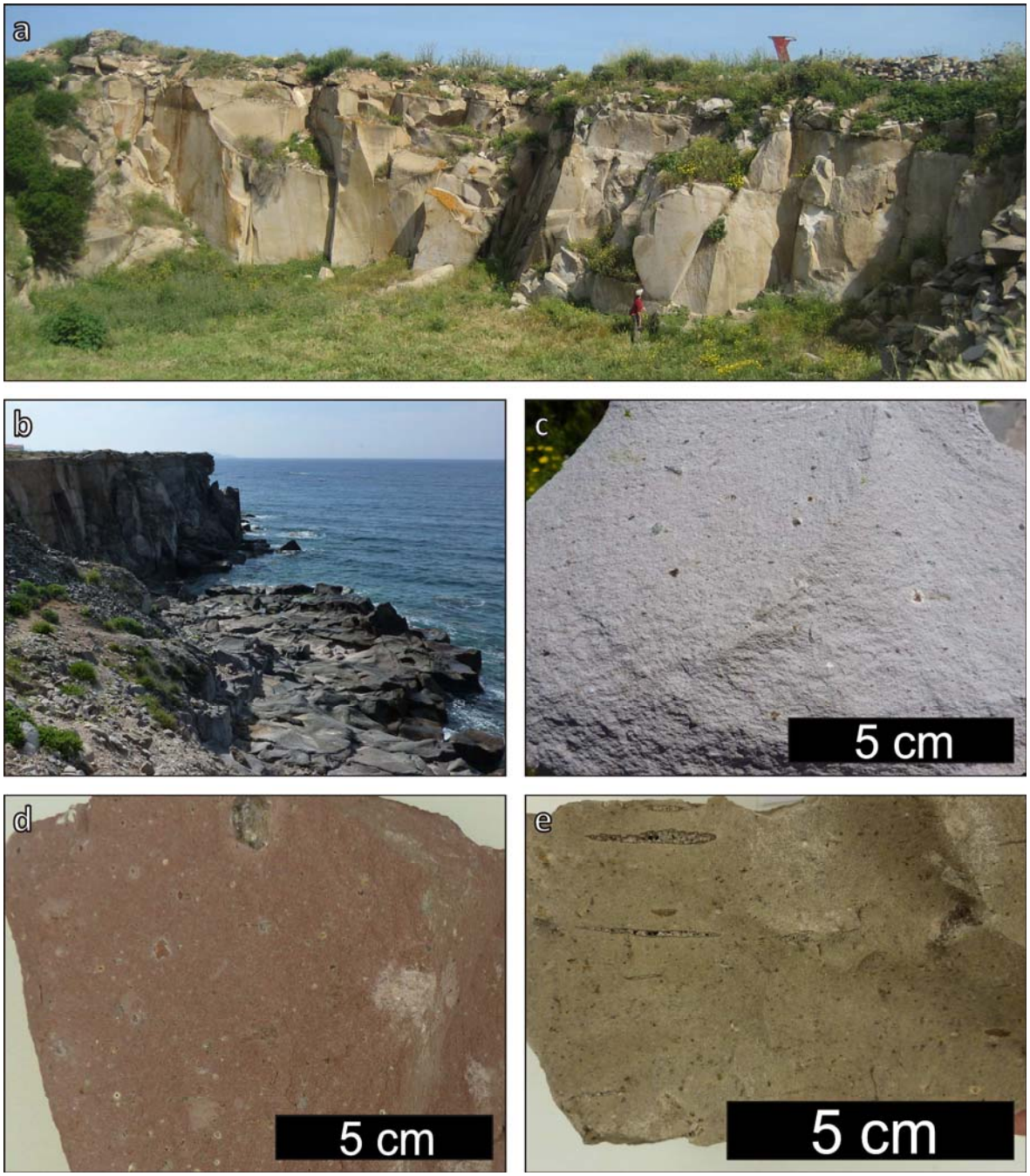

Figure 5.21: Appearance of Punta Mingosa unit in the field and in hand specimen. a) quarry in PM, see person for scale; b) cliffs of PM in the southern coast of San Pietro Island; c), d) and e) hand specimens of different PM facies

identify them. For this purpose a methodology for unit recognition based on whole rock geochemistry has been developed for the Sulcis. This methodology helped in unit recognition and correlation and so to obtain the volcanostratigraphic and cartographic results described above. It is explained in Chapter 8, in the discussion part of this Thesis.

Some scarcely welded units can be difficult to differentiate from each other. This is the case for CM and AC, and some facies of the CA unit. These units are massive, pumice and lithic rich, being

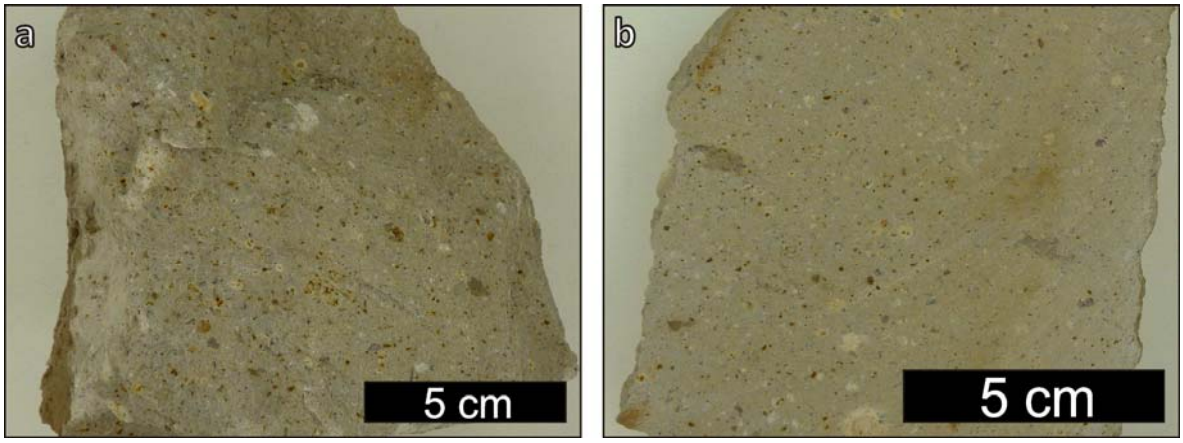

Figure 5.22: Punta Geniò/Colonne unit in a) hand specimen and b) rock slice

in some cases very similar. Distinction between CM and AC is usually done thanks to identification of its stratigraphic position since CM unit is at the base of the sequence and they are separated by a welded unit (LE). CA can also be very similar to the non-welded non-eutaxitic facies of the top of MC unit, from which it is difficult to differentiate. The problem is minor because these two units occur in different areas, presenting overlap only in northern Santo Antioco Island. MZ unit, which is most usually non-welded and presents a wide variety of facies, is easy to identify thanks to the presence of bronze biotite, which is a diagnostic character of this unit because, although present as accessory phase in some other units, this mineral is only macroscopically visible in significant amounts in this one. The last scarcely welded unit in the sequence, PA, is usually not difficult to identify because it is stratigraphically separated from the other scarcely welded units by several welded ones, and is overlain by the SP unit, which has a very characteristic base with a thick basal vitrophyre; this facilitates the recognition of the stratigraphic position of PA unit. In addition, unlike the rest of the scarcely welded units, PA has a relatively poor lithic content.

Most of the identification problems, though, arise when dealing with welded units. Several ignimbrites present welded porphyritic eutaxitic facies with variable amounts of flattened pumices, and even share an overall brownish colour (Fig. 5.24). These facies can be seen in LE, SE, MC, NU, PC, MCR and SP. Although each unit presents some particularities, within unit variability frequently produces very similar facies. LE and SE are very similar, although its stratigraphic position can be usually correctly established, allowing a correct identification, especially in the northern mainland. MC can be similar to the less eutaxitic facies of NU, especially when its pumice content is low. The less eutaxitic facies of NU can be also easily misinterpreted as MCR or PC. The extremely welded pumice-poor facies of NU are quite characteristic because all the other welded units usually present abundant pumices, which can be scarcely to extremely flattened. Only the

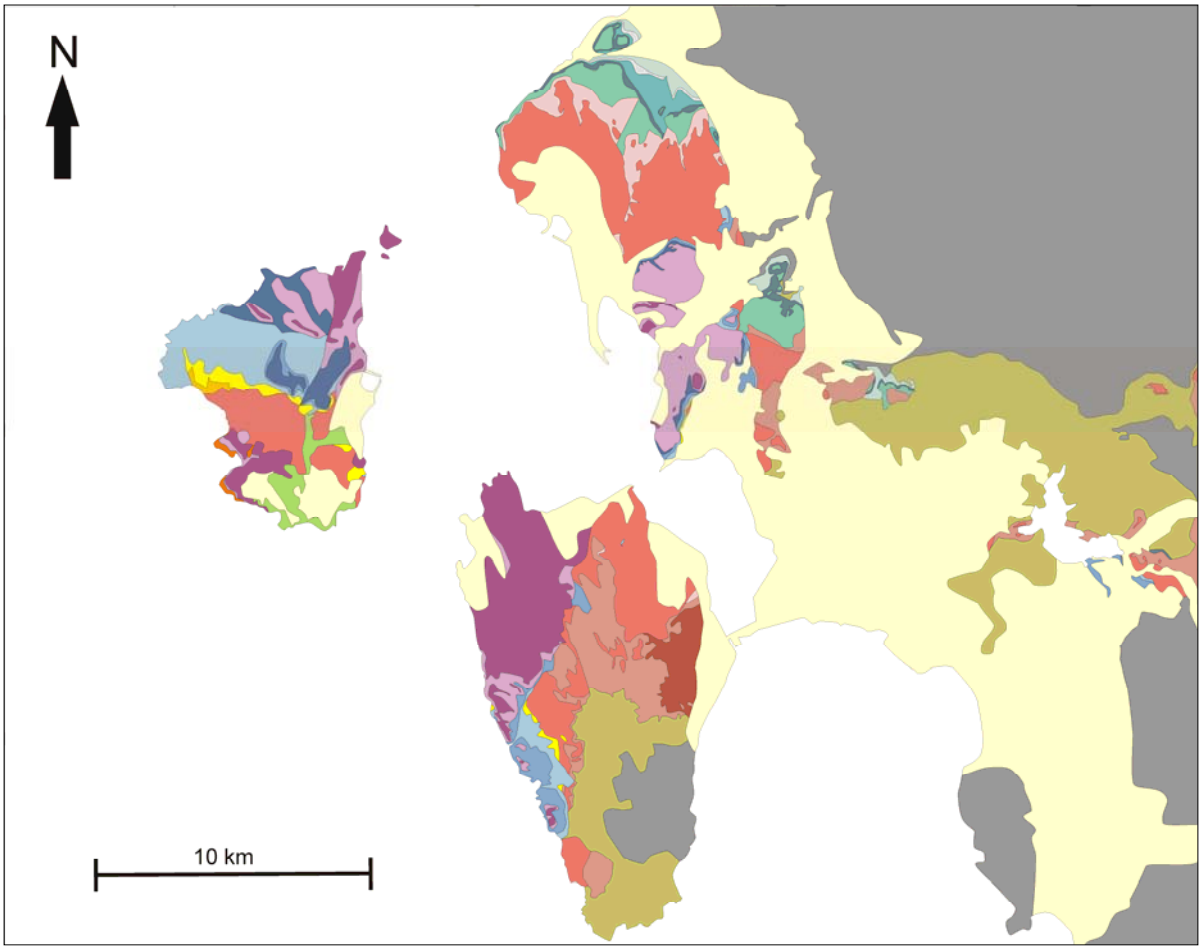

Figure 5.23: Simplified map of the Oligo-Miocene volcanism in the Sulcis area. The basement is depicted in grey and the post-volcanic materials in pale yellow

Unit	Outcropping area	Main characteristics
CL/PG	Southern San Pietro Island	Colonne/Punta Genniò: moderately welded cineritic ignimbrite
PM	Southern San Pietro Island	Punta Mingosa: moderately welded aphyric cineritic ignimbrite
SP	Widespread unit present in central mainland and the two islands	Serra di Paringianu: extremely welded and eutaxitic ignimbrite with abundant extremely flattened light and dark grey pumices. Basal vitrophyre. Grey non-welded facies in northern San Pietro and Santo Antioco islands
PA	Central mainland and both islands	Paringianu: scarcely to moderately welded complex ignimbritic unit. Mostly cineritic. Low porphyricity and pumice content.
CF	San Pietro Island and central mainland	Carloforte: strongly welded and eutaxitic ignimbrite with abundant sanidine-bearing black pumices. Also grey and white pumices.
MU	Central and southern mainland and in the two islands.	Monte Ulmus: stronlgy welded and eutaxitic aphyric ignimbritic unit with occasional scarce black flattened pumices. Basal vitrophyre.
CO	Central mainland and the two islands, most expressed in San Pietro	Comendites: complex unit. Lava flows and variably welded ignimbrites with or without basal vitrophyre. May contain quartz phenocrysts
MZ	Central mainland and in the two minor islands	Matzaccara: variably welded complex ignimbritic unit. Presents bronze-coloured biotite.
MCR	Western San Pietro Island	Montagna di Capo Rosso: lava flows and moderately welded lithic rich ignimbrites.
PC	Western San Pietro Island	Punta dei Cannoni: moderately to strongly welded, eutaxitic and porphyritic ignimbritic unit. Abundant big (several dm) pumices.
NU	Widespread, found in all the studied area	Nuraxi: extremely welded and eutaxitic ignimbrite. Scarce extremely flattened grey pumices. Rheomorphic structures are abundant. Basal vitrophyre.
CA	Northern mainland and scarcely in northern Santo Antioco	Conca is Angius: slightly welded complex ignimbritic unit with abundant pumices and accidental lithics. Degassing structures present.
MC	Whole southern and eastern mainland (Carbonia, Narcao) and Santo Antioco Island	Monte Crobu: moderately to extremely welded and eutaxitic ignimbrite with abundant to very abundant grey and occasionally black strongly flattened pumices. Rheomorphic. Basal vitrophyre.
MLN	Eastern Santo Antioco Island	Monte la Noce: lava flows, cinerites and moderately to extremely welded ignimbrites with basal vitrophyre. Aphyric.
SE	Northern and central mainland	Seruci: highly welded and eutaxitic ignimbrite with dm-sized pumices. Basal vitrophyre.
AC	Widespread from northern mainland to Giba-Narcao graben	Acqua sa Canna: poorly welded ignimbrite formed by several flow units with pumice normal grading.
LE	Northern mainland	Lenzu: strongly welded and eutaxitic ignimbrite with abundant dm-sized big pumices. Basal vitrophyre.
CM	Northern and central mainland	Corona Maria: scarcely to moderately welded and eutaxitic ignimbrite with abundant pumices and lithic fragments. Basal vitrophyre.
AND	Southern Santo Antioco Island and Giba-Narcao graben	Andesites: lava flows and domes with associated breccias.

Table 5.1: Summary of the outcropping area and main characteristics of the described units arranged according to its stratigraphic position

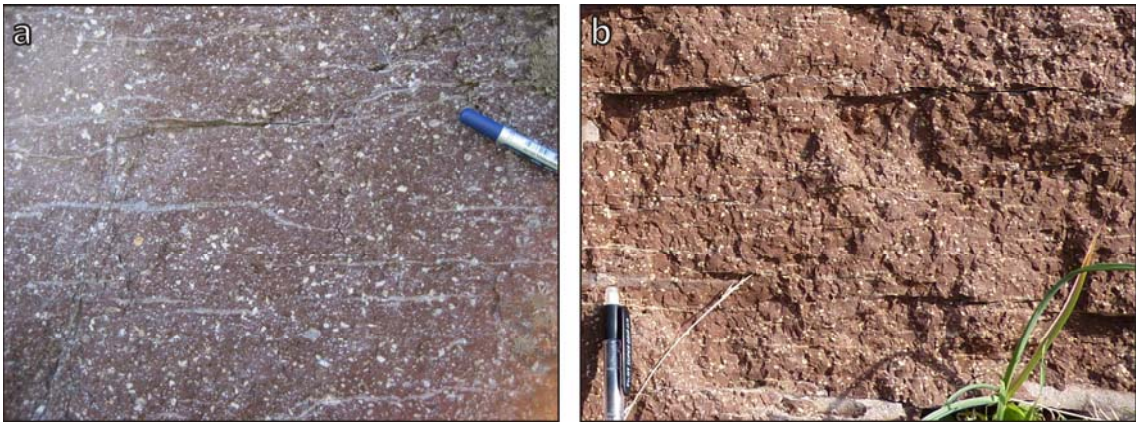

Figure 5.24: Example of strong similarity between two different units. Extremely welded and eutaxitic facies of NU (a) and SP (b) units

base of SP presents a pumice poor facies which could be regarded as similar, but its thickness is small, just a few meters, and, being just above the thick characteristic vitrophyre of this unit, its identification as SP is easy. On the other hand, the more eutaxitic and pumice-bearing facies of NU are very similar to those of SP and SE. NU can be separated from the other two units in this facies because SP and SE typically present two pumice populations (light and dark grey) whereas NU typically presents a single population of pumices. SE and SP are stratigraphically very separated, both present characteristic vitrophyres, and the extremely eutaxititc facies in SP are dominant, while they are not in SE; all of this factors facilitate unit identification.

MCR and PC could be confused with LE, SE or MC, but the geographical separation between these units (PC and MCR only crop out in western San Pietro, and LE and SE in the mainland) avoids any identification problems. Regarding CO, some ignimbritic facies may resemble this generic facies, but the phenocryst assemblage, formed by sanidine and quartz, is usually enough to allow a correct unit identification. The other peralkaline unit, MU, is characteristic for being aphyric. CF unit is the most easily identified welded unit because of the presence of the porphyritic black pumices, which are a diagnostic feature. MC and MU may also present big black pumices; in MU these only occur in western Santo Antioco Island and share the aphyric character of this unit, so misidentification is not possible. Regarding MC, its pumices may present feldspar phenocrysts, but in less quantity than those in CF, and, moreover, CF and MC units occur in different areas within the Sulcis. The PM unit is usually easily identified thanks to its welded cineritic appearance and by being geographically restricted to southern San Pietro Island. It can only be regarded as similar to some welded facies of PA unit, which, however, usually presents more abundant pumices.

5.3 UNIT MORPHOLOGIES

The areal extension and final shape of the bodies corresponding to each unit are variable. Lava flows and domes corresponding to Andesites and CO were strongly conditioned by previous relief features, following valleys, while at the same time they generated new reliefs themselves. On the other hand, ignimbritic units were variably conditioned by topography depending on its volume and on the energy of the pyroclastic density current that generated them. Low energy pyroclastic density currents concentrate in topographic lows such as valleys, while high-energy ones tend to propagate over most of the topography (Fig 5.25). It has to be borne in mind at this point that in the area where ignimbrites were emplaced in the Sulcis there were no big topographic highs except for the Iglesiente horst (which limited ignimbrite expansion to the E) and the andesitic and comenditic domes and flows. In all cases ignimbrites were preferentially deposited in topographic lows such as valleys, thus tending to smooth the relief. The result was that small volume ignimbrites are mostly confined to valleys and lows, while high-volume deposits can completely smooth the topography and generate flat top ignimbritic mantles known as ignimbritic mesas (Fig. 5.26). Some fault activity contemporary to the Oligo-Miocene volcanic activity has been found in the Sulcis mainland (Assorgia et al., 1992a), as well as evidences of erosion of ignimbritic deposits between eruptions. These two factors modified the relief and generated irregularities which were subsequently smoothed out by the next ignimbrite. Figure 5.27 is a cross-section of the northern mainland Sulcis showing the widespread flat disposition of ignimbrites which progressively cover a topographic high by onlap.

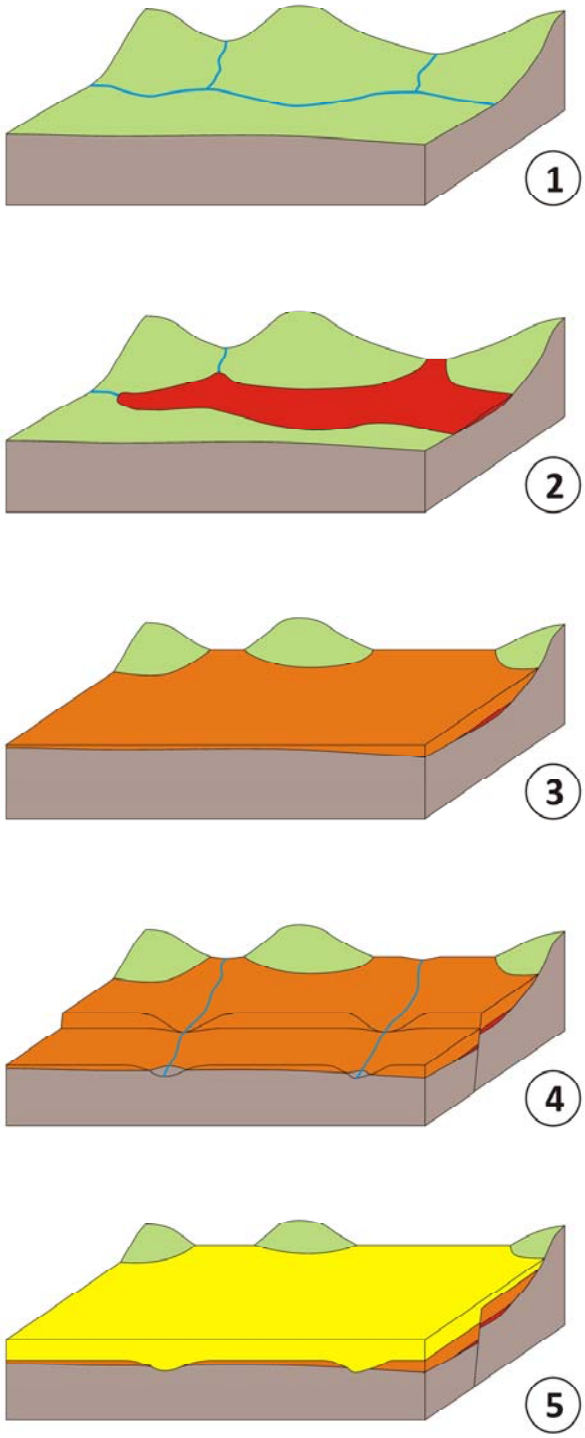

Figure 5.25: Simplified figure on ignimbrite emplacement. 1) original relief; 2) emplacement of a low energy pyroclastic density current deposit filling the lower parts of the fluvial valley; 3) deposition of a high volume ignimbrite which infills the valley; 4) erosion and faulting; 5) deposition of a second high volume ignimbrite which smoothes the relief again

Figure 5.26: Ignimbritic mesa in northern Sulcis mainland. The top layer is Seruci unit. The relief in the background is the Iglesiente horst

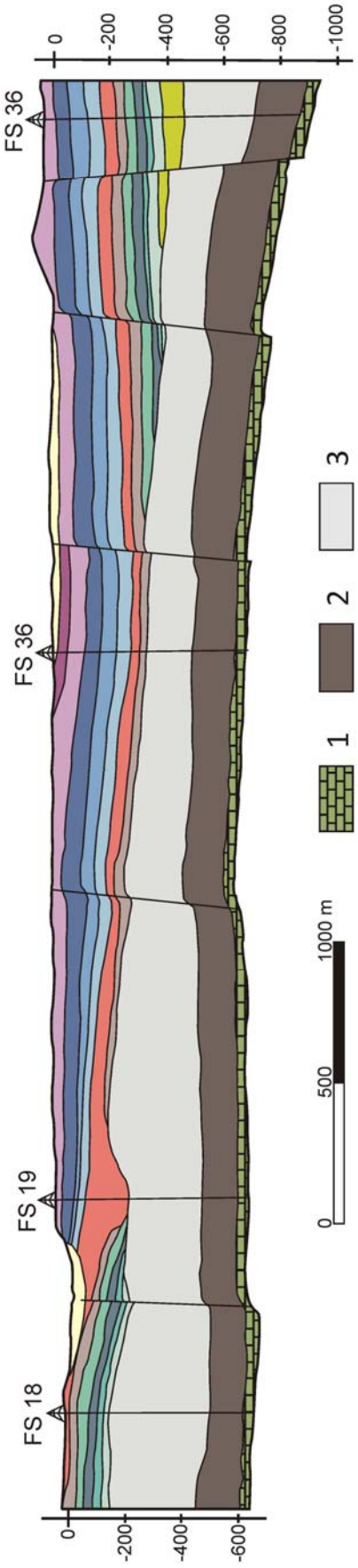

Figure 5.27: Cross-section of northern Sulcis mainland. 1) Paleocene miliolitic limestones; 2) Cuisian-Lutecian paralic deposits with interbedding of coal layers; 3) Cixerri Fm., Middle Eocene-Middle Oligocene. FS are prospective boreholes made by the Carbosulcis SpA. Figure modified from Assorgia et al. (1990b)

CHAPTER 6: PETROGRAPHY AND MINERAL CHEMISTRY

6.1 INTRODUCTION

A description of the main petrographic characteristics and the chemical composition of the mineral phases of each unit is provided in this chapter. On first place, though, a brief introduction to the petrographic characteristics of lava and pyroclastic flow deposits is given.

Lava flows (and domes) are usually porphyritic rocks formed by phenocrysts in a groundmass. Components of the groundmass may be smaller crystals (microphenocrysts), glass, and a crypto- to microcrystalline aggregate of crystals that are the product of late crystallisation or devitrification processes. Enclaves may be present, consisting in mingled batches of another magma (cognate enclaves), as well as xenoliths and xenocrysts. The amount of glass in a lava flow depends on the cooling history of the rock and on the composition of the magma; in general terms the higher the silica content in a magma, the more difficult it is to crystallize. For this reason basaltic lava flows usually present less content in glass (known as sideromelane) than rhyolitic ones (where it is known as obsidian).

Ignimbrites, on the other hand, are fragmental deposits. This means that they are not massive lava bodies, but an accumulation of pyroclasts which may be completely incoherent, or partly cohesive due to compaction, welding, devitrification or alteration. Pyroclasts include glass shards, pumices (or equivalents of more basic composition), crystals and crystal fragments, xenoliths and lithic fragments from the vent. Additionally, pyroclastic density currents or lava flows may collect ground material during transport; these fragments are known as accidental lithic fragments. From now on, the term enclave is used as a generic term assigned to any foreign body included in the deposit, and it may include xenoliths or rock fragments captured by the lava during fragmentation

and transport. Fragmentation of magma occurs when during eruption vesicles formed in the ascending magma progressively expand due to volatile exsolution and pressure decrease until magma collapses and ceases being a liquid containing gas bubbles to become a gas carrying lava fragments (magmatic fragmentation). Shards are ash-sized glass fragments that correspond to the walls that separated gas bubbles; they typically present platy and tricuspid shapes. Pumices are bigger shreds of lava that were not so finely fragmented; they may present sizes from a few millimeters to several meters (they form the lapilli and bomb size fraction of the juvenile pyroclasts). Pumices are usually highly vesicular, although they may collapse and lose gas on deposition and compaction, and may contain crystals. Crystals carried by the magma are phenocrysts and xenocrysts. During eruption and magma fragmentation, crystals tend to separate from the melt and become free pyroclasts, especially when fragmentation is intensive. During fragmentation and transport crystals break forming diverse size crystal fragments.

Depending on the viscosity of the glass on deposition, glass pyroclasts may deform due to flow stresses and compaction, and even weld together. Stretching and flattening of glass fragments generate the eutaxitic texture, which can be seen at macroscopic and microscopic scale. Welding may vary from non-existing, giving a loose character to the deposit, to extreme, in which case the ignimbrite resembles a massive lava flow where shards cannot be recognised. Perlitic texture may appear in both lavas and welded ignimbrites due to thermal contraction. Compaction and thermal history of a deposit condition the devitrification and alteration of it.

High-temperature devitrification processes in lavas and welded ignimbrites produce spherulites, lithophysae, and micropoikilitic (sensu Lofgren, 1971) and microgranular textures. Spherulites are radial aggregates of acicular crystals (typically feldspar and/or quartz or cristobalite in silicic rocks), whose morphology depends on the temperature of formation. Spherulites usually range in size from 0.1 to 2 cm. Lithophysae are macroscopic structures similar to spherulites but with a void in the centre, and may reach some tens of centimeters in diameter. In ignimbrites they usually appear low in the deposit, mostly in the vitrophyre by water absorption and saturation.

6.2 PETROGRAPHY AND MINERAL CHEMISTRY

6.2.1 Andesites (AND)

Despite the wide range in composition, age and emplacement mechanisms, andesitic lavas share some common characteristics: most of them are holocrystalline and porphyritic with idio- to hypidiomorphic phenocrysts ranging in size from less than a millimeter to several mm (Fig. 6.1). Phenocrysts consist dominantly of plagioclase (An_{55-85}) (Fig. 6.2) (Table 6.1), which may be zoned, and minor pyroxene (usually less than 3 vol % but up to 10 vol %). The groundmass is formed by

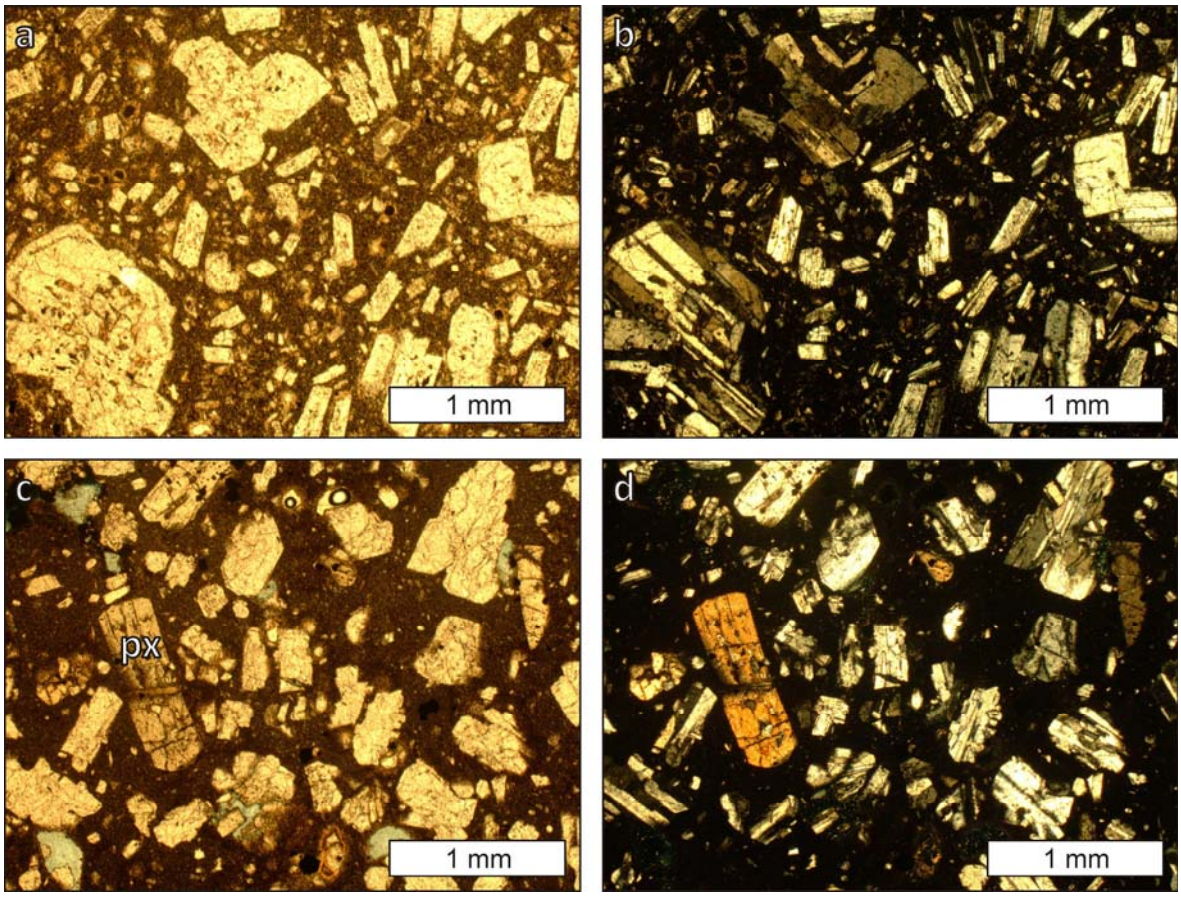

Figure 6.1: Microscope pictures of andesitic samples. a) and c) plain-polarized light; b) and d) same pictures under cross-polarized light

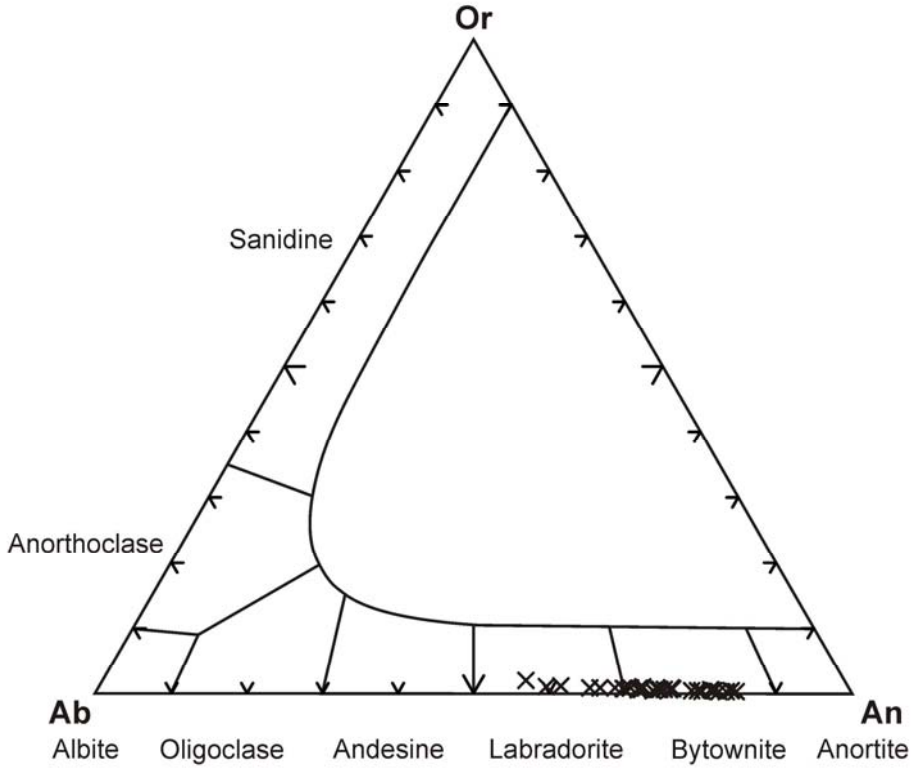

Figure 6.2: Feldspar compositions for AND unit

Unit	AND		CM		LE				AC		SE		MLN		MC	
Feldspar	pl	pl	pl	pl	pl	pl	sa	sa	pl	pl	pl	pl	pl	pl	pl	pl
Sample	VS-723	VS-723	VS-703	VS-703	VS-702	VS-702	VS-702	VS-702	VS-782	VS-782	VS-783	VS-783	VS-774	VS-774	VS-790	VS-790
Oxides (%)																
SiO_2	46.70	50.36	51.77	58.48	55.44	60.35	63.43	64.51	52.31	57.16	57.52	61.08	56.24	58.60	57.22	62.87
TiO_2	0.03	0.01	0.07	0.01	0.04	0.02	0.06	0.04	0.05	0.05	0.05	0.03	0.03	0.03	0.04	0.00
Al_2O_3	33.31	30.85	30.01	25.62	27.09	23.95	19.13	18.90	29.30	25.74	26.15	24.18	27.20	25.58	26.53	22.13
Fe_2O_3	0.43	0.51	0.61	0.37	0.27	0.27	0.19	0.16	0.47	0.32	0.24	0.28	0.24	0.31	0.29	0.13
MgO	0.00	0.04	0.06	0.04	0.02	0.02	0.00	0.01	0.05	0.06	0.01	0.00	0.04	0.00	0.01	0.00
CaO	16.94	14.24	13.57	8.07	9.78	6.01	0.54	0.44	12.18	8.35	8.49	5.70	9.52	7.62	8.95	3.93
Na_2O	1.98	3.90	4.12	6.59	6.00	7.12	3.82	3.66	5.00	7.47	6.74	7.73	6.74	7.72	6.32	8.63
K_2O	0.04	0.14	0.28	0.98	0.65	1.40	10.30	10.68	0.30	0.68	0.74	1.27	0.40	0.72	0.55	2.10
BaO	0.04	0.04	0.00	0.14	0.00	0.17	2.12	0.96	0.00	0.08	0.11	0.04	0.00	0.00	0.13	0.04
Rb_2O	0.08	0.06	0.00	0.11	0.04	0.09	0.08	0.07	0.06	0.06	0.03	0.11	0.11	0.09	0.11	0.09
Sum	99.56	100.13	100.49	100.41	99.32	99.39	99.68	99.43	99.73	99.97	100.07	100.41	100.52	100.67	100.14	99.93
Cations																
Si	2.16	2.30	2.35	2.62	2.52	2.72	2.94	2.97	2.39	2.58	2.59	2.72	2.53	2.62	2.57	2.81
Ti	0.00	0.00	0.00	0.00	0.00	0.00	0.00	0.00	0.00	0.00	0.00	0.00	0.00	0.00	0.00	0.00
Al	1.82	1.66	1.61	1.35	1.45	1.27	1.04	1.03	1.58	1.37	1.39	1.27	1.44	1.35	1.41	1.17
Fe^{3+}	0.02	0.02	0.02	0.01	0.01	0.01	0.01	0.01	0.02	0.01	0.01	0.01	0.01	0.01	0.01	0.00
Mg	0.00	0.00	0.00	0.00	0.00	0.00	0.00	0.00	0.00	0.00	0.00	0.00	0.00	0.00	0.00	0.00
Ca	0.84	0.70	0.66	0.39	0.48	0.29	0.03	0.02	0.60	0.40	0.41	0.27	0.46	0.37	0.43	0.19
Ba	0.00	0.00	0.00	0.00	0.00	0.00	0.04	0.02	0.00	0.00	0.00	0.00	0.00	0.00	0.00	0.00
Na	0.18	0.35	0.36	0.57	0.53	0.62	0.34	0.33	0.44	0.65	0.59	0.67	0.59	0.67	0.55	0.75
K	0.00	0.01	0.02	0.06	0.04	0.08	0.61	0.63	0.02	0.04	0.04	0.07	0.02	0.04	0.03	0.12
Rb	0.00	0.00	0.00	0.00	0.00	0.00	0.00	0.00	0.00	0.00	0.00	0.00	0.00	0.00	0.00	0.00
Sum	5.02	5.04	5.02	5.01	5.03	5.00	5.01	4.99	5.04	5.07	5.03	5.01	5.05	5.06	5.01	5.04
An mol%	82.35	66.34	63.53	38.13	45.68	29.23	2.74	2.22	56.43	36.82	39.36	26.89	42.90	33.95	42.53	17.83
Ab mol%	17.42	32.88	34.91	56.35	50.71	62.66	35.06	33.49	41.92	59.61	56.55	65.98	54.96	62.24	54.35	70.83
Or mol%	0.23	0.78	1.56	5.51	3.61	8.11	62.20	64.29	1.65	3.57	4.08	7.13	2.15	3.82	3.11	11.34

Table 6.1: Representative analyses of feldspars. For each feldspar in each unit end-member compositions are given. For pl it is according to SiO_2 content, and for ano and sa it is according to K_2O and Na_2O. Cation calculations made by the Xmas Plus of SAMx program

Unit	MC		CA				NU				PC					
Feldspar	sa	sa	pl	pl	sa	sa	pl	pl	sa	sa	pl 1	pl 1	pl2	pl2	ano	ano
Sample	VS-790	VS-790	VS-787	VS-788	VS-788	VS-788	VS-757	ISP-124	ISP-124	VS-757	ISP-218	ISP-218	ISP-230	ISP-230	ISP-218	ISP-218
Oxides (%)																
SiO_2	64.70	65.87	59.79	62.21	65.08	65.71	56.70	63.03	65.48	64.83	59.95	62.86	54.58	62.13	62.66	64.31
TiO_2	0.04	0.00	0.02	0.01	0.03	0.01	0.10	0.04	0.04	0.06	0.05	0.02	0.08	0.06	0.03	0.03
Al_2O_3	18.98	18.57	24.22	22.81	18.91	18.49	26.78	22.62	18.96	19.04	24.15	22.05	27.84	22.31	21.39	20.55
Fe_2O_3	0.13	0.11	0.18	0.27	0.07	0.17	0.34	0.38	0.21	0.27	0.34	0.32	0.41	0.43	0.28	0.22
MgO	0.01	0.01	0.00	0.00	0.00	0.02	0.02	0.01	0.02	0.00	0.02	0.00	0.02	0.00	0.00	0.00
CaO	0.37	0.28	6.42	4.78	0.32	0.21	8.97	4.31	0.59	0.86	6.48	4.29	10.53	4.20	3.56	2.43
Na_2O	4.04	3.77	7.56	7.97	3.72	3.70	6.23	8.01	5.01	6.15	7.42	7.72	5.30	7.94	7.48	7.17
K_2O	10.55	11.11	0.93	1.48	10.82	11.06	0.60	1.96	8.89	7.40	1.18	2.27	0.46	2.33	3.40	4.97
BaO	0.70	0.03	0.05	0.00	1.08	0.00	0.19	0.22	0.49	0.45	0.07	0.21	0.12	0.12	0.29	0.19
Rb_2O	0.00	0.00	0.09	0.08	0.00	0.00	0.08	0.04	0.00	0.13	0.09	0.03	0.06	0.05	0.04	0.00
Sum	99.53	99.74	99.27	99.61	100.05	99.38	100.02	100.64	99.70	99.21	99.74	99.77	99.40	99.58	99.13	99.89
Cations																
Si	2.97	3.00	2.70	2.78	2.98	3.00	2.56	2.80	2.97	2.95	2.69	2.81	2.48	2.79	2.83	2.89
Ti	0.00	0.00	0.00	0.00	0.00	0.00	0.00	0.00	0.00	0.00	0.00	0.00	0.00	0.00	0.00	0.00
Al	1.03	1.00	1.29	1.20	1.02	1.00	1.42	1.18	1.02	1.02	1.28	1.16	1.49	1.18	1.14	1.09
Fe^{3+}	0.01	0.00	0.01	0.01	0.00	0.01	0.01	0.01	0.01	0.01	0.01	0.01	0.01	0.02	0.01	0.01
Mg	0.00	0.00	0.00	0.00	0.00	0.00	0.00	0.00	0.00	0.00	0.00	0.00	0.00	0.00	0.00	0.00
Ca	0.02	0.01	0.31	0.23	0.02	0.01	0.43	0.21	0.03	0.04	0.31	0.21	0.51	0.20	0.17	0.12
Ba	0.01	0.00	0.00	0.00	0.02	0.00	0.00	0.00	0.01	0.01	0.00	0.00	0.00	0.00	0.01	0.00
Na	0.36	0.33	0.66	0.69	0.33	0.33	0.55	0.69	0.44	0.54	0.65	0.67	0.47	0.69	0.66	0.63
K	0.62	0.65	0.05	0.09	0.63	0.64	0.04	0.11	0.52	0.43	0.07	0.13	0.03	0.13	0.20	0.29
Rb	0.00	0.00	0.00	0.00	0.00	0.00	0.00	0.00	0.00	0.00	0.00	0.00	0.00	0.00	0.00	0.00
Sum	5.01	4.99	5.02	5.00	4.99	4.98	5.01	5.01	4.99	5.02	5.02	5.00	5.01	5.02	5.02	5.02
An mol%	1.83	1.38	30.27	22.80	1.61	1.05	42.80	20.39	2.91	4.13	30.40	20.46	50.95	19.68	16.84	11.40
Ab mol%	36.12	33.56	64.51	68.80	33.77	33.36	53.79	68.57	44.79	53.51	63.00	66.64	46.40	67.32	64.02	60.85
Or mol%	62.05	65.06	5.22	8.40	64.62	65.60	3.41	11.04	52.29	42.36	6.59	12.89	2.65	13.00	19.14	27.75

Table 6.1: (Continuation)

Unit	MCR				MZ		CO		MU				PU			
Feldspar	pl	pl	sa	sa	pl	pl	sa	sa	sa 1	sa 1	sa 2	sa 2	sa 1	sa 1	sa 2	sa 2
Sample	ISP-132	ISP-132	ISP-132	ISP-132	VS-760	VS-760	ISP-150	ISP-150	ISP-185	ISP-127	ISP-185	ANT-27	ISP-104	ISP-104	ISP-72	ISP-104
Oxides (%)																
SiO_2	57.54	60.17	64.27	64.69	56.42	61.99	66.41	67.19	66.14	67.68	64.53	66.73	61.29	65.37	66.53	66.55
TiO_2	0.10	0.03	0.08	0.02	0.08	0.04	0.05	0.01	0.03	0.03	0.07	0.02	0.09	0.05	0.02	0.00
Al_2O_3	25.67	24.51	19.18	19.06	26.78	22.69	18.87	19.06	18.83	18.29	20.54	18.93	22.62	19.19	18.82	18.68
Fe_2O_3	0.37	0.43	0.22	0.19	0.45	0.35	0.33	0.28	0.25	0.23	0.22	0.27	0.36	0.17	0.30	0.24
MgO	0.01	0.01	0.00	0.04	0.00	0.00	0.00	0.00	0.00	0.00	0.00	0.01	0.02	0.00	0.00	0.01
CaO	8.25	6.60	0.69	0.91	8.92	4.66	0.00	0.08	0.25	0.21	2.01	0.51	4.09	0.65	0.28	0.22
Na_2O	6.78	7.51	5.13	6.04	6.36	8.42	6.78	7.66	7.35	7.17	6.78	6.86	7.26	5.74	7.34	6.81
K_2O	0.80	1.12	9.36	8.07	0.51	1.64	6.99	5.86	6.85	6.57	5.83	6.65	3.46	8.08	7.27	6.70
BaO	0.00	0.31	1.32	0.70	0.11	0.21	0.00	0.00	0.00	0.00	0.31	0.00	0.87	0.21	0.06	0.00
Rb_2O	0.08	0.07	0.00	0.00	0.08	0.05	0.00	0.00	0.01	0.00	0.00	0.00	0.06	0.00	0.00	0.00
Sum	99.60	100.77	100.26	99.72	99.72	100.05	99.43	100.14	99.70	100.18	100.29	99.98	100.11	99.45	100.62	99.21
Cations																
Si	2.60	2.68	2.94	2.95	2.55	2.77	2.99	2.99	2.98	3.02	2.90	2.99	2.77	2.96	2.98	3.00
Ti	0.00	0.00	0.00	0.00	0.00	0.00	0.00	0.00	0.00	0.00	0.00	0.00	0.00	0.00	0.00	0.00
Al	1.37	1.29	1.03	1.02	1.43	1.20	1.00	1.00	1.00	0.96	1.09	1.00	1.20	1.03	0.99	0.99
Fe^{3+}	0.01	0.01	0.01	0.01	0.02	0.01	0.01	0.01	0.01	0.01	0.01	0.01	0.01	0.01	0.01	0.01
Mg	0.00	0.00	0.00	0.00	0.00	0.00	0.00	0.00	0.00	0.00	0.00	0.00	0.00	0.00	0.00	0.00
Ca	0.40	0.32	0.03	0.04	0.43	0.22	0.00	0.00	0.01	0.01	0.10	0.02	0.20	0.03	0.01	0.01
Ba	0.00	0.01	0.02	0.01	0.00	0.00	0.00	0.00	0.00	0.00	0.01	0.00	0.02	0.00	0.00	0.00
Na	0.59	0.65	0.45	0.53	0.56	0.73	0.59	0.66	0.64	0.62	0.59	0.60	0.64	0.50	0.64	0.60
K	0.05	0.06	0.55	0.47	0.03	0.09	0.40	0.33	0.39	0.37	0.33	0.38	0.20	0.47	0.42	0.39
Rb	0.00	0.00	0.00	0.00	0.00	0.00	0.00	0.00	0.00	0.00	0.00	0.00	0.00	0.00	0.00	0.00
Sum	5.03	5.02	5.04	5.04	5.02	5.03	5.00	5.00	5.03	4.99	5.02	5.00	5.04	5.00	5.05	4.99
An mol%	38.42	30.66	3.27	4.24	42.40	21.33	0.00	0.38	1.15	1.00	9.47	2.45	19.16	3.15	1.26	1.07
Ab mol%	57.14	63.14	43.96	50.96	54.71	69.74	59.58	66.27	61.28	61.76	57.82	59.56	61.54	50.28	59.78	60.05
Or mol%	4.44	6.20	52.77	44.80	2.89	8.94	40.42	33.35	37.57	37.24	32.71	37.99	19.30	46.57	38.96	38.87

Table 6.1: (Continuation)

Unit	PA		SP				PM				CL			
Feldspar	sa	sa	pl	pl	ano	ano	pl	pl	sa	sa	pl	pl	sa	sa
Sample	VS-789	VS-789	ANT-12	ANT-12	ANT-12	ANT-12	ISP-215	ISP-215	ISP-215	ISP-215	ISP-210	ISP-210	ISP-210	ISP-210
Oxides (%)														
SiO_2	65,39	65,26	59,94	62,79	63,37	63,85	64,23	65,36	67,21	66,73	61,42	62,89	64,91	65,54
TiO_2	0,00	0,00	0,06	0,00	0,03	0,03	0,02	0,04	0,02	0,04	0,02	0,03	0,02	0,04
Al_2O_3	18,69	18,91	24,50	22,26	22,06	20,67	21,89	20,21	17,97	18,43	23,13	22,08	18,59	18,53
Fe_2O_3	0,11	0,15	0,45	0,28	0,29	0,19	0,22	0,15	0,72	0,24	0,25	0,18	0,11	0,14
MgO	0,00	0,00	0,03	0,05	0,00	0,01	0,00	0,00	0,01	0,00	0,00	0,00	0,00	0,00
CaO	0,25	0,39	6,52	3,76	3,56	2,48	3,56	2,21	0,04	0,24	5,50	4,27	0,28	0,30
Na_2O	5,67	6,36	7,75	8,09	8,36	7,34	9,37	9,14	6,27	7,35	7,96	8,06	3,82	4,52
K_2O	8,67	7,84	0,99	2,16	2,44	4,10	1,35	2,34	7,93	6,48	1,00	1,46	10,62	9,95
BaO	0,00	0,00	0,00	0,03	0,19	0,36	0,03	0,04	0,00	0,00	0,03	0,08	1,28	0,25
Rb_2O	0,00	0,00	0,06	0,04	0,00	0,04	0,06	0,04	0,00	0,00	0,12	0,12	0,00	0,00
Sum	98,78	98,92	100,31	99,45	100,31	99,07	100,73	99,53	100,17	99,52	99,43	99,17	99,63	99,28
Cations														
Si	2,99	2,97	2,68	2,81	2,82	2,89	2,84	2,91	3,02	3,00	2,76	2,82	2,98	2,99
Ti	0,00	0,00	0,00	0,00	0,00	0,00	0,00	0,00	0,00	0,00	0,00	0,00	0,00	0,00
Al	1,01	1,02	1,29	1,18	1,16	1,10	1,14	1,06	0,95	0,98	1,22	1,17	1,01	1,00
Fe^{3+}	0,00	0,01	0,02	0,01	0,01	0,01	0,01	0,01	0,02	0,01	0,01	0,01	0,00	0,01
Mg	0,00	0,00	0,00	0,00	0,00	0,00	0,00	0,00	0,00	0,00	0,00	0,00	0,00	0,00
Ca	0,01	0,02	0,31	0,18	0,17	0,12	0,17	0,11	0,00	0,01	0,27	0,21	0,01	0,02
Ba	0,00	0,00	0,00	0,00	0,00	0,01	0,00	0,00	0,00	0,00	0,00	0,00	0,02	0,01
Na	0,50	0,56	0,67	0,70	0,72	0,64	0,80	0,79	0,55	0,64	0,69	0,70	0,34	0,40
K	0,51	0,46	0,06	0,12	0,14	0,24	0,08	0,13	0,45	0,37	0,06	0,08	0,62	0,58
Rb	0,00	0,00	0,00	0,00	0,00	0,00	0,00	0,00	0,00	0,00	0,00	0,00	0,00	0,00
Sum	5,01	5,03	5,03	5,01	5,02	5,00	5,03	5,01	5,00	5,01	5,01	4,99	4,99	5,00
An mol%	1,20	1,84	30,01	17,93	16,49	12,01	16,09	10,26	0,19	1,13	26,07	20,73	1,41	1,48
Ab mol%	49,25	54,20	64,56	69,81	70,06	64,34	76,64	76,80	54,48	62,57	68,28	70,83	34,85	40,24
Or mol%	49,55	43,96	5,43	12,26	13,45	23,65	7,27	12,94	45,33	36,30	5,64	8,44	63,74	58,28

Table 6.1: (Continuation)

plagioclase microcrysts and minor pyroxene and opaque minerals in a cryptocrystalline matrix. Pyroxenes are mostly enstatite (Wo_{2-5}, En_{53-72}, Fs_{26-44}) (Fig. 6.3) (Table 6.2), but augite (Wo_{40-42}, En_{36-43}, Fs_{15-22}) may be abundant in some andesites, coexisting with enstatite (pyroxene nomenclature sensu Morimoto et al., 1989). Opaque minerals are Fe-Ti spinel, in this unit and in the rest of the sequence. Mineral assemblage may include very scarce small olivine crystals presenting disequilibrium textures and accessory apatite. Enclaves are frequent, most of them with andesitic composition, but also as cumulates rich in pyroxene.

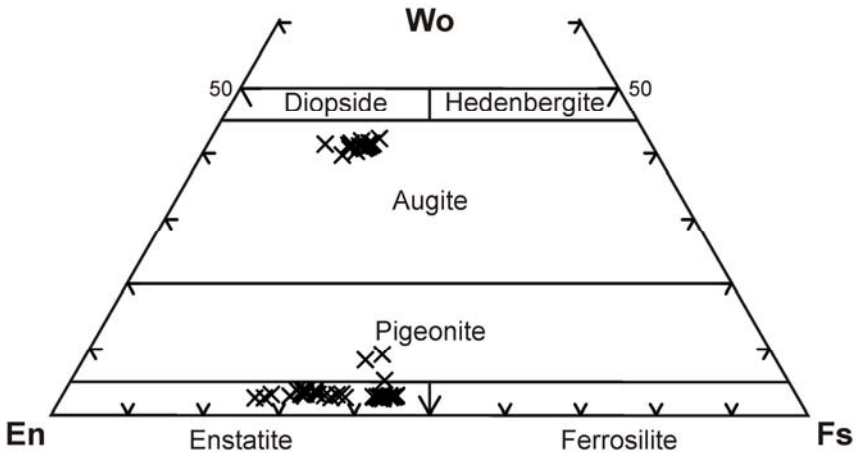

Figure 6.3: Pyroxene compositions from AND unit

6.2.2 Corona Maria (CM)

The CM is, for most of its volume, an eutaxitic porphyritic scarcely to moderately welded ignimbrite formed by pumices, crystals and enclaves in a shard groundmass (Fig. 6.4). Eutaxitic texture is evidenced by pumice flattening (fiammes), crystal orientation, and shard deformation. In the upper portions of the deposit fiammes are present, while shards are neither oriented nor flattened. Pumices are dark red in colour, may contain crystals equals to those in the groundmass, and have variable vesiculation, although always scarce. Phenocrysts assemblage is formed dominantly by plagioclase (Fig. 6.5), minor amounts of clinopyroxene (Fig. 6.6), opaque minerals and accessory titanite; with the presence in some samples of accessory biotite (#Mg 18-19) (Table 6.3) and amphibole (calcic amphibole, hastingsite; sensu Leake et al., 1997) (Fig. 6.7) (Table 6.4) (when present, they represent less than 1 vol %). Crystal content varies between 10 and 30 vol %. All of it consists of crystal fragments of originally idio- to hipidiomorphic phenocrysts grown free or in glomerules. Plagioclase (An_{37-64}) is twinned following Albite law and typically shows zoning

Unit	AND				CM		LE		SE				PC			
Pyroxene	opx	opx	cpx	cpx	cpx	cpx	opx	opx	opx	opx	cpx	cpx	opx	opx	cpx	cpx
Sample	VS-723	VS-723	VS-724	VS-722	VS-47	VS-47	VS-221	VS-365	VS-398	VS-398	VS-398	VS-398	ISP-230	ISP-230	ISP-230	ISP-230
Oxides (%)																
SiO_2	51.00	52.34	48.72	51.95	49.98	50.65	48.95	51.97	51.10	52.98	49.23	51.42	52.83	53.32	50.79	52.93
TiO_2	0.21	0.17	0.79	0.38	0.48	0.43	0.16	0.25	0.27	0.23	0.84	0.48	0.42	0.40	0.94	0.35
Al_2O_3	1.17	3.17	4.17	1.77	1.52	1.30	0.44	0.66	1.76	0.90	3.99	1.91	0.89	0.85	2.76	0.95
Cr_2O_3	0.03	0.03	0.01	0.01	0.00	0.00	0.02	0.01	0.06	0.01	0.00	0.00	0.04	0.02	0.04	0.05
Fe_2O_3(c)	2.50	2.96	4.08	1.00	3.22	2.40	2.76	3.55	3.30	1.41	3.40	1.95	1.96	0.97	4.33	1.16
FeO(c)	24.85	13.63	8.18	11.84	12.91	12.23	30.61	16.96	18.57	19.17	8.58	8.99	18.22	19.00	5.48	7.95
MnO	0.84	0.43	0.31	0.41	0.48	0.35	1.16	0.72	0.50	0.63	0.33	0.45	1.13	1.05	0.49	0.75
MgO	18.82	26.35	13.13	12.94	11.79	12.64	13.86	23.80	22.60	23.37	13.26	14.66	23.69	23.64	14.98	14.89
CaO	1.38	1.29	19.35	20.09	19.06	19.27	1.59	1.58	1.43	1.50	19.35	19.61	1.49	1.41	20.42	20.78
Na_2O	0.03	0.00	0.48	0.31	0.29	0.24	0.03	0.05	0.03	0.03	0.49	0.26	0.01	0.02	0.59	0.36
K_2O	0.00	0.02	0.02	0.00	0.00	0.00	0.00	0.00	0.01	0.00	0.00	0.00	0.00	0.00	0.01	0.02
Sum	100.83	100.39	99.23	100.70	99.73	99.52	99.59	99.56	99.64	100.24	99.46	99.74	100.67	100.70	100.83	100.19
Cations																
Si	1.93	1.89	1.85	1.95	1.92	1.93	1.95	1.93	1.91	1.96	1.86	1.93	1.94	1.96	1.87	1.97
Ti	0.01	0.01	0.02	0.01	0.01	0.01	0.01	0.01	0.01	0.01	0.02	0.01	0.01	0.01	0.03	0.01
Al/Al IV	0.05	0.11	0.16	0.05	0.07	0.06	0.02	0.03	0.08	0.04	0.14	0.07	0.04	0.04	0.12	0.03
Al VI	0.00	0.02	0.03	0.03	0.00	0.00	0.00	0.00	0.00	0.00	0.04	0.01	0.00	0.00	0.00	0.01
Cr	0.00	0.00	0.00	0.00	0.00	0.00	0.00	0.00	0.00	0.00	0.00	0.00	0.00	0.00	0.00	0.00
Fe^{3+}	0.07	0.08	0.12	0.03	0.09	0.07	0.08	0.10	0.09	0.04	0.10	0.06	0.05	0.03	0.12	0.03
Fe^{2+}	0.79	0.41	0.26	0.37	0.41	0.39	1.02	0.53	0.58	0.59	0.27	0.28	0.56	0.58	0.17	0.25
Mn	0.03	0.01	0.01	0.01	0.02	0.01	0.04	0.02	0.02	0.02	0.01	0.01	0.04	0.03	0.02	0.02
Mg	1.06	1.42	0.74	0.72	0.67	0.72	0.82	1.32	1.26	1.29	0.75	0.82	1.30	1.29	0.82	0.82
Ca	0.06	0.05	0.79	0.81	0.78	0.79	0.07	0.06	0.06	0.06	0.78	0.79	0.06	0.06	0.81	0.83
Na	0.00	0.00	0.04	0.02	0.02	0.02	0.00	0.00	0.00	0.00	0.04	0.02	0.00	0.00	0.04	0.03
K	0.00	0.00	0.00	0.00	0.00	0.00	0.00	0.00	0.00	0.00	0.00	0.00	0.00	0.00	0.00	0.00
Sum	4.00	4.00	4.00	4.00	4.00	4.00	4.00	4.00	4.00	4.00	4.00	4.00	4.00	4.00	4.00	4.00
Wo (Ca) mol %	2.79	2.53	41.07	41.54	39.56	39.84	3.34	3.10	2.86	2.97	41.05	40.23	2.93	2.78	41.70	42.32
En (Mg) mol %	53.02	71.87	38.77	37.22	34.04	36.36	40.49	64.93	62.78	64.43	39.13	41.84	64.70	64.94	42.56	42.18
Fs (Fe. Mn) mol %	44.18	25.60	20.16	21.23	26.40	23.80	56.17	31.97	34.36	32.60	19.82	17.93	32.38	32.27	15.74	15.50

Table 6.2: Representative analyses of pyroxenes. For each pyroxene in each unit end-member compositions are given according to SiO_2 content. Cation calculations done with Piro-Max (D'Antonio, M., personal communication). (c): calculated

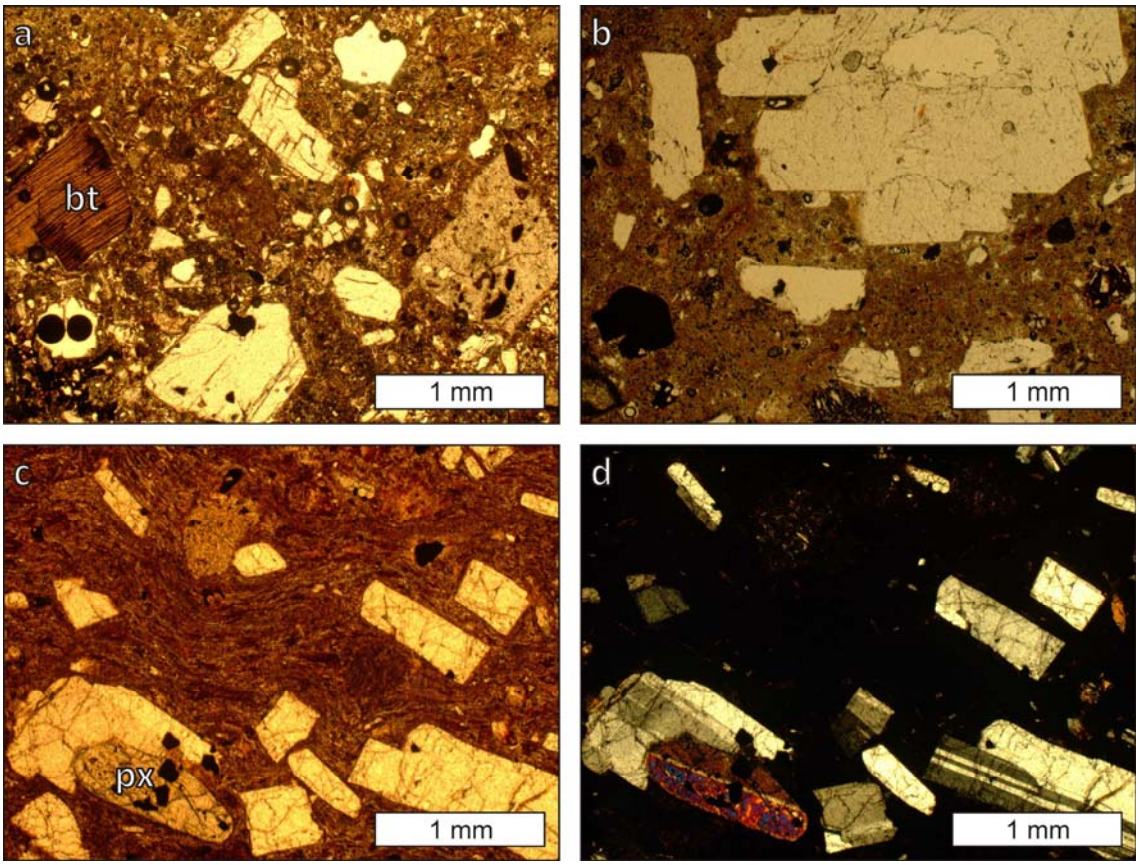

Figure 6.4: Microscope pictures of CM unit. a) and b) non-welded facies under plain-polarized light; c and d) welded facies, same picture under plain and cross-polarized light

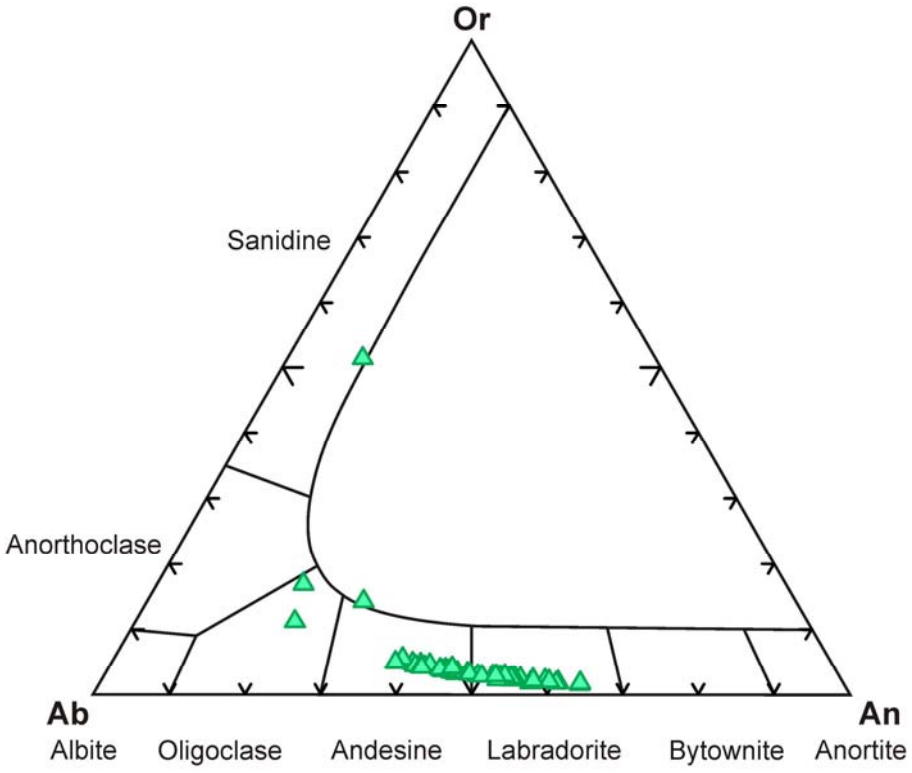

Figure 6.5: Feldspar compositions for CM unit

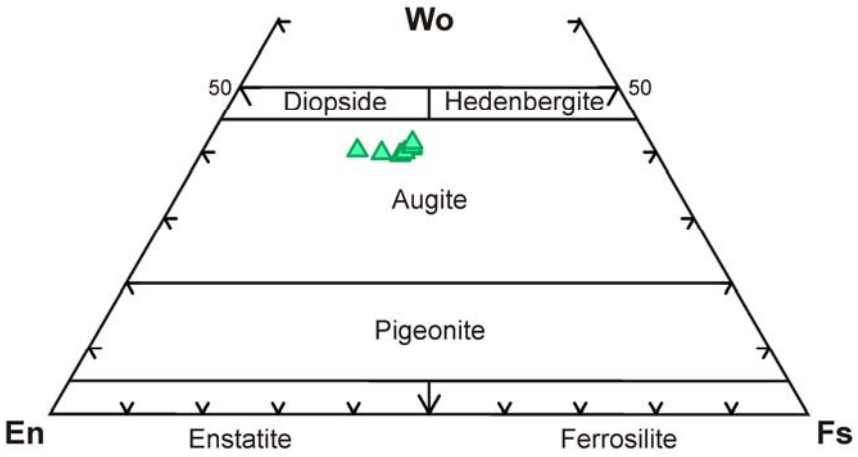

Figure 6.6: Pyroxene compositions for CM unit

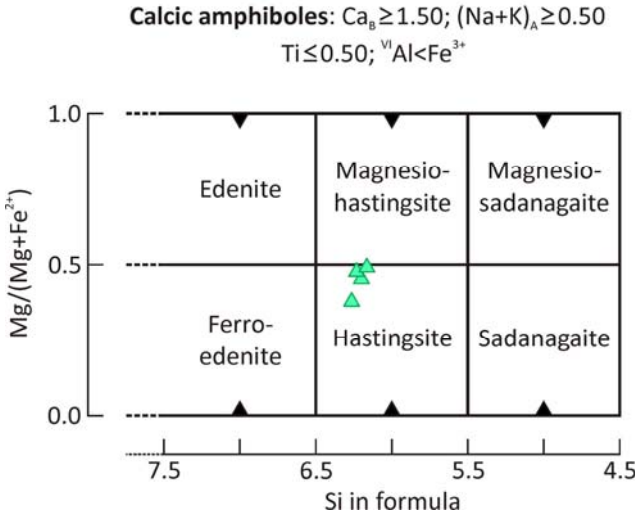

Figure 6.7: Amphibole compositions for CM unit

(either normal or oscillatory), and in some cases may present homogeneous cores. Clinopyroxenes are augite and diposide (Wo_{39-41}, En_{31-39}, Fs_{20-27}) and appear as big tabular twinned crystals. Titanite presents signs of disequilibrium, like corrosion. Enclaves are andesite fragments, either xenoliths or accidental lithic fragments, with characteristics like the ones described before for this type of rocks. Enclave size varies from less than a millimeter to several centimeters, and its abundance greatly varies within the unit. Shards forming the groundmass are usually not preserved, having been replaced by devitrification products, usually a crypto to microcrystalline aggregate of feldspar. When preserved, plastic deformation of shards is evident, flattening and accommodating them to crystals and pumices.

Unit	CM		AC		MLN		MZ	
Sample	VS-32	VS-32	VS-782	VS-782	VS-775	VS-775	VS-760	VS-760
Oxides (%)								
SiO_2	33.66	33.79	36.32	35.93	34.58	35.41	37.63	36.74
TiO_2	5.77	5.77	5.41	5.90	4.69	4.74	5.79	5.80
Al_2O_3	13.25	13.14	13.33	13.30	14.11	14.05	13.06	13.60
Cr_2O_3	0.00	0.00	0.00	0.02	0.00	0.00	0.01	0.02
FeO	27.07	26.97	17.36	17.10	23.77	23.74	13.03	13.27
MnO	0.19	0.21	0.13	0.10	0.18	0.19	0.23	0.16
MgO	5.94	5.85	13.40	13.13	9.02	8.95	16.31	15.54
CaO	0.01	0.02	0.02	0.04	0.03	0.01	0.00	0.04
Na_2O	0.53	0.55	0.90	0.91	0.59	0.62	0.94	0.83
K_2O	8.49	8.37	8.29	8.12	8.24	8.44	8.78	8.49
BaO	0.84	1.02	0.63	1.09	0.79	0.64	0.81	0.73
Rb_2O	0.00	0.00	0.00	0.00	0.00	0.00	0.09	0.07
NiO	0.07	0.00	0.05	0.00	0.00	0.02	0.01	0.04
H_2O(c)	3.75	3.74	3.96	3.95	3.84	3.88	4.07	4.01
Sum Ox%	99.58	99.42	99.80	99.58	99.84	100.70	100.78	99.34
Cations								
Si	5.39	5.42	5.50	5.46	5.40	5.47	5.54	5.49
Ti	0.70	0.70	0.62	0.68	0.55	0.55	0.64	0.65
Al/Al IV	2.50	2.48	2.38	2.38	2.60	2.53	2.27	2.40
Al VI	0.00	0.00	0.00	0.00	0.00	0.03	0.00	0.00
Cr	0.00	0.00	0.00	0.00	0.00	0.00	0.00	0.00
Fe^{2+}	3.63	3.62	2.20	2.17	3.11	3.07	1.61	1.66
Mn^{2+}	0.03	0.03	0.02	0.01	0.02	0.03	0.03	0.02
Mg	1.42	1.40	3.02	2.97	2.10	2.06	3.58	3.46
Ca	0.00	0.00	0.00	0.01	0.01	0.00	0.00	0.01
Na	0.17	0.17	0.27	0.27	0.18	0.19	0.27	0.24
K	1.73	1.71	1.60	1.57	1.64	1.66	1.65	1.62
Ba	0.05	0.06	0.04	0.07	0.05	0.04	0.05	0.04
Rb	0.00	0.00	0.00	0.00	0.00	0.00	0.01	0.01
Ni	0.01	0.00	0.01	0.00	0.00	0.00	0.00	0.01
OH	4.00	4.00	4.00	4.00	4.00	4.00	4.00	4.00
Sum	19.62	19.59	19.63	19.59	19.66	19.63	19.64	19.59
XMg	0.28	0.28	0.58	0.58	0.40	0.40	0.69	0.68
Oct	5.77	5.74	5.86	5.84	5.78	5.74	5.86	5.80
Int	1.95	1.95	1.91	1.91	1.88	1.89	1.97	1.91

Table 6.3: Representative analyses of biotite. Water and cation calculations made by the Xmas Plus of SAMx program

CM vitrophyre is porphyritic (15-20 vol % plagioclase phenocrysts up to 5 mm) and contains abundant mm- to cm-sized strongly flattened pumices altered to reddish dark colours. Lithic fragments may be abundant with sizes up to centimeters.

6.2.3 Lenzu (LE)

LE unit is a strongly welded eutaxitic porphyritic ignimbrite formed by a shard groundmass containing mainly feldspar phenocrysts, with flattened pumices and very scarce lithic fragments (Fig. 6.8). Pumices occur as scarcely vesicular fiamme usually devitrified to crypto- to

Unit	CM		AC		SE		MC		NU		CO					
Population											amp 1	amp 1	amp 2	amp 2	amp 3	amp 3
Sample	VS-32	VS-32	VS-782	VS-782	VS-375	VS-375	VS-765	VS-765	VS-757	VS-757	ISP-150	ISP-150	ISP-150	ISP-150	PI-42	PI-42
Oxides (%)																
SiO_2	40.44	40.09	42.53	41.45	43.76	44.15	43.37	44.60	44.81	46.27	49.17	49.35	49.20	50.27	46.01	47.41
TiO_2	2.84	3.02	3.21	3.40	1.05	1.07	1.34	1.30	1.07	0.99	0.69	0.75	1.52	1.03	1.74	1.87
$Al2O_3$	9.54	10.34	9.71	9.85	5.89	5.74	6.31	5.48	5.46	4.76	0.33	0.32	0.58	0.38	1.35	1.34
Cr_2O_3	0.00	0.00	0.00	0.01	0.01	0.00	0.02	0.00	0.04	0.00	0.00	0.04	0.00	0.03	0.04	0.00
Fe_2O_3(c)	7.01	7.23	6.85	6.00	9.46	9.59	7.93	8.12	10.67	8.56	4.60	5.00	1.91	2.88	5.53	4.87
FeO(c)	15.69	14.84	9.80	10.37	13.58	13.06	14.86	13.96	11.70	12.03	29.08	28.78	28.13	28.40	28.29	29.10
MnO	0.30	0.36	0.29	0.27	0.73	0.84	0.80	0.68	0.95	0.97	1.74	1.71	1.64	1.57	0.92	1.02
MgO	7.97	7.94	12.18	12.17	9.80	9.90	9.15	10.02	10.46	10.95	0.95	1.08	2.98	2.16	1.70	1.45
CaO	10.46	10.20	10.79	11.04	10.06	9.92	10.17	10.08	9.68	9.51	2.88	2.82	3.94	3.23	5.40	5.35
Na_2O	2.26	2.28	2.45	2.60	2.56	2.51	2.41	2.37	2.53	2.58	6.81	6.83	6.76	6.60	5.08	4.94
K_2O	1.05	1.13	0.98	0.98	1.10	1.01	1.15	1.07	1.08	1.02	1.28	1.34	1.20	1.32	1.14	1.12
NiO	0.02	0.01	0.00	0.00	0.00	0.01	0.05	0.00	0.01	0.05	0.01	0.03	0.02	0.00	0.08	0.07
H_2O(c)	1.95	1.95	2.03	2.01	1.97	1.97	1.95	1.97	1.99	1.99	1.86	1.87	1.89	1.89	1.85	1.88
Sum	99.51	99.40	100.84	100.16	99.96	99.77	99.49	99.64	100.44	99.68	99.40	99.93	99.76	99.76	99.12	100.42
Cations																
Si	6.23	6.16	6.27	6.18	6.68	6.73	6.67	6.80	6.75	6.97	7.92	7.90	7.82	7.97	7.47	7.57
Ti	0.33	0.35	0.36	0.38	0.12	0.12	0.15	0.15	0.12	0.11	0.08	0.09	0.18	0.12	0.21	0.22
Al	1.73	1.87	1.69	1.73	1.06	1.03	1.14	0.98	0.97	0.85	0.06	0.06	0.11	0.07	0.26	0.25
Cr	0.00	0.00	0.00	0.00	0.00	0.00	0.00	0.00	0.00	0.00	0.00	0.01	0.00	0.00	0.01	0.00
Fe^{3+}	0.80	0.83	0.77	0.68	1.09	1.09	0.90	0.93	1.21	0.95	0.56	0.60	0.22	0.35	0.64	0.55
Fe^{2+}	2.04	1.91	1.20	1.29	1.73	1.67	1.93	1.78	1.47	1.54	3.92	3.86	3.75	3.76	3.87	3.92
Mn	0.04	0.05	0.04	0.03	0.09	0.11	0.10	0.09	0.12	0.12	0.24	0.23	0.22	0.21	0.13	0.14
Mg	1.83	1.82	2.68	2.71	2.23	2.25	2.10	2.27	2.35	2.46	0.23	0.26	0.70	0.51	0.41	0.34
Ca	1.73	1.68	1.70	1.76	1.64	1.62	1.68	1.65	1.56	1.54	0.50	0.48	0.67	0.55	0.94	0.91
Na	0.68	0.68	0.70	0.75	0.76	0.74	0.72	0.70	0.74	0.76	2.13	2.12	2.08	2.03	1.60	1.53
K	0.21	0.22	0.18	0.19	0.21	0.20	0.23	0.21	0.21	0.20	0.26	0.27	0.24	0.27	0.24	0.23
Sum	15.61	15.58	15.59	15.70	15.62	15.56	15.62	15.55	15.51	15.49	15.88	15.87	16.00	15.85	15.78	15.67

Table 6.4: Representative analyses of amphiboles. amp 1) sodic amphibole phenocrysts; amp 2) matrix poikilitic sodic-calcic amphiboles; amp 3) sodic-calcic amphibole phenocrysts. Water and cation calculations made by the Xmas Plus of SAMx program. (c): calculated

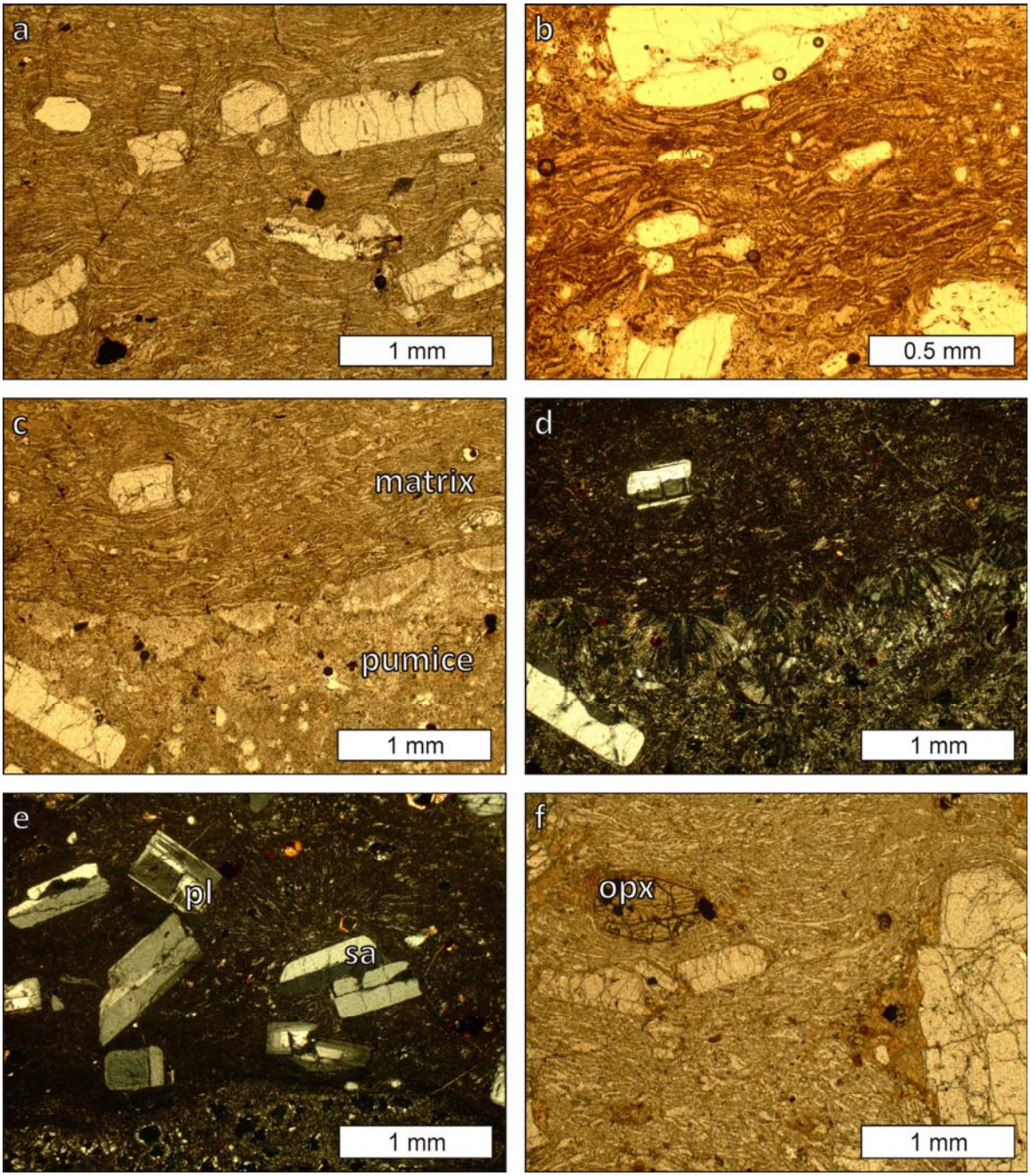

Figure 6.8: Microscope pictures of LE unit. a) and b) eutaxitic welded shard groundmass with feldspars under plain-polarized light; c) and d) difference between matrix and pumices, same picture under plain- (c) and cross- (d) polarized light; e) feldspars under cross-polarized light; f) orthopyroxene, picture under plain-polarized light

microcrystalline aggregates of feldspar and crystalline silica, including spherulites. Fiamme may contain crystals like those found in the groundmass. Porphyricity of this unit (10-20 vol %) is given by a mineral assemblage dominated by feldspars (plagioclase and sanidine in similar amounts) (Fig. 6.9) up to some mm in size, minor opaque minerals, and accessory orthopyroxene (Fig. 6.10). Zircons can be found in opaque minerals. Plagioclase (An_{29-46}) is milky in hand specimen, presents normal zoning and twinning following albite law, and occurs both as free crystals and in

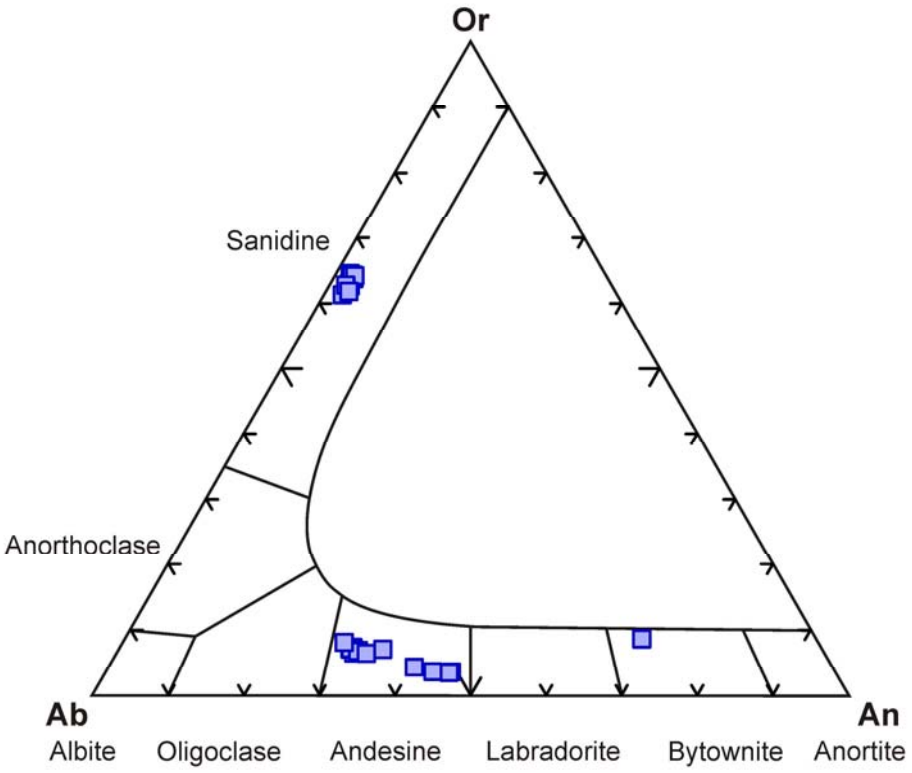

Figure 6.9: Feldspar compositions for LE unit

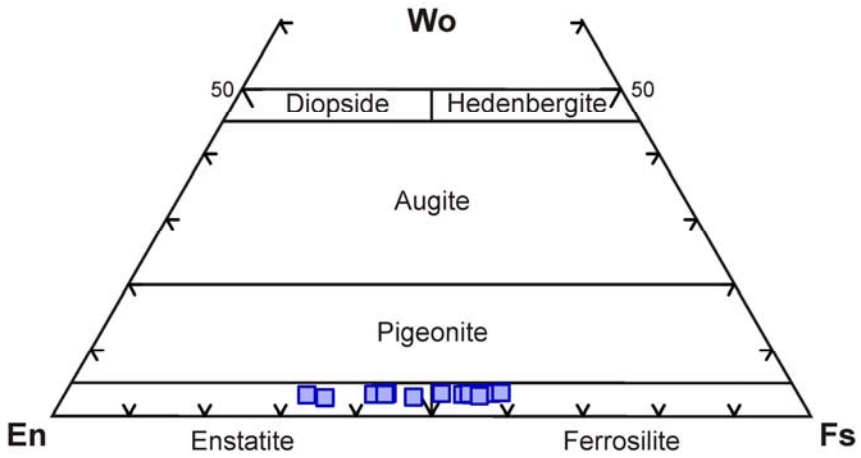

Figure 6.10: Pyroxene compositions for LE unit

glomerules. Sanidine (Or_{61-65}) occurs as clear crystals twinned following Carlsbad law. Orthopyroxenes (enstatite/ferrosilite, Wo_3, En_{39-65}, Fs_{32-57}) occur in some facies as short prisms.

Amphibole xenocrysts may appear; they are usually altered, in clear instability, and may appear free or in glomerules with plagioclase crystals. They present magnesiohastingsite composition,

which is similar to that of amphiboles in CM. All crystals are fragments of the original hipidio- to idiomorphic tabular phenocrysts. The groundmass is scarcely devitrified so the shards are still observable. They are strongly flattened and welded. Spherulites may be present.

LE vitrophyre is porphyritic, it contains about 10 vol % of feldspar phenocrysts free or in glomerules. No pumices or lithic fragments occur.

6.2.4 Acqua sa Canna (AC)

AC is a poorly to moderately welded porphyritic ignimbritic deposit with several facies resulting from the different flows that form it. However, most flows share the same mineral assemblage and texture (Fig. 6.11). Crystal orientation and pumice flattening mark an eutaxitic texture. Porphyricity (10-20 vol %) is given by phenocryst fragments of plagioclase, with minor biotite and opaque minerals (both less than 1 vol %). Plagioclase (An_{37-56}) (Fig. 6.12) occurs as hypidiomorphic crystals with normal zoning (although oscillatory zoning may appear in the bigger crystals) and twinning following albite law. Plagioclase crystals are dominantly free, with scarce glomerules. Compositional variation within a single plagioclase crystal is large, covering most of the compositional range observable in the sample. Biotite crystals (#Mg 41-44) are fresh usually deformed plates. Accessory amphibole (calcic amphibole, magnesiohastingsite) (Fig. 6.13) crystals are rarely found. The groundmass is formed by fine shards mostly devitrified to a cryptocrystalline aggregate of crystalline silica and feldspar, so original shards shape and structure can barely be seen. Pumices are flattened, with shredded edges, containing vesicles up to 10-20 vol %, and invariably devitrified to a microgranular aggregate of crystalline silica and feldspar. They may contain crystals equal to those in the matrix. Andesitic enclaves may be present.

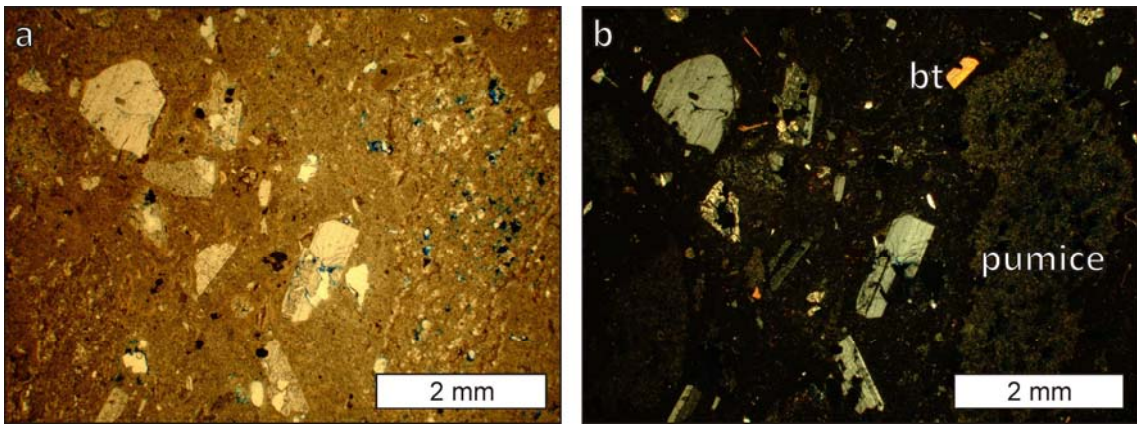

Figure 6.11: Microscope pictures of AC unit. Same picture of typical scarcely welded facies under plain- (a) and cross- (b) polarized light

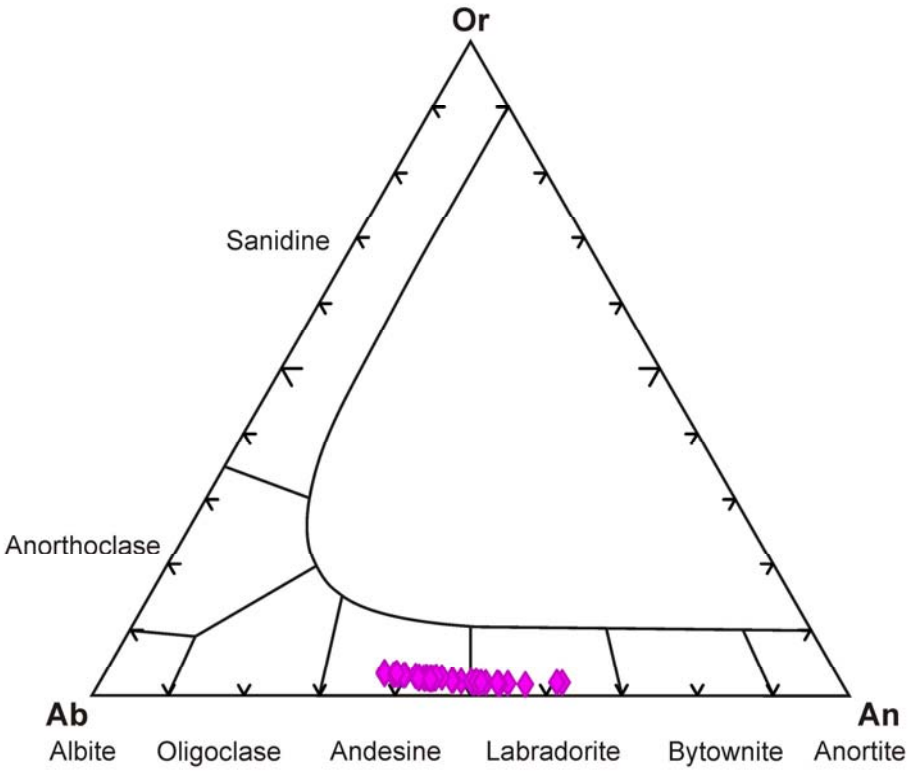

Figure 6.12: Feldspar compositions for AC unit

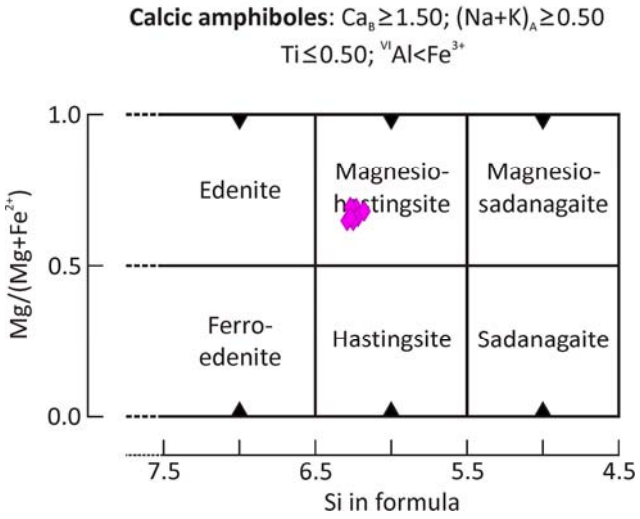

Figure 6.13: Amphibole compositions for AC unit

6.2.5 Seruci (SE)

SE is a strongly welded and eutaxitic porphyritic ignimbrite (Fig. 6.14). Eutaxitic texture is macroscopically evidenced by a strong pumice flattening, and microscopically also by crystal orientation and strong shard flattening. Pumices are very variable in size (cm to dm) and are

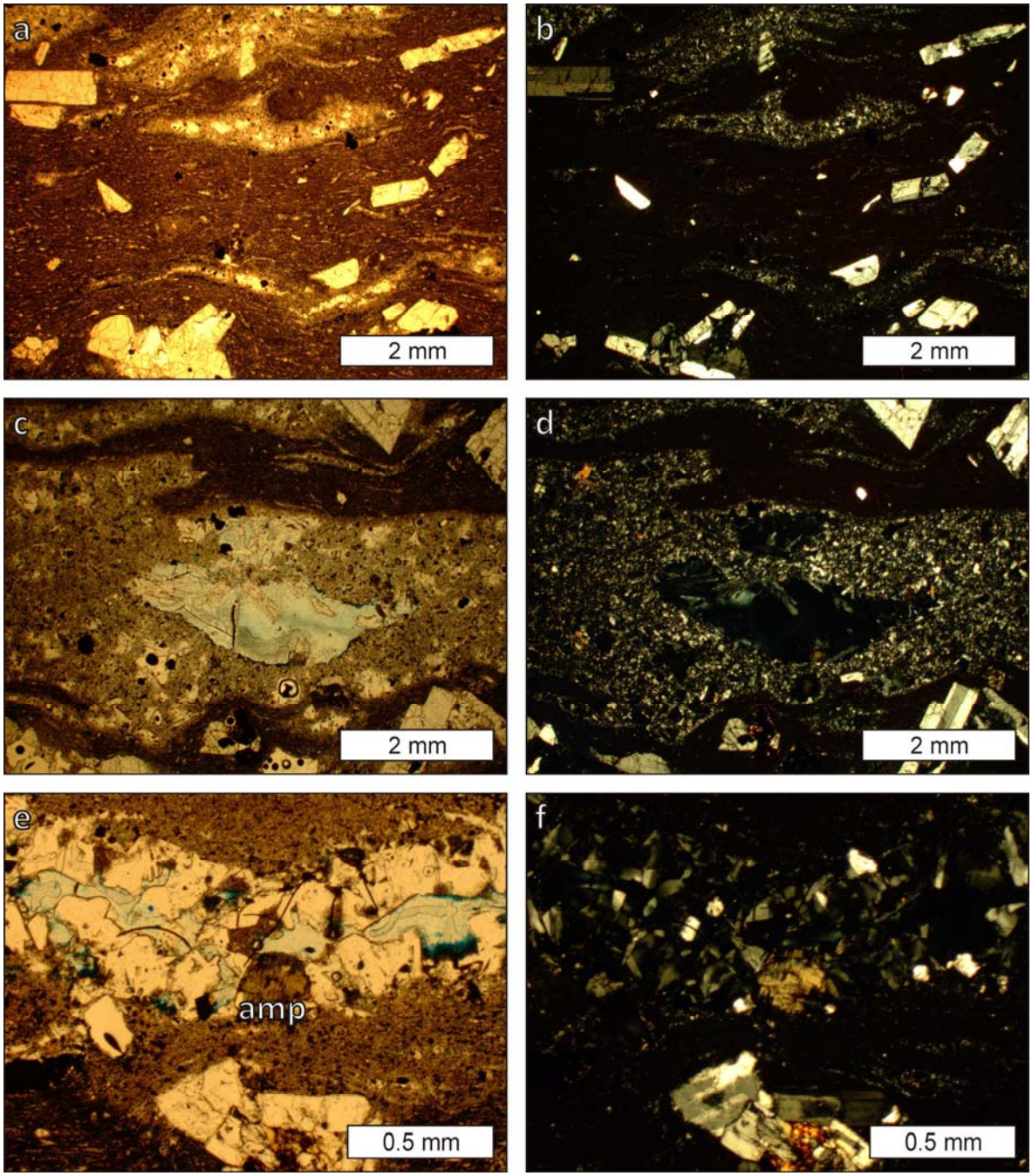

Figure 6.14: Microscope pictures of SE unit. a) welded eutaxitic matrix with oriented phenocrysts and fiamme; c) devitrified pumice with acicular crystals in vesicle; e) late amphibole in a vesicle; pictures a), c) and e) are with plain-polarized light; b), c) and f) equivalent pictures under cross-polarized light

vesicular (up to 20-30 vol %). They are devitrified to a microcrystalline aggregate of crystalline silica and feldspar, and long prismatic silica crystals may be present partially filling vesicles (miarolitic texture, sensu Lofgren, 1971); amphibole (calcic amphibole, edenite) (Fig. 6.15) hypidiomorphic crystals may also occur in vesicles. Pumices may contain phenocrysts equivalent to those in the groundmass. Mineral assemblage consists of plagioclase and opaque minerals, forming about 10-20 vol % of the rock. Plagioclase (An_{26-40}) (Fig. 6.16) crystals present no or little

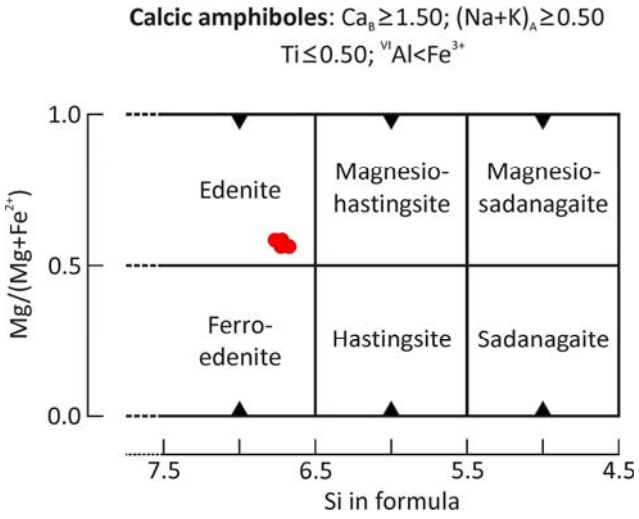

Figure 6.15: Amphibole compositions for SE unit

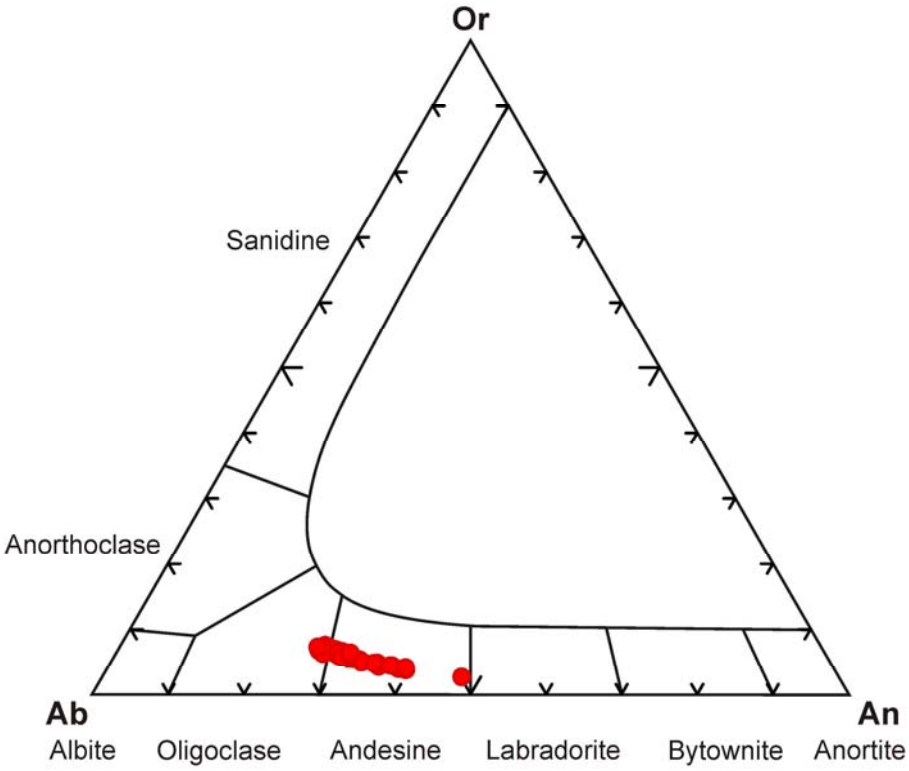

Figure 6.16: Feldspar compositions for SE unit

zoning, which is normal except for few big crystals with oscillatory zoning. Apart from plagioclase crystals, some scarce reddish brown crystals occur showing signs of instability such as corrosion and alteration; alteration makes impossible the recognition of this mineral, though a former exfoliation can be recognised so they probably were pyroxene or amphibole. Shard groundmass is mostly preserved, although incipient devitrification may have occurred locally. Shards are strongly flattened and welded. Pyroxenes may be present in a particular facies as hypidiomorphic

accessory phases; these are enstatite (Wo_3, En_{60-65}, Fs_{32-37}) and augite (Wo_{40-41}, En_{39-42}, Fs_{17-20}) (Fig. 6.17)

SE unit vitrophyre is porphyritic (10 vol % plagioclase phenocrysts) and may present abundant (more than 5 %) lithic fragments up to a cm in size and strongly flattened mm- to cm-sized pumices. This vitrophyre can be very similar to that of CM.

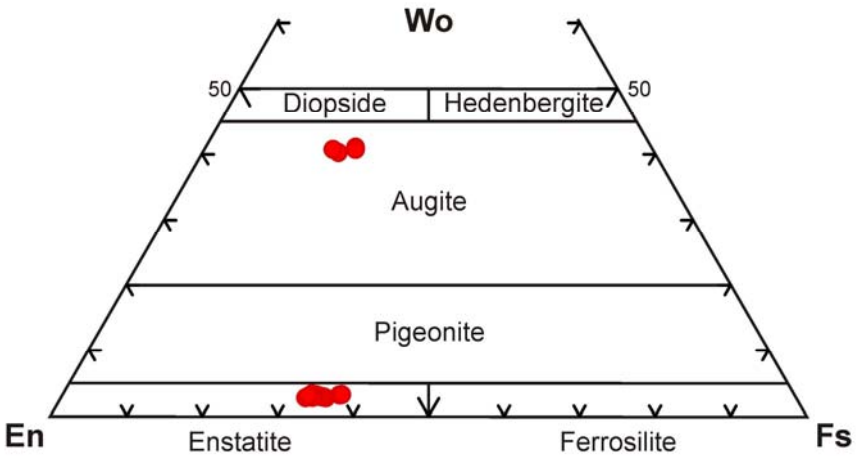

Figure 6.17: Pyroxene compositions for SE unit

6.2.6 Monte la Noce (MLN)

Monte la Noce unit is present as consolidated cineritic deposits, as lava flows, and locally as an extremely welded ignimbrite (Fig. 6.18). All types are aphyric to scarcely porphyritic. Cinerites are very fine grained, and are composed of a cryptocrystalline devitrified matrix containing plagioclase microlites and small opaque minerals. Crystal content is below 3 vol %. In ignimbritic facies small vesicular pumices and scarce plagioclase and biotite phenocrysts (< 1mm) and microcrysts may appear. Pumices are flattened, giving the rock an eutaxitic texture. They are affected by a coarser devitrification than matrix (microcrystalline). Original ash pyroclasts cannot be recognised in the matrix. Vesicles are partially filled by prismatic crystalline silica (miarolitic texture). Plagioclase crystals (An_{34-43}) (Fig. 6.19) are fragments of originally idiomorphic to hipidiomorphic phenocrysts, which are variable in appearance; they may have no to strong zoning, which may be normal or oscillatory. All crystals are twinned following albite law. Biotite (#Mg 27-28) is usually partially altered and is very scarce (far less than 1 vol %). Crystals can be found in the matrix or in pumices and represent less than 3 vol % of the sample.

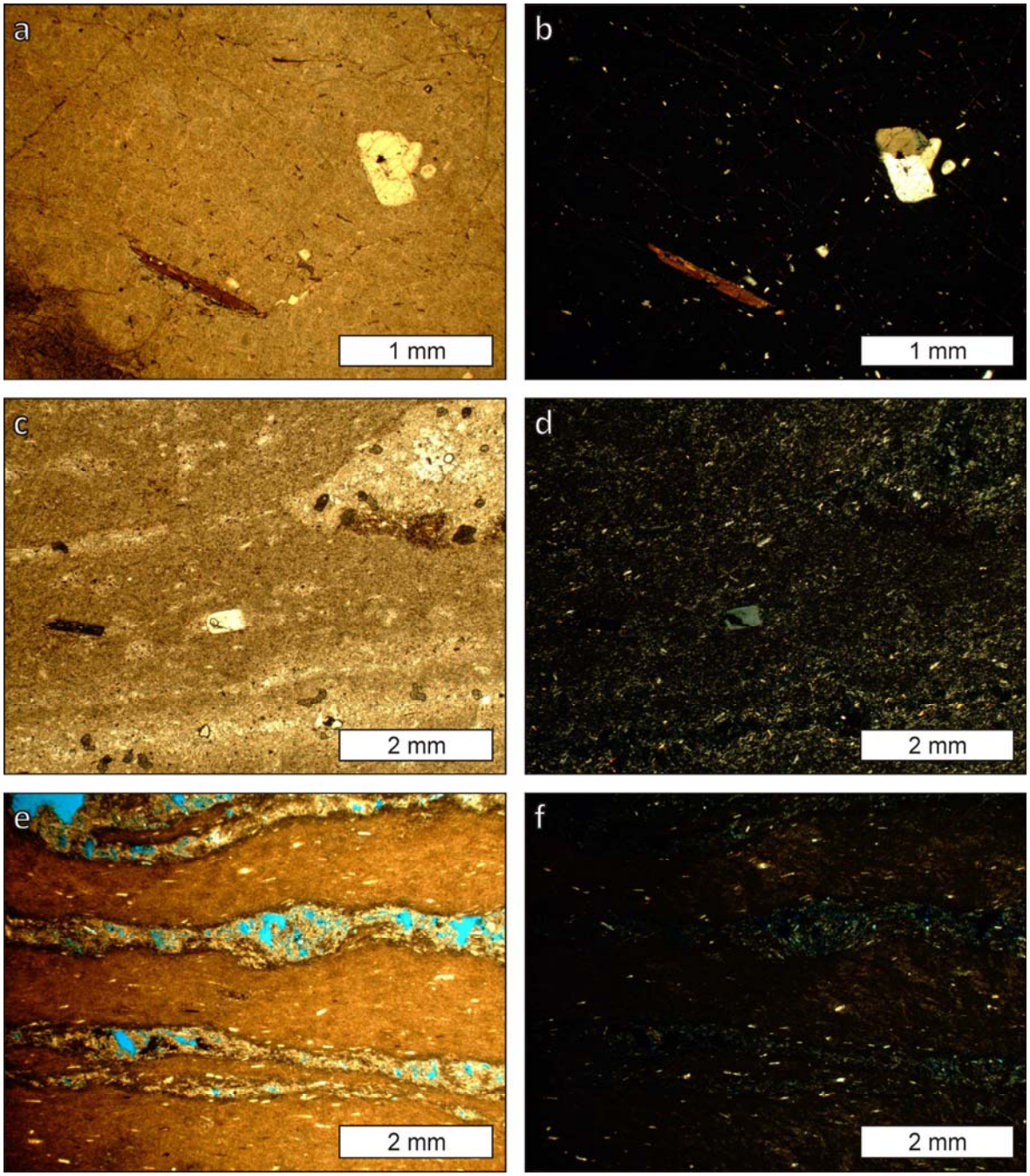

Figure 6.18: Microscope pictures of MLN unit. a) vitrophyre with bt and plg; c) extremely welded and eutaxitic facies of an ignimbrite; e) lava flow facies. Vesiculated bands resemble pumices; b), d) and f) correspond to the same areas in pictures at the left under cross-polarized light

The vitrophyre in the welded ignimbrite is strongly aphyric, containing only accessory phenocrysts of plagioclase and biotite. Locally, microlites less than 200 µm long and perlitic texture can be observed.

Lava flows present almost aphyric fluidal textures evidenced by bands of vesiculated lava few mm-thick which resemble pumitic material. Rock is aphyric except for scarce plagioclase

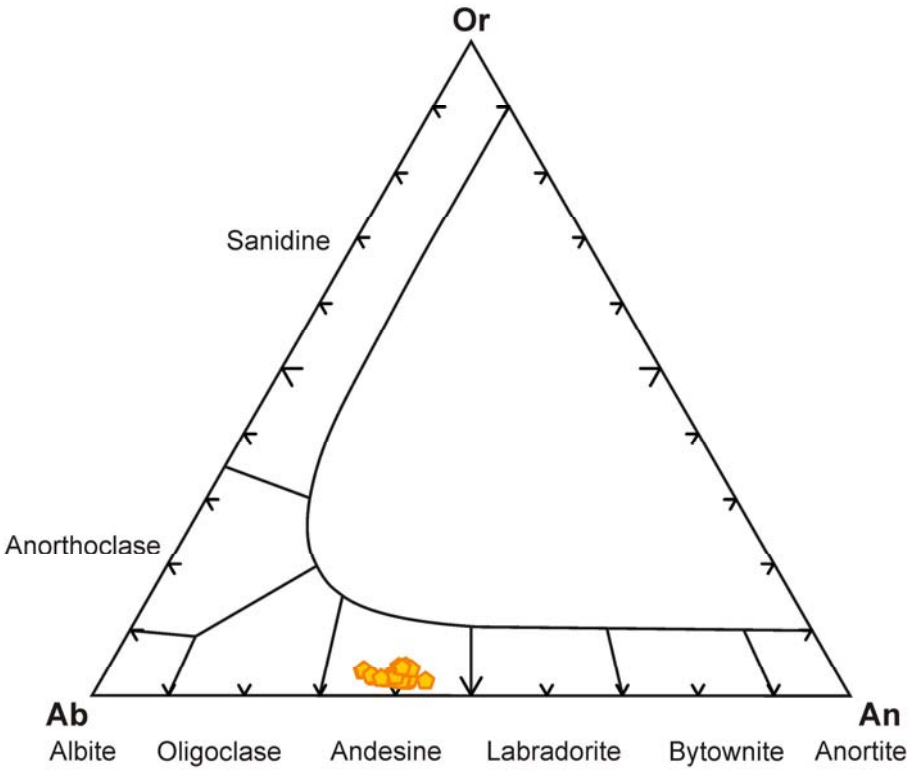

Figure 6.19: Feldspar compositions for MLN unit

microlites, which are oriented following flow structures. The groundmass is devitrified to a cryptocrystalline aggregate of felsic minerals (crystalline silica and feldspar), while vesicular bands are more coarsely devitrified.

6.2.7 Monte Crobu (MC)

The Monte Corbu unit presents variety of facies, from extremely to poorly welded, and from containing few pumices to a pumice-dominated deposit. Welded facies dominate, being the scarcely welded ones only at the top of the ignimbrite (Fig. 6.20).

The vitrophyre of MC unit is very poor in crystals and these are small feldspars (<1mm). For most of its volume the MC unit is a strongly welded porphyritic eutaxitic ignimbrite with abundant pumices. Porphyricity (10 to 20 vol %) is given by mm-sized (up to 5 mm) feldspar hypidiomorphic phenocrysts fragments and scarce (<1 vol %) opaque minerals. Sanidine largely dominates over plagioclase. Sanidine (Or_{54-65}) (Fig. 6.21) appears homogeneous with twinning following Carlsbad law. Plagioclase crystals (An_{18-38}, but up to An_{61} (probably xenocrysts)) are twinned following albite law, and may show normal zoning. In some samples amphibole (calcic amphibole, edenite) (Fig. 6.22) appears as a late phase in the mineral assemblage (probably as a vapour phase, contemporary to high temperature devitrification). It may crystallise as allotriomorphic crystals in

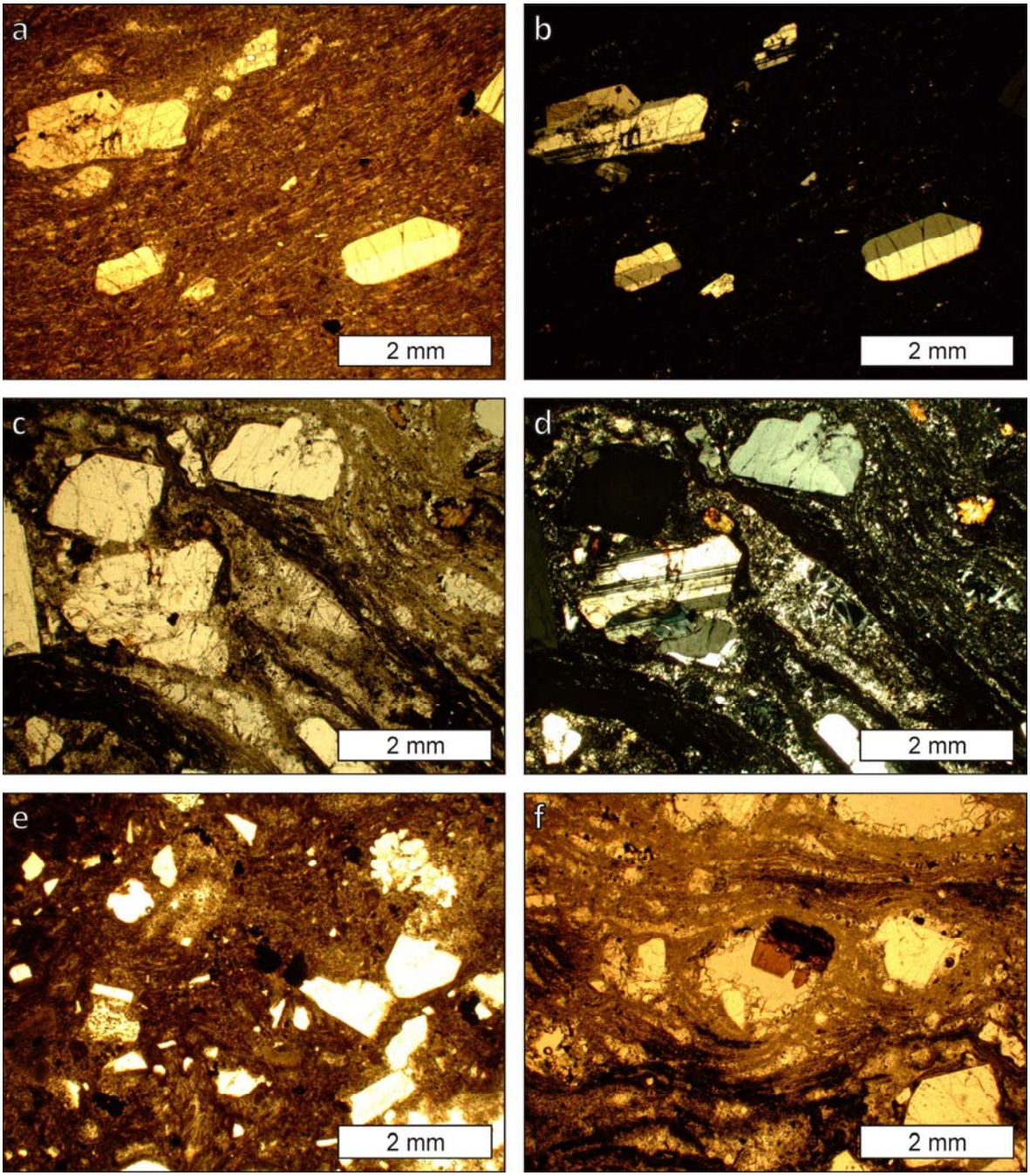

Figure 6.20: Microscope pictures of MC unit. a) and b) strongly welded and eutaxitic facies with oriented phenocrysts under plain- (a) and cross- (b) polarized light. No pumices are present in the picture; c) and d) pumice dominated facies under plain- (c) and cross- (d) polarized light; e) scarcely welded upper facies of the unit in Santo Antioco Island under plain-polarized light; f) amphibole in a vesicle as a late crystallising phase under plain-polarized light

the groundmass, but it crystallises preferentially as hypidiomorphic crystals in vesicles. Pumices are strongly flattened and show variable vesicularity. They may be grey or black. Grey pumices contain the same crystals as the groundmass, but in slightly smaller amount. Black pumices also present sanidine and plagioclase, but in this case sanidine crystals are strongly corroded and embayed, whereas plagioclase crystals remain mostly intact. Plagioclases in black pumices present

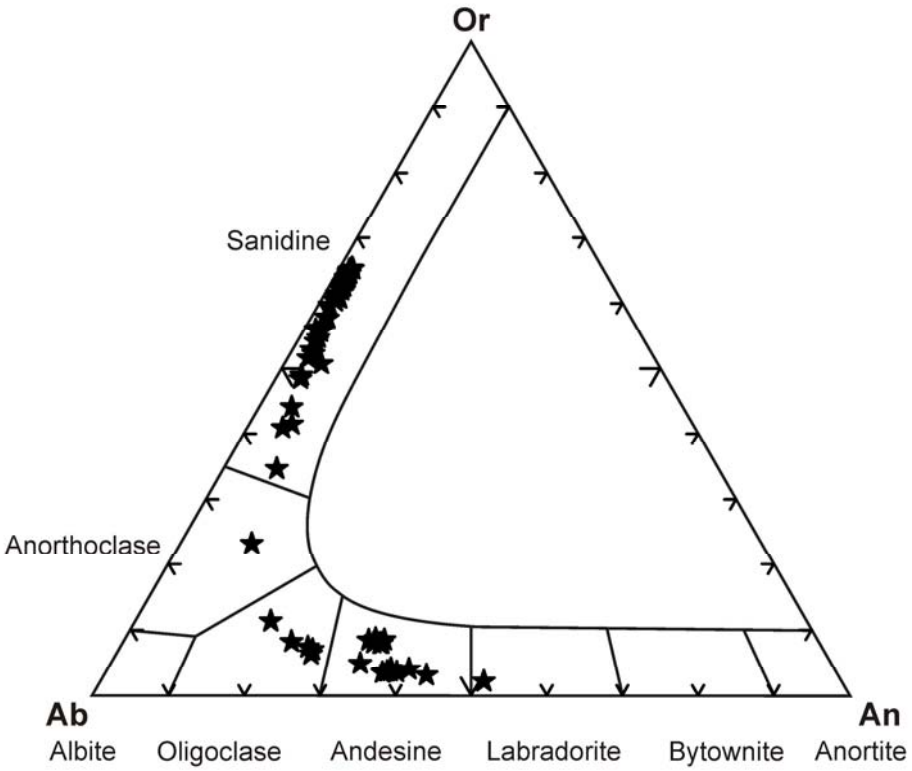

Figure 6.21: Feldspar compositions for MC unit

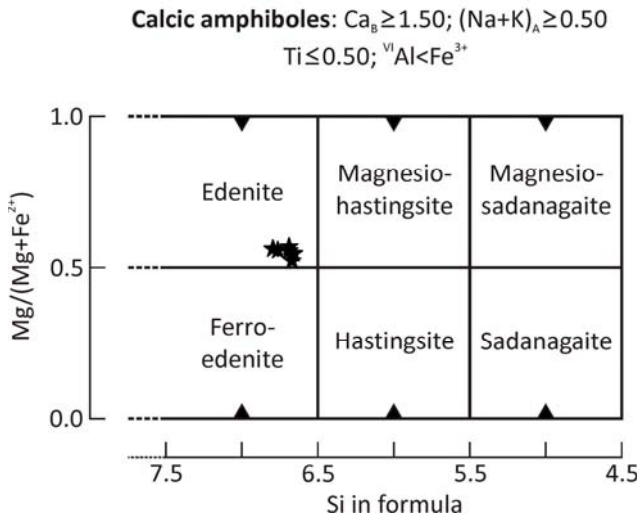

Figure 6.22: Amphibole compositions for MC unit

slightly more Or-rich compositions than those in the groundmass. The groundmass is of a reddish-brown colour; it is formed by flattened shards and may present small vesicles. Devitrification affects both shards and pumices in variable degree. Pumices are devitrified to a coarser microcrystalline granular aggregate of feldspars and crystalline silica. Vesicles are filled with aggregates of prismatic and acicular crystalline silica and feldspar. Sanidines may present a thin overgrowing formed during devitrification.

Non-welded cineritic facies are formed by the same components but show less welding and deformation of shards and pumices, being only slightly eutaxitic. These facies are more affected by devitrification.

6.2.8 Conca is Angius (CA)

CA is a non- to slightly welded unit formed by shards, crystals, pumices and abundant variable size (mm to cm) lithic fragments (Fig. 6.23). Porphyricity is about 10 vol % and is given by hypidiomorphic fragments of sanidine and plagioclase crystals with slight dominance of sanidine. Sanidine (Or_{62-65}) (Fig. 6.24) appears as homogeneous crystals with twinning following Carlsbad law. Plagioclase crystals (An_{23-30}) are twinned following albite law, and may show normal zoning. Opaque minerals occur (<1 vol %). Pumices are variable in shape and size, but show little deformation and abundant vesiculation. They are strongly devitrified. The cineritic groundmass is heavily devitrified to a crypto- to microcrystalline granular aggregate of crystalline silica and feldspar, but in some places the original texture of undeformed shards can be observed. Vesicles

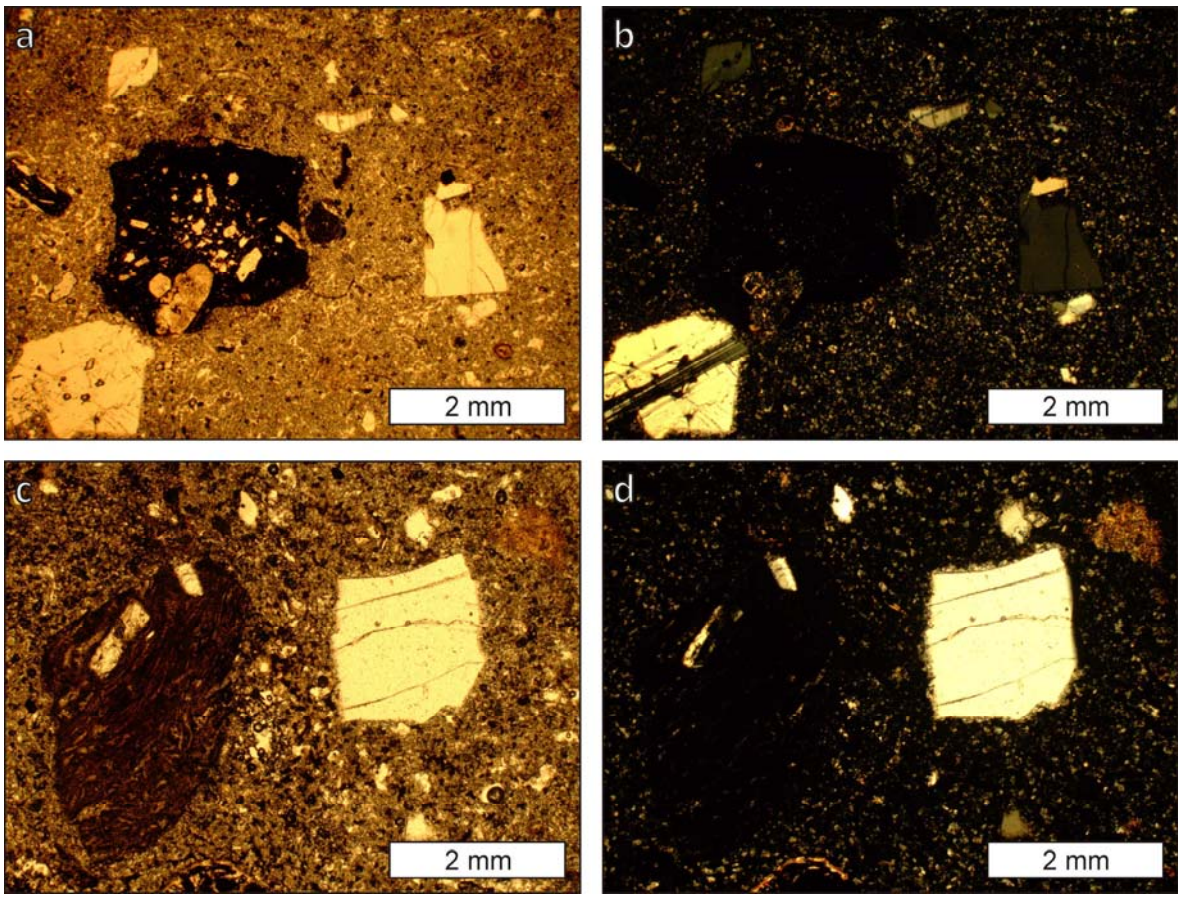

Figure 6.23: Microscope pictures of CA unit. a) non-welded facies with phenocrysts fragments and an andesitic lithic fragment; c) same facies, with a lithic fragment of extremely welded and eutaxitic ignimbrite; b) and d) equivalent pictures under cross-polarized light

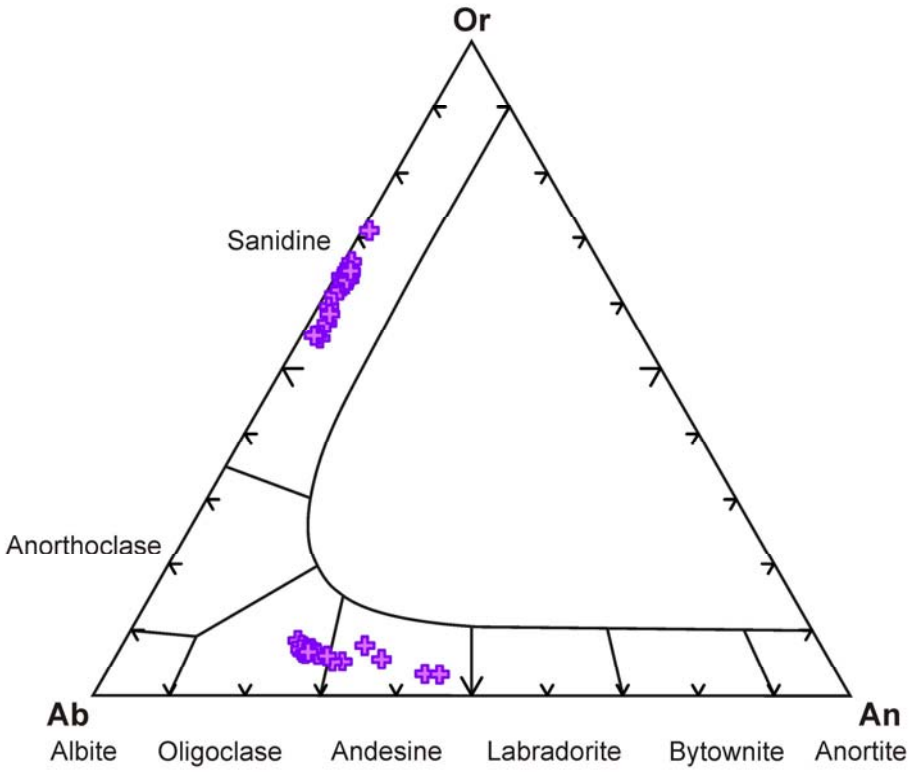

Figure 6.24: Feldspar compositions in CA unit

in the groundmass and pumices are irregular, equidimensional and are empty (have not been filled by vapour phase or devitrification crystals). Enclaves belong to all the units having erupted before the CA, being from andesite lava fragments to extremely welded ignimbrite pieces.

6.2.9 Nuraxi (NU)

NU unit is a rather homogeneous reddish-brown strongly eutaxitic ignimbrite characterised by an extreme welding and high porphyricity (Fig. 6.25). Pumices are scarce and appear as extremely flattened light grey fiamme which may contain crystals equal to those in the groundmass. Enclaves are very scarce in this unit.

The vitrophyre has very scarce crystal content, lower than 3 vol %. But this content increases upwards in the main body of the ignimbrite, being for most of its volume between 20 and 30 vol %. A detailed description of this vitrophyre and its forming mechanisms is given in Gimeno et al. (1996). Mineral assemblage in NU unit is formed by feldspars, with accessory opaque minerals and clinopyroxene. Feldspars are sanidine and plagioclase in varying ratios, from dominating sanidine to dominating plagioclase. Crystals are hypidiomorphic fragments of tabular phenocrysts up to some mm in size. Sanidines (Or_{41-53}) (Fig. 6.26) may present or not twinning following Carlsbad law and are found as free crystals. Plagioclases (An_{20-43}) are milky and may present normal zoning and twinning following albite law. Plagioclases occur both as free crystals and in

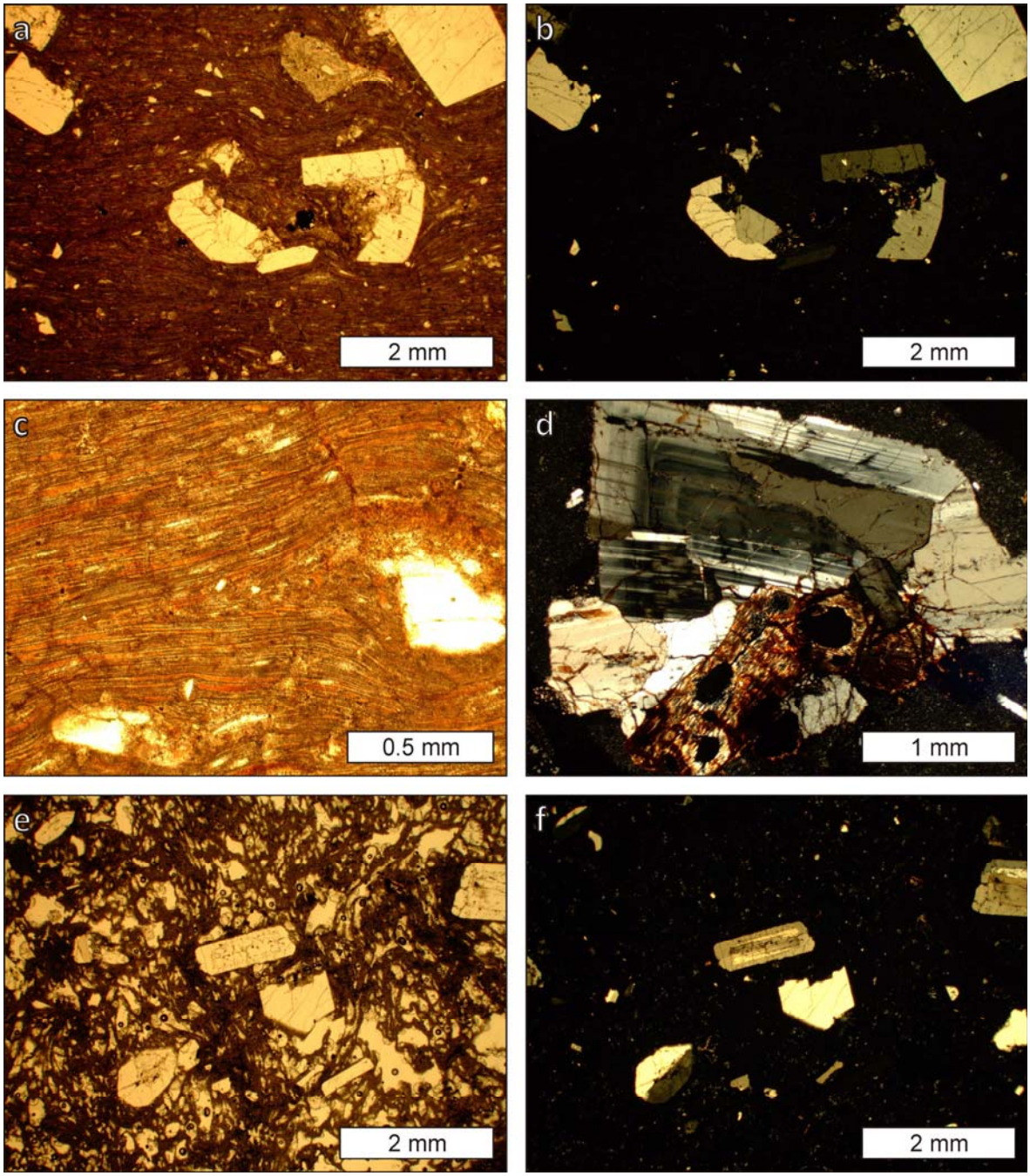

Figure 6.25: Microscope pictures of NU unit. a) and b) characteristic extremely welded and eutaxitic facies under plain- (a) and cross- (b) polarized light; c) detail of the shard groundmass; d) plagioclase glomerule which also contains an altered mafic mineral under cross-polarized light; e) vesicled facies from the upper region of the ignimbrite in western Santo Antioco Island under plain-polarized light. There are two idiomorphic plagioclase crystals in the centre and upper right corner presenting sanidine mantle, which is better appreciated in picture f) under cross-polarized light

glomerules up to a 7-8 mm in size, and may have a mantle of sanidine overgrowing a plagioclase core. Opaque minerals occur as small hypidiomorphic phenocrysts. Pyroxenes are most commonly altered to oxides aggregates (it has not been possible to obtain the chemical composition of a fresh clinopyroxene). The groundmass is formed by completely flattened shards marking a

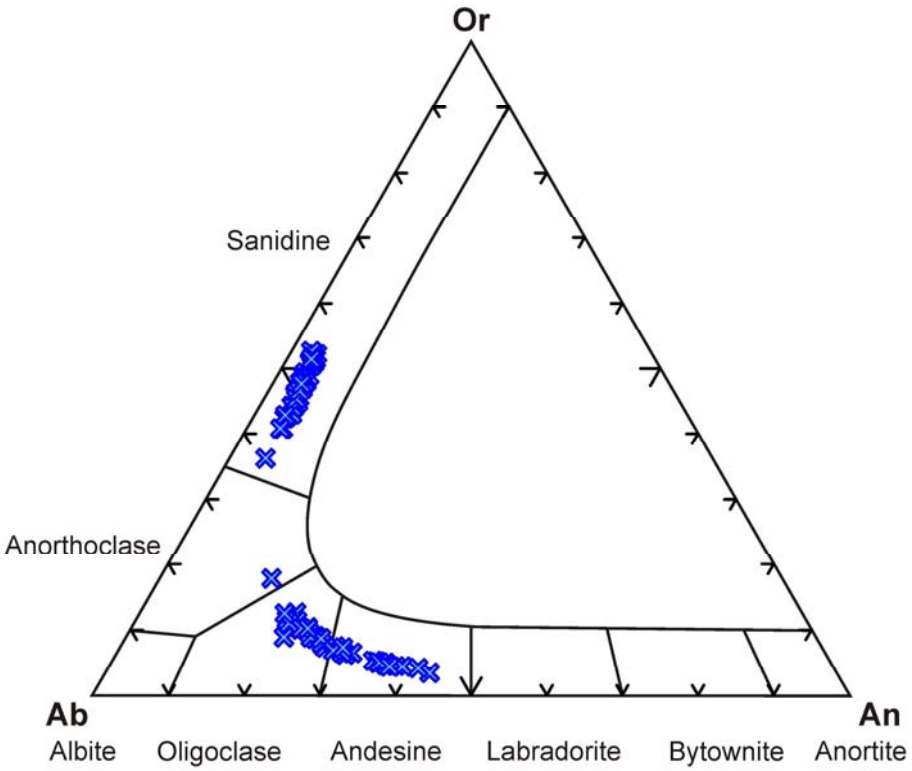

Figure 6.26: Feldspar compositions for NU unit

microeutaxitic texture, which may present flow structures. Despite the very strong welding, the groundmass commonly shows some degree of devitrification to a microspherulitic or crypto- to microgranular aggregates formed by crystalline silica and feldspar. Devitrification becomes more intense towards the upper less welded part of the unit. Pumices are devitrified to coarser aggregates than the groundmass, and usually present flattened vesicles partially to totally filled by prismatic hypidiomorphic crystals of silica and feldspar, and occasionally amphibole (calcic amphibole, edenite) (Fig. 6.27) (miarolitic texture).

Upper less welded facies can be found at the top of the ignimbrite showing abundant vesiculation (10 vol %), and being strongly devitrified.

6.2.10 Punta dei Cannoni (PC)

PC ignimbrite is formed by several flow deposits changing in colour, pumice and lithics contents and welding that share, however, a very similar microscopic texture. PC is a highly porphyritic and welded eutaxitic unit presenting abundant cm to dm-sized moderately flattened pumices (Fig. 6.28). Enclaves are scarce.

Porphyricity is given by a high crystal content (up to 50 vol %) of dominantly feldspar phenocrysts hypidiomorphic to allotriomorphic fragments. Opaque minerals and pyroxenes are also present

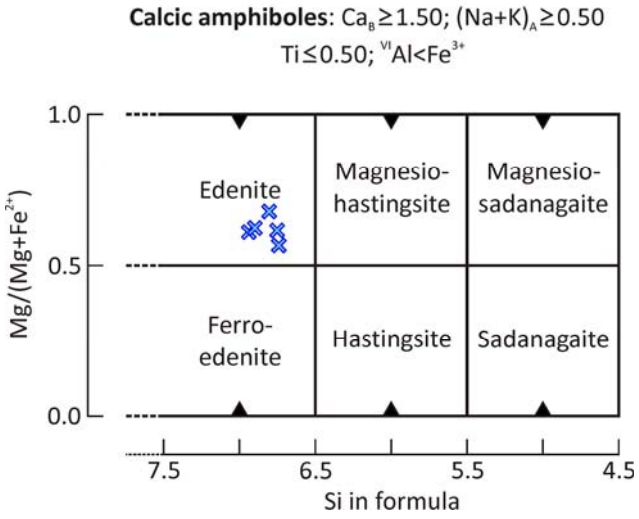

Figure 6.27: Amphibole compositions in NU unit

and can amount up to 3-5 vol %. Feldspars are plagioclase and anorthoclase mm in size (up to half centimeter), which can be found either free or in glomerules (especially plagioclase). The distribution of feldspars is not homogeneous throughout the unit; in the brown part of the unit anorthoclase is the dominant feldspar, with only scarce plagioclase crystals, whereas in the black levels found in the middle of the unit plagioclase is the only feldspar. Plagioclases (An_{20-35}) (Fig. 6.29) show scarce twinning following albite law, whereas anorthoclases (An_{11-17}, Ab_{61-65}, Or_{19-28}) are finely twinned following albite and pericline laws. Both minerals present abundant fracturing and internal corrosion. Some re-equilibration with melt took place, because zoning may follow open fractures and embayments. The combination of original zoning, zoning due to re-equilibration, and some degree of physical deformation of crystals, produces complex extinction patterns when crystals are observed under cross-polarized light. Opaque minerals are several times smaller than feldspars and present hypidiomorphic to idiomorphic morphologies. Pyroxenes (dominant diopside (Wo_{40-43}, En_{41-43}, Fs_{15-19}) and minor enstatite (Wo_3, En_{65}, Fs_{32})) (Fig. 6.30) are most commonly altered, and have only been found fresh in the black level in the middle of the unit. They can be found free in the groundmass or forming glomerules with plagioclase. In the black levels cumulitic bodies exist formed by plagioclase and pyroxene crystals with the same compositions than those free in the groundmass.

Pumices are vesicular (up to 10-20 vol %) with small round vesicles which may be partially to totally filled by crystalline silica and feldspar aggregates. Pumices also present a high porphyricity (20-30 vol %), being crystals the same as in the equivalent groundmass. The grey ellipsoidal bodies are thought to be pumices, for they are microvesiculated with spherical vesicles partially to totally

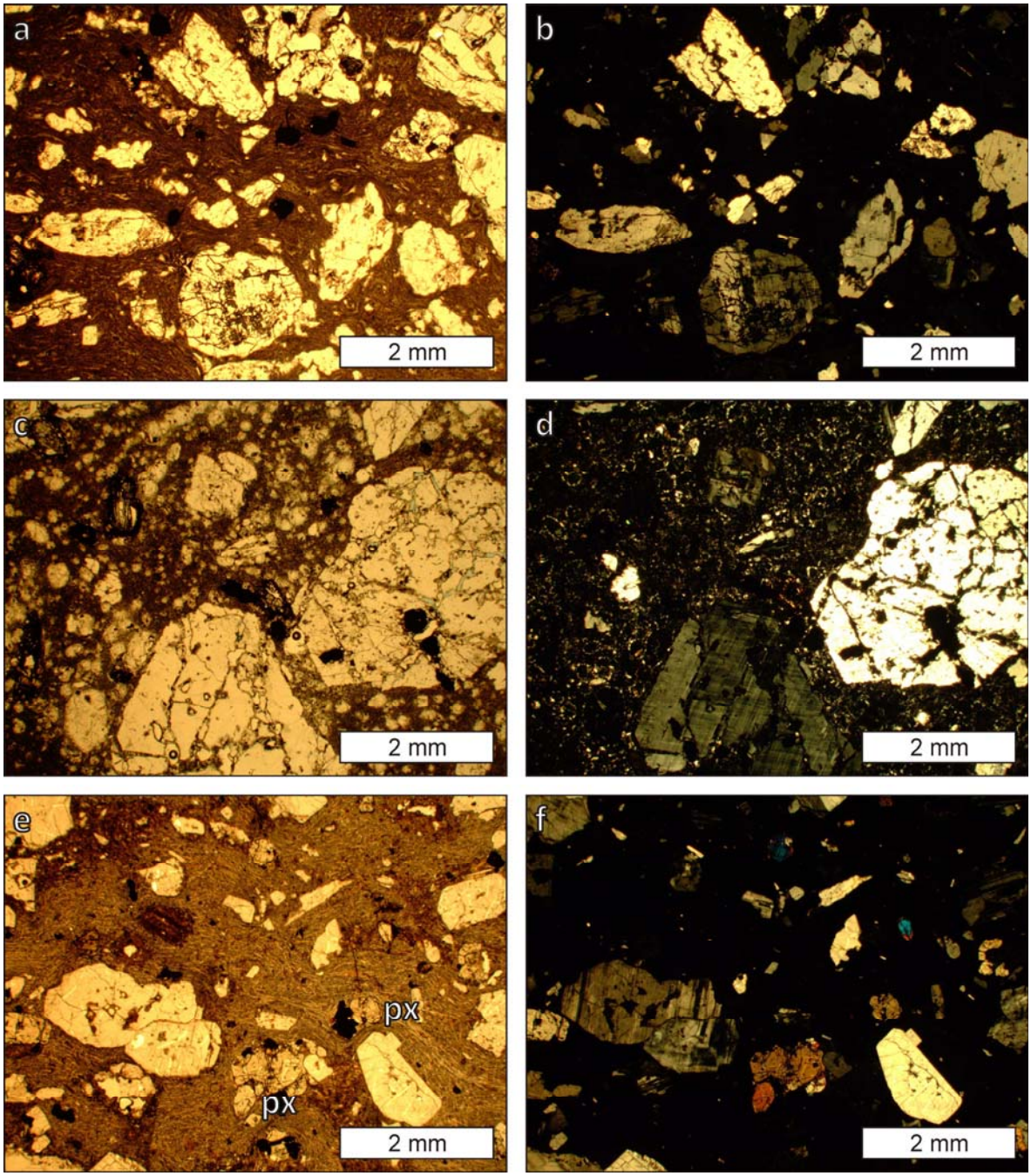

Figure 6.28: Microscope pictures of PC unit. a) crystal-rich welded facies with shard groundmass; c) crystal-rich pumice; e) black facies with pyroxenes, two of them are labelled; b), d) and f) equivalent pictures in cross-polarized light

filled by crystalline silica. These bodies contain the same mineral assemblage as the brown groundmass.

Groundmass is formed by strongly flattened welded shards showing microeutaxitic texture. Devitrification varies from almost inexistent to almost complete, forming a cryptocrystalline granular aggregate of crystalline silica and feldspars. Pumices are always devitrified to coarser aggregates.

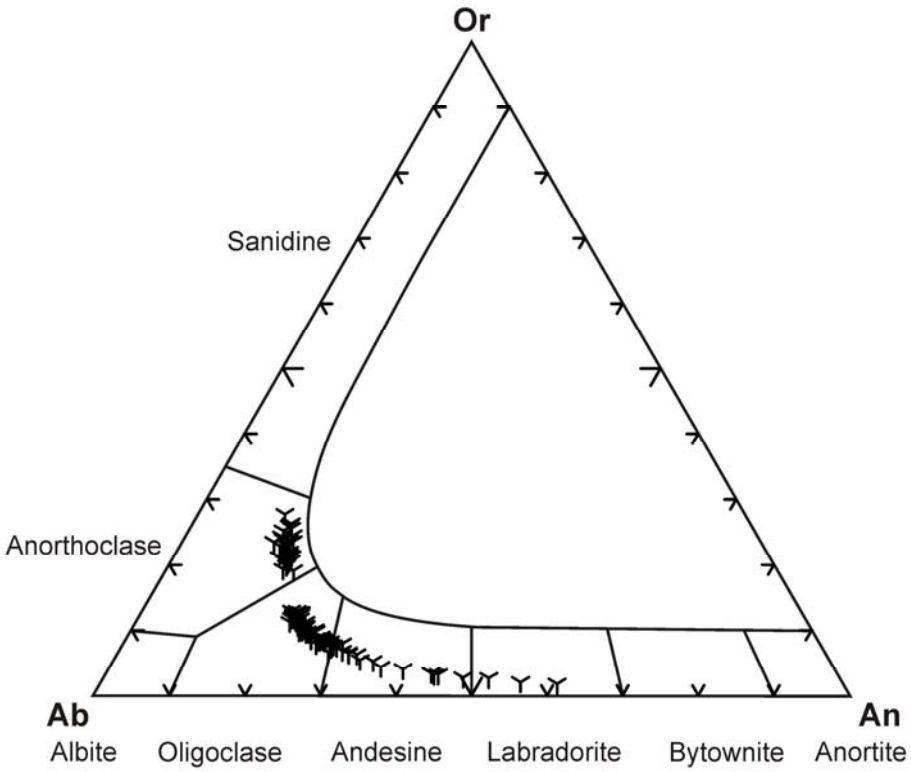

Figure 6.29: Feldspar compositions for PC unit

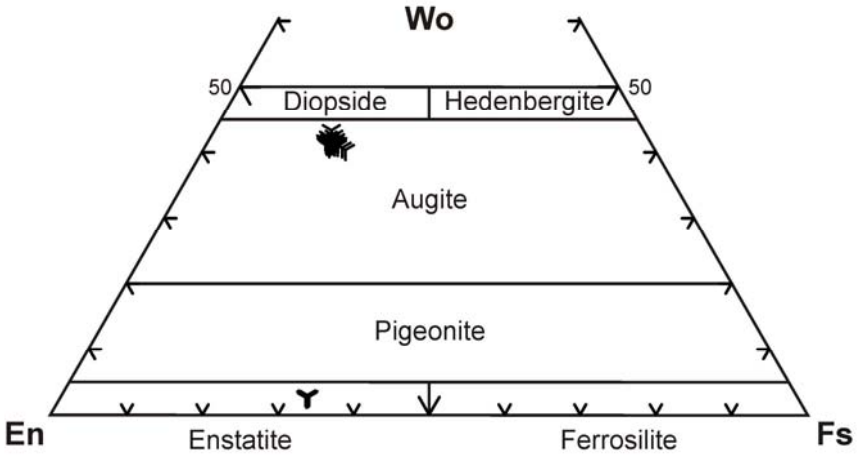

Figure 6.30: Pyroxene compositions for PC unit

6.2.11 Montagna di Capo Rosso (MCR)

The ignimbritic deposits in the MCR unit are moderately welded porphyritic ignimbrites which may be lithic-rich (Fig. 6.31). The high lithic content (5 to 20 vol %) contrasts with the units among which it is deposited, that present very scarce lithics.

Porphyricity (10 to 20 vol %) is given by sanidine (Or_{44-53}) (Fig. 6.32) and plagioclase (An_{21-38}) crystal fragments. Crystal sizes are very variable due to strong fragmentation, ranging from a few mm to <<1mm. Sanidine may present twinning following Carlsbad law, and only some plagioclases show

twinning following albite law. Sanidine is far more abundant than plagioclase, and plagioclase crystals may present sanidine mantles. Opaque minerals are moderately abundant (1-3 vol %). Zircons have been found associated with opaque crystals. The groundmass is heavily devitrified to microgranular aggregates of crystalline silica and feldspar.

Lithic fragments present a wide variety in texture and composition. Some present rounded sharp edges, whereas others appear to have undergone some degree of plastic deformation on

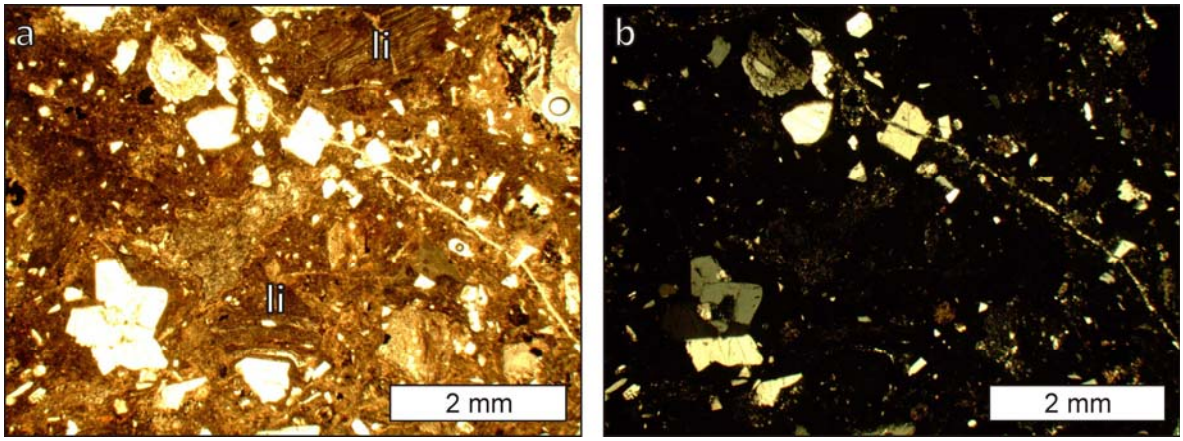

Figure 6.31: Microscope pictures of MCR unit. Moderately welded porphyritic facies with two lithic fragments under plain- (a) and cross- (b) polarized light

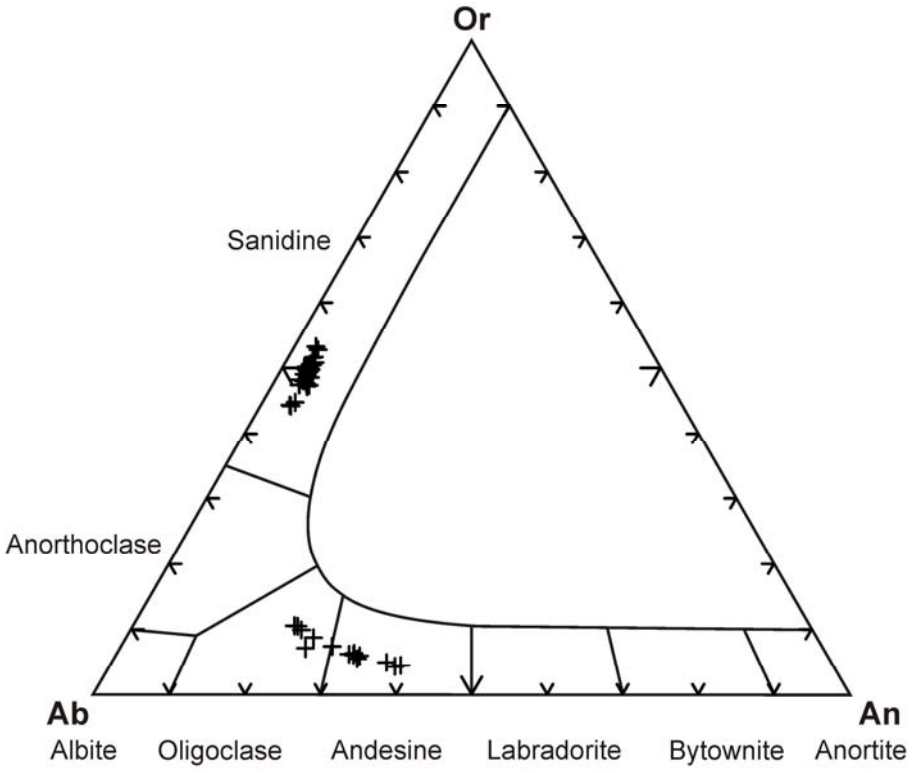

Figure 6.32: Feldspar compositions for MCR unit

emplacement or compaction, being moderately flattened. It is suggested that some of the lithic fragments may be in fact cannibalised fragments of previously deposited portions of the ignimbrite.

6.2.12 Matzaccara (MZ)

The MZ unit is formed by several flow deposits grey in colour which are characterised by the presence of bronze-coloured biotite phenocrysts accompanying plagioclase and opaque minerals crystals (Fig. 6.33). Apart from sharing a common mineralogy, the flows present strong facies diversity, from ash deposits to extremely welded ignimbrites.

Porphyricity varies from less than 3 to 20 vol %. Crystals are oriented with the depositional surface. Plagioclase phenocryst fragments are the dominant phase, with far less biotite and accessory opaques. Plagioclase (An_{21-45}) (Fig. 6.34) occurs as crystals presenting twinning following albite law, and may present zoning, which may be normal or oscillatory. In some facies, plagioclase crystals may present a thin overgrowing of sanidine (Or_{35-42}), which affects only a portion of the crystals. Biotite crystals (#Mg 53-56) are mostly fresh, being only slightly altered to

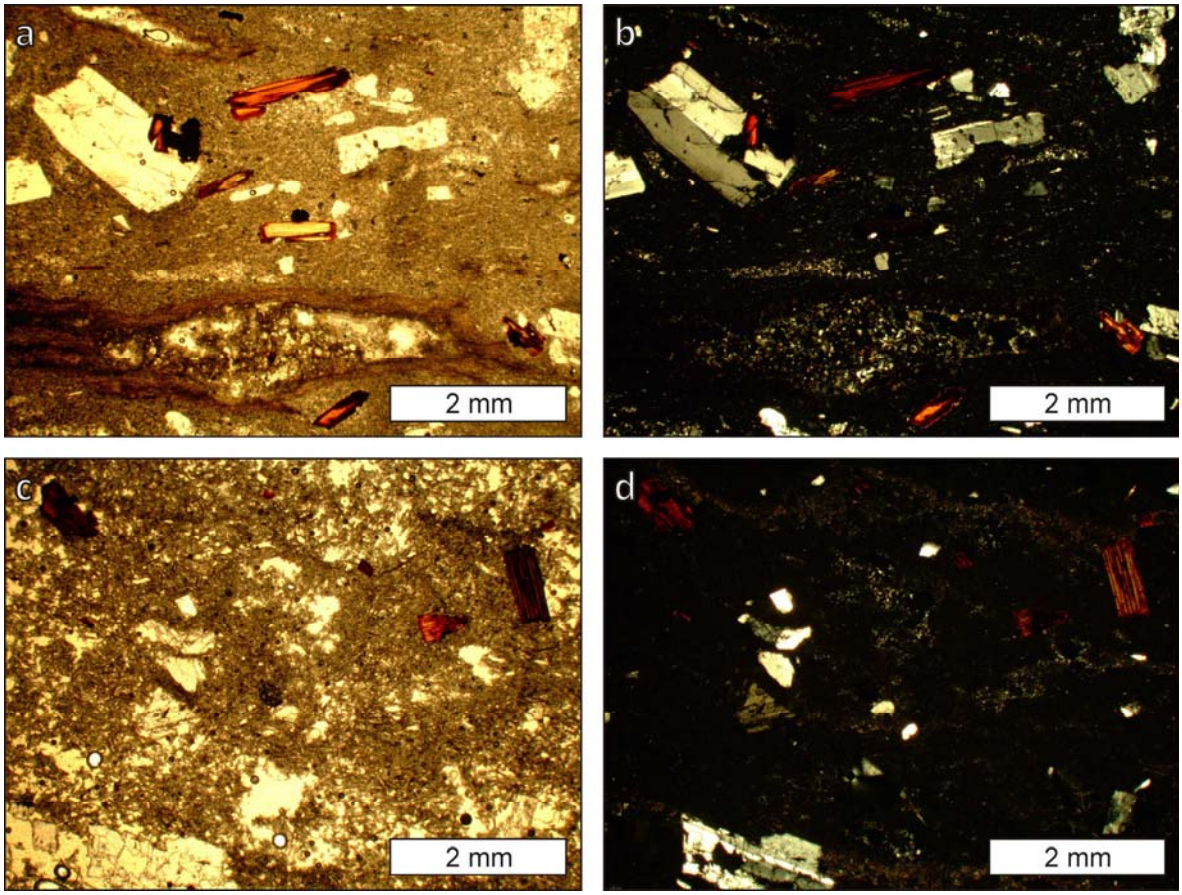

Figure 6.33: Microscope pictures of MZ unit. a) welded facies with dark pumices from San Pietro Island; c) cineritic facies from Santo Antioco Island; b) and d) equivalent pictures under cross-polarized light

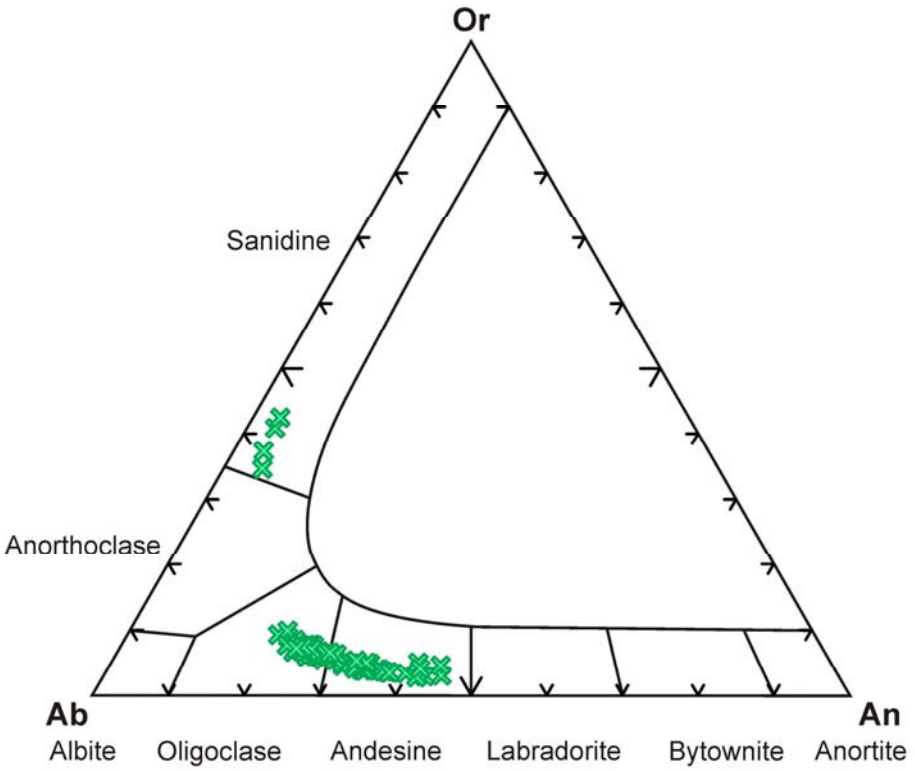

Figure 6.34: Feldspar compositions for MZ unit

oxides. The groundmass containing the phenocrysts is formed by shards of fine ash size, variably devitrified to cryptocrystalline granular or spherulitic aggregates of feldspar and crystalline silica. In welded facies shards may be partially preserved showing a microeutaxitic texture. Pumice content is very variable, from inexistent to 10-20 vol %. When present, pumices are flattened and vesicled, and always devitrified to coarser aggregates than the groundmass. Its colour may vary from light grey to dark reddish grey. Pumices define an eutaxitic texture both at macro and microscale.

6.2.13 Comendites (CO)

Comenditic unit occur as pyroclastic deposits and as lava flows (Fig. 6.35). Mineral assemblage is the same for both populations and consists of sanidine (Or_{35-40}) (Fig. 6.36), with minor quartz and accessory amphiboles and opaque minerals.

Pyroclastic deposits are eutaxitic and vary in porphyricity from less than 5 to 20-30 vol %. Sanidines are short tabular hypidiomorphic to allotriomorphic fragments of phenocrysts which present no zoning and may present twinning following Carlsbad law. Crystal size may reach 5 mm. Quartz is present as hypidiomorphic crystal fragments. Two populations of amphiboles may be recognised: brown prismatic hypidiomorphic phenocrysts and late crystallising green amphiboles.

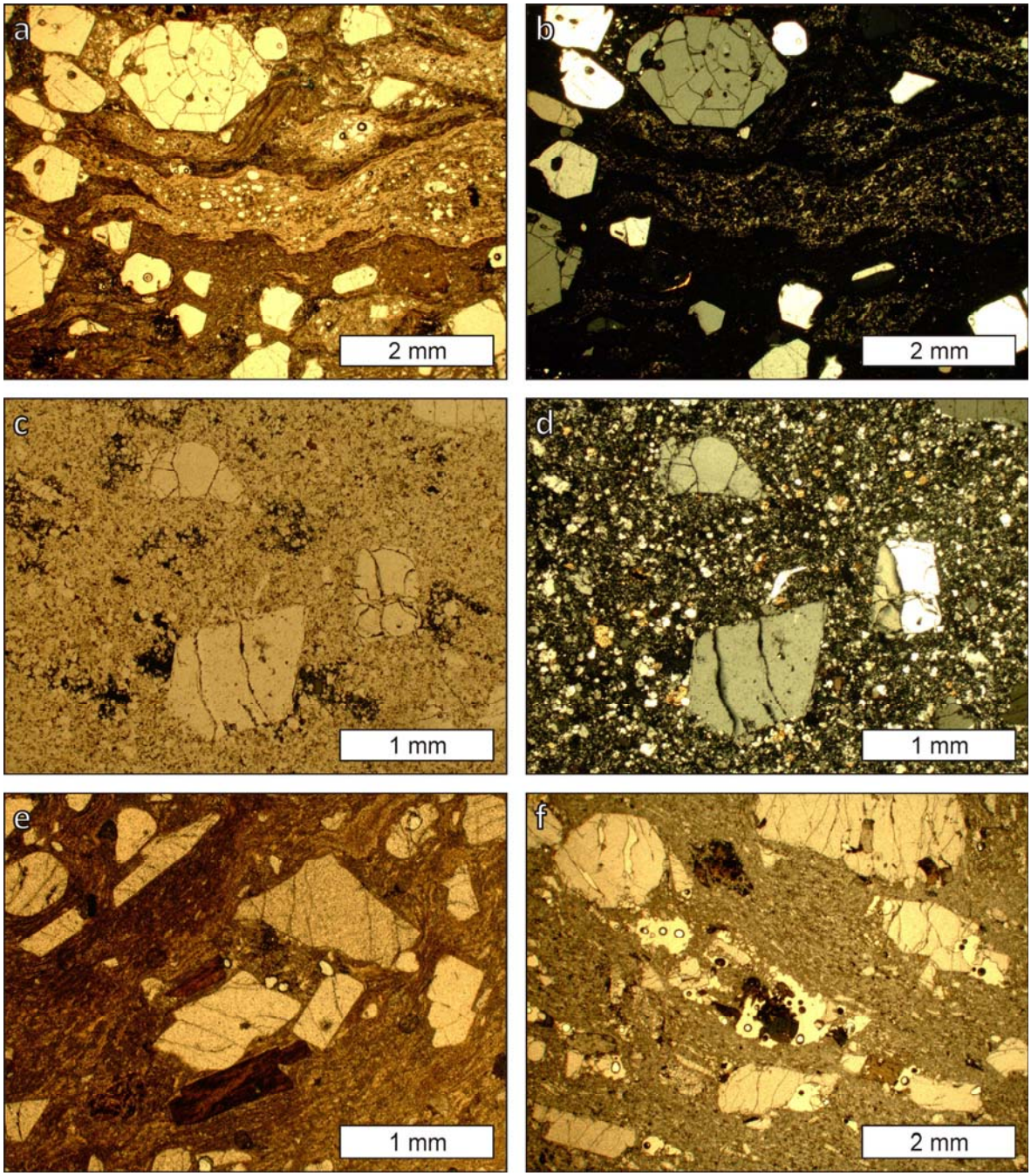

Figure 6.35: Microscope pictures of CO unit. a) and b) pyroclastic welded facies with pumices under plain- (a) and cross- (b) polarized light, the black patches are poikilitic amphibole; c) and d) lava flow facies with poikilitic amphibole under plain- (c) and cross- (d) polarized light; e) pyroclastic facies with amphibole phenocrysts under plain-polarized light; f) pyroclastic facies with amphibole crystals grown in vesicles under plain-polarized light

Its chemical composition was determined in lava flow samples. Green amphiboles seem to have crystallised during devitrification of the groundmass or as a vapour phase in form of allotriomorphic poikilitic flakes. When crystallisation of the green amphibole takes place in a vesicle, crystals tend to develop hypidiomorphic morphologies. Green amphiboles always represent less than 3 vol %, usually less than 1 vol %. The groundmass is formed by shards which

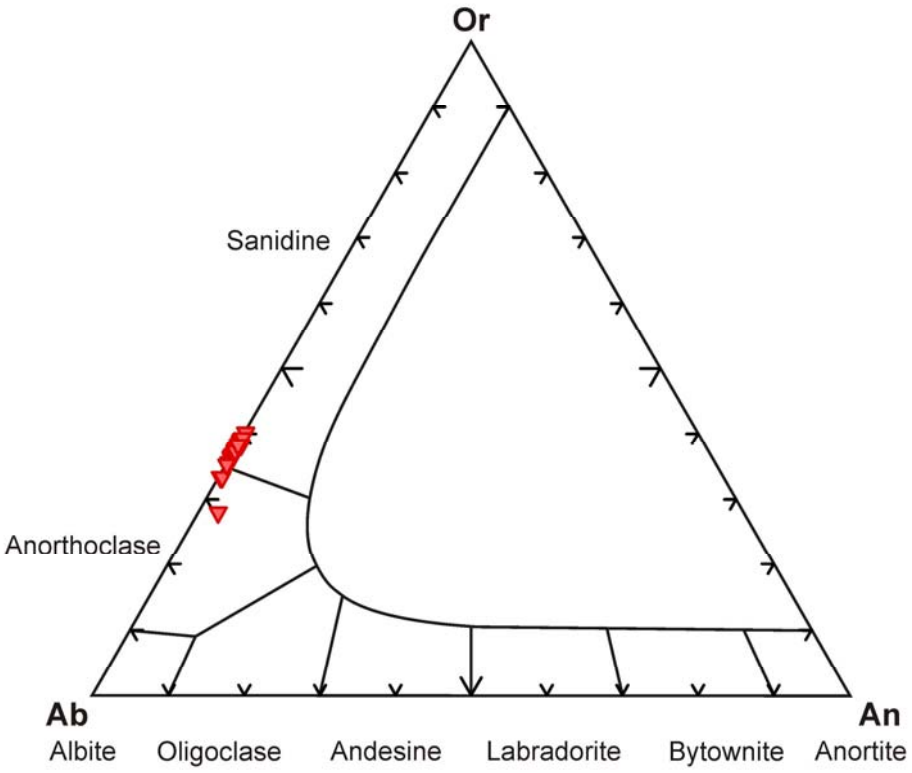

Figure 6.36: Feldspar compositions for CO unit

are variably welded and devitrified. All welding and devitrification degrees occur. The less welded deposits may present up to 20 vol % porosity. Devitrification is to granular crypto- to micro-crystalline felsic aggregates. Pumice content is very variable. When present, pumices are strongly flattened and vesicular with small rounded to elongated vesicles. Pumices are always devitrified to coarser aggregates than the groundmass, and may contain crystals equals to those in the groundmass. Several vitrophyres are present, with variable crystal content, from aphyric to 20 vol % phenocrysts; small pumices may also be present.

Lava flows present high porphyricity, with a content up to 50 vol % in phenocrysts, which as in pyroclastic deposits are dominated by sanidine up to 5 mm long. Sanidine accounts for up to 60-70 vol % of the phenocrysts (Cioni and Funedda, 2005), and it may macroscopically show a blue reflection. Comenditic lavas are holocrystalline, their groundmass is completely devitrified to a microgranular felsic texture. Amphiboles occur as phenocrysts (sodic amphibole, arfvedsonite; partially reabsorbed phenocrysts of sodic-calcic amphibole, ferrorichterite and katophorite) (Fig. 6.37 and Fig. 6.38) in glomerules with sanidine and as green poikilitic flakes (sodic-calcic amphibole, ferrorichterite).

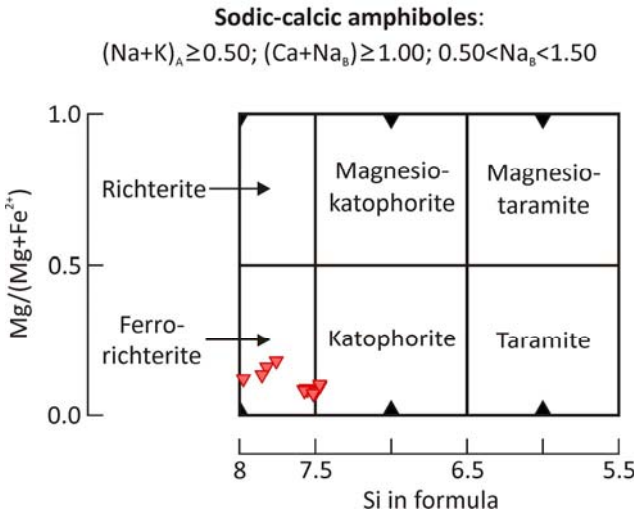

Figure 6.37: Sodic-calcic amphibole compositions in CO unit

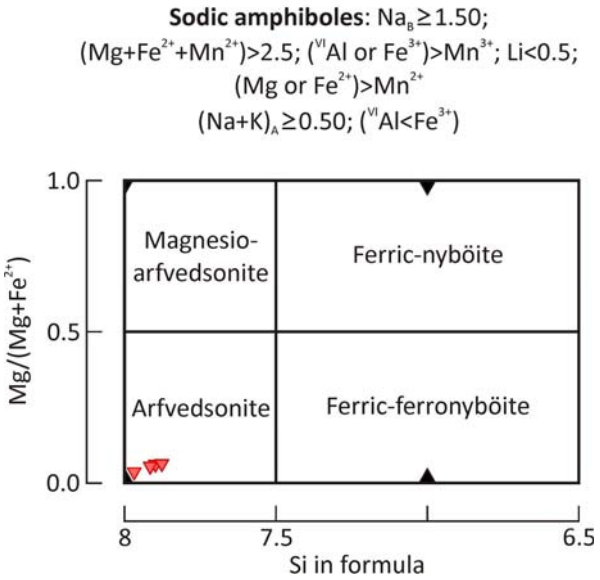

Figure 6.38: Sodic amphibole compositions in CO unit

6.2.14 Monte Ulmus (MU)

Monte Ulmus unit is a strongly welded ignimbrite characterised by a very low porphyricity, which is always less than 3 vol %, and usually less than 1 vol % (Fig. 6.39). Pumice content is also very scarce except for a pumice-rich facies in Santo Antioco.

Porphyricity is given by hypidiomorphic sanidine (Or_{37-41}) (Fig. 6.40) phenocryst fragments usually less than 2 mm in size. Two compositional populations can be seen in Figure 6.40, one with very scarce An content, similar to that in CO, and another with more than 5 % An. However, these do not correspond to two crystal populations; instead, An-rich sanidine is found as zones in regular sanidine crystals. Both populations are represented in Table 6.1. But for the An-rich zones in some

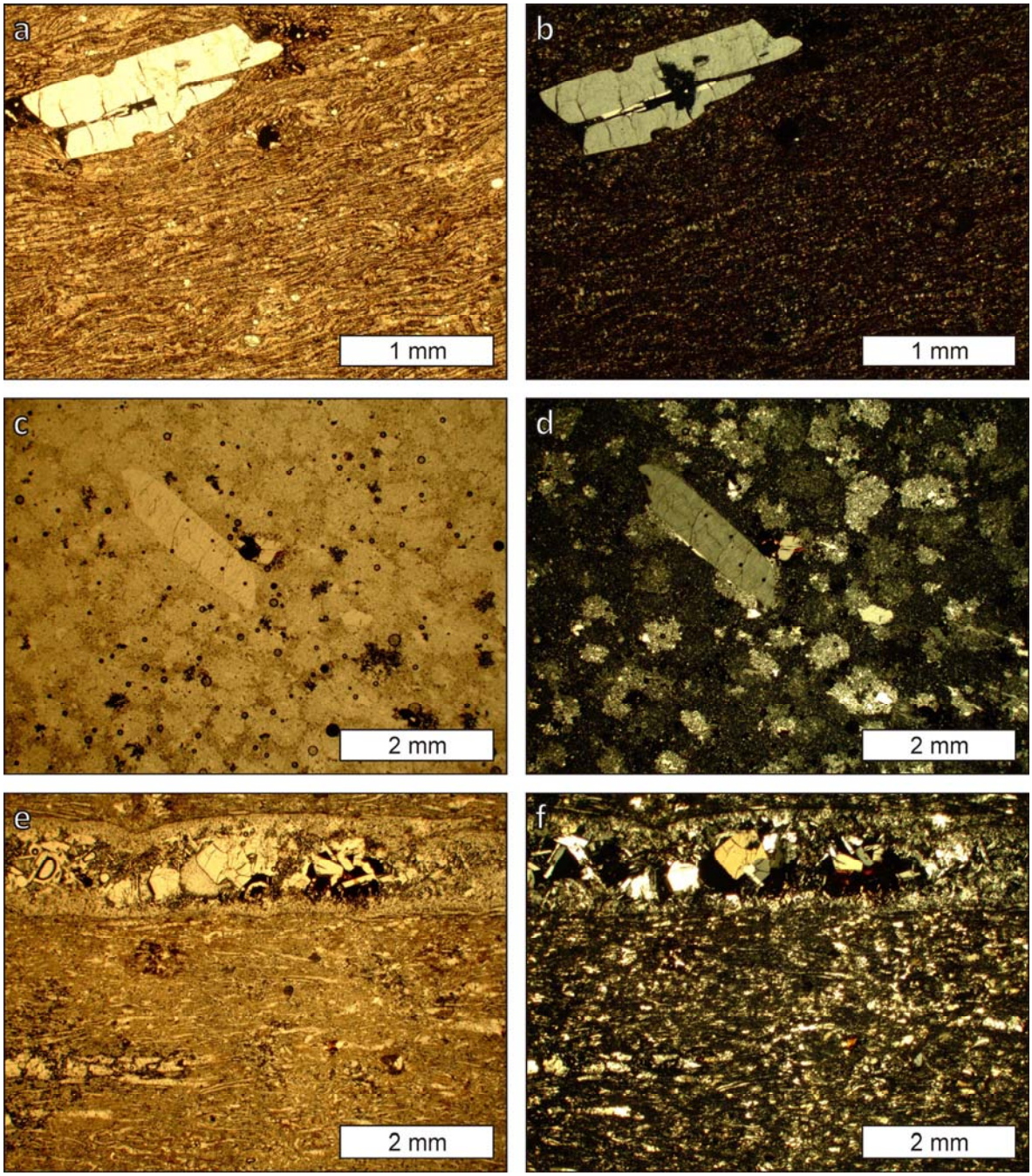

Figure 6.39: Microscope pictures of MU unit. a) base of MU unit in Santo Antioco Island, in pink facies above vitrophyre; c) green facies in Santo Antioco Island with micropoikilitic devitrification texture. Dark patches are altered poikilitic amphibole; e) moderately condensed facies in San Pietro Island showing growth of acicular felsic crystals and amphiboles (altered) in vesicles (miarolitic texture); b), d) and f) equivalent pictures in cross-polarized light

crystals, sanidines are homogeneous and may present twinning following Carlsbad law. Quartz is an accessory phase, like opaque minerals. Occasionally zircon crystals may be found as inclusions in feldspars or opaque minerals. Very small alkaline amphibole flakes can be found growing in the matrix like the ones described for commendites; these are most usually altered to opaque aggregates. The groundmass is formed by flattened welded shards that may be preserved to

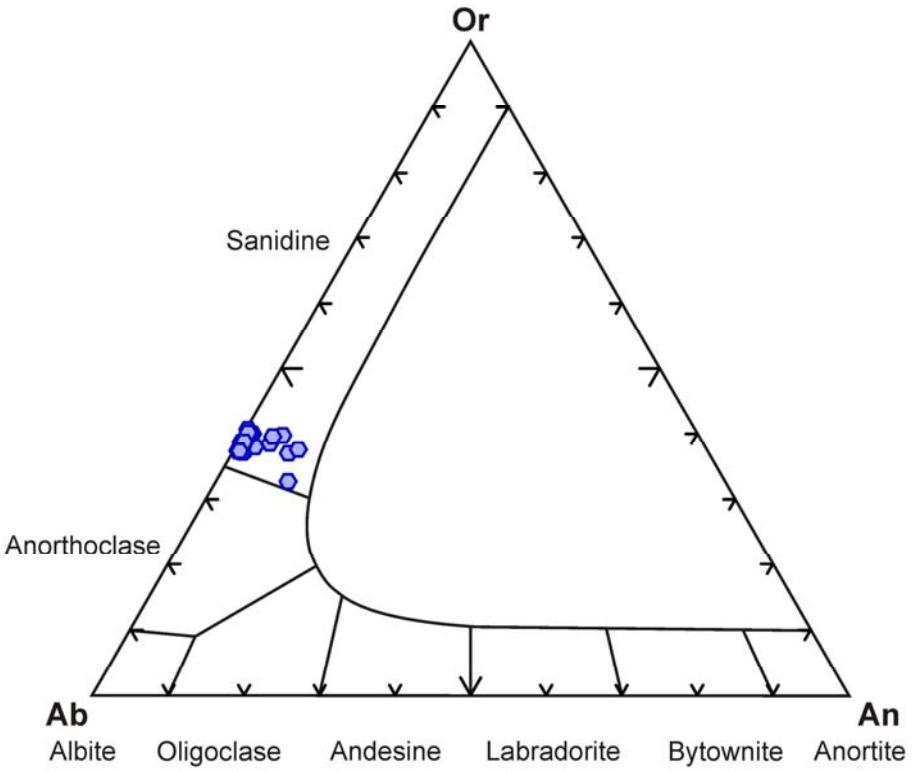

Figure 6.40: Feldspar compositions for MU unit

completely devitrified to microgranular or spherulitic aggregates. In western Santo Antioco MU presents a devitrification pattern that is only found in this unit; the pyroclastic texture is completely obliterated and the groundmass appears formed by a microgranular felsic aggregate displaying round irregular poikilitic patches with homogeneous extinction (micropoikilitic texture, sensu Lofgren, 1971).

Pumices appear strongly to extremely flattened, with vesiculation concentrated in few big flattened vesicles in the middle part of the pumices. Vesicles may be partially filled with hypidiomorphic prismatic silica crystals. Pumices are always devitrified and may show spherulites.

MU vitrophyre is mostly aphyric, with phenocrysts content below 1 vol %. Locally, lithic-rich facies with abundant cm-sized flattened altered pumices occur in San Pietro Island.

6.2.15 Carloforte (CF)

CF unit is a moderately to strongly welded moderately eutaxitic ignimbrite characterised by the presence of vesicular porphyritic black pumices (Fig. 6.41). The sizes of pumices (either black or white) and lithic fragments strongly decrease with distance from the inferred emission site close to the east of La Piramide sector in eastern San Pietro Island, their abundance becoming also lower. Pumices are always strongly flattened (fiamme) with shredded edges.

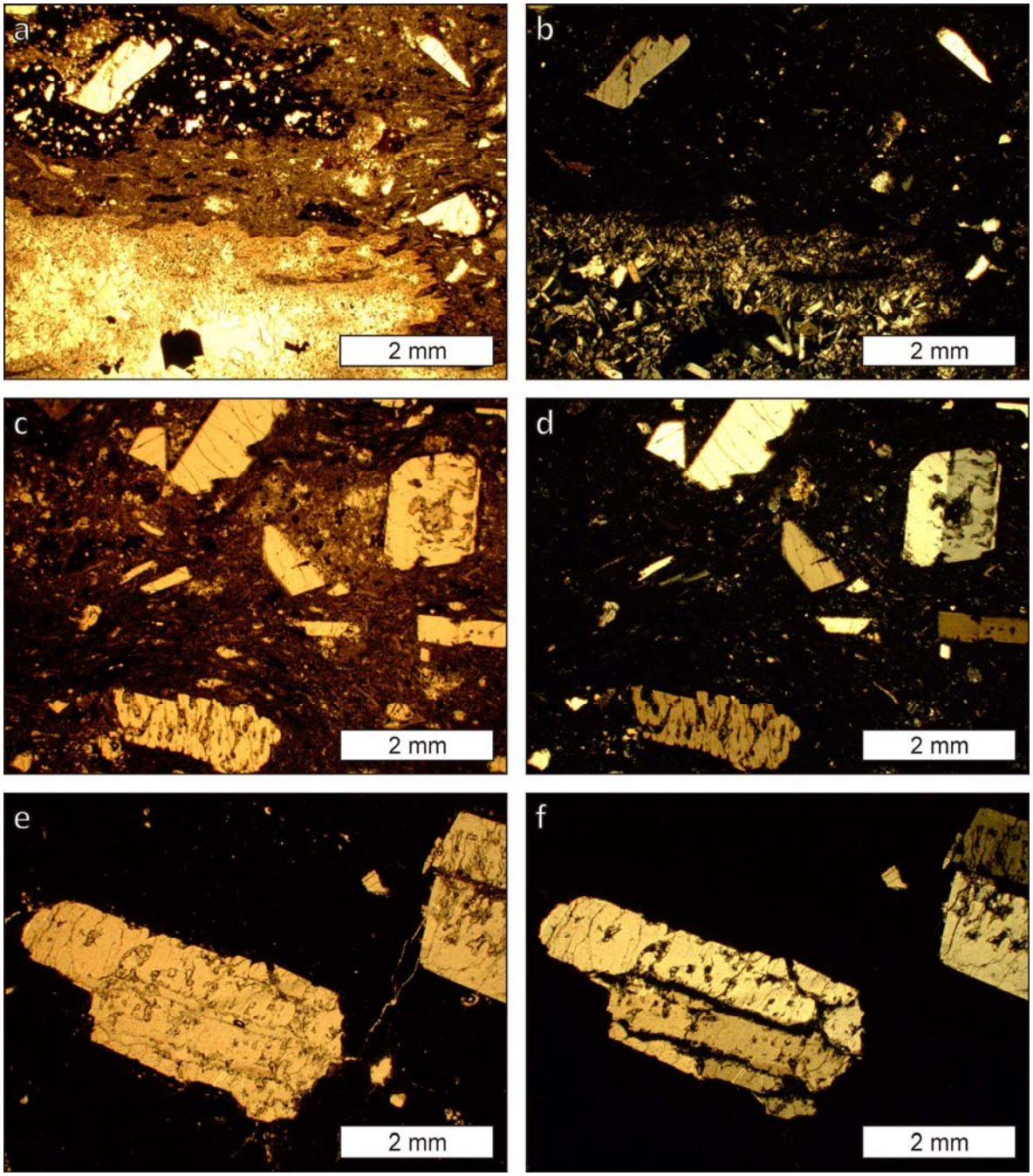

Figure 6.41: Microscope pictures of CF unit. a) strongly welded facies with black and white pumices; c) shard groundmass containing phenocrysts fragments; e) black pumice with big sanidine phenocrysts showing reabsorption texture; b), d) and f) equivalent pictures under cross-polarized light

Black pumices are vesicled (5 to 30 vol %) and contain abundant (up to 30 vol %) clear tabular sanidine (Or_{35-45}) (Fig. 6.42) phenocrysts of up to 1 cm in size that may present twinning following Carlsbad law. They present an An content between 3 and 10 %, which is higher than the one displayed by another sanidine population found only in the matrix, which has a more limited An content (less than 2 %) and a more restricted composition (Or_{37-42}), also showing twinning (both populations are shown in Table 6.2). They show signs of reabsorption, displaying incipient sieve

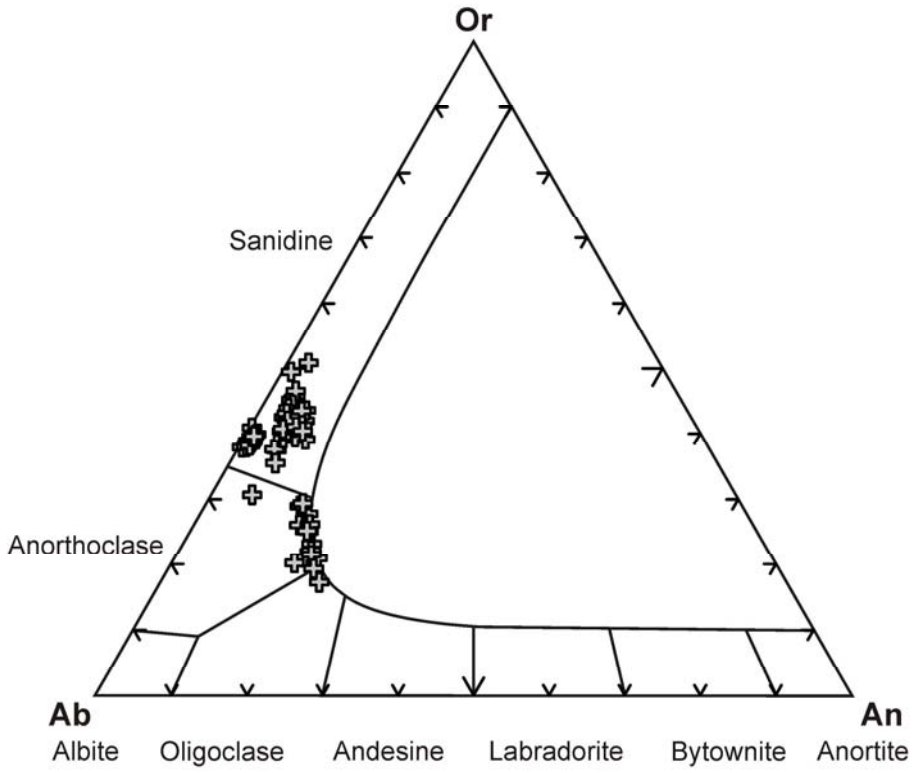

Figure 6.42: Feldspar compositions for CF unit

texture preferentially in the central parts of crystals. Some re-equilibration with the melt took place because slight zoning is evident following corrosion channels. Black pumices are usually not devitrified. Big white pumices may be strongly vesicled (up to 40 vol %) with small rounded vesicles and big vesiculation planes that concentrated gas forming big flattened bubbles which are partially filled by prismatic crystalline silica and minor sanidine crystals (miarolitic texture). Small white pumices tend to have a big central vesicle probably produced by reinflation, which is also partially filled. White pumices are mostly aphyric and devitrified to a microgranular felsic aggregate.

Apart from pumices, the ignimbrite is porphyritic (usually 10 to 20 vol %) with clear tabular sanidine phenocrysts fragments which may show different corrosion degrees, and compositions comprising the two populations previously described. Corroded crystals resemble those found in black pumices. Accessory opaque minerals and extremely scarce strongly corroded anorthoclase, which probably has a xenocryst origin, can be found.

Components are in a cineritic shard groundmass which is partially to totally devitrified to a felsic cryptocrystalline granular aggregate. Shard flattening and welding is strong except in the upper or more distal facies, where deformation is less evident and groundmass porosity appears, the unit gradually losing its eutaxitic character.

6.2.16 Paringianu (PA)

The PA unit is formed by several flow deposits. It is mainly cineritic, with low porphyricity (usually less than 10 vol %), and scarce (usually less than 5 vol %) lithic and pumice content (Fig. 6.43). Pumices may appear as undeformed strongly vesiculated equidimentional pumices or, in some very specific facies, as fiamme. They are always devitrified to a microgranular aggregate of crystalline silica and feldspar. Welding degree varies from inexistent to slight. Porphyricity is given by sanidine (Or_{41-50}) (Fig. 6.44) phenocrysts fragments with accessory plagioclase (An_{16-20}) and opaque minerals. Plagioclase crystals are usually present as nuclei with sanidine (Or_{36-38}) mantles. Zircon and biotite crystals may be found. The groundmass is formed by undeformed to moderately flattened shards usually devitrified to cryptocrystalline felsic granular aggregates, although axiolithic and spherulitic aggregates may occur.

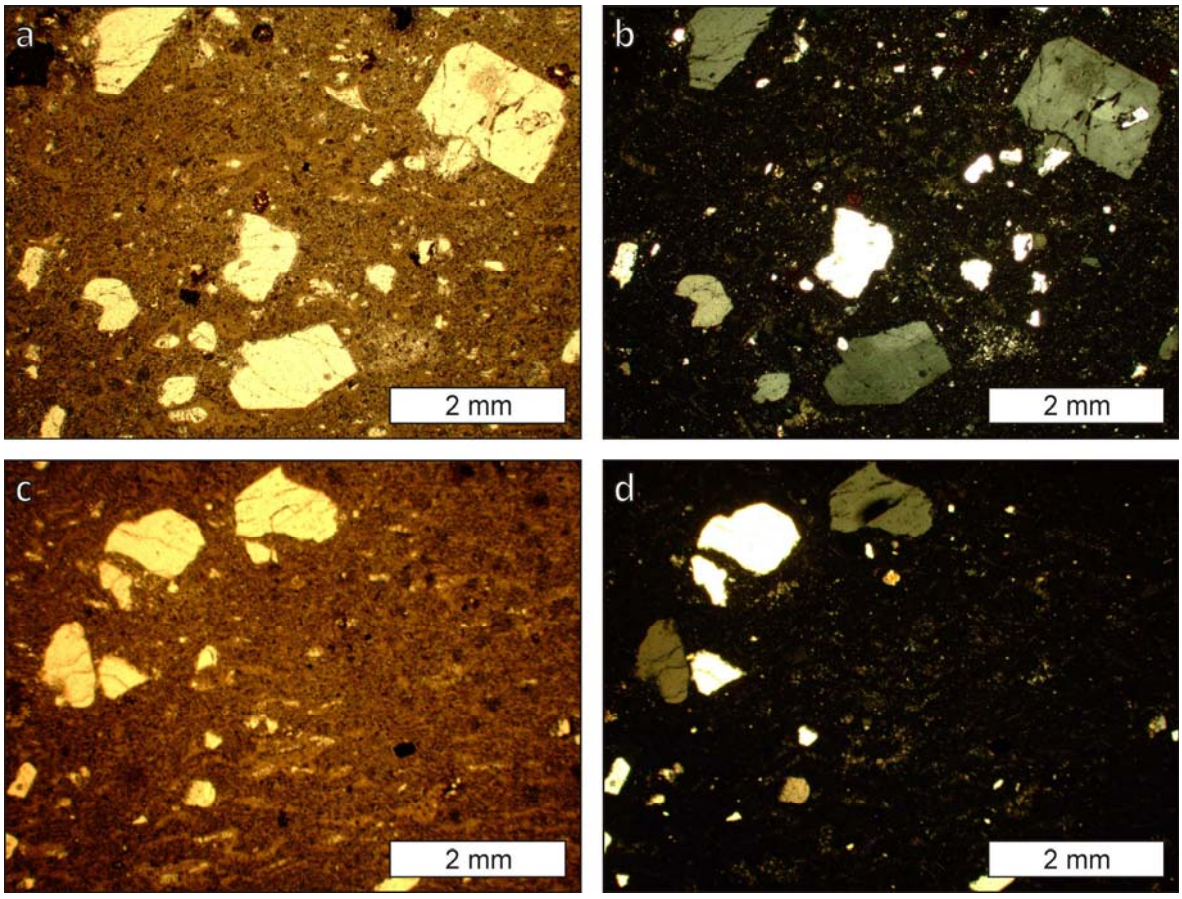

Figure 6.43: Microscope pictures of PA unit. Scarcely to moderately welded facies from San Pietro Island (a) and entroterra (c); b) and d) equivalent pictures under cross-polarized light

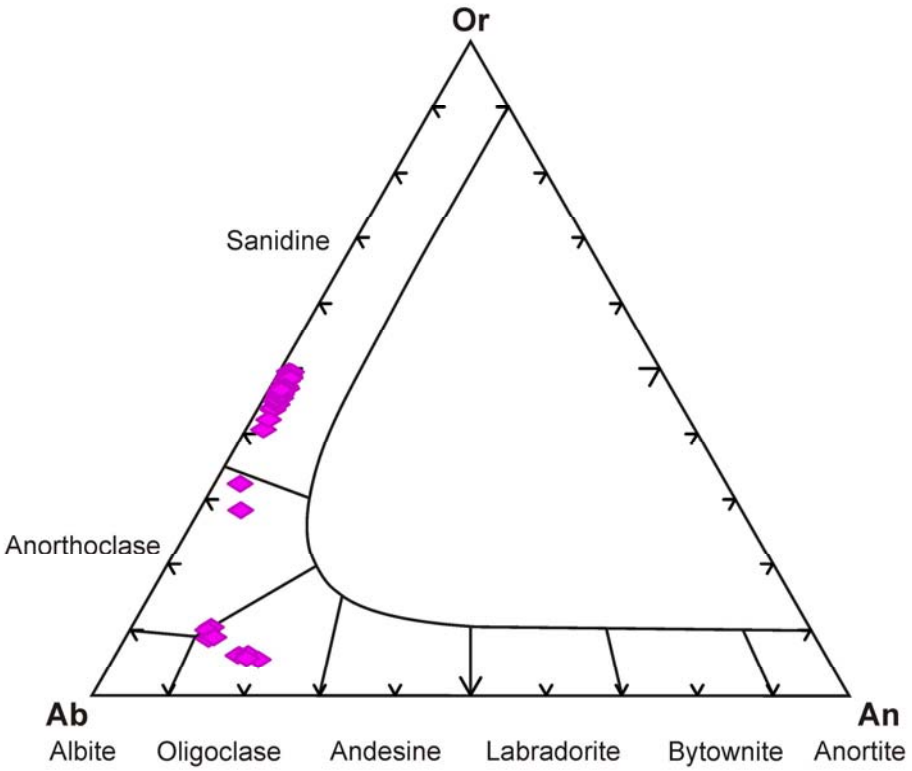

Figure 6.44: Feldspar compositions for PA unit

6.2.17 Serra di Paringianu (SP)

The SP unit is an extremely welded porphyritic strongly eutaxitic ignimbrite for most of its volume. An exception to this are the non-welded facies found in northern San Pietro and Santo Antioco islands (Fig. 6.45).

The dominant welded facies are formed by a groundmass of strongly flattened welded shards containing between less than 1 and 20 vol % crystals up to 5 mm in size, and up to 20 vol % extremely flattened grey pumices varying in length from a few mm to several dm. Porphyricity is given by plagioclase and anorthoclase (continuum between An_{10-32} and Or_{5-30}) (Fig. 6.46) hypidiomorphic phenocrysts fragments, which are found free (dominant) or in glomerules. Most crystals are twinned following albite law, with some anorthoclases following also pericline law, and may present normal zoning. Altered pyroxenes and amphiboles and opaque minerals occur as accessory phases accompanying feldspars. Pumices may be slightly vesicled and contain crystals equal to those in the groundmass. Devitrification mostly affects pumices, which are devitrified to microgranular felsic aggregates, while the glass in the shard groundmass is mostly preserved and only in some samples may present a slight cryptocrystalline devitrification. Locally, spherulitic devitrification may be found.

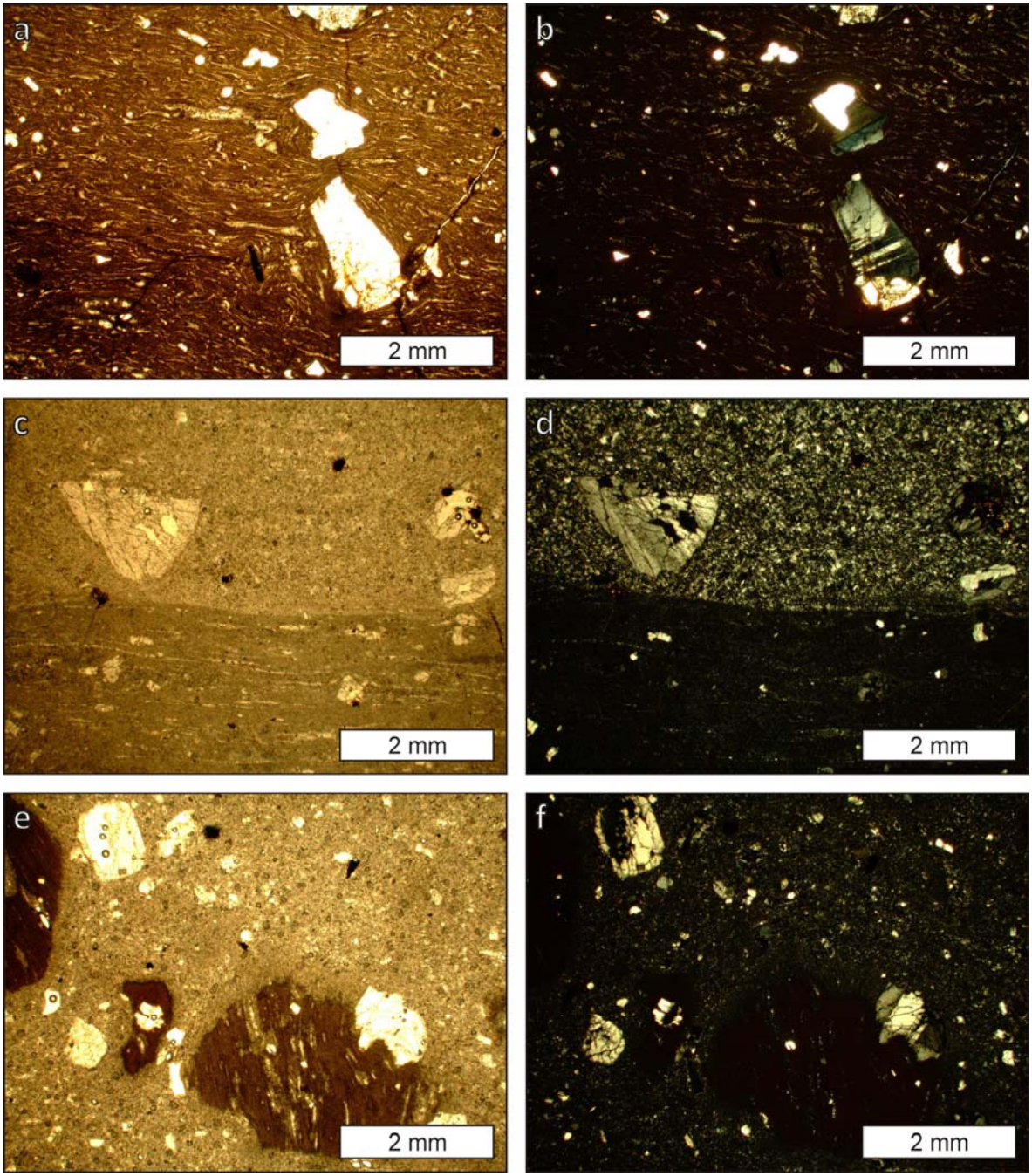

Figure 6.45: Microscope pictures of SP unit. a) strongly welded and eutaxitic brown facies with evidences of rheomorphic flow; c) contact between pumice (upper half) and shard groundmass (lower half) in typical SP facies; e) non-welded facies from San Pietro containing lithic fragments of strongly welded and eutaxitic ignimbrite; b), d) and f) equivalent pictures under cross-polarized light

The non-welded facies consist of a slightly welded, mostly undeformed shard matrix containing the same crystals as the welded facies, variable pumices, and abundant maroon lithic fragments. The lithics are fragments of extremely welded ignimbrite with the same characteristics as the welded facies of the SP unit. Its size varies from less than a mm to some dm.

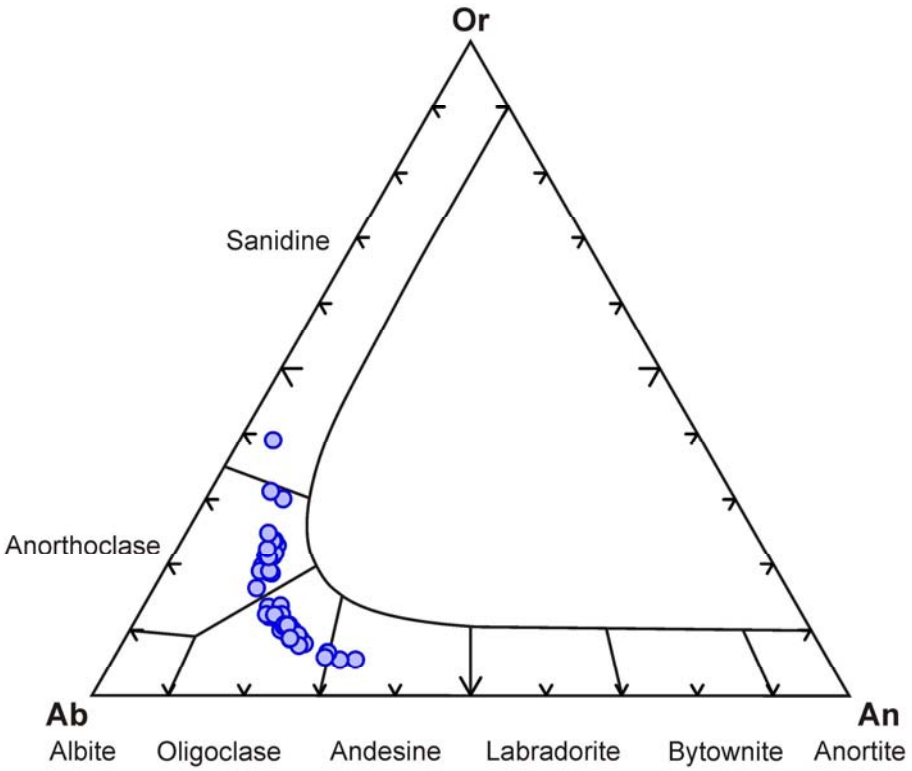

Figure 6.46: Feldspar compositions for SP unit

The vitrophyre of this unit has a low crystal content (1-5 vol %) given by feldspar phenocrysts (few) and small (<0.5 mm) phenocrysts fragments (dominant).

6.2.18 Punta Mingosa (PM)

PM is a moderately welded cineritic ignimbrite (Fig. 6.47). It is formed by a groundmass of shards containing very scarce (less than 3 vol %, mostly far less than 1 vol %) crystals and less than 1 vol % enclaves and pumices. Shards may present no to strong flattening, and are devitrified to a cryptocrystalline felsic aggregate. Devitrification may appear in the more microeutaxitic facies as axiolitic growths following single shards profiles. Porphyricity is given by sanidine, anorthoclase and plagioclase phenocrysts fragments, none of them clearly dominating. Sanidines (Or_{35-49}) (Fig. 6.48) present twinning following Carlsbad law, while anorthoclase and plagioclase (An_{10-17}) show twinning following albite law and may present normal zoning. Anorthoclase and plagioclase may form glomerules. Accessory opaque minerals and zircon occur, and occasionally remnants of altered mafic minerals also appear.

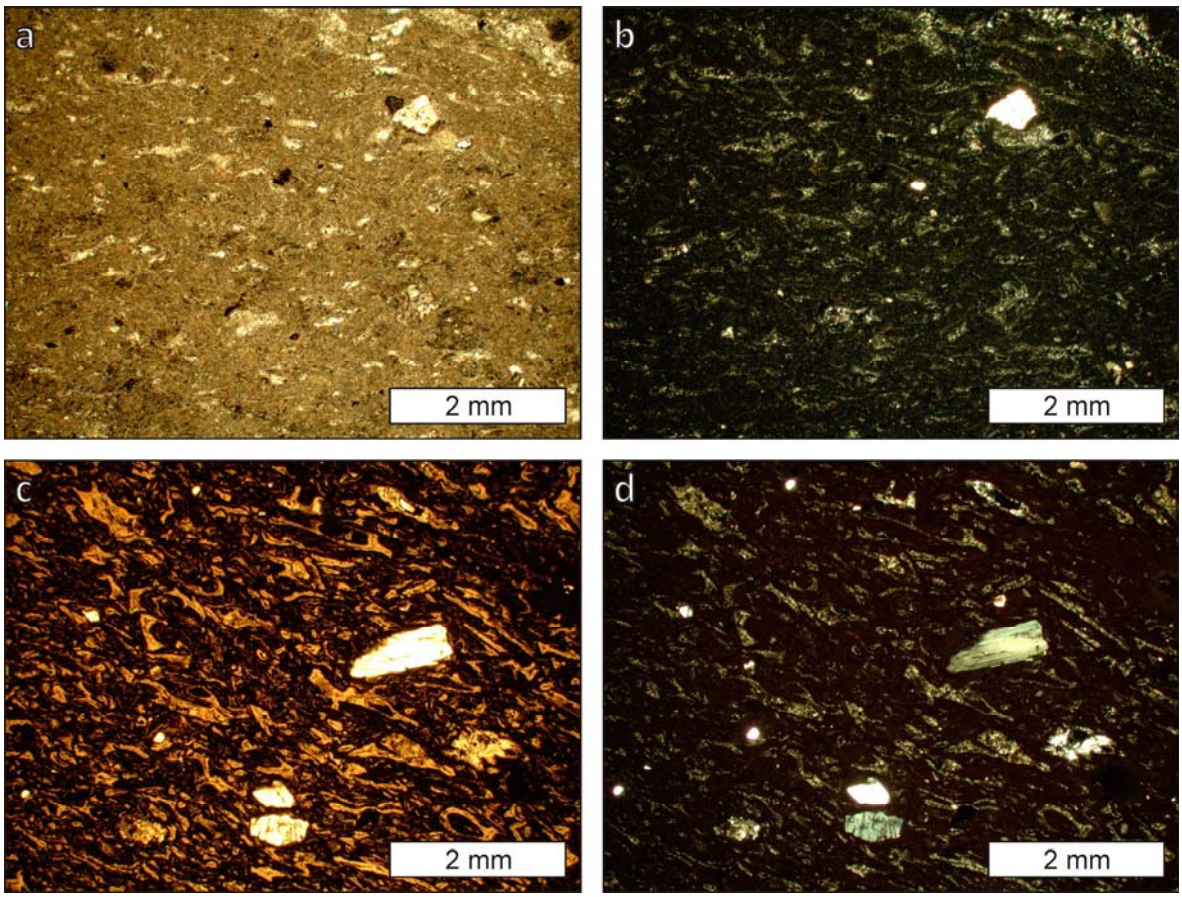

Figure 6.47: Microscope pictures of PM unit. Moderately welded ignimbrite in fine (a) and coarser (c) facies; b) and d) equivalent pictures under cross-polarized light

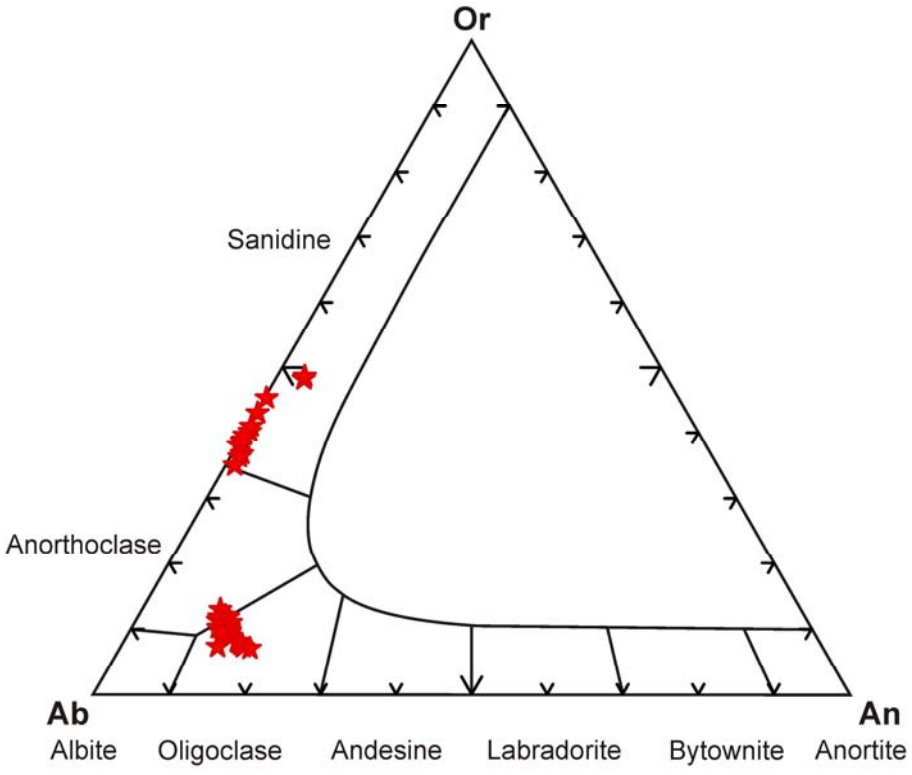

Figure 6.48: Feldspar compositions for PM unit

6.2.19 Punta Geniò and Colonne (PG/CL)

PG and CL units are cineritic moderately welded ignimbrites with 10 vol % porphyricity (Fig. 6.49). Groundmass is formed by scarcely deformed shards partially to totally devitrified to cryptocrystalline felsic granular aggregates which may completely obliterate its original texture. Porosity is abundant among shards. Porphyricity is given by sanidine and plagioclase phenocrysts fragments in similar proportions. Sanidine (Or_{58-64}) (Fig. 6.50) occurs as free crystals with twinning following Carlsbad law. Plagioclase (An_{21-26}) may appear as free crystals or forming glomerules, with twinning following albite law and normal zoning. Less than 1 vol % opaque minerals accompany feldspars. Zircon may be found as inclusions in opaque minerals.

6.2.20 Summary figures

In the previous descriptions diagrams showing mineral compositions only contained one unit at the same time for a better visualization. Figures 6.51, 6.52 and 6.53 show the same diagrams but with all units represented in them at the same time.

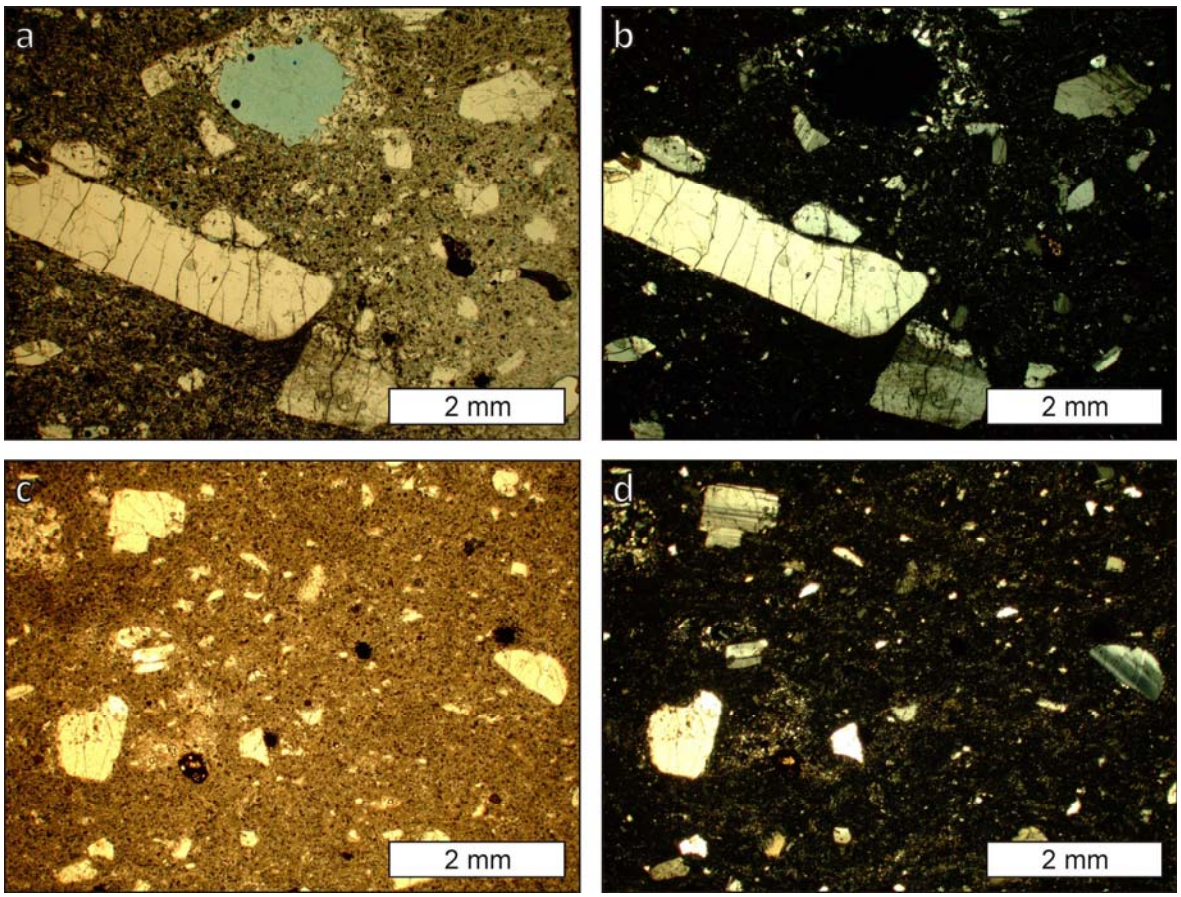

Figure 6.49: Microscope pictures of PG/CL units. a) and c) plain polarized light; b) and d) equivalent pictures under cross-polarized light

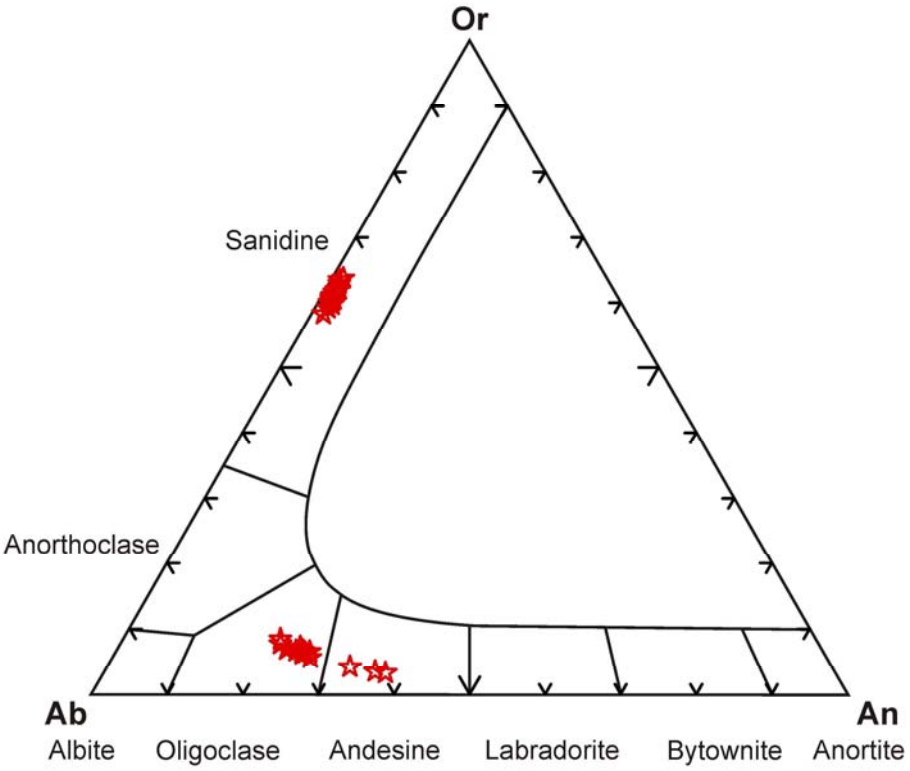

Figure 6.50: Feldspar compositions for PG/CL units

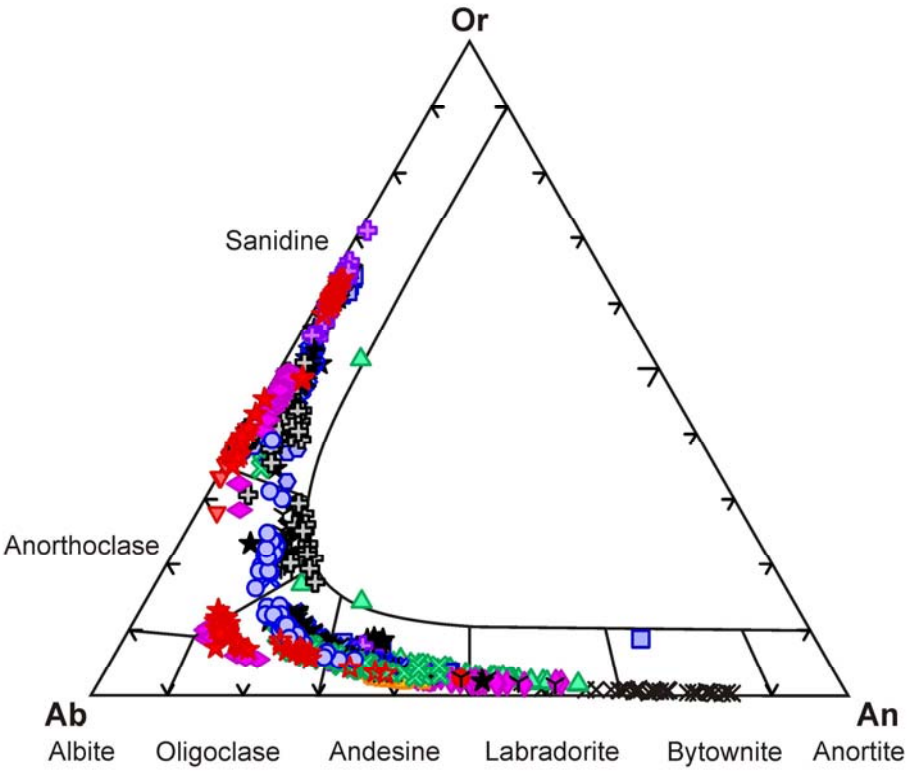

Figure 6.51: Feldspar compositions for all units

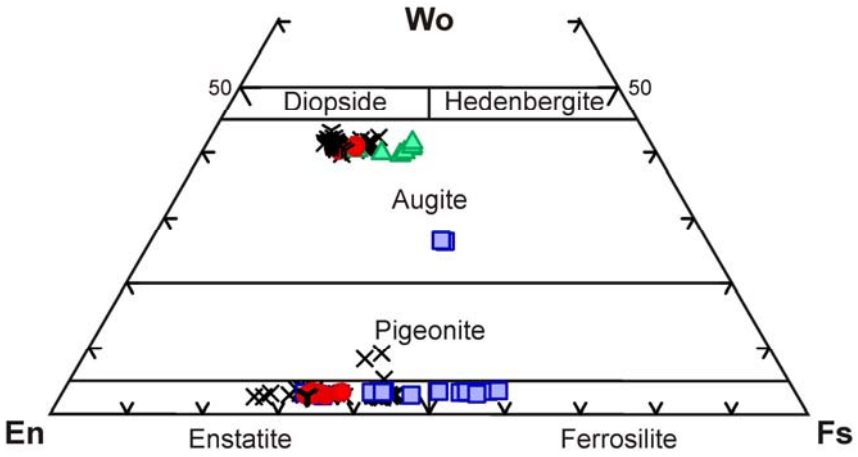

Figure 6.52: Pyroxene compositions for all units presenting them

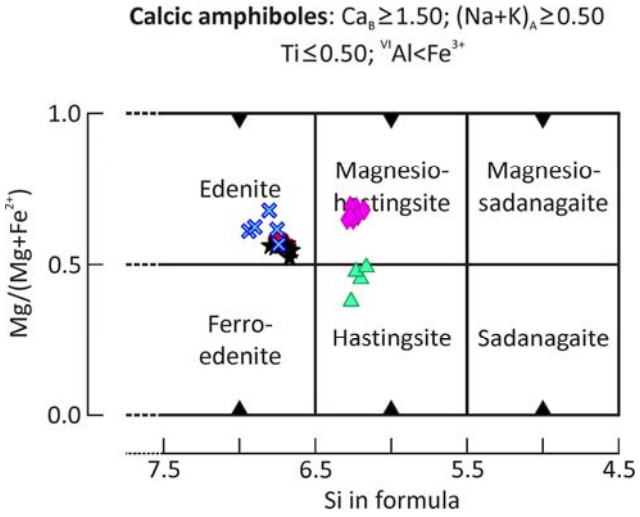

Figure 6.53: Calcic amphibole compositions for all units presenting them

CHAPTER 7: WHOLE ROCK GEOCHEMISTRY

7.1 INTRODUCTION

Data obtained from the whole rock geochemical analyses are presented in this chapter. It must be borne in mind that new sampling and sample selection was done taking into account already available data, which therefore had to be incorporated into the study. New data have allowed a revision of previously published geochemical data, whose aim has been to collect all data that could be incorporated into a comprehensive geochemical database of the Oligocene-Miocene volcanism from the Sulcis area. Subsequent work on the interpretation of the petrogenesis of this magma suite as well as on the development a method for unit recognition based on whole rock geochemistry has been done based on this final database.

In the first section of this chapter new data are presented. Then it is described which of the literature data have been selected to be in the geochemical database. Finally, an initial examination of the results is made by employing the new database. Interpretation of geochemical data will be subsequently dealt with in the corresponding chapters of the discussion part of this Thesis.

7.2 NEW WHOLE ROCK GEOCHEMICAL DATA

In Tables 7.1 and 7.2 results of the geochemical analyses carried out for this study on major and trace elements are reported. However, not all the performed analyses are presented. Only those whose major element sum is over 98 wt % and LOI value is under 2.5 wt % have been considered of enough quality to be used in subsequent work and are therefore shown. A LOI of 2.5 wt % is the limit value fixed in Le Maitre et al. (1989) for a rock which is considered to be fresh. A value above this number means that the rock has been altered to a degree in which mobile elements content may have been distorted, making data unusable for geochemical interpretation.

Sample	FS-22/5	FS-22/8	FS-23/3	FS-24/6	FS-26CFb	FS-30/4	FS-30/2	FS-30/5	FS-30/1	FS-30/3	FS-30/16	FS-32/3	FS-32/2	FS-35/7	FS-37/8
Unit	CO rhyolite	CO rhyolite	NU rhyolite	LE rhyolite	PA rhyolite	SE rhyolite	SE rhyolite	SE rhyolite	SE rhyolite	SE rhyolite	LE rhyolite	SE rhyolite	SE rhyolite	CM rhyolite	CO rhyolite
Major elements (wt %)															
SiO_2	70.69	74.02	71.92	66.53	74.57	69.44	68.19	69.44	69.22	69.42	66.74	70.12	69.09	74.05	73.61
TiO_2	0.37	0.48	0.37	0.50	0.18	0.39	0.47	0.38	0.43	0.37	0.45	0.37	0.42	0.22	0.24
Al_2O_3	12.38	10.23	13.98	15.17	13.80	14.78	15.14	14.95	14.93	14.83	14.78	14.83	14.91	12.02	12.42
Fe_2O_3	4.55	4.17	2.10	3.13	0.74	3.48	3.87	3.23	3.61	3.70	3.65	3.37	3.77	2.88	3.00
MnO	0.06	0.09	0.05	0.06	0.01	0.04	0.04	0.03	0.03	0.04	0.06	0.04	0.04	0.06	0.12
MgO	0.18	<LL	0.12	0.38	<LL	0.01	0.23	0.11	0.25	0.08	0.47	<LL	0.14	<LL	<LL
CaO	0.20	0.09	0.52	2.11	0.22	1.10	1.24	1.17	1.23	1.10	2.06	1.03	1.23	0.04	0.04
Na_2O	4.69	4.15	3.89	3.29	4.40	3.89	3.69	3.82	3.69	3.87	3.24	3.58	3.86	4.21	4.93
K_2O	4.97	4.52	5.87	4.98	5.02	5.11	4.96	5.04	5.11	5.16	4.81	5.13	4.93	4.78	4.98
P_2O_5	0.03	0.02	0.05	0.11	0.02	0.08	0.09	0.07	0.10	0.08	0.10	0.02	0.04	0.02	0.02
LOI	0.85	0.58	0.37	2.03	0.98	0.77	1.04	0.79	0.82	0.69	1.97	0.59	0.68	0.53	0.24
Total	98.97	98.35	99.24	98.29	99.94	99.09	98.96	99.03	99.42	99.34	98.33	99.08	99.11	98.81	99.60
Agpaicity index	1.06	1.15	0.91	0.71	0.92	0.81	0.76	0.79	0.78	0.81	0.71	0.77	0.78	1.01	1.09
Fe_2O_3/FeO^*	0.5	0.5	0.5	0.5	0.5	0.5	0.5	0.5	0.5	0.5	0.5	0.5	0.5	0.5	0.5
Mineral norm (wt %)															
qz	21.69	32.40	23.62	22.00	27.34	22.80	22.72	23.23	23.09	22.45	22.85	25.13	22.63	28.84	24.84
or	30.20	27.83	35.29	30.89	30.00	31.00	30.26	30.58	30.94	31.21	29.87	31.15	29.90	29.06	29.75
ab	39.30	30.37	35.54	31.01	39.97	35.87	34.21	35.23	33.96	35.58	30.58	33.04	35.58	38.45	38.80
an	-	-	2.29	10.24	0.97	5.07	5.75	5.49	5.59	5.05	10.06	5.12	6.00	-	-
crn	-	-	0.45	0.91	0.86	1.17	1.87	1.40	1.49	1.20	0.85	1.75	1.21	-	-
di	0.66	0.26	-	-	-	-	-	-	-	-	-	-	-	0.06	0.05
hyp	4.04	3.50	1.48	2.92	0.32	2.20	3.02	2.29	2.90	2.59	3.66	2.12	2.74	2.05	2.74
acm	3.21	3.76	-	-	-	-	-	-	-	-	-	-	-	0.36	2.62
mag	0.31	-	0.69	1.07	0.24	1.16	1.30	1.08	1.20	1.23	1.24	1.12	1.26	0.83	-
ilm	0.53	0.70	0.52	0.73	0.25	0.56	0.68	0.54	0.61	0.53	0.66	0.53	0.60	0.32	0.34
ttn	-	-	-	-	-	-	-	-	-	-	-	-	-	-	-
ap	0.06	0.04	0.11	0.24	0.04	0.17	0.19	0.15	0.21	0.17	0.22	0.04	0.09	0.04	0.04
rt	-	-	-	-	-	-	-	-	-	-	-	-	-	-	-
NMS	-	1.13	-	-	-	-	-	-	-	-	-	-	-	-	0.81
%An	-	-	6.06	24.82	2.37	12.38	14.38	13.49	14.12	12.44	24.75	13.41	14.42	-	-

Table 7.1: Major element composition and CIPW norm of selected samples of the Sulcis Oligo-Miocene volcanism. Rock classification following Le Maitre et al. (2002). <DL: below detection limit; <LL: below the lower limit of the calibration range

Sample	ANT-1	ANT-2	ANT-3	ANT-4	ANT-5	ANT-8	ANT-9	ANT-10	ANT-11	ANT-12	ANT-13	ANT-14	ANT-15	ANT-16a	ANT-16b
Unit	NU rhyolite	NU rhyolite	NU rhyolite	NU rhyolite	MC rhyolite	PA rhyolite	SP rhyolite	SP rhyolite	SP rhyolite	SP rhyolite	MC rhyolite	MC rhyolite	NU rhyolite	NU rhyolite	NU rhyolite
Major elements (wt %)															
SiO_2	69.66	68.41	69.06	69.37	67.72	68.10	71.58	70.51	70.60	70.08	72.31	68.12	68.93	69.39	69.62
TiO_2	0.50	0.50	0.51	0.51	0.43	0.45	0.38	0.36	0.37	0.37	0.20	0.40	0.50	0.58	0.51
Al_2O_3	15.01	15.32	15.39	15.21	15.66	15.37	14.35	14.53	14.31	14.96	13.94	15.22	15.26	15.26	15.27
Fe_2O_3	2.51	2.67	2.65	2.59	3.39	2.03	2.26	2.43	2.38	2.46	2.16	3.26	2.65	2.26	2.14
MnO	0.03	0.15	0.06	0.03	0.07	0.03	0.06	0.05	0.04	0.02	0.03	0.04	0.04	0.03	0.02
MgO	<LL	0.17	0.20	<LL	0.19	0.21	0.21	0.16	0.18	<LL	<LL	0.22	0.08	<LL	0.23
CaO	0.95	1.14	0.75	0.78	0.98	0.60	0.73	0.68	0.49	0.72	0.57	0.95	0.99	0.93	0.97
Na_2O	4.05	4.26	3.77	3.90	3.67	3.87	4.30	4.29	4.18	4.46	3.34	3.41	4.11	4.15	4.23
K_2O	5.63	5.54	5.82	5.74	6.01	5.88	5.54	5.46	5.54	5.36	5.93	5.78	5.55	5.51	5.62
P_2O_5	0.09	0.06	0.03	0.07	0.10	0.74	0.08	0.07	0.11	0.05	0.05	0.06	0.07	0.05	0.04
LOI	0.42	0.54	1.02	0.58	0.88	2.08	0.14	0.54	0.86	0.48	0.50	1.02	0.54	0.48	0.44
Total	98.84	98.72	99.23	98.77	99.08	99.33	99.61	99.05	99.04	98.95	99.00	98.47	98.70	98.62	99.07
Agpaicity index	0.85	0.85	0.81	0.83	0.80	0.83	0.91	0.89	0.90	0.88	0.85	0.78	0.84	0.84	0.85
Fe_2O_3/FeO^*	0.5	0.5	0.5	0.5	0.5	0.5	0.5	0.5	0.5	0.5	0.5	0.5	0.5	0.5	0.5
Mineral norm (wt %)															
qz	20.92	18.07	21.19	21.41	19.18	22.08	21.56	21.17	22.16	20.24	26.98	22.01	19.95	20.63	19.51
or	33.96	33.37	35.17	34.73	36.41	35.83	33.00	32.81	33.43	32.21	35.95	35.38	33.50	33.27	33.66
ab	37.13	38.99	34.61	35.86	33.75	35.80	38.89	39.22	38.37	40.73	30.73	31.72	37.69	38.09	38.50
an	4.19	5.41	3.62	3.47	4.32	-1.92	3.10	2.94	1.73	3.33	2.58	4.45	4.56	4.42	4.62
crn	0.84	0.43	1.80	1.50	1.77	3.74	0.18	0.56	0.92	0.68	1.24	2.01	0.97	0.98	0.64
di	-	-	-	-	-	-	-	-	-	-	-	-	-	-	-
hyp	1.24	2.03	1.96	1.29	2.63	1.54	1.83	1.85	1.85	1.37	1.41	2.63	1.59	0.95	1.57
acm	-	-	-	-	-	-	-	-	-	-	-	-	-	-	-
mag	0.83	0.88	0.88	0.86	1.13	0.68	0.74	0.80	0.79	0.81	0.72	1.10	0.88	0.75	0.70
ilm	0.71	0.70	0.72	0.73	0.61	0.65	0.53	0.50	0.52	0.52	0.29	0.58	0.71	0.82	0.71
ttn	-	-	-	-	-	-	-	-	-	-	-	-	-	-	-
ap	0.19	0.12	0.05	0.15	0.21	1.60	0.17	0.15	0.24	0.10	0.10	0.13	0.15	0.10	0.08
rt	-	-	-	-	-	-	-	-	-	-	-	-	-	-	-
NMS	-	-	-	-	-	-	-	-	-	-	-	-	-	-	-
%An	10.13	12.18	9.46	8.82	11.34	-5.66	7.38	6.98	4.30	7.57	7.73	12.31	10.78	10.39	10.71

Table 7.1: (Continuation)

Sample	ANT-16c	ANT-17	ANT-18	ANT-19	ANT-20	ANT-21 T	ANT-22	ANT-23	ANT-24	ANT-25	ANT-26	ANT-26+	ANT-27	ANT-30	ANT-31
Unit	NU rhyolite	MU rhyolite	MU rhyolite	MU rhyolite	MU rhyolite	MU rhyolite	MU rhyolite	MU rhyolite	SP rhyolite	MU rhyolite	MU rhyolite	MU rhyolite	MU rhyolite	MU rhyolite	MU rhyolite
Major elements (wt %)															
SiO_2	69.75	71.88	73.67	73.04	73.10	72.79	71.49	71.89	71.48	72.30	74.91	72.24	72.75	72.84	72.18
TiO_2	0.46	0.20	0.19	0.20	0.20	0.19	0.23	0.19	0.36	0.20	0.23	0.29	0.19	0.18	0.20
Al_2O_3	14.88	14.09	11.93	12.60	12.51	12.64	12.71	12.50	14.83	11.42	10.82	12.29	12.55	12.60	12.70
Fe_2O_3	2.45	2.14	2.98	2.98	2.95	3.03	3.00	2.99	2.51	3.94	3.66	2.88	2.81	2.82	3.08
MnO	0.04	0.04	0.04	0.07	0.07	0.08	0.11	0.11	0.02	0.13	0.09	0.10	0.10	0.05	0.09
MgO	<LL	0.15	0.13	<LL	<LL	<LL	0.13	<LL	<LL	0.59	<LL	0.29	0.33	0.31	0.33
CaO	0.84	0.51	0.09	0.19	0.07	<LL	0.19	0.29	0.51	0.27	0.15	0.33	0.14	0.08	0.12
Na_2O	3.98	3.43	4.15	4.48	4.19	4.29	4.22	4.31	4.22	4.35	4.08	5.07	5.10	5.15	5.01
K_2O	5.57	5.87	4.63	4.82	4.98	5.11	5.11	5.03	5.63	4.43	4.70	4.88	5.06	5.01	5.09
P_2O_5	0.05	0.03	0.06	0.07	0.03	0.05	0.06	0.06	0.07	0.08	0.04	0.09	0.06	0.07	0.05
LOI	0.44	0.88	1.22	0.49	0.70	0.68	0.98	0.68	0.54	1.64	0.74	0.55	1.00	0.72	0.63
Total	98.44	99.19	99.07	98.92	98.78	98.83	98.22	98.03	100.15	99.35	99.40	99.01	100.09	99.83	99.48
Agpaicity index	0.84	0.85	0.99	1.00	0.98	0.99	0.98	1.00	0.88	1.05	1.09	1.11	1.10	1.10	1.08
Fe_2O_3/FeO^*	0.5	0.5	0.5	0.5	0.5	0.5	0.5	0.5	0.5	0.5	0.5	0.5	0.5	0.5	0.5
Mineral norm (wt %)															
qz	21.82	26.15	29.21	25.93	27.24	26.00	24.80	25.18	22.19	26.61	31.42	23.53	23.06	23.11	22.06
or	33.72	35.56	28.28	29.16	30.27	31.00	31.30	30.78	33.51	27.09	28.59	29.33	30.19	29.87	30.47
ab	36.66	31.61	38.53	41.15	38.70	39.55	39.29	39.89	38.20	37.43	32.28	38.92	38.98	39.54	39.76
an	3.95	2.37	0.03	0.05	0.16	-0.30	0.57	-	2.07	-	-	-	-	-	-
crn	1.01	1.40	0.09	-	0.20	0.19	0.04	-	1.15	-	-	-	-	-	-
di	-	-	-	0.39	-	-	-	0.85	-	0.68	0.38	0.85	0.24		0.22
hyp	1.29	1.85	2.47	1.91	2.09	2.18	2.54	1.81	1.42	4.91	3.25	2.95	3.42	3.43	3.68
acm	-	-	-	-	-	-	-	0.12	-	2.40	3.26	2.54	2.45	2.46	2.70
mag	0.82	0.71	1.00	0.99	0.99	1.01	1.01	0.96	0.82	0.42	-	-	-	-	-
ilm	0.65	0.28	0.27	0.29	0.29	0.26	0.32	0.27	0.50	0.29	0.33	0.41	0.27	0.25	0.28
ttn	-	-	-	-	-	-	-	-	-	-	-	-	-	-0.04	-
ap	0.10	0.06	0.13	0.14	0.06	0.10	0.13	0.13	0.15	0.17	0.09	0.19	0.13	0.15	0.11
rt	-	-	-	-	-	-	-	-	-	-	-	-	-	0.01	-
NMS	-	-	-	-	-	-	-	-	-	-	0.41	1.27	1.26	1.22	0.73
%An	9.72	6.98	0.08	0.11	0.40	-0.77	1.43	-	5.13	-	-	-	-	-	-

Table 7.1: (Continuation)

Sample	ANT-35	ANT-36	ANT-37	ANT-38	ANT-41	ANT-47	ANT-48	ANT-49	ANT-50	ANT-54	ANT-55	ANT-57	ANT-62	ANT-64	ANT-65
Unit	SP rhyolite	SP rhyolite	SP rhyolite	MU rhyolite	CO rhyolite	MU rhyolite	MU rhyolite	MU rhyolite	MU rhyolite	MU rhyolite	MU rhyolite	CO rhyolite	MZ rhyolite	MZ rhyolite	NU rhyolite
Major elements (wt %)															
SiO_2	69.95	70.38	70.15	71.98	73.52	72.74	72.59	73.00	73.65	73.19	72.70	74.27	72.77	72.19	69.26
TiO_2	0.32	0.36	0.35	0.18	0.21	0.19	0.19	0.18	0.18	0.18	0.19	0.22	0.38	0.44	0.51
Al_2O_3	13.95	14.21	14.27	12.81	10.65	12.78	12.76	12.70	12.76	12.79	12.74	11.31	12.42	13.20	15.10
Fe_2O_3	2.39	2.30	2.41	3.00	3.18	2.99	3.18	2.83	2.90	2.56	2.80	3.32	1.78	2.04	2.79
MnO	0.05	0.04	0.03	0.10	0.08	0.07	0.05	0.06	0.09	0.03	0.02	0.05	0.08	0.07	0.03
MgO	0.26	0.29	0.27	0.27	0.60	0.09<LL	0.11<LL	0.15	0.08<LL	0.11<LL	0.11<LL	0.14	0.37	0.37	0.17
CaO	0.59	0.51	0.55	0.13	0.89	0.15	0.06	0.05	0.08	0.19	0.18	0.08	0.68	0.63	0.95
Na_2O	4.73	4.48	6.02	5.24	3.75	4.46	4.46	4.68	4.48	4.40	4.37	4.19	3.57	3.62	4.13
K_2O	5.50	5.61	5.52	5.16	4.61	5.16	5.14	5.05	5.15	5.09	5.05	4.77	5.02	5.14	5.70
P_2O_5	0.08	0.06	0.18	0.05	0.02	0.02	0.01	0.02	0.02	0.02	0.02	0.03	0.02	0.01	0.05
LOI	1.08	0.87	1.04	1.01	1.58	0.72	0.71	0.82	0.46	0.86	0.91	0.68	2.11	1.21	0.67
Total	98.90	99.11	100.79	99.93	99.09	99.34	99.24	99.54	99.84	99.39	99.06	99.04	99.17	98.91	99.35
Agpaicity index	0.98	0.95	1.11	1.11	1.05	1.01	1.01	1.04	1.01	1.00	0.99	1.07	0.91	0.87	0.86
Fe_2O_3/FeO^*	0.5	0.5	0.5	0.5	0.5	0.5	0.5	0.5	0.5	0.5	0.5	0.5	0.5	0.5	0.5
Mineral norm (wt %)															
qz	18.53	19.63	14.83	21.37	30.24	24.40	24.32	23.96	25.10	25.42	25.28	29.42	29.32	27.80	19.34
or	33.17	33.75	32.32	30.79	28.35	31.09	31.01	30.36	30.83	30.68	30.61	29.00	30.88	31.38	34.25
ab	43.36	40.96	44.88	39.83	32.16	40.09	40.15	40.18	39.74	40.30	40.21	34.59	33.38	33.59	37.68
an	0.60	2.13	-	-	-	-	-	-	-	0.14	0.25	-	3.15	3.16	4.50
crn	-	-	-	-	-	-	-	-	-	-	-	-	-	0.63	0.58
di	1.48	0.04	1.23	0.26	3.57	0.48	0.17	0.10	0.22	0.53	0.41	0.15	0.16	-	-
hyp	1.43	2.10	1.98	3.44	2.81	2.27	2.62	2.88	2.38	1.78	2.00	3.38	1.92	2.10	1.91
acm	-	-	2.07	2.62	2.31	0.60	0.63	2.07	0.78	-	-	2.95	-	-	-
mag	0.79	0.76	-	-	0.21	0.77	0.82	0.16	0.66	0.85	0.93	-	0.60	0.68	0.92
ilm	0.46	0.51	0.48	0.25	0.30	0.26	0.26	0.26	0.25	0.26	0.26	0.31	0.54	0.63	0.72
ttn	-	-	-	-	-	-	-	-	-	-	-	-	-	-	-
ap	0.17	0.13	0.37	0.11	0.04	0.04	0.02	0.04	0.04	0.04	0.04	0.06	0.04	0.02	0.10
rt	-	-	-	-	-	-	-	-	-	-	-	-	-	-	-
NMS	-	-	1.84	1.32	-	-	-	-	-	-	-	0.14	-	-	-
%An	1.37	4.95	-	-	-	-	-	-	-	0.35	0.61	-	8.62	8.61	10.66

Table 7.1: (Continuation)

Sample	ANT-66	ANT-67	ANT-68	ANT-70	ANT-71	ANT-79	ANT-81	ANT-82	ANT-85	ANT-90	ANT-94	ANT-95	ANT-96	ANT-99	ANT-100
Unit	NU rhyolite	SP rhyolite	NU rhyolite	MZ rhyolite	MC rhyolite	SP rhyolite	SP rhyolite	SP rhyolite	CO rhyolite	CO rhyolite	CO rhyolite	CO rhyolite	CO rhyolite	MU rhyolite	CO rhyolite
Major elements (wt %)															
SiO_2	68.71	71.46	69.49	68.42	71.15	70.65	71.18	70.32	72.38	73.47	74.26	74.22	73.75	73.14	73.93
TiO_2	0.50	0.34	0.50	0.53	0.19	0.34	0.37	0.36	0.25	0.21	0.23	0.20	0.23	0.18	0.21
Al_2O_3	15.64	14.50	15.21	15.70	14.38	14.42	15.05	14.65	12.12	10.60	11.21	10.80	11.56	12.01	11.20
Fe_2O_3	2.79	2.22	2.66	2.64	2.17	2.25	2.31	2.36	3.44	4.19	3.15	3.74	3.23	2.82	3.31
MnO	0.03	0.03	0.03	0.06	0.03	0.04	0.02	0.02	0.06	0.13	0.09	0.13	0.05	0.03	0.09
MgO	0.1<LL	0.10<LL	0.11<LL	0.28	0.09<LL	0.19	0.07<LL	0.09<LL	0.21	0.11<LL	0.15	0.12<LL	0.13<LL	0.17	0.11<LL
CaO	0.67	0.52	0.80	0.86	0.48	0.60	0.75	0.61	0.11	0.20	0.13	0.14	0.13	0.10	0.15
Na_2O	3.89	4.28	4.19	4.76	3.24	4.38	4.41	4.40	4.06	4.25	4.05	4.18	4.21	4.32	4.26
K_2O	5.80	5.71	5.76	5.26	6.02	5.64	5.66	5.55	4.77	4.69	4.75	4.74	4.77	4.76	4.69
P_2O_5	0.02	0.02	0.03	0.02	0.02	0.03	0.02	0.03	0.02	0.02	0.03	0.02	0.03	0.03	0.01
LOI	1.11	0.50	2.00	0.88	0.91	0.75	0.73	0.51	1.07	0.90	0.68	0.66	0.78	1.09	0.43
Total	99.25	99.68	100.77	99.39	98.66	99.27	100.54	98.88	98.48	98.76	98.69	98.94	98.87	98.63	98.39
Agpaicity index	0.81	0.91	0.86	0.86	0.82	0.92	0.89	0.90	0.98	1.14	1.05	1.11	1.05	1.02	1.08
Fe_2O_3/FeO*	0.5	0.5	0.5	0.5	0.5	0.5	0.5	0.5	0.5	0.5	0.5	0.5	0.5	0.5	0.5
Mineral norm (wt %)															
qz	20.47	21.40	19.33	16.62	26.25	20.20	20.02	20.25	27.72	30.01	30.12	30.44	28.56	27.42	29.40
or	35.08	34.10	34.55	31.46	36.71	33.86	33.54	33.38	29.29	28.77	29.01	28.93	29.08	29.06	28.65
ab	35.76	38.85	38.20	43.23	30.06	39.92	39.72	40.18	37.84	31.27	34.28	31.97	36.03	38.75	34.55
an	3.27	2.48	3.83	4.16	2.30	2.80	3.58	2.86	0.43	-	-	-	-	-	-
crn	2.00	0.42	0.77	0.74	1.94	0.12	0.39	0.43	0.15	-	-	-	-	-	-
di	-	-	-	-	-	-	-	-	-	0.70	0.38	0.47	0.37	0.25	0.56
hyp	1.74	1.51	1.66	2.12	1.70	1.81	1.44	1.55	3.00	4.04	3.13	3.74	3.01	2.58	3.17
acm	-	-	-	-	-	-	-	-	-	3.76	2.64	3.34	2.35	1.10	2.96
mag	0.93	0.73	0.88	0.87	0.73	0.74	0.75	0.78	1.16	-	0.06	-	0.20	0.53	-
ilm	0.71	0.48	0.71	0.75	0.27	0.48	0.51	0.51	0.36	0.30	0.32	0.29	0.33	0.25	0.30
ttn	-	-	-	-	-	-	-	-	-	-	-	-	-	-	-
ap	0.04	0.04	0.06	0.04	0.04	0.06	0.04	0.06	0.04	0.04	0.05	0.04	0.06	0.06	0.02
rt	-	-	-	-	-	-	-	-	-	-	-	-	-	-	-
NMS	-	-	-	-	-	-	-	-	-	1.09	-	0.78	-	-	0.39
%An	8.38	5.99	9.12	8.78	7.11	6.56	8.26	6.64	1.13	-	-	-	-	-	-

Table 7.1: (Continuation)

Sample	ANT-101	ANT-105	ANT-106	ANT-108	ANT-109	ANT-110	SU-1	SU-2	SU-3	SU-4	SU-5	SU-8	SU-12a	SU-12b	SU-13b
Unit	CO	CO	CO	MU	MU	MU	NU	NU	NU	NU	NU	NU	NU	NU	NU
	rhyolite	rhyolite	rhyolite	rhyolite	rhyolite	rhyolite	rhyolite	rhyolite	rhyolite	rhyolite	rhyolite	rhyolite	rhyolite	rhyolite	rhyolite
Major elements (wt %)															
SiO_2	73.67	71.58	72.82	71.34	71.15	73.13	71.09	70.97	71.04	70.30	70.23	68.80	71.90	71.43	71.50
TiO_2	0.21	0.23	0.23	0.20	0.18	0.17	0.41	0.44	0.41	0.44	0.48	0.51	0.38	0.39	0.40
Al_2O_3	11.16	11.45	11.35	13.44	13.06	12.76	13.71	13.72	13.81	14.15	14.33	14.99	13.70	13.82	13.78
Fe_2O_3	3.31	3.72	3.44	3.18	3.18	3.03	2.11	2.11	2.10	2.68	2.71	2.65	2.21	2.16	2.11
MnO	0.03	0.09	0.07	0.05	0.07	0.07	0.06	0.06	0.04	0.02	0.03	0.02	0.03	0.06	0.05
MgO	0.11<LL	0.29	0.22	0.12<LL	0.17	0.12<LL	0.24	0.24	0.24	0.21	0.37	0.16	0.22	0.22	0.25
CaO	0.08	0.09	0.10	0.05	0.02<LL	0.06	0.63	0.65	0.40	0.45	0.52	0.86	0.44	0.57	0.54
Na_2O	4.01	4.39	4.49	4.12	4.71	4.45	3.89	3.94	3.74	3.62	3.61	3.99	3.82	3.94	3.81
K_2O	4.71	4.95	4.77	5.30	5.22	5.03	5.80	5.74	5.81	5.75	5.80	5.60	5.81	5.79	5.78
P_2O_5	0.03	0.03	0.01<LL	0.02	0.02	0.02	0.05	0.05	0.04	0.03	0.04	0.06	0.04	0.05	0.05
LOI	0.71	2.42	1.45	1.32	1.08	0.80	0.36	0.20	0.76	0.92	0.80	0.68	0.54	0.32	0.48
Total	98.01	99.22	98.93	99.11	98.84	99.63	98.33	98.09	98.37	98.55	98.89	98.31	99.07	98.72	98.73
Agpaicity index	1.05	1.10	1.10	0.93	1.02	1.00	0.92	0.92	0.90	0.86	0.85	0.84	0.92	0.92	0.91
Fe_2O_3/FeO^*	0.5	0.5	0.5	0.5	0.5	0.5	0.5	0.5	0.5	0.5	0.5	0.5	0.5	0.5	0.5
Mineral norm (wt %)															
qz	30.18	25.90	27.53	24.56	21.45	25.17	22.91	22.79	24.22	24.22	23.57	20.56	24.28	23.05	23.95
or	29.02	30.48	29.16	32.25	31.63	30.29	35.17	34.82	35.39	35.07	35.18	34.04	35.07	34.92	34.98
ab	34.48	34.72	35.01	38.14	41.55	40.67	35.85	36.28	34.63	33.58	33.31	36.81	35.05	36.11	35.04
an	-	-	-	0.10	-	-	2.88	2.90	1.81	2.10	2.36	3.99	1.97	2.56	2.42
crn	-	-	-	1.00	-	-	-	-	0.82	1.38	1.43	1.07	0.47	0.18	0.44
di	0.17	0.22	0.36	-	-	0.14	0.02	0.04	-	-	-	-	-	-	-
hyp	3.16	4.28	3.65	2.57	3.13	2.45	1.79	1.72	1.78	2.04	2.48	1.79	1.81	1.81	1.82
acm	2.42	3.36	3.08	-	1.46	0.01	-	-	-	-	-	-	-	-	-
mag	0.21	-	-	1.06	0.51	1.00	0.70	0.70	0.70	0.90	0.90	0.88	0.73	0.72	0.70
ilm	0.30	0.33	0.32	0.28	0.25	0.23	0.59	0.63	0.58	0.63	0.68	0.73	0.54	0.55	0.56
ttn	-	-	-	-	-0.02	-	-	-	-	-	-	-	-	-	-
ap	0.07	0.05	0.02	0.04	0.04	0.04	0.10	0.11	0.08	0.06	0.09	0.13	0.07	0.10	0.10
rt	-	-	-	-	0.01	-	-	-	-	-	-	-	-	-	-
NMS	-	0.66	0.86	-	-	-	-	-	-	-	-	-	-	-	-
%An	-	-	-	0.25	-	-	7.43	7.39	4.97	5.90	6.61	9.77	5.33	6.63	6.45

Table 7.1: (Continuation)

Sample	SU-13bis a	SU-13bis b	SU-14a	SU-14b	SU-15b	SU-15c	SU-16	SU-13a	VS-145	VS-146	VS-147	VS-148	VS-149	VS-159	VS-161
Unit	NU rhyolite	NU rhyolite	NU rhyolite	NU rhyolite	NU rhyolite	NU rhyolite	NU trachyte	NU rhyolite	NU rhyolite	NU rhyolite	NU rhyolite	NU rhyolite	NU rhyolite	NU rhyolite	NU rhyolite
Major elements (wt %)															
SiO_2	71.31	70.77	70.13	70.34	71.41	70.93	66.46	71.43	68.75	69.28	69.09	69.23	69.37	71.93	69.86
TiO_2	0.45	0.45	0.45	0.43	0.41	0.38	0.77	0.38	0.56	0.55	0.56	0.66	0.59	0.46	0.48
Al_2O_3	14.10	13.93	14.01	14.38	14.05	13.83	16.27	13.97	14.72	14.93	14.69	14.69	14.80	13.31	14.43
Fe_2O_3	2.01	2.39	2.40	2.51	1.67	2.16	2.67	2.13	2.51	2.47	2.56	2.37	2.42	2.21	2.40
MnO	0.02	0.02	0.03	0.02	0.01	0.04	0.02	0.60	0.05	0.03	0.05	0.03	0.03	0.04	0.04
MgO	0.18	0.19	0.23	0.21	0.11	0.23	0.27	0.24	0.47	0.46	0.42	0.46	0.32	0.40	0.33
CaO	0.48	0.48	0.45	0.55	0.28	0.47	1.09	0.65	0.92	0.96	0.90	0.88	0.88	0.47	0.69
Na_2O	3.76	3.67	3.63	3.66	3.34	3.74	3.81	4.16	4.18	4.28	4.35	4.23	4.43	4.34	4.55
K_2O	5.86	5.78	5.86	5.87	6.25	5.84	5.98	5.61	5.65	5.67	5.70	5.74	5.74	5.59	5.76
P_2O_5	0.04	0.03	0.03	0.02	0.11	0.03	0.02	0.12	0.14	0.14	0.19	0.15	0.17	0.11	0.11
LOI	0.70	0.80	1.00	0.88	0.78	0.62	1.42	0.42	0.83	-0.41	0.62	0.58	0.67	0.83	0.84
Total	98.89	98.49	98.19	98.85	98.40	98.26	98.75	99.70	98.75	98.32	99.12	99.01	99.42	99.66	99.46
Agpaicity index	0.89	0.88	0.88	0.86	0.87	0.90	0.78	0.92	0.88	0.88	0.91	0.90	0.91	0.99	0.95
Fe_2O_3/FeO^*	0.5	0.5	0.5	0.5	0.5	0.5	0.5	0.5	0.5	0.5	0.5	0.5	0.5	0.5	0.5
Mineral norm (wt %)															
qz	24.06	24.34	23.74	23.31	26.11	23.86	17.44	21.85	18.90	18.54	18.18	18.88	18.01	22.30	18.07
or	35.48	35.24	35.89	35.66	38.11	35.54	36.36	33.55	34.12	33.96	34.19	34.50	34.35	33.49	34.49
ab	34.55	33.96	33.74	33.75	30.93	34.57	35.19	37.77	38.35	38.91	39.70	38.64	40.30	39.55	41.36
an	2.21	2.29	2.15	2.67	0.67	2.20	5.41	2.47	3.74	3.93	3.31	3.45	3.30	0.33	1.99
crn	0.88	0.93	1.06	1.19	1.77	0.66	1.82	0.19	0.44	0.37	0.19	0.31	0.12	-	-
di	-	-	-	-	-	-	-	-	-	-	-	-	-	1.05	0.58
hyp	1.44	1.75	1.91	1.94	1.03	1.83	1.74	2.69	2.53	2.41	2.40	2.19	1.94	1.68	1.82
acm	-	-	-	-	-	-	-	-	-	-	-	-	-	-	-
mag	0.67	0.80	0.81	0.84	0.56	0.72	0.89	0.70	0.83	0.81	0.84	0.78	0.80	0.73	0.79
ilm	0.64	0.65	0.65	0.61	0.58	0.55	1.10	0.54	0.79	0.77	0.79	0.94	0.83	0.64	0.67
ttn	-	-	-	-	-	-	-	-	-	-	-	-	-	-	-
ap	0.07	0.05	0.05	0.04	0.24	0.06	0.04	0.25	0.29	0.29	0.39	0.32	0.36	0.22	0.23
rt	-	-	-	-	-	-	-	-	-	-	-	-	-	-	-
NMS	-	-	-	-	-	-	-	-	-	-	-	-	-	-	-
%An	6.00	6.32	5.98	7.34	2.11	5.99	13.33	6.14	8.89	9.18	7.70	8.19	7.57	0.83	4.58

Table 7.1: (Continuation)

Sample	VS-163	VS-165	VS-167	VS-168	VS-169	VS-170	VS-177	VS-178	VS-179	VS-180	VS-715	VS-716	VS-720	VS-721	VS-722
Unit	NU rhyolite	NU rhyolite	NU rhyolite	NU rhyolite	NU rhyolite	NU rhyolite	NU rhyolite	NU rhyolite	NU rhyolite	NU rhyolite	AND b. andesite	AND b. andesite	AND andesite	AND ancesite	AND andesite
Major elements (wt %)															
SiO_2	69.13	69.09	68.88	69.23	69.31	69.02	68.80	69.41	69.35	68.86	53.28	54.48	57.39	56.92	56.84
TiO_2	0.56	0.51	0.52	0.54	0.54	0.54	0.60	0.52	0.56	0.68	0.99	0.92	0.82	0.81	0.83
Al_2O_3	14.70	14.82	14.88	14.72	14.88	14.98	14.76	14.99	14.66	14.71	18.40	18.32	17.73	17.87	17.95
Fe_2O_3	2.40	2.47	2.34	2.27	2.37	2.26	2.38	2.21	2.58	2.54	9.61	9.21	8.61	8.59	8.66
MnO	0.03	0.03	0.02	0.02	0.03	0.02	0.03	0.02	0.03	0.04	0.15	0.15	0.16	0.17	0.14
MgO	0.43	0.35	0.33	0.40	0.37	0.33	0.38	0.44	0.35	0.36	3.32	3.88	2.44	2.86	2.55
CaO	0.97	0.95	0.98	0.90	0.94	1.01	0.94	0.99	0.91	1.02	8.89	8.35	6.89	7.27	7.25
Na_2O	4.22	4.50	4.12	4.30	4.25	4.16	4.20	4.53	4.18	4.31	2.10	2.51	2.72	2.70	2.63
K_2O	5.66	5.61	5.55	5.57	5.58	5.56	5.55	5.58	5.63	5.46	1.13	1.17	1.77	1.62	1.63
P_2O_5	0.16	0.15	0.17	0.14	0.14	0.14	0.22	0.14	0.15	0.20	0.21	0.21	0.23	0.23	0.23
LOI	0.73	0.71	0.90	0.83	0.73	0.59	0.87	0.68	0.62	0.83	1.16	0.31	0.65	0.38	0.72
Total	98.95	99.17	98.66	98.91	99.14	98.59	98.70	99.49	99.02	98.99	99.21	99.49	99.38	99.39	99.40
Agpaicity index	0.89	0.91	0.86	0.89	0.88	0.86	0.87	0.90	0.88	0.88	0.25	0.29	0.36	0.35	0.34
Fe_2O_3/FeO^*	0.5	0.5	0.5	0.5	0.5	0.5	0.5	0.5	0.5	0.5	0.3	0.3	0.35	0.35	0.35
Mineral norm (wt %)															
qz	19.01	17.59	19.97	19.17	19.31	19.71	19.62	17.60	19.64	19.14	9.89	8.76	13.23	12.19	12.89
or	34.07	33.65	33.58	33.58	33.55	33.58	33.58	33.31	33.90	32.90	6.95	7.10	10.80	9.84	9.98
ab	38.59	40.98	37.88	39.35	38.83	38.14	38.58	41.09	38.26	39.47	19.68	23.16	25.25	24.95	24.43
an	3.85	3.74	3.88	3.60	3.82	4.16	3.28	4.04	3.60	3.83	39.20	36.24	32.10	32.89	33.57
crn	0.29	-	0.81	0.37	0.53	0.70	0.75	0.04	0.44	0.39	-	-	-	-	-
di	-	0.04	-	-	-	-	-	-	-	-	4.44	3.92	1.41	2.21	1.73
hyp	2.28	2.16	2.01	2.12	2.12	1.90	2.07	2.18	2.20	2.04	15.71	16.95	13.31	14.06	13.47
acm	-	-	-	-	-	-	-	-	-	-	-	-	-	-	-
mag	0.79	0.81	0.78	0.75	0.78	0.75	0.79	0.72	0.85	0.84	2.23	2.10	2.23	2.22	2.25
ilm	0.79	0.71	0.74	0.77	0.77	0.77	0.86	0.72	0.80	0.97	1.44	1.32	1.18	1.16	1.19
ttn	-	-	-	-	-	-	-	-	-	-	-	-	-	-	-
ap	0.33	0.32	0.35	0.30	0.30	0.30	0.47	0.30	0.32	0.43	0.45	0.45	0.50	0.49	0.49
rt	-	-	-	-	-	-	-	-	-	-	-	-	-	-	-
NMS	-	-	-	-	-	-	-	-	-	-	-	-	-	-	-
%An	9.07	8.35	9.29	8.38	8.95	9.84	7.83	8.95	8.61	8.85	66.58	61.01	55.97	56.86	57.88

Table 7.1: (Continuation)

Sample	VS-723	VS-724	VS-725	VS-726	VS-727	VS-728	VS-729	VS-732	VS-742	VS-745	VS-751	VS-752	VS-753	VS-757	VS-758
Unit	AND andesite	AND b. andesite	AND andesite	AND b. andesite	MC rhyolite	NU rhyolite	NU rhyolite	NU rhyolite	MC rhyolite	MU rhyolite	CO rhyolite	MZ trachyte	NU rhyolite	NU rhyolite	AND b. andesite
Major elements (wt %)															
SiO_2	57.62	53.11	57.05	51.93	68.57	69.75	68.29	68.62	70.53	72.20	74.00	66.80	69.33	69.76	55.71
TiO_2	0.82	0.92	0.75	1.08	0.37	0.46	0.47	0.46	0.24	0.18	0.24	0.56	0.46	0.48	0.80
Al_2O_3	18.05	18.04	18.32	19.12	14.89	14.58	15.30	15.06	13.84	12.32	11.03	15.58	14.49	14.62	18.43
Fe_2O_3	8.58	9.29	7.54	9.62	3.03	2.47	2.69	2.55	2.31	2.87	3.14	2.80	2.39	2.60	8.51
MnO	0.13	0.17	0.15	0.15	0.10	0.06	0.03	0.05	0.10	0.10	0.05	0.05	0.03	0.07	0.14
MgO	2.33	4.33	2.31	3.63	0.26	0.19	0.17	0.20	0.22	0.18	0.18	0.42	0.19	0.22	2.96
CaO	7.06	8.55	7.28	9.24	1.24	0.88	1.00	1.00	0.91	0.11	0.14	1.20	0.96	1.11	7.45
Na_2O	2.74	2.48	2.79	2.49	3.71	4.08	4.09	4.15	3.47	4.48	4.00	4.31	4.09	4.09	2.78
K_2O	1.74	0.92	1.57	1.12	6.04	5.49	5.75	5.66	5.68	4.86	4.30	5.45	5.49	5.48	1.60
P_2O_5	0.23	0.21	0.26	0.18	0.08	0.02	0.07	0.02	0.04	0.02	0.03	0.06	0.08	0.08	0.22
LOI	0.60	0.70	1.32	0.92	0.93	0.88	0.85	0.95	1.18	1.22	1.11	1.38	0.68	0.80	0.80
Total	99.87	98.69	99.31	99.45	99.22	98.84	98.69	98.69	98.50	98.52	98.21	98.58	98.16	99.29	99.37
Agpaicity index	0.35	0.28	0.34	0.28	0.85	0.87	0.85	0.86	0.86	1.02	1.02	0.83	0.87	0.87	0.34
Fe_2O_3/FeO^*	0.35	0.3	0.35	0.3	0.5	0.5	0.5	0.5	0.5	0.5	0.5	0.5	0.5	0.5	0.3
Mineral norm (wt %)															
qz	13.21	7.69	13.14	5.51	19.00	21.13	18.60	18.72	24.62	25.19	31.88	16.35	20.79	20.61	9.90
or	10.56	5.65	9.64	6.82	36.54	33.22	34.82	34.28	34.76	29.70	26.56	33.09	33.40	32.99	9.76
ab	25.30	23.13	26.04	23.14	34.11	37.51	37.59	38.21	32.30	39.84	36.39	39.76	37.77	37.42	25.74
an	32.82	36.74	34.12	39.01	5.76	4.32	4.59	4.96	4.41	-	-	5.70	4.37	5.08	34.19
crn	-	-	-	-	0.21	0.44	0.79	0.37	0.49	-	-	0.64	0.30	0.16	-
di	1.38	4.73	1.34	5.76	-	-	-	-	-	0.37	0.42	-	-	-	1.99
hyp	12.86	18.16	12.12	15.61	2.68	1.87	1.89	1.93	2.22	2.77	2.71	2.61	1.75	2.02	14.85
acm	-	-	-	-	-	-	-	-	-	1.39	0.90	-	-	-	-
mag	2.21	2.14	1.96	2.21	1.01	0.82	0.89	0.85	0.78	0.44	0.73	0.93	0.80	0.86	1.95
ilm	1.17	1.32	1.09	1.56	0.53	0.65	0.67	0.65	0.34	0.26	0.35	0.80	0.65	0.68	1.15
ttn	-	-	-	-	-	-	-	-	-	-	-	-	-	-	-
ap	0.50	0.45	0.55	0.39	0.17	0.04	0.15	0.03	0.09	0.03	0.05	0.13	0.17	0.17	0.48
rt	-	-	-	-	-	-	-	-	-	-	-	-	-	-	-
NMS	-	-	-	-	-	-	-	-	-	-	-	-	-	-	-
%An	56.47	61.36	56.71	62.77	14.46	10.32	10.88	11.49	12.01	-	-	12.53	10.36	11.96	57.05

Table 7.1: (Continuation)

Sample	VS-759	VS-760	VS-761	VS-762	VS-763	VS-765	VS-766	VS-773	VS-775	VS-780	VS-781	VS-782	VS-783	VS-784	VS-785
Unit	MC rhyolite	MZ trachyte	MZ rhyolite	MZ rhyolite	MLN rhyolite	MC rhyolite	MC rhyolite	MLN rhyolite	MLN rhyolite	MLN rhyolite	CF rhyolite	AC trachyte	SE rhyolite	LE rhyolite	CM trachyte
Major elements (wt %)															
SiO_2	74.05	65.94	71.35	68.13	69.30	70.01	70.66	72.43	70.29	72.22	74.28	64.17	70.19	69.24	62.44
TiO_2	0.18	0.68	0.41	0.53	0.27	0.27	0.26	0.12	0.10	0.11	0.23	0.82	0.40	0.45	0.81
Al_2O_3	12.86	16.04	13.50	15.61	15.92	14.81	14.66	14.30	13.72	14.09	12.24	16.61	14.91	14.95	17.56
Fe_2O_3	1.92	3.39	1.74	2.69	3.02	2.62	2.38	1.99	1.93	2.04	2.92	5.14	3.49	3.59	6.07
MnO	0.02	0.07	0.04	0.05	0.07	0.07	0.05	0.03	0.05	0.04	0.04	0.05	0.04	0.02	0.11
MgO	0.09<LL	0.97	0.57	0.40	0.22	0.17	0.12	0.15	0.15	0.16	0.19	0.72	0.23	0.20	0.64
CaO	0.64	1.33	0.65	0.82	1.64	0.75	0.81	1.24	1.34	1.34	0.14	3.30	1.20	1.14	3.34
Na_2O	3.33	3.94	3.79	4.69	3.71	3.81	3.82	3.42	3.25	3.71	4.13	3.93	4.16	3.27	3.88
K_2O	5.43	5.91	5.21	5.32	4.26	6.04	5.95	4.45	4.48	4.42	4.84	4.06	5.14	5.61	3.89
P_2O_5	0.02	0.03	0.02	0.04	0.05	0.03	0.02	0.03	0.03	0.03	0.02	0.23	0.13	0.03	0.11
LOI	0.59	1.59	1.56	1.43	1.09	0.69	0.54	0.74	3.47	0.67	1.03	1.09	0.69	1.24	2.00
Total	99.11	99.86	98.82	99.69	99.52	99.26	99.25	98.88	98.78	98.80	100.04	100.09	100.56	99.73	100.83
Agpaicity index	0.88	0.80	0.88	0.86	0.67	0.86	0.87	0.73	0.74	0.77	0.98	0.65	0.83	0.77	0.60
Fe_2O_3/FeO^*	0.5	0.5	0.5	0.5	0.5	0.5	0.5	0.5	0.5	0.5	0.5	0.5	0.5	0.5	0.5
Mineral norm (wt %)															
qz	30.32	14.45	25.64	16.50	25.32	20.87	21.71	30.58	30.00	28.55	28.60	15.85	21.17	23.81	14.50
or	32.98	35.56	31.79	31.87	25.77	36.36	35.80	27.07	28.07	26.82	29.17	24.47	30.62	34.07	23.52
ab	30.70	35.99	35.18	42.70	34.15	34.85	34.94	31.60	30.93	34.21	37.83	35.99	37.62	30.21	35.61
an	3.11	6.50	3.17	3.90	8.01	3.60	3.94	6.14	6.89	6.64	0.55	15.18	5.18	5.62	16.23
crn	0.46	0.92	0.57	0.82	2.63	0.81	0.57	1.90	1.34	0.96	0.03	0.33	0.69	1.69	1.30
di	-	-	-	-	-	-	-	-	-	-	-	-	-	-	-
hyp	1.51	4.44	2.43	2.49	2.65	2.20	1.86	1.82	1.91	1.92	2.48	4.85	2.75	2.70	5.45
acm	-	-	-	-	-	-	-	-	-	-	-	-	-	-	-
mag	0.64	1.12	0.58	0.89	1.00	0.87	0.78	0.66	0.66	0.68	0.97	1.70	1.14	1.20	2.01
ilm	0.25	0.96	0.58	0.74	0.38	0.38	0.36	0.17	0.14	0.15	0.33	1.16	0.56	0.64	1.15
ttn	-	-	-	-	-	-	-	-	-	-	-	-	-	-	-
ap	0.04	0.06	0.04	0.07	0.10	0.06	0.04	0.06	0.06	0.06	0.04	0.48	0.26	0.06	0.24
rt	-	-	-	-	-	-	-	-	-	-	-	-	-	-	-
NMS	-	-	-	-	-	-	-	-	-	-	-	-	-	-	-
%An	9.19	15.29	8.27	8.36	19.01	9.35	10.12	16.27	18.21	16.25	1.43	29.66	12.10	15.68	31.30

Table 7.1: (Continuation)

Sample	VS-786	VS-787	VS-788	VS-789	VS-790	VS-791	VS-792	VS-793	VS-794	VS-795	VS-797	VS-798	VS-801	VS-802	VS-803
Unit	CM trachyte	CA rhyolite	CA rhyolite	PA rhyolite	MC rhyolite	AND andesite	AND andesite	MC rhyolite	AND andesite	AND b. andesite	MLN rhyolite	MLN rhyolite	MC rhyolite	CA rhyolite	MC rhyolite
Major elements (wt %)															
SiO_2	62.63	70.98	71.45	74.97	70.71	56.12	58.19	74.61	55.87	55.40	73.88	73.75	73.75	69.56	69.36
TiO_2	0.83	0.30	0.27	0.12	0.36	0.86	0.76	0.16	0.81	0.84	0.13	0.14	0.17	0.41	0.41
Al_2O_3	18.09	14.89	14.77	13.36	14.89	18.29	17.88	13.12	18.44	18.97	14.02	14.13	13.48	14.83	15.18
Fe_2O_3	6.25	2.71	2.66	1.53	2.91	8.20	8.39	1.96	8.35	9.43	1.94	2.04	1.94	3.23	3.16
MnO	0.07	0.04	0.02	0.05	0.05	0.12	0.15	0.02	0.14	0.16	0.03	0.07	0.02	0.10	0.07
MgO	0.49	0.21	0.36	0.17	0.23	3.26	2.53	0.14	2.87	3.15	0.15	0.16	0.24	0.35	0.21
CaO	2.72	0.72	0.72	0.33	0.96	7.37	6.71	0.59	7.37	7.89	1.22	1.33	0.54	1.15	1.18
Na_2O	3.55	3.25	2.93	4.16	3.78	2.69	2.80	3.37	2.73	2.52	3.45	3.54	3.10	3.62	3.85
K_2O	4.00	6.12	5.80	5.03	5.91	1.65	1.66	5.62	1.59	1.34	4.65	4.55	5.69	5.74	5.91
P_2O_5	0.02	0.03	0.03	0.02	0.04	0.23	0.20	0.02	0.22	0.21	0.03	0.03	0.02	0.07	0.07
LOI	2.14	1.37	1.81	1.05	0.77	0.87	0.56	0.65	1.20	0.74	0.68	0.73	1.05	0.92	0.50
Total	100.78	100.59	100.78	100.76	100.59	99.64	99.80	100.24	99.67	100.62	100.16	100.44	99.98	99.96	99.90
Agpaicity index	0.56	0.80	0.75	0.92	0.85	0.34	0.36	0.89	0.34	0.29	0.76	0.76	0.83	0.82	0.84
Fe_2O_3/FeO^*	0.5	0.5	0.5	0.5	0.5	0.35	0.35	0.5	0.35	0.3	0.5	0.5	0.5	0.5	0.5
Mineral norm (wt %)															
qz	17.38	24.54	27.83	28.09	21.38	10.69	13.85	29.62	10.55	10.02	30.74	30.09	30.21	21.43	19.39
or	24.28	36.79	35.05	29.93	35.22	10.04	10.06	33.72	10.33	8.07	27.92	27.24	34.42	34.54	35.35
ab	32.79	29.67	26.94	37.66	34.24	24.87	25.87	30.71	25.30	23.15	31.47	32.20	28.46	33.06	35.00
an	13.75	3.47	3.47	1.53	4.54	33.93	32.23	2.82	34.23	37.35	5.93	6.47	2.58	5.35	5.47
crn	3.40	1.87	2.72	0.58	0.68	-	-	0.54	-	-	1.32	1.17	1.46	0.82	0.52
di	-	-	-	-	-	1.74	0.53	-	1.58	1.03	-	-	-	-	-
hyp	5.09	2.29	2.68	1.52	2.39	14.90	13.79	1.68	14.12	16.60	1.74	1.89	1.93	3.00	2.50
acm	-	-	-	-	-	-	-	-	-	-	-	-	-	-	-
mag	2.09	0.90	0.88	0.50	0.95	2.11	2.16	0.65	2.16	2.14	0.64	0.67	0.64	1.07	1.04
ilm	1.19	0.42	0.38	0.16	0.50	1.23	1.08	0.23	1.16	1.19	0.18	0.20	0.24	0.58	0.58
ttn	-	-	-	-	-	-	-	-	-	-	-	-	-	-	-
ap	0.04	0.05	0.05	0.03	0.08	0.50	0.43	0.04	0.48	0.45	0.06	0.06	0.04	0.15	0.15
rt	-	-	-	-	-	-	-	-	-	-	-	-	-	-	-
NMS	-	-	-	-	-	-	-	-	-	-	-	-	-	-	-
%An	29.54	10.47	11.40	3.90	11.71	57.70	55.47	8.40	57.50	61.73	15.86	16.73	8.33	13.92	13.51

Table 7.1: (Continuation)

Sample	VS-804	VS-805a	VS-805b	VS-806	VS-808	VS-810	VS-811	VS-812	VS-813	VS-814	VS-816	VS-817	VS-819	VS-821	VS-822
Unit	MC rhyolite	MC rhyolite	MC rhyolite	MC rhyolite	MU rhyolite	SP rhyolite	SP rhyolite	SP rhyolite	SP rhyolite	SP rhyolite	SP rhyolite	SP rhyolite	PA rhyolite	PA rhyolite	PA rhyolite
Major elements (wt %)															
SiO_2	67.50	67.88	68.98	68.76	73.13	69.87	69.58	70.36	70.51	70.46	69.81	69.91	74.15	74.83	74.25
TiO_2	0.42	0.41	0.40	0.37	0.18	0.38	0.43	0.37	0.39	0.41	0.40	0.40	0.11	0.12	0.12
Al_2O_3	16.10	15.94	15.75	15.25	12.57	15.29	15.59	14.75	15.09	15.02	15.39	15.22	12.87	13.15	12.84
Fe_2O_3	2.63	3.35	2.84	2.87	2.93	2.34	2.68	2.55	2.20	2.48	2.37	2.52	1.40	0.59	1.55
MnO	0.03	0.04	0.04	0.07	0.04	0.05	0.03	0.03	0.03	0.04	0.05	0.05	0.02	0.01<LL	0.01<LL
MgO	0.31	0.20	0.12	0.51	0.19	0.30	0.15	0.14	0.16	0.21	0.26	0.17	0.23	0.09<LL	0.32
CaO	0.65	0.55	0.60	0.98	0.06	0.60	0.57	0.59	0.68	0.59	0.58	0.82	0.34	0.45	0.35
Na_2O	3.51	3.16	3.43	3.40	4.53	4.49	4.32	4.34	4.33	4.01	3.83	4.55	3.64	3.82	3.40
K_2O	6.41	6.58	6.57	5.59	5.03	5.68	5.53	5.56	5.59	5.83	5.76	5.50	4.96	5.10	5.02
P_2O_5	0.03	0.03	0.03	0.04	0.03	0.02	0.04	0.02	0.02	0.03	0.02	0.04	0.02	0.02	0.01
LOI	1.97	1.57	1.22	1.39	0.59	0.48	0.97	0.69	0.85	0.88	1.09	0.47	1.10	1.02	1.39
Total	99.53	99.68	99.96	99.21	99.27	99.47	99.85	99.39	99.81	99.93	99.55	99.63	98.81	99.18	99.25
Agpaicity index	0.79	0.77	0.81	0.76	1.03	0.89	0.84	0.89	0.87	0.86	0.81	0.88	0.88	0.90	0.86
Fe_2O_3/FeO^*	0.5	0.5	0.5	0.5	0.5	0.5	0.5	0.5	0.5	0.5	0.5	0.5	0.5	0.5	0.5
Mineral norm (wt %)															
qz	19.09	20.87	20.44	22.85	24.91	18.39	19.89	20.36	20.34	21.27	21.94	18.46	31.10	30.27	32.08
or	38.97	39.97	39.55	34.03	30.27	33.83	33.10	33.36	33.37	34.88	34.70	32.74	30.23	30.86	30.64
ab	32.38	29.15	31.41	31.41	39.69	40.68	39.25	39.57	39.28	36.45	35.07	41.20	33.71	35.13	31.54
an	3.15	2.61	2.84	4.72	-	2.85	2.61	2.84	3.29	2.74	2.78	3.81	1.64	2.13	1.73
crn	2.55	3.03	2.21	2.18	-	0.80	1.72	0.62	0.82	1.26	2.06	0.44	1.06	0.65	1.35
di	-	-	-	-	0.06	-	-	-	-	-	-	-	-	-	-
hyp	2.33	2.62	1.99	3.24	2.88	2.13	1.87	1.84	1.60	1.95	2.04	1.89	1.60	0.55	1.94
acm	-	-	-	-	1.43	-	-	-	-	-	-	-	-	-	-
mag	0.88	1.12	0.94	0.96	0.43	0.76	0.88	0.84	0.72	0.81	0.78	0.82	0.47	0.19	0.52
ilm	0.59	0.58	0.56	0.52	0.26	0.53	0.60	0.52	0.54	0.57	0.57	0.55	0.16	0.16	0.17
ttn	-	-	-	-	-	-	-	-	-	-	-	-	-	-	-
ap	0.05	0.06	0.06	0.09	0.06	0.04	0.07	0.04	0.03	0.06	0.04	0.08	0.03	0.04	0.02
rt	-	-	-	-	-	-	-	-	-	-	-	-	-	-	-
NMS	-	-	-	-	-	-	-	-	-	-	-	-	-	-	-
%An	8.87	8.21	8.28	13.05	-	6.54	6.23	6.70	7.73	7.00	7.34	8.47	4.64	5.71	5.19

Table 7.1: (Continuation)

Sample	VS-823	VS-826	VS-828	VS-832	VS-834	VS-836	VS-837	VS-838	ISP-1	ISP-2	ISP-12	ISP-41	ISP-43c	ISP-45	ISP-46
Unit	CO rhyolite	MC rhyolite	CA rhyolite	NU rhyolite	MU rhyolite	AND andesite	NU rhyolite	LE rhyolite	PM rhyolite	PM rhyolite	PM rhyolite	CO rhyolite	CO rhyolite	CO rhyolite	CO rhyolite
Major elements (wt %)															
SiO_2	74.48	68.19	68.65	68.61	73.47	58.26	70.13	67.95	74.67	74.32	73.97	73.58	73.58	75.52	75.51
TiO_2	0.24	0.38	0.37	0.52	0.20	0.65	0.48	0.45	0.11	0.12	0.11	0.27	0.27	0.14	0.16
Al_2O_3	11.48	14.88	14.49	14.79	12.82	17.78	14.38	14.64	13.35	13.53	13.86	10.61	10.43	11.39	11.53
Fe_2O_3	2.88	3.03	2.99	2.75	2.09	6.50	2.58	3.65	1.88	1.80	1.50	4.96	5.34	2.94	3.10
MnO	0.05	0.03	0.06	0.06	0.04	0.08	0.04	0.03	0.03	0.02	0.02	0.20	0.12	0.05	0.07
MgO	0.14	0.82	1.06	0.26	0.09<LL	2.19	0.20	0.17	0.15	0.09<LL	0.08<LL	0.17	0.15	0.13	0.07<LL
CaO	0.10	0.79	0.68	1.07	0.16	6.54	0.99	1.36	0.35	0.37	0.35	0.20	0.11	0.06	0.04
Na_2O	3.85	2.74	2.80	3.96	4.50	2.58	4.00	4.02	3.98	4.12	4.42	4.55	4.26	4.30	4.21
K_2O	4.83	5.90	5.82	5.75	5.11	2.75	5.52	5.04	5.06	5.17	5.11	4.65	4.83	4.55	4.72
P_2O_5	0.03	0.08	0.08	0.09	0.02	0.21	0.08	0.10	0.02	0.02	0.02	0.01	0.04	0.00<LL	0.01<LL
LOI	0.85	2.49	2.25	0.71	0.63	0.95	0.61	0.87	0.80	0.67	0.75	0.62	0.97	0.74	0.50
Total	98.90	99.31	99.22	98.54	99.12	98.47	98.99	98.26	100.38	100.11	100.17	99.81	100.09	99.79	99.90
Agpaicity index	1.01	0.73	0.75	0.86	1.01	0.41	0.87	0.82	0.90	0.91	0.92	1.18	1.17	1.05	1.04
Fe_2O_3/FeO^*	0.5	0.5	0.5	0.5	0.5	0.35	0.5	0.5	0.5	0.5	0.5	0.5	0.5	0.5	0.5
Mineral norm (wt %)															
qz	31.06	25.23	25.47	19.40	25.31	13.35	21.64	20.37	28.67	27.22	25.56	28.66	29.38	30.43	30.16
or	29.50	36.41	35.84	34.85	30.78	16.93	33.34	30.82	30.22	30.84	30.40	28.14	29.32	27.43	28.39
ab	35.34	25.72	26.18	36.51	40.56	24.10	36.67	37.36	36.12	37.34	40.00	31.18	29.21	36.06	35.72
an	-	3.53	2.95	4.85	-	30.06	4.49	6.31	1.63	1.76	1.59	-	-	-	-
crn	-	3.15	2.91	0.36	-	-	0.25	0.38	0.82	0.59	0.53	-	-	-	-
di	0.25	-	-	-	0.54	1.89	-	-	-	-	-	0.76	0.23	0.24	0.11
hyp	2.29	4.22	4.92	2.18	1.47	10.59	1.91	2.69	1.73	1.47	1.23	4.92	5.40	3.01	2.94
acm	0.31	-	-	-	0.51	-	-	-	-	-	-	4.40	4.75	2.60	2.24
mag	0.85	1.03	1.01	0.91	0.50	1.70	0.85	1.22	0.62	0.59	0.49	-	-	-	0.18
ilm	0.34	0.55	0.54	0.74	0.28	0.94	0.68	0.64	0.16	0.16	0.15	0.38	0.39	0.19	0.23
ttn	-	-	-	-	-	-	-	-	-	-	-	-	-	-	-
ap	0.06	0.17	0.17	0.19	0.04	0.45	0.17	0.22	0.03	0.03	0.04	0.02	0.09	-	0.02
rt	-	-	-	-	-	-	-	-	-	-	-	-	-	-	-
NMS	-	-	-	-	-	-	-	-	-	-	-	1.55	1.25	0.03	-
%An	-	12.05	10.12	11.72	-	55.50	10.90	14.45	4.33	4.49	3.83	-	-	-	-

Table 7.1: (Continuation)

Sample	ISP-47	ISP-48	ISP-54	ISP-55b	ISP-65	ISP-67	ISP-70	ISP-75	ISP-76	ISP-79	ISP-80	ISP-81	ISP-83	ISP-85	ISP-87
Unit	MZ rhyolite	MCR rhyolite	CO rhyolite	MU rhyolite	NU rhyolite	CF rhyolite	CF trachyte	CF rhyolite	CO rhyolite	CO rhyolite	MU rhyolite	MU rhyolite	CF rhyolite	PA rhyolite	PA rhyolite
Major elements (wt %)															
SiO_2	69.09	69.49	75.36	74.91	70.91	74.13	64.76	73.09	74.06	73.16	70.12	72.07	67.32	73.04	73.16
TiO_2	0.57	0.47	0.22	0.18	0.47	0.17	0.70	0.17	0.25	0.29	0.15	0.14	0.49	0.14	0.11
Al_2O_3	15.69	15.12	11.22	12.01	14.69	11.99	16.78	12.62	9.99	12.66	12.57	12.69	15.52	13.70	13.85
Fe_2O_3	2.72	2.75	3.52	2.86	2.82	2.67	3.75	2.93	5.54	3.24	2.87	3.01	3.21	0.84	1.29
MnO	0.09	0.04	0.08	0.05	0.05	0.02	0.07	0.05	0.11	0.05	0.09	0.02	0.03	0.01<LL	0.01
MgO	0.38	0.57	0.15	0.17	0.28	0.17	0.26	0.15	0.16	0.1<LL	0.16	0.15	0.16	0.24	0.16
CaO	0.87	0.73	0.07	0.09	0.65	0.12	0.54	0.08	0.17	0.15	0.35	0.07	0.31	0.37	0.28
Na_2O	4.58	3.13	3.70	4.35	3.72	4.18	5.61	4.48	4.28	4.53	2.98	4.42	4.99	4.54	3.49
K_2O	5.40	6.32	4.62	4.77	5.83	4.68	6.34	4.94	4.55	5.13	5.57	4.94	5.72	4.93	5.21
P_2O_5	0.03	0.07	0.05	0.02	0.02	0.03	0.05	0.02	0.06	0.03	0.01<LL	0.03	0.03	0.02	0.04
LOI	0.79	1.64	1.02	1.10	0.80	0.96	0.67	0.62	0.88	0.58	3.91	0.89	0.95	1.75	1.59
Total	100.17	100.30	99.99	100.49	100.22	99.09	99.52	99.12	100.02	99.90	98.75	98.41	98.70	99.57	99.18
Agpaicity index	0.85	0.79	0.99	1.03	0.85	1.00	0.96	1.01	1.20	1.03	0.87	0.99	0.93	0.93	0.82
Fe_2O_3/FeO^*	0.5	0.5	0.5	0.5	0.5	0.5	0.5	0.5	0.5	0.5	0.5	0.5	0.5	0.5	0.5
Mineral norm (wt %)															
qz	17.46	22.86	33.03	28.40	22.91	29.18	5.14	25.42	31.01	24.43	29.19	24.91	13.88	24.99	30.39
or	32.05	38.19	28.08	28.60	34.92	28.47	37.48	29.80	27.65	30.75	35.23	30.10	34.41	29.73	31.77
ab	41.30	28.70	34.21	38.00	33.86	38.60	50.36	40.58	28.50	39.33	28.67	40.97	45.61	41.61	32.37
an	4.12	3.25	0.02	-	3.11	0.16	1.90	-	-	-	1.76	0.19	1.34	1.74	1.20
crn	0.90	2.21	0.14	-	1.25	-	-	-	-	-	1.22	0.01	0.72	0.30	2.31
di	-	-	-	0.26	-	0.21	0.36	0.22	0.40	0.47	-	-	-	-	-
hyp	2.43	3.09	2.92	2.66	2.32	2.20	2.46	2.49	5.55	2.54	2.70	2.56	2.22	1.13	1.29
acm	-	-	-	1.35	-	-	-	0.39	4.94	1.51	-	-	-	-	-
mag	0.89	0.91	1.17	0.44	0.93	0.89	1.22	0.82	-	0.50	1.00	1.01	1.06	0.28	0.43
ilm	0.79	0.66	0.32	0.25	0.66	0.24	0.98	0.23	0.35	0.41	0.22	0.19	0.70	0.19	0.16
ttn	-	-	-	-	-	-	-	-	-	-	-	-	-	-	-
ap	0.06	0.14	0.11	0.04	0.04	0.05	0.10	0.04	0.12	0.05	0.02	0.05	0.06	0.04	0.08
rt	-	-	-	-	-	-	-	-	-	-	-	-	-	-	-
NMS	-	-	-	-	-	-	-	-	1.47	-	-	-	-	-	-
%An	9.07	10.16	0.06	-	8.42	0.41	3.64	-	-	-	5.80	0.46	2.86	4.02	3.57

Table 7.1: (Continuation)

Sample	ISP-88	ISP-89	ISP-94	ISP-95	ISP-97	ISP-100	ISP-116	ISP-118	ISP-120	ISP-121	ISP-124	ISP-126	ISP-127	ISP-128	ISP-130
Unit	MU rhyolite	CF rhyolite	SP rhyolite	CF rhyolite	SP rhyolite	CF rhyolite	CO rhyolite	CO rhyolite	NU rhyolite	NU rhyolite	NU rhyolite	MU rhyolite	MU rhyolite	CF rhyolite	CF rhyolite
Major elements (wt %)															
SiO_2	69.95	70.11	70.18	68.57	69.90	74.47	75.34	68.03	69.25	69.36	70.06	70.29	73.79	71.85	74.49
TiO_2	0.25	0.29	0.33	0.48	0.36	0.19	0.20	0.51	0.45	0.45	0.48	0.20	0.18	0.31	0.19
Al_2O_3	13.13	13.90	14.40	15.30	15.21	11.93	11.00	14.29	15.05	14.83	15.07	13.18	12.74	13.55	12.93
Fe_2O_3	3.25	3.03	2.30	3.34	1.67	2.54	3.40	4.47	2.60	2.63	2.81	3.27	2.91	3.41	2.28
MnO	0.07	0.03	0.06	0.07	0.03	0.04	0.03	0.03	0.04	0.04	0.05	0.08	0.02	0.03	0.01
MgO	0.27	0.18	0.25	0.12	0.11<LL	0.10<LL	0.16	0.52	0.20	0.41	0.17	0.30	0.11<LL	0.18	0.12
CaO	0.37	0.24	0.82	0.31	0.62	0.08	0.09	1.14	0.66	0.70	0.78	0.30	0.08	0.22	0.08
Na_2O	2.89	4.63	4.54	5.07	4.82	4.07	3.90	4.13	3.70	3.68	3.98	2.69	4.55	4.75	4.36
K_2O	5.21	5.33	5.53	5.73	5.64	4.72	4.63	4.92	6.29	5.76	5.86	5.13	4.97	5.25	4.95
P_2O_5	0.02	0.03	0.04	0.03	0.02	0.02	0.03	0.06	0.02	0.02	0.02	0.01	0.02	0.03	0.02
LOI	4.55	0.90	0.44	0.64	0.86	0.92	0.71	2.28	0.78	0.95	0.62	4.73	1.04	0.84	1.10
Total	99.93	98.64	98.87	99.64	99.23	99.06	99.47	100.37	99.02	98.80	99.88	100.17	100.39	100.40	100.51
Agpaicity index	0.79	0.96	0.93	0.95	0.92	0.99	1.04	0.85	0.86	0.83	0.86	0.76	1.01	1.00	0.97
Fe_2O_3/FeO*	0.5	0.5	0.5	0.5	0.5	0.5	0.5	0.5	0.5	0.5	0.5	0.5	0.5	0.5	0.5
Mineral norm (wt %)															
qz	30.57	20.04	18.97	14.34	17.25	30.18	32.13	19.77	20.17	22.06	20.49	32.42	25.45	21.03	27.32
or	32.82	32.25	33.18	34.10	33.70	28.71	28.17	29.87	37.99	34.96	35.06	32.39	29.72	31.25	29.61
ab	27.65	42.58	41.36	45.81	43.77	37.62	33.66	38.10	33.99	33.93	36.15	25.77	40.71	42.97	39.60
an	1.86	1.05	2.63	1.35	2.98	0.25	-	5.42	3.19	3.41	3.79	1.52	-	0.18	0.30
crn	2.46	0.17	-	0.30	0.10	0.06	-	0.29	1.14	1.50	0.90	3.14	-	-	0.32
di	-	-	0.99	-	-	-	0.21	-	-	-	-	-	0.22	0.56	-
hyp	3.11	2.44	1.56	2.28	1.11	2.03	3.18	4.21	1.98	2.58	1.98	3.31	2.31	2.40	1.80
acm	-	-	-	-	-	-	1.88	-	-	-	-	-	0.55	-	-
mag	1.12	1.01	0.76	1.09	0.55	0.85	0.43	1.49	0.86	0.88	0.92	1.13	0.75	1.12	0.75
ilm	0.37	0.41	0.47	0.67	0.50	0.27	0.29	0.73	0.63	0.64	0.68	0.30	0.25	0.44	0.27
ttn	-	-	-	-	-	-	-	-	-	-	-	-	-	-	-
ap	0.03	0.05	0.08	0.06	0.04	0.04	0.06	0.13	0.04	0.04	0.04	0.02	0.04	0.06	0.03
rt	-	-	-	-	-	-	-	-	-	-	-	-	-	-	-
NMS	-	-	-	-	-	-	-	-	-	-	-	-	-	-	-
%An	6.29	2.41	5.98	2.87	6.37	0.66	-	12.44	8.58	9.14	9.48	5.57	-	0.43	0.76

Table 7.1: (Continuation)

Sample	ISP-132	ISP-136	ISP-137	ISP-140	ISP-150	ISP-154	ISP-156	ISP-159	ISP-160	ISP-162	ISP-164	ISP-173	ISP-175	ISP-179	ISP-182
Unit	MCR rhyolite	MCR rhyolite	MCR rhyolite	MZ rhyolite	CO rhyolite	MZ trachyte	NU rhyolite	NU rhyolite	NU rhyolite	NU rhyolite	CO rhyolite	MU rhyolite	MU rhyolite	MU rhyolite	CF rhyolite
Major elements (wt %)															
SiO_2	69.11	69.24	70.20	70.76	75.90	66.87	70.23	70.74	70.76	70.91	71.80	72.04	71.29	74.59	72.60
TiO_2	0.68	0.64	0.47	0.49	0.15	0.83	0.57	0.52	0.51	0.53	0.32	0.19	0.18	0.18	0.48
Al_2O_3	15.25	14.90	14.89	14.98	11.25	15.34	14.97	14.63	14.01	14.55	12.14	12.22	12.47	12.64	13.60
Fe_2O_3	2.50	3.38	2.48	2.40	2.73	4.10	2.89	2.88	2.80	2.74	4.21	3.13	3.02	2.50	2.00
MnO	0.09	0.09	0.06	0.06	0.05	0.08	0.04	0.05	0.04	0.07	0.06	0.09	0.09	0.01	0.02
MgO	0.67	0.77	0.36	0.58	0.13	0.64	0.36	0.35	0.31	0.29	0.56	0.12<LL	0.18	0.14	0.18
CaO	0.95	0.78	0.75	0.81	0.22	0.93	1.00	0.82	0.79	0.75	0.32	0.32	0.33	0.14	0.31
Na_2O	3.34	3.31	3.74	4.10	4.38	3.58	4.00	3.93	3.83	3.88	4.55	2.90	2.83	4.37	4.43
K_2O	5.99	5.78	5.94	5.33	4.43	6.44	5.67	5.72	5.66	5.80	4.90	5.56	5.51	5.01	5.03
P_2O_5	0.15	0.14	0.08	0.02	0.00<LL	0.02	0.12	0.10	0.09	0.08	0.03	0.01<LL	0.01	0.04	0.02
LOI	1.59	2.00	0.99	1.13	0.52	1.25	0.84	0.90	0.71	0.71	1.21	4.23	4.36	0.91	1.20
Total	100.30	101.02	99.95	100.63	99.74	100.06	100.66	100.60	99.49	100.28	100.07	100.79	100.25	100.52	99.83
Agpaicity index	0.79	0.79	0.84	0.84	1.07	0.84	0.85	0.86	0.89	0.87	1.05	0.88	0.85	1.00	0.94
Fe_2O_3/FeO^*	0.5	0.5	0.5	0.5	0.5	0.5	0.5	0.5	0.5	0.5	0.5	0.5	0.5	0.5	0.5
Mineral norm (wt %)															
qz	22.32	23.14	21.77	21.81	31.11	16.49	20.67	21.72	22.85	22.13	23.02	31.19	31.18	26.98	24.80
or	36.09	34.85	35.66	31.74	26.68	38.82	33.71	34.09	34.09	34.62	29.54	34.69	34.59	29.93	30.21
ab	30.61	30.33	34.08	37.06	35.91	32.75	36.18	35.58	35.09	35.19	38.04	27.45	26.96	39.68	40.44
an	3.79	3.02	3.25	3.89	-	4.57	4.24	3.45	3.40	3.21	-	1.61	1.67	0.06	1.41
crn	2.14	2.36	1.27	1.16	-	0.94	0.78	0.81	0.40	0.82	-	1.02	1.48	-	0.41
di	-	-	-	-	0.89	-	-	-	-	-	1.12	-	-	0.30	-
hyp	2.95	3.98	2.32	2.83	2.47	3.85	2.44	2.48	2.32	2.22	4.58	2.69	2.78	1.89	1.36
acm	-	-	-	-	2.40	-	-	-	-	-	2.88	-	-	-	-
mag	0.83	1.12	0.82	0.78	-	1.36	0.94	0.94	0.93	0.90	0.31	1.07	1.04	0.82	0.66
ilm	0.97	0.90	0.66	0.68	0.21	1.18	0.79	0.72	0.72	0.75	0.45	0.27	0.27	0.25	0.67
ttn	-	-	-	-	-	-	-	-	-	-	-	-	-	-	-
ap	0.32	0.30	0.17	0.04	-	0.04	0.24	0.21	0.19	0.17	0.06	0.02	0.02	0.08	0.04
rt	-	-	-	-	-	-	-	-	-	-	-	-	-	-	-
NMS	-	-	-	-	0.34	-	-	-	-	-	-	-	-	-	-
%An	11.01	9.04	8.71	9.51	-	12.26	10.49	8.83	8.83	8.36	-	5.53	5.84	0.16	3.36

Table 7.1: (Continuation)

Sample	ISP-185	ISP-186	ISP-189	ISP-190	ISP-192	ISP-200	ISP-203	ISP-208	ISP-209	ISP-209 bis	ISP-210	ISP-211	ISP-212	ISP-214	ISP-215
Unit	MU rhyolite	MU rhyolite	CF trachyte	CF trachyte	PM rhyolite	NU rhyolite	NU rhyolite	PC rhyolite	MZ rhyolite	CL rhyolite	CL rhyolite	NU rhyolite	NU rhyolite	PM rhyolite	PM rhyolite
Major elements (wt %)															
SiO_2	74.08	74.17	64.70	65.51	74.08	70.27	70.96	68.62	69.23	73.74	74.14	71.07	70.78	74.57	74.37
TiO_2	0.19	0.19	0.73	0.67	0.11	0.50	0.49	0.73	0.54	0.28	0.27	0.49	0.49	0.11	0.12
Al_2O_3	12.82	12.86	17.44	16.80	14.16	15.36	15.13	15.50	15.56	13.49	13.42	14.98	15.32	13.70	14.03
Fe_2O_3	2.80	3.02	3.84	3.65	1.29	2.56	2.46	3.72	2.64	1.90	1.98	2.55	2.26	1.89	1.97
MnO	0.02	0.03	0.04	0.05	0.02	0.04	0.03	0.05	0.05	0.02	0.02	0.04	0.04	0.04	0.03
MgO	0.18	0.14	0.18	0.20	0.09<LL	0.31	0.20	0.25	0.37	0.13<LL	0.09<LL	0.19	0.18	0.10<LL	0.14
CaO	0.09	0.08	0.55	0.38	0.32	1.08	0.98	1.19	0.88	0.80	0.73	0.89	0.93	0.39	0.34
Na_2O	4.33	4.34	5.50	5.65	4.00	3.94	3.91	3.75	4.68	3.58	3.60	4.15	4.03	4.03	3.61
K_2O	4.97	4.93	6.46	6.41	5.35	5.82	5.94	5.75	5.29	5.25	5.35	5.72	5.94	5.13	5.19
P_2O_5	0.02	0.03	0.06	0.06	0.01	0.08	0.06	0.13	0.02	0.02	0.02	0.04	0.06	0.02	0.02
LOI	1.27	1.05	0.88	0.69	0.93	0.85	0.66	0.84	0.62	0.68	0.57	0.50	0.60	0.78	1.28
Total	100.75	100.82	100.35	100.05	100.34	100.79	100.81	100.51	99.86	99.88	100.17	100.59	100.61	100.75	101.07
Agpaicity index	0.98	0.97	0.92	0.97	0.87	0.83	0.85	0.80	0.86	0.86	0.87	0.87	0.85	0.89	0.82
Fe_2O_3/FeO^*	0.5	0.5	0.5	0.5	0.5	0.5	0.5	0.5	0.5	0.5	0.5	0.5	0.5	0.5	0.5
Mineral norm (wt %)															
qz	26.74	26.89	5.28	5.70	27.28	20.33	21.06	19.95	17.45	28.68	28.69	20.71	20.38	27.88	29.96
or	29.72	29.42	37.94	37.66	31.90	34.55	35.19	34.37	31.41	31.59	32.05	33.87	35.21	30.53	31.00
ab	39.39	39.36	49.09	50.50	36.24	35.55	35.19	34.10	42.23	32.74	32.76	37.38	36.30	36.41	32.76
an	0.32	0.20	2.30	1.52	1.51	4.86	4.49	5.12	4.26	3.91	3.54	4.18	4.27	1.82	1.55
crn	0.22	0.36	0.61	0.01	1.38	0.88	0.71	1.39	0.66	0.56	0.49	0.48	0.76	0.95	2.13
di	-	-	-	-	-	-	-	-	-	-	-	-	-	-	-
hyp	2.37	2.45	2.39	2.39	1.10	2.14	1.76	2.55	2.34	1.45	1.40	1.79	1.56	1.61	1.74
acm	-	-	-	-	-	-	-	-	-	-	-	-	-	-	-
mag	0.92	0.99	1.24	1.18	0.42	0.83	0.80	1.22	0.86	0.63	0.65	0.83	0.73	0.62	0.65
ilm	0.27	0.26	1.01	0.93	0.15	0.69	0.69	1.03	0.75	0.39	0.38	0.68	0.68	0.15	0.17
ttn	-	-	-	-	-	-	-	-	-	-	-	-	-	-	-
ap	0.04	0.06	0.12	0.11	0.02	0.17	0.13	0.28	0.04	0.04	0.04	0.07	0.12	0.04	0.04
rt	-	-	-	-	-	-	-	-	-	-	-	-	-	-	-
NMS	-	-	-	-	-	-	-	-	-	-	-	-	-	-	-
%An	0.81	0.51	4.48	2.92	4.01	12.03	11.31	13.05	9.17	10.67	9.76	10.05	10.52	4.76	4.52

Table 7.1: (Continuation)

Sample	ISP-216	ISP-218	ISP-220	ISP-223	ISP-225	ISP-226	ISP-227	ISP-230	ISP-233a	ISP-233b	ISP-237	ISP-241	ISP-244	ISP-246	ISP-247
Unit	SP rhyolite	PC rhyolite	PC rhyolite	PC trachyte	PC trachyte	PC trachyte	PC trachyte	PC trachyte	PC trachyte	PC rhyolite	CF rhyolite	PA rhyolite	CF rhyolite	PA rhyolite	CF rhyolite
Major elements (wt %)															
SiO_2	69.42	69.21	71.03	66.37	66.11	67.10	66.61	64.17	63.81	71.00	74.02	74.97	72.58	74.18	72.93
TiO_2	0.37	0.68	0.62	0.93	0.92	0.85	0.86	0.89	0.85	0.18	0.42	0.13	0.29	0.14	0.29
Al_2O_3	14.46	15.19	14.46	16.87	16.84	16.17	15.45	15.69	15.89	12.50	12.88	13.84	13.63	14.14	13.09
Fe_2O_3	2.39	3.72	3.05	3.67	3.91	3.83	4.74	4.85	4.65	2.90	2.91	1.41	3.12	2.05	3.37
MnO	0.06	0.02	0.02	0.02	0.02	0.03	0.04	0.08	0.08	0.09	0.04	0.01<LL	0.06	0.02	0.07
MgO	0.26	0.22	0.17	0.35	0.20	0.25	0.33	1.18	1.18	0.32	0.16	0.10<LL	0.13<LL	0.15	0.12<LL
CaO	0.94	1.56	1.59	1.97	1.96	2.00	2.21	2.60	2.57	0.43	0.21	0.32	0.17	0.25	0.11
Na_2O	3.79	4.55	4.36	5.14	5.14	4.84	4.66	4.33	4.27	3.29	4.38	3.66	4.72	2.93	4.54
K_2O	5.13	4.64	4.28	4.29	4.52	4.52	4.11	4.04	4.17	5.54	4.85	5.08	5.26	5.24	5.14
P_2O_5	0.04	0.18	0.17	0.13	0.16	0.20	0.24	0.22	0.21	0.09	0.03	0.02	0.03	0.02	0.03
LOI	4.04	0.95	1.15	0.95	0.79	0.96	1.41	2.70	3.07	4.22	0.60	1.24	0.76	1.75	0.63
Total	100.89	100.91	100.88	100.68	100.54	100.73	100.64	100.72	100.73	100.54	100.48	100.77	100.73	100.85	100.29
Agpaicity index	0.81	0.82	0.82	0.78	0.79	0.79	0.78	0.73	0.73	0.91	0.97	0.83	0.99	0.74	0.99
Fe_2O_3/FeO^*	0.5	0.5	0.5	0.5	0.5	0.5	0.5	0.5	0.5	0.5	0.5	0.5	0.5	0.5	0.5
Mineral norm (wt %)															
qz	23.82	19.41	23.74	13.80	12.95	15.49	16.95	14.75	14.36	27.74	26.69	31.00	21.86	33.85	23.78
or	31.50	27.58	25.55	25.36	26.73	26.82	24.61	24.44	25.30	34.46	28.91	30.42	31.21	31.72	30.66
ab	35.32	41.10	39.52	46.18	46.20	43.60	42.42	39.82	39.42	31.05	39.73	33.26	42.52	26.96	41.16
an	4.58	6.58	6.86	8.91	8.70	8.66	9.28	11.73	11.67	1.60	0.83	1.45	0.48	1.11	0.20
crn	1.21	0.31	0.19	0.56	0.33	0.18	-	0.02	0.22	0.62	0.14	2.00	-	3.63	-
di	-	-	-	-	-	-	0.19	-	-	-	-	-	0.12	-	0.13
hyp	2.14	2.49	1.92	2.45	2.20	2.41	3.26	5.89	5.82	3.08	2.10	1.18	2.33	1.81	2.50
acm	-	-	-	-	-	-	-	-	-	-	-	-	-	-	-
mag	0.81	1.21	1.00	1.19	1.27	1.25	1.56	1.61	1.55	0.99	0.95	0.46	1.02	0.68	1.10
ilm	0.54	0.95	0.87	1.29	1.28	1.19	1.22	1.26	1.21	0.26	0.59	0.18	0.41	0.20	0.41
ttn	-	-	-	-	-	-	-	-	-	-	-	-	-	-	-
ap	0.09	0.38	0.35	0.27	0.32	0.41	0.51	0.47	0.45	0.20	0.06	0.04	0.06	0.04	0.06
rt	-	-	-	-	-	-	-	-	-	-	-	-	-	-	-
NMS	-	-	-	-	-	-	-	-	-	-	-	-	-	-	-
%An	11.47	13.80	14.79	16.17	15.84	16.57	17.94	22.75	22.85	4.90	2.05	4.18	1.12	3.96	0.48

Table 7.1: (Continuation)

Sample	ISP-252	ISP-254	ISP-255	ISP-258	ISP-259	ISP-260	ISP-261	ISP-262	ISP-263	ISP-265	ISP-266	ISP-267	ISP-268	ISP-269
Unit	NU rhyolite	MZ rhyolite	CO rhyolite	PC rhyolite	PC rhyolite	PC trachyte	PC trachyte	PC trachyte	CO rhyolite	CF rhyolite	CO rhyolite	CO rhyolite	trachyandesite	MZ rhyolite
Major elements (wt %)														
SiO_2	70.42	69.70	74.00	68.95	68.68	67.66	67.58	68.49	74.11	70.38	76.29	73.19	56.49	70.86
TiO_2	0.49	0.53	0.26	0.66	0.68	0.85	0.72	0.67	0.26	0.52	0.16	0.31	1.99	0.49
Al_2O_3	15.11	15.15	10.39	14.81	15.16	15.34	15.98	15.50	10.73	14.43	11.27	11.24	15.77	14.80
Fe_2O_3	2.72	2.74	5.31	3.70	3.71	4.33	4.03	3.71	4.73	3.45	2.89	4.59	9.55	2.46
MnO	0.03	0.17	0.10	0.08	0.05	0.05	0.05	0.03	0.09	0.06	0.09	0.08	0.13	0.05
MgO	0.32	0.42	0.10<LL	0.46	0.31	0.35	0.25	0.15	0.14	0.20	0.06<LL	0.13	2.23	0.37
CaO	0.81	0.75	0.11	1.78	1.68	2.11	1.67	1.34	0.11	0.33	0.11	0.23	5.77	0.84
Na_2O	3.92	4.19	4.55	4.39	4.52	4.45	4.64	4.50	4.41	4.72	4.58	4.45	3.97	4.12
K_2O	5.72	5.61	4.73	4.46	4.75	4.31	4.87	5.13	4.80	5.34	4.50	4.78	2.67	5.72
P_2O_5	0.05	0.03	0.02	0.18	0.18	0.21	0.14	0.15	0.04	0.03	0.02	0.03	0.69	0.03
LOI	0.96	0.99	0.53	0.78	0.63	0.87	0.76	0.67	0.67	1.03	0.55	1.11	0.96	0.69
Total	100.54	100.25	100.08	100.23	100.31	100.51	100.66	100.31	100.06	100.47	100.51	100.12	100.19	100.41
Agpaicity index	0.84	0.86	1.21	0.81	0.83	0.78	0.81	0.84	1.16	0.94	1.10	1.11	0.60	0.88
Fe_2O_3/FeO^*	0.5	0.5	0.5	0.5	0.5	0.5	0.5	0.5	0.5	0.5	0.5	0.5	0.4	0.5
Mineral norm (wt %)														
qz	21.43	19.56	29.55	20.00	18.37	18.48	16.12	17.76	29.28	19.23	31.01	27.04	7.61	20.60
or	34.12	33.49	28.56	26.64	28.29	25.76	28.87	30.52	28.97	31.79	26.88	28.94	16.18	33.97
ab	35.54	37.97	29.40	39.90	40.87	40.37	41.81	40.69	30.89	42.70	35.32	33.93	36.60	37.22
an	3.73	3.54	-	7.64	7.12	9.20	7.41	5.75	-	1.43	-	-	17.84	4.00
crn	1.23	1.00	-	-	-	0.03	0.42	0.51	-	0.42	-	-	-	0.41
di	-	-	0.37	0.09	0.09	-	-	-	0.24	-	0.36	0.75	5.57	-
hyp	2.28	2.76	5.11	3.22	2.73	3.10	2.76	2.31	4.69	2.51	2.72	4.20	9.16	2.25
acm	-	-	4.69	-	-	-	-	-	4.18	-	2.53	4.06	-	-
mag	0.89	0.90	-	1.21	1.21	1.42	1.31	1.21	-	1.13	-	-	2.72	0.80
ilm	0.69	0.74	0.36	0.92	0.95	1.19	1.01	0.94	0.37	0.73	0.22	0.44	2.84	0.69
ttn	-	-	-	-	-	-	-	-	-	-	-	-	-	-
ap	0.11	0.06	0.03	0.38	0.37	0.44	0.28	0.31	0.07	0.06	0.03	0.06	1.47	0.06
rt	-	-	-	-	-	-	-	-	-	-	-	-	-	-
NMS	-	-	1.93	-	-	-	-	-	1.30	-	0.93	0.58	-	-
%An	9.49	8.52	-	16.07	14.83	18.56	15.06	12.38	-	3.24	-	-	32.77	9.70

Table 7.1: (Continuation)

Sample	FS-22/5	FS-22/8	FS-23/3	FS-24/6	FS-26CFb	FS-30/4	FS-30/2	FS-30/5	FS-30/1	FS-30/3	FS-30/16	FS-32/3	FS-32/2	FS-35/7	FS-37/8
Unit	CO	CO	NU	LE	PA	SE	SE	SE	SE	SE	LE	SE	SE	CM	CO
	rhyolite	rhyolite	rhyolite	rhyolite	rhyolite	rhyolite	rhyolite	rhyolite	rhyolite	rhyolite	rhyolite	rhyolite	rhyoite	rhyolite	rhyolite
As	-	-	-	13.6	-	-	4.61	9.37	-	-	14.6	12.4	13.8	15.1	-
Ba	-	-	-	-	-	-	-	-	-	-	-	-	-	-	-
Be	-	-	-	3.14	-	-	2.30	2.71	-	-	3.07	3.22	3.06	5.78	-
Bi	-	-	-	0.10	-	-	0.04	0.05	-	-	0.08	0.01	0.07	0.08	-
Ce	-	-	-	-	-	-	-	-	-	-	-	-	-	-	-
Co	-	-	-	-	-	-	-	-	-	-	-	-	-	-	-
Cr	-	-	-	18.4	-	-	21.8	17.5	-	-	19.1	18.9	21.9	16.7	-
Cs	-	-	-	6.55	-	-	3.73	4.32	-	-	7.91	2.83	3.12	3.47	-
Cu	-	-	-	7.98	-	-	9.24	5.12	-	-	6.99	5.54	6.46	2.59	-
Dy	-	-	-	9.72	-	-	8.28	8.62	-	-	10.1	9.17	8.10	13.4	-
Er	-	-	-	5.28	-	-	4.25	4.46	-	-	5.55	4.51	4.34	7.45	-
Eu	-	-	-	1.71	-	-	1.99	2.10	-	-	1.62	1.99	1.99	0.14	-
Ga	-	-	-	-	-	-	-	-	-	-	-	-	-	-	-
Gd	-	-	-	11.0	-	-	9.36	10.4	-	-	11.3	11.0	9.07	14.4	-
Ge	-	-	-	1.55	-	-	1.33	1.58	-	-	1.60	1.56	1.60	2.04	-
Hf	-	-	-	9.83	-	-	6.13	10.9	-	-	10.1	3.79	10.1	20.7	-
Ho	-	-	-	1.80	-	-	1.49	1.52	-	-	1.85	1.57	1.46	2.45	-
La	-	-	-	59.7	-	-	47.6	61.1	-	-	60.9	62.2	53.8	91.3	-
Li	-	-	-	11.5	-	-	24.2	17.2	-	-	16.4	17.5	21.8	25.5	-
Lu	-	-	-	0.71	-	-	0.53	0.59	-	-	0.74	0.53	0.58	1.09	-
Mo	-	-	-	3.35	-	-	2.03	2.57	-	-	3.69	2.66	2.32	4.49	-
Nb	-	-	-	-	-	-	-	-	-	-	-	-	-	-	-
Nd	-	-	-	56.2	-	-	45.8	54.5	-	-	57.1	56.2	47.5	77.8	-
Ni	-	-	-	1.95	-	-	2.77	1.43	-	-	2.14	1.64	1.88	1.20	-
Pb	-	-	-	-	-	-	-	-	-	-	-	-	-	-	-
Pr	-	-	-	14.4	-	-	11.5	14.2	-	-	14.8	14.7	12.4	21.5	-
Rb	-	-	-	-	-	-	-	-	-	-	-	-	-	-	-
Sb	-	-	-	1.98	-	-	1.00	1.20	-	-	1.90	1.57	1.73	0.63	-
Sc	-	-	-	11.7	-	-	14.7	9.67	-	-	11.6	9.47	10.0	3.87	-
Sm	-	-	-	11.1	-	-	9.28	10.6	-	-	11.4	11.0	9.27	14.8	-
Sn	-	-	-	-	-	-	-	-	-	-	-	-	-	-	-
Sr	-	-	-	-	-	-	-	-	-	-	-	-	-	-	-
Ta	-	-	-	0.64	-	-	0.87	0.75	-	-	0.80	0.50	0.50	0.31	-
Tb	-	-	-	1.64	-	-	1.40	1.51	-	-	1.72	1.61	1.37	2.22	-
Te	-	-	-	0.22	-	-	0.44	0.11	-	-	0.26	0.08	0.12	0.08	-
Th	-	-	-	-	-	-	-	-	-	-	-	-	-	-	-
Tl	-	-	-	0.91	-	-	0.46	0.50	-	-	0.93	0.36	0.48	0.74	-
Tm	-	-	-	0.74	-	-	0.58	0.61	-	-	0.77	0.59	0.61	1.10	-
U	-	-	-	5.87	-	-	2.56	3.62	-	-	5.20	2.03	3.55	6.51	-
V	-	-	-	-	-	-	-	-	-	-	-	-	-	-	-
W	-	-	-	-	-	-	-	-	-	-	-	-	-	-	-
Y	-	-	-	-	-	-	-	-	-	-	-	-	-	-	-
Yb	-	-	-	4.83	-	-	3.67	4.05	-	-	4.99	3.79	3.98	7.33	-
Zn	-	-	-	-	-	-	-	-	-	-	-	-	-	-	-
Zr	-	-	-	-	-	-	-	-	-	-	-	-	-	-	-

Table 7.2: Trace element compositions of rocks from the Sulcis. Concentrations in µg/g (ppm). <DL: below detection limit; >UL: above the upper limit; <LL: below the lower limit of the calibration range

Sample	ANT-1	ANT-2	ANT-3	ANT-4	ANT-5	ANT-8	ANT-9	ANT-10	ANT-11	ANT-12	ANT-13	ANT-14	ANT-15	ANT-16a	ANT-16b
Unit	NU rhyolite	NU rhyolite	NU rhyolite	NU rhyolite	MC rhyolite	PA rhyolite	SP rhyolite	SP rhyolite	SP rhyolite	SP rhyolite	MC rhyolite	MC rhyolite	NU rhyolite	NU rhyolite	NU rhyolite
As	-	-	-	-	-	2.98	5.62	-	-	4.96	-	-	-	-	-
Ba	1070	1170	949	936	1250	802	622	694	683	786	217	1220	1120	1040	1110
Be	-	-	-	-	-	2.40	3.86	-	-	3.18	-	-	-	-	-
Bi	-	-	-	-	-	0.04	0.04	-	-	0.05	-	-	-	-	-
Ce	102	102	91.8	103	149	84.7	93.8	100	92.7	106	113	117	111	106	112
Co	29.3	52.5	29.7	22.8	31.2	22.6	41.5	86.0	69.4	17.7	28.3	17.2	27.8	35.7	33.7
Cr	35.6	30.1	27.4	26.1	27.5	8.07	9.36	22.9	34.6	7.36	38.0	32.4	29.6	25.1	30.1
Cs	-	-	-	-	-	1.73	4.07	-	-	1.62	-	-	-	-	-
Cu	<DL	<DL	<DL	<DL	<DL	6.33	4.37	<DL	<DL	3.69	<DL	<DL	<DL	<DL	<DL
Dy	-	-	-	-	-	5.37	6.48	-	-	5.14	-	-	-	-	-
Er	-	-	-	-	-	3.42	3.87	-	-	2.49	-	-	-	-	-
Eu	-	-	-	-	-	1.11	0.82	-	-	1.08	-	-	-	-	-
Ga	16.0	16.2	16.0	16.2	16.7	15.2	15.8	15.6	16.0	16.1	16.0	16.6	16.1	15.4	15.3
Gd	-	-	-	-	-	5.89	7.15	-	-	6.63	-	-	-	-	-
Ge	-	-	-	-	-	1.21	1.53	-	-	1.40	-	-	-	-	-
Hf	-	-	-	-	-	10.1	12.1	-	-	5.43	-	-	-	-	-
Ho	-	-	-	-	-	1.06	1.23	-	-	0.86	-	-	-	-	-
La	-	-	-	-	-	50.4	53.9	-	-	54.2	-	-	-	-	-
Li	-	-	-	-	-	2.48	15.3	-	-	5.93	-	-	-	-	-
Lu	-	-	-	-	-	0.58	0.61	-	-	0.31	-	-	-	-	-
Mo	4.80	4.80	3.90	3.10	2.00	3.24	5.53	5.50	3.90	3.86	4.10	3.10	3.50	2.90	3.00
Nb	38.7	38.1	40.0	40.2	27.9	41.0	43.7	41.9	42.5	41.0	31.8	28.4	37.1	37.8	38.1
Nd	-	-	-	-	-	33.5	38.1	-	-	37.5	-	-	-	-	-
Ni	<DL	<DL	<DL	<DL	<DL	1.21	0.49	<DL	<DL	0.70	<DL	<DL	<DL	<DL	<DL
Pb	-	-	-	-	-	7.70	18.2	19.3	20.8	15.6	25.8	29.4	16.9	19.3	18.8
Pr	-	-	-	-	-	9.86	10.9	-	-	11.0	-	-	-	-	-
Rb	165	164	175	172	161	150	174	165	166	152	202	168	165	158	162
Sb	-	-	-	-	-	0.50	0.65	-	-	0.51	-	-	-	-	-
Sc	-	-	-	-	-	4.15	4.53	-	-	4.39	-	-	-	-	-
Sm	-	-	-	-	-	5.77	6.90	-	-	6.70	-	-	-	-	-
Sn	3.2	3.5	3.9	3.7	1.4	1.0	2.2	2.8	2.6	1.9	2.7	3.9	2.1	0.3	0.9
Sr	92.3	105	81.4	81.2	75.8	80.4	38.0*	51.4	49.0	77.1	35.4	74.5	102	95.2	96.6
Ta	-	-	-	-	-	2.95	4.48	-	-	3.49	-	-	-	-	-
Tb	-	-	-	-	-	0.87	1.08	-	-	0.92	-	-	-	-	-
Te	-	-	-	-	-	0.09	0.12	-	-	0.06	-	-	-	-	-
Th	22.3	19.7	22.1	21.3	21.2	22.1	23.6	22.6	24.0	22.8	26.5	22.0	21.1	19.9	20.4
Tl	-	-	-	-	-	0.64	0.67	-	-	0.41	-	-	-	-	-
Tm	-	-	-	-	-	0.53	0.56	-	-	0.33	-	-	-	-	-
U	-	-	-	-	-	4.86	6.20	-	-	2.77	-	-	-	-	-
V	23.7	23.4	22.7	22.5	23.8	17.7	15.8	17.6	16.9	18.0	14.7	25.4	20.7	23.2	21.9
W	182	277	164	197	254	64.3	402	651	211	141	172	137	119	185	169
Y	38.8	35.4	36.1	37.6	42.7	26.5	31.2	27.8	27.9	25.8	50.8	38.7	38.7	32.3	33.5
Yb	-	-	-	-	-	3.81	3.94	-	-	2.19	-	-	-	-	-
Zn	47.3	57.4	57.2	42.6	69.8	32.1	53.6	53.0	45.1	37.6	39.5	59.7	40.8	37.1	37.5
Zr	438	433	442	434	428	401	407	414	398	415	236	410	426	417	421

Table 7.2: (Continuation)

Sample	ANT-16c	ANT-17	ANT-18	ANT-19	ANT-20	ANT-21 T	ANT-22	ANT-23	ANT-24	ANT-25	ANT-26	ANT-26+	ANT-27	ANT-30	ANT-31
Unit	NU rhyolite	MU rhyolite	MU rhyolite	MU rhyolite	MU rhyolite	MU rhyolite	MU rhyolite	MU rhyolite	SP rhyolite	MU rhyolite	MU rhyolite	MU rhyolite	MU rhyolite	MU rhyolite	MU rhyolite
As	-	-	-	-	-	12.6	-	-	-	-	-	-	-	-	-
Ba	975	197	26.6	44.3	30.6	40.4*	62.8	65.8	634	73.8	57.5	58.6	37.4	30.8	26.3
Be	-	-	-	-	-	5.72	-	-	-	-	-	-	-	-	-
Bi	-	-	-	-	-	0.04	-	-	-	-	-	-	-	-	-
Ce	106	80.8	139	158	145	131	177	180	117	290	237	162	159	112	202
Co	37.9	23.2	57.4	40.5	23.2	43.2	19.0	24.9	40.7	22.7	29.6	22.3	25.4	31.5	16.6
Cr	27.2	27.2	23.1	25.1	23.4	18.7	26.1	31.0	22.3	45.3	27.6	42.8	56.3	41.1	52.4
Cs	-	-	-	-	-	3.86	-	-	-	-	-	-	-	-	-
Cu	<DL	<DL	<DL	<DL	<DL	2.60	<DL	<DL	<DL	<DL	<DL	<DL	<DL	<DL	<DL
Dy	-	-	-	-	-	14.0	-	-	-	-	-	-	-	-	-
Er	-	-	-	-	-	7.56	-	-	-	-	-	-	-	-	-
Eu	-	-	-	-	-	0.19	-	-	-	-	-	-	-	-	-
Ga	15.6	16.6	20.2	21.4	20.6	20.2	21.4	21.7	15.6	23.6	21.7	21.4	21.9	19.5	21.3
Gd	-	-	-	-	-	15.3	-	-	-	-	-	-	-	-	-
Ge	-	-	-	-	-	2.29	-	-	-	-	-	-	-	-	-
Hf	-	-	-	-	-	18.3	-	-	-	-	-	-	-	-	-
Ho	-	-	-	-	-	2.50	-	-	-	-	-	-	-	-	-
La	-	-	-	-	-	92.7	-	-	-	-	-	-	-	-	-
Li	-	-	-	-	-	12.5	-	-	-	-	-	-	-	-	-
Lu	-	-	-	-	-	1.06	-	-	-	-	-	-	-	-	-
Mo	3.50	3.30	3.60	5.50	3.00	2.65	2.80	2.70	4.10	2.50	1.80	4.30	4.00	2.30	3.00
Nb	39.7	32.1	76.9	80.8	79.5	77.9	81.2	83.7	41.5	144	102	79.9	79.6	72.1	79.3
Nd	-	-	-	-	-	80.3	-	-	-	-	-	-	-	-	-
Ni	<DL	<DL	<DL	<DL	<DL	1.50	<DL	<DL	<DL	<DL	<DL	<DL	<DL	<DL	<DL
Pb	19.6	29.1	20.6	26.7	28.7	48.5	79.4	30.5	15.6	66.1	25.9	34.0	24.3	30.5	26.1
Pr	-	-	-	-	-	21.9	-	-	-	-	-	-	-	-	-
Rb	170	215	183	192	189	187	194	202	158	169	251	198	201	182	198
Sb	-	-	-	-	-	1.17	-	-	-	-	-	-	-	-	-
Sc	-	-	-	-	-	3.77	-	-	-	-	-	-	-	-	-
Sm	-	-	-	-	-	15.3	-	-	-	-	-	-	-	-	-
Sn	2.7	1.6	6.7	7.3	6.7	5.9	4.7	6.8	1.7	12.3	8.1	5.2	4.1	4.4	5.9
Sr	85.4	33.9	23.6	19.2	28.5	11.8*	25.9	19.9	53.5	23.1	19.6	19.8	21.1	19.7	20.1
Ta	-	-	-	-	-	5.62	-	-	-	-	-	-	-	-	-
Tb	-	-	-	-	-	2.36	-	-	-	-	-	-	-	-	-
Te	-	-	-	-	-	0.07	-	-	-	-	-	-	-	-	-
Th	22.6	24.2	23.2	23.0	23.4	23.4	23.5	23.1	22.2	34.1	31.5	23.3	22.1	21.6	22.7
Tl	-	-	-	-	-	0.93	-	-	-	-	-	-	-	-	-
Tm	-	-	-	-	-	1.08	-	-	-	-	-	-	-	-	-
U	-	-	-	-	-	4.94	-	-	-	-	-	-	-	-	-
V	21.9	16.8	12.8	14.1	20.0	24.5	20.6	14.6	23.5	13.4	14.4	16.0	14.1	14.8	15.8
W	214	112	264	434	195	305	137	200	274	170	241	158	207	195	64.3
Y	41.8	29.1	64.6	54.0	56.9	61.8	56.0	69.9	35.8	122	92.4	64.9	59.0	56.5	71.1
Yb	-	-	-	-	-	7.17	-	-	-	-	-	-	-	-	-
Zn	43.5	39.3	93.8	97.8	89.9	76.8	90.3	96.0	40.7	210	154	90.3	94.3	91.9	112
Zr	432	234	578	603	599	562	602	604	407	1260	947	592	585	533	604

Table 7.2: (Continuation)

Sample	ANT-35	ANT-36	ANT-37	ANT-38	ANT-41	ANT-47	ANT-48	ANT-49	ANT-50	ANT-54	ANT-55	ANT-57	ANT-62	ANT-64	ANT-65
Unit	SP	SP	SP	MU	CO	MU	MU	MU	MU	MU	MU	CO	MZ	MZ	NU
	rhyolite	rhyolite	rhyolite	rhyolite	rhyolite	rhyolite	rhyolite	rhyolite	rhyolite	rhyolite	rhyolite	rhyolite	rhyolite	rhyolite	rhyolite
As	-	-	-	-	-	-	-	-	-	-	-	3.32	3.89	4.51	14.3
Ba	664	650	777	68.7	<LL	<LL	<LL	<LL	<LL	<LL	<LL	25.5*	810	961	1150
Be	-	-	-	-	-	-	-	-	-	-	-	6.81	2.48	2.10	3.13
Bi	-	-	-	-	-	-	-	-	-	-	-	0.02	0.01	0.01	0.09
Ce	99.1	116	100	178	199	163	151	114	195	188	159	236	91.0	102	122
Co	40.5	48.4	18.0	8.0	16.7	25.4	18.6	36.4	36.8	26.5	32.2	25.6	34.2	21.0	21.9
Cr	37.2	31.0	36.1	32.1	<LL	<LL	<LL	<LL	<LL	<LL	<LL	6.86	17.7	17.5	18.6
Cs	-	-	-	-	-	-	-	-	-	-	-	2.11	2.01	1.97	2.51
Cu	<DL	<DL	<DL	<DL	<LL	<LL	<LL	<LL	<LL	<LL	<LL	2.80	4.07	4.33	5.04
Dy	-	-	-	-	-	-	-	-	-	-	-	16.2	7.11	7.01	7.55
Er	-	-	-	-	-	-	-	-	-	-	-	8.96	3.91	3.90	3.80
Eu	-	-	-	-	-	-	-	-	-	-	-	0.42	1.68	1.81	1.92
Ga	15.8	16.0	15.9	22.0	23.6	23.6	23.5	23.7	25.4	25.4	25.1	24.7	13.0	14.2	15.6
Gd	-	-	-	-	-	-	-	-	-	-	-	17.1	8.36	7.94	9.20
Ge	-	-	-	-	-	-	-	-	-	-	-	2.00	1.25	1.31	1.56
Hf	-	-	-	-	-	-	-	-	-	-	-	21.2	4.45	3.69	6.98
Ho	-	-	-	-	-	-	-	-	-	-	-	2.96	1.31	1.32	1.26
La	-	-	-	-	-	-	-	-	-	-	-	105	47.9	46.1	57.9
Li	-	-	-	-	-	-	-	-	-	-	-	19.4	24.4	27.6	33.8
Lu	-	-	-	-	-	-	-	-	-	-	-	1.29	0.49	0.51	0.50
Mo	5.10	4.90	3.70	3.70	<LL	<LL	<LL	<LL	<LL	<LL	<LL	1.38	0.55	0.51	2.53
Nb	42.6	43.6	41.6	82.7	99.0	88.1	90.5	86.2	92.6	94.4	95.0	107	34.0	35.9	42.4
Nd	-	-	-	-	-	-	-	-	-	-	-	85.8	41.5	40.1	51.1
Ni	<DL	<DL	<DL	<DL	<LL	<LL	<LL	<LL	<LL	<LL	<LL	0.57	2.50	1.61	1.51
Pb	20.8	26.5	22.9	30.6	22.2	39.9	39.2	37.3	21.0	47.9	55.3	24.1	20.2	14.2	19.8
Pr	-	-	-	-	-	-	-	-	-	-	-	23.7	10.7	10.6	14.2
Rb	171	172	160	204	208	210	216	214	227	225	226	214	145	151	184
Sb	-	-	-	-	-	-	-	-	-	-	-	0.38	0.64	0.60	2.13
Sc	-	-	-	-	-	-	-	-	-	-	-	2.02	3.30	3.81	6.57
Sm	-	-	-	-	-	-	-	-	-	-	-	16.3	7.85	7.57	9.46
Sn	1.8	5.1	2.1	6.1	8.7	7.4	9.5	6.8	8.6	7.9	7.6	6.7	1.34*	1.23*	3.4
Sr	50.0	50.3	55.9	23.7	45.1	<LL	<LL	<LL	<LL	<LL	<LL	9.05*	79.4	95.0	99.2
Ta	-	-	-	-	-	-	-	-	-	-	-	13.2	0.18	0.17	0.44
Tb	-	-	-	-	-	-	-	-	-	-	-	2.69	1.21	1.16	1.29
Te	-	-	-	-	-	-	-	-	-	-	-	0.09	0.04	0.10	0.09
Th	23.8	23.9	22.9	23.7	13.0	23.9	25.3	21.0	18.4	18.6	20.4	20.4	13.7	14.7	17.0
Tl	-	-	-	-	-	-	-	-	-	-	-	0.42	0.30	0.29	0.51
Tm	-	-	-	-	-	-	-	-	-	-	-	1.28	0.53	0.53	0.52
U	-	-	-	-	-	-	-	-	-	-	-	2.02	3.30	2.74	4.46
V	19.5	21.2	20.3	17.7	9.0	16.1	21.7	11.6	11.8	8.2	10.8	10.1	17.2	20.3	22.9
W	272	278	116	62.1	172	219	194	240	308	238	257	245	131	138	135
Y	30.7	35.7	26.8	62.2	60.0	59.3	64.7	65.0	73.5	60.8	54.5	74.9	42.3	44.5	36.1
Yb	-	-	-	-	-	-	-	-	-	-	-	8.67	3.37	3.38	3.45
Zn	51.8	50.8	40.8	91.9	101	92.6	86.6	115	93.7	125	123	118	30.9	38.7	44.7
Zr	407	410	405	612	699	673	675	642	687	700	700	791	377	416	493

Table 7.2: (Continuation)

Sample	ANT-66	ANT-67	ANT-68	ANT-70	ANT-71	ANT-79	ANT-81	ANT-82	ANT-85	ANT-90	ANT-94	ANT-95	ANT-96	ANT-99	ANT-100
Unit	NU rhyolite	SP rhyclite	NU rhyolite	MZ rhyolite	MC rhyolite	SP rhyolite	SP rhyolite	SP rhyolite	CO rhyolite	CO rhyolite	CO rhyolite	CO rhyolite	CO rhyolite	MU rhyolite	CO rhyolite
As	-	-	-	6.33	-	5.81	-	5.92	-	-	4.15	-	-	-	-
Ba	1160	619	1100	1100	210	583	830	714	<LL	<LL	49.7*	<LL	<LL	<LL	<LL
Be	-	-	-	2.71	-	3.26	-	3.08	-	-	5.68	-	-	-	-
Bi	-	-	-	0.01	-	0.08	-	0.01	-	-	0.08	-	-	-	-
Ce	140	91.1	136	94.4	128	111	98.4	107	200	293	231	230	224	192	157
Co	13.4	36.2	36.0	15.9	23.5	43.7	25.8	25.0	30.2	21.8	19.0	43.8	32.6	27.0	51.6
Cr	<LL	<LL	<LL	18.7	<LL	18.4	<LL	18.2	<LL	<LL	18.6	<LL	<LL	<LL	<LL
Cs	-	-	-	4.08	-	3.08	-	1.05	-	-	1.91	-	-	-	-
Cu	<LL	<LL	<LL	7.01	<LL	4.61	<LL	5.04	<LL	<LL	2.65	5.3	<LL	<LL	9.1
Dy	-	-	-	6.89	-	8.12	-	8.03	-	-	17.2	-	-	-	-
Er	-	-	-	3.35	-	4.68	-	3.91	-	-	8.70	-	-	-	-
Eu	-	-	-	1.98	-	1.03	-	1.31	-	-	0.56	-	-	-	-
Ga	15.9	15.9	16.0	17.1	17.2	15.1	16.2	16.2	26.5	25.4	26.3	25.3	26.1	23.7	25.0
Gd	-	-	-	8.28	-	8.76	-	9.39	-	-	20.0	-	-	-	-
Ge	-	-	-	1.55	-	1.62	-	1.53	-	-	2.16	-	-	-	-
Hf	-	-	-	6.54	-	12.6	-	4.50	-	-	25.2	-	-	-	-
Ho	-	-	-	1.17	-	1.48	-	1.35	-	-	2.96	-	-	-	-
La	-	-	-	55.0	-	62.1	-	58.5	-	-	129	-	-	-	-
Li	-	-	-	25.5	-	14.7	-	8.67	-	-	26.7	-	-	-	-
Lu	-	-	-	0.40	-	0.70	-	0.50	-	-	1.15	-	-	-	-
Mo	<LL	<LL	<LL	2.33	<LL	3.25	<LL	3.17	<LL	<LL	0.83	<LL	<LL	<LL	<LL
Nb	43.0	47.7	43.3	43.4	36.1	45.2	47.9	46.2	96.7	187	108	168	65.4	86.8	107
Nd	-	-	-	45.2	-	46.4	-	48.1	-	-	107	-	-	-	-
Ni	<LL	<LL	<LL	1.51	<LL	0.85	<LL	1.14	<LL	<LL	1.67	<LL	<LL	<LL	<LL
Pb	21.9	18.5	22.0	16.9	29.7	23.6	52.7	21.7	23.0	49.5	47.5	54.9	21.5	29.1	24.3
Pr	-	-	-	12.4	-	13.3	-	13.3	-	-	29.5	-	-	-	-
Rb	196	199	192	171	235	184	207	178	197	350	232	284	213	209	219
Sb	-	-	-	0.79	-	0.63	-	0.61	-	-	0.36	-	-	-	-
Sc	-	-	-	5.63	-	4.36	-	3.93	-	-	2.23	-	-	-	-
Sm	-	-	-	8.37	-	8.47	-	9.15	-	-	20.2	-	-	-	-
Sn	<LL	<LL	3.4	3.33*	3.2	4.5	2.6	3.25*	7.5	18.8	9.0	15.0	7.5	9.5	10.1
Sr	82.1	43.6	91.9	121	32.3	40.4*	75.9	64.5	<LL	<LL	6.75*	<LL	<LL	<LL	<LL
Ta	-	-	-	0.30	-	0.34	-	0.39	-	-	2.00	-	-	-	-
Tb	-	-	-	1.20	-	1.34	-	1.39	-	-	2.99	-	-	-	-
Te	-	-	-	0.05	-	0.04	-	0.06	-	-	0.12	-	-	-	-
Th	17.3	19.9	18.7	16.0	25.2	18.9	16.6	19.7	13.1	29.3	16.1	23.4	15.6	16.8	14.3
Tl	-	-	-	0.21	-	0.48	-	0.27	-	-	0.70	-	-	-	-
Tm	-	-	-	0.45	-	0.68	-	0.54	-	-	1.18	-	-	-	-
U	-	-	-	4.08	-	6.57	-	3.21	-	-	2.26	-	-	-	-
V	21.3	12.7	20.7	23.8	11.0	13.1	17.8	17.8	15.1	8.5	12.9	10.0	12.1	9.4	8.4
W	132	257	181	117	185	247	166	191	281	241	260	383	326	222	345
Y	52.3	29.8	42.7	33.2	53.1	39.2	38.5	39.7	55.8	>UL	75.6	>UL	52.8	66.4	70.7
Yb	-	-	-	2.91	-	4.63	-	3.59	-	-	7.86	-	-	-	-
Zn	46.8	36.8	53.0	51.4	39.6	55.3	76.7	75.8	101	251	129	211	107	101	123
Zr	498	424	483	480	275	433	444	453	695	>UL	807	1320	625	656	782

Table 7.2: (Continuation)

Sample	ANT-101	ANT-105	ANT-106	ANT-108	ANT-109	ANT-110	SU-1	SU-2	SU-3	SU-4	SU-5	SU-8	SU-12a	SU-12b	SU-13b
Unit	CO rhyolite	CO rhyolite	CO rhyolite	MU rhyolite	MU rhyolite	MU rhyolite	NU rhyolite	NU rhyolite	NU rhyolite	NU rhyolite	NU rhyolite	NU rhyolite	NU rhyolite	NU rhyolite	NU rhyolite
As	-	-	4.07	9.60	8.10	5.50	-	27.2	26.2	-	-	-	-	-	-
Ba	<LL	<LL	12.9*	12.8*	9.02*	15.8*	-	-	-	-	-	-	343	-	691
Be	-	-	5.04	7.77	6.17	6.06	-	4.11	4.10	-	-	-	-	-	-
Bi	-	-	0.19	0.07	0.03	0.01	-	0.05	0.31	-	-	-	-	-	-
Ce	250	191	215	142	124	132	-	-	-	-	-	-	117	-	132
Co	31.6	17.4	30.8	20.5	17.6	28.3	-	-	-	-	-	-	73.2	-	31.9
Cr	<LL	<LL	17.9	7.26	6.93	7.50	-	18.1	22.4	-	-	-	-	-	-
Cs	-	-	0.96	3.49	2.94	2.83	-	8.80	8.03	-	-	-	-	-	-
Cu	<LL	<LL	2.54	2.67	2.14	2.50	-	3.91	3.63	-	-	-	<DL	-	<DL
Dy	-	-	14.5	15.8	11.3	11.9	-	11.0	10.9	-	-	-	-	-	-
Er	-	-	8.59	9.27	6.06	6.40	-	6.26	6.12	-	-	-	-	-	-
Eu	-	-	0.39	0.20	0.20	0.15	-	1.23	1.36	-	-	-	-	-	-
Ga	25.4	24.2	25.6	24.0	25.0	23.1	-	-	-	-	-	-	16.0	-	16.1
Gd	-	-	15.1	16.0	12.5	13.3	-	11.8	12.0	-	-	-	-	-	-
Ge	-	-	2.17	1.94	1.95	1.93	-	1.84	1.71	-	-	-	-	-	-
Hf	-	-	22.0	19.8	13.0	12.2	-	13.6	13.4	-	-	-	-	-	-
Ho	-	-	2.74	3.06	2.09	2.22	-	2.04	1.99	-	-	-	-	-	-
La	-	-	94.3	96.7	76.7	89.7	-	71.6	73.1	-	-	-	-	-	-
Li	-	-	39.0	16.3	21.5	21.9	-	51.8	35.2	-	-	-	-	-	-
Lu	-	-	1.33	1.31	0.81	0.81	-	0.93	0.87	-	-	-	-	-	-
Mo	<LL	<LL	0.59	3.63	1.62	1.59	-	5.20	2.01	-	-	-	4.40	-	2.80
Nb	100	105	105	98.2	95.5	88.9	-	-	-	-	-	-	47.0	-	45.1
Nd	-	-	77.3	81.2	64.4	71.2	-	61.3	63.6	-	-	-	-	-	-
Ni	<LL	<LL	1.20	1.26	0.84	2.19	-	1.36	2.87	-	-	-	4.40	-	5.10
Pb	21.3	23.3	17.7	27.2	36.5	27.6	-	-	-	-	-	-	31.6	-	31.9
Pr	-	-	21.4	22.2	17.7	19.8	-	16.8	17.5	-	-	-	-	-	-
Rb	229	215	221	231	235	221	-	-	-	-	-	-	218	-	210
Sb	-	-	0.42	0.84	0.67	0.54	-	2.99	2.87	-	-	-	-	-	-
Sc	-	-	2.18	4.17	3.77	3.80	-	6.84	6.68	-	-	-	-	-	-
Sm	-	-	15.0	15.6	12.4	13.1	-	11.5	12.2	-	-	-	-	-	-
Sn	6.6	10.1	9.2	7.9	7.8	6.8	-	-	-	-	-	-	3.2	-	<DL
Sr	<LL	<LL	<LL	<LL	<LL	7.49*	-	-	-	-	-	-	33.2	-	57.5
Ta	-	-	1.33	5.24	3.97	7.47	-	3.13	2.61	-	-	-	-	-	-
Tb	-	-	2.38	2.58	1.96	2.00	-	1.80	1.84	-	-	-	-	-	-
Te	-	-	0.12	0.07	0.02	0.02	-	0.09	0.08	-	-	-	-	-	-
Th	18.2	20.3	17.9	20.8	18.4	16.6	-	-	-	-	-	-	26.6	-	24.8
Tl	-	-	0.08	0.82	0.72	0.65	-	0.98	1.00	-	-	-	-	-	-
Tm	-	-	1.25	1.29	0.83	0.86	-	0.92	0.88	-	-	-	-	-	-
U	-	-	4.65	4.66	4.18	4.47	-	7.08	7.37	-	-	-	-	-	-
V	9.8	8.0	7.4	9.3	8.7	8.5	-	-	-	-	-	-	15.6	-	19.6
W	367	113	221	107	95.3	179	-	-	-	-	-	-	560	-	406
Y	76.0	84.2	82.3	92.3	71.0	75.8	-	-	-	-	-	-	45.8	-	46.9
Yb	-	-	8.51	8.70	5.43	5.42	-	6.20	5.87	-	-	-	-	-	-
Zn	129	175	119	107	106	127	-	-	-	-	-	-	63.5	-	61.7
Zr	778	950	799	675	681	654	-	-	-	-	-	-	427	-	461

Table 7.2: (Continuation)

Sample	SU-13bis a	SU-13bis b	SU-14a	SU-14b	SU-15b	SU-15c	SU-16	SU-13a	VS-145	VS-146	VS-147	VS-148	VS-149	VS-159	VS-161
Unit	NU rhyolite	NU rhyolite	NU rhyolite	NU rhyolite	NU rhyolite	NU rhyolite	NU trachyte	NU rhyolite	NU rhyolite	NU rhyolite	NU rhyolite	NU rhyolite	NU rhyolite	NU rhyolite	NU rhyolite
As	-	-	-	-	-	-	-	-	-	-	-	-	-	-	-
Ba	654	-	686	-	391	-	-	-	1100	1090	951	930	933	378	917
Be	-	-	-	-	-	-	-	-	-	-	-	-	-	-	-
Bi	-	-	-	-	-	-	-	-	-	-	-	-	-	-	-
Ce	98.4	-	104	-	114	-	-	-	95.6	114	111	102	113	112	119
Co	67.9	-	68.1	-	80.2	-	-	-	47.1	32.8	35.2	39.5	38.9	84.7	27.3
Cr	-	-	-	-	-	-	-	-	29.8	26.5	32.5	38.3	31.7	21.9	28.0
Cs	-	-	-	-	-	-	-	-	-	-	-	-	-	-	-
Cu	<DL	-	<DL	-	<DL	-	-	-	<DL	<DL	<DL	<DL	<DL	<DL	<DL
Dy	-	-	-	-	-	-	-	-	-	-	-	-	-	-	-
Er	-	-	-	-	-	-	-	-	-	-	-	-	-	-	-
Eu	-	-	-	-	-	-	-	-	-	-	-	-	-	-	-
Ga	15.8	-	16.1	-	16.0	-	-	-	16.9	16.4	15.7	15.8	15.5	15.4	16.8
Gd	-	-	-	-	-	-	-	-	-	-	-	-	-	-	-
Ge	-	-	-	-	-	-	-	-	-	-	-	-	-	-	-
Hf	-	-	-	-	-	-	-	-	-	-	-	-	-	-	-
Ho	-	-	-	-	-	-	-	-	-	-	-	-	-	-	-
La	-	-	-	-	-	-	-	-	-	-	-	-	-	-	-
Li	-	-	-	-	-	-	-	-	-	-	-	-	-	-	-
Lu	-	-	-	-	-	-	-	-	-	-	-	-	-	-	-
Mo	2.40	-	2.10	-	3.50	-	-	-	1.20	1.70	4.90	4.70	4.70	3.50	0.70
Nb	43.9	-	44.9	-	46.1	-	-	-	34.0	34.0	40.8	38.3	39.2	29.4	38.4
Nd	-	-	-	-	-	-	-	-	-	-	-	-	-	-	-
Ni	4.90	-	6.20	-	3.80	-	-	-	<DL	<DL	<DL	<DL	<DL	<DL	<DL
Pb	29.0	-	38.2	-	37.3	-	-	-	24.9	23.9	22.1	21.9	24.1	21.3	27.2
Pr	-	-	-	-	-	-	-	-	-	-	-	-	-	-	-
Rb	199	-	199	-	207	-	-	-	170	168	182	175	175	194	184
Sb	-	-	-	-	-	-	-	-	-	-	-	-	-	-	-
Sc	-	-	-	-	-	-	-	-	-	-	-	-	-	-	-
Sm	-	-	-	-	-	-	-	-	-	-	-	-	-	-	-
Sn	4.8	-	1.4	-	2.7	-	-	-	<DL	<DL	4.1	2.8	4.3	<DL	<DL
Sr	56.5	-	60.8	-	34.9	-	-	-	104	107	76.0	75.8	77.5	41.2	78.4
Ta	-	-	-	-	-	-	-	-	-	-	-	-	-	-	-
Tb	-	-	-	-	-	-	-	-	-	-	-	-	-	-	-
Te	-	-	-	-	-	-	-	-	-	-	-	-	-	-	-
Th	24.0	-	23.5	-	27.3	-	-	-	20.3	18.8	21.9	20.2	22.2	23.1	23.5
Tl	-	-	-	-	-	-	-	-	-	-	-	-	-	-	-
Tm	-	-	-	-	-	-	-	-	-	-	-	-	-	-	-
U	-	-	-	-	-	-	-	-	-	-	-	-	-	-	-
V	19.4	-	18.7	-	15.6	-	-	-	26.1	25.6	21.5	20.2	21.4	23.4	22.2
W	370	-	400	-	641	-	-	-	251	222	238	231	281	389	211
Y	32.8	-	33.6	-	45.5	-	-	-	40.5	37.4	38.2	37.1	37.5	46.1	42.6
Yb	-	-	-	-	-	-	-	-	-	-	-	-	-	-	-
Zn	56.5	-	66.5	-	68.0	-	-	-	61.4	54.6	53.1	48.4	49.2	53.1	60.9
Zr	440	-	459	-	418	-	-	-	439	424	433	418	424	395	443

Table 7.2: (Continuation)

Sample	VS-163	VS-165	VS-167	VS-168	VS-169	VS-170	VS-177	VS-178	VS-179	VS-180	VS-715	VS-716	VS-720	VS-721	VS-722
Unit	NU rhyolite	NU rhyolite	NU rhyolite	NU rhyolite	NU rhyolite	NU rhyolite	NU rhyolite	NU rhyolite	NU rhyolite	NU rhyolite	AND b. andesite	AND b. andesite	AND andesite	AND andesite	AND andesite
As	15.4	-	-	-	-	-	-	12.6	-	-	-	1.71	2.03	-	2.89
Ba	1200	1200	1110	1100	1200	1240	863	1260	858	1000	237	302	375	401	417
Be	3.22	-	-	-	-	-	-	3.17	-	-	-	0.99	1.27	-	1.25
Bi	0.08	-	-	-	-	-	-	0.03	-	-	-	0.01	-	-	0.01
Ce	102	113	115	113	108	105	83.8	115	103	99.2	33.6	38.2*	38.0	39.2	46.2*
Co	80.2	25.9	32.5	31.7	32.1	31.0	53.4	44.4	30.7	37.5	36.2	35.8	45.6	36.2	32.6
Cr	7.31	29.5	26.9	54.4	28.1	29.4	32.1	7.88	32.6	35.4	<LL	36.1	20.3	<LL	24.8
Cs	3.20	-	-	-	-	-	-	2.87	-	-	-	1.16	1.84	-	1.43
Cu	5.24	<DL	<DL	<DL	<DL	<DL	<DL	4.72	<DL	<DL	25.6	28.3	19.6	12.9	17.1
Dy	8.16	-	-	-	-	-	-	7.49	-	-	-	5.07	5.36	-	5.09
Er	4.35	-	-	-	-	-	-	3.86	-	-	-	2.91	3.05	-	2.93
Eu	1.71	-	-	-	-	-	-	1.85	-	-	-	1.44	1.45	-	1.49
Ga	17.9	17.5	16.8	16.9	17.0	16.9	14.3	17.3	15.1	15.8	18.4	18.4	18.3	19.0	19.4
Gd	9.56	-	-	-	-	-	-	8.95	-	-	-	5.15	5.72	-	5.64
Ge	1.49	-	-	-	-	-	-	1.43	-	-	-	1.54	1.48	-	1.44
Hf	8.18	-	-	-	-	-	-	7.22	-	-	-	4.51	4.42	-	4.36
Ho	1.46	-	-	-	-	-	-	1.33	-	-	-	0.98	1.02	-	0.97
La	59.6	-	-	-	-	-	-	58.6	-	-	-	18.1	24.6	-	23.2
Li	33.7	-	-	-	-	-	-	16.9	-	-	-	10.7	12.9	-	9.11
Lu	0.58	-	-	-	-	-	-	0.48	-	-	-	0.43	0.45	-	0.41
Mo	3.28	1.50	0.80	0.60	1.30	2.00	4.30	3.30	4.40	3.60	<LL	0.81	1.11	<LL	1.07
Nb	29.8	35.6	33.6	34.5	34.4	34.0	35.0	32.3	37.7	39.9	8.4	9.9	11.0	10.6	10.7
Nd	50.0	-	-	-	-	-	-	48.5	-	-	-	21.8	25.9	-	25.5
Ni	1.17	<DL	<DL	<DL	<DL	<DL	<DL	0.90	<DL	<DL	<LL	7.43	4.05	<LL	4.32
Pb	24.6	20.6	21.8	20.4	18.8	18.7	21.0	27.1	41.1	25.4	10.4	12.9	11.9	13.1	11.9
Pr	13.6	-	-	-	-	-	-	13.2	-	-	-	5.09	6.32	-	6.13
Rb	181	174	163	167	166	162	150	160	165	168	41.9	36.7	64.0	58.5	57.7
Sb	1.75	-	-	-	-	-	-	1.97	-	-	-	0.10	0.12	-	0.15
Sc	7.59	-	-	-	-	-	-	7.83	-	-	-	28.9	19.2	-	21.5
Sm	9.42	-	-	-	-	-	-	9.22	-	-	-	4.90	5.51	-	5.47
Sn	4.45*	0.5	<DL	<DL	<DL	<DL	2.4	5.04*	1.0	3.4	<LL	1.41*	1.46*	2.2	1.27*
Sr	109	102	102	102	107	107	77.1	115	79.1	95.5	336	298	315	325	325
Ta	3.85	-	-	-	-	-	-	2.27	-	-	-	0.70	0.66	-	0.71
Tb	1.42	-	-	-	-	-	-	1.30	-	-	-	0.83	0.88	-	0.86
Te	0.10	-	-	-	-	-	-	0.04	-	-	-	1.28	1.32	-	0.97
Th	20.8	21.9	19.4	19.8	19.4	19.4	19.5	19.6	19.1	20.8	5.20	4.80	6.50	7.50	6.60
Tl	0.53	-	-	-	-	-	-	0.50	-	-	-	0.13	0.19	-	0.23
Tm	0.60	-	-	-	-	-	-	0.52	-	-	-	0.41	0.43	-	0.42
U	4.51	-	-	-	-	-	-	4.01	-	-	-	0.61	1.00	-	0.91
V	24.3	22.5	23.8	23.6	23.8	25.3	24.8	29.4	23.3	21.9	221	185	115	136	123
W	422	203	240	215	227	242	299	305	237	265	136	162	125	185	133
Y	35.6	39.8	41.1	37.2	33.7	37.1	26.1	34.5	35.4	35.8	19.7	23.5	25.4	22.9	23.3
Yb	3.95	-	-	-	-	-	-	3.44	-	-	-	2.78	2.96	-	2.71
Zn	60.0	49.7	53.1	47.5	48.2	54.4	63.1	80.7	146	73.4	109	99.8	101	97.5	94.8
Zr	440	437	421	422	436	435	394	451	428	432	112	144	146	143	141

Table 7.2: (Continuation)

Sample	VS-723	VS-724	VS-725	VS-726	VS-727	VS-728	VS-729	VS-732	VS-742	VS-745	VS-751	VS-752	VS-753	VS-757	VS-758
Unit	AND andesite	AND b. andesite	AND andesite	AND b. andesite	MC rhyolite	NU rhyolite	NU rhyolite	NU rhyolite	MC rhyolite	MU rhyolite	CO rhyolite	MZ trachyte	NU rhyolite	NU rhyolite	AND b. andesite
As	-	2.19	-	1.93	-	-	-	-	-	14.1	4.07	-	-	12.9	2.04
Ba	340	293	288	238	1480	1280	1220	1330	917	115*	74.8*	1090	983	1100	392
Be	-	0.94	-	0.95	-	-	-	-	-	7.11	4.44	-	-	3.26	1.48
Bi	-	0.01	-	0.02	-	-	-	-	-	0.05	0.02	-	-	0.01	0.02
Ce	33.6	36.6*	28.6	31.9*	97.7	98.3	102	97.8	100	169	155	135	99.1	101	42.6*
Co	34.6	42.2	41.8	36.2	34.7	24.7	24.2	56.4	38.1	46.2	48.5	34.1	40.9	26.5	35.9
Cr	<LL	41.2	<LL	36.5	<LL	<LL	<LL	<LL	<LL	7.40	8.08	<LL	<LL	7.42	20.2
Cs	-	0.92	-	1.09	-	-	-	-	-	4.34	3.15	-	-	2.96	2.10
Cu	9.20	32.2	10.0	37.4	<LL	<LL	<LL	<LL	<LL	2.32	3.61	8.9	<LL	4.44	19.8
Dy	-	5.04	-	4.85	-	-	-	-	-	14.1	11.4	-	-	7.72	4.98
Er	-	2.92	-	2.78	-	-	-	-	-	8.09	6.32	-	-	4.03	2.74
Eu	-	1.41	-	1.30	-	-	-	-	-	0.16	0.45	-	-	1.83	1.46
Ga	17.5	18.8	16.2	19.2	20.8	21.6	21.6	21.9	19.8	25.7	28.5	22.8	20.4	20.9	20.2
Gd	-	5.04	-	4.81	-	-	-	-	-	14.5	11.7	-	-	8.89	5.41
Ge	-	1.52	-	1.46	-	-	-	-	-	1.91	1.74	-	-	1.39	1.41
Hf	-	4.23	-	3.33	-	-	-	-	-	18.1	14.3	-	-	5.64	3.94
Ho	-	0.97	-	0.93	-	-	-	-	-	2.67	2.15	-	-	1.39	0.94
La	-	17.4	-	14.4	-	-	-	-	-	86.5	67.5	-	-	56.5	23.5
Li	-	7.66	-	9.65	-	-	-	-	-	6.67	14.1	-	-	19.1	19.1
Lu	-	0.41	-	0.39	-	-	-	-	-	1.18	0.92	-	-	0.50	0.38
Mo	<LL	0.90	<LL	0.72	<LL	<LL	<LL	<LL	<LL	3.37	2.46	<LL	<LL	2.81	0.92
Nb	10.9	10.2	10.5	8.7	31.5	42.9	43.8	44.6	32.8	86.4	78.7	44.7	42.4	42.2	10.4
Nd	-	21.4	-	18.7	-	-	-	-	-	72.0	58.1	-	-	47.2	24.0
Ni	<LL	7.28	<LL	8.99	<LL	<LL	<LL	<LL	<LL	1.80	1.73	<LL	<LL	0.89	3.07
Pb	10.7	8.9	11.9	7.40	28.3	37.8	18.6	39.5	50.9	35.8	18.8	17.2	24.0	18.8	12.8
Pr	-	4.89	-	4.28	-	-	-	-	-	19.8	15.7	-	-	12.8	5.81
Rb	56.5	34.5	53.0	36.3	195	184	193	190	180	210	160	175	180	182	60.5
Sb	-	0.09	-	0.08	-	-	-	-	-	0.92	0.57	-	-	1.74	0.40
Sc	-	31.9	-	33.1	-	-	-	-	-	4.05	2.87	-	-	7.64	21.4
Sm	-	4.76	-	4.47	-	-	-	-	-	14.0	11.5	-	-	8.93	5.02
Sn	<LL	1.24*	<LL	1.41*	5.7	4.2	2.3	2.4	13.1	5.5	6.1	3.1	2.4	4.2	1.71*
Sr	300	307	281	318	93.2	105	112	113	58.3	13.1*	16.7*	122	94.7	108	298
Ta	-	0.66	-	0.67	-	-	-	-	-	9.28	11.5	-	-	3.38	0.71
Tb	-	0.82	-	0.78	-	-	-	-	-	2.27	1.83	-	-	1.33	0.83
Te	-	1.89	-	1.31	-	-	-	-	-	0.11	0.09	-	-	0.11	1.33
Th	5.20	4.10	5.80	3.50	15.4	15.8	15.4	15.2	16.3	16.2	9.20	14.8	14.8	15.1	6.90
Tl	-	0.15	-	0.13	-	-	-	-	-	0.75	0.36	-	-	0.45	0.26
Tm	-	0.41	-	0.38	-	-	-	-	-	1.18	0.92	-	-	0.55	0.38
U	-	0.49	-	0.54	-	-	-	-	-	5.79	3.54	-	-	3.62	1.02
V	127	182	97.5	249	19.3	22.9	23.0	22.9	14.8	15.2	14.1	23.7	25.0	22.5	161
W	174	271	231	196	132	174	186	183	194	201	353	136	301	138	197
Y	22.3	23.7	21.0	23.1	40.0	31.8	42.7	30.3	38.9	71.3	62.9	46.3	38.3	42.0	23.8
Yb	-	2.74	-	2.50	-	-	-	-	-	7.77	6.12	-	-	3.54	2.56
Zn	97.0	98.5	85.1	94.8	72.7	54.0	53.4	57.8	56.4	93.8	108	46.3	58.5	44.4	93.5
Zr	138	141	153	113	446	473	500	500	404	630	612	512	464	451	135

Table 7.2: (Continuation)

Sample	VS-759	VS-760	VS-761	VS-762	VS-763	VS-765	VS-766	VS-773	VS-775	VS-780	VS-781	VS-782	VS-783	VS-784	VS-785
Unit	MC rhyolite	MZ trachyte	MZ rhyolite	MZ rhyolite	MLN rhyolite	MC rhyolite	MC rhyolite	MLN rhyolite	MLN rhyolite	MLN rhyolite	CF rhyolite	AC trachyte	SE rhyolite	LE rhyolite	CM trachyte
As	-	4.70	-	5.56	2.19	11.1	9.93	2.62	2.30	5.65	9.58	5.37	14.2	23.7	-
Ba	209	1040	793	944	983	930	905	918	863	873	121	890	1100	779	856
Be	-	3.44	-	2.53	2.10	4.49	2.92	1.83	2.61	2.57	4.26	2.14	3.91	4.72	-
Bi	-	0.01	-	0.02	-	-	-	0.07	0.06	0.03	0.30	0.01	-	0.14	-
Ce	97.9	108	80.5	132	86.9	121	120	90.8	87.9	95.8	136	89.6	134	120	81.2
Co	46.2	51.4	18.2	28.8	23.3	26.0	18.2	14.9	43.0	23.5	20.8	15.2	8.4	8.7	12.1
Cr	<LL	17.9	<LL	18.5	17.8	17.9	17.5	19.0	17.4	18.4	17.6	12.6	8.08	10.6	<LL
Cs	-	2.08	-	2.77	1.15	4.38	4.14	3.69	4.53	3.46	3.24	3.08	3.40	6.44	-
Cu	<LL	12.1	<LL	7.46	5.15	4.94	3.87	3.33	3.02	3.70	3.91	8.68	4.82	6.51	5.80
Dy	-	10.5	-	10.5	3.55	12.3	9.15	4.07	3.78	4.25	10.2	7.62	8.03	10.4	-
Er	-	5.60	-	5.35	1.83	6.37	4.60	2.27	2.08	2.33	6.07	3.95	3.89	5.74	-
Eu	-	2.63	-	2.20	0.97	1.86	1.48	1.06	0.83	0.96	0.34	2.03	1.92	1.45	-
Ga	18.9	21.7	19.9	21.2	15.5	16.0	14.7	14.5	13.7	13.4	20.3	19.1	18.6	18.4	20.3
Gd	-	12.6	-	12.4	4.83	13.7	10.6	5.69	4.83	5.49	10.1	9.03	9.81	11.8	-
Ge	-	1.42	-	1.53	1.41	1.56	1.53	1.45	1.36	1.46	1.79	1.14	1.51	1.56	-
Hf	-	5.54	-	5.39	8.57	2.17	1.92	5.78	5.81	6.02	14.9	6.09	2.40	9.10	-
Ho	-	1.99	-	1.89	0.60	2.20	1.58	0.71	0.67	0.74	1.97	1.38	1.38	1.94	-
La	-	68.6	-	77.3	45.0	71.9	64.9	57.8	50.2	52.9	60.7	46.9	58.3	65.4	-
Li	-	37.9	-	25.1	15.2	29.2	17.8	9.33	17.8	14.3	27.2	17.6	15.8	21.2	-
Lu	-	0.65	-	0.61	0.27	0.81	0.56	0.33	0.34	0.35	0.90	0.51	0.45	0.78	-
Mo	6.00	0.38	<LL	1.14	0.26	1.96	1.41	1.37	2.09	1.77	2.83	2.06	2.28	3.10	<LL
Nb	31.1	39.8	42.0	44.0	19.9	33.4	33.1	17.2	16.9	17.2	74.9	26.1	30.7	28.7	26.2
Nd	-	57.1	-	60.9	29.4	70.9	57.3	35.9	30.0	32.9	50.3	44.6	51.7	62.2	-
Ni	<LL	2.77	<LL	2.91	1.84	1.69	1.21	1.60	1.13	1.36	1.38	3.89	2.11	2.84	<LL
Pb	27.9	16.6	19.8	18.2	25.2	28.2	26.5	22.6	21.1	23.3	38.2	17.4	22.4	48.7	37.7
Pr	-	14.7	-	16.2	8.67	18.6	15.5	10.8	9.09	9.87	13.7	11.4	13.8	16.4	-
Rb	197	175	160	174	125	205	192	146	144	138	196	127	167	198	121
Sb	-	0.81	-	0.99	0.22	1.59	1.41	0.29	0.21	0.30	1.78	0.74	1.32	2.44	-
Sc	-	5.50	-	5.29	3.00	9.72	8.36	2.69	1.55	2.28	4.04	13.6	10.0	11.1	-
Sm	-	11.0	-	11.5	4.82	14.5	11.1	5.69	4.70	5.29	9.83	8.91	9.97	12.2	-
Sn	5.6	2.8	3.2	2.59*	1.21*	1.63*	4.3	4.8	3.9	3.7	7.9	2.1	4.1	3.7	8.4
Sr	31.2	192	82.9	118	172	41.7*	50.1	134	136	136	31.3*	273	127	96.6	254
Ta	-	0.23	-	0.39	0.41	0.13	0.18	0.26	0.15	0.41	1.01	3.92	1.78	1.79	-
Tb	-	1.82	-	1.83	0.63	2.10	1.58	0.72	0.65	0.72	1.67	1.32	1.41	1.77	-
Te	-	0.17	-	0.08	0.11	0.03	0.06	0.06	0.08	0.08	0.09	0.15	0.08	0.07	-
Th	20.6	10.7	14.8	14.9	15.8	17.5	19.1	19.1	17.7	17.4	15.2	17.1	22.4	22.9	10.8
Tl	-	0.42	-	0.26	0.48	0.52	0.48	0.46	0.58	0.56	0.63	0.55	0.53	0.90	-
Tm	-	0.71	-	0.69	0.25	0.87	0.62	0.32	0.31	0.34	0.89	0.55	0.52	0.80	-
U	-	3.55	-	2.96	2.31	2.82	1.90	2.79	3.80	3.53	5.21	1.86	1.64	4.40	-
V	13.7	28.6	17.3	20.7	9.8	13.7	15.6	8.9	7.6	10.1	12.4	50.9	15.1	26.2	35.5
W	178	207	89.0	82.1	68.4	157	154	118	258	187	120	88.5	99.3	78.1	38.9
Y	39.7	84.9	>UL	63.6	17.5	58.0	44.0	21.0	18.9	22.9	56.5	39.9	42.4	54.8	24.7
Yb	-	4.30	-	4.22	1.79	5.67	4.00	2.20	2.19	2.33	5.94	3.48	3.30	5.30	-
Zn	38.4	74.6	34.5	62.2	52.9	51.9	48.6	38.7	51.7	47.5	115	73.8	74.6	69.2	88.3
Zr	232	486	416	476	306	442	408	182	186	191	607	327	410	409	310

Table 7.2: (Continuation)

Sample	VS-786	VS-787	VS-788	VS-789	VS-790	VS-791	VS-792	VS-793	VS-794	VS-795	VS-797	VS-798	VS-801	VS-802	VS-803
Unit	CM trachyte	CA rhyolite	CA rhyolite	PA rhyolite	MC rhyolite	AND andesite	AND andesite	MC rhyolite	AND andesite	AND b. andesite	MLN rhyolite	MLN rhyolite	MC rhyolite	CA rhyolite	MC rhyolite
As	4.00	-	16.1	4.90	19.0	-	-	-	-	-	-	-	-	-	-
Ba	863	806	444	40.5	1380	534	428	112	685	391	893	997	144	130	1570
Be	4.00	-	3.31	3.66	3.11	-	-	-	-	-	-	-	-	-	-
Bi	0.01	-	0.17	0.01	0.05	-	-	-	-	-	-	-	-	-	-
Ce	65.1	100	162	106	122	31.5	23.4	152	35.7	37.6	93.4	89.2	141	115	112
Co	10.7	6.2	5.2	15.3	12.1	24.2	31.3	29.1	23.4	25.8	11.8	11.9	9.3	16.7	14.7
Cr	10.4	<LL	9.84	7.48	8.63	<LL	<LL	<LL	<LL	<LL	<LL	<LL	<LL	<LL	<LL
Cs	1.67	-	4.63	3.73	4.69	-	-	-	-	-	-	-	-	-	-
Cu	9.94	<LL	5.27	3.08	4.54	16.5	11.8	<LL	19.5	14.0	<LL	<LL	<LL	<LL	<LL
Dy	5.63	-	9.50	5.17	9.00	-	-	-	-	-	-	-	-	-	-
Er	2.93	-	5.13	2.91	4.69	-	-	-	-	-	-	-	-	-	-
Eu	1.93	-	0.97	0.23	1.77	-	-	-	-	-	-	-	-	-	-
Ga	20.6	16.6	16.5	15.4	16.1	19.8	19.6	17.3	19.4	20.2	15.6	16.4	16.9	17.6	17.3
Gd	6.70	-	10.8	5.94	10.3	-	-	-	-	-	-	-	-	-	-
Ge	1.17	-	1.34	1.55	1.45	-	-	-	-	-	-	-	-	-	-
Hf	6.44	-	6.55	4.18	5.81	-	-	-	-	-	-	-	-	-	-
Ho	1.00	-	1.73	0.95	1.60	-	-	-	-	-	-	-	-	-	-
La	39.7	-	68.6	51.0	59.5	-	-	-	-	-	-	-	-	-	-
Li	13.2	-	37.7	14.9	16.5	-	-	-	-	-	-	-	-	-	-
Lu	0.39	-	0.68	0.44	0.59	-	-	-	-	-	-	-	-	-	-
Mo	1.24	<LL	1.13	1.69	2.05	<LL	<LL	6.20	<LL	<LL	5.10	<LL	6.10	<LL	<LL
Nb	27.0	34.8	38.3	39.7	35.2	11.7	11.6	36.0	11.7	10.4	16.5	17.1	36.0	30.7	31.0
Nd	34.1	-	56.3	31.9	52.6	-	-	-	-	-	-	-	-	-	-
Ni	3.83	<LL	5.73	2.63	2.32	<LL	<LL	<LL	<LL	<LL	<LL	<LL	<LL	<LL	<LL
Pb	22.4	21.3	27.2	69.7	26.9	13.2	14.4	39.3	14.2	11.1	23.9	23.1	25.8	62.0	25.7
Pr	8.90	-	15.5	9.50	13.9	-	-	-	-	-	-	-	-	-	-
Rb	125	230	225	198	202	65.1	69.1	230	68.5	59.1	149	148	225	176	183
Sb	1.25	-	2.46	0.86	1.63	-	-	-	-	-	-	-	-	-	-
Sc	17.7	-	9.88	1.68	11.8	-	-	-	-	-	-	-	-	-	-
Sm	6.79	-	10.8	5.58	10.3	-	-	-	-	-	-	-	-	-	-
Sn	4.9	2.8	7.2	3.7	3.4	2.1	2.4	3.6	<LL	<LL	2.1	4.5	8.5	3.6	3.4
Sr	234	69.3	65.2	12.6*	75.3	321	264	26.5	295	284	123	132	32.6	89.9	87.6
Ta	2.60	-	1.98	3.94	1.84	-	-	-	-	-	-	-	-	-	-
Tb	0.98	-	1.60	0.87	1.52	-	-	-	-	-	-	-	-	-	-
Te	0.18	-	0.05	0.07	0.04	-	-	-	-	-	-	-	-	-	-
Th	11.5	19.4	22.6	24.0	13.2	5.50	4.20	27.6	6.30	4.60	21.6	20.2	24.9	16.5	16.5
Tl	0.42	-	1.21	0.17	0.99	-	-	-	-	-	-	-	-	-	-
Tm	0.40	-	0.73	0.43	0.64	-	-	-	-	-	-	-	-	-	-
U	2.29	-	4.99	3.95	3.60	-	-	-	-	-	-	-	-	-	-
V	34.1	17.0	16.9	7.5	16.1	143	113	13.9	138	151	9.7	10.2	9.6	20.9	21.3
W	30.3	80.7	47.8	83.6	107	86.7	204	158	110	92.8	128	132	124	128	140
Y	28.2	41.5	53.8	29.6	51.0	23.4	27.1	49.7	25.6	20.5	22.0	26.1	43.7	47.3	42.5
Yb	2.65	-	4.68	2.90	4.13	-	-	-	-	-	-	-	-	-	-
Zn	80.1	53.9	95.4	111	71.2	99.5	100	46.4	94.4	107	40.1	50.4	48.7	77.6	65.8
Zr	318	347	304	201	460	130	135	247	135	110	180	190	261	455	485

Table 7.2: (Continuation)

Sample	VS-804	VS-805a	VS-805b	VS-806	VS-808	VS-810	VS-811	VS-812	VS-813	VS-814	VS-816	VS-817	VS-819	VS-821	VS-822
Unit	MC rhyolite	MC rhyolite	MC rhyolite	MC rhyolite	MU rhyolite	SP rhyolite	SP rhyolite	SP rhyolite	SP rhyolite	SP rhyolite	SP rhyolite	SP rhyolite	PA rhyolite	PA rhyolite	PA rhyolite
As	-	-	-	-	-	-	-	-	-	-	-	-	-	-	-
Ba	1450	1470	1500	1470	<LL	836	829	781	814	788	788	899	<LL	<LL	152
Be	-	-	-	-	-	-	-	-	-	-	-	-	-	-	-
Bi	-	-	-	-	-	-	-	-	-	-	-	-	-	-	-
Ce	102	98.0	99.4	121	138	104	98.6	113	95.2	120	98.2	123	75.3	99.0	125
Co	7.8	10.0	33.1	10.4	20.5	8.2	7.6	19.8	8.2	9.1	8.3	8.7	8.4	8.8	7.1
Cr	<LL	<LL	<LL	<LL	<LL	<LL	<LL	<LL	<LL	<LL	<LL	<LL	<LL	<LL	<LL
Cs	-	-	-	-	-	-	-	-	-	-	-	-	-	-	-
Cu	<LL	<LL	<LL	<LL	<LL	<LL	<LL	<LL	<LL	<LL	<LL	<LL	<LL	<LL	<LL
Dy	-	-	-	-	-	-	-	-	-	-	-	-	-	-	-
Er	-	-	-	-	-	-	-	-	-	-	-	-	-	-	-
Eu	-	-	-	-	-	-	-	-	-	-	-	-	-	-	-
Ga	18.4	18.2	17.6	18.6	22.1	16.8	17.7	16.1	16.6	16.6	16.7	16.8	17.5	17.6	17.3
Gd	-	-	-	-	-	-	-	-	-	-	-	-	-	-	-
Ge	-	-	-	-	-	-	-	-	-	-	-	-	-	-	-
Hf	-	-	-	-	-	-	-	-	-	-	-	-	-	-	-
Ho	-	-	-	-	-	-	-	-	-	-	-	-	-	-	-
La	-	-	-	-	-	-	-	-	-	-	-	-	-	-	-
Li	-	-	-	-	-	-	-	-	-	-	-	-	-	-	-
Lu	-	-	-	-	-	-	-	-	-	-	-	-	-	-	-
Mo	<LL	<LL	<LL	<LL	<LL	<LL	<LL	5.70	<LL	<LL	<LL	<LL	<LL	<LL	<LL
Nb	31.0	33.1	31.0	32.0	91.5	45.3	46.2	47.9	46.9	47.5	46.6	46.2	41.1	40.0	41.0
Nd	-	-	-	-	-	-	-	-	-	-	-	-	-	-	-
Ni	<LL	<LL	<LL	<LL	<LL	<LL	<LL	<LL	<LL	<LL	<LL	<LL	<LL	<LL	<LL
Pb	34.1	29.2	29.1	176	20.2	18.8	32.3	24.3	33.7	28.0	28.3	24.1	26.2	15.3	19.5
Pr	-	-	-	-	-	-	-	-	-	-	-	-	-	-	-
Rb	200	201	207	187	219	190	182	183	179	195	188	180	200	205	200
Sb	-	-	-	-	-	-	-	-	-	-	-	-	-	-	-
Sc	-	-	-	-	-	-	-	-	-	-	-	-	-	-	-
Sm	-	-	-	-	-	-	-	-	-	-	-	-	-	-	-
Sn	2.6	5.4	4.5	58.7	7.8	2.8	2.5	<LL	6.0	<LL	3.9	3.5	2.7	<LL	<LL
Sr	75.4	69.0	58.4	138	22.5	73.9	82.0	70.6	76.8	73.4	77.3	95.2	21.5	20.3	26.3
Ta	-	-	-	-	-	-	-	-	-	-	-	-	-	-	-
Tb	-	-	-	-	-	-	-	-	-	-	-	-	-	-	-
Te	-	-	-	-	-	-	-	-	-	-	-	-	-	-	-
Th	14.9	16.0	14.7	18.6	19.0	17.9	17.6	18.1	16.7	16.1	17.4	16.6	24.6	26.3	23.9
Tl	-	-	-	-	-	-	-	-	-	-	-	-	-	-	-
Tm	-	-	-	-	-	-	-	-	-	-	-	-	-	-	-
U	-	-	-	-	-	-	-	-	-	-	-	-	-	-	-
V	18.1	19.9	14.2	20.2	11.5	12.2	22.1	23.5	24.6	15.2	15.5	13.8	6.3	8.1	7.8
W	50.7	65.5	159	76.1	182	102	78.4	112	90.8	84.9	66.4	84.8	71.1	72.8	61.0
Y	41.5	40.7	33.7	52.1	66.5	32.8	33.3	40.7	34.6	33.9	36.5	36.1	23.7	18.9	25.3
Yb	-	-	-	-	-	-	-	-	-	-	-	-	-	-	-
Zn	69.4	72.4	51.0	51.6	89.7	41.4	68.5	64.1	70.5	64.2	57.5	70.2	72.1	43.0	57.6
Zr	491	496	559	438	703	469	489	474	480	475	483	474	188	193	188

Table 7.2: (Continuation)

Sample	VS-823	VS-826	VS-828	VS-832	VS-834	VS-836	VS-837	VS-838	ISP-1	ISP-2	ISP-12	ISP-41	ISP-43c	ISP-45	ISP-46
Unit	CO rhyolite	MC rhyolite	CA rhyolite	NU rhyolite	MU rhyolite	AND andesite	NU rhyolite	LE rhyolite	PM rhyolite	PM rhyolite	PM rhyolite	CO rhyolite	CO rhyolite	CO rhyolite	CO rhyolite
As	-	-	-	-	-	-	-	-	4.15	2.61	2.96	2.92	-	-	-
Ba	<LL	1450	1140	1440	247	590	1230	969	<LL	<LL	<LL	<LL	<LL	<LL	<LL
Be	-	-	-	-	-	-	-	-	2.83	2.99	2.11	9.97	-	-	-
Bi	-	-	-	-	-	-	-	-	0.01	0.01	-	0.11	-	-	-
Ce	140	106	83.9	121	175	43.7	132	110	87.3	98.8	95.4	285	323	46.8	133
Co	9.2	5.7	12.8	13.5	16.2	23.1	17.8	15.3	21.6	15.2	21.7	22.8	23.7	32.8	36.2
Cr	<LL	<LL	<LL	<LL	<LL	<LL	<LL	<LL	7.66	7.79	18.1	16.9	<LL	<LL	<LL
Cs	-	-	-	-	-	-	-	-	3.12	2.92	2.86	3.86	-	-	-
Cu	<LL	<LL	<LL	<LL	<LL	20.3	<LL	<LL	3.12	3.49	2.95	4.14	<LL	<LL	<LL
Dy	-	-	-	-	-	-	-	-	5.55	6.08	7.71	35.0	-	-	-
Er	-	-	-	-	-	-	-	-	3.16	3.24	3.79	19.5	-	-	-
Eu	-	-	-	-	-	-	-	-	0.18	0.29	0.58	1.01	-	-	-
Ga	26.2	17.8	18.4	17.8	24.5	20.9	17.9	19.5	17.1	16.6	15.6	22.5	25.0	23.7	24.3
Gd	-	-	-	-	-	-	-	-	6.39	7.41	9.87	43.6	-	-	-
Ge	-	-	-	-	-	-	-	-	1.38	1.45	1.48	3.00	-	-	-
Hf	-	-	-	-	-	-	-	-	5.57	6.95	4.21	40.9	-	-	-
Ho	-	-	-	-	-	-	-	-	1.02	1.07	1.29	6.23	-	-	-
La	-	-	-	-	-	-	-	-	51.8	60.0	74.9	470	-	-	-
Li	-	-	-	-	-	-	-	-	10.1	9.02	16.7	75.5	-	-	-
Lu	-	-	-	-	-	-	-	-	0.44	0.47	0.48	2.59	-	-	-
Mo	<LL	<LL	<LL	<LL	<LL	<LL	<LL	<LL	1.79	1.84	0.99	0.31	<LL	<LL	<LL
Nb	79.7	29.7	29.1	45.1	89.1	12.3	44.4	31.8	38.2	35.1	29.4	166	188	112	116
Nd	-	-	-	-	-	-	-	-	34.1	43.2	55.1	302	-	-	-
Ni	<LL	<LL	<LL	<LL	<LL	<LL	<LL	<LL	1.25	4.59	1.88	1.76	<LL	<LL	<LL
Pb	11.8	25.0	21.9	21.1	21.2	20.7	16.6	16.7	21.8	19.3	16.9	42.4	44.5	11.4	23.6
Pr	-	-	-	-	-	-	-	-	9.88	12.2	15.1	84.1	-	-	-
Rb	229	186	193	193	234	122	195	177	195	192	184	310	334	290	289
Sb	-	-	-	-	-	-	-	-	0.44	0.45	0.51	0.53	-	-	-
Sc	-	-	-	-	-	-	-	-	2.51	2.21	2.14	1.41	-	-	-
Sm	-	-	-	-	-	-	-	-	6.15	7.68	9.91	46.1	-	-	-
Sn	10.0	<LL	2.0	2.6	5.7	<LL	2.8	2.6	3.2	2.5	3.7	13.6	17.6	10.1	11.2
Sr	14.8<LL	72.7	69.2	105	20.1	392	98.8	141	11.4*	14.5*	15.4*	<LL	<LL	<LL	<LL
Ta	-	-	-	-	-	-	-	-	4.37	4.20	0.32	1.34	-	-	-
Tb	-	-	-	-	-	-	-	-	0.94	1.06	1.37	5.94	-	-	-
Te	-	-	-	-	-	-	-	-	0.04	0.02	0.13	0.18	-	-	-
Th	20.6	14.9	15.3	16.5	22.6	7.00	18.2	16.2	21.8	21.2	21.1	20.3	28.8	19.4	19.7
Tl	-	-	-	-	-	-	-	-	0.42	0.28	0.40	0.47	-	-	-
Tm	-	-	-	-	-	-	-	-	0.45	0.46	0.52	2.68	-	-	-
U	-	-	-	-	-	-	-	-	3.85	4.30	3.26	6.29	-	-	-
V	7.7	20.2	23.6	25.7	11.9	107	25.7	30.1	9.5	8.6	11.1	7.3	7.7	6.8	7.3
W	92.1	35.4	86.6	108	135	94.1	146	149	141	117	152	275	191	303	318
Y	57.8	31.4	37.1	43.7	52.0	20.1	43.3	46.2	33.6	31.3	35.2	>UL	>UL	120	78.5
Yb	-	-	-	-	-	-	-	-	3.03	3.24	3.38	17.5	-	-	-
Zn	108	58.4	59.7	50.1	99.5	81.7	45.4	79.8	58.8	51.1	51.7	274	271	142	151
Zr	757	462	404	526	721	175	502	411	258	255	249	1440	>UL	918	934

Table 7.2: (Continuation)

Sample	ISP-47	ISP-48	ISP-54	ISP-55b	ISP-65	ISP-67	ISP-70	ISP-75	ISP-76	ISP-79	ISP-80	ISP-81	ISP-83	ISP-85	ISP-87
Unit	MZ rhyolite	MCR rhyclite	CO rhyolite	MU rhyolite	NU rhyolite	CF rhyolite	CF trachyte	CF rhyolite	CO rhyolite	CO rhyolite	MU rhyolite	MU rhyolite	CF rhyolite	PA rhyolite	PA rhyolite
As	5.11	-	-	-	-	9.23	4.57	-	-	-	9.95	12.3	3.61	3.74	-
Ba	1110	1190	<LL	<LL	939	31.0*	400	<LL	87.4	<LL	414	14.8*	583	69.2*	<LL
Be	2.19	-	-	-	-	4.58	1.61	-	-	-	5.44	5.47	2.34	2.09	-
Bi	0.03	-	-	-	-	-	0.02	-	-	-	0.13	0.04	-	0.01	-
Ce	117	131	313	161	113	164	38.9*	173	340	186	198	204	108	150	91.1
Co	19.3	13.2	11.2	20.8	11.3	40.1	11.1	20.3	18.5	19.4	30.1	20.1	16.2	44.8	17.8
Cr	17.4	<LL	<LL	<LL	<LL	18.9	18.6	<LL	<LL	<LL	17.2	18.1	17.5	19.1	<LL
Cs	2.65	-	-	-	-	1.57	1.31	-	-	-	4.30	3.76	2.19	2.01	-
Cu	4.44	<LL	<LL	<LL	<LL	2.85	5.80	<LL	<LL	<LL	2.47	2.69	4.67	3.96	<LL
Dy	8.33	-	-	-	-	14.1	2.86	-	-	-	15.1	16.7	8.45	5.37	-
Er	3.96	-	-	-	-	7.44	1.42	-	-	-	8.55	9.33	4.21	3.04	-
Eu	2.21	-	-	-	-	0.53	1.91	-	-	-	0.19	0.25	1.66	0.32	-
Ga	15.8	18.7	25.2	22.5	17.3	20.2	18.0	22.8	27.6	25.5	21.0	21.2	19.7	16.3	15.3
Gd	10.6	-	-	-	-	15.4	3.42	-	-	-	15.7	17.6	9.66	6.23	-
Ge	1.49	-	-	-	-	1.75	1.33	-	-	-	2.09	2.04	1.41	1.44	-
Hf	3.98	-	-	-	-	2.89	5.52	-	-	-	21.0	20.3	3.63	4.41	-
Ho	1.38	-	-	-	-	2.56	0.50	-	-	-	2.82	3.11	1.45	0.97	-
La	65.5	-	-	-	-	91.0	19.7	-	-	-	96.5	111	58.1	54.0	-
Li	17.2	-	-	-	-	5.32	14.5	-	-	-	6.52	16.8	10.3	16.7	-
Lu	0.44	-	-	-	-	0.96	0.17	-	-	-	1.26	1.34	0.51	0.43	-
Mo	0.92	<LL	<LL	<LL	<LL	2.43	1.45	<LL	<LL	<LL	6.66	3.85	0.87	0.43	<LL
Nb	43.6	45.1	135	84.8	43.5	83.3	32.7	87.3	172	86.3	90.9	93.0	56.2	41.1	40.2
Nd	55.1	-	-	-	-	79.7	17.8	-	-	-	80.4	91.5	50.8	33.3	-
Ni	1.62	<LL	<LL	<LL	<LL	1.30	0.64	<LL	<LL	<LL	0.65	0.90	0.93	1.23	<LL
Pb	14.0	77.1	21.9	30.5	30.2	21.3	13.0	21.1	25.4	23.4	28.0	32.4	15.9	14.7	18.0
Pr	14.6	-	-	-	-	21.7	4.61	-	-	-	22.1	25.2	13.7	10.2	-
Rb	176	216	255	198	205	163	76.9	208	283	173	230	219	140	179	191
Sb	0.87	-	-	-	-	0.68	0.50	-	-	-	0.42	0.94	0.64	0.76	-
Sc	5.17	-	-	-	-	3.96	8.19	-	-	-	3.43	3.15	7.40	2.32	-
Sm	10.4	-	-	-	-	15.3	3.47	-	-	-	15.6	17.4	9.81	5.89	-
Sn	2.22*	4.1	12.4	8.4	4.6	3.39*	2.2	7.2	13.3	6.2	7.7	7.6	2.3	1.70*	<LL
Sr	153	73.1	<LL	20.1	72.6	18.0*	14.5*	24.8	<LL	<LL	14.6*	<LL	29.0*	20.6*	<LL
Ta	1.08	-	-	-	-	0.65	0.48	-	-	-	0.77	0.79	0.87	0.17	-
Tb	1.50	-	-	-	-	2.39	0.51	-	-	-	2.51	2.79	1.46	0.91	-
Te	0.14	-	-	-	-	0.08	0.02	-	-	-	0.11	0.11	0.05	0.07	-
Th	12.5	25.8	31.2	23.3	24.5	16.5	5.00	16.7	24.4	15.9	17.4	15.8	11.0	25.4	24.6
Tl	0.67	-	-	-	-	0.18	0.25	-	-	-	2.22	0.81	0.30	0.17	-
Tm	0.51	-	-	-	-	1.01	0.19	-	-	-	1.23	1.34	0.57	0.44	-
U	2.89	-	-	-	-	3.19	1.22	-	-	-	6.72	6.08	2.01	4.21	-
V	18.2	21.5	8.7	8.4	21.0	9.3	16.7	8.8	8.3	9.6	6.8	9.8	14.6	12.7	9.0
W	142	49.1	113	176	106	183	90.2	155	133	190	234	131	75.1	111	53.6
Y	42.3	37.9	94.0	64.6	43.9	74.0	13.5	68.1	>UL	76.8	70.2	79.3	43.0	28.9	28.6
Yb	3.18	-	-	-	-	6.53	1.21	-	-	-	8.40	8.85	3.59	3.00	-
Zn	40.6	71.3	123	98.5	66.0	57.3	89.9	98.1	237	89.4	125	90.1	74.5	44.3	55.2
Zr	471	476	1050	651	474	649	197	656	1440	618	683	693	415	214	204

Table 7.2: (Continuation)

Sample	ISP-88	ISP-89	ISP-94	ISP-95	ISP-97	ISP-100	ISP-116	ISP-118	ISP-120	ISP-121	ISP-124	ISP-126	ISP-127	ISP-128	ISP-130
Unit	MU rhyolite	CF rhyolite	SP rhyolite	CF rhyolite	SP rhyolite	CF rhyolite	CO rhyolite	CO rhyolite	NU rhyolite	NU rhyolite	NU rhyolite	MU rhyolite	MU rhyolite	CF rhyolite	CF rhyolite
As	-	-	-	-	-	3.58	2.89	-	19.6	25.1	-	9.40	-	-	-
Ba	68.7	279	714	505	809	58.6*	10.3*	513	1050	1120	1520	18.5*	<LL	173	<LL
Be	-	-	-	-	-	4.23	6.39	-	3.09	3.02	-	5.78	-	-	-
Bi	-	-	-	-	-	-	0.01	-	0.08	0.02	-	0.07	-	-	-
Ce	160	125	108	156	132	177	243	132	169	117	99.2	196	123	160	110
Co	11.2	17.1	47.7	11.4	36.5	34.8	23.3	22.0	8.6	12.4	13.9	14.6	17.4	11.3	13.5
Cr	<LL	<LL	<LL	<LL	<LL	17.8	18.1	<LL	18.7	18.2	<LL	8.58	<LL	<LL	<LL
Cs	-	-	-	-	-	1.79	2.01	-	4.30	4.01	-	5.01	-	-	-
Cu	<LL	<LL	<LL	<LL	<LL	2.33	2.79	<LL	5.67	4.69	<LL	3.36	<LL	<LL	<LL
Dy	-	-	-	-	-	12.4	19.9	-	10.6	10.4	-	13.4	-	-	-
Er	-	-	-	-	-	6.45	11.9	-	5.72	5.28	-	7.67	-	-	-
Eu	-	-	-	-	-	0.25	0.48	-	2.02	2.07	-	0.17	-	-	-
Ga	22.3	20.5	14.6	19.3	14.9	20.5	23.8	22.2	14.8	14.5	17.8	24.6	24.2	22.7	27.3
Gd	-	-	-	-	-	13.3	19.8	-	12.2	12.3	-	14.3	-	-	-
Ge	-	-	-	-	-	1.72	2.02	-	1.63	1.59	-	1.98	-	-	-
Hf	-	-	-	-	-	2.82	28.3	-	12.1	6.64	-	19.1	-	-	-
Ho	-	-	-	-	-	2.19	3.85	-	1.88	1.79	-	2.51	-	-	-
La	-	-	-	-	-	85.3	116	-	75.8	68.0	-	89.5	-	-	-
Li	-	-	-	-	-	13.5	32.2	-	26.8	23.4	-	10.6	-	-	-
Lu	-	-	-	-	-	0.80	1.69	-	0.79	0.62	-	1.11	-	-	-
Mo	6.30	<LL	<LL	<LL	<LL	2.49	0.82	<LL	1.90	1.98	<LL	6.41	5.00	<LL	5.70
Nb	78.7	74.0	49.8	63.0	47.5	83.8	115	64.0	47.3	46.7	43.8	91.3	91.0	78.6	82.0
Nd	-	-	-	-	-	70.6	95.9	-	64.3	62.3	-	74.1	-	-	-
Ni	<LL	<LL	<LL	<LL	<LL	1.24	1.00	<LL	1.03	1.26	<LL	2.02	<LL	<LL	<LL
Pb	34.7	26.4	21.7	25.3	49.1	20.6	20.1	31.5	40.8	33.7	45.1	28.8	29.3	27.0	32.3
Pr	-	-	-	-	-	19.9	26.5	-	17.6	16.7	-	20.6	-	-	-
Rb	202	184	195	156	183	206	247	134	221	231	201	216	218	188	214
Sb	-	-	-	-	-	0.41	0.32	-	2.22	2.02	-	0.44	-	-	-
Sc	-	-	-	-	-	2.75	1.98	-	7.97	7.42	-	4.84	-	-	-
Sm	-	-	-	-	-	13.4	18.7	-	12.2	12.4	-	14.1	-	-	-
Sn	6.4	6.3	5.2	<LL	<LL	3.5	8.7	5.4	7.9	4.4	<LL	6.8	8.6	5.9	7.0
Sr	26.1	28.6	50.6	36.8	73.0	17.1*	7.10*	109	80.2	84.5	98.3	11.0*	<LL	27.7	<LL
Ta	-	-	-	-	-	0.62	1.10	-	0.46	0.23	-	6.94	-	-	-
Tb	-	-	-	-	-	2.06	3.20	-	1.79	1.77	-	2.20	-	-	-
Te	-	-	-	-	-	0.02	0.16	-	0.03	0.14	-	0.10	-	-	-
Th	17.8	13.6	18.7	14.0	17.0	16.7	16.5	13.8	17.6	16.6	19.8	21.3	21.4	16.1	16.6
Tl	-	-	-	-	-	0.37	0.43	-	1.62	0.71	-	1.63	-	-	-
Tm	-	-	-	-	-	0.87	1.72	-	0.81	0.71	-	1.12	-	-	-
U	-	-	-	-	-	4.67	2.54	-	5.91	4.41	-	6.07	-	-	-
V	9.5	11.7	13.1	15.2	13.3	9.1	10.0	19.5	20.1	20.4	20.6	7.1	9.2	12.4	11.1
W	90.9	116	>UL	83.4	163	210	238	125	102	103	136	121	109	100	111
Y	69.4	55.4	37.3	37.5	29.0	65.2	99.7	60.6	51.3	52.5	47.6	70.9	48.2	58.6	55.6
Yb	-	-	-	-	-	5.55	11.4	-	5.29	4.42	-	7.46	-	-	-
Zn	157	97.7	58.3	72.7	29.9	84.2	140	110	62.6	61.9	79.6	132	89.1	113	69.1
Zr	605	564	465	472	467	648	906	531	492	493	491	722	690	600	666

Table 7.2: (Continuation)

Sample	ISP-132	ISP-136	ISP-137	ISP-140	ISP-150	ISP-154	ISP-156	ISP-159	ISP-160	ISP-162	ISP-164	ISP-173	ISP-175	ISP-179	ISP-182
Unit	MCR rhyolite	MCR rhyolite	MCR rhyolite	MZ rhyolite	CO rhyolite	MZ trachyte	NU rhyolite	NU rhyolite	NU rhyolite	NU rhyolite	CO rhyolite	MU rhyolite	MU rhyolite	MU rhyolite	CF rhyolite
As	-	20.9	-	-	1.53	9.61	-	-	-	-	-	-	-	4.21	2.95
Ba	1320	996	1120	1340	2.59*	1050	1330	939	919	1010	<LL	<LL	<LL	34.4*	760
Be	-	3.54	-	-	7.90	2.30	-	-	-	-	-	-	-	6.03	1.90
Bi	-	0.01	-	-	-	0.01	-	-	-	-	-	-	-	0.01	-
Ce	184	96.9	117	97.1	214	106	110	99.3	130	143	182	173	189	227	57.5
Co	9.1	6.8	11.5	7.9	34.9	18.1	24.3	29.7	20.5	15.9	19.3	24.2	21.0	19.5	11.2
Cr	<LL	8.68	<LL	<LL	18.3	17.9	<LL	<LL	<LL	<LL	<LL	<LL	<LL	7.41	17.8
Cs	-	5.22	-	-	4.58	2.57	-	-	-	-	-	-	-	3.42	1.91
Cu	7.2	5.58	<LL	<LL	2.27	7.56	<LL	<LL	<LL	<LL	<LL	<LL	<LL	2.29	3.86
Dy	-	7.56	-	-	19.2	9.40	-	-	-	-	-	-	-	18.8	4.55
Er	-	3.98	-	-	11.5	4.79	-	-	-	-	-	-	-	9.44	2.61
Eu	-	1.75	-	-	0.09	2.36	-	-	-	-	-	-	-	0.40	1.53
Ga	17.7	16.9	17.5	17.1	23.8	15.2	17.4	17.3	16.5	17.0	25.8	22.1	21.2	23.8	17.1
Gd	-	8.58	-	-	18.2	10.8	-	-	-	-	-	-	-	21.2	4.87
Ge	-	1.45	-	-	2.37	1.19	-	-	-	-	-	-	-	1.80	1.22
Hf	-	7.37	-	-	24.2	3.94	-	-	-	-	-	-	-	7.68	2.34
Ho	-	1.36	-	-	3.72	1.66	-	-	-	-	-	-	-	3.28	0.85
La	-	52.9	-	-	91.9	58.8	-	-	-	-	-	-	-	118	29.4
Li	-	21.0	-	-	64.4	31.5	-	-	-	-	-	-	-	21.0	7.12
Lu	-	0.54	-	-	1.65	0.56	-	-	-	-	-	-	-	1.22	0.38
Mo	<LL	2.16	<LL	<LL	0.59	1.42	<LL	<LL	<LL	<LL	<LL	8.10	8.50	1.33	1.42
Nb	43.0	41.7	46.0	43.6	105	39.7	44.7	46.0	45.7	47.1	93.0	88.4	89.1	90.9	44.9
Nd	-	45.1	-	-	79.6	53.2	-	-	-	-	-	-	-	105	26.2
Ni	<LL	1.72	<LL	<LL	0.64	1.90	<LL	<LL	<LL	<LL	<LL	<LL	<LL	2.21	0.73
Pb	55.1	24.5	25.1	21.0	30.8	38.3	29.9	20.3	19.5	29.0	21.9	28.3	25.6	27.2	13.5
Pr	-	12.2	-	-	22.2	13.7	-	-	-	-	-	-	-	27.4	7.06
Rb	196	210	225	171	286	189	195	207	207	212	196	226	227	223	112
Sb	-	3.04	-	-	0.65	1.04	-	-	-	-	-	-	-	0.60	0.57
Sc	-	9.03	-	-	2.62	8.97	-	-	-	-	-	-	-	4.02	5.89
Sm	-	8.65	-	-	17.1	10.6	-	-	-	-	-	-	-	21.0	5.07
Sn	3.6	2.62*	5.1	4.5	8.7	1.37*	7.4	4.4	<LL	20.7	6.2	7.0	6.7	6.9	3.3
Sr	112	81.6	83.4	113	4.26*	149	113	88.9	82.0	88.5	24.2	<LL	<LL	22.3*	33.9*
Ta	-	5.91	-	-	0.87	0.31	-	-	-	-	-	-	-	4.05	0.19
Tb	-	1.28	-	-	3.09	1.61	-	-	-	-	-	-	-	3.23	0.76
Te	-	0.06	-	-	0.10	0.10	-	-	-	-	-	-	-	0.02	0.00
Th	16.6	15.9	17.8	15.6	20.1	12.8	16.0	17.9	17.6	17.7	11.7	16.3	16.2	16.2	10.8
Tl	-	0.74	-	-	0.51	1.06	-	-	-	-	-	-	-	0.73	0.21
Tm	-	0.57	-	-	1.69	0.62	-	-	-	-	-	-	-	1.28	0.37
U	-	3.95	-	-	7.98	2.79	-	-	-	-	-	-	-	4.27	2.04
V	46.8	33.8	22.7	22.4	7.0	39.9	28.4	22.3	24.0	20.0	11.7	6.7	6.5	10.3	15.4
W	63.3	54.3	116	95.9	346	125	149	160	137	123	218	176	167	137	103
Y	53.2	40.5	42.5	45.3	99.8	51.3	41.5	49.7	50.8	44.6	88.8	74.8	77.3	99.3	28.3
Yb	-	3.74	-	-	11.3	3.92	-	-	-	-	-	-	-	8.29	2.51
Zn	108	89.1	124	61.1	156	79.1	97.9	46.3	42.8	38.2	140	121	122	116	43.9
Zr	473	454	478	462	825	405	486	480	471	498	732	669	676	696	333

Table 7.2: (Continuation)

Sample	ISP-185	ISP-186	ISP-189	ISP-190	ISP-192	ISP-200	ISP-203	ISP-208	ISP-209	ISP-209 bis	ISP-210	ISP-211	ISP-212	ISP-214	ISP-215
Unit	MU rhyolite	MU rhyolite	CF trachyte	CF trachyte	PM rhyolite	NU rhyolite	NU rhyolite	PC rhyolite	MZ rhyolite	CL rhyolite	CL rhyolite	NU rhyolite	NU rhyolite	PM rhyolite	PM rhyolite
As	-	-	3.02	-	2.44	-	-	-	6.46	3.08	5.19	-	-	-	-
Ba	<LL	<LL	547	160	49.9*	1160	1170	1360	1230	546	507	1250	1260	<LL	<LL
Be	-	-	1.10	-	2.69	-	-	-	2.76	2.62	3.29	-	-	-	-
Bi	-	-	0.01	-	0.01	-	-	-	0.01	0.01	0.02	-	-	-	-
Ce	153	169	39.5*	158	100	113	113	118	126	79.8	91.0	129	132	110	125
Co	9.5	15.2	11.0	13.0	14.3	19.4	10.4	11.8	17.1	26.1	21.8	15.8	13.6	9.1	<LL
Cr	<LL	<LL	16.4	<LL	18.0	<LL	<LL	<LL	17.5	7.77	7.73	<LL	<LL	<LL	<LL
Cs	-	-	1.67	-	2.67	-	-	-	3.04	3.77	4.22	-	-	-	-
Cu	<LL	<LL	6.86	<LL	2.55	<LL	18.4	<LL	5.10	4.35	3.69	<LL	<LL	<LL	<LL
Dy	-	-	2.98	-	7.75	-	-	-	9.20	3.46	5.71	-	-	-	-
Er	-	-	1.38	-	4.42	-	-	-	4.57	2.08	3.19	-	-	-	-
Eu	-	-	2.18	-	0.32	-	-	-	2.34	0.64	0.73	-	-	-	-
Ga	23.2	24.2	19.1	21.0	16.6	16.4	16.8	17.2	15.3	14.3	14.7	16.2	17.0	17.2	17.7
Gd	-	-	3.67	-	8.77	-	-	-	10.8	4.10	6.82	-	-	-	-
Ge	-	-	1.37	-	1.40	-	-	-	1.46	1.21	1.21	-	-	-	-
Hf	-	-	5.37	-	4.86	-	-	-	5.98	2.69	3.41	-	-	-	-
Ho	-	-	0.48	-	1.47	-	-	-	1.57	0.66	1.07	-	-	-	-
La	-	-	22.2	-	68.5	-	-	-	66.5	37.5	56.2	-	-	-	-
Li	-	-	11.3	-	11.1	-	-	-	14.5	13.8	10.1	-	-	-	-
Lu	-	-	0.17	-	0.57	-	-	-	0.55	0.31	0.42	-	-	-	-
Mo	<LL	<LL	1.70	<LL	0.67	<LL	<LL	<LL	1.29	2.10	1.44	<LL	<LL	<LL	5.00
Nb	92.6	86.8	31.9	46.0	35.1	44.5	45.3	44.4	43.7	24.4	26.4	47.0	47.8	37.1	37.8
Nd	-	-	19.6	-	46.1	-	-	-	56.4	22.4	35.7	-	-	-	-
Ni	<LL	<LL	1.53	<LL	2.27	<LL	<LL	<LL	1.45	2.00	1.56	<LL	<LL	<LL	<LL
Pb	29.3	17.3	25.2	17.0	19.6	28.7	36.9	20.9	20.1	23.9	31.5	27.1	38.4	21.2	21.7
Pr	-	-	5.13	-	13.1	-	-	-	15.1	6.78	10.0	-	-	-	-
Rb	213	220	77.8	188	191	193	198	202	168	203	211	192	209	186	190
Sb	-	-	0.63	-	0.31	-	-	-	0.84	0.29	0.35	-	-	-	-
Sc	-	-	8.06	-	1.77	-	-	-	5.37	1.88	1.73	-	-	-	-
Sm	-	-	3.85	-	8.22	-	-	-	10.9	3.84	6.17	-	-	-	-
Sn	6.8	7.5	4.1	2.5	1.07*	5.0	3.9	<LL	2.12*	0.70*	0.90*	3.9	4.3	3.8	3.8
Sr	<LL	23.3	17.8*	<LL	11.9*	119	107	152	127	95.2	87.8	122	104	22.9	22.8
Ta	-	-	1.15	-	0.25	-	-	-	0.16	4.07	3.43	-	-	-	-
Tb	-	-	0.53	-	1.31	-	-	-	1.57	0.58	0.98	-	-	-	-
Te	-	-	0.10	-	0.05	-	-	-	0.12	0.07	0.08	-	-	-	-
Th	18.0	19.2	4.70	6.40	23.7	15.6	14.1	13.8	12.1	28.1	26.9	14.7	16.3	22.1	22.8
Tl	-	-	0.73	-	0.38	-	-	-	1.48	0.21	0.10	-	-	-	-
Tm	-	-	0.18	-	0.61	-	-	-	0.61	0.31	0.45	-	-	-	-
U	-	-	1.42	-	4.06	-	-	-	3.10	3.03	3.72	-	-	-	-
V	8.2	8.1	16.2	15.7	9.6	22.3	21.6	36.2	20.9	17.4	16.7	20.6	19.0	7.1	8.4
W	81.5	115	70.7	118	94.3	137	135	118	145	182	189	159	135	78.4	53.3
Y	53.0	60.0	11.8	27.1	43.1	43.9	43.6	68.6	45.9	25.3	37.5	114	51.0	32.2	31.0
Yb	-	-	1.16	-	3.91	-	-	-	3.86	2.06	2.89	-	-	-	-
Zn	105	97.5	121	99.6	58.6	73.4	177	55.6	62.4	39.0	49.6	65.2	105	51.7	55.4
Zr	694	668	194	204	261	473	486	473	475	239	234	488	498	256	258

Table 7.2: (Continuation)

Sample	ISP-216	ISP-218	ISP-220	ISP-223	ISP-225	ISP-226	ISP-227	ISP-230	ISP-233a	ISP-233b	ISP-237	ISP-241	ISP-244	ISP-246	ISP-247
Unit	SP rhyolite	PC rhyolite	PC rhyolite	PC trachyte	PC trachyte	PC trachyte	PC trachyte	PC trachyte	PC trachyte	PC rhyolite	CF rhyolite	PA rhyolite	CF rhyolite	PA rhyolite	CF rhyolite
As	-	-	5.96	-	-	-	9.05	-	-	-	-	-	-	6.99	4.22
Ba	744	646	606	739	704	664	723	661	662	1020	402	<LL	133	47.5*	122
Be	-	-	2.77	-	-	-	3.12	-	-	-	-	-	-	2.44	4.26
Bi	-	-	0.07	-	-	-	0.01	-	-	-	-	-	-	0.03	0.02
Ce	87.2	105	79.8	97.2	93.4	91.1	81.0	89.3	76.5	180	116	104	202	90.7	165
Co	17.0	37.7	37.0	18.4	16.5	21.3	21.1	24.3	19.1	12.6	10.0	8.1	18.5	<LL	13.7
Cr	<LL	<LL	8.64	<LL	<LL	<LL	8.63	<LL	<LL	<LL	<LL	<LL	<LL	8.94	7.47
Cs	-	-	3.51	-	-	-	3.10	-	-	-	-	-	-	2.65	2.62
Cu	<LL	<LL	7.99	4.3	<LL	<LL	10.8	<LL	10.0	<LL	<LL	<LL	<LL	3.12	3.35
Dy	-	-	6.32	-	-	-	6.12	-	-	-	-	-	-	4.25	12.0
Er	-	-	3.49	-	-	-	3.30	-	-	-	-	-	-	2.38	6.07
Eu	-	-	1.46	-	-	-	1.60	-	-	-	-	-	-	0.22	0.60
Ga	16.2	18.1	15.9	19.6	18.8	18.3	18.1	17.8	18.2	22.4	18.0	16.5	21.5	16.4	20.2
Gd	-	-	7.06	-	-	-	7.14	-	-	-	-	-	-	4.97	13.8
Ge	-	-	1.24	-	-	-	1.27	-	-	-	-	-	-	1.33	1.70
Hf	-	-	6.65	-	-	-	7.45	-	-	-	-	-	-	5.25	5.33
Ho	-	-	1.15	-	-	-	1.11	-	-	-	-	-	-	0.78	2.12
La	-	-	44.7	-	-	-	44.3	-	-	-	-	-	-	44.9	81.2
Li	-	-	11.0	-	-	-	14.2	-	-	-	-	-	-	9.61	11.0
Lu	-	-	0.47	-	-	-	0.46	-	-	-	-	-	-	0.38	0.77
Mo	5.70	<LL	3.26	<LL	<LL	<LL	2.48	<LL	<LL	8.20	<LL	5.90	<LL	1.66	1.69
Nb	46.5	50.3	44.8	47.2	49.4	49.8	46.7	49.4	49.4	91.1	53.7	42.2	83.7	41.7	78.3
Nd	-	-	36.5	-	-	-	36.5	-	-	-	-	-	-	27.4	71.7
Ni	<LL	<LL	1.91	<LL	<LL	<LL	3.95	<LL	<LL	<LL	<LL	<LL	<LL	1.87	2.02
Pb	18.0	16.0	15.6	16.1	31.7	25.4	21.9	31.1	25.5	25.8	15.8	23.9	22.1	37.2	22.3
Pr	-	-	9.78	-	-	-	9.78	-	-	-	-	-	-	8.47	19.4
Rb	182	158	139	138	151	150	135	138	146	219	130	193	198	199	189
Sb	-	-	0.70	-	-	-	1.29	-	-	-	-	-	-	0.93	0.71
Sc	-	-	5.46	-	-	-	7.42	-	-	-	-	-	-	2.17	5.83
Sm	-	-	6.83	-	-	-	6.82	-	-	-	-	-	-	4.77	13.7
Sn	<LL	4.1	1.65*	<LL	5.2	<LL	3.3	7.6	4.0	7.9	3.9	4.2	7.3	3.0	5.5
Sr	77.1	157	158	290	280	224	232	220	217	46.4	36.0	20.5	26.2	15.0*	22.7*
Ta	-	-	5.95	-	-	-	6.77	-	-	-	-	-	-	4.68	2.82
Tb	-	-	1.06	-	-	-	1.06	-	-	-	-	-	-	0.71	2.04
Te	-	-	0.06	-	-	-	0.21	-	-	-	-	-	-	0.03	0.06
Th	15.1	12.4	11.2	10.0	11.4	12.3	10.1	11.4	10.2	15.4	9.60	23.6	17.4	24.8	13.0
Tl	-	-	0.22	-	-	-	0.26	-	-	-	-	-	-	0.27	0.25
Tm	-	-	0.49	-	-	-	0.46	-	-	-	-	-	-	0.37	0.83
U	-	-	3.39	-	-	-	3.11	-	-	-	-	-	-	3.81	3.49
V	14.6	31.8	34.2	64.5	56.8	52.5	58.8	56.2	58.3	8.2	13.5	8.7	12.7	8.2	9.4
W	139	143	192	105	119	109	129	128	120	111	78.2	63.9	107	38.0	136
Y	56.7	46.6	35.3	41.0	34.5	36.6	35.7	38.7	38.6	74.9	49.0	25.2	64.9	25.6	68.2
Yb	-	-	3.21	-	-	-	3.06	-	-	-	-	-	-	2.49	5.31
Zn	53.3	75.1	62.5	70.4	85.8	146	94.1	138	145	123	95.2	57.1	78.7	69.5	91.9
Zr	456	415	363	404	427	426	392	420	421	682	392	205	623	213	585

Table 7.2: (Continuation)

Sample	ISP-252	ISP-254	ISP-255	ISP-258	ISP-259	ISP-260	ISP-261	ISP-262	ISP-263	ISP-265	ISP-266	ISP-267	ISP-268	ISP-269
Unit	NU rhyolite	MZ rhyolite	CO rhyolite	PC rhyolite	PC rhyolite	PC trachyte	PC trachyte	PC trachyte	CO rhyolite	CF rhyolite	CO rhyolite	CO rhyolite	trachyandesite	MZ rhyolite
As	19.7	10.6	-	-	14.6	-	-	-	-	-	-	5.30	6.44	-
Ba	1160	1090	<LL	640	632	660	644	649	<LL	804	<LL	23.8*	648	960
Be	3.29	3.17	-	-	3.88	-	-	-	-	-	-	5.95	4.24	-
Bi	0.03	0.05	-	-	0.56	-	-	-	-	-	-	0.01	0.03	-
Ce	165	113	185	98.4	101	83.4	121	120	279	66.0	189	227	73.9	116
Co	13.6	16.1	14.3	21.3	26.5	12.8	16.1	14.1	16.6	7.6	28.6	18.6	20.9	20.2
Cr	7.89	7.60	<LL	<LL	10.7	<LL	<LL	<LL	<LL	<LL	<LL	7.05	9.17	<LL
Cs	4.85	5.03	-	-	2.72	-	-	-	-	-	-	2.57	2.29	-
Cu	4.30	15.2	<LL	<LL	9.11	4.6	4.7	<LL	<LL	<LL	<LL	3.29	19.0	<LL
Dy	9.81	12.7	-	-	7.34	-	-	-	-	-	-	20.0	18.6	-
Er	5.02	6.43	-	-	3.98	-	-	-	-	-	-	11.4	12.0	-
Eu	1.96	2.39	-	-	1.41	-	-	-	-	-	-	0.56	2.97	-
Ga	16.7	16.8	23.4	17.6	17.6	17.5	18.4	18.8	22.7	18.9	24.0	23.9	19.9	15.7
Gd	11.7	14.3	-	-	8.22	-	-	-	-	-	-	20.1	16.8	-
Ge	1.53	1.48	-	-	1.44	-	-	-	-	-	-	2.09	1.43	-
Hf	7.45	2.94	-	-	7.89	-	-	-	-	-	-	28.7	6.28	-
Ho	1.74	2.23	-	-	1.33	-	-	-	-	-	-	3.73	3.99	-
La	70.7	81.8	-	-	52.4	-	-	-	-	-	-	114	50.6	-
Li	18.3	15.9	-	-	11.8	-	-	-	-	-	-	31.0	14.0	-
Lu	0.63	0.76	-	-	0.55	-	-	-	-	-	-	1.71	1.40	-
Mo	2.09	2.22	<LL	<LL	2.22	<LL	<LL	<LL	<LL	<LL	5.70	1.63	1.72	<LL
Nb	45.7	43.3	189	48.9	52.6	46.9	52.2	55.7	133	48.8	116	121	33.0	45.0
Nd	61.8	80.4	-	-	42.6	-	-	-	-	-	-	99.8	58.7	-
Ni	1.98	2.75	<LL	<LL	1.88	<LL	<LL	<LL	<LL	<LL	<LL	0.92	3.29	<LL
Pb	21.3	18.4	19.7	89.8	27.1	17.9	20.4	19.9	32.5	16.6	33.0	19.9	12.7	22.0
Pr	16.4	21.5	-	-	11.5	-	-	-	-	-	-	27.1	13.4	-
Rb	204	184	351	153	164	134	169	185	288	119	298	242	93.1	174
Sb	4.19	1.22	-	-	1.28	-	-	-	-	-	-	0.43	0.65	-
Sc	7.55	7.64	-	-	6.49	-	-	-	-	-	-	2.64	22.6	-
Sm	11.5	15.1	-	-	7.92	-	-	-	-	-	-	19.7	13.3	-
Sn	4.4	5.7	16.1	4.2	3.1	4.0	<LL	2.3	14.0	4.2	11.3	10.7	2.43*	4.0
Sr	94.9	120	<LL	160	149	206	163	140	<LL	42.8	<LL	14.2*	414	131
Ta	1.26	1.52	-	-	6.27	-	-	-	-	-	-	9.51	5.19	-
Tb	1.70	2.16	-	-	1.24	-	-	-	-	-	-	3.25	2.85	-
Te	0.03	0.07	-	-	0.09	-	-	-	-	-	-	0.13	0.64	-
Th	15.6	14.0	24.7	11.9	13.9	11.6	13.0	15.7	19.5	9.90	21.2	15.7	7.40	13.3
Tl	0.58	0.78	-	-	0.50	-	-	-	-	-	-	0.24	0.28	-
Tm	0.67	0.87	-	-	0.56	-	-	-	-	-	-	1.67	1.61	-
U	3.93	2.73	-	-	4.10	-	-	-	-	-	-	2.62	2.26	-
V	21.2	25.1	8.1	38.0	40.1	53.8	40.5	36.0	10.0	16.0	5.7	9.0	166	24.4
W	144	107	156	178	193	85.0	104	126	213	77.3	267	168	69.0	164
Y	52.2	73.9	>UL	37.3	40.2	37.2	43.7	45.8	107	31.5	107	101	>UL	68.2
Yb	4.35	5.52	-	-	3.75	-	-	-	-	-	-	11.4	9.70	-
Zn	66.0	81.1	287	71.8	88.8	62.8	75.3	63.9	201	78.1	149	167	151	55.8
Zr	492	451	>UL	400	421	409	432	451	1240	353	877	1060	253	450

Table 7.2: (Continuation)

However, there are exceptions to this; among the studied materials there are the vitrophyres, which in fresh condition may present a water content of up to 7 wt % (Smith et al., 2001), this water being dissolved in fresh glass and not in alteration minerals. Therefore, vitrophyre analyses are presented showing LOI values above 2.5 wt %. Silicification of ignimbrites is a recurrent process; data showing that rock had undergone a silicification process have been rejected.

CIPW norm was calculated using the integrated software in Igpet (Carr, 2005) following the Irvine and Baragar (1971) method.

In total, 281 whole rock analyses are presented. Analyses from samples FS, SU, ANT-1 to ANT-38, and VS-145 to VS-180 were performed in previous studies by the research group but never got published.

7.3 LITERATURE DATA

Several published studies providing data from the Sulcis area (Araña et al., 1974; Assorgia et al., 1994; Morra et al., 1994; Cioni and Funedda, 2005; and Conte et al., 2010) have been revised to collect useful geochemical analyses. Moreover, two unpublished studies from the research group (Roselló, 2005; Ramon, 2009) have also been revised. Criteria for incorporating geochemical data into the new database have been several. Regarding analyses quality, they have to present a LOI value lower than 2.5 wt % (except for vitrophyres), and major elements must add up to more than 98 wt %. A further requirement has been that sample unit origin has to be specified (subsequent revision of the attribution of samples to a specific unit has been carried out based on geochemistry following the criteria explained in Chapter 8). Finally, each analysis has been checked for consistency with the rest of the database. Next, the result of the selection process is provided.

Araña et al. (1974): Analyses from Araña et al. (1974) lack trace element data, and but for one sample (SS-60) LOI values are higher than 3 wt %. Only SS-60 has been selected.

Assorgia et al. (1994): data from two peralkaline units (CO and MU) are provided in this study. It has not been possible to rule out analyses based on major elements sum because results appear normalised to 100 wt %. However, when compared with data from other studies, these are consistent, so all of them have been used; it has to be mentioned, though, that some CO show a Nb content higher than the average.

Morra et al. (1994): this work provides a lot of analyses representing all units outcropping at the Sulcis mainland. It has not been possible to rule out analyses based on major elements sum because results appear normalised to 100 wt % (an exception to this is 36/268 which sums more

than 103 wt % and has been consequently ruled out). Based on LOI value, analyses from samples 37/403.5, 385.60, 393.20, 392.60, 387.60, 402.3, 393.5, 37/T, 15/28, 10/12, 33/P, 37/Q, 31/12, 7/3, 26/G, 30/20, 48/19bis, 7/1, 10/9, 37/324.5, 48/14bis, 26/6, 1/5, 17/3, 16/8, 15/5, 26/C, 21/3 have been rejected. Finally, major element data from samples 327.5, 326.5, 324, 37/324, 328.7, 37/L, 378.80, 379.70, 378, 37/375.00, 398.40 and 345.5 (belonging to upper parts of CM, AC and LE units) have been rejected because these samples show characteristics that evidence a moderate degree of alteration (especially modification of Na_2O (decrease) and K_2O (decrease or increase) contents). Trace elements of these samples have to be used cautiously. Finally, samples 36/Bbis and 37/I have been discarded because it is believed that there is a unit misidentification.

Cioni and Funedda (2005): the four analyses provided by these authors from the analysis of comenditic lava flows from San Pietro Island have been incorporated into the database.

Conte et al. (2010): this work presents analyses from andesites cropping out at Santo Antioco Island. All of them have been used.

Roselló (2005): data from PI-11, PI-15, PI-18, PI-19, PI-21 and PI-43 have been ruled out based on LOI and major element sum criteria. PI-38, PI-39, PI-40, PI-41 and PI-42 data have been discarded because sampling location and unit are not known.

Ramon (2009): data from samples L-2, L-3, L-5, L-6, L-21, L-31, L-35 and L-43 have been rejected based on LOI and major element sum criteria. Samples L-9, L-19, L-30 and L-62 show evidences of silicification and have been, therefore, discarded.

7.4 WHOLE ROCK GEOCHEMISTRY

7.4.1 Major elements

Major elements are the raw material for petrogenetic modelling in igneous petrology, but in the case of volcanic rocks they are also essential for rock classification. Petrography is usually not enough to classify volcanic rocks, especially when dealing with pyroclastic deposits. Many classification systems have been proposed over the years. One of the most used is that by Le Maitre et al. (1989), who proposed a classification for volcanic rocks based on whole rock major element geochemistry using as a main tool the Total Alkalis versus Silica diagram (TAS) defined by Le Bas et al. (1986).

Samples from the Sulcis have been classified following Le Maitre (2002). Figure 7.1 is the TAS diagram used in the classification process, in which whole rock analyses have been plotted after normalization to 100 wt % in an anhydrous basis with Fe distributed between FeO and Fe_2O_3 following Middlemost (1989) (for better visualization several plots have been made). Two

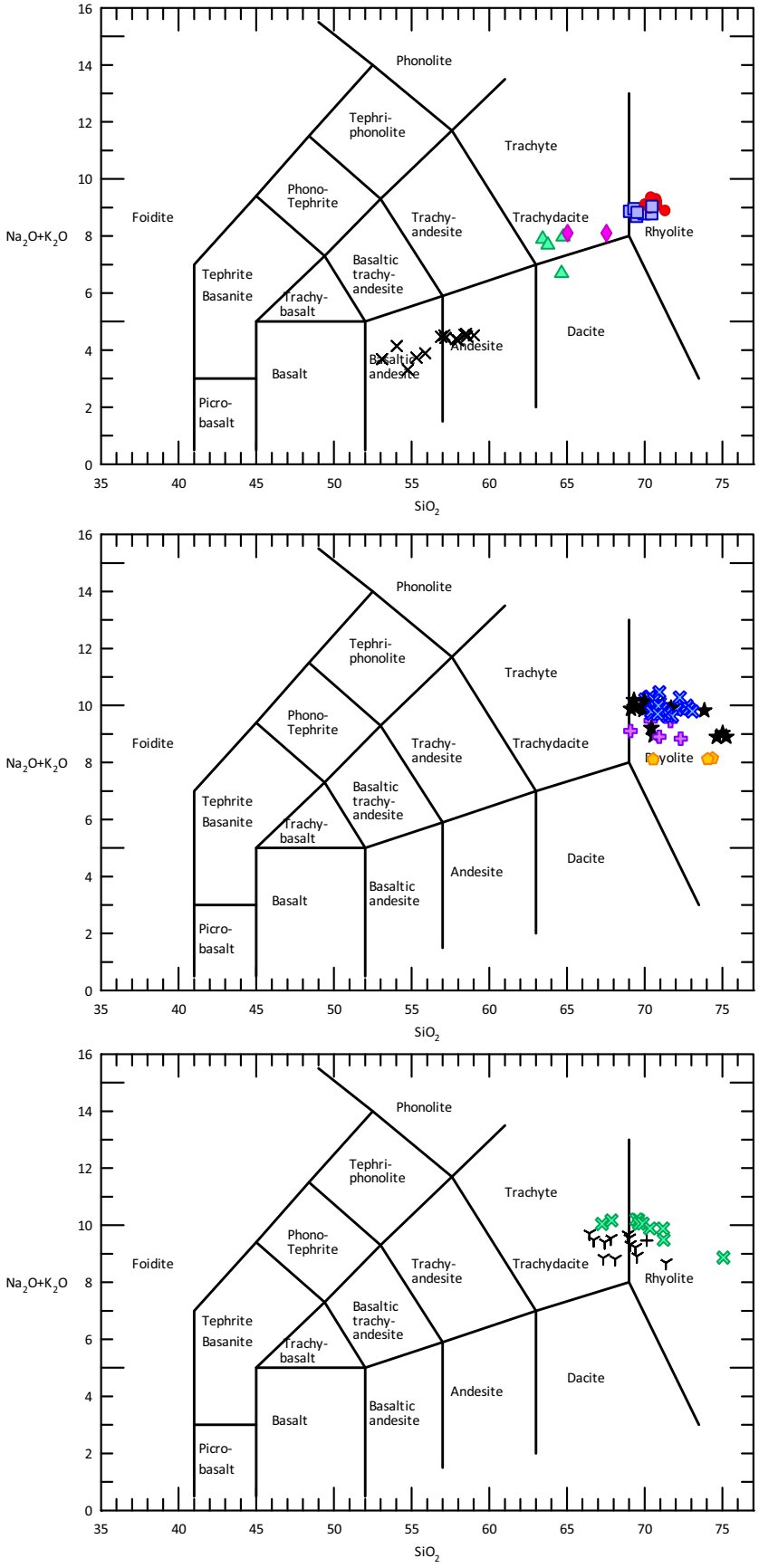

Figure 7.1: TAS diagrams showing the classification of units from AND to MZ. Contents in wt %

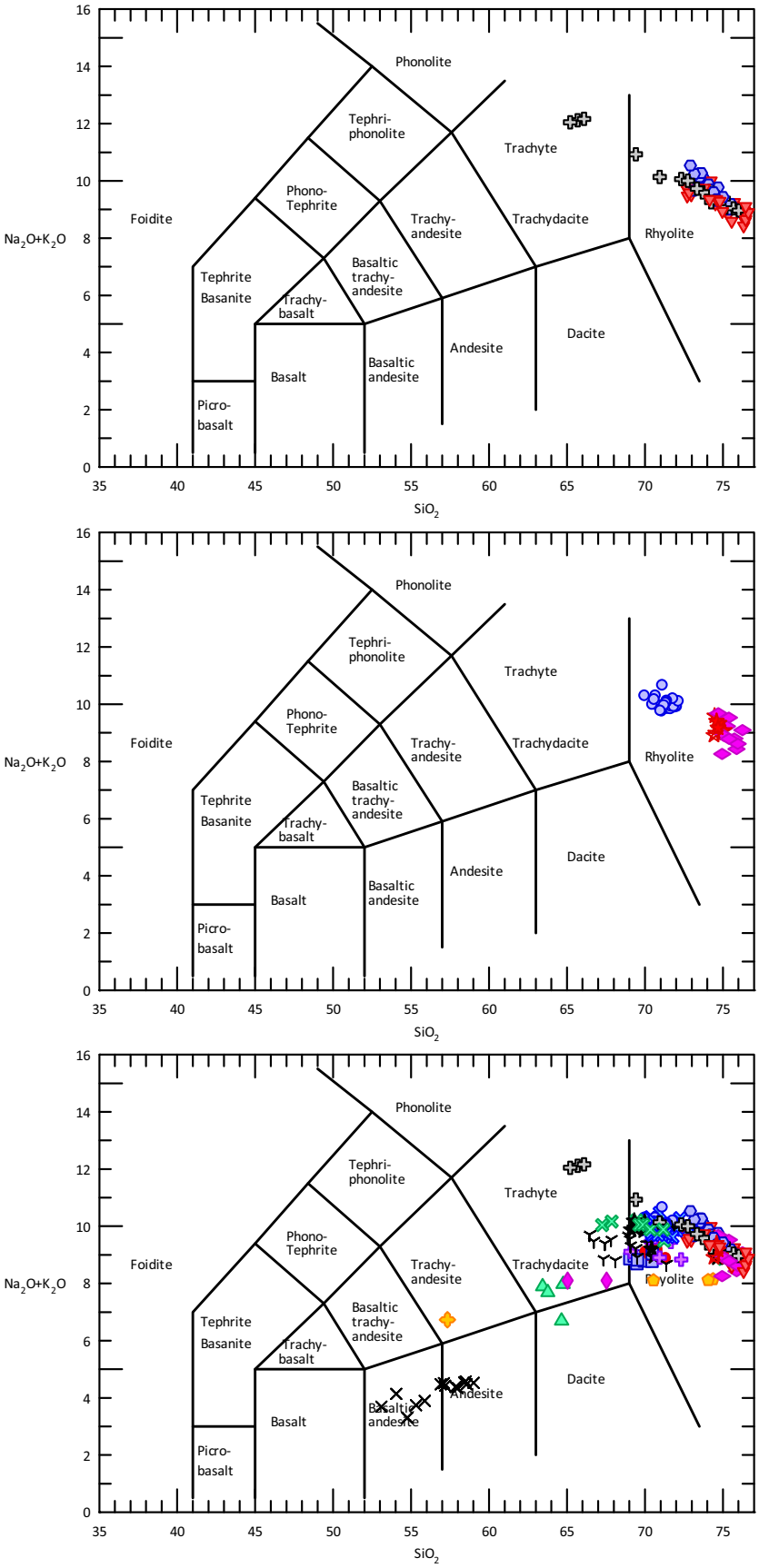

Figure 7.1: (Continuation) TAS diagrams showing the classification of units from CO to CL units. The diagram at the bottom includes all units

principal groups are seen in the diagram, one formed by the andesitic lower part of the Oligo-Miocene sequence (basalts to andesites), and the other one by the upper ignimbritic sequence (mainly rhyolites and minor trachytes and dacites). Only CM, AC and some samples from PC and MZ units fall in the trachyte field. Samples from the CF unit in the trachyte field correspond to crystal-rich black pumice samples and a mixing line can be observed between pumice and groundmass composition.

Contrary to what could be expected, there isn't a single continuous trend connecting the whole sequence. Instead, several main trends can be observed (Fig. 7.2): an ascending one defined by the andesitic sequence, another ascending one separated from the first one formed by the ignimbrites with lower silica content, and a third one marked by the more silica-rich units. The inflexion between the second and third trend is at about 72 wt % silica. Sample represented by a yellow cross is from a lava flow found at the stratigraphic level of CO.

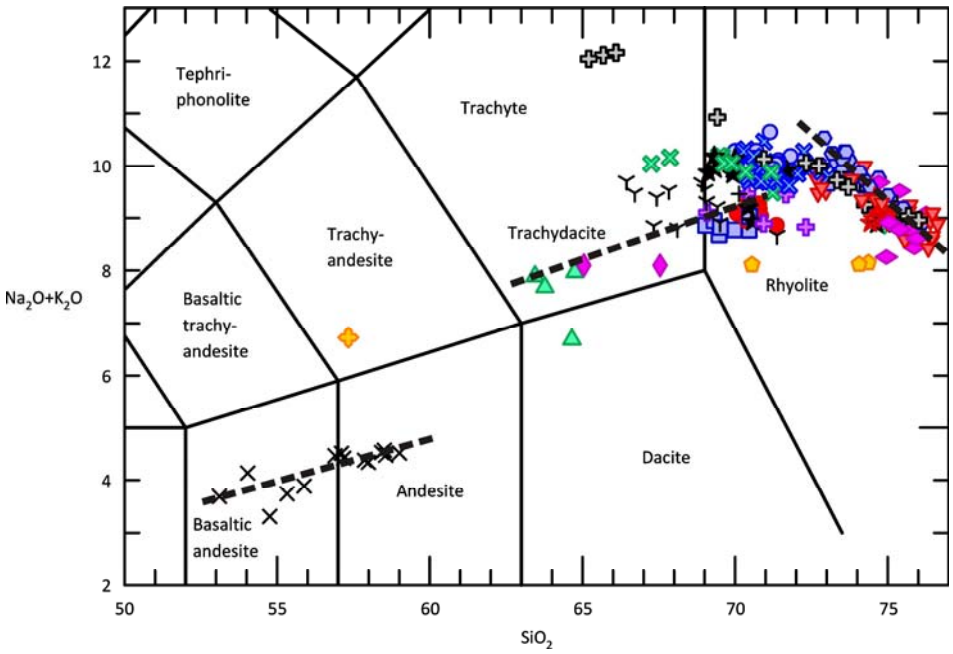

Figure 7.2: Zoom on the TAS diagram showing the main trends observable in the Sulcis data. Contents in wt %

The occurrence of several trends in this suite is also observable in the variation diagrams of major elements versus silica (Fig. 7.3). Multiple trends can be seen in these diagrams. These show negative correlations of major elements with silica for all elements but for Na and K, which show a positive correlation, with some exceptions. Interpretation of these trends will be tackled in the chapter on the petrogenesis of the suite.

Figure 7.4 is a diagram of agpaicity index versus silica (values can be seen in Table 7.1). Several of the ignimbritic units have an alkalinity close to peralkalinity, but only CO, MU and CF cross the

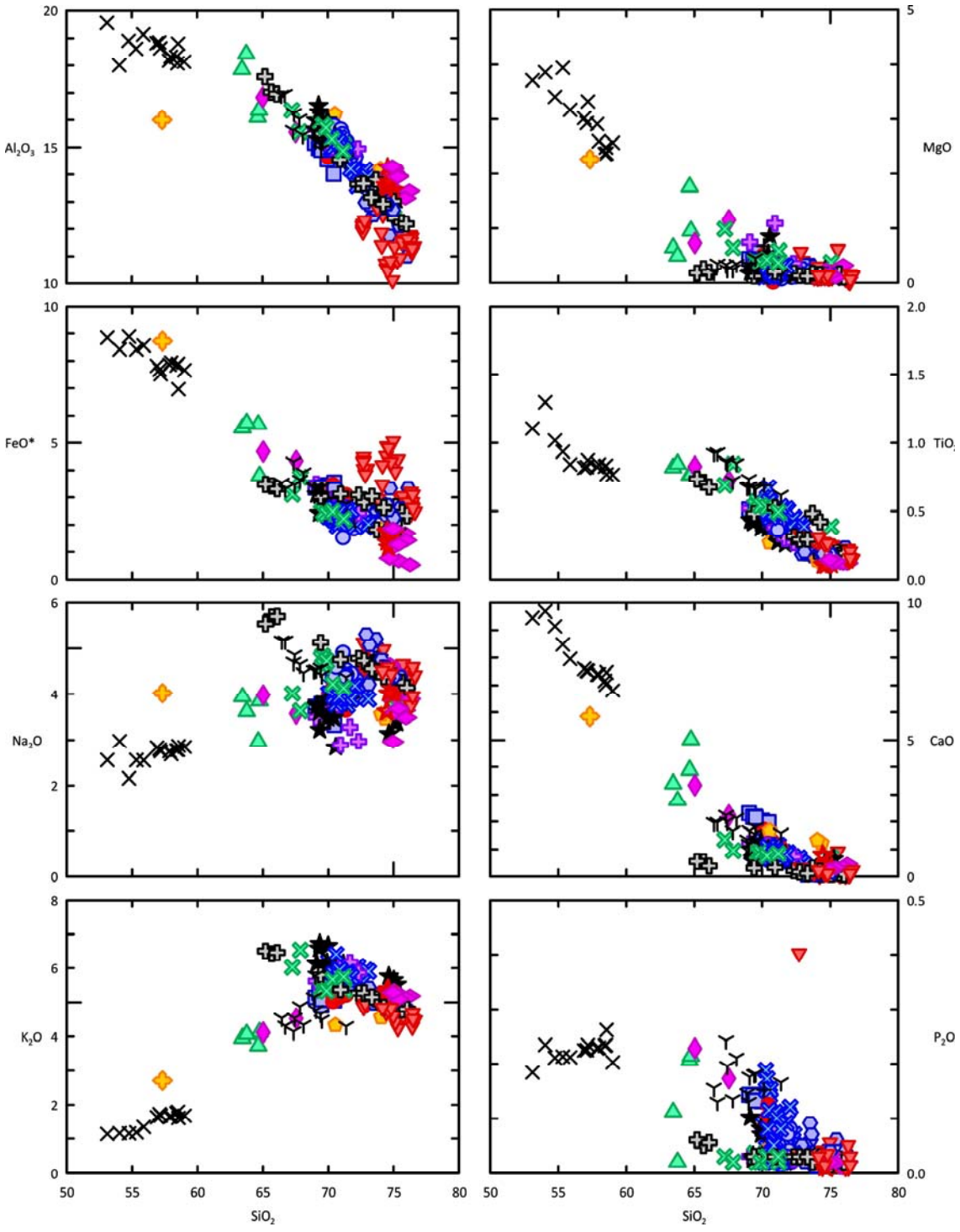

Figure 7.3: Harker diagrams of major elements versus silica content. FeO* is total iron. Contents in wt %

limit, with a maximum value of 1.21. Peralkaline samples were classified into comenditic or pantelleritic types following the Al_2O_3 versus total iron as FeO diagram (Macdonald, 1974a); all samples but three plot in the comenditic field (Fig. 7.5).

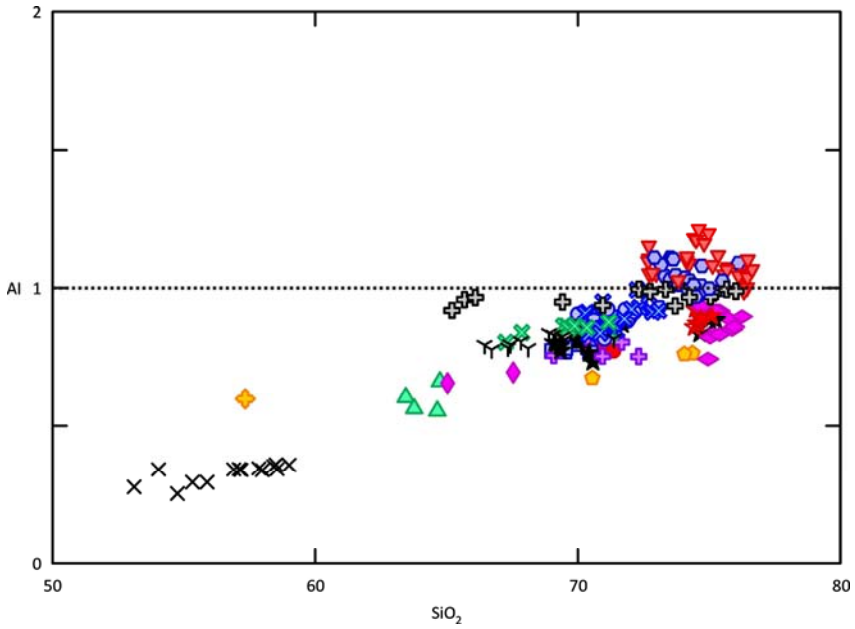

Figure 7.4: Agpaicity index versus silica (wt %). 1 is the limit for peralkalinity

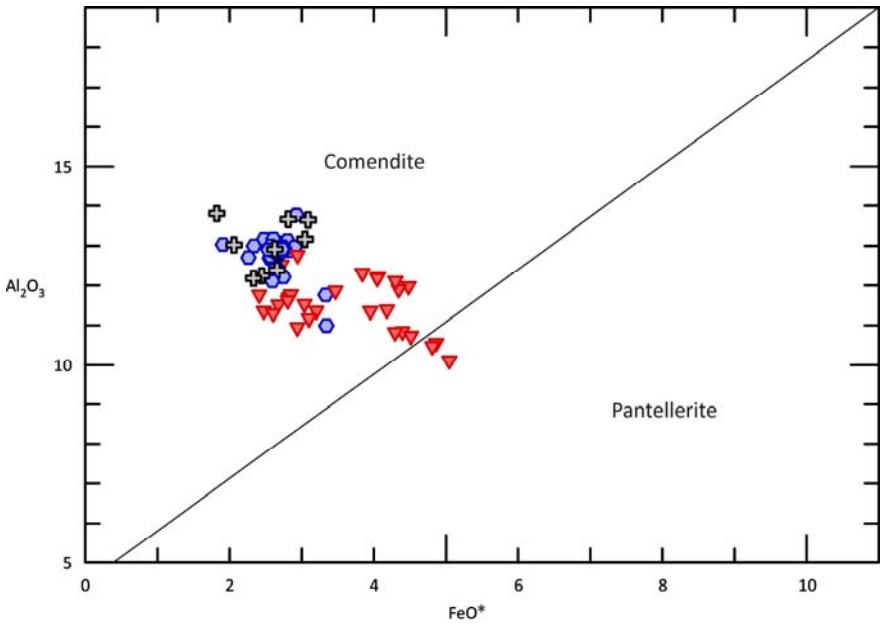

Figure 7.5: Classification of peralkaline rocks into comendites and pantellerites based on MacDonald (1974a)

Finally, all rocks were represented in the K_2O versus SiO_2 diagram provided in Le Maitre (2002), which is a simplification of that of Peccerillo and Taylor (1976) (Fig. 7.6). Andesites fall in the medium-K field, whereas the rest of the sequence falls in the high-K field. Na_2O/K_2O ratio (Fig. 7.7) shows that in the ignimbritic sequence potassium dominates over sodium except for some samples belonging to the PC unit. CO, MU and CF units are close to the 1:1 ratio. In Andesites Na_2O dominates.

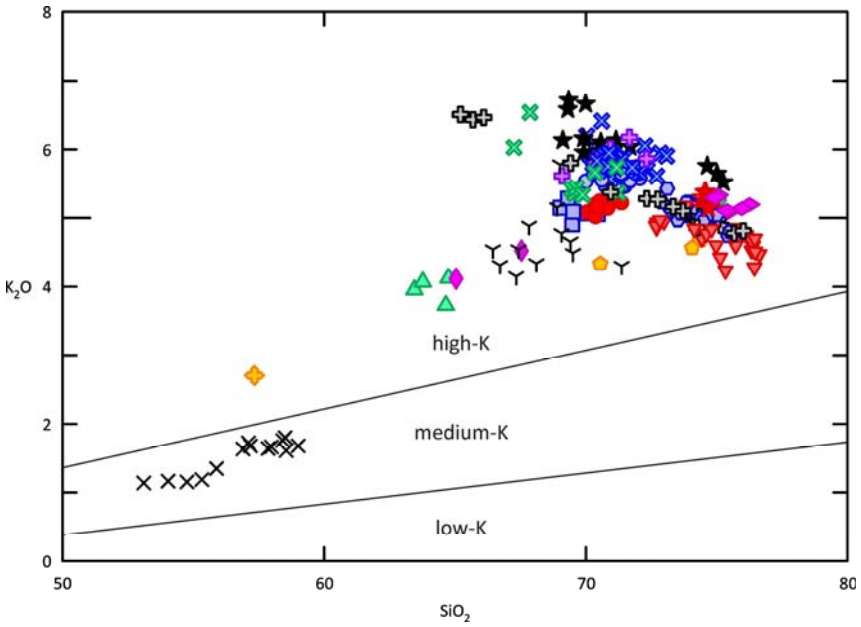

Figure 7.6: Division of the basalt-rhyolite series into low-K, medium-K and high-K types (Le Maitre et al., 2002)

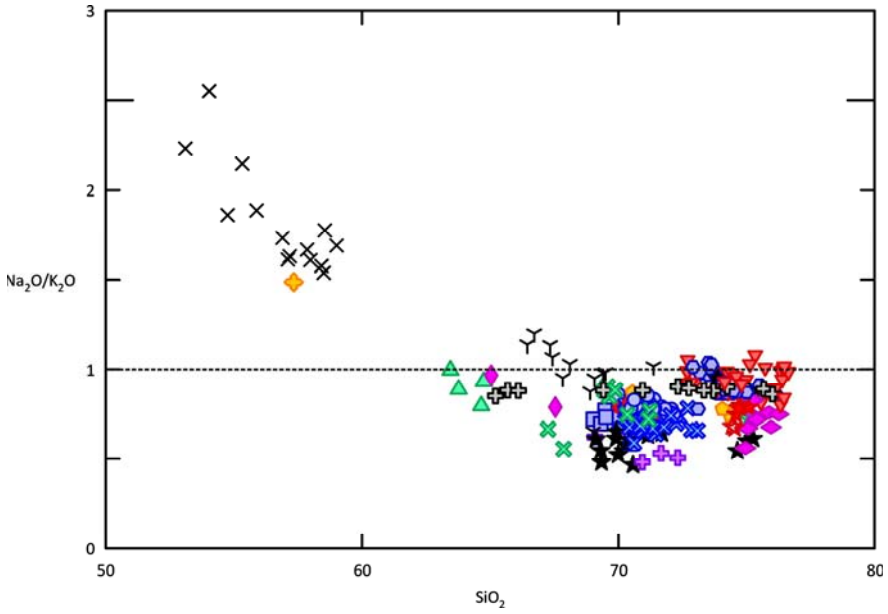

Figure 7.7: Na_2O/K_2O vs. SiO_2 (wt %) diagram

7.4.2 Trace elements

The diverse geochemical behaviour that trace elements have during magma generation and evolution (distribution coefficient), together with the higher number of elements (compared to major elements), make these elements a powerful tool to study magma source, generation and evolution, including fractional crystallisation and assimilation processes. Information is obtained through the comparison between single trace elements as well as from the comparison of ratios

between two elements. A detailed description and interpretation of trace element contents will be given in the corresponding discussion chapter.

Trace elements relations may be visualised using either variation diagrams or multielemental diagrams. Variation diagrams are binary diagrams comparing two elements or element ratios. In Figure 7.8 some variation diagrams of trace elements against silica are shown. Selected trace elements are those providing more information in this suite of rocks. Ba and Sr are compatible elements entering the crystal net of feldspars. Trends of these two elements mark whether feldspar fractionation is taking place (negative correlation) or not (positive correlation). An opposite behaviour is that of Nb and Rb, which are incompatible elements. Incompatible elements content in melt gets progressively higher with crystallisation because these are not constituents of any of the mineral phases and therefore get concentrated in the liquid phase. Zr is an incompatible element that can, under specific conditions, form a mineral phase on its own (zircon). If these conditions are reached (such as for PA and PM units) Zr is extracted from the melt; if not, it behaves as a typical incompatible element.

Another way of studying trace elements is using multielemental diagrams, also known as spider diagrams or spidergrams. In these diagrams trace element content of the studied sample is compared to that of a reference composition (for example primitive mantle or chondrite compositions). Profiles drawn in these diagrams can be compared with profiles from magma suites from various geodynamic settings to interpret which setting the studied magma suite is related to. Changes in profiles in a magma suite may represent variations in the magma source or evolution.

Diagram in Figure 7.9 sorts trace elements by incompatibility (the more incompatible are at the left end of the diagram) and compares its content to that of the primitive mantle composition (Sun and McDonough, 1989). The more incompatible the element, the more enriched in the sample it is, giving to the profiles a descending trend towards the more compatible elements. There are some exceptions to this trend: Ba, Nb, Sr, P, Eu and Ti form negative anomalies, and Pb and K form positive ones. While positive anomalies remain more or less constant throughout the sequence, negative anomalies increase (but for Nb) with the degree of differentiation of the rock. Negative anomalies of Ba, Sr and Eu are related to the incorporation of these elements in feldspars (thus feldspar crystallisation and fractionation deepens the anomaly), and those of P and Ti are caused by the precipitation of apatite and spinel respectively. The profile depicted by the Sulcis Oligo-Miocene volcanic suite is similar to that of typical calc-alkaline magma suites, like that of the Carpathians (Fig. 7.10).

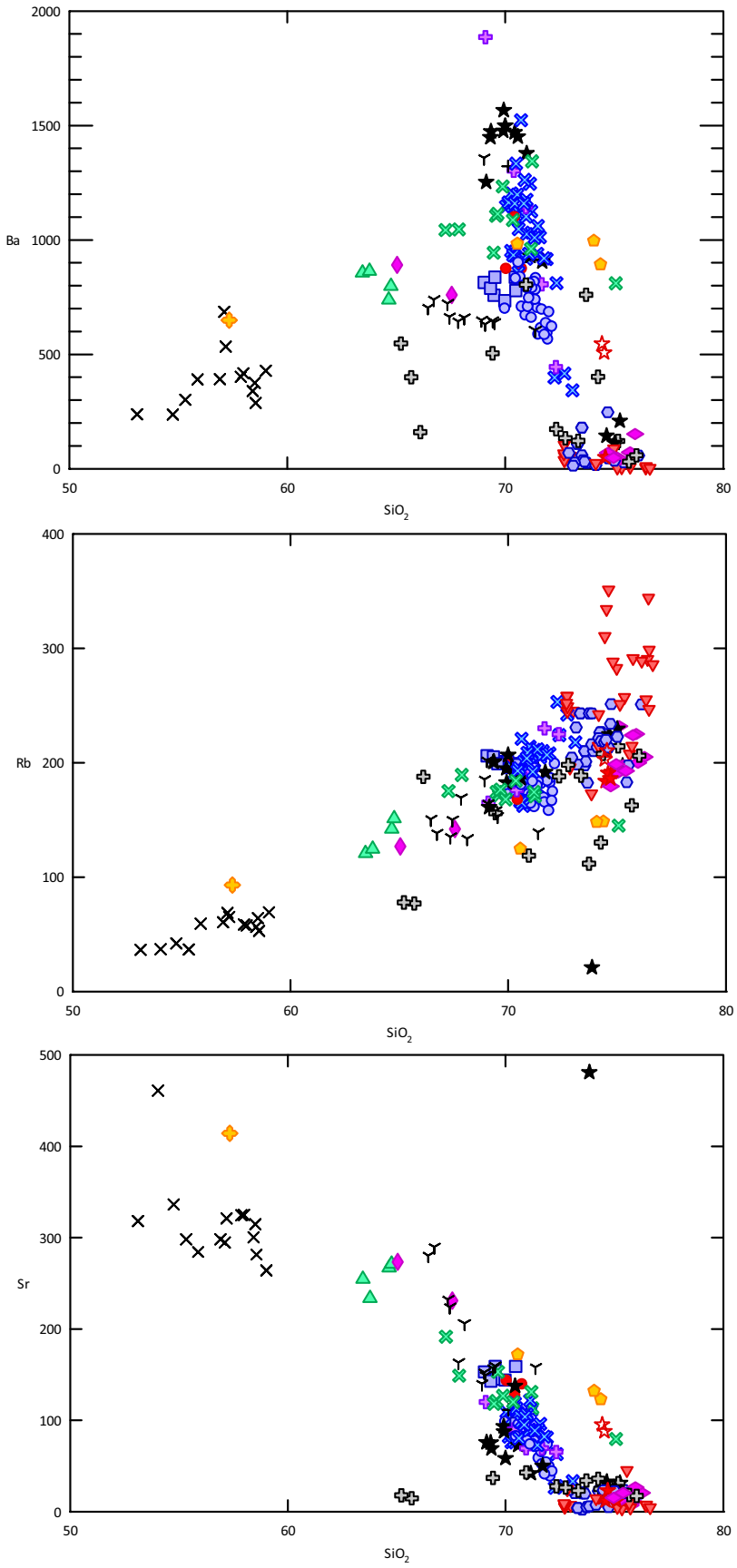

Figure 7.8: Variation diagrams of trace elements (content in ppm) versus silica (wt %)

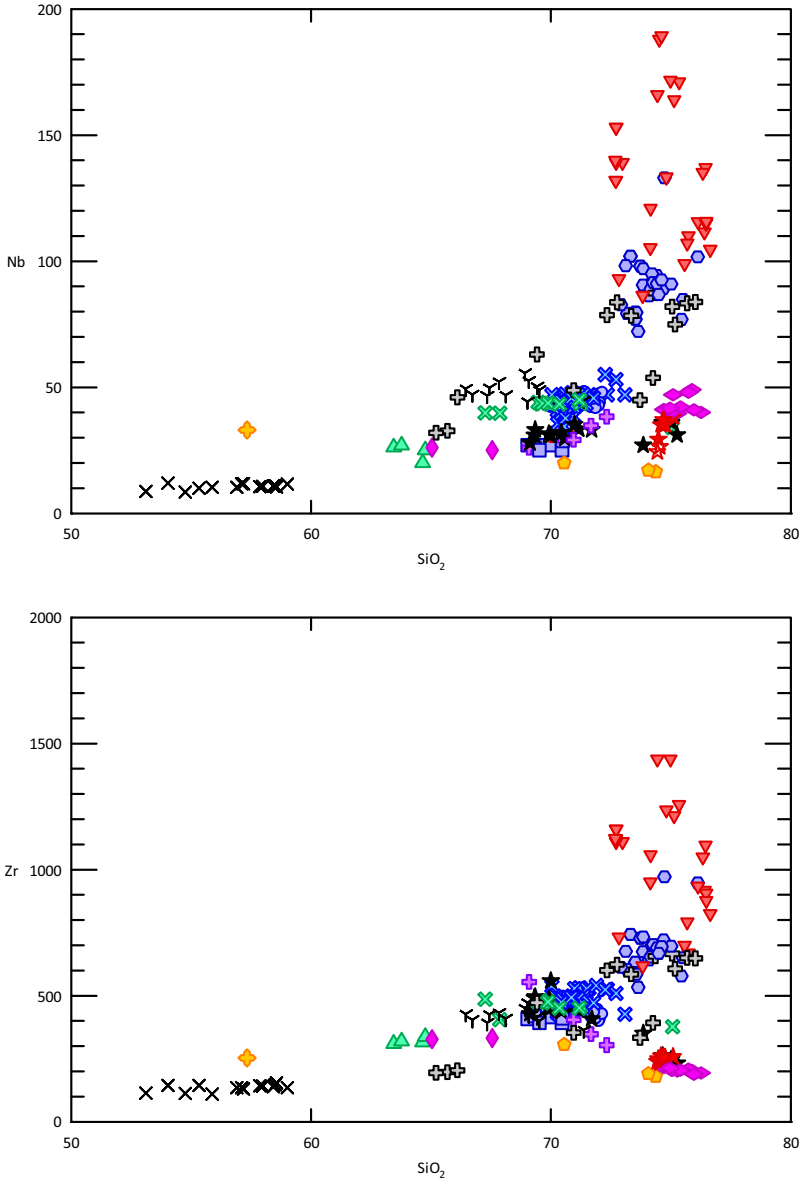

Figure 7.8: (Continuation)

Some spidergrams focus on REE. Figure 7.11 presents REE content normalized to chondrite composition (Sun and McDonough, 1989). Although they all behave as incompatible elements (but for Eu in feldspars), there is a slight decrease in incompatibility from light REE (LREE) to heavy REE (HREE), which generally produces a profile descending from the LREE to the HREE. Rocks from the Sulcis present a profile with a descending trend from LREE to medium-REE (Sm to Ho, MREE), and a more flat zone at the HREE. Values for $(La/Ho)_N$ are from 3.5 to 13 (with a maximum of 18), while $(Ho/Lu)_N$ presents values from 0.93 to 1.4. Eu anomaly reaches a maximum in $(Eu/Eu^*)_N$ of 0.01.

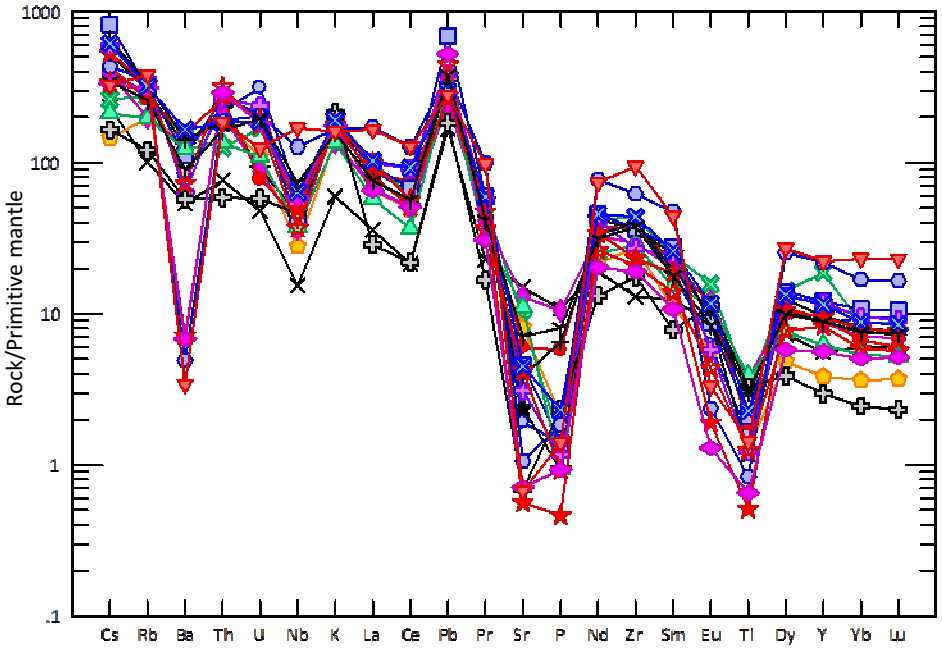

Figure 7.9: Primitive mantle-normalized spider diagram. Normalizing values of Sun and McDonough (1989)

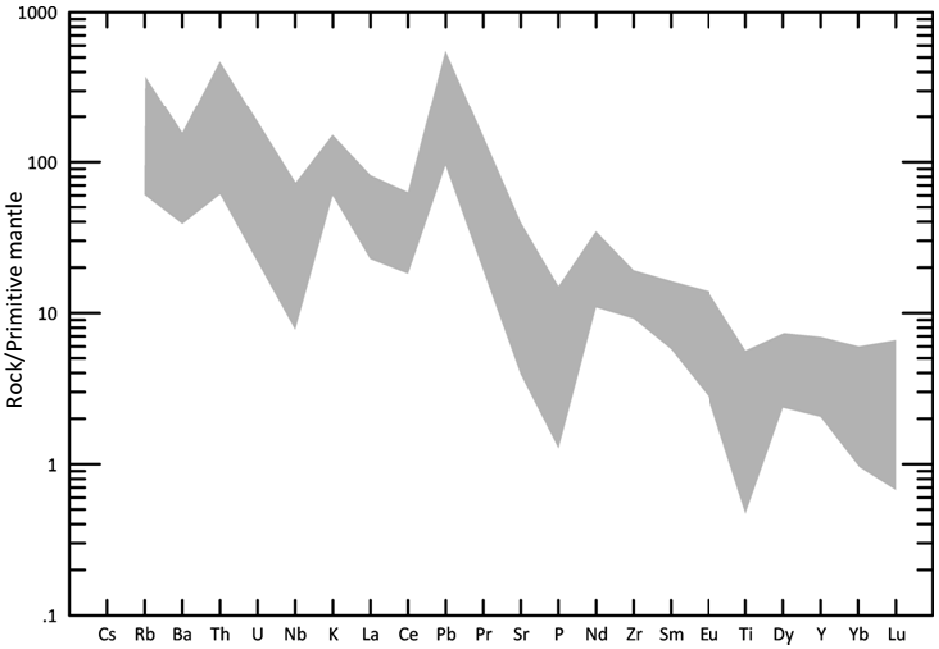

Figure 7.10: Primitive mantle spider diagram (Sun and McDonough, 1989). Shade represents data from the Carpathians by Harangi et al. (2007)

7.4.3 Isotopic ratios

Strontium, Nd and Pb isotopic data have been obtained in this study (Table 7.3) and collected from literature. Initially used in geochronology, radiogenic isotopes have become a powerful tool for petrogenetic studies because isotopic ratios provide information that trace elements cannot. Differently from major and trace elements, isotopic ratios are not affected by partial melting or

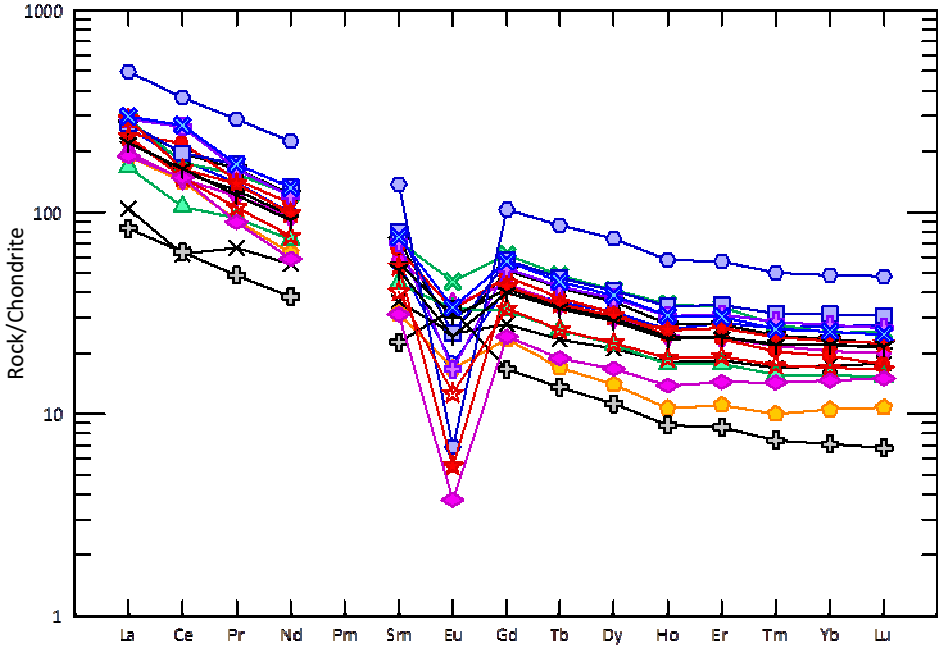

Figure 7.11: Chondrite-normalized spider diagram (Sun and McDonough, 1989)

crystal fractionation processes. The reason is that mass difference between isotopes of a single element (this is valid only for heavy elements such as the ones being studied in the present work) is too small for fractionation to be significant. Being independent of fractionation, isotopic ratios of a given magma are determined only by magma source composition, contamination processes and age. Therefore, they are capable of tracing magma source even in highly evolved rocks like the ones being worked with in this study.

The best way to visualize isotopic ratios in a stratigraphic sequence is in a diagram of isotopic ratio versus stratigraphic position (Fig. 12 to 16). Initial $^{87}Sr/^{86}Sr$ ($^{87}Sr/^{86}Sr_i$) values have been calculated using for age correction a $^{87}Rb/^{86}Sr$ value calculated from the Rb/Sr obtained from ICP data and an age of 18 Ma for andesites, 16 Ma for CM to SE units, 15.5 Ma for MLN to NU units, and 15 Ma for PC to CL. Peralkaline units present very low Sr and high Rb contents. Analytical error on measuring Sr when its content is very low has a strong effect on calculating the Rb/Sr, and therefore on the age correction of $^{87}Sr/^{86}Sr$ values. Peak values for peralkaline units observable in the diagram are due to this effect. Not taking into account this peak, the general trend for $^{87}Sr/^{86}Sr_i$ is a descending one. The opposite trend is found for Nd and Pb isotopic ratios. Age correction for these two elements has not been made because the studied materials are not old enough to have undergone a significant variation of the isotopic ratios. $^{143}Nd/^{144}Nd$ presents an ascending approximately linear trend. Lead isotopes also present an ascending trend, but it is not linear, it appears segmented. This is especially evident in the $^{207}Pb/^{204}Pb$ diagram, where three small descending trends originate within the general ascending one.

Sample	Unit	$^{87}Sr/^{86}Sr$	$^{143}Nd/^{144}Nd$	$^{206}Pb/^{204}Pb$	$^{207}Pb/^{204}Pb$	$^{208}Pb/^{204}Pb$	$^{207}Pb/^{206}Pb$	$^{208}Pb/^{206}Pb$	Age	$(^{87}Sr/^{86}Sr)_i$
ANT 12	SP	0.706611 ± 0.000006	0.512693 ± 0.000003	18.871 ±0.0040	15.695 ± 0.0040	39.006 ±0.0140	0.831688 ± 0.000072	2.06695 ± 0.00036	15	0.705255
ANT 57	CO	0.729451 ± 0.000005	0.512694 ± 0.000003	18.902 ±0.0017	15.722 ± 0.0020	39.143 ±0.0070	0.830321 ± 0.000034	2.06724 ± 0.00018	15	0.713501
ANT 110	MU	0.731066 ± 0.000004	0.512618 ± 0.000003	18.868 ±0.0002	15.685 ± 0.0002	38.992 ±0.0006	0.831269 ± 0.000004	2.06651 ± 0.00001	15	0.710925
VS 721	AND	0.707533 ± 0.000004	0.512355 ± 0.000004	18.570 ±0.0005	15.676 ± 0.0005	38.746 ±0.0017	0.844150 ± 0.000006	2.08650 ± 0.00004	18	0.707399
VS 757	NU	0.708074 ± 0.000005	0.512535 ± 0.000004	18.771 ±0.0004	15.700 ± 0.0004	38.928 ±0.0012	0.836404 ± 0.000005	2.07387 ± 0.00027	15.5	0.706949
VS 762	MZ	0.707192 ± 0.000007	0.512614 ± 0.000004	18.725 ±0.0040	15.693 ± 0.0040	38.859 ±0.0120	0.838063 ± 0.000047	2.07518 ± 0.00022	15	0.706224
VS763	MLN	0.707267 ± 0.000006	0.512453 ± 0.000004	18.709 ±0.0003	15.676 ± 0.0003	38.865 ±0.0007	0.737774 ± 0.000005	2.07731 ± 0.00002	15.5	0.706776
VS782	AC	0.706916 ± 0.000005	0.512495 ± 0.000003	18.718 ±0.0005	15.688 ± 0.0005	38.876 ±0.0015	0.838099 ± 0.000008	2.07691 ± 0.00003	16.5	0.706646
VS783	SE	0.707662 ± 0.000005	0.512506 ± 0.000003	18.719 ±0.0008	15.683 ± 0.0010	38.872 ±0.0031	0.837817 ± 0.000016	2.07661 ± 0.00008	16.5	0.706901
VS784	LE	0.709245 ± 0.000005	0.512471 ± 0.000004	18.464 ±0.0002	15.695 ± 0.0004	38.655 ±0.0010	0.850048 ± 0.000008	2.09356 ± 0.00003	16.5	0.708273
VS786	CM	0.707863 ± 0.000007	0.512450 ± 0.000005	18.725 ±0.0005	15.696 ± 0.0005	38.904 ±0.0017	0.838241 ± 0.000010	2.07763 ± 0.00005	16.5	0.707569
VS788	CA	0.710482 ± 0.000006	0.512472 ± 0.000006	18.719 ±0.0003	15.672 ± 0.0002	38.800 ±0.0006	0.837241 ± 0.000004	2.07275 ± 0.00001	15.5	0.707830
VS789	PA	0.717806 ± 0.000006	0.512672 ± 0.000003	18.239 ±0.0028	15.656 ± 0.0034	38.312 ±0.0130	0.858339 ± 0.000062	2.10046 ± 0.00030	15	0.707183
VS790	MC	0.709708 ± 0.000006	0.512510 ± 0.000004	18.720 ±0.0006	15.679 ± 0.0005	38.818 ±0.0013	0.837573 ± 0.000006	2.07360 ± 0.00002	15.5	0.708077
ISP 71	CF	0.716069 ± 0.000006	0.512706 ± 0.000004	18.855 ±0.0017	15.668 ± 0.0020	38.943 ±0.0070	0.830975 ± 0.000036	2.06538 ± 0.00019	15	0.710342
ISP 75	CF	0.716736 ± 0.000005	0.512608 ± 0.000004	18.900 ±0.0042	15.722 ± 0.0050	39.118 ±0.0016	0.831828 ± 0.000086	2.06972 ± 0.00043	15	0.710094
ISP 136	MCR	0.708877 ± 0.000005	0.512535 ± 0.000005	18.763 ±0.0018	15.696 ± 0.0020	38.902 ±0.0068	0.836534 ± 0.000036	2.07329 ± 0.00018	15	0.707356
ISP 150	CO	0.754174 ± 0.000005	0.512685 ± 0.000003	18.874 ±0.0007	15.687 ± 0.0006	38.985 ±0.0017	0.831152 ± 0.000008	2.06556 ± 0.00003	15	0.709799
ISP 179	MU	0.717596 ± 0.000006	0.512624 ± 0.000004	18.852 ±0.0003	15.659 ± 0.0003	38.909 ±0.0009	0.830647 ± 0.000005	2.06388 ± 0.00002	15	0.711110
ISP 192	PM	0.717585 ± 0.000006	0.512596 ± 0.000003	18.851 ±0.0007	15.701 ± 0.0007	39.062 ±0.0012	0.832920 ± 0.000012	2.07212 ± 0.00006	15	0.706641
ISP 209	MZ	0.707206 ± 0.000006	0.512556 ± 0.000004	18.781 ±0.0004	15.691 ± 0.0004	38.912 ±0.0014	0.835469 ± 0.000006	2.07184 ± 0.00003	15	0.706334
ISP 210	PG	0.707526 ± 0.000005	0.512590 ± 0.000005	18.780 ±0.0003	15.664 ± 0.0004	38.874 ±0.0012	0.834048 ± 0.000006	2.06990 ± 0.00003	15	0.706186
ISP 227	PC	0.705482 ± 0.000006	0.512649 ± 0.000003	18.800 ±0.0020	15.704 ± 0.0023	38.960 ±0.0080	0.835340 ± 0.000020	2.07233 ± 0.00021	15	0.705170
ISP247	CF	0.714227 ± 0.000005	0.512619 ± 0.000005	18.736 ±0.0003	15.665 ± 0.0003	38.811 ±0.0007	0.836078 ± 0.000004	2.07146 ± 0.00001	15	0.708810
ISP 252	NU	0.708544 ± 0.000005	0.512543 ± 0.000003	18.778 ±0.0008	15.710 ± 0.0007	38.959 ±0.0018	0.836585 ± 0.000016	2.07467 ± 0.00003	15.5	0.707419
ISP 254	MZ	0.707574 ± 0.000006	0.512649 ± 0.000006	18.788 ±0.0006	15.693 ± 0.0006	38.922 ±0.0020	0.835282 ± 0.000009	2.07164 ± 0.00005	15	0.706455

Table 7.3: Isotope ratios for the studied rocks. $(^{87}Sr/^{86}Sr)_i$ have been calculated for the ages shown in Ma using Sr/Rb ICP values

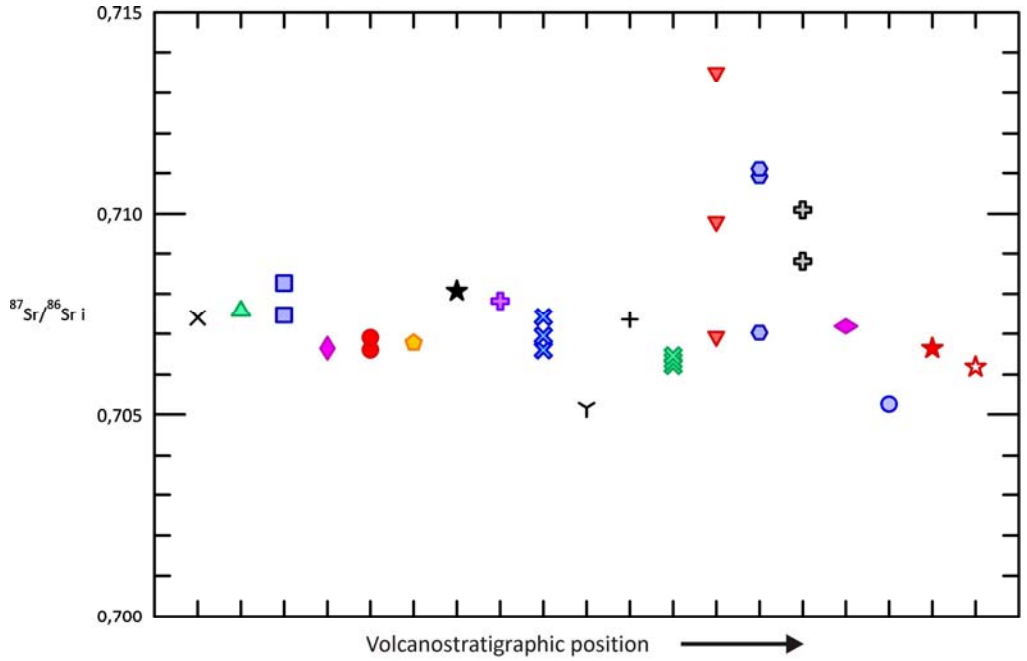

Figure 7.12: Calculated initial $^{87}Sr/^{86}Sr$ ratios

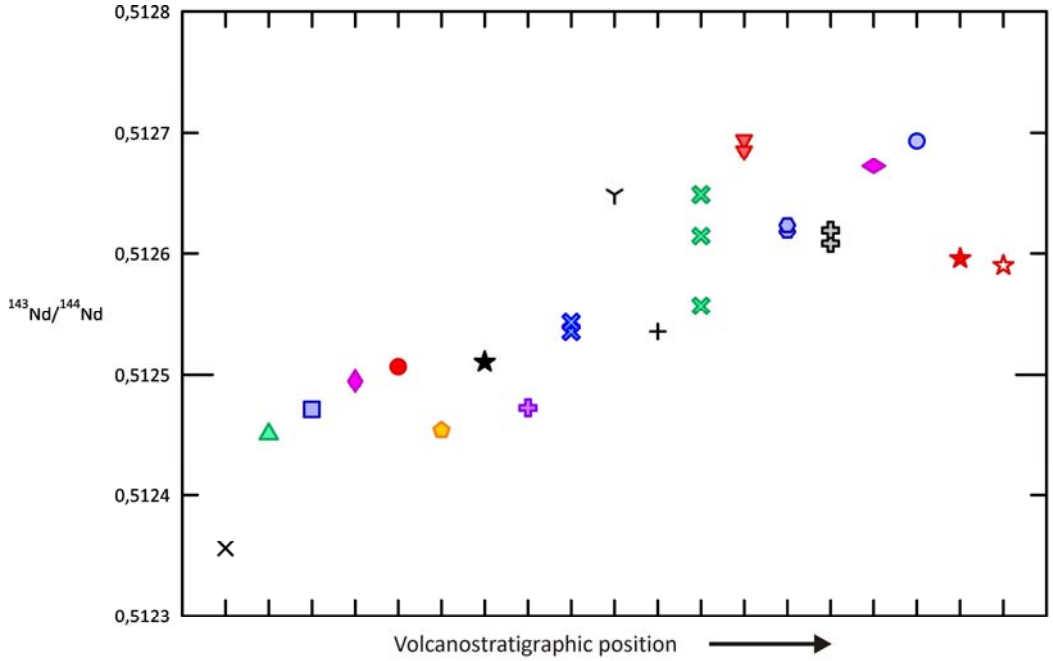

Figure 7.13: $^{143}Nd/^{144}Nd$ isotope ratios

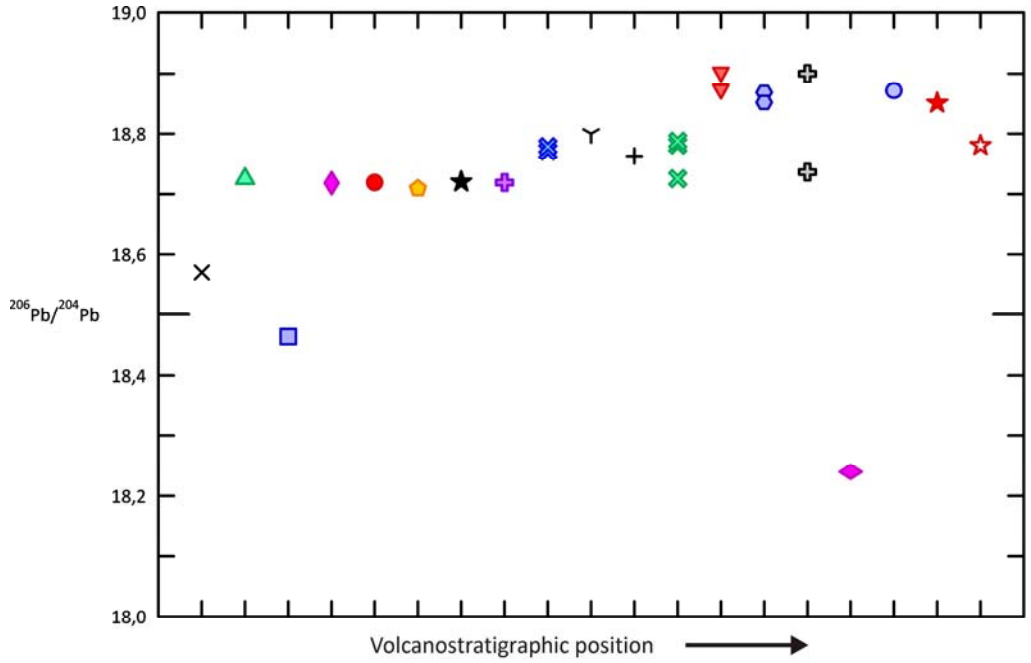

Figure 7.14: $^{206}Pb/^{204}Pb$ isotope ratios

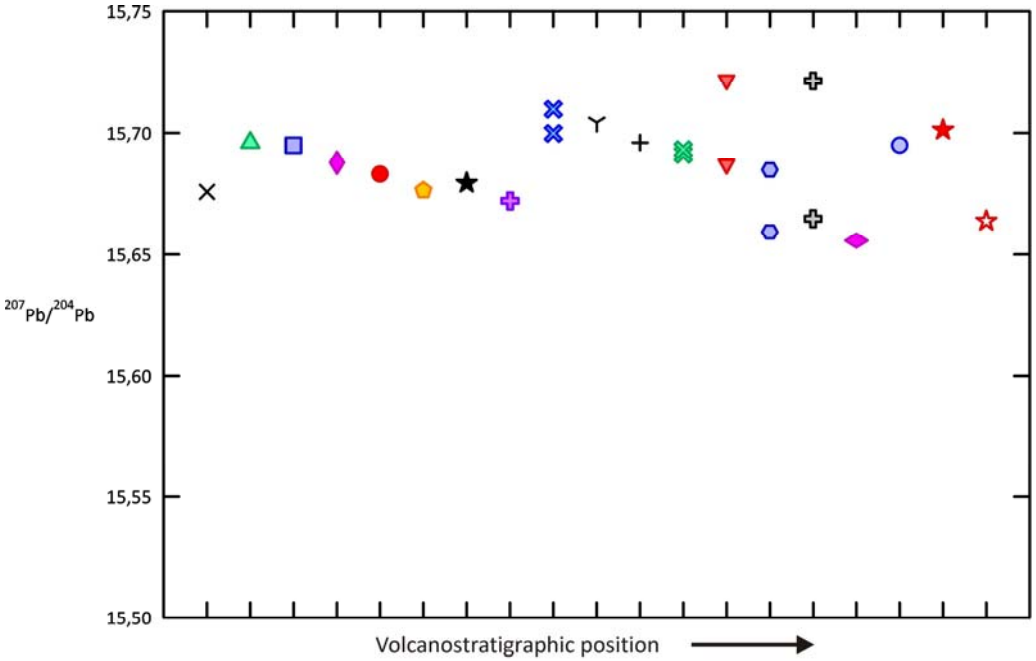

Figure 7.15: $^{207}Pb/^{204}Pb$ isotope ratios

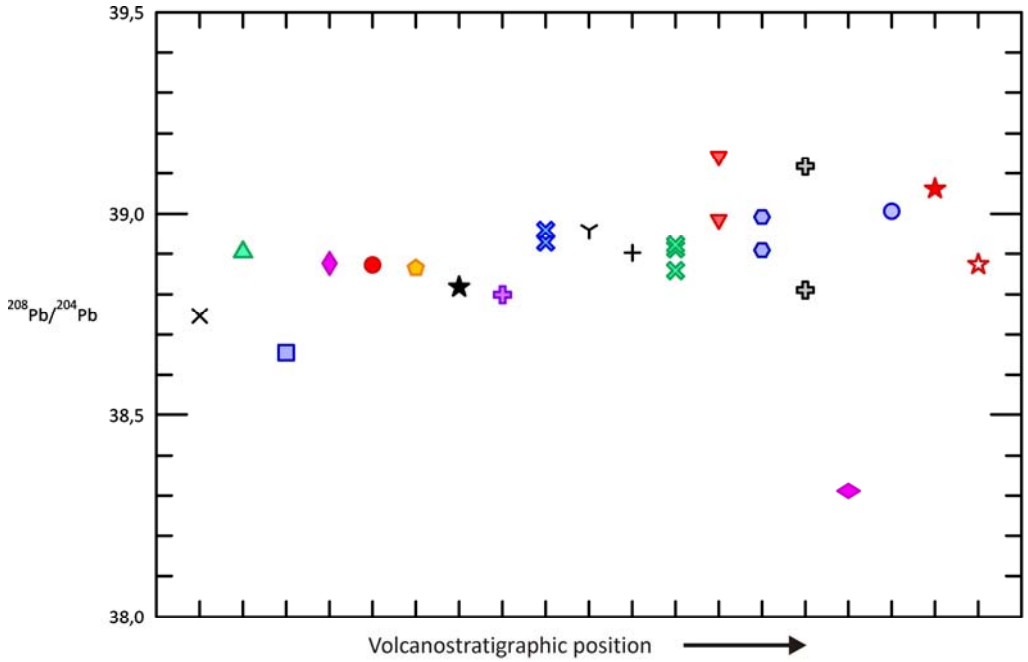

Figure 7.16: $^{208}Pb/^{204}Pb$ isotope ratios

PART IV: DISCUSSION

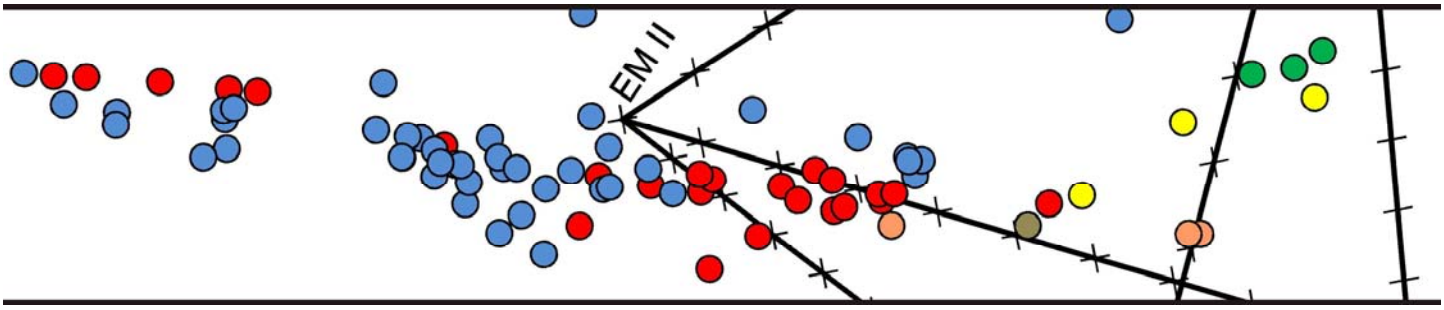

CHAPTER 8: UNIT RECOGNITION

8.1 INTRODUCTION

Traditionally, whole rock geochemistry of ignimbrites has not been regarded as useful either for petrogenetic studies or chemical characterization of deposits due to the pyroclastic nature of these materials. During transport and deposition of pyroclastic density currents segregation of primary pyroclastic components and incorporation of external bodies may occur. Segregation may be due to several factors including particle characteristics as viscosity, shape or density among others, and causes concentration or depletion of certain components in different stratigraphic positions of the ignimbrite, producing a geochemical heterogeneity in a deposit formed from an initially homogeneous magma. Entrapment of external bodies (accidental clasts) changes the overall chemistry of the ignimbrite. Another drawback of working with ignimbrites is that pyroclastic deposits are more easily affected by alteration and weathering than lavas. For these reasons whole rock geochemistry of an ignimbrite fragment is usually not considered to be representative of the initial magma composition. This is why lava flows have always been preferred for study and, when working with ignimbritic deposits was unavoidable, glass analyses have been performed to characterise the original melt.

But, if fresh samples are collected and a careful extraction of foreign bodies is performed previous to grinding the sample, whole rock geochemical analysis can be used for petrogenetic studies as well as for chemical ignimbrite characterisation and recognition. It is proposed that whole rock geochemistry may be a valid tool for unit recognition, even in samples belonging to different facies of the same unit. To demonstrate this, a protocol has been established for the identification of ignimbritic units from the Oligo-Miocene volcanism of the Sulcis area based mainly on whole rock geochemistry.

8.2 GEOCHEMISTRY-BASED UNIT RECOGNITION

When doing fieldwork, most of the time macroscopic characteristics of ignimbrites (components, colour, stratigraphy, etc.) are enough to recognise a given ignimbritic unit. Moreover, additional information may be obtained from petrographic study if needed. However, in some cases deficient outcrop availability together with stratigraphic and petrographic similarity between two or more units, or the occurrence of an unrecognised facies of a previously defined unit make unit recognition more difficult. It is in these cases when whole rock geochemistry may represent a powerful tool for unit identification.

The selection of chemical elements which are reliable for unit chemical characterisation is very important. Ignimbrites show varying welding degrees, from non-welded to extremely welded, so being differently affected by alteration and weathering. Non- or poorly welded deposits are strongly affected by alteration thus making major element, as well as mobile trace element, data practically useless for discrimination between units. For this reason most of the elements used in unit identification have been those considered immobile, especially Ti, Zr, Y and Nb. Th, Rb, Sr and Zn, though more mobile, have been used in some cases for discrimination between unit pairs because they have been seen to be useful. In the diagrams shown in this chapter trace element concentrations are in ppm, and TiO_2 is in wt %.

8.2.1 Solving unit pairs problems

When working in the Sulcis area most doubts in unit recognition arise from the similarity between unit pairs. If the ignimbritic sequence is divided in two halves (below and above the Nuraxi unit), the two similar units almost always belong to only one of the two halves. Since it is usually easy to recognise in which of the two halves of the sequence the problem unit is, a methodology using discrimination diagrams for solving unit pairs problems has been developed considering the two halves of the sequence separately.

Lower half of the sequence

The lower half of the sequence contains all the units from Andesites to Nuraxi, which crop out in Sulcis mainland and Santo Antioco Island. The main problem in this part of the sequence is the macroscopic similarity that exists between the following units pairs: CM/AC, LE/SE, SE/NU, MLN/MC, MC/CA and MC/NU. To solve identification problems some diagrams can be used.

CM/AC: these units are especially rich in lithic fragments. If a careful lithic fragment removal is not made before grinding the sample, resulting chemical data will appear in diagrams more spread out than they should. The available data do not allow at the moment for a precise differentiation

between these two units, there is always some overlap. However, although Th data for these units are scarce, in the Y vs. Th diagram (Fig. 8.1) these two units can be distinguished due to the higher content in these elements in AC with respect to CM.

LE/SE: These two units are very similar in the field. Discrimination between them is possible using the Nb vs. Zr/TiO_2 diagram (Fig. 8.2).

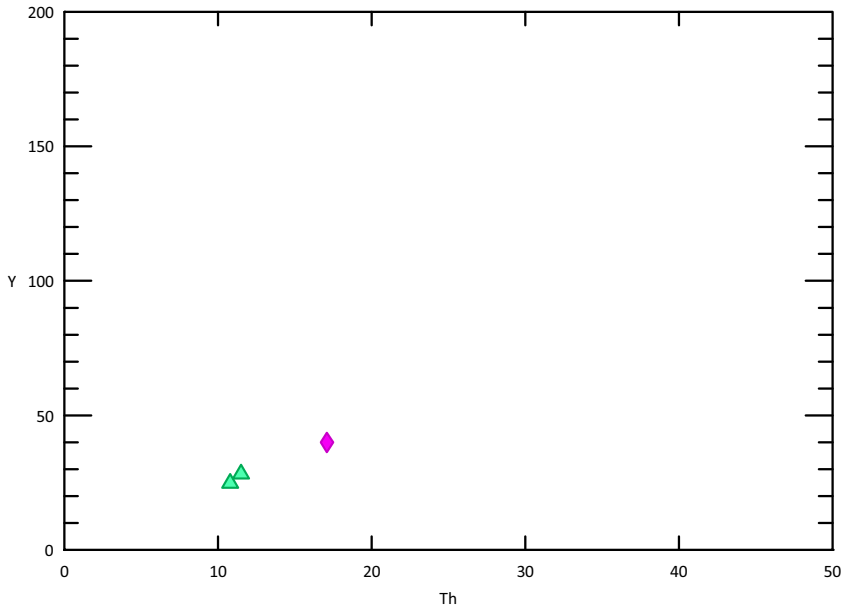

Figure 8.1: The Y vs. Th diagram allows differentiation between CM and AC units

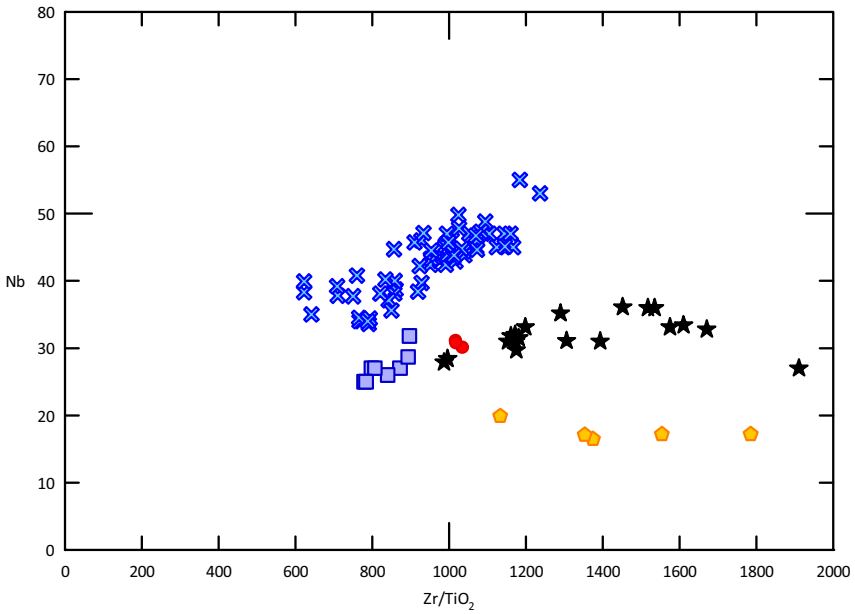

Figure 8.2: The Nb vs. Zr/TiO_2 diagram allows discrimination between the LE/SE, SE/NU, MLN/MC and MC/NU unit pairs

SE/NU: sometimes these two units can be misidentified in pumice-poor facies. The Nb vs. Zr/TiO_2 diagram (Fig. 8.2) allows discrimination between them.

MLN/MC: welded eutaxitic facies of MLN ignimbrites can be misidentified as MC unit. Discrimination between them can be done using the Nb vs. Zr/TiO_2 diagram (Fig. 8.2).

MC/CA: in general these units are easily distinguishable macroscopically. But in some places upper facies of MC can be confused with CA. Unfortunately, since correct and precise identification in the places where this confusion occurs is not available yet, it is not possible to provide a tool for chemical identification. Even in clear samples differentiation of these two units using chemistry has not been possible, there is always some overlap.

MC/NU: in most cases these units can be correctly identified in the field. With some pumice poor facies, though, this is not possible. It is then when the Nb vs. Zr/TiO_2 diagram (Fig. 8.2) allows differentiation between them.

Upper half of the sequence

It contains all units from NU to the end of the sequence. Identification problems arise from the similarity between the following unit pairs: NU/MCR, NU/PC, NU/SP, CO/MU, PM/PG-CL.

NU/MCR: the Rb vs. Zr/TiO_2 diagram must be used (Fig. 8.3).

NU/PC: easily distinguishable using the plot Nb vs. Zr/TiO_2 (Fig. 8.4)

NU/SP: the most useful diagram is Rb vs. Zr/TiO_2 (Fig. 8.3).

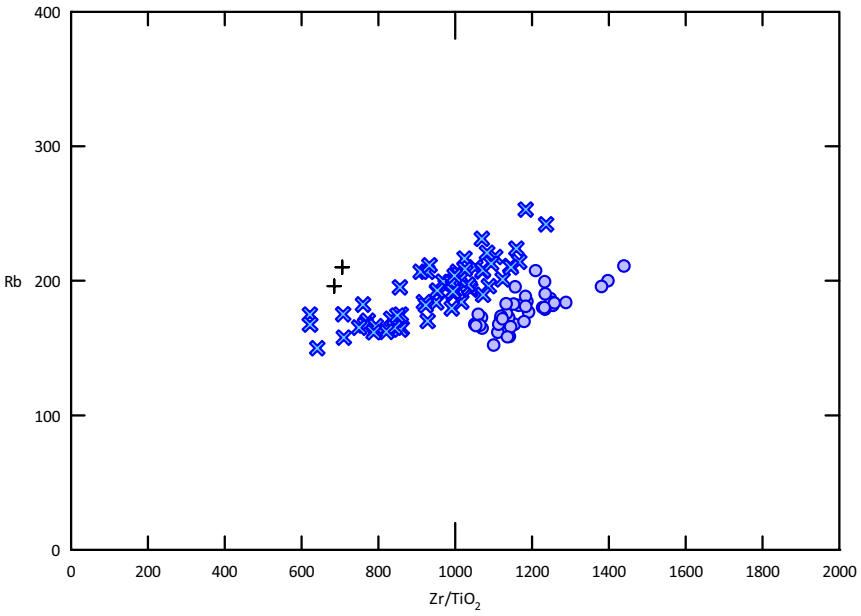

Figure 8.3: Rb vs. Zr/TiO_2 diagram to solve the MCR/NU and NU/SP unit differentiation

CO/MU: there is always some overlap in trace element binary diagrams between these two units, mostly due to the wide chemical compositions displayed by the CO unit, which is formed by several lava and pyroclastic deposits. The Nb vs. Rb diagram is the one that better separates them (Fig. 8.5).

PM/PG: these units are chemically very different, as can be seen in the Nb vs. Zr/TiO_2 plot (Fig. 8.4).

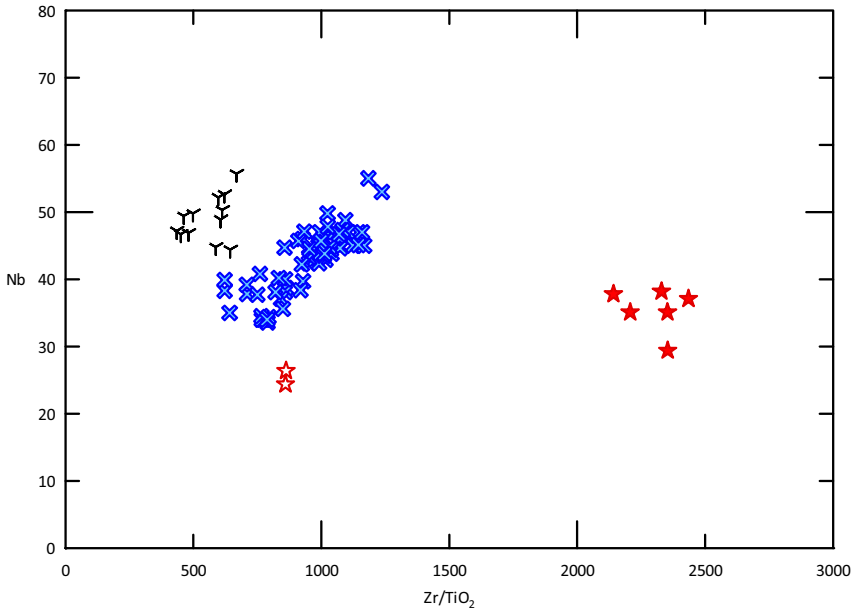

Figure 8.4: Nb vs. Zr/TiO_2 diagram to solve NU/PC and PM/PG similarities

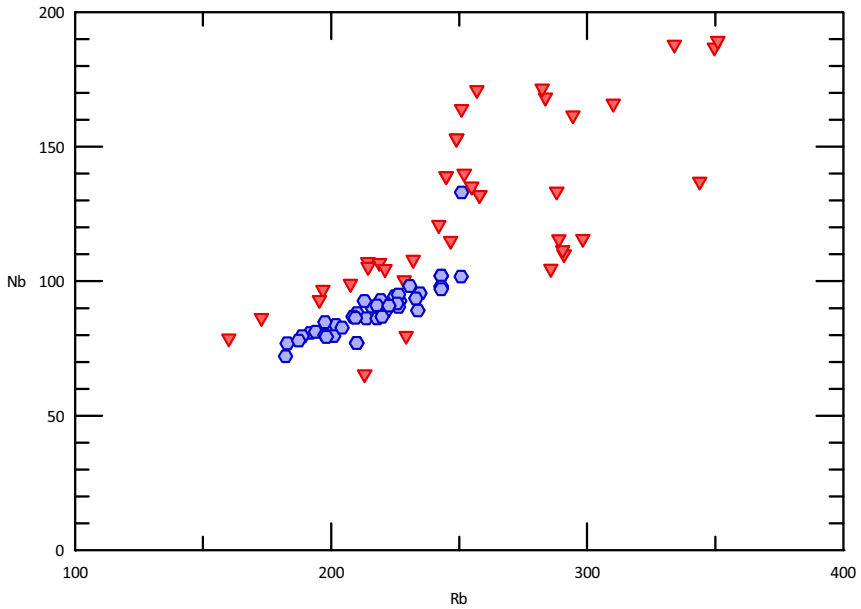

Figure 8.5: Nb vs. Rb diagram to solve the CO/MU similarity

8.2.2 More difficult cases

On some occasions even an approximate identification of a unit is not possible. This may occur with small and isolated outcrops, or with isolated samples, from boreholes for example. In these cases a more exhaustive examination of the chemical data is needed. A methodology has been developed which makes it possible to identify most units using only its whole rock chemistry.

Before explaining the procedure to discriminate between units using geochemical data, it is important to mention that in four cases whole rock data are not enough to identify a unit. The first cases are the above-mentioned CM/AC and MC/CA problems. The third one is the Matzaccara unit (MZ). It has been impossible to chemically isolate this unit from the others. MZ unit shows a wide compositional range for most elements, thus overlapping other unit's fields. However, there is a character that makes this unit easily recognisable: the presence of abundant biotite. In most units biotite is very scarce or inexistent. It is considered that the presence of abundant biotite, which is a feature easily observable in hand specimen, is enough to recognise MZ and therefore this unit is excluded from the protocol for unit recognition. The last case concerns the Carloforte (CF) unit. As explained in the description of the units, this particular ignimbrite is characterised by the presence of abundant porphyritic black pumices. Black pumices and the rest of the rock show two different chemical compositions. Because of this, whole rock analyses are plotted along a mixing line connecting both ends. The richer in pumices the ignimbrite, the more basic the whole rock composition is. Basic compositions are easy to distinguish chemically from other units. However, the most pumice-impoverished facies show compositions almost equal to those of the Monte Ulmus unit, they are chemically undistinguishable, and the only criterion to differentiate them is the presence of the black pumices. It is to be said, though, that black pumices in the CF unit are a characteristic feature of this unit, like biotite for MZ. Apart from these four cases, the rest of the units can be recognised using the following methodology, which uses a set of binary diagrams.

The first diagram to be used is the Nb vs. Zr/TiO_2 (Fig. 8.6). In this diagram two main areas can be distinguished: one comprising CO+MU+CF (A.1), and the other comprising all the other units plus the basic terms of CF unit (A.2). On a closer look to A.2 (Fig. 8.7), many other areas can be delimited; A.3: Andesites; A.4: CM + AC; A.5: LE + PG-CL; A.6: SE + MC + CA; A.7 MLN; A.8: PC + MCR + CF; A.9: NU + MCR + SP; A.10: PA; A.11: PM.

Areas 3, 7, 10 and 11 are delimited by a single unit each. Therefore, if a sample falls into one of these 4 areas the unit can be immediately identified. In the case of PA unit, which is poorly to non-welded, it is easily affected by weathering, plotting outside the above-mentioned area. Only

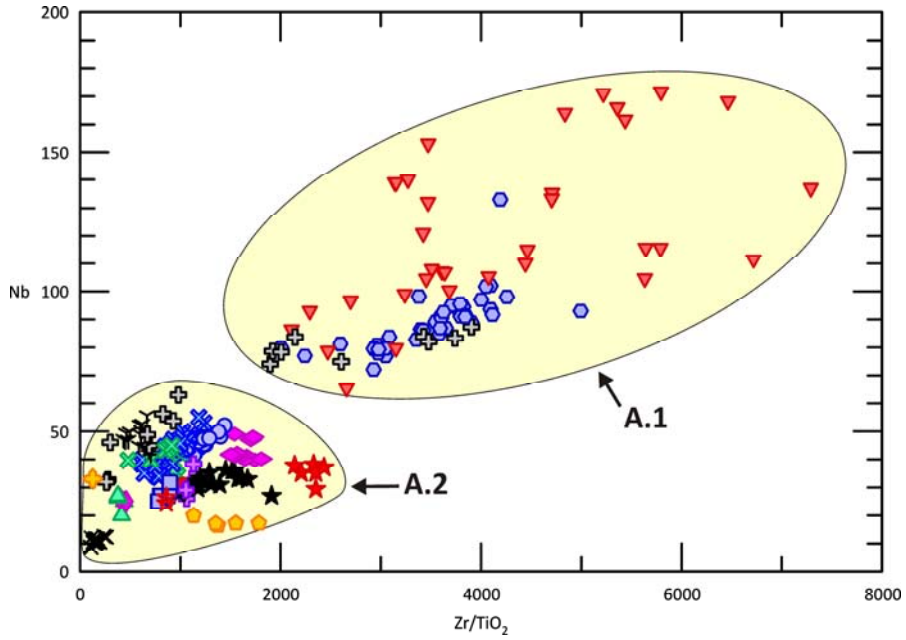

Figure 8.6: Initial discrimination diagram

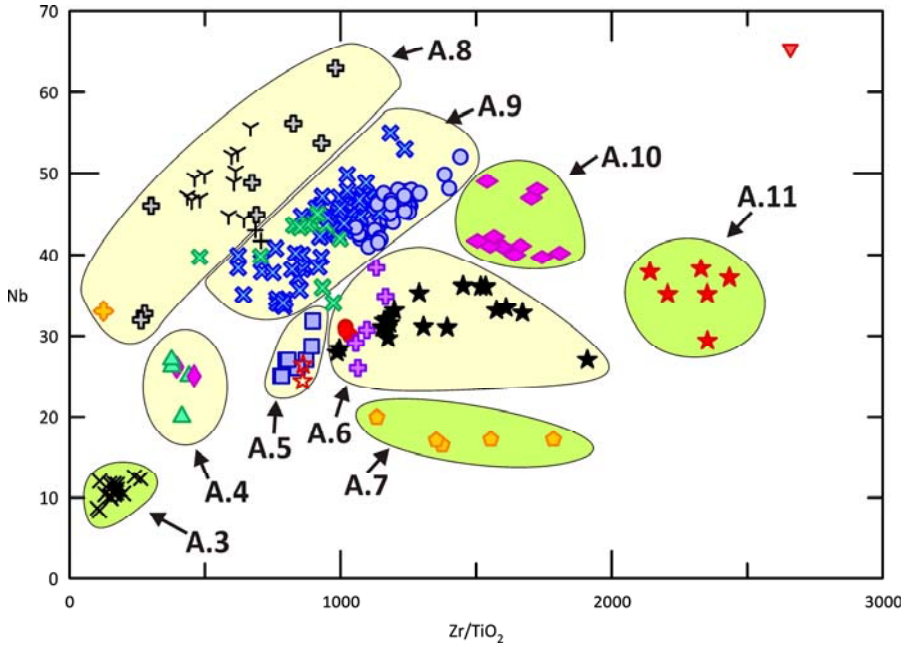

Figure 8.7: Zoom to Area 2

fresh samples of PA unit can be classified using this plot. With samples falling into other areas, one or more other diagrams must be used.

Area 1: as explained before, the Rb vs. Nb diagram (Fig. 8.5) is the best one to differentiate between CO and MU units.

Area 4: as mentioned in the previous section, an attempt to discriminate between the CM and AC can be done using the Y vs. Th diagram (Fig. 8.1).

Area 5: to discriminate between LE and PG-CL the Zn vs. Zr diagram is used (Fig. 8.8). It has to be noted that at the moment LE unit has only been identified in the mainland, whereas PG-CL is a local unit of San Pietro Island.

Area 6: three units are present in this area: SE, MC and CA. As mentioned before, it has not been possible to chemically differentiate between MC from CA at the moment. The Sr/Zr vs. Zr/TiO_2 diagram (Fig. 8.9) separates SE from the other two units.

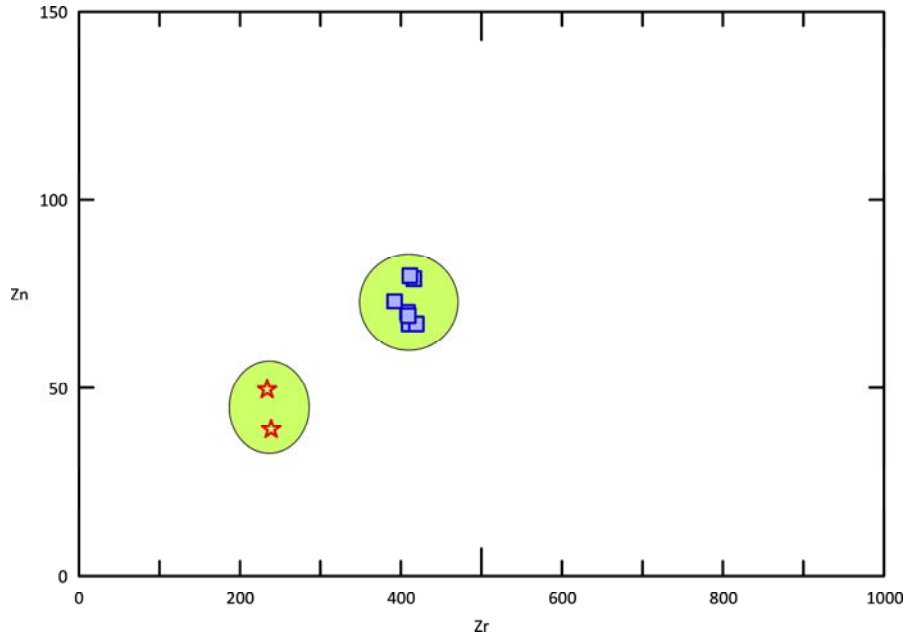

Figure 8.8: Zn vs. Zr diagram for solving Area 5

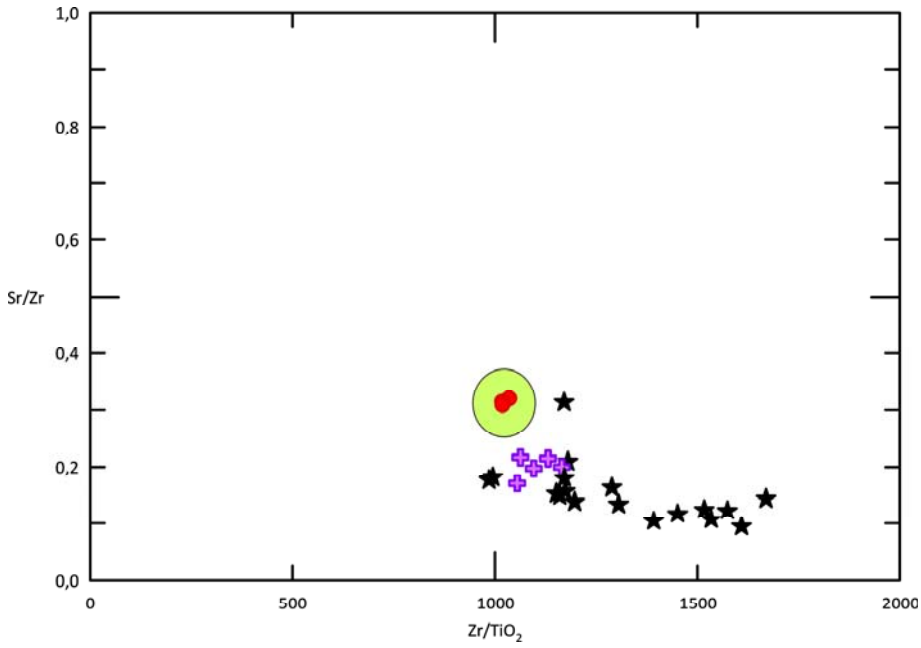

Figure 8.9: Diagram for solving Area 6

Area 8: the Sr vs. Zr/TiO_2 diagram (Fig. 8.10) allows differentiation between PC, MCR and CF units.

Area 9: to differentiate between MCR, NU and SP the Rb vs. Zr/TiO_2 diagram has to be used (Fig. 8.11).

Figure 8.12 is a flow diagram summarizing the explained procedure for unit recognition based on whole rock geochemistry.

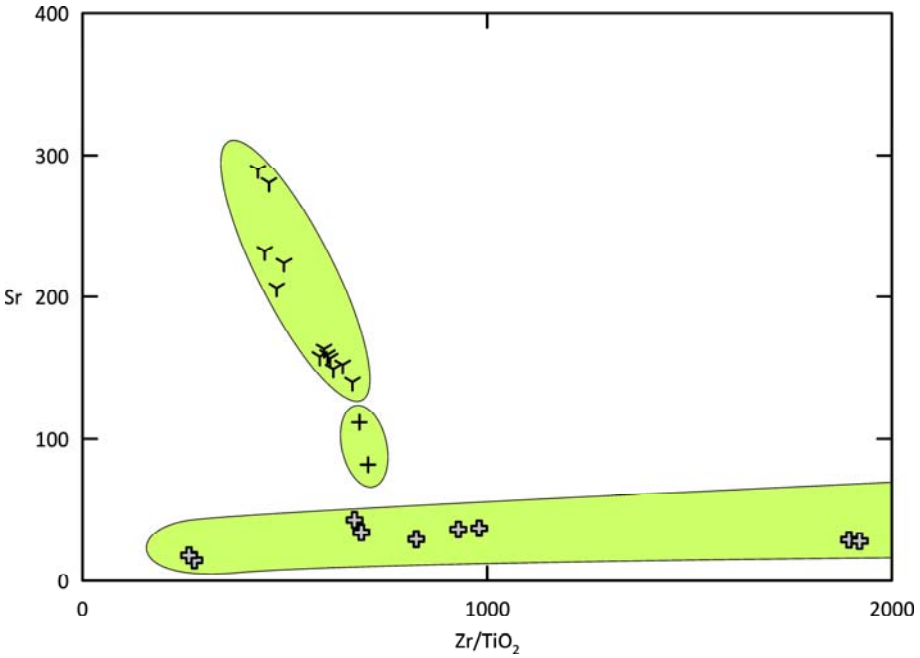

Figure 8.10: Diagram for solving Area 8

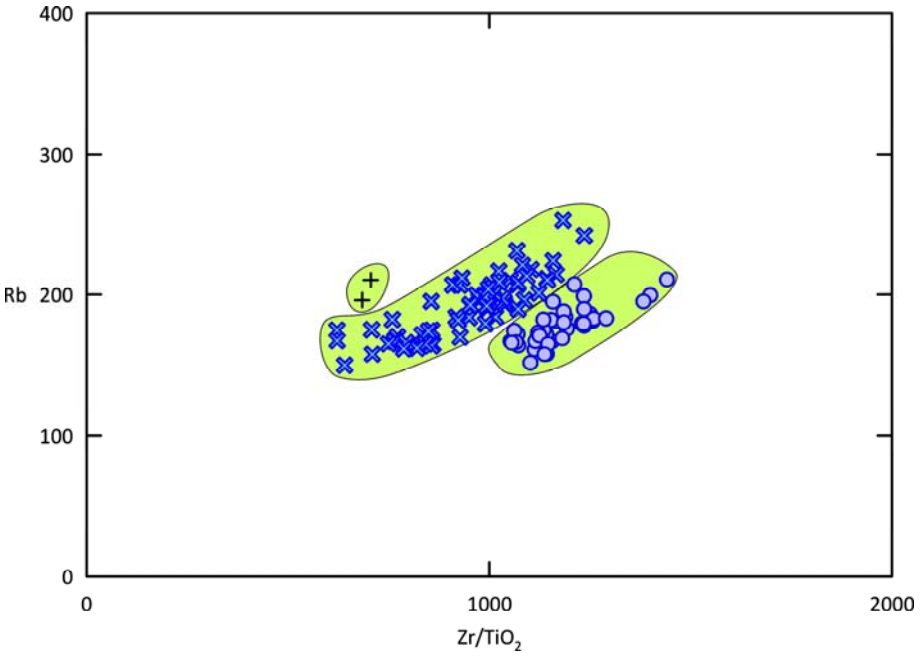

Figure 8.11: Diagram for solving Area 9

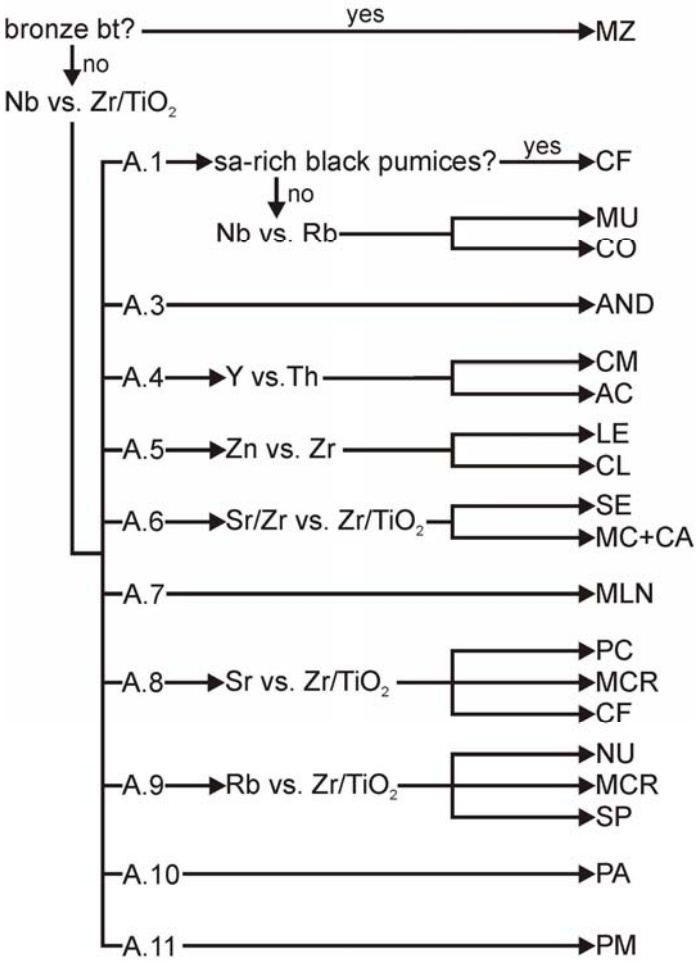

Figure 8.12: Procedure for whole rock geochemistry-based unit recognition

8.2.3 Applicability to altered samples

The previous methodology has been designed to be used in samples which present good analysis quality and little signs of alteration or weathering. Sometimes, though, identification of special samples is needed to solve specific stratigraphic or cartographic problems. In this section the applicability of the previous diagrams to altered samples will be discussed by including all the available analyses (fresh and altered samples) into the diagrams. For this purpose previously rejected data from altered samples have been incorporated into the geochemical database, coming both from literature and our own data (available in Appendix 6). This part of the discussion does not pretend to be a systematic revision of the effects of silicification and alteration of the studied materials. Moreover, it must be kept in mind that no specific sampling of altered rocks has been made for this purpose, so altered samples included are most probably not representative of the real variability in chemical composition that alteration can produce. Therefore, the results of the following discussion are only for guidance.

Solving unit pairs

A Y vs. Th diagram has been proposed to discriminate between CM and AC units. Despite the fact that these two units are usually affected by alteration, especially in their upper parts, no Y and Th data are available for altered samples, so the effect of weathering in this specific case cannot be observed.

The Nb vs. Zr/TiO_2 diagram is used to solve LE/SE, SE/NU, MLN/MC and MC/NU similarities. As can be seen in Figure 8.13, it keeps its usefulness.

The Rb vs. Zr/TiO_2 diagram (Fig. 8.14) is used to solve the MCR/NU and NU/SP unit pairs. Discrimination between NU and SP units is apparently not affected by alteration. This is mostly due to the high welding degree of both units, which prevents extensive fluid circulation and alteration which could significantly modify their chemical composition. On the other hand, MCR may overlap with NU. The trend defined by MCR samples approximately parallels those of NU and SP, suggesting that chemical variation could be more related to within-unit variation rather than to alteration.

The Nb vs. Zr/TiO_2 diagram (Fig. 8.15) is used to solve NU/PC and PM/PG similarities. Only some altered samples are available for NU, and only one for PM. Thus, the projection of data does not change significantly. NU samples appear more widespread, but without overlapping other units. The PM altered sample presents a lower Zr/TiO_2 ratio, still far, though, from those of the other units.

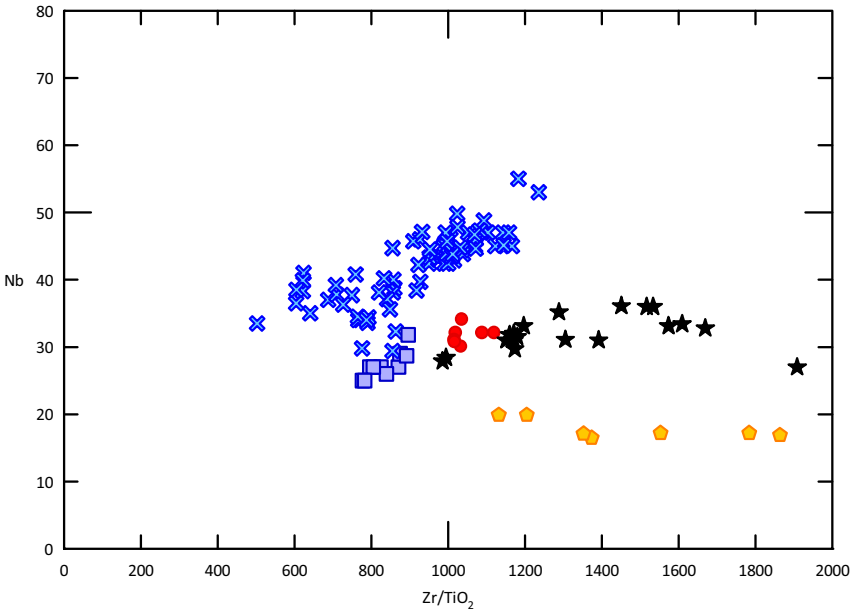

Figure 8.13: Nb vs. Zr/TiO_2 diagram for solving LE/SE, SE/NU, MLN/MC and MC/NU pairs

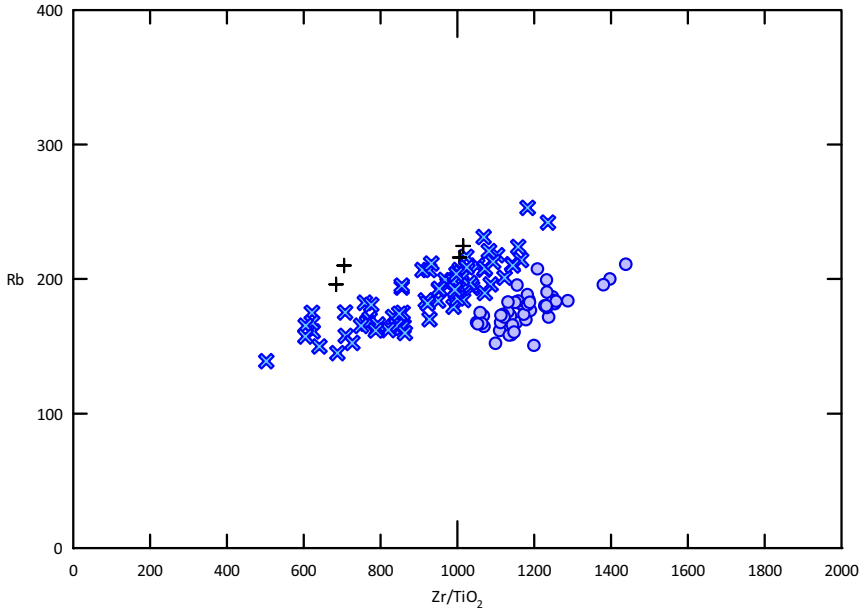

Figure 8.14: Rb vs. Zr/TiO_2 diagram to solve MCR/NU and NU/SP unit pairs

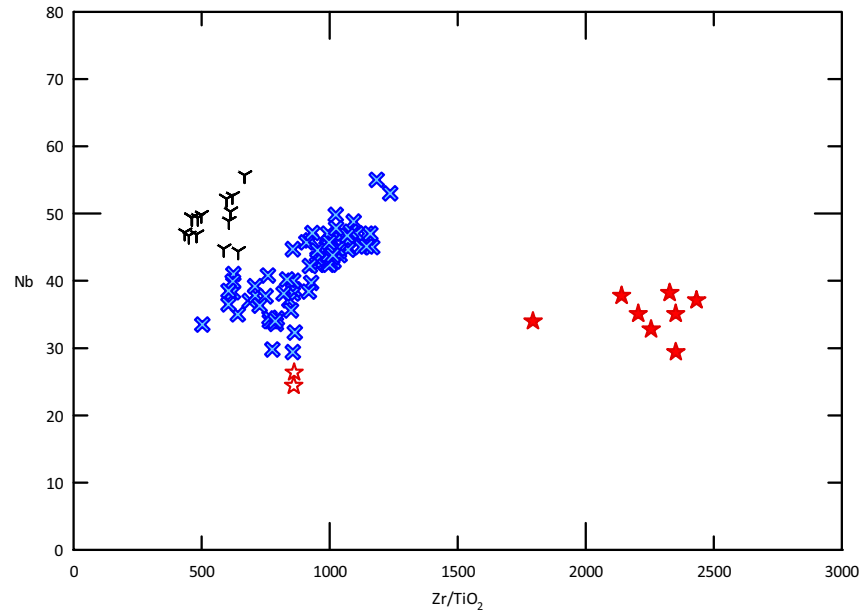

Figure 8.15: Nb vs. Zr/TiO_2 diagram for solving NU/PC and PM/PG similarities

The Nb vs. Rb diagram (Fig. 8.16) is used to differentiate between CO and MU. 13 silicified samples, 12 with high LOIs, and some samples previously rejected due to its incoherent dispersion, are added to the previously depicted samples. New samples are projected within the corresponding chemical trends, with a tendency to be at the lower regions of it, showing that the main effect of silicification and incorporation of water into alteration minerals is the decrease in concentration of both Rb and Nb, but without highly distorting Nb/Rb ratios. The MU samples falling outside the main trend were analysed in previous studies and, but for the two with the

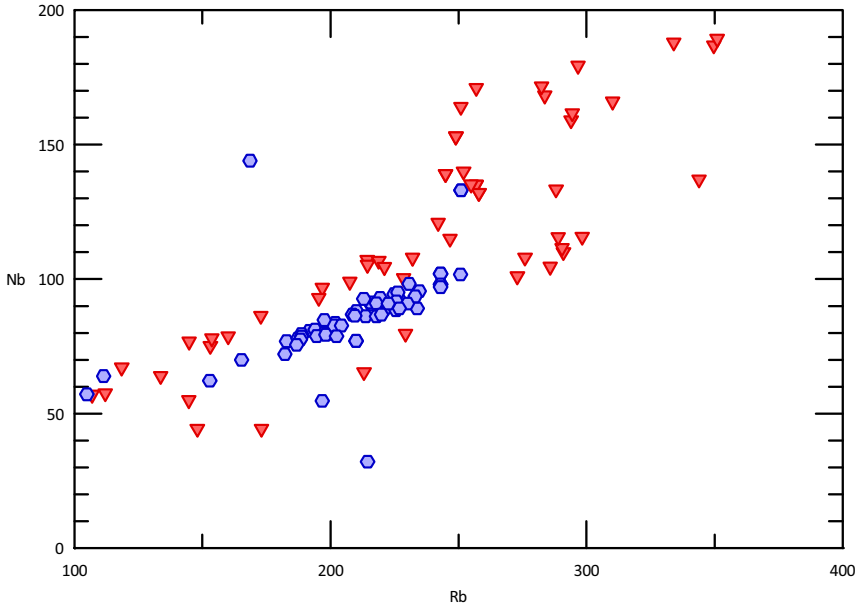

Figure 8.16: Nb vs. Rb diagram used to differentiate between CO and MU

lowest Rb content, present no evident signs of alteration. It is thought that its deviation from the main trend is most probably caused by wrong selection of the sample before grinding.

More difficult cases

Separation into A.1 and A.2 can still be made. Area 1 is solved with the Nb vs. Rb (Fig. 8.16) diagram. Area 2 can still be subdivided (Fig. 8.17), but many samples fall outside their previously defined corresponding sectors. This fact is especially evident with altered samples from the PA unit, which plot far from the fresh ones. The main problems are: some CM and AC samples fall outside A.4, although deviation is scarce, without overlapping with other areas and can, therefore, be still correctly identified. Some NU data fall outside A.9; those which project into the A.5 are problematical, they overlap with LE samples. Some CO data appear within A.8 and A.9. Altered PA samples overlap with A.8 and A.9. Finally, the only data available for altered PM falls outside A.11 and could be misidentified with A.6.

The A.5 is solved using the Zn vs. Zr diagram (Fig. 8.18). As can be seen, those NU samples falling in A.5 separate slightly from LE in the proposed diagram; therefore, they can be differentiated from LE if the depicted LE field is reduced.

The diagram for solving A.6 can still be used (Fig. 8.19); only a small modification of the area covered by SE is needed. The CA sample falling by the SE area has a LOI of 4.69, but despite the relatively high weathering still falls close to the rest of the CA.

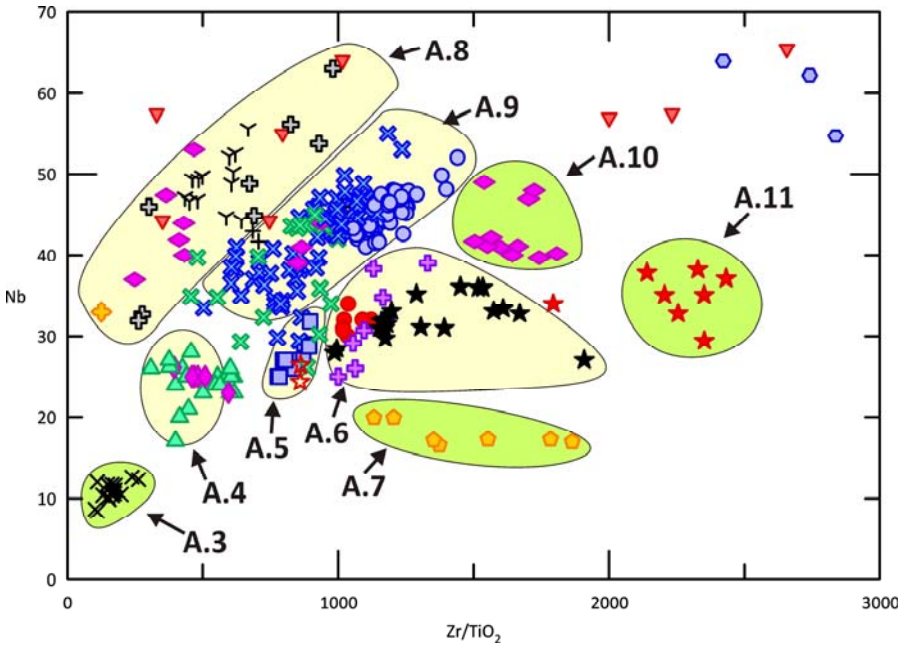

Figure 8.17: Subdivision of A.2

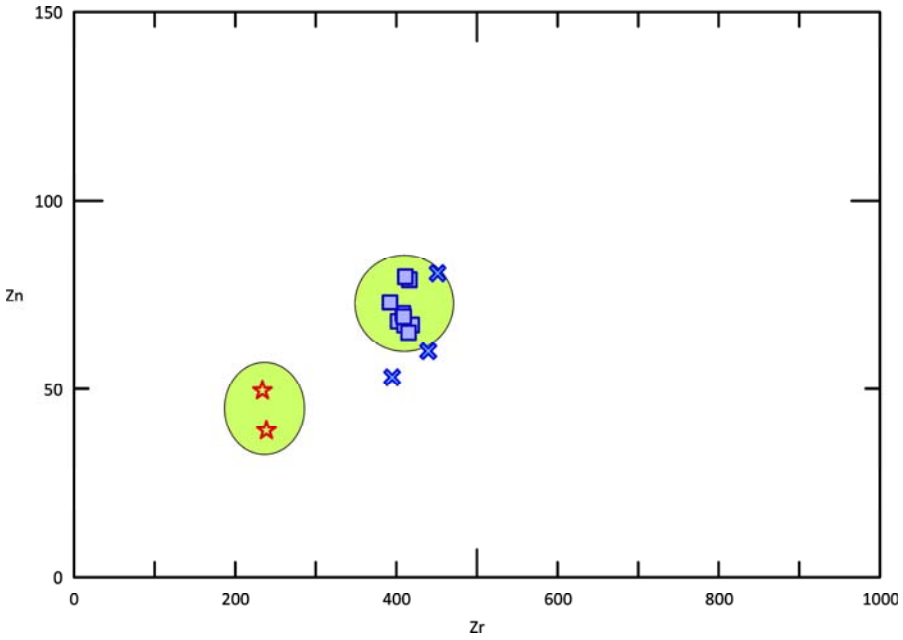

Figure 8.18: Zn vs. Zr diagram for solving A.5

The diagram for solving A.8 (Fig. 8.20) has lost most of its utility due to the dispersion shown by altered CO and PA samples. This diagram can still be used for separating PC from MCR, but is useless for any other purpose. New diagrams have been searched to try to separate the different units but none have been found. The enrichment in Sr and the depletion in Zr/TiO_2 altered CO and PA samples show are remarkable. Since both units are very poor in Sr (with concentrations typically below 30 ppm), this strong enrichment must have been caused by a Sr input supplied by

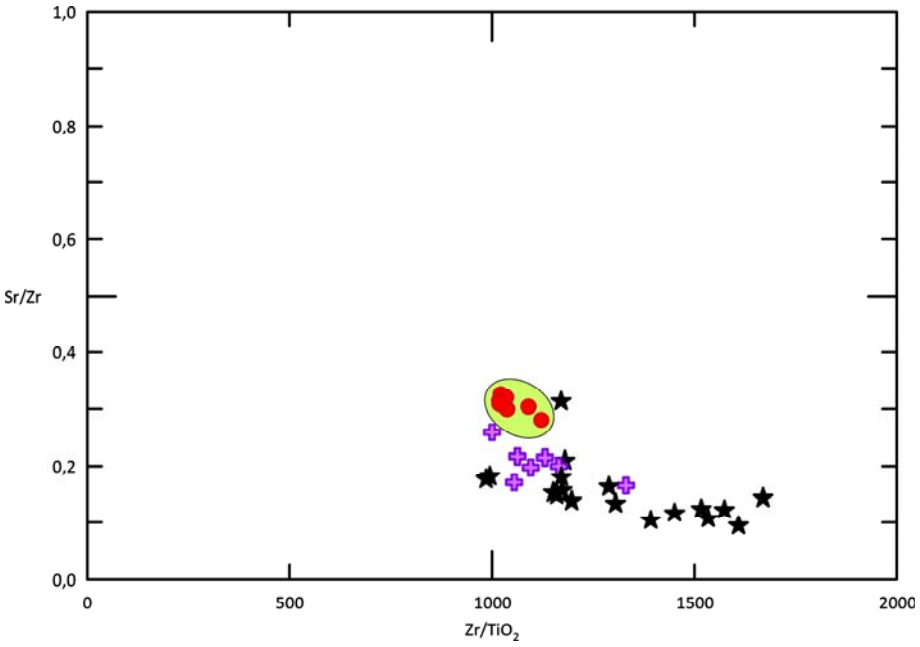

Figure 8.19: Sr/Zr vs. Zr/TiO_2 diagram for solving A.6

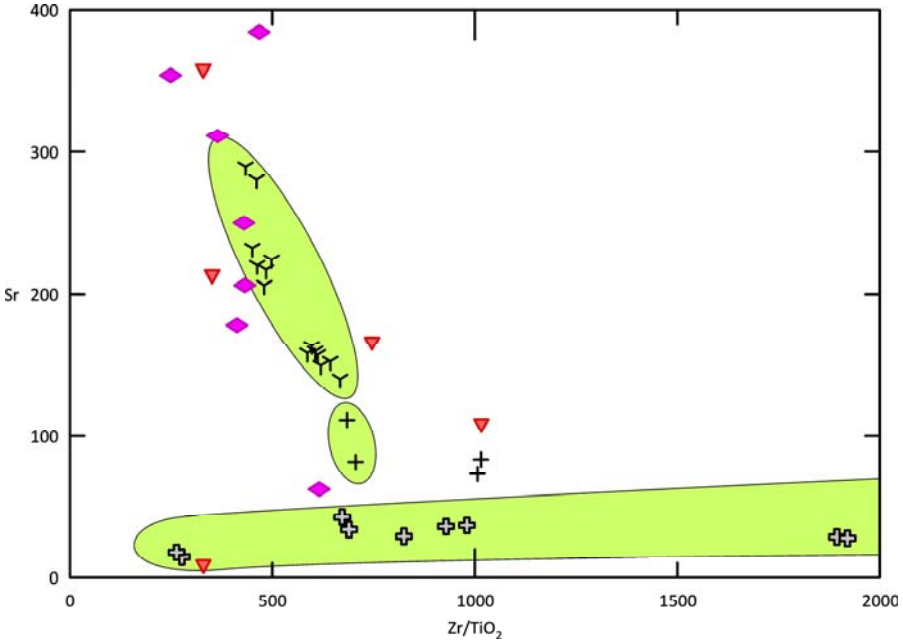

Figure 8.20: Sr vs. Zr/TiO_2 for solving A.8

alteration fluids. A similar behaviour has been observed with other elements, thus showing the strong impact that alteration can produce on the chemistry of poorly welded units. In terms of unit identification, in this case geochemistry alone is not enough for the differentiation of these units; however, CO and PA are macroscopically very different from PC and MCR, and more especially in the case of these altered samples, which belong to non- to poorly-welded facies, so the combination of macroscopic observation and geochemistry is enough for unit recognition.

The last diagram used is that for the study of A.9 (Fig. 8.21). This particular diagram keeps its utility except for the previously discussed overlapping of some MCR samples with the NU unit. Apparently altered CO and PA samples plot slightly separated from the NU data.

Most of the diagrams designed through observation of fresh samples are still of use when incorporating altered rocks. Therefore, it is shown that the election of the discriminating elements was appropriate, because alteration did not substantially change their concentrations and ratios within the studied rocks. As could be expected, strongest modifications in whole rock chemistry are observed in the least welded rocks, which have undergone stronger alteration processes (as seen for some CO and PA samples), whereas little alteration affected welded facies.

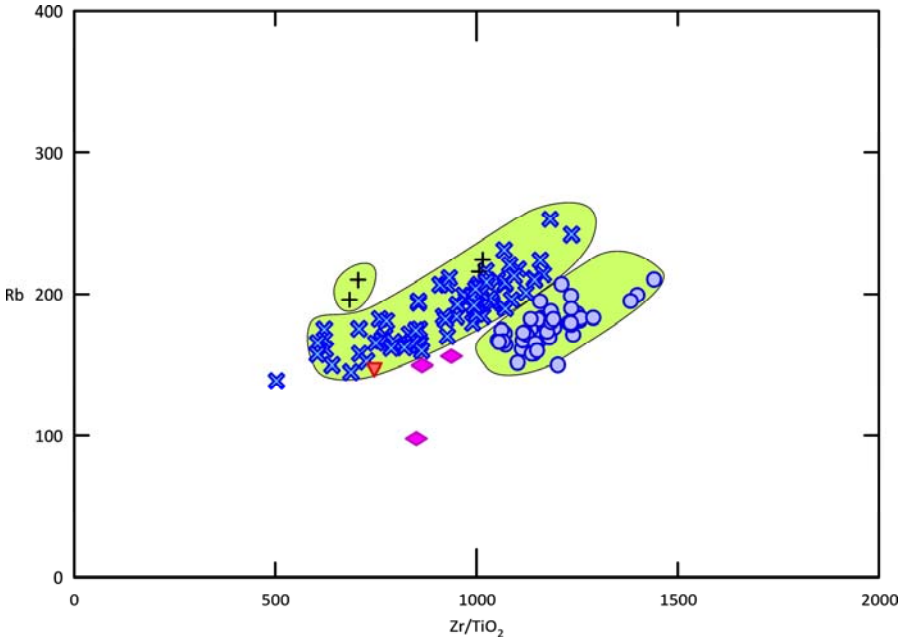

Figure 8.21: Rb vs. Zr/TiO_2 diagram for solving A.9

8.3 CONCLUSIONS

The methodologies explained above for unit recognition based on whole rock geochemistry have proven to be a very useful tool in this study area. During field work doubts on unit identification have arisen which basic observation of outcrops and samples could not solve. Geochemistry has allowed to correctly identify units and so to solve doubts in mapping. Moreover, correlation of macroscopically different facies belonging to the same unit has been possible due to the shared geochemistry. Even in facies containing what appeared to be enclaves, geochemistry has shown that the supposed enclaves were in fact fragments of the same unit that had been cannibalised (brown lithics in SP unit). Another use has been to allow a revision of geochemical data from literature. It has allowed checking if unit attribution was correct. Finally, and probably the most

significant demonstration of its usefulness occurred when a small sample recovered from a new prospective borehole drilled by the Carbosulcis SpA mining company in 2010 was successfully recognised, immediately providing information on the stratigraphic position of the drilling front. All these facts demonstrate that geochemical characterisation of ignimbritic units is possible despite their apparent heterogeneity, and that it can be used for unit identification both for academic and commercial purposes, not only here but probably also in other areas with ignimbritic piles.

CHAPTER 9: PETROGENESIS I. FROM ROCK TO MAGMA

9.1 INTRODUCTION

Since the work by Coulon (1977) the abundant Oligo-Miocene volcanism in Sardinia was interpreted as calc-alkaline of orogenic affinity formed by partial melting of a mantle source caused by subduction. This hypothesis was assumed for most of the volcanic sequence in Sardinia, although some more evolved materials were initially interpreted to have formed from a different source. For example, Coulon et al. (1978) and Beccaluva et al. (1989) claimed that the acid ignimbritic successions in Northern Sardinia were products of partial melting of the continental crust.

In the Sulcis area the lower andesitic sequence is covered by an acid ignimbritic sequence which has the particularity of reaching a peralkaline composition; peralkaline rocks represent 10-15% of the Sulcis succession, and a much lesser proportion of the Oligo-Miocene volcanic sequence of Sardinia (only 1% according to Lustrino et al. (2004)). Despite the wide compositional range in the Sulcis area, and the fact that peralkaline rocks have never been described as belonging to calc-alkaline suites, the upper sequence in the Sulcis was also considered to be of orogenic origin since the first geochemical studies (Assorgia et al., 1990b). Morra et al. (1994) did the first petrogenetic modelling for the Sulcis, centred in the ignimbritic sequence and genetically linking this upper sequence with the andesitic lower one.

This first petrogenetic discussion chapter is focused on formation of the magmas that generated the Oligo-Miocene volcanic suite in the Sulcis, with emphasis on the ignimbritic sequence and its relation to the lower andesitic terms. In Appendix 5 a summary of the two petrogenetic models

available for the Sulcis are presented; Conte et al. (2010) on the origin of the andesitic suite in Santo Antioco, and Morra et al. (1994).

9.2 MAGMA SOURCE

Subduction-related environments can produce melt in several settings; the three melting mechanisms explained in the introduction chapter of this thesis may be involved. Melting by reducing liquidus temperature is the dominant mechanism. It affects the mantle wedge, which melts due to water release from the slab. Melting by temperature increase may occur in the slab itself (both in the basaltic material and the sediment on top of it), which can melt if a high enough temperature is reached. It may also occur when any of the mantle-generated magmas reaches the overlying continental crust; at this point it may get stagnated, heating crustal rocks to their melting point, thus generating a magma which has not a mantle origin. Finally, melting by pressure release also occurs. Roll-back of the slab may generate extensional tectonics in back-arc settings which promote melting. The last and less common mechanism occurs when the slab breaks apart favouring an ascent of asthenospheric mantle through a slab window. The adiabatic ascent may be enough to produce melting.

Apart from the magma generated by melting of the continental crust or subducted sediments, all the generated magmas have a major element geochemical composition very similar to each other. In addition, from the generation of the magma to its cooling as a rock major elements may be strongly modified by processes inherent in magma evolution such as crystal fractionation. Therefore, the study of major elements is not adequate for distinguishing magma origins. Instead, the tools for this purpose are the study of trace elements and isotope ratios, which are less affected by magma evolution.

9.2.1 Trace elements

Profiles in normalised spider diagrams are deeply influenced by the tectonic environment in which a magma is formed. Both mantle chemical and mineralogical compositions, as well as the degree of partial melting, influence the shape of the trace element profiles. Determination of magma origin using trace element profiles ideally should be done studying only primitive magmas, because crystal fractionation and crustal contamination progressively modify the profile during magma evolution. In the studied region, however, there is a lack of mafic rocks attributable to primitive magmas, so the determination must be done with the available data.

Figure 9.1 represents Sulcis rocks normalised to primitive mantle (Sun and McDonough, 1989). Both the andesitic and the ignimbritic sequence present parallel profiles (except for Ba, Sr, P, Eu

and Ti, which are influenced by crystal fractionation), so they were probably originated in a source of a similar composition. A profile with enrichment in LILE compared to HFSE is typical of magmas generated in the mantle in subduction zones (Fig. 9.2, Carpathians), where fluids released from the slab metasomatise the mantle wedge placed immediately above. This profile is shared with the rest of the Sardinian Miocene volcanic suite.

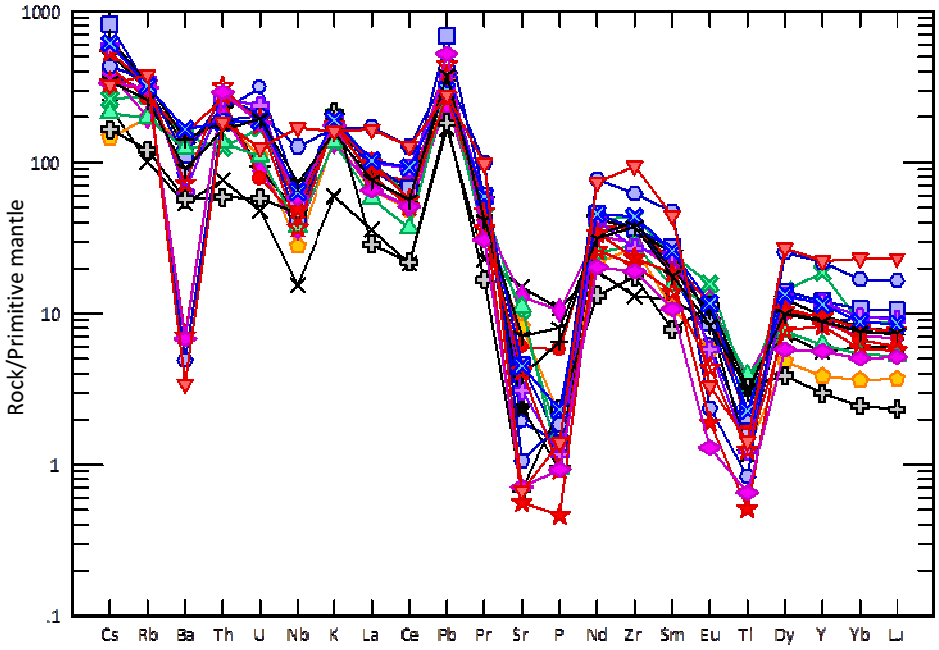

Figure 9.1: Primitive mantle-normalized spider diagram for the Sulcis rocks. Normalizing values of Sun and McDonough (1989)

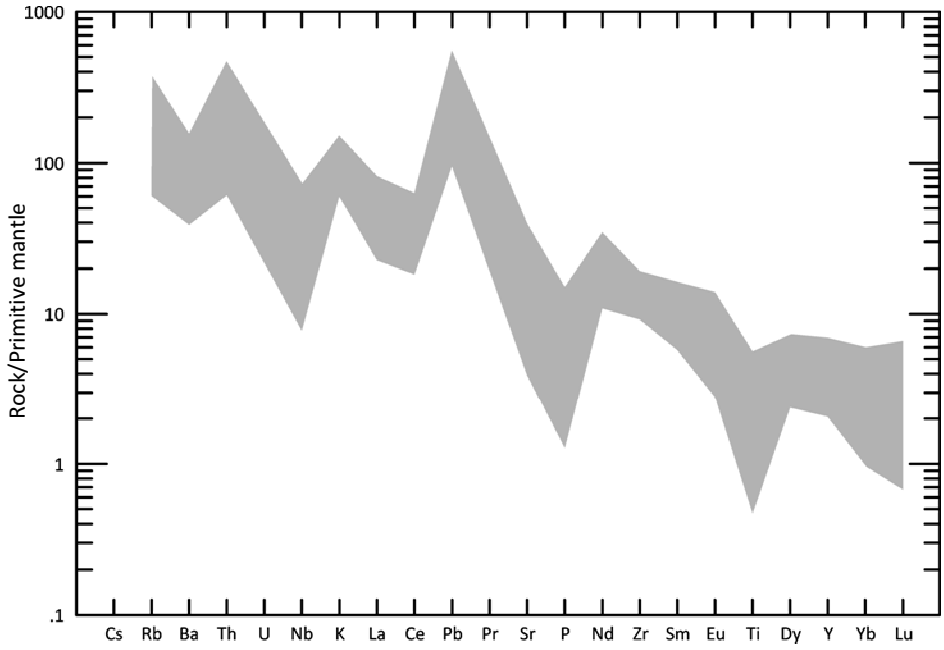

Figure 9.2: Rock/primitive mantle spider diagram. Normalizing values of Sun and McDonough (1989). Shade represents data from the Carpathians by Harangi et al. (2007)

With regard to mantle mineralogical composition, chondrite-normalised REE spider diagrams provide some clues (Fig. 9.3). The profiles depicted by samples from the Sulcis area are concave, with relative enrichment of LREE (steeper slope from La to Sm) and a flat end at the HREE part. The flat region in HREE indicates that garnet was not a residual phase during melting, and therefore it was probably not present. The stronger enrichment in LREE relative to heavier REE indicates that the main phases in the source region were olivine and pyroxenes. Although it is not evidenced in this diagram, water-bearing phases such as phlogopite or amphibole may be found in mantle regions that have undergone metasomatism by aqueous fluids. Mantle xenoliths bearing phlogopite have been found in Plio-Pleistocene magmas (Lustrino et al., 1999). Hornblende enhances the pattern produced by olivine and pyroxenes, whereas phlogopite does not produce a relative enrichment of any REE. It should be borne in mind, though, that observed profiles are not the original ones, because magmas underwent fractional crystallisation, as clearly evidenced by the strong negative Eu anomaly (mainly caused by feldspar fractionation), so this mantle mineralogical composition is just a hypothesis.

9.2.2 Isotope ratios

The isotopic ratios in a magma are only influenced by the isotopic composition of the magma source, and by the contamination and magma mixing processes, thus being highly useful to characterise source regions when assimilation effects are small, regardless of the evolutionary stage of the magma.

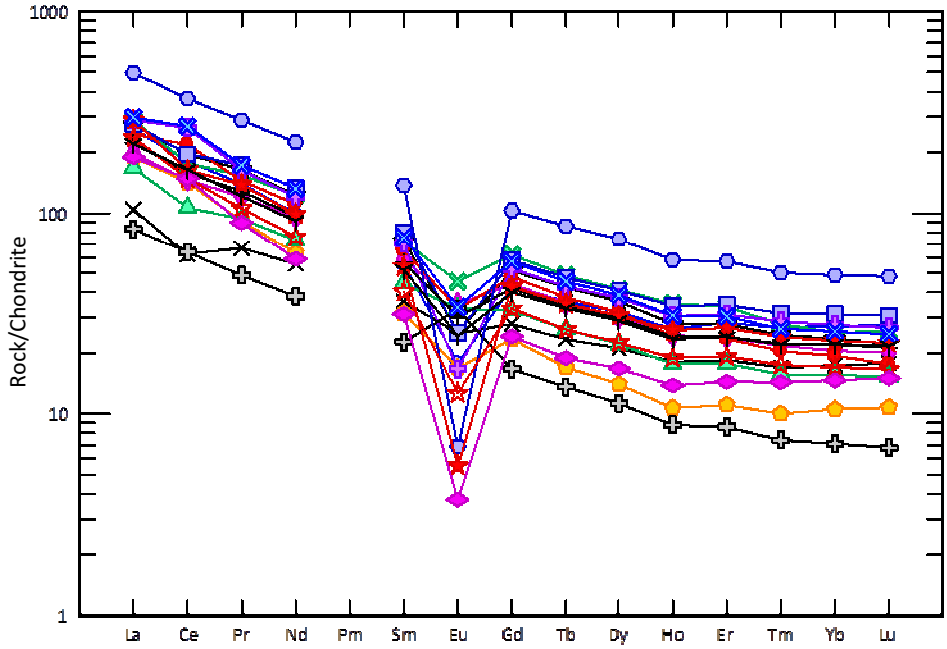

Figure 9.3: Chondrite-normalized spider diagram (Sun and McDonough, 1989)

Diagrams of isotope ratios versus stratigraphic position (Figures 9.4 to 9.8) show linear trends for all isotopes except ^{207}Pb. These trends can be better explained by a progressive change in the isotopic composition of the magma source rather than by contamination processes of magmas with a single original isotopic signature. If contamination by crustal assimilation was considered the origin of the isotopic variety, isotopic ratios would depend on the degree of magma differentiation and not on its stratigraphic position (the more evolved a magma is, the more time it has spent in the crust and more assimilation has occurred). Moreover, strongly differentiated magmas present extremely low Sr values, thus becoming very sensitive to Sr isotopic contamination, which, however, does not become evident (Fig. 9.9, diagram $^{87}Sr/^{86}Sr_i$ vs. Sr). Therefore, crustal contamination is considered to have had a small effect, only significant in the case of ^{207}Pb, which is the most sensitive isotope to contamination. Downes et al. (2001) in a study on the Monte Arcuentu andesitic suite, which is some 50 km N of Sulcis area and therefore expected to have formed under very similar conditions, found, based on Sr, Nd and O isotopes (no Pb isotope data are available) and trace elements, that the geochemical signature of these materials was consistent with mantle contamination by subducted sediments, and that contamination by upper crust assimilation was minor. This is another argument in favour of the predominant mantle signature of Sulcis magmas, at least until the andesite differentiation degree.

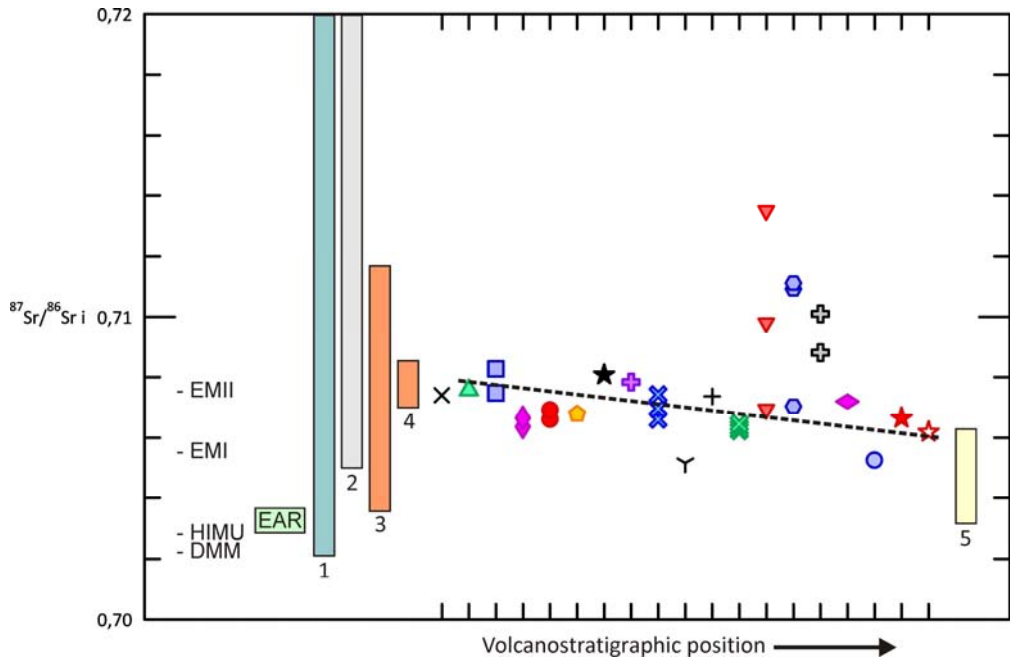

Figure 9.4: Initial $^{87}Sr/^{86}Sr$ ratios. 1: oceanic sediments (Othman et al., 1989; Plank and Langmuir, 1998); 2: continental crust (Rutter, 1987; Tommasini et al., 1995); 3: Oligo-Miocene volcanism of Sardinia (Morra et al. ,1997; Downes et al., 2001; Lustrino et al., 2004); 4: Andesitic sequence of Santo Antioco Island (Conte et al., 2010); 5: Plio-Pleistocene magmatism of Sardinia (Lustrino et al., 1996, 2000, 2007a). Mantle components by Hart et al. (1992). EAR includes component C (Hanan and Graham, 1996), FOZO (Stracke et al., 2005) and EAR (Lustrino and Wilson, 2007)

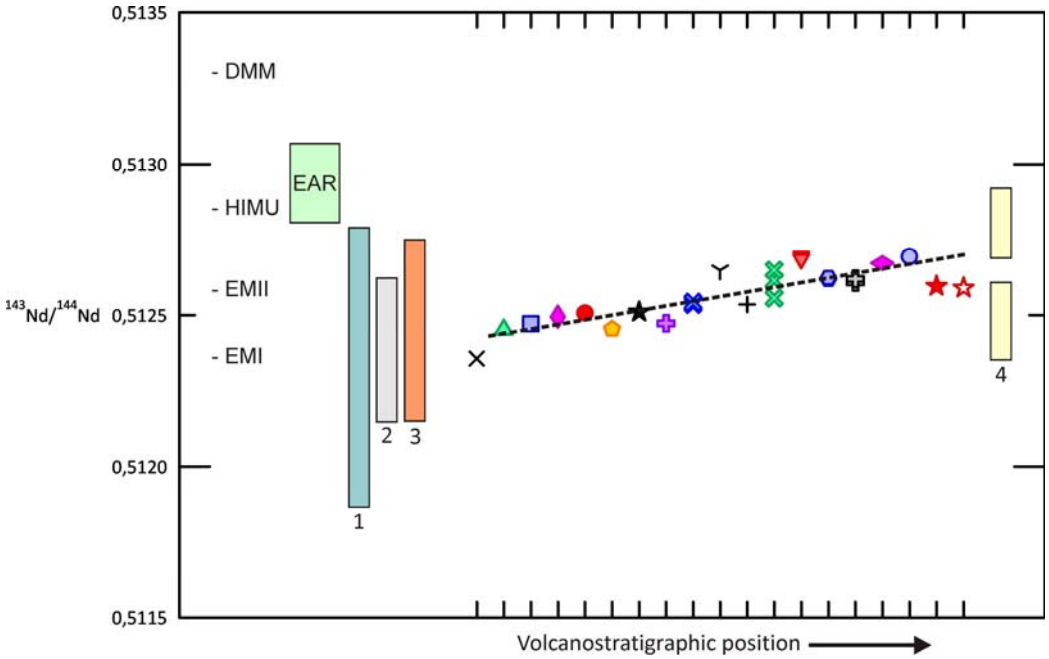

Figure 9.5: $^{143}Nd/^{144}Nd$ ratios. 1: oceanic sediments (Othman et al., 1989; Plank and Langmuir, 1998); 2: continental crust (Rutter, 1987; Tommasini et al., 1995); 3: Oligo-Miocene volcanism of Sardinia (Morra et al. ,1997; Downes et al., 2001; Lustrino et al., 2004); 4: Plio-Pleistocene magmatism of Sardinia (Lustrino et al., 1996, 2000, 2007a). Mantle components by Hart et al. (1992). EAR includes component C (Hanan and Graham, 1996), FOZO (Stracke et al., 2005) and EAR (Lustrino and Wilson, 2007)

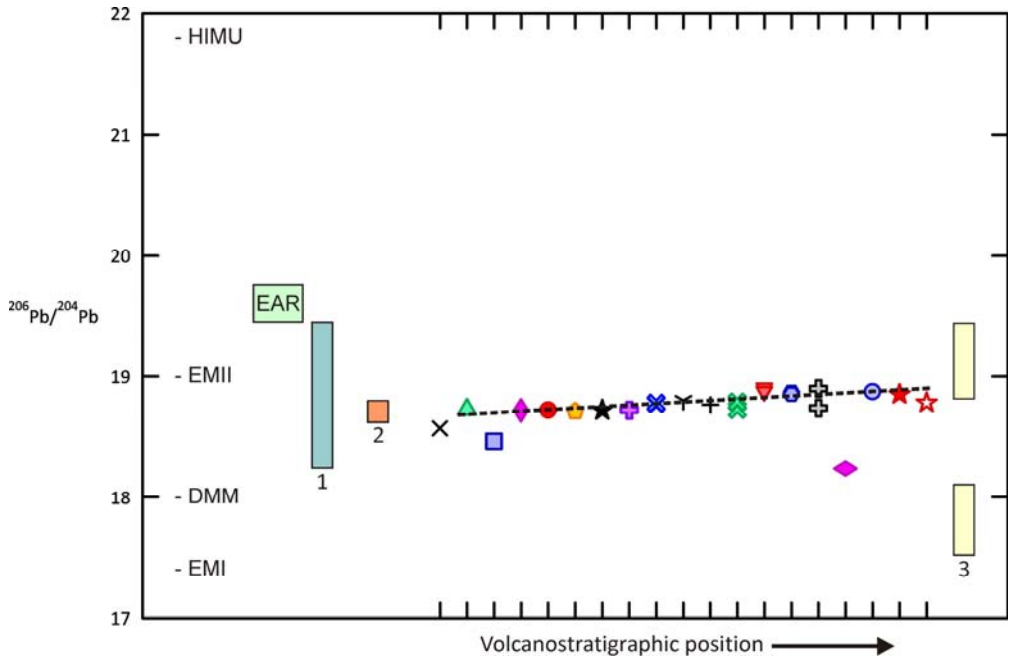

Figure 9.6: $^{206}Pb/^{204}Pb$ ratios. 1: oceanic sediments (Othman et al., 1989; Plank and Langmuir, 1998); 2: Oligo-Miocene volcanism of Sardinia (only two samples, by Morra et al. (1997)); 3: Plio-Pleistocene magmatism of Sardinia (Lustrino et al., 1996, 2000). Mantle components by Hart et al. (1992). EAR includes component C (Hanan and Graham, 1996), FOZO (Stracke et al., 2005) and EAR (Lustrino and Wilson, 2007)

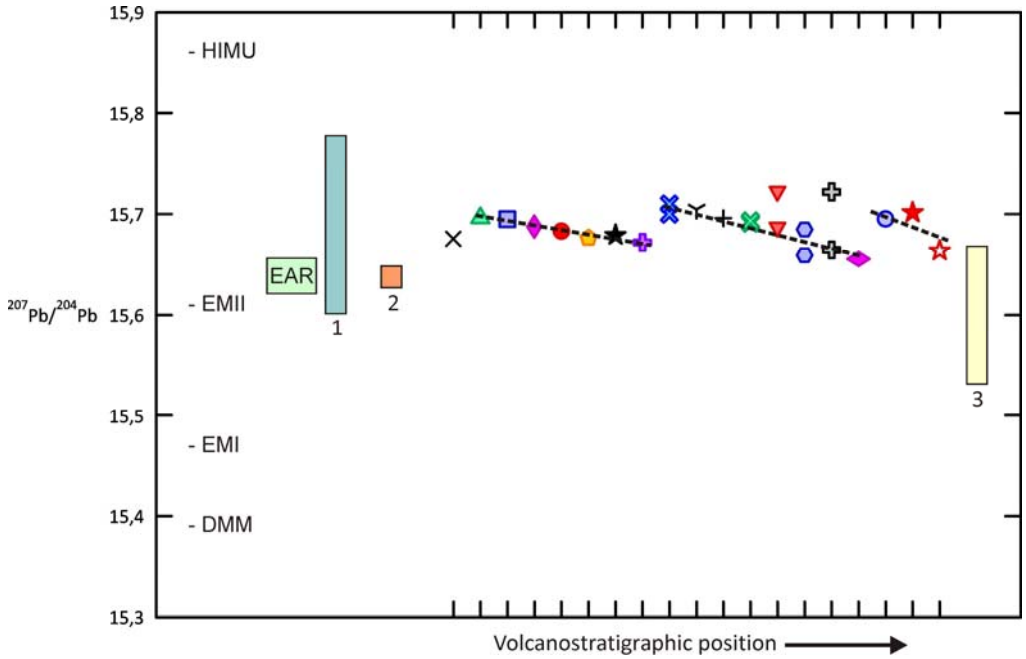

Figure 9.7: $^{207}Pb/^{204}Pb$ ratios. 1: oceanic sediments (Othman et al., 1989; Plank and Langmuir, 1998); 2: Oligo-Miocene volcanism of Sardinia (only two samples, by Morra et al. (1997)); 3: Plio-Pleistocene magmatism of Sardinia (Lustrino et al., 1996, 2000). Mantle components by Armienti and Gasperini (2007). EAR includes component C (Hanan and Graham, 1996), FOZO (Stracke et al., 2005) and EAR (Lustrino and Wilson, 2007)

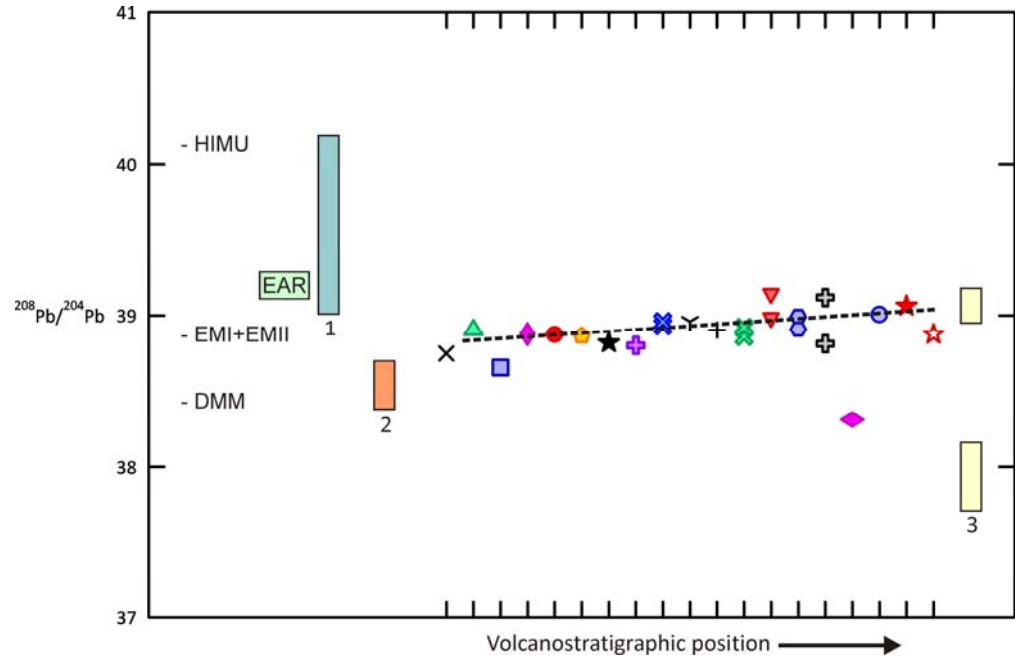

Figure 9.8: $^{208}Pb/^{204}Pb$ ratios. 1: oceanic sediments (Othman et al., 1989; Plank and Langmuir, 1998); 2: Oligo-Miocene volcanism of Sardinia (only two samples, by Morra et al. (1997)); 3: Plio-Pleistocene magmatism of Sardinia (Lustrino et al., 1996, 2000). Mantle components by Armienti and Gasperini (2007). EAR includes component C (Hanan and Graham, 1996), FOZO (Stracke et al., 2005) and EAR (Lustrino and Wilson, 2007)

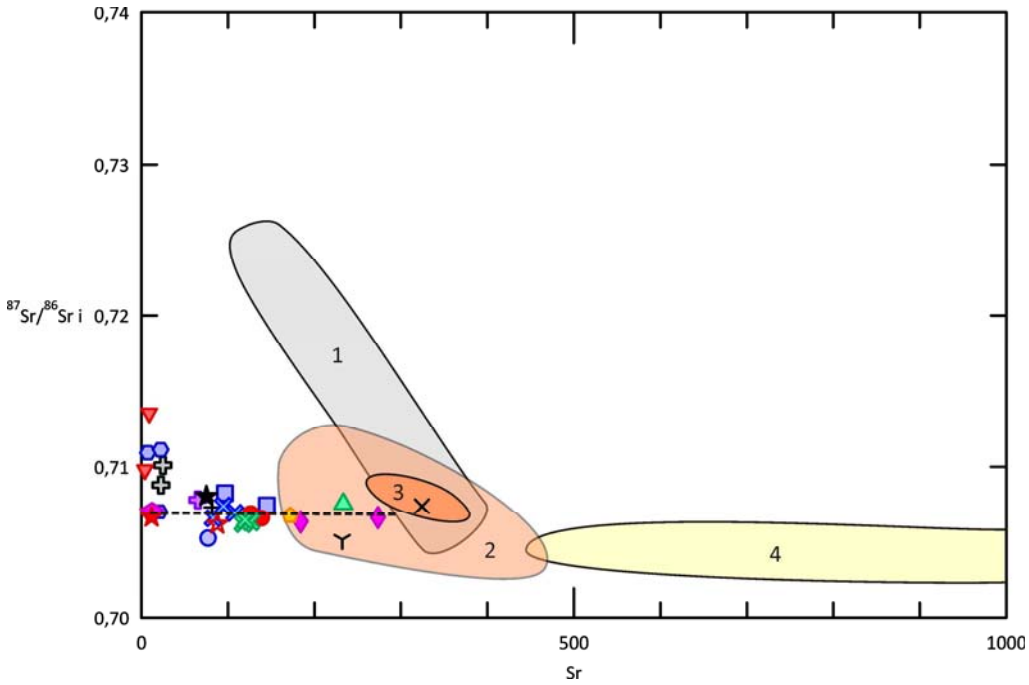

Figure 9.9: Initial $^{87}Sr/^{86}Sr$ ratios vs. Sr concentration (ppm). 1: continental crust (Rutter, 1987; Tommasini et al., 1995); 2: Oligo-Miocene volcanism of Sardinia (Morra et al. ,1997; Downes et al., 2001; Lustrino et al., 2004); 3: Andesitic sequence of Santo Antioco Island (Conte et al., 2010); 4: Plio-Pleistocene magmatism of Sardinia (Lustrino et al., 1996, 2000, 2007a)

Having ruled out crustal contamination as the main origin of isotope ratios variety, another mechanism needs to be proposed. In the $^{87}Sr/^{86}Sr_i$ vs. $^{143}Nd/^{144}Nd$ diagram (Fig. 9.10) data from Sulcis and the rest of Oligo-Miocene magmatism plot in a mixing line that has as end-members mantle compositions on one side and continental crust/oceanic sediment compositions on the other. This trend can be interpreted as being the result of a mantle source whose isotopic signature is modified by influence of an incoming component, probably fluids carrying the isotopic signature of oceanic sediment plus altered MORB from the subducting slab. Identification of possible end-member compositions and mixing trends is typically done by using binary diagrams (Fig. 9.11), but projection of a 3D space (Sr, Nd, Pb) onto a planar surface may produce false sample groupings and apparent trends. Tetrahedral projections are in this sense much more reliable (Armienti and Gasperini, 2007; Armienti and Longo, 2011). Isotopic trend in tetrahedral projection (Fig. 9.12) confirms this subduction influence on mantle magma source isotopic composition. The progressive change in isotope ratios with time of Sulcis data would reflect a change in the magma source region from a mantle with higher influence of subducted materials to another one which has been less modified. Although this trend is well marked in isotopes, it cannot be so easily detected using trace elements, which show subduction-like profiles throughout the whole sequence because, as isotopes show, slab-fluids influence decreases but does not disappear.

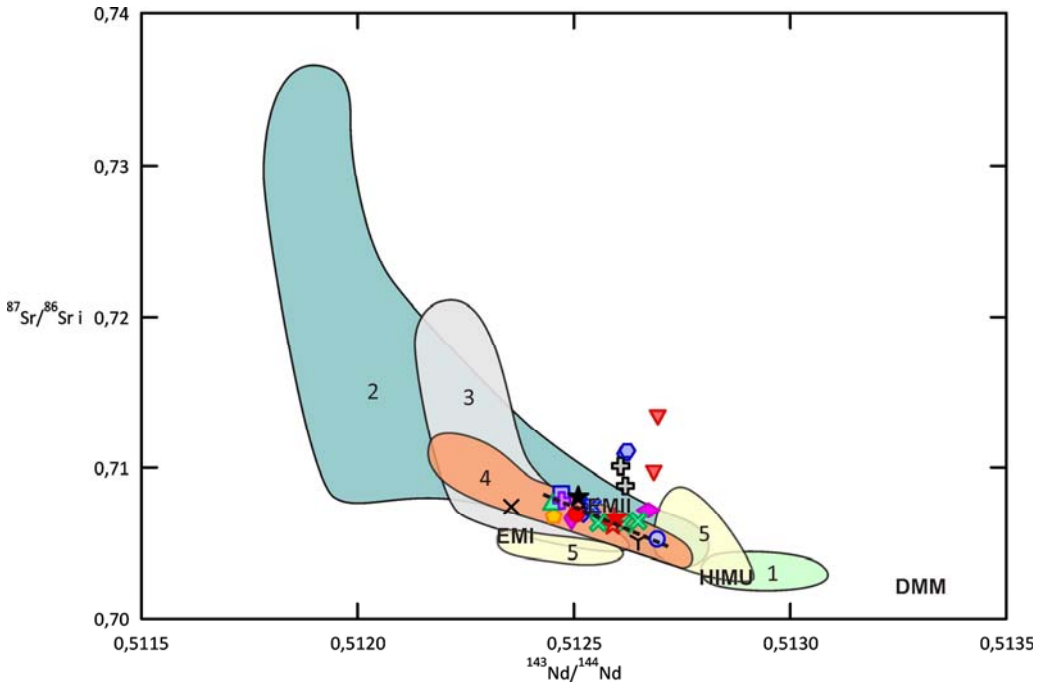

Figure 9.10: Initial $^{87}Sr/^{86}Sr$ ratios vs. $^{143}Nd/^{144}Nd$. 1: component C (Hanan and Graham, 1996), FOZO (Stracke et al., 2005) and EAR (Lustrino and Wilson, 2007); 2: oceanic sediments (Othman et al., 1989; Plank and Langmuir, 1998); 3: continental crust (Rutter, 1987; Tommasini et al., 1995); 4: Oligo-Miocene volcanism of Sardinia (Morra et al., 1997; Downes et al., 2001; Lustrino et al., 2004); 5: Plio-Pleistocene magmatism of Sardinia (Lustrino et al., 1996, 2000, 2007a). Mantle components by Hart et al. (1992)

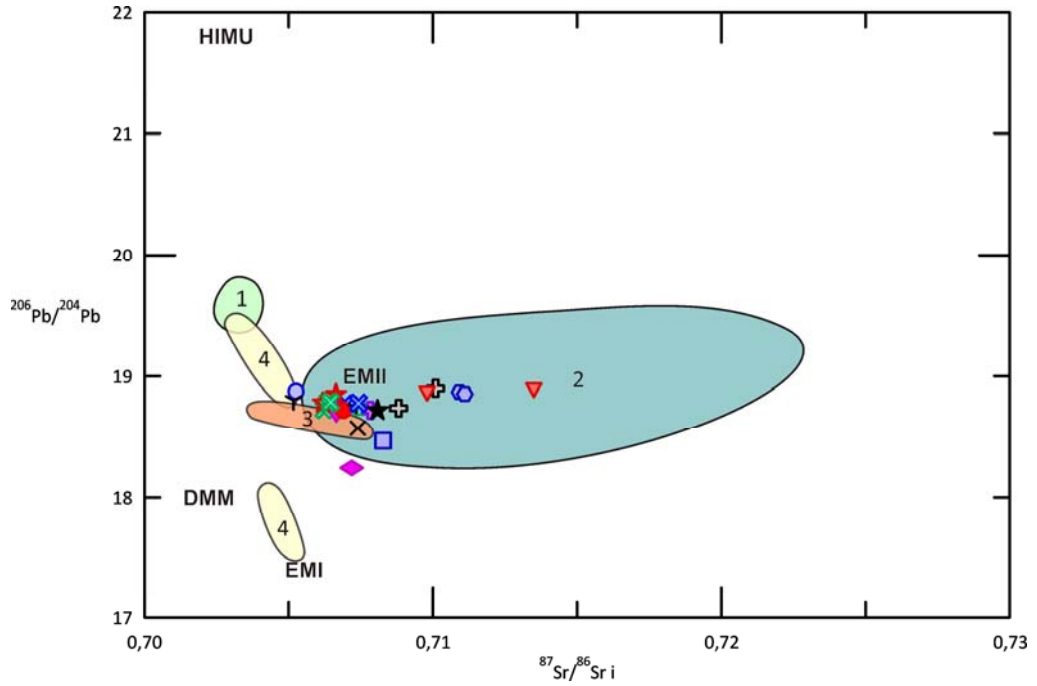

Figure 9.11: $^{206}Pb/^{204}Pb$ vs. initial $^{87}Sr/^{86}Sr$. 1: component C (Hanan and Graham, 1996), FOZO (Stracke et al., 2005) and EAR (Lustrino and Wilson, 2007); 2: oceanic sediments (Othman et al., 1989; Plank and Langmuir, 1998); 3: Oligo-Miocene volcanism of Sardinia (only two samples, by Morra et al. (1997)); 4: Plio-Pleistocene magmatism of Sardinia (Lustrino et al., 1996, 2000). Mantle components by Hart et al. (1992)

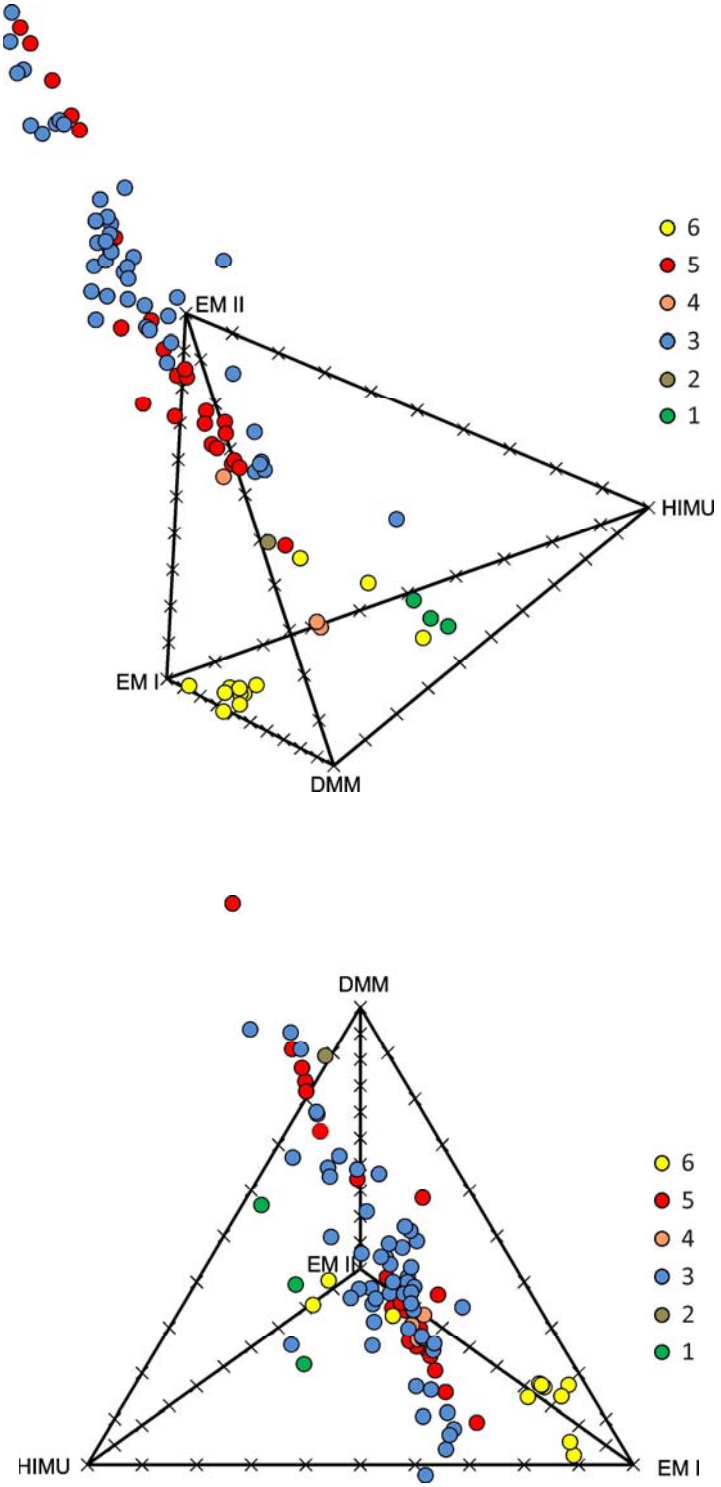

Figure 9.12: Tetrahedral diagram; the same diagram is shown in three different views. Mantle components by Hart et al. (1992) and Armienti and Gasperini (2007); 1: component C (Hanan and Graham, 1996), FOZO (Stracke et al., 2005) and EAR (Lustrino and Wilson, 2007); 2: altered MORB (Hawkesworth et al., 1991); 3: oceanic sediments (Othman et al., 1989; Plank and Langmuir, 1998); 4: Oligo-Miocene volcanism of Sardinia (Morra et al., 1997); 5: Sulcis Oligo-Miocene volcanism from this study; 6: Plio-Pleistocene magmatism of Sardinia (Lustrino et al., 1996, 2000)

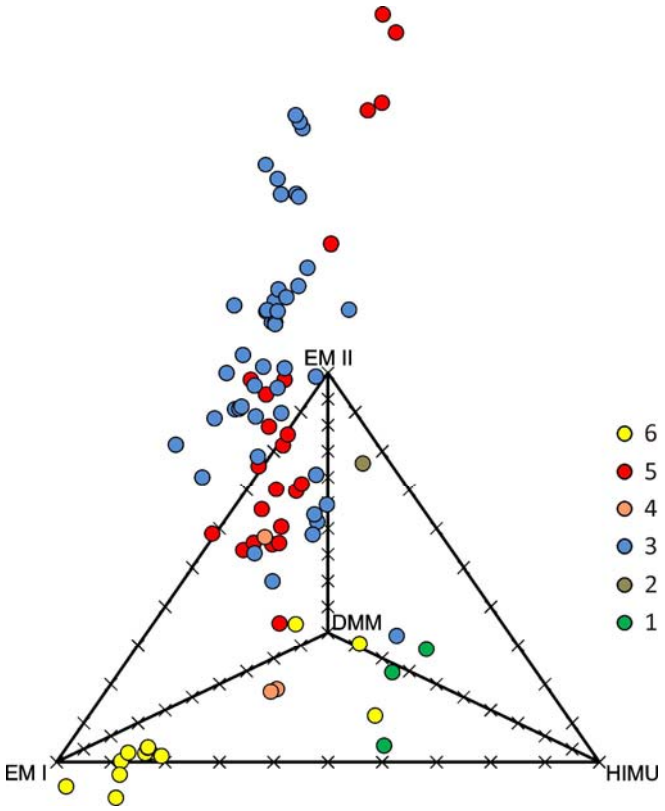

Figure 9.12: (Continuation)

The next step is to characterise the end-members of this mixing trend. In the first instance the mantle component is tackled. The study of Tertiary-Quaternary anorogenic magmatism from the Euro-Mediterranean region, which extends also into the Atlantic domain, has revealed the presence of a common HIMU-like signature for most of the materials erupted in the last 100 Ma, even in diverse tectonic environments (Piromallo et al., 2008) (Fig. 9.13). A common mantle reservoir with rather uniform composition has been invoked to explain such fact, and different names have been given to this mantle component: Component A (Wilson and Downes, 1991), EAR (Cebria and Wilson, 1995), Low Velocity Component (LVC) (Hoernle et al., 1995), Focal Zone (FOZO) component (Bell et al., 2004), Common sublithospheric Mantle Reservoir (CMR) (Lustrino and Wilson, 2007) or component C (Cadoux et al., 2007) (From now on this mantle component will be referred to as EAR-like). This common reservoir is placed in the top 400 km of the mantle beneath the Euro-Mediterranean region, and according to Harangi et al. (2006) and Piromallo et al. (2008) could be the result of a mantle contamination episode triggered by the rise of the Central Atlantic Plume (CAP) head since Cretaceous times.

However, the mantle beneath Sardinia appears to be different from that in the rest of the Mediterranean region. Anorogenic magmatism in Sardinia is anomalous within the circum-Mediterranean region affected by the CAP, because unlike all other anorogenic magmas, which

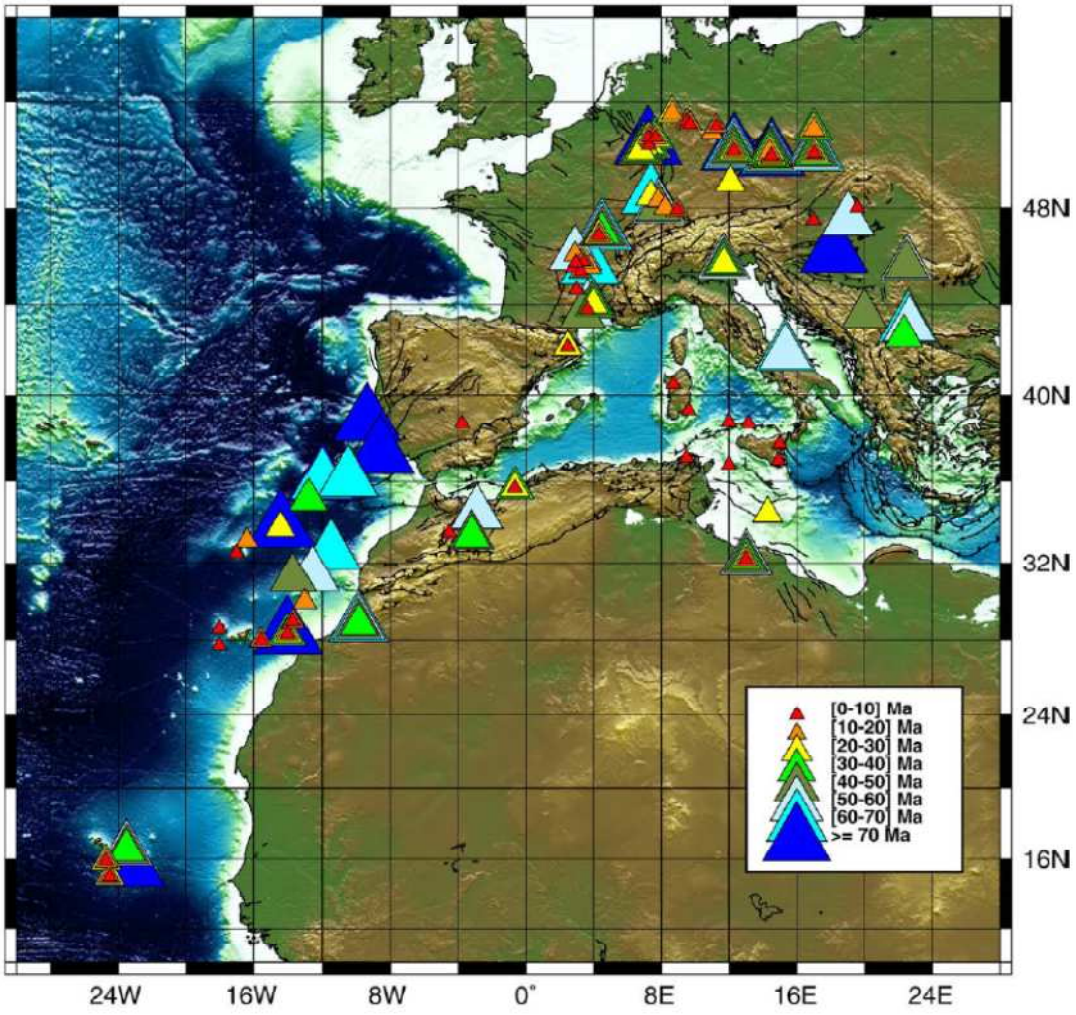

Figure 9.13: Location of the alkali basalts showing the common OIB-HIMU signature in eastern Atlantic and Euro-Mediterranean regions. Figure from Piromallo et al. (2008)

show EAR-like compositions differently mixed with other mantle compositions (Lustrino and Wilson, 2007), Sardinian magmas present a composition close to the EMI end-member (Fig. 9.12), showing only a small trend that could be regarded as the result of some mixing between the EMI end-member and an EAR-like or HIMU mantle component. There are only two exceptions within the Sardinian anorogenic magmatism, the very scarce Radiogenic Pb Volcanics (RPV, Lustrino et al., 2000) and volcanics from Isola del Toro (Lustrino et al., 2007a), which present compositions closer to the EAR-like end-member. These could be interpreted as the only occurrences of the EAR-like component in Sardinia. The origin of this EMI signature has been addressed in several pieces of research. Beccaluva et al. (2001) suggest that the mantle source of this magmatism underwent several partial melting events prior to Mesozoic (based in ages calculated using models contemplating DMM and CHUR), and argue that refertilization was related to a subsequent metasomatism produced by fluids ascending through the lithosphere, which do not

carry subduction signature and are therefore thought to have been highly alkaline melts with an isotopic signature close to EM. The model suggested by Lustrino et al. (2000) regards the EMI signature as being the result of mixing between a depleted mantle (DMM) with low $^{87}Sr/^{86}Sr$ and high $^{143}Nd/^{144}Nd$ with partial melts originated in delaminated ancient (Precambrian) lower crust (Lustrino et al. 2000, 2004, 2007b; Lustrino, 2005; Fedele et al., 2007). As another hypothesis, Gasperini et al. (2000) proposed that magmas in the Logudoro area (northern Sardinia) originated from a DMM mantle source which was modified by subduction and assimilation of a large oceanic plateau which included rocks rich in cumulate plagioclase.

Regarding the mantle source of the Oligo-Miocene volcanism, this has been traditionally thought to be a DMM mantle source modified by subduction fluids (Coulon, 1977; Dostal et al. 1982; Morra et al. 1994, 1997; Downes et al. 2001; Franciosi et al., 2003; Lustrino et al., 2004, 2011). The isotopic trend depicted by the Oligo-Miocene magmatism in tetrahedral projection (Fig. 9.12), instead, appears to have as mantle end-member a composition which can be interpreted as falling into a mixing line between the EAR-like composition and EMI, being closer to the EAR-like composition. Considering that the EAR-like component has been found in most of the Euro-Mediterranean region, that the RPV fall close to this component composition, and that both Oligo-Miocene and Plio-Pleistocene magmatisms present mixing trends which are compatible with the EAR-like composition being one of the end-members, it is not unrealistic to think that the CAP event did also affect the mantle under Sardinia.

Since the Oligo-Miocene and Plio-Pleistocene magmatisms have two very distinct isotopic signatures it is evident that the mantle beneath Sardinia has at least two main reservoirs. As the origin of the alkaline Plio-Pleistocene suite was by decompression melting, magmas must be expected to have been formed at shallower levels than Oligo-Miocene subduction magmas. Therefore, a possible explanation would be the presence beneath Sardinia of a diffusely "stratified" mantle with an upper region with an isotopic composition close to that of the EMI end-member, and a lower one that, having initially a similar composition, was affected first by the CAP metasomatic episode, which introduced an EAR-like component to this region that became dominant, and subsequently by the metasomatism caused by the slab-released fluids.

The particularities of Sardinian magmatism cause the identification of the widespread EAR-like component to be difficult in this area because Oligo-Miocene magma sources were modified by subduction fluids, and anorogenic magmatism sampled above the significantly CAP-modified mantle. The presence of the EMI component under Sardinia had been previously interpreted as a lateral variation in mantle composition (Panza et al., 2007), thus considering that the EAR-like component was not present in Sardinia (except for the RPV). Now it is seen that the CAP episode

also affected the mantle under Sardinia, and that the very scarce sampling of it by the anorogenic magmatism is not due to a lateral (as proposed by Panza et al. (2007)) but to a depth mantle compositional variation. Whether the CAP-modified mantle is deeper under Sardinia than in other areas and/or the Plio-Pleistocene magma source is shallower compared to other anorogenic magmatic events remains an open question.

Therefore, it is proposed that the mantle magma source of the Oligo-Miocene volcanism consisted in a mixture between EAR-like and EMI compositions that was subsequently metasomatised by slab-released fluids.

The other end-member in the Oligo-Miocene magmatism isotopic mixing trend is more difficult to characterise, since it could have any composition of the ones depicted by the oceanic sediment data shown in Figure 9.12, or most probably be a mixture between altered MORB and sediment compositions. In a mixture between these two components, fluids released by subducted sediments have more influence in the resulting isotope composition of the mantle wedge than fluids released by the altered oceanic crust because their isotopic compositions are more different from those of the mantle wedge. Regelous et al. (2010) illustrate this fact with a case from the northern Tonga arc, in the Pacific.

9.2.3 Mantle composition and fluid effect

To constrain the composition of the mantle in which the studied magmas were generated it is necessary to take into account the different components and events that generated the final composition. That is, the EMI and EAR-like mantle components, and the effect of subduction-released fluids.

Regarding the pre-subduction trace element composition, it has been argued that this mantle source probably represented a mixture between the EMI and EAR-like components. The EMI end-member composition can be deduced from the Plio-Pleistocene anorogenic magmatism of Sardinia, which presents trace element profiles in mantle-normalised spider diagrams similar to those of OIB (Fig. 9.14) but with a positive anomaly in Pb. Some scarce samples present evidences for having originated in slightly subduction-modified mantle regions; these are not considered here. Anorogenic magmas generated in the EAR-like portion of the mantle are scarcely represented in the available data from Sardinia (as seen in Fig. 9.12), but there is plenty of data from other alkaline provinces around the circum-Mediterranean area (Piromallo et al., 2008) (Fig. 9.15). These also show OIB-like profiles, consistently with the proposed plume origin of the contamination episode that generated this end-member. Therefore, the mantle source in which

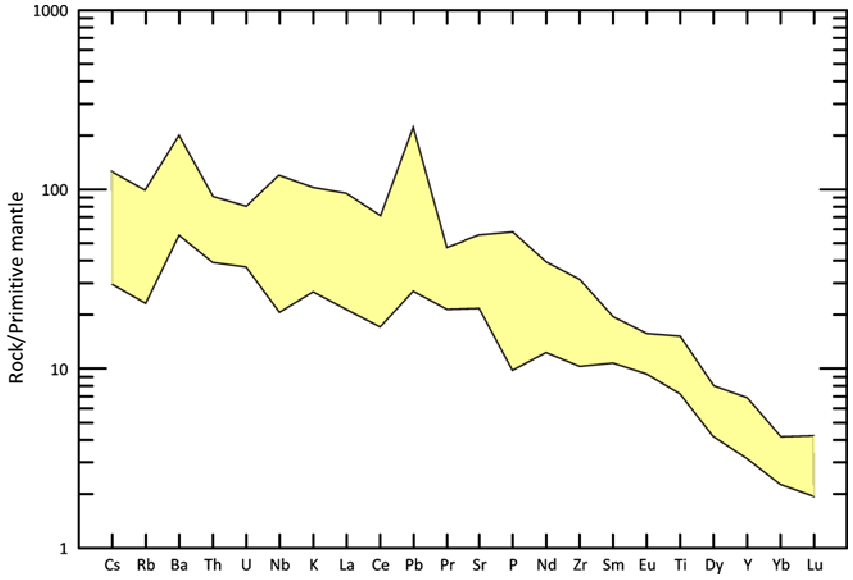

Figure 9.14: Anorogenic magmatism of Sardinia with >7 wt % MgO. Primitive mantle-normalized spider diagram; normalizing values by Sun and McDonough (1989). Data origin in Fig. 9.18

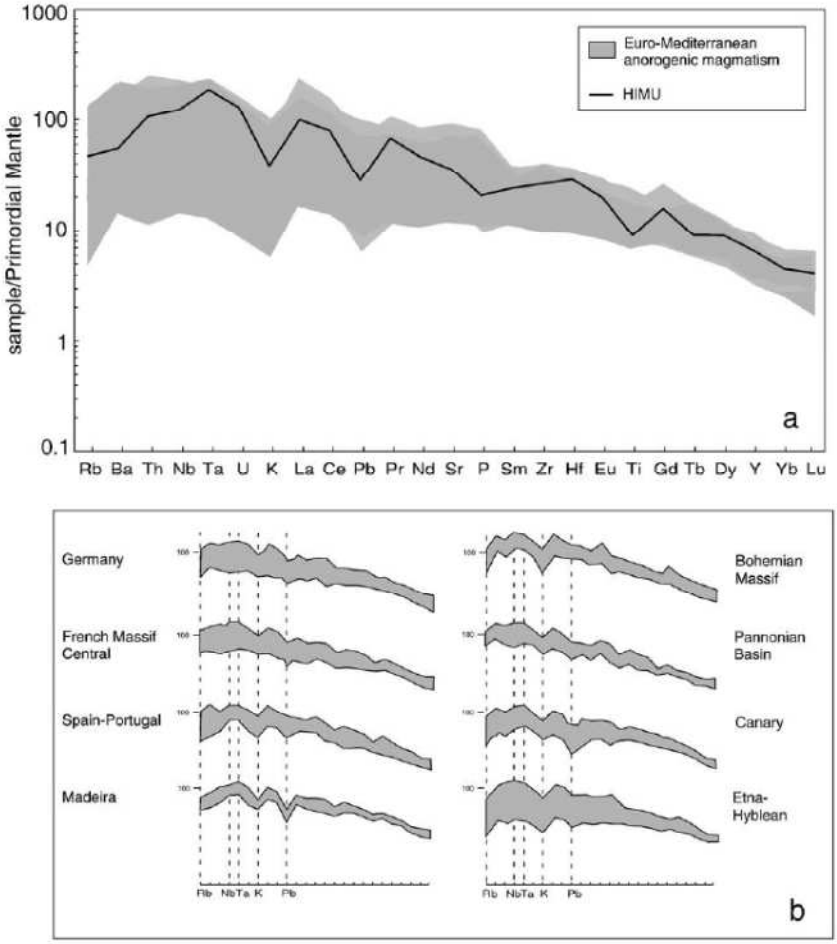

Figure 9.15: Figure from Piromallo et al. (2008) showing primitive mantle-normalized patterns for the Euro-Mediterranean region as a whole (a) and in separate areas (b). All areas show homogeneity in composition

the studied magmas were generated had, before subduction fluids modified it, a trace element composition such that OIB-like magmas would be generated by partial melting. That is, an undepleted and/or refertilised mantle.

Modification of the original mantle source by metasomatism was caused by fluids released by the subducting slab, which may have been dominantly two: aqueous fluids released by the subducting oceanic slab and overlying sediments, and partial melts of the sediments. Both fluid types affect differently the mantle wedge composition. Fluid expulsion from subducting slabs is a complex process controlled by many factors such as the chemical and mineralogical composition of sediments, crust and lithospheric mantle, and its mineralogical evolution to adapt to the increasing P and T conditions on subduction (Schmidt and Poli, 2003). The amount of water that can be stored by the water-bearing phases of a rock decreases with pressure until water saturation is reached and hydrous fluids expulsion begins. Chemical composition of the aqueous fluid depends on the mineral phases that have released it, on the fluid/rock equilibration, and on element solubility. Aqueous solutions are typically enriched in mobile elements (LILE) relative to immobile ones (HFSE), thus producing enrichment in LILE elements in the mantle wedge while HFSE contents remain nearly constant. Partial melts of sediment occur when a sufficient temperature is reached. Composition of the resulting melt depends on the original composition of sediments, melting degree and partition coefficients of each element (its incompatibility), these melts being enriched in incompatible elements.

As seen before, magmas generated from the mantle source previous to fluid metasomatism would present Th, U and Nb normalised contents close to each other. However, in the post-metasomatism magmas there is a strong Nb negative anomaly relative to the other two elements. Considering that all three elements are immobile, aqueous fluids cannot be the origin of such anomaly, and therefore the participation of sediment partial melts must be invoked. Subducted sediments always present a negative Nb anomaly when normalised to primitive mantle compositions (Fig. 9.16), which, added to the lower incompatibility of this element, especially when rutile is present as a residual phase (Class et al., 2000), results in the impoverishment of Nb in the partial melts relative to Th and U. The contribution of sediment partial melts to mantle wedge metasomatism is also supported by the Nd isotope ratios, which show sediment compositions as one of the end-members conditioning its composition. Since Nd, as other REE, is immobile in aqueous fluids, it is not transferred from the slab to the mantle wedge in significant amounts unless sediment partial melting occurs. Thus, aqueous fluids released from the subducting oceanic crust influenced the final Sr and Pb isotopic ratios, whereas the Nd isotopic ratio was only influenced by sediment partial melt. A last factor can be considered: contamination

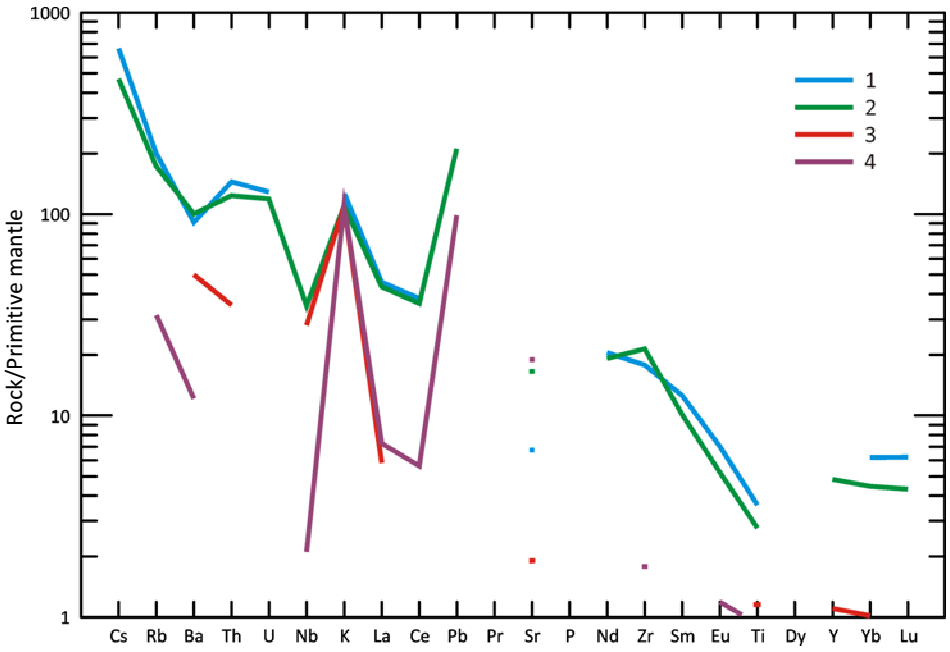

Figure 9.16: Sediment compositions in primitive mantle-normalized spider diagram; normalizing values by Sun and McDonough (1989). 1: North American Shale Composite (Gromet et al., 1984), 2: average upper crust (Taylor and McLennan, 1981); 3: average Phanerozoic quartz arenite (Boryta and Condie, 1990); 4: average Phanerozoic limestone (Condie et al., 1991)

that generated the EAR-like mantle compositions was produced by a mantle plume, which affected the thermal structure of the upper mantle. Although this event took place in late Cretaceous times (Piromallo et al., 2008), mantle regions affected by this plume probably still present higher temperatures than the surrounding mantle, thus favouring the melting of subducted sediments at a lower depth; seismic waves velocity anomalies found below the circum-Mediterranean area (Hoernle et al., 1995) have been interpreted as being caused by a temperature positive anomaly of up to 150°C (Lustrino and Wilson, 2007).

However, according to some authors sediment partial melting does not have to be necessary involved to explain HFSE anomalies observed in the Sulcis and other subduction environments. The anomalously high recycling of Th and of some other immobile elements such as Be into the mantle wedge in subduction zones has been traditionally explained by the occurrence of sediment partial melts (Schmidt and Poli, 2003), as seen before. But Schmidt and Poli (2003) argue that if the subducting lithosphere is studied as a whole, the water released by the non-sedimentary lithosphere can account for the mobilization of significant amounts of immobile elements. All the water released by the oceanic lithosphere must cross the sediment layer to reach the mantle wedge, thus resulting in much higher water/sediment ratios than if just sediment-released water is contemplated. Even if element mobility is small, the large amount of

water leaching the sediment is capable of significantly transfering immobile elements into the mantle wedge without the participation of sediment partial melts. Calculations made for a case study show that more than 60% of the ^{10}Be (which only occurs in sediments and is traditionally considered immobile) can be transferred to the mantle wedge in this way. Therefore, considering this hypothesis of sediment leaching by altered-MORB-derived water solutions, the observed mantle wedge metasomatism could be explained in terms of aqueous fluids effect, without the necessary intervention of melts.

The calculation of the relative contributions of each reservoir to the final mantle composition, as well as the order of release of each fluid phase into the mantle wedge are beyond the scope of this study and will not be tackled; examples of case studies in other regions can be found in works such as those of Class et al. (2000), Duggen et al. (2007) or Regelous et al. (2010).

9.3 MAGMA GENERATION

As has been seen, trace element contents and isotope ratios indicate that Oligo-Miocene magmas in Sardinia were generated in a mantle reservoir with an original composition between EMI and EAR-like, which was subsequently metasomatised by slab-released fluids. After characterising the composition of the magma source, the investigation of the melting mechanisms generating the studied magmas must be addressed.

Since the work by Coulon (1977) the Oligo-Miocene magmatism was regarded as being the consequence of subduction of an oceanic plate under Sardinia. In subduction environments the release of aqueous fluids from the slab into the mantle wedge causes melting by the decrease of the melting point, which is the main magma generation mechanism. The resulting calc-alkaline melts present the typical trace element patterns previously explained, and are characterised by a subalkaline character, which they share with the tholeiitic suites. In Figure 9.17 a Total Alkalis versus Silica (TAS) diagram presents Oligo-Miocene magmatism from Sardinia compared to the typical compositions shown by orogenic calc-alkaline suites, in this case represented by a suite from the Carpathians. As can be seen in this figure both magmatisms overlap in the subalkaline field, thus confirming the hypothesis by Coulon (1977). However, although the andesitic sequence of the Sulcis area can be related to the rest of the Sardinian Oligo-Miocene magmatism, the ignimbritic sequence is clearly separated from the subduction-related trends, falling into the transitional area between subalkaline and alkaline magmas. Two hypotheses may be proposed at this point to explain this fact. The ignimbritic sequence can be considered to be genetically related to andesites through some mechanism of magma evolution (assimilation and fractional

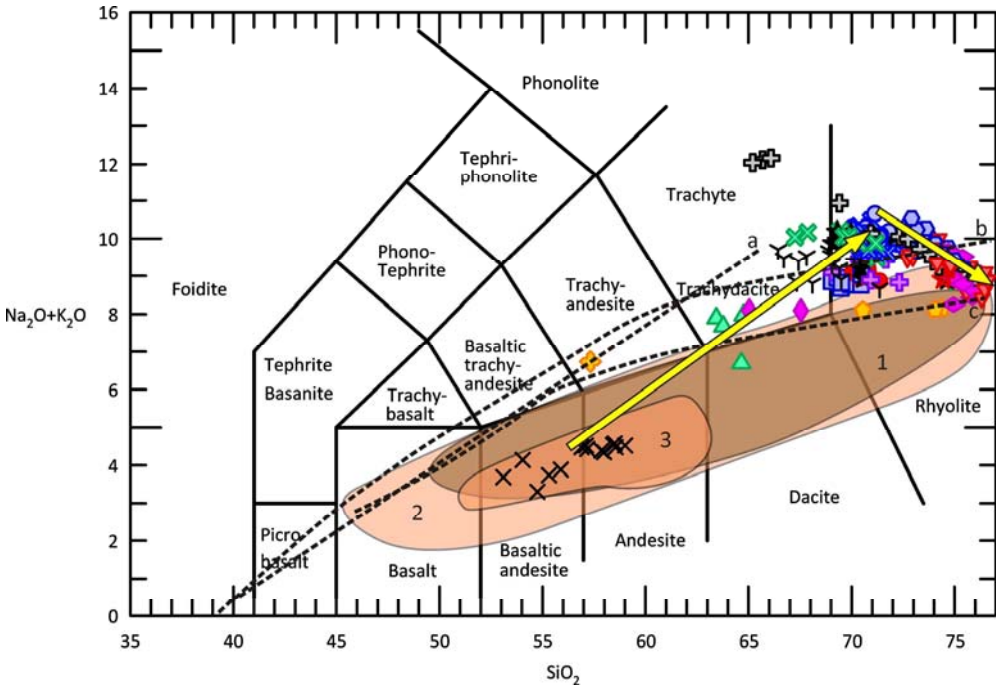

Figure 9.17: TAS diagram showing typical compositions shown by orogenic calc-alkaline suites, as well as samples from the present study. Contents in wt %. 1: calc-alkaline suite from the Carpathians (Harangi et al., 2007); 2: Oligo-Miocene magmatism from Sardinia (Coulon et al., 1973; Coulon, 1977; Dostal et al., 1982; Brotzu et al., 1997b; Conte 1997; Lonis et al., 1997; Morra et al., 1997; Mattioli et al., 2000; Downes et al., 2001; Lustrino et al,. 2004, 2009; Guarino et al., 2011); 3: Andesitic sequences from Santo Antioco Island and Narcao area (Brotzu, 1997a; Conte et al., 2010). Dash lines are the subdivision of volcanic rocks into alkaline (above) and subalkaline (below) proposed by: a) MacDonald (1968); b) Irvine and Baragar (1971); c) Kuno (1966). Yellow arrows represent the petrogenetic hypothesis by Morra et al. (1994), discussed and rejected in this work (see text for explanation)

crystallisation) which caused its departure from the typical trends as proposed by Morra et al. (1994), or rather that it originated from a different parental magma.

The Subcommission on the Systematics of Igneous Rocks agreed in the early 80's that the classification of volcanic rocks should be based on modal composition in order to be consistent with the classification of plutonic rocks proposed by Streckeisen (1978). However, the usually incomplete crystallisation of volcanic rocks means that this method cannot be always successfully applied. Thus, an alternative classification method was proposed based on whole rock geochemistry using the total alkalis versus silica diagram. The TAS classification diagram (Le Bas et al., 1986) was designed using an extensive geochemical database, and boundaries between fields were established trying to fit the limits between rock types while keeping a simple array of straight lines. The basic pattern of the diagram is based on two main diverging lines, and several transversal lines which depart from different silica contents. The two main diverging lines separate three sectors with different silica saturation in the CIPW norm. Rock compositions which plot in the lower (oversaturated) sector (basaltic andesite to rhyolite) are almost exclusively

quartz-normative, while rocks in the upper sector are almost exclusively nepheline-normative. The array with which the diagram was designed implies that each of the three main sectors contains commonly associated rock types. That means that, generally, the evolutionary trend of co-magmatic rocks is subparallel to the silica saturation lines. The transversal lines subdividing the main sectors into smaller fields may be regarded as approximate lines of equal evolution (Zanettin, 1984).

The hypothesis by Morra et al. (1994), which genetically relates the upper ignimbritic sequence to andesites, implies strong changes in silica saturation. Although several mechanisms have been proposed to explain changes in silica saturation and departures from the typical evolutionary trends in the TAS diagram, the most common situation is that of trends being subparallel to the silica-saturation lines as can be seen in Figure 9.17 for the Carpathians. Therefore, it is considered that andesites are not the parental magmas for the ignimbritic sequence and that the melting mechanisms must be somewhat different.

In mantle-derived melts alkalinity is usually a consequence of the partial melting degree, which conditions the mineral phases and proportions between them that melt. In subduction settings, water release causes high partial melting degrees which produce calc-alkaline subalkaline melts. In extensional settings alkalinity of the generated magmas is most dependent on opening rates, which condition melting degrees. Low extensional rates produce little melting and alkaline magmas. As extension increases, melting degree increases and alkalinity is reduced, first to transitional magmas and finally to subalkaline ones, the most typical of which are the tholeiitic suites in ridge environments. Since most of the transitional and alkaline magmas are generated in extensional settings, it can be thought that extension had a key influence in the generation of the Sulcis ignimbritic sequence. However, an extensional setting was present in Sardinia during the occurrence of most of the Oligo-Miocene volcanism, it was not only present in the Sulcis.

At the beginning of the subduction process east of Sardinia, when the Corsica-Sardinia microplate was still part of the European continental margin, Sardinia was under a compressive stress field. With the beginning of the roll-back in Oligocene times, the stress field progressively changed to extensional, generating a rift system which finally produced the detachment of Sardinia from the continental margin, allowing its drifting and rotation to its present position. The Sardinian Rift and associated structures were originated during this rifting process and evolved during the movement of Sardinia towards its current position. The Oligo-Miocene evolution of the Sardinian Rift occurred between 28 and 15 Ma (Cherchi and Montadert, 1982; Lecca et al., 1997) and consisted in the development of several sub-basins which were filled by thick orogenic volcanic sequences and continental and marine sediments (Sau et al., 2005).

Lecca et al. (1997) recognized several stages in the evolution of the Sardinian Rift:

a) Pre-Rift phase: characterised by strike-slip and/or transpressive regime during collisional phases (upper Eocene-Oligocene) with emplacement of pre-Aquitanian andesitic sequences (28 to 24 Ma) in an early proto-rift. In southern Sardinia andesites cover the pre-existing Eocene continental basins. There are no evidences of significant basins associated to pre-Aquitanian volcanism. There is reactivation of NW-trending late-Hercynian fault patterns with important left-lateral components. This reactivation of NW trending faults may promote extensional movements along E-W trending fault zones (i.e. Arcuentu area, where less evolved basaltic varieties suggest shorter residence times of magmas)
b) 1st Rift phase (Aquitanian-Burdigalian) (24-18 Ma): from strike-slip to transtensive up to extensional regimes. In western Sardinia the Liguro-Provençal basin opens and syn-rift sediments are deposited from Upper Oligocene to Aquitanian times (Cherchi and Montadert, 1982; Burrus, 1989; Gorini et al., 1993). Since the Aquitanian post-rift sediments are deposited (Gorini et al., 1993) and oceanic crust is formed (Burdigalian, Burrus (1989)) during the rotation of the Corsica-Sardinia microplate. Volcanic activity occurs mainly in central and northern Sardinia, with important outpouring of ignimbrites. There is an increase of the extensional movements within the rift producing structural highs and basins. Basins are first infilled by continental sediments and subsequently by marine epicontinental silicoclastic sediments in southern and northern Sardinia. The NE trending transtensive major faults are active in central and northern Sardinia, whereas the southern branch of the Sardinian rift is involved in important subsidence along the NW trending faults. This phase is contemporary to the climax of the Sardinia-Corsica microplate rotation (Montigny et al., 1981).
c) 2nd Rift phase (upper Burdigalian-Langhian) (18-15 Ma): extensional collapse phase linked to the eastward jump of the subduction and of the back-arc extension, which moves from the Liguro-Provençal basin to the future Tyrrhenian basin. In central and northern Sardinia the transtensive structures evolve to a more pronounced extensional regime favouring the marine transgression of upper Burdigalian. In southern Sardinia the transtensive regime jumps out of the main branch of the Sardinian rift. To the west it affects the Sulcis area, where the emplacement of the ignimbritic sequence occurs. To the east, it initiates the formation of the northern Tyrrhenian basin (Sau et al., 2005). In the northern sector of the Tyrrhenian basin syn-rift deposits are 20 to 15 Ma old by the Corsica margin. In the southern sector syn-rift deposits are progressively younger (10-12

to 5 Ma old) from the Sardinian margin to the Vavilov basin (Wezel et al., 1981; Kastens et al., 1988; Sartori, 1990). According to Argnani and Savelli (1999) the first sediments in western Sardinia indicating the opening of the southern Tyrrhenian are from late Tortonian. In this stage volcanic activity occurred only in western sectors of the Rift. Important changes in the chemical character of volcanics are documented by the occurrence of very primitive basalts (high-Mg basalts from Montresta (Morra et al., 1997) and Villanovaforru (Mattioli et al., 2000) areas, 17 Ma) and peralkaline rhyolites in the Sulcis area (15 Ma).

d) Upper Miocene: final extensional arrangements of the Sardinia-Corsica microplate lead to the lowering and tilting of western Sardinia continental margin. In this stage, the Sulcis area constitutes a horst block without appreciable tilting.

During Tortonian to Quaternary times the rift faults are partially reactivated, especially in central and southern Sardinia (Ottana and Campidano grabens). Lowering of presently submerged basins occurs, including parts of the Sulcis area (Sau et al., 2005).

Therefore, most of the orogenic magmatism in Sardinia was formed and emplaced under extensional tectonics, and having a calc-alkaline subalkaline character. Even the climax in extension, which occurred during the rotation of the Corsica-Sardinia microplate, was accompanied by a climax in orogenic magmatism related to the increased subduction rates. In this sense, the chemical character of subduction-related subalkaline magmatism was not significantly affected by the extensional tectonics. The only appreciable change is the occurrence of special magmas, such as the high-Mg basalts, which can be considered as primitive magmas that were able to reach the surface without significant stagnation and evolution thanks to the extensional setting. So, what caused the change in alkalinity of the ignimbritic sequence in the Sulcis, which apparently formed under the same conditions and from a mantle of the same composition as the rest of the Oligo-Miocene magmatism?

Over the past decades the study of peralkaline magmatism has shown that these magmas almost exclusively occur in mildly extensional settings and oceanic islands (Macdonald, 1974b; Mahood, 1984). The presence of peralkaline magmas in active subduction-related environments is restricted to back-arc positions (Bowden, 1974) as in the Northwestern Mexican Volcanic Belt (Nelson and Hegre, 1990; Vidal-Solano et al., 2007) or Mayor Island, New Zealand (Houghton et al., 1992). Occasionally, they are found in the arc itself once subduction has stopped and tectonics change from compressive to extensional, as in the D'Entrecasteaux Islands, Papua New Guinea (Smith, 1976; Smith et al., 1977). They never appear in the arc contemporaneously with the calc-

alkaline magmas. The only exception to this has been, until now, the Sulcis suite, which was directly related to subduction-generated magmas (Morra et al., 1994). Considering the apparent exceptionality of the studied suite in the global context of peralkaline magmas, it is thought that this hypothesis needs to be revised. It needs to be studied if the ignimbritic suite containing comendites could be related to an anorogenic magmatism rather than to the orogenic one as suggested by Morra et al. (1994).

The TAS diagram in Figure 9.18 presents the fields occupied by the orogenic and anorogenic Cenozoic magmatism of Sardinia. Despite the wide range of compositions shown by the anorogenic magmatism, most of it has an alkaline character, plotting in the trachybasalt-trachyte evolutionary path. Samples in the transitional to subalkaline fields belong mostly to the evolved terms of the Monte Arci volcanic complex. This complex presents a main series of basaltic andesites to rhyolites erupted in reverse order, with the occurrence of some mafic-inclusion bearing trachytes in the middle of the sequence (Cioni et al., 1982; Montanini and Melli, 1992). The subalkaline magmas of Monte Arci partly overlap with the Oligo-Miocene orogenic magmas and have the particularity of presenting trace element patterns in normalised diagrams similar to those of the orogenic magmatism. If Monte Arci is not considered, the Sulcis ignimbritic sequence

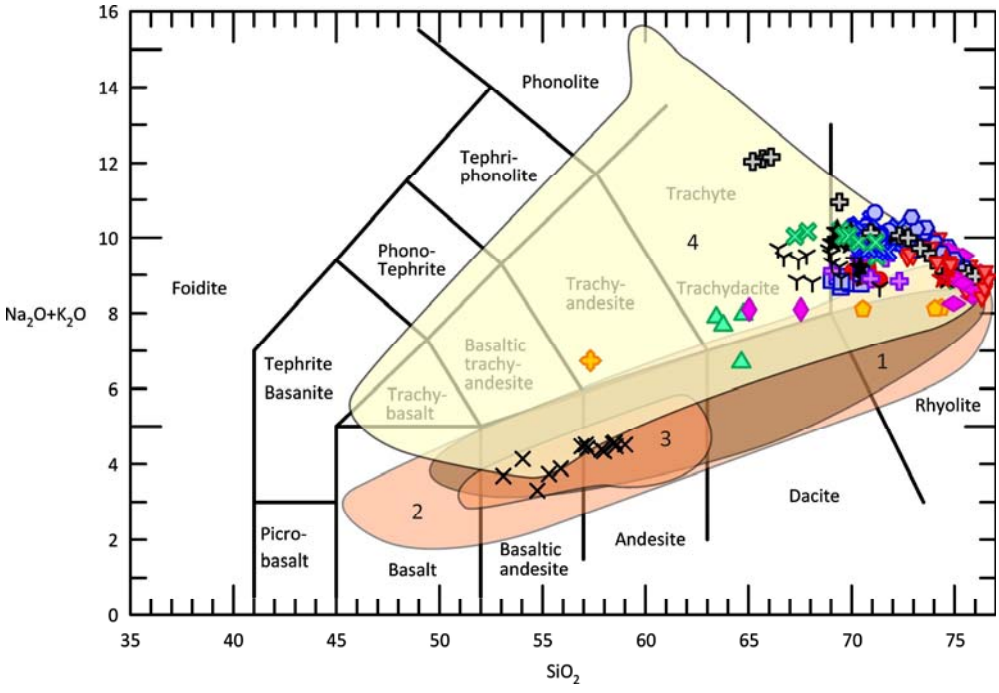

Figure 9.18: TAS diagram presenting the fields occupied by orogenic and anorogenic magmatism of Sardinia. 1: calc-alkaline suite from the Carpathians (Harangi et al., 2007); 2: Oligo-Miocene magmatism from Sardinia (references in Fig. 9.17); 3: Andesitic sequences from Santo Antioco Island and Narcao area (Brotzu, 1997a; Conte et al., 2010); 4: Anorogenic magmatism (Cioni et al., 1982; Dostal et al., 1982; Rutter, 1987; Montanini and Meli, 1992; Montanini et al., 1994; Lustrino et al., 1996, 2000, 2002; Lustrino, 2000; Fedele et al., 2007)

plots in the TAS between the two main groups of magmatism (alkaline and calc-alkaline), and thus could be considered to have a transitional character between the two magmatic types. However, as evidenced by the Monte Arci samples, in this case the TAS diagram is not capable of clearly differentiating between orogenic and anorogenic magmatism based on its alkalinity.

The search for a diagram capable of differentiating between orogenic and anorogenic magmatism has ended in the use of two elements, Nb and Zr, which proved to be very useful in the previous chapter on unit recognition. In this case either Zr alone or Zr/TiO_2 may be used with similar results; for simplification Zr will be used. A Nb vs. Zr diagram was already used by Leat et al. (1986) to study the basalt-subalkaline/peralkaline rhyolite provinces in the Southern British Caledonides. Figure 9.19 presents the areas covered by the two magmatisms, which are clearly differentiated. Except for mafic inclusion-bearing trachytes from Monte Arci, which display an anomalously high Zr content, both magmatisms are separated by an approximate value of Nb/Zr = 0.1; ratios for orogenic and anorogenic magmatisms are below and above this value respectively. The cause for this separation of the two fields needs to be further investigated, but in this case it appears to be exclusively related to the fluid or decompression melting mechanism of the mantle magma source. No relation with alkalinity, mantle trace element chemical composition or isotopic signature has been found. For example, as seen before, the Monte Arci basaltic andesite-rhyolite

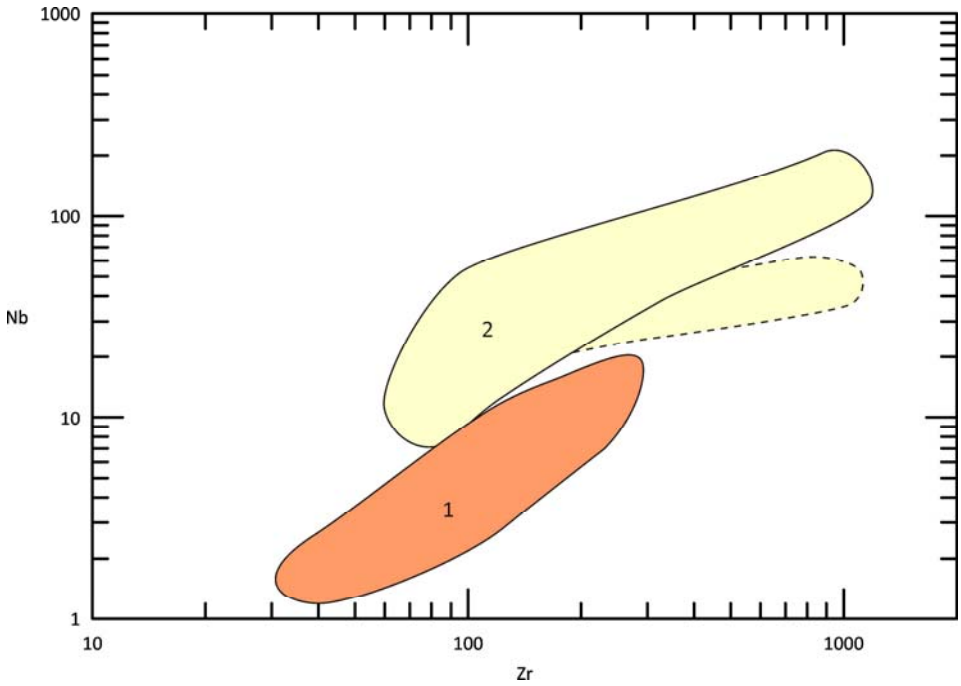

Figure 9.19: Areas covered by both the orogenic (1) and anorogenic (2) magmatism of Sardinia. Concentrations in ppm. Dashed line contains the mafic inclusion-bearing trachytes of the Monte Arci complex, which present anomalous Zr contents. Separation between both fields approximately follows Nb/Zr = 0.1

suite overlaps with the orogenic magmatism in the TAS diagram, and presents trace element profiles in mantle normalised diagrams equivalent to those of the subduction-generated magmatism. However, in the Nb vs. Zr diagram these "problematic" samples are right in the middle of the anorogenic field. The same happens with other anorogenic samples presenting subduction signature, confirming that separation of both fields is not due to different mantle composition caused by metasomatism. Isotope ratios confirm that the Nb/Zr ratio is not modified by subduction metasomatism, but also shows that it is neither affected by the CAP contamination event (Fig. 9.20 and 9.21). In Figure 9.20 the orogenic magmatism is represented by samples from the Arcuentu and Montresta areas. Arcuentu magmas present a wide range in $^{143}Nd/^{144}Nd$ caused by a variable amount of subduction-related contamination of the mantle source, which does not produce changes in the Nb/Zr ratio. This is not completely surprising since both elements are immobile and therefore scarcely and similarly mobilised by aqueous fluids. In the case of anorogenic magmatism, and considering as reference values the compositions of the regular Unradiogenic Pb Volcanics (UPV, Lustrino et al., 2000), originated in the EMI mantle, RPV represent the modification of the EMI source by the CAP event, and Monte Arci magmas represent the contamination by subduction, producing higher and lower Nd isotopic ratios respectively. Despite the range in Nb/Zr ratios within each population of anorogenic magmas, neither of the two contamination events which affected the mantle source produced significant changes in Nb/Zr. Although fewer samples are available for study, the same observations can be made with Pb isotopes (Fig. 9.21).

The exact significance of the different Nb/Zr ratios between orogenic and anorogenic magmatisms in Sardinia will be carefully addressed in future studies. At the moment, it has been ruled out that the origin of different ratios for both magmatisms could be due to different mantle compositions, thus confirming that they are only caused by the melting mechanism. Since all evidences confirm the utility of the Nb vs. Zr diagram to differentiate between orogenic and anorogenic magmatisms in Sardinia, it will be used to study the Sulcis suite. Figures 9.22 and 9.23 present the studied samples from the Sulcis area in the diagrams shown in Figures 9.19 and 9.20. In these diagrams samples from the andesitic sequence fall in the orogenic magmatism field, thus confirming its orogenic origin. Samples from the ignimbritic sequence, however, cover the space between both magmatisms. The lower ignimbrites (previous to NU unit) are close to the orogenic field; on the other hand peralkaline units are clearly in the anorogenic field. Overall, the ignimbritic sequence of the Sulcis appears to depict a transition between orogenic and anorogenic magmatisms. Samples from PA and PM are displaced relative to equivalent units due to a low Zr content caused by zircon fractionation. The occurrence of peralkaline units in the anorogenic field

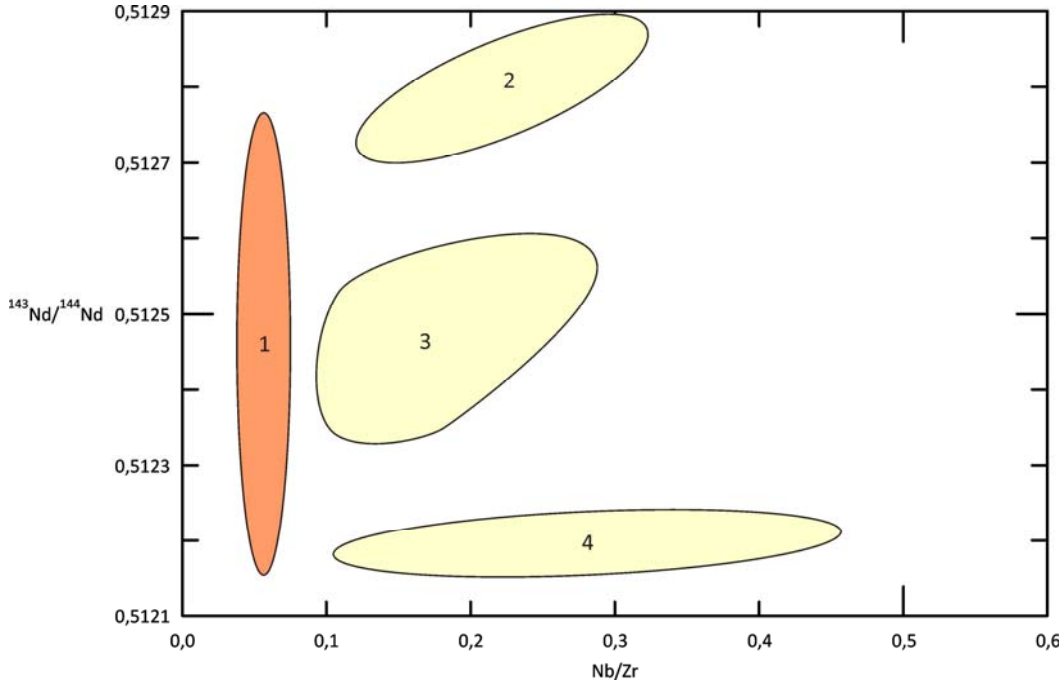

Figure 9.20: This diagram shows the independence between the Nd isotope ratio and the Nb/Zr ratio. 1: orogenic magmatism, available data only include Montresta (Morra et al., 1997) and Arcuentu (Downes et al., 2001) areas; 2: RPV plus samples from Isola del Toro (Lustrino et al., 2000, 2007a); 3) regular anorogenic magmatism (UPV) (Lustrino et al., 2000, 2002; Fedele et al., 2007); 4) Monte Arci complex (Montanini et al., 1994)

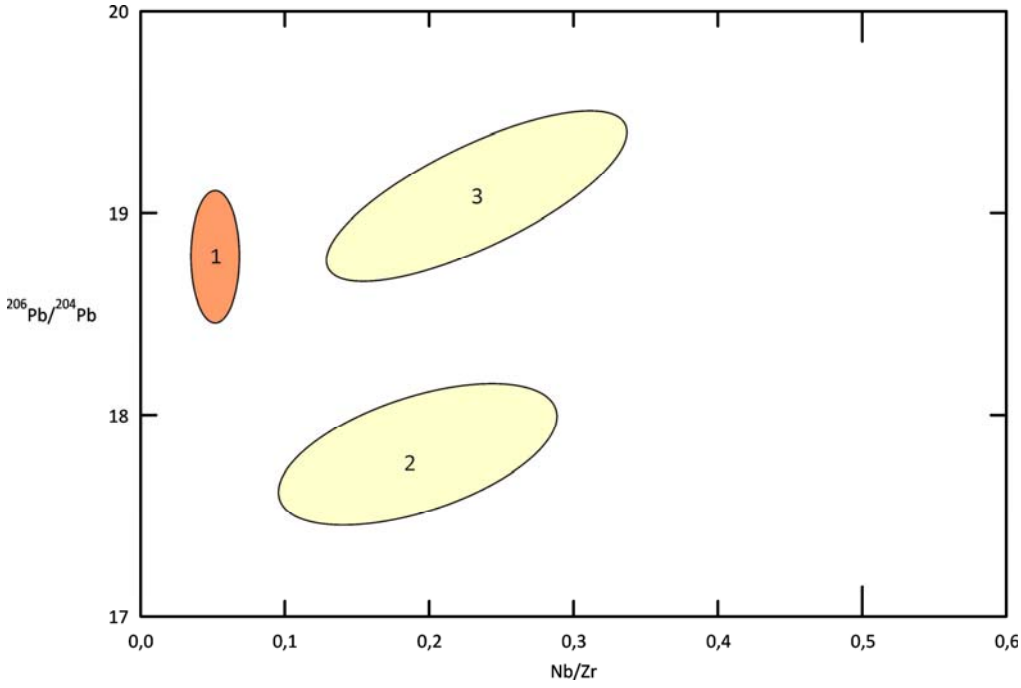

Figure 9.21: 1: orogenic magmatism, available data only include Montresta and Arcuentu areas (Morra et al., 1997; Downes et al., 2001); 2: RPV (Lustrino et al., 2000); 3) regular anorogenic magmatism (UPV) (Lustrino et al., 2000, 2002)

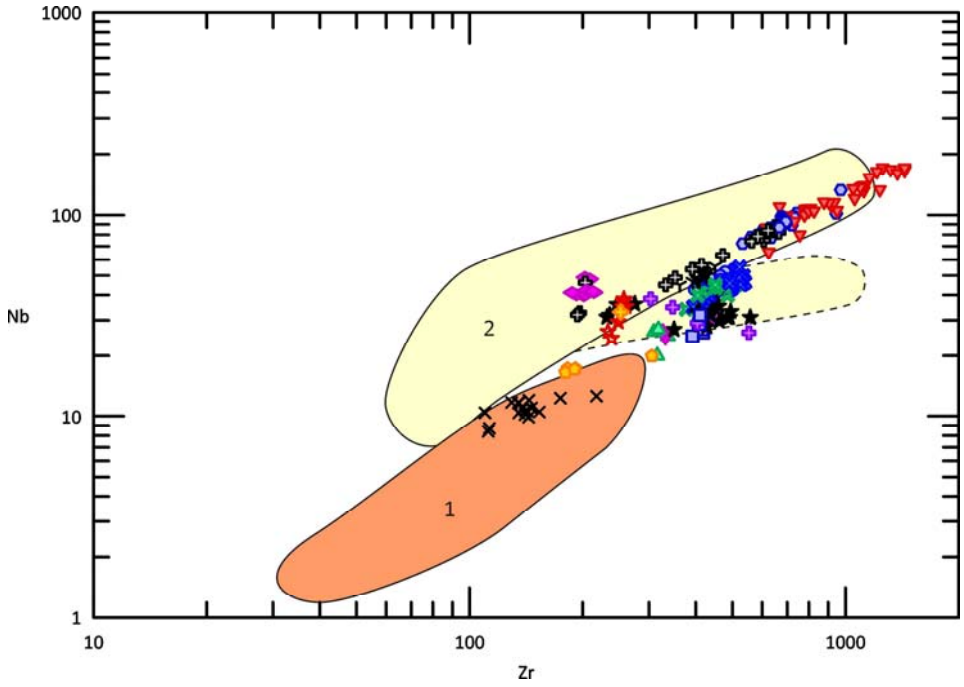

Figure 9.22: Samples from the Sulcis area in the Nb vs. Zr diagram. Concentrations in ppm. 1) orogenic magmatism; 2) anorogenic magmatism

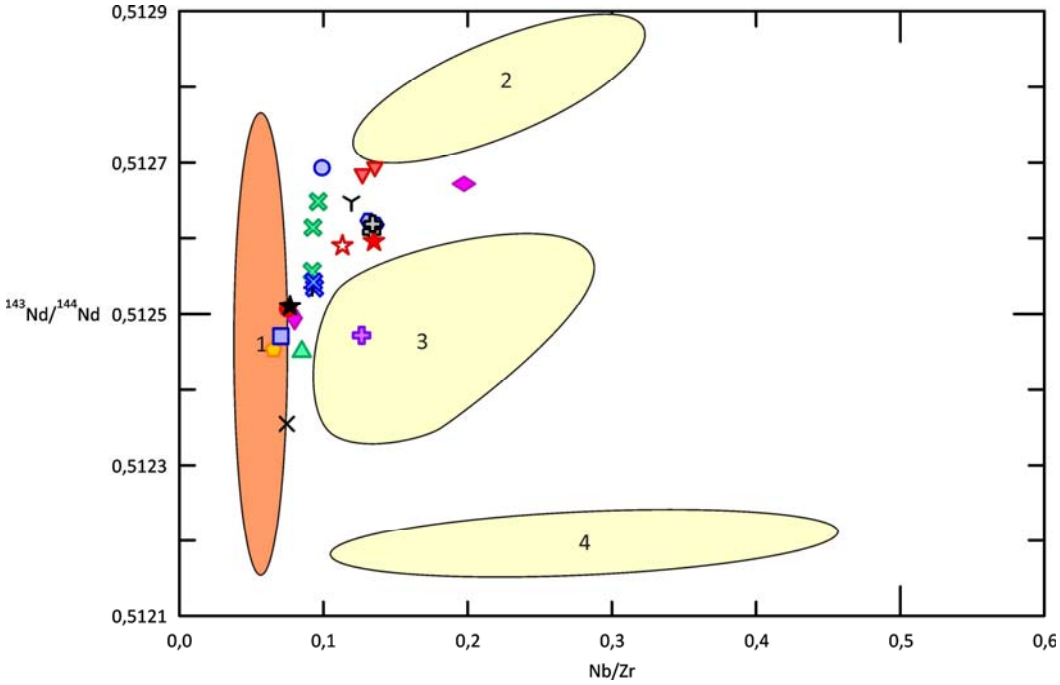

Figure 9.23: Samples from the Sulcis area in the $^{143}Nd/^{144}Nd$ vs. Nb/Zr diagram. 1: orogenic magmatism, available data only include Montresta and Arcuentu areas; 2: RPV plus samples from Isola del Toro; 3) regular anorogenic magmatism (UPV); 4) Monte Arci complex

of these diagrams rules out the orogenic character of this peralkaline suite, which is consistent with observations made all over the world of peralkaline rocks having originated only in anorogenic environments. Figure 9.24 is a TAS diagram showing the area occupied by magmatic series which produced peralkaline melts in subduction environments; the Sulcis ignimbritic sequence falls within the depicted field. If the trachytic samples from Monte Arci are also included in the definition of the anorogenic magmatism field in the Nb vs. Zr diagram, this field expands, including all the ignimbritic sequence from the Sulcis, so it could be stated that the whole sequence belongs to an anorogenic suite.

At the beginning of this section it was observed that the Sulcis ignimbritic suite presents higher alkalinity than the rest of the Oligo-Miocene magmatism, being in the transitional area between subalkaline and alkaline magmas. It was explained that, despite the fact that transitional to alkaline magmas are usually associated to extensional settings, the occurrence of extensional tectonics during the emplacement of the Sulcis suite alone could not account for its different alkalinity, as the rest of the orogenic suite was also generated under extensional tectonics. Apparently extension-related processes cannot alter the alkalinity of orogenic magmas; released fluids maintain high melting degrees in the mantle wedge which preclude any increase in alkalinity. However, it has now been seen that the Sulcis ignimbritic suite was not related to subduction anymore, which explains that under similar extensional tectonics generated magmas

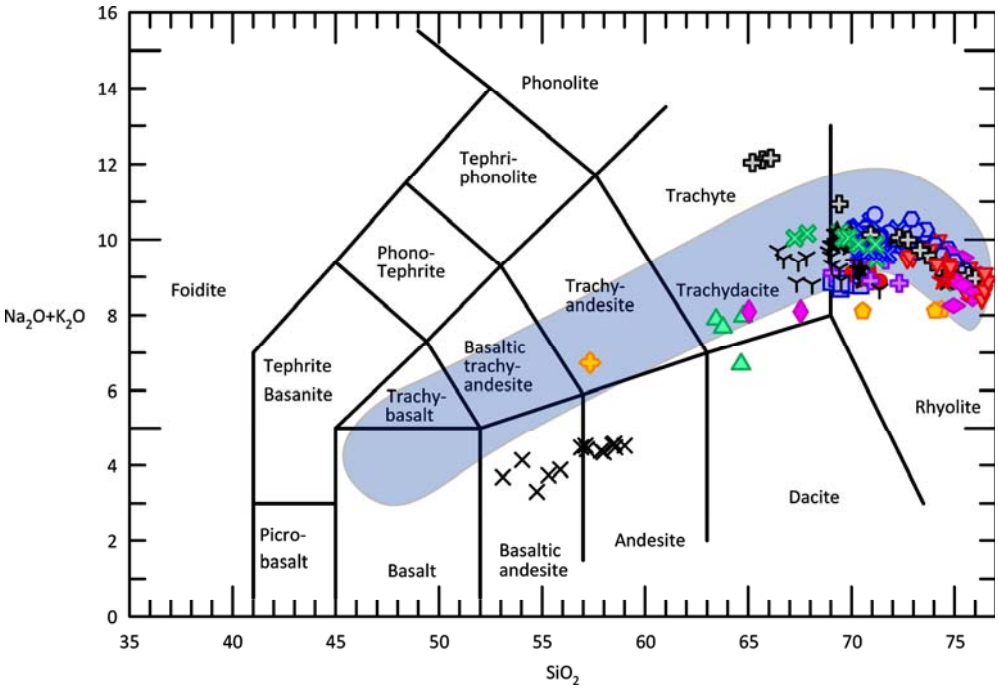

Figure 9.24: TAS diagram showing the field occupied by peralkaline suites associated to subduction environments (Smith, 1976; Nelson and Hegre, 1990; Kiminami and Imaoka, 2006)

were significantly more alkaline, even producing peralkaline rocks. Increased alkalinity was, then, apparently due to the decreasing influence of subduction fluids controlling mantle melting. The decrease in the subduction signature was already observed earlier in this chapter from the observation of isotope ratios. It is though that in the Sulcis area while subduction was active andesitic orogenic magmas were generated, even during increased extensional tectonics. At some point the subduction influence stopped, so there was a decrease in the supply of subduction fluids, which caused melting to be progressively more controlled by extension. At the beginning the mantle source was equal to that present when subduction was active, thus generating nearly orogenic magmas. With time and progressive melting, the mantle source was progressively depleted in subduction fluids, thus generating magmas which tended towards anorogenic affinity. At this point alkalinity in the generated magmas was controlled by both the extensional rate and the residual presence of subduction fluids in the mantle source. The progressive change in the melting mechanism (from fluid to extension dominated) and varying extension rates, produced batches of magma with varying alkalinity, which can be observed in the TAS diagram (Fig. 9.25). In this diagram it can be seen that the ignimbritic sequence in the Sulcis area does not correspond to a single evolutionary trend but to some nearly parallel ones. Only the sequence with higher alkalinity was capable of producing peralkaline magmas (CO, MU, PU), while other slightly less alkaline batches produced strongly evolved magmas but without peralkalinity. The presence of several evolutionary trends can also be observed in other diagrams such as in the Nb vs. Rb (Fig. 9.26).

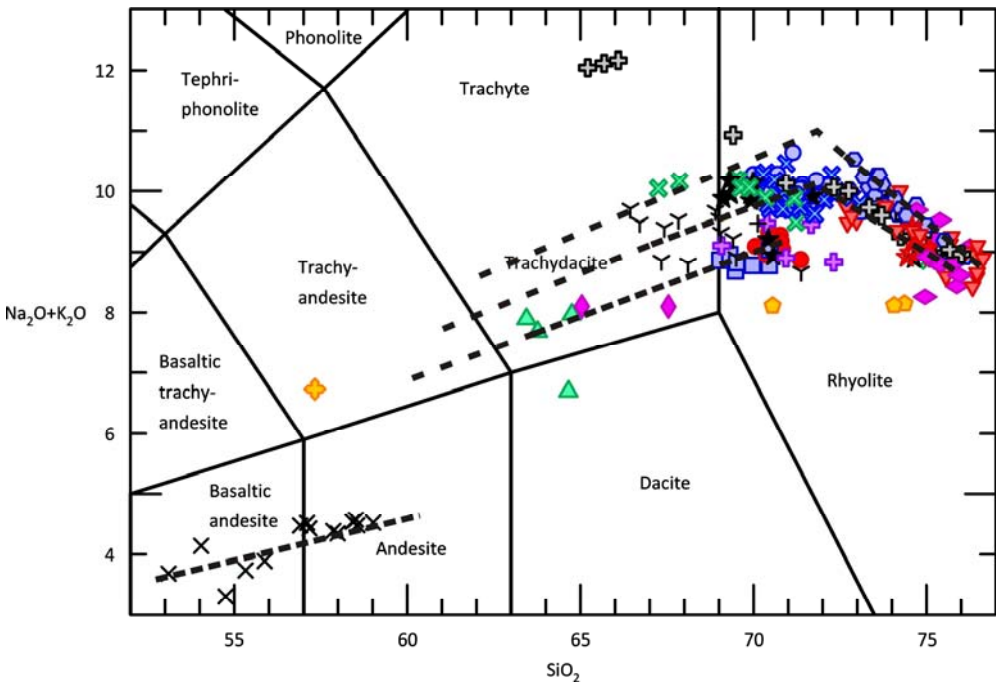

Figure 9.25: Zoom on the TAS diagram. Several evolutionary trends can be observed in the Sulcis ignimbritic suite

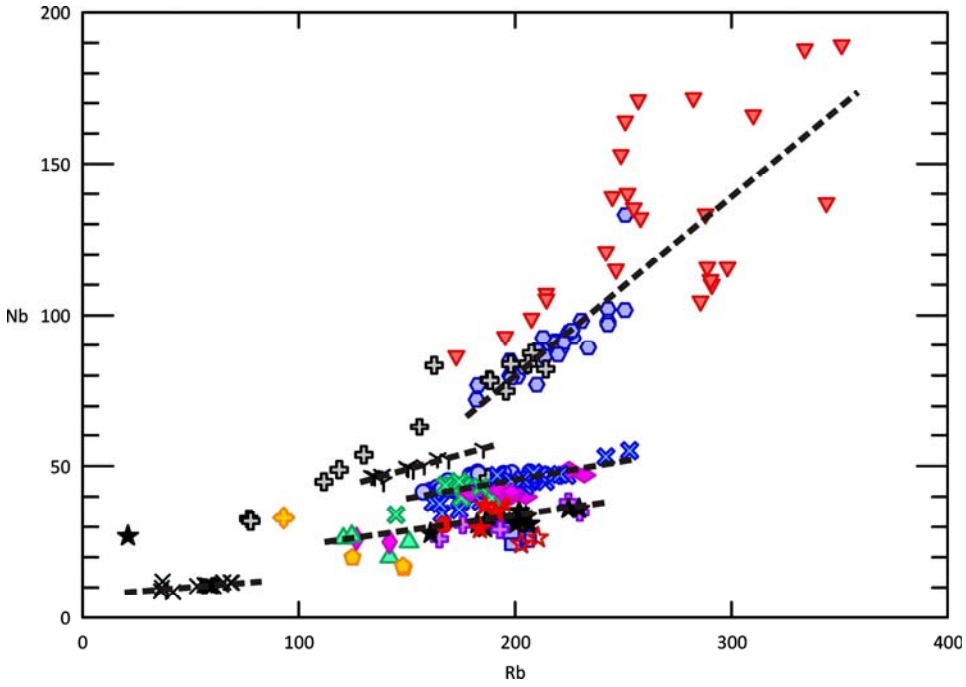

Figure 9.26: Nb vs. Rb diagram showing the multiple evolutionary trends in the Sulcis magmatism. Concentrations in ppm

A way to assess the degree of partial melting controlling alkalinity is to study the ratios between incompatible immobile elements such as REE. Although REE behave in a very similar way, LREE tend to be more incompatible than HREE, so for primitive magmas, the lower the melting degree the higher LREE/HREE ratios are. But in the Sulcis area there are no primitive magmas and original REE ratios are modified by fractional crystallisation. Even if the effect of fractional crystallisation could be weighted and reduced, small heterogeneities in mantle chemical and mineralogical compositions would make it difficult to evaluate the effect of the different degrees of partial melting. These small heterogeneities, combined with varied melting mechanisms, partial melting degrees and magma evolutionary trends are what have provided the existing magma batches with slightly different chemical compositions that have made possible the unit differentiation based on whole rock geochemistry explained in the previous chapter.

9.4 GEODYNAMIC SIGNIFICANCE OF THE SULCIS MAGMATISM

Several processes may be responsible for the end in the influence of the subduction on the Sulcis magmatism; a strong slow down or stop of the subduction, a retreat of the slab relative to the Sulcis area produced, for example, by the elongation of the Sardinian crust due to extensional tectonics, a slab break, or a combination of them all. Next it will be attempted to solve the question on what caused the shift towards anorogenic magmatism in the Sulcis area.

The most recent and reliable datings for the Sulcis ignimbritic sequence are those performed by Pasci et al. (2001) using the $^{40}Ar/^{39}Ar$ method, which produced an age of 15.76±0.16 Ma for NU unit, and 15.1±0.2 Ma for SP. These two datings constrain the age of the upper half of the sequence at between 15 and 16 Ma. The beginning of the ignimbritic activity is much less constrained, for only K/Ar datings are available. Those by Morra et al. (1994) suggest a maximum age around 17 Ma. Considering an emplacement age between 17 and 15 Ma for the whole sequence, the Sulcis represents one of the youngest Oligo-Miocene magmatic manifestations in Sardinia. In fact, until recent times the Sulcis magmatism was considered the last occurrence of the orogenic magmatism in Sardinia (Lustrino et al., 2007a). However, recent datings have shown that orogenic magmatism was present in other areas of Sardinia contemporaneously to that in the Sulcis, and even later. Dating of a series of isolated andesitic lava domes in NW Sardinia produced ages around 15 Ma (terminal andesites in Gattacceca et al. (2007)). And Lustrino et al. (2009) dated a sample from Cuguttada which showed an age of 12.24±0.98 Ma. These datings were performed using the $^{40}Ar/^{39}Ar$ method and are thus considered to be more reliable than previous K/Ar datings. Regarding older manifestations of the orogenic magmatism, datings have shown a climax in magmatic activity around 20 to 18 Ma, coinciding with the climax in rotation of Sardinia. Apparently, after 17 Ma magmatic activity was greatly reduced, being mostly represented by the Sulcis magmatism and finally only by some sporadic events as those of the terminal andesites and Cuguttada. The presence of magmatic orogenic activity at 16-18 Ma is at the moment difficult to assure because the only datings presenting these ages are K/Ar; there is a lack of systematic $^{40}Ar/^{39}Ar$ dating of the whole Oligo-Miocene magmatism in part because this method has been used in Sardinia only in studies published after the year 2000. Available $^{40}Ar/^{39}Ar$ data show ages above 18 Ma in all cases but for the two explained exceptions. It is clear at least, though, that orogenic activity occurred in Sardinia contemporaneously (terminal andesites) and after (Cuguttada) the emplacement of the anorogenic Sulcis ignimbritic sequence. Therefore, whichever process caused the transition from orogenic to anorogenic magmatism in the Sulcis, it was restricted to that area. This fact rules out a general stop or slow down of the subduction, for this process would have affected the whole orogenic magmatism.

The second mechanism proposed to explain the transition from orogenic to anorogenic magmatism in the Sulcis area has been the retreat of the subduction zone away from the Sulcis caused by the progressive elongation of the Corsica-Sardinian microplate. This process could appropriately explain the occurrence of this transition in just one place along Sardinia. Considering this hypothesis, as the trench moved eastward away from the Sulcis, a similar displacement of the manifestations of orogenic volcanism should be expected, at the same time

that in back-arc positions the transition between orogenic and anorogenic magmatism took place. However, no signs of Oligo-Miocene magmatic activity with appropriate ages have been found E of the Sulcis. Therefore this mechanism is also ruled out. To further constrain the process involved, revision of posterior magmatism and geodynamic activity in the area is required.

The Plio-Pleistocene magmatism of Sardinia has been related to the extensional setting caused by the opening of the Tyrrhenian (Sartori et al., 1989), which was caused by the reactivation of the roll-back that caused the drifting and rotation of Sardinia (Serri, 1990). This extension produced in southern Sardinia the formation of the Campidano graben. Lustrino et al. (2007a) studied and dated the Isola del Toro (10 km south of Santo Antioco Island), which is made of alkaline anorogenic magmas and presents an age of 11.83±0.1 Ma. The authors claimed it to be the oldest manifestation of the anorogenic magmatism in Sardinia. Considering the anorogenic character of the Sulcis ignimbritic magmatism discussed previously, and the geographic proximity of the Isola del Toro to the Sulcis, it is suggested that magmas that formed this island were related to the same process that generated the anorogenic magmatism in the Sulcis, and not to an early manifestation of the Plio-Pleistocene anorogenic suite. The older manifestations of the true Plio-Pleistocene anorogenic magmatism are found in southern Sardinia (Capo Ferrato, Rio Girone and Guspini) and correspond to the RPV (Lustrino et al., 2000); these are dated at 6.5 to 4.5 Ma (Lustrino et al., 2007b). RPV are volumetrically minor in the context of the whole anorogenic suite and are related to the beginning of the opening of the southern Tyrrhenian. The rest of the anorogenic Plio-Pleistocene magmatism was active between 5 and 0.1 Ma and presents two periods of increased activity at 5-2 and 1.2-0.1 Ma, which have been related to the higher extensional tectonics that caused the opening of the Vavilov and Marsili basins respectively in the southern Tyrrhenian area (Argnani and Savelli, 1999) (Fig. 9.27).

The Tyrrhenian Sea is divided into two parts by a major E-W structural discontinuity at 41°N (Wezel, 1985). Both sectors are characterised by different direction and rates of extension, which reached in the southern part the oceanic stage (Vavilov and Marsili basins) (Serri, 1990). The northern region is shallower and is characterised by lower extension rates (calculated at approximately 1.3 cm/a) and the occurrence of acidic crustal-derived magmatism, whereas the southern region is deeper and is characterised by higher extension rates (up to 4.8 cm/a) and the presence of basic mantle-derived magmatism forming magmatic arcs and ocean floor in back-arc positions (Argnani and Savelli, 1999). Sardinia is located mostly south of the 41°N discontinuity and its evolution was thus mainly controlled by the opening of southern Tyrrhenian. First evidences of rifting in western Sardinia marking the opening of southern Tyrrhenian date back to late Tortonian-early Messinian (Argnani and Savelli, 1999). The rifting progressed as the trench

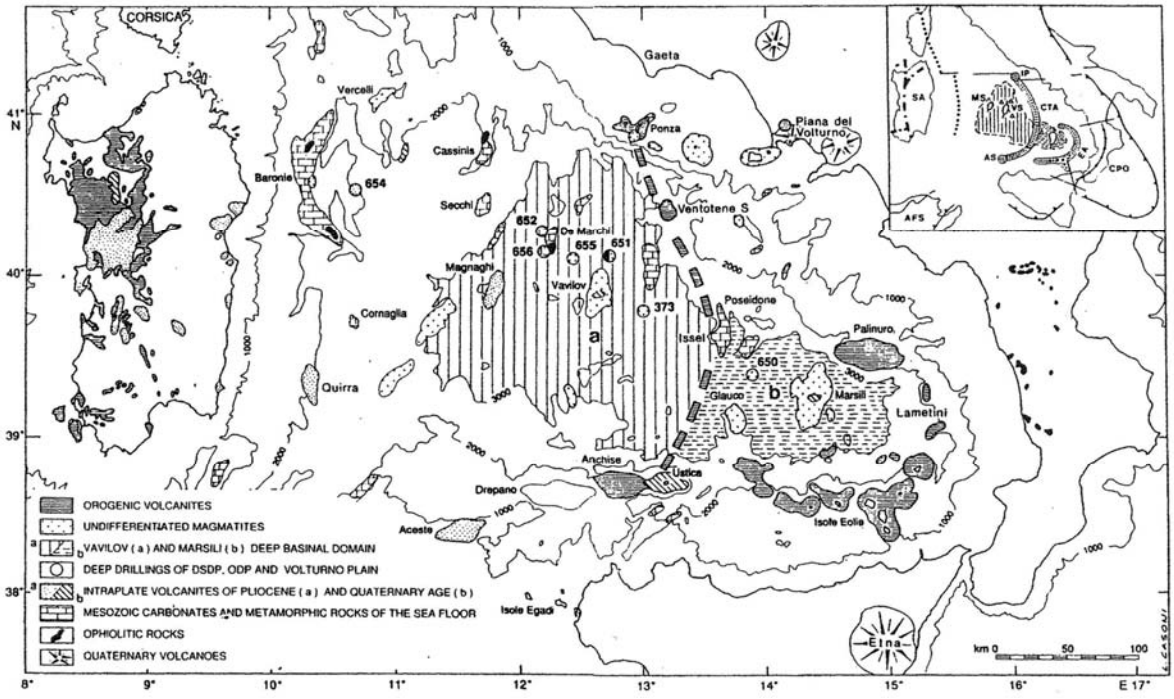

Figure 9.27: Magmatism in Sardinia and southern Tyrrhenian area. a) Vavilov basin; b) Marsili basin. Extracted from Argnani and Savelli (1999)

migrated SE, thinning the continental crust until the formation of the Vavilov oceanic floor. Orogenic magmas were formed in arc positions. Remnants of this arc are currently present between the Vavilov and Marsili basins; recovered samples show ages between 5 and 2 Ma (Argnani and Savelli, 1999). As roll-back migration of the trench progressed a second back-arc basin opened (Marsili), leaving part of the volcanic arc behind, and migrating the rest of it to its current position: the islands and seamounts of the Aeolian area, where radiometric datings show ages from 1 Ma to present (Argnani and Savelli, 1999). Therefore, the opening of the Tyrrhenian was not continuous but instead consisted of two main cycles separated by some hundred thousand years as shown by the two separated Plio-Pleistocene volcanic climaxes in Sardinia and the gap in ages of the Vavilov and Marsili basins and the two volcanic arcs.

Provided data evidence that there is a clear gap in tectonic and volcanic activity between Oligo-Miocene and late Miocene-Pleistocene volcanism of the Sardo-Tyrrhenian area. Extensional tectonics related to the drift and rotation of the Corsica-Sardinia microplate strongly decreased after 18 Ma, after the main rotation phase occurred. The mid to late Burdigalian period is characterised by reduced tectonics, consequence of the final stages of microplate rotation (Speranza et al., 2002) with post-rift deposition in late Burdigalian-Langhian (Sowerbutts and Underhill, 1998). Volcanics in Isola del Toro may represent one of the last consequences of Oligo-Miocene extensional tectonics. Orogenic magmatic activity has its last known manifestation in

Sardinia in the rocks from Cuguttada at around 12 Ma. Therefore, until the first extensional evidences in late Tortonian-Messinian, and the first RPV at 6.5 Ma, there is a gap of nearly 6 Ma in both tectonic and magmatic activity. Such a long interruption in the roll-back activity is difficult to conceive without the participation of some processes affecting the normal subduction progression.

Two processes are envisaged as possibly responsible for this gap and for the cessation in the rotation of the Corsica-Sardinia microplate: collision of the drifting trench and microplate with other plates and/or breaking of the subducting slab. When the Corsica-Sardinia microplate detached from the European continental margin, trench retreat caused a SE-ward drift of the plate. Rotation began later and was most probably produced by different roll-back velocities along the subduction caused by varying properties of the subduction slab and/or collision of the north-eastern margin of the drifting plate with the Italian continental margin. Regardless of the mechanism, the natural evolution of the subduction would have been the progressive consumption of the subducting oceanic crust, which would probably have ended in the complete collision and suturation of the Corsica-Sardinia microplate and the Italian peninsula. However, rotation of the Corsica-Sardinia microplate slowed down after 18 Ma, and ended approximately at 16 Ma (Speranza et al., 2002), leaving this block in its current position. The main explanation for the cessation in rotation could be the collision of the trench and some of the pulled blocks with the African plate. At this point subduction would get stuck, blocked, at the two ends: in the north by the Italian peninsula, and in the south by the African plate. This blocking would not only cause the cessation in the rotation of the studied microplate, but most likely also a strong reduction or almost complete cessation in the subduction, so accounting for the end of magmatism. In this model, after collision occurred stresses would build up until finally breaking the blocking area, thus permitting the trench to continue retreating and to form the Tyrrhenian sea. Drawbacks for this hypothesis are the presence of a deep trough between Sardinia and Africa, which apparently is not consistent with a significant collision between the two plates, the fact that this process would affect all the volcanism in Sardinia and not only that of the Sulcis, and the absence of young orogenic magmatism in Sardinia, especially in the east. If subduction merely stopped for some time, it should be expected to find orogenic magmatism forming upon reactivation, migrating from W to E with time as the trench retreated. The other possible explanation, which is not incompatible with this one, is the breaking of the subducting slab. The hypothesis is that as the Corsica-Sardinia microplate rotated and approached its final position, the subducting slab broke apart.

The Corsica-Sardinia microplate is only one of the many continental microplates that were detached from the European/Iberian continental margin by the roll-back retreat of the studied subduction (Gennesseaux and Stanley, 1983; Séranne, 1999; Zeck, 1999; Edel et al., 2001). Blocks in the southern portion of the trench (south of Sardinia) migrated SE, rotated clockwise and finally collided with the African plate, as the Kabylies did. Blocks in the northern portion drifted SE, rotated counter-clockwise, left Corsica and Sardinia in its current position, and later continued its movement SE-ward as the trench continued to retreat; this is the case for the Calabrian microplate. The trench segment between the two sectors moving differently was the one undergoing higher subduction velocity and having longer subducted slab length, so it was probably subjected to stronger tectonic stresses. Séranne (1999) proposes the presence of a transform zone separating both sectors, the North Balearic Transform Zone (NBTZ). Either if a transform zone actually divided the subducting slab or if the slab was in structural continuity but subject to strong stresses, the slab region present between the Corsica-Sardinia microplate and the Kabylies most probably represented a weaker portion of the subducting slab where breaking of it could start. The proposed hypothesis is that at some point during the rotation of the Corsica-Sardinia microplate the slab under Sardinia broke, and that the breaking started S of Sardinia, either at the NBTZ if it existed, or at the weaker region separating the northern and southern sectors of the slab. The fracture would progress from S to N, progressively shearing the lower region of the subducting slab and rapidly sinking it into the mantle thanks to the slab pull, generating a slab window (Fig. 9.28). The beginning of the breaking is thought to be caused by the slab pull having surpassed the breaking threshold of the slab, and/or maybe being triggered by collision of the trench with the African plate. Breaking of the slab would produce a reduction in the slab pull, which in turn would cause a slowdown in the subduction velocity and consequently in the roll-back retreat and rotation of the microplate. From the point of view of the magma genesis, for this model to work the breaking of the slab would have to be significantly above the fluid-production depth. The sinking of the broken slab portion would be faster than the arrival of new subducting crust, thus generating a slab window and causing a stop in the supply of subduction fluids in the regions with broken slab, while more to the north, where the slab was still in continuity or just recently broken, the supply would still continue. Thus, this mechanism can explain the temporal coexistence of orogenic and anorogenic magmatism in Sardinia. The magmatism in the Sulcis would reflect the breaking of the slab and the transition from orogenic to anorogenic magmatism while in northern Sardinia there was coeval orogenic magmatism, which would represent the magmas generated in portions of the mantle where subduction was still producing fluids. The strong decrease in orogenic magmatism activity would be caused by the severe slow down in subduction velocity. It is probable that if extensional tectonics had continued

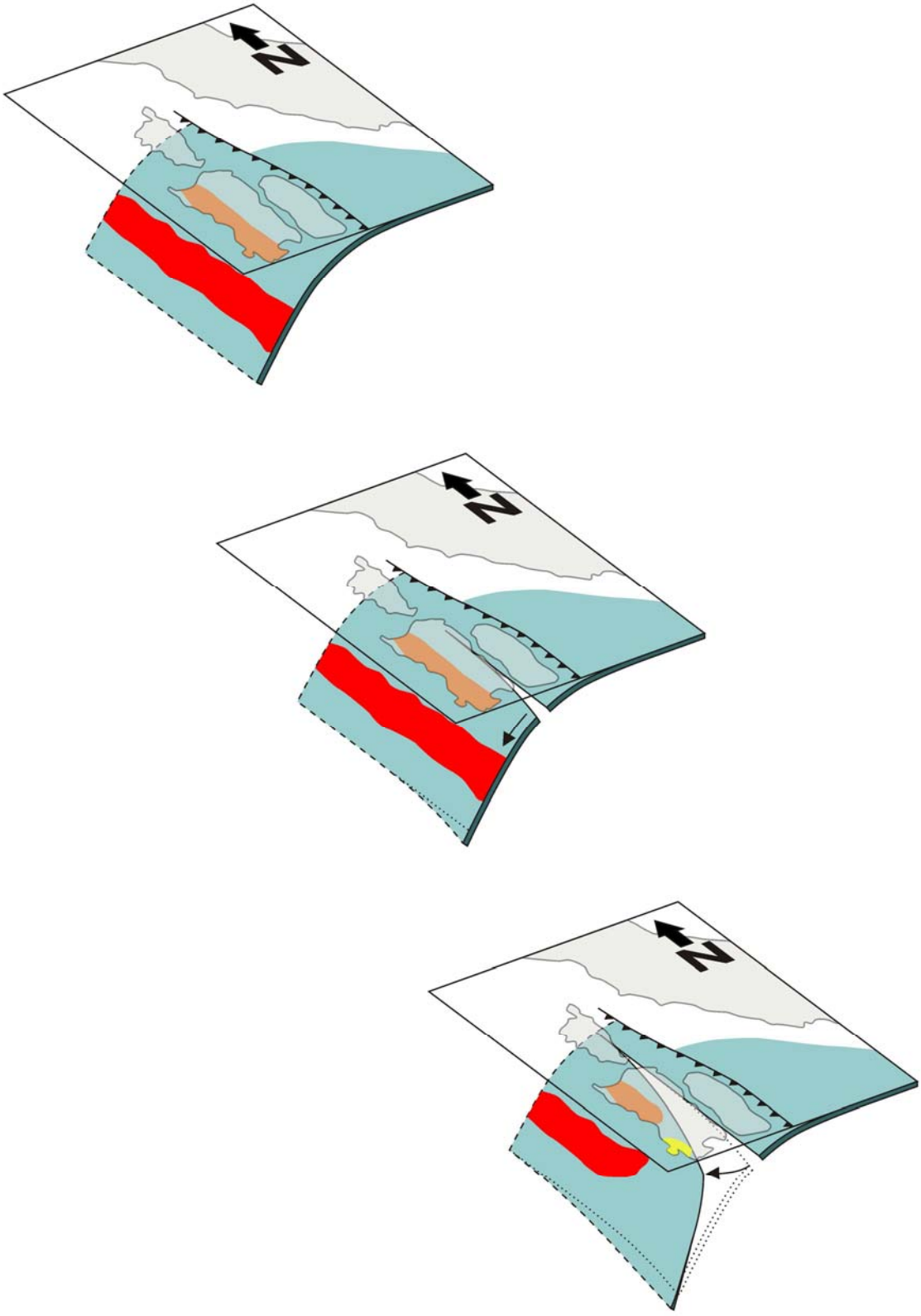

Figure 9.28: Schematic diagram of the proposed hypothesis on the evolution of the subduction. The red area represents the zone of fluid release and orogenic magma production. The orange area is the zone where orogenic volcanism in Sardinia occurs. The yellow area represents the anorogenic magmatism in the Sulcis, which occurs contemporaneously with the orogenic one

for some time, anorogenic magmas would have progressed from the Sulcis to the north, following the progressive slab breaking and sinking. According to this model, observed cessation in magmatism and almost absent tectonic activity in Sardinia after the Oligo-Miocene cycle was caused by a complete break off of a significant portion of the slab. Only after some millions of years the slab pull was capable of reactivating the roll-back mechanism, which finally generated the Tyrrhenian back-arc basin. The absence of Plio-Pleistocene orogenic magmatism in Sardinia fits perfectly in this model. It has been considered that slab break off occurred above the fluid-production depth; therefore, when subduction and roll-back reactivated some time was needed for the new slab to reach this depth so it could start generating orogenic magmas again. This gap in magma production was enough for the magma production zone to move from under western Sardinia (where it was previous to the slab break off) to under what currently is the Tyrrhenian. Magmas generated in this second stage of roll-back are the ones that formed the remnants of volcanic arc found between the Vavilov and Marsili basins, and could also probably be found on the rifted continental crust present between the eatern coast of Sardinia and the Vavilov basin.

The opening of a slab window usually causes an ascent of the asthenosphere beneath the slab to fill the gap. On some occasions adiabatic ascent of this asthenosphere may produce melting. In the Sulcis area, though, no evidence has been found for such melts, either as erupted materials or in the form of trace element or isotopic contamination of the source area of the ignimbritic magmatism.

9.5 CONCLUSIONS

The study of whole rock geochemical data has allowed us to obtain information on the nature of the mantle beneath Sardinia and on the processes affecting its composition, on the melting mechanisms which generated both the Oligo-Miocene and Plio-Pleistocene magmatisms, and on their geodynamic significance.

Regarding mantle composition and structure, it is proposed that the mantle beneath Sardinia presented in pre-Late Cretaceous times an EMI signature which was subsequently modified by the CAP event in Late Cretaceous and by subduction-released fluids from Oligocene to Miocene. The CAP event metasomatised the existing mantle by introducing a HIMU signature which produced a change in composition of the mantle from EMI towards EAR-like. Metasomatism was not complete and left a diffusely stratified mantle with an upper part presenting an EMI signature and a lower more EAR-like region, both of them having an OIB mantle source-like composition. Subduction released into the mantle wedge hydrous fluids and partial melts carrying sediment

and MORB isotope and trace element compositions, which introduced mostly into the more EAR-like mantle a subduction signature.

Oligo-Miocene orogenic magmas were produced in the subduction-modified more EAR-like mantle portion by lowering of the melting temperature due to the input of subduction fluids. Increased extensional tectonics during the rotation of the Corsica-Sardinia microplate resulted in a higher volume of erupted magmas but not in a modification of its subalkaline calc-alkaline character. The andesitic lower sequence in the Sulcis shared its orogenic origin with the rest of the Oligo-Miocene magmatism in Sardinia. The ignimbritic sequence, instead, unlike all the previous petrogenetic theories considering it as part of the orogenic magmatism, is thought to represent a transition from orogenic to anorogenic magmatism. It is suggested that the transition was due to a change in the melting mechanism from fluid- to extension-controlled related to the cessation in the subduction influence below the Sulcis. This process produced a modification in alkalinity of the generated magmas, which changed in character from subalkaline to transitional or mildly alkaline, promoting the generation of peralkaline magmas. Until now comendites in the Sulcis were the only example of peralkaline magmas interpreted to have originated from orogenic magmatism; the interpretation of these magmas as anorogenic rules out this exceptionality, considering these magmas as one more regular occurrence of peralkalinity in anorogenic environment. The production in the Sulcis of transitional to anorogenic magmas was contemporaneous with the continuation, although strongly reduced, of the orogenic activity in northern parts of Sardinia. The mechanism proposed to explain the simultaneous occurrence of both magmatism types is the formation of a slab break-off which started south of Sardinia and progressed northward opening a slab window. Slab break-off not only explains the occurrence of anorogenic magmas, but also the strong slowdown in subduction and roll back of the trench, which produced the 6 Ma-long pause in magmatic and tectonic activity between the end of the Corsica-Sardinia rotation and the opening of the southern Tyrrhenian basin.

Plio-Pleistocene magmas in Sardinia were anorogenic and were formed mostly in the upper EMI mantle by pressure release due to extensional tectonics related to the opening of the southern Tyrrhenian basin.

CHAPTER 10: PETROGENESIS II. FROM MAGMA TO ROCK

The discussion on source and melting mechanisms of the magmas in the Sulcis area and its geodynamic significance has been tackled in the first part of this petrogenetic discussion section. In this chapter, which complements the previous one, the evolution of magmas from their formation to its eruption is discussed.

10.1 INTRODUCTION

Partial melting in the mantle produces small quantities of melt, which is located in intergranular positions. As melting progresses, melts tend to concentrate in increasingly bigger magma pockets, which can finally become big enough as to move through the mantle driven by density differences. Since the density of basaltic magmas generated by partial melting is lower than that of the surrounding mantle, magmas ascend towards the surface. During its ascent through the mantle and crust, cooling and contact with wall rock promote magma evolution by processes of fractional crystallisation and assimilation. Ascent history of magmas is conditioned by its density and by the density and structure of the mantle and crust, as well as by the tectonic setting, and typically involves stagnation at one or several structural levels in magma chambers, which favours its evolution, including magma mixing as a third factor conditioning magma composition. Progressive cooling and crystallisation of stagnated magma in the end turn the magma chamber into a crystalline plutonic body. Volcanic eruptions represent events during which the magma chamber is opened and part of its content is expelled at the surface, being rapidly solidified so stopping its magmatic evolution. Thus, volcanic rocks formed during a single eruption represent samples of the cooling magma at a given evolutionary stage. In places where a magma chamber is

periodically tapped by eruptions the resulting volcanic rocks show the same magma at different evolutionary stages, allowing a detailed study of the evolution of that particular melt.

10.2 EVOLUTIONARY TRENDS AND MAGMA BATCHES

In a typical case, multiple sampling of a magma chamber by successive eruptions shows in geochemical diagrams linear evolutionary trends which are the product of magma chemistry modification mainly by crystal fractionation of a mineral assemblage with an overall composition different from that of the melt, usually more primitive. As a result, magma chemistry is progressively modified towards more evolved compositions so the younger the eruption the more differentiated the erupted products are. In the Sulcis suite, though, several evolutionary trends have been observed representing magmas of different original compositions, and even in a single trend some units may present more primitive compositions than older ones (AC relative to LE for instance), evidencing several successive differentiation processes. These facts show that the Sulcis suite is the product of the evolution of several magma batches.

In the TAS diagram of the Sulcis suite (Fig. 10.1) the presence of several evolutionary trends is clearly seen. As explained in the previous chapter, this magmatic suite cannot be attributed to a single evolutionary trend as proposed by Morra et al. (1994), but instead it is the product of the evolution of several magma batches with slightly different initial chemical composition. Trends in the TAS represent the evolution of batches with different initial alkalinity (the origin of these

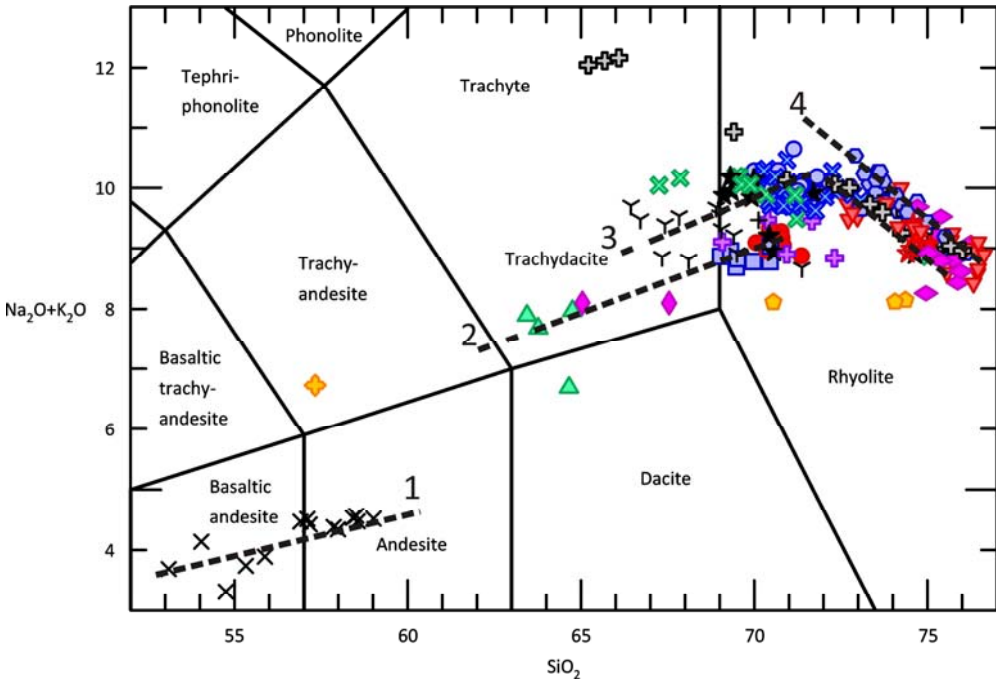

Figure 10.1: Zoom of the TAS diagram showing the presence of several evolutionary trends in the Sulcis suite. Contents in wt %

differences has been discussed in the previous chapter), which produced subparallel trends. Four main trends are depicted, which does not mean these to be the only ones present. Trend one is marked by the evolution of the orogenic suite, represented by rocks of basaltic andesite and andesite compositions. In other areas of Sardinia the evolution of this magmatism produced more evolved compositions than those in the Sulcis, reaching the rhyolite field. Trend two is marked by the first transitional to anorogenic rocks occurring in the Sulcis, those of the basal ignimbritic units (CM, LE, AC and SE). This trend was run at least twice, from CM to LE and from AC to SE. Therefore, between LE and AC there was an input of primitive magma in the system. The third trend can be subdivided in two parts by the inflexion it shows at approximately 72 wt % SiO_2. The lower silica part does not present a clear linear trend, but instead there is a cluster of data around the position of the NU unit. This trend represents the evolution of a second population of magmas which were more alkaline than those that generated the lower ignimbritic units of trend two. To this trend belong important units such as NU and SP, and evidently includes the evolution of several magma batches separated in time because several more evolved units erupted between these two ignimbrites. The upper half of the trend, richer in silica, is shown by two of the more evolved units in this suite, PA and PM, which, however, did not reach peralkalinity. Its origin has been tentatively linked to the evolution of magmas similar to those in the first half of the trend, and as a whole the third trend represents the most alkaline magmas that do not reach peralkaline compositions. The last trend depicted in the diagram is marked by the peralkaline units (CO, MU, and pumice poor facies of CF). This trend is located parallel to and above the upper half of the third trend, and could be regarded as equivalent to it but belonging to a more alkaline suite which, if more magmas belonging to it had been erupted, would probably depict a lower half equivalent to that in the third trend but in more alkaline positions. A second possibility would be to consider the peralkaline units as having originated by further evolution of the more alkaline magmas belonging to the third trend while PA and PM would form from the less alkaline ones. These two possibilities are discussed in the last section of this chapter.

Among other evidences, changes in alkalinity and returns to more primitive compositions mark the arrival of new batches of magma. Figure 10.2 presents the silica content along the volcanostratigraphic sequence, evidencing arrival of new more primitive magmas to the system. Study of diagrams as those in Figures 10.1, 10.2 or Nb vs. Rb (Fig. 10.3) and of differences in phenocryst assemblages allows us to infer the minimum number of magma inputs that formed the ignimbritic sequence of the Sulcis area. CM, LE, AC and SE plot along a common trend where LE and SE could be regarded as having evolved from CM and AC respectively. In this sense CM and LE, and AC and SE could be considered to have formed from two different magma batches, both

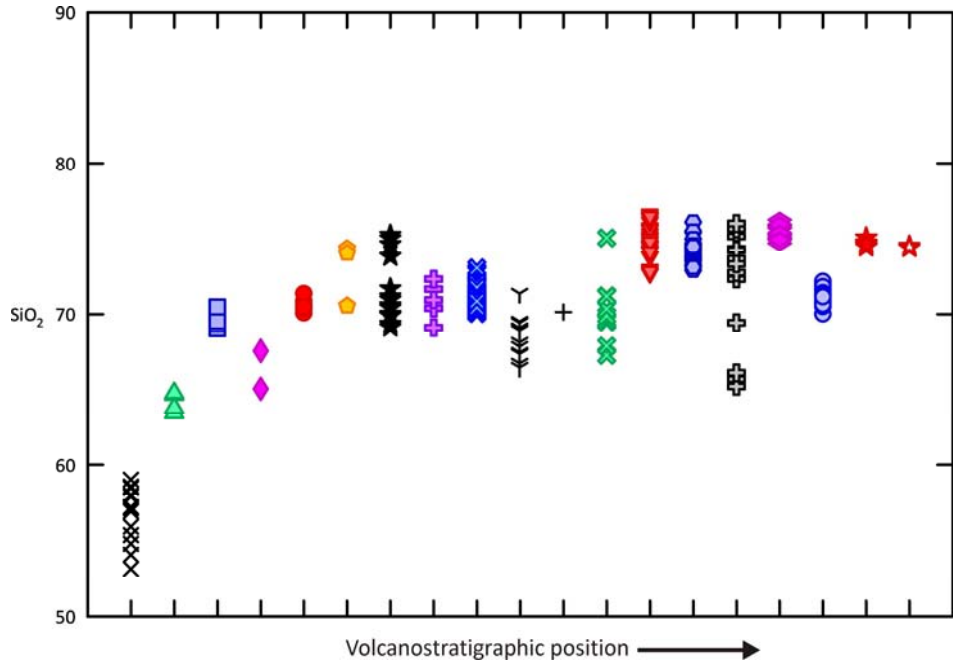

Figure 10.2: Change in the silica content (wt %) along the volcanostratigraphic sequence

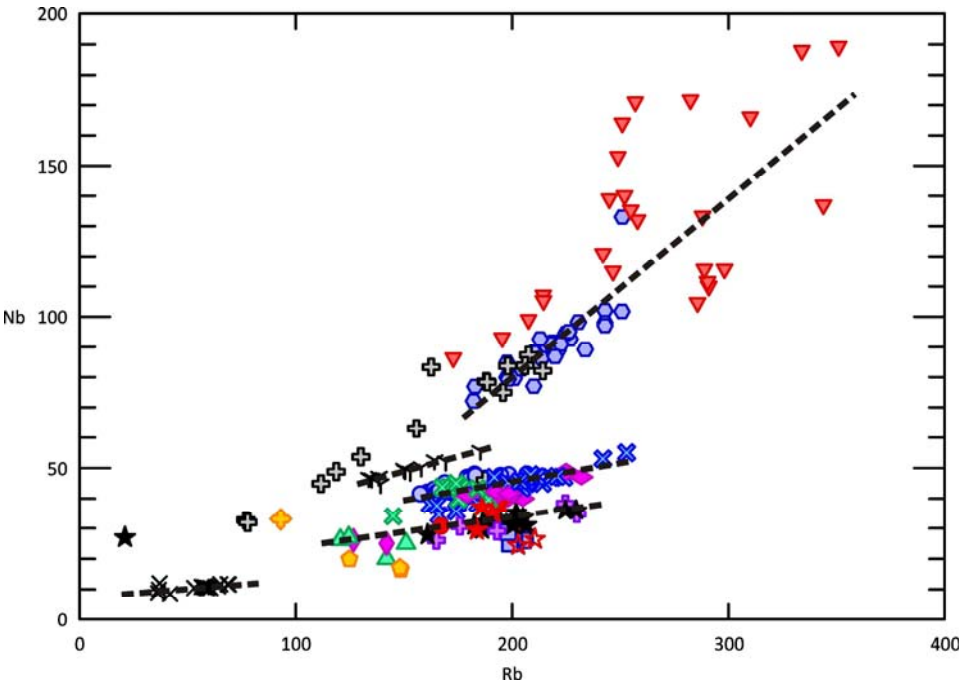

Figure 10.3: Nb vs. Rb diagram showing several evolution trends. Contents in ppm

of them having been sampled twice. MLN presents lower alkalinity and its feldspars (plagioclase) are more anorthitic than those in SE; therefore it was formed from a new magma input. MC formed from a magma more alkaline than that of MLN and the rest of the lower ignimbrites. In some facies MC presents dark pumices; their chemistry has not been yet analysed because they have been found in altered or silicified condition, but they could represent a late input of new magma into the chamber, which mingled with the one previously present. This new magma might

belong to the new magma batch that subsequently formed CA unit, which is very similar to MC in whole rock chemistry but that presents slightly more primitive compositions, which is also evidenced by feldspar compositions. NU unit formed from a magma slightly more alkaline than that of MC and CA, and is clearly separated from them in diagrams separating the different trends such as the Nb vs. Rb. PC is more primitive than NU, and represents a bit more alkaline magma which had the particularity of being impoverished in K_2O with respect to Na_2O if compared to other units with a similar evolutionary degree. This had consequences in the crystallising feldspar assemblage, which will be later discussed. Little can be said of MCR unit except that it was formed from a magma more similar to that of NU, but being less evolved. MZ is a complex unit formed by several ignimbrites sharing a similar chemistry and thus thought to have formed from the same magma batch. Special characteristics of this magma, such as a high water content, produced a chemistry similar to but less evolved than that of NU with the presence of abundant biotite, which is only found in significant amounts in this unit. Peralkaline units (CO, MU and CF) were formed from the most alkaline magmas. It is at the moment difficult to assess whether the several ignimbrites and lava flows forming CO originated from one or several magma batches; a more detailed volcanostratigraphic and geochemical study needs to be done. MU presents slightly different compositions and is less evolved than CO, thus representing a new magma batch. MU, like MC, presents dark pumices which could be regarded as the product of magma mingling by a late input of probably less evolved magma. CF unit depicts in geochemical diagrams a mixing trend between a composition very similar to that of MU and the composition of the black pumices which are the characteristic feature of this unit. Feldspar phenocrysts in the black pumices did not crystallise from the black melt, as evidenced by the instability textures that present and by the Eu positive anomaly of black pumices whole rock analyses. These crystals were collected by the incoming magma probably from a cumulate. It is difficult to calculate the original composition of the black melt, but subtraction of feldspar compositions from black pumice whole rock composition results in a reduction of alkalinity while maintaining approximately constant the SiO_2 content. Therefore, black pumices represent the arrival of a markedly more primitive magma to a peralkaline magma chamber. Considering evidences suggesting almost simultaneous eruption of CF and MU units (in San Pietro Island condensed MU is extremely welded and shows vitrophyre formation in a deposit less than a meter thick; these features are considered to have been difficult to form without the heat and load contribution of the next ignimbrite, CF unit, which is thus thought to have been emplaced immediately after), and the very similar composition of MU and the peralkaline end-member of the CF unit, it is thought that both units originated from the same magma chamber, but with black pumices marking a new input of magma. PA unit represents a new magma that also reached high levels of differentiation, but which presented a less alkaline

composition. SP was formed by a more primitive magma than PA. Finally, PM and CL units are also highly evolved, only slightly less than PA, and could be regarded as having evolved from the remnants of the SP magma. However, in the Nb vs. Rb diagram these last units fall in a different trend, thus suggesting that they originated from a different magma batch. It is seen, so, that except for LE and SE units, which can be considered as formed from the same magmas batches than the immediately previously erupted units (CM and AC respectively), the rest of the units of the ignimbritic sequence reflect each one the input and evolution of a new magma. The study of the presence of one or several magma chambers, its evolution and interaction, the effects of new magma arrivals, the causes of such a limited sampling of each magma batch and of the absence of the primitive terms of this magmatic suite, among other issues, needs to be addressed to gain a better understanding of the magmatic system but is beyond the scope of this work. It will be tackled in the future.

10.3 GENERIC MAGMA EVOLUTION

Factors controlling magma composition and evolution are mainly three: fractional crystallisation, assimilation and magma mixing. Typically fractional crystallisation is the one having a stronger effect.

10.3.1 Fractional crystallisation

The occurrence of fractional crystallisation as a mechanism for magma evolution may be evidenced either by the products of crystal fractionation (crystal cumulates in a magma chamber, which can be sampled as xenoliths in volcanic materials or studied in presently exposed magma chambers) or by the effect it has on the chemical composition of magmas. Trends in binary diagrams are the product of the fractionation of given mineral assemblages, which may change as the magma evolves. The current fractionating assemblage at the time of eruption is recorded as phenocrysts in the volcanic rock.

Harker diagrams of major element versus silica contents show the evolutionary trends for the studied magmas (Fig. 10.4). Although it has been argued before that magmatism from the Sulcis presents several evolutionary trends, these are the product of similar mineral fractionating assemblages. The observed trends are the result of only slightly different initial magma compositions, which produced small variations in the fractionation assemblages and thus in the evolutionary trends. Keeping this fact in mind, these trends are similar enough as to use them together to interpret which have been the mineral phases involved in magma evolution. Until quartz crystallisation and fractionation is reached (in this study case it only occurs with

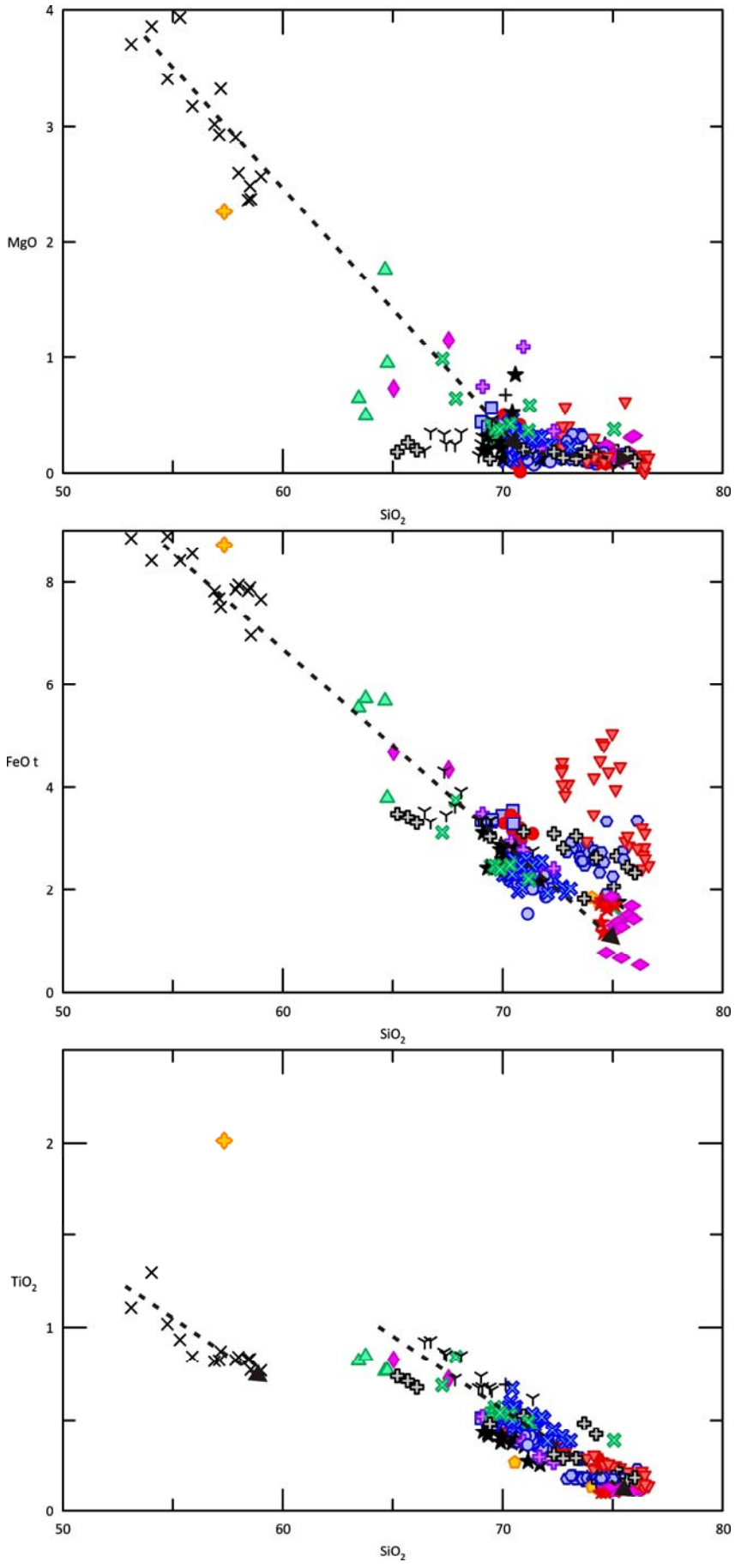

Figure 10.4: Major elements versus silica. Concentrations in wt %

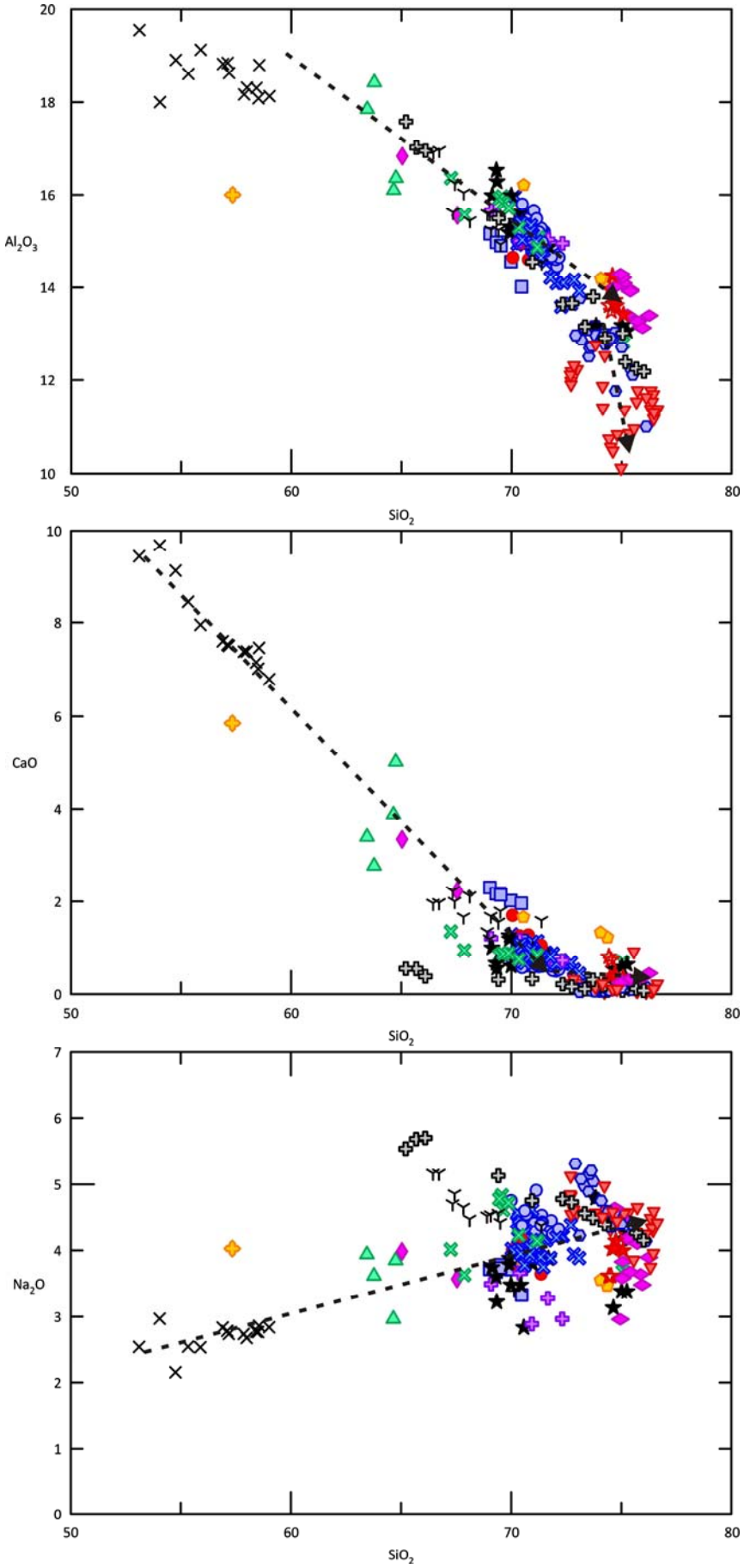

Figure 10.4: (Continuation)

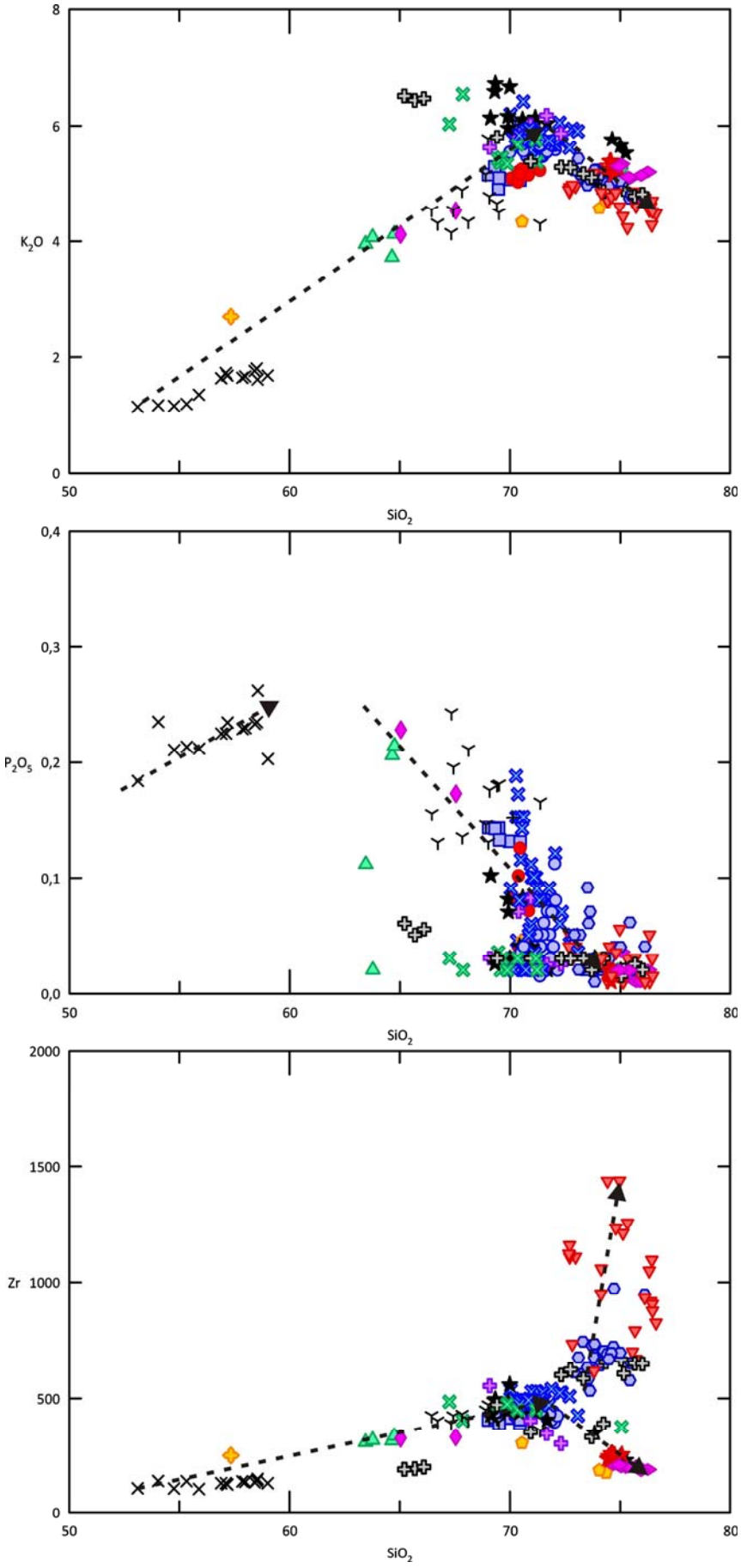

Figure 10.4: (Continuation). Zr concentration is in ppm

peralkaline units), crystal fractionation produces enrichment in SiO_2, whose content can be regarded as an indicator of the magma evolutionary stage.

Magnesium content drops rapidly from the more mafic Andesites to the ignimbrites containing about 70 wt % SiO_2. This drop is attributable to abundant fractionation of Mg-rich mafic minerals, such as olivine, pyroxene, amphibole or biotite. Regarding olivine, it is only found as accessory unstable remnants in andesites, so it cannot be a main fractionating phase for andesitic melts, although it probably played an important role in reaching andesitic compositions starting from the initial basaltic melts. Amphibole is only found as accessory phenocrysts in CM and AC units, and altered in SP, and biotite only occurs significantly in MZ unit. Therefore, the main fractionating mafic phase must have been pyroxene, which is found as phenocrysts in units containing less than ca. 70 % silica. The decrease in the slope of MgO content trends after this SiO_2 content indicates that at this point in evolution pyroxene stopped being a significant fractionating phase. In the analysed pyroxenes MgO dominates over FeOt, thus explaining the stronger depletion in MgO compared to FeOt, which presents a steadier decrease. Occasionally, in the more water-rich magmas amphibole or biotite may have had a stronger influence.

Iron content drops at an approximately constant rate for the whole sequence, except for comendites. Iron may fractionate as component of both silicate mafic minerals (pyroxenes, amphiboles and biotite) and spinel. Since pyroxene fractionation ceases to be significant after 70 wt % SiO_2, amphibole, biotite and spinel may be responsible for the FeOt content decrease above this value. Comendites show a marked enrichment in iron content, typical of peralkaline magmas by fractionation of an almost exclusively felsic mineral assemblage. In peralkaline magmas strong iron enrichment in the melt is thought to be possible thanks to the complexing of the iron ions with unbound alkalis, which stabilises it (Noble, 1968).

Titanium is mainly fractionated in spinel and biotite. Spinel is present throughout the sequence, while biotite only occurs occasionally. Andesitic and ignimbritic sequences depict two clearly separated trends.

Trends in Al_2O_3, CaO, Na_2O and K_2O evidence the fractionation of feldspars. Al_2O_3 content draws a steady decrease, reflecting constant fractionation of feldspars (Al-bearing mafic phases contain less Al_2O_3 than magma so its fractionation tends to counteract the feldspar effect). The relative depletion in Al_2O_3 of comendites can be interpreted as the product of continuous feldspar fractionation at nearly constant silica content (which is buffered by the fractionation of quartz). The strong depletion in CaO shows that plagioclase is a major fractionating phase for most of the sequence, as reflected also by its presence as phenocrysts in all units but comendites. The

decreasing slope in the CaO diagram reflects not only the decrease in the relevance of plagioclase fractionation in the more silica-rich magmas, but also the increasingly lower content in CaO of the fractionating plagioclase; plagioclase fractionating in the more silica-rich units reaches oligoclase compositions. K_2O shows an inflection at about 72 wt % SiO_2 from positive to negative correlation with silica. This inflection marks the evolutionary point where alkali feldspar becomes the main fractionating phase. The trend in the Na_2O diagram has a positive correlation with silica, but samples appear more disperse than with other elements. Increasing Ba, Sr, and Eu negative anomalies in spider diagrams confirm the major role of feldspar fractionation (Fig. 10.5). A special case is that of CF unit, whose black pumices are enriched in feldspars collected by the magma, probably from a cumulate, which produces positive Eu anomalies in spider diagrams.

To conclude with major elements, P_2O_5 presents a positive correlation with silica in andesites, and negative in the ignimbrites. The negative correlation is the result of apatite fractionation. This mineral has only been found as an accessory phase in some units, although chemistry demonstrates that it was significantly fractionated throughout most of the ignimbritic sequence.

Finally, zircon has been found as an accessory phase in petrographic observations in some units, so it could have acted as a fractionating phase. However, fractionation was not enough as to deplete Zr in the melt; there is a progressive enrichment of Zr in the magmas, shown by a positive correlation between Zr and SiO_2; the only exceptions are PA, PM and MLN units, which are depleted in this element.

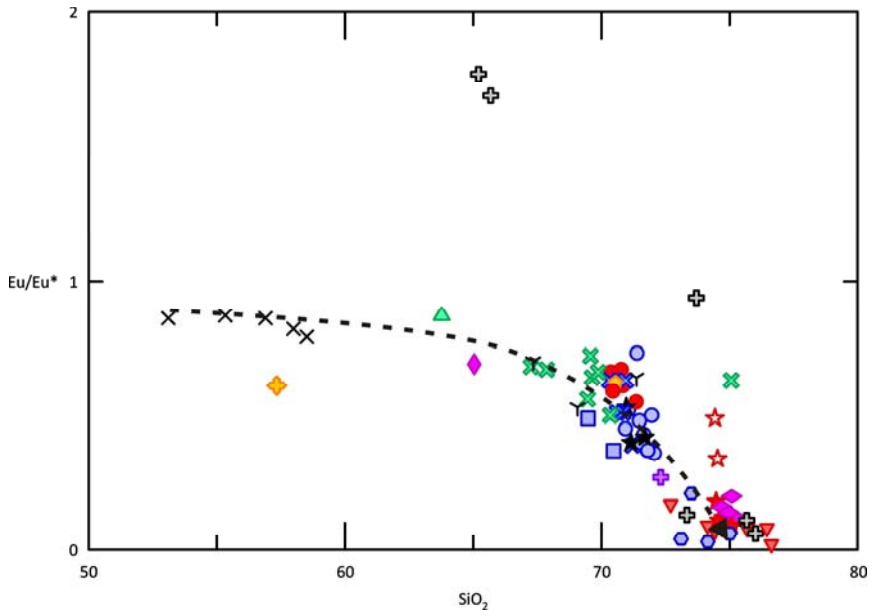

Figure 10.5: Eu anomaly (Eu/Eu*) versus silica content (wt %). Eu* is the expected Eu concentration if no anomaly existed; it is calculated using Sm and Gd normalised values

10.3.2 Assimilation

It has been discussed in the previous chapter that according to isotopic ratios significant assimilation did not occur, so this process didn't play a significant role in magma evolution. The inexistence of any important geochemical distortion in trace element diagrams seems to confirm this hypothesis. Contamination was, however, present, as evidenced by $^{207}Pb/^{204}Pb$ isotopic ratio. The basement in Sardinia consists of Hercynian rocks, with abundant granitoids, and with the presence, in the Sulcis area, of a thick metasedimentary sequence including a thick pile (up to 2000 m) of Cambrian carbonates (cropping out at the Iglesiente horst) and Cretaceous limestones (cropping out at Santo Antioco Island). The short half-life of ^{235}U (compared to ^{238}U and ^{232}Th) quickly modifies the original isotopic ratios of these rocks to compositions farther away from those of an incoming mantle-generated magma. This fact, combined with the abundant content of Pb in basement rocks (which include important Pb-Zn-Ba ore deposits hosted by Cambrian carbonates), make incoming magmas very sensitive to ^{207}Pb contamination. $^{207}Pb/^{204}Pb$ ratios in the studied rocks show the combined effect of initial magma composition and contamination (Fig. 10.6). Where more than one sample per unit has been analysed, it can be seen that these may present isotopic variation. In CO it is not unexpected, because this unit consists of several ignimbrites and lava flows, thus representing magmas erupted over a period of time. Instead, MU is a single eruption unit, which therefore may show the presence of isotopic heterogeneities within the magma chamber. These can be the product of several processes such as differential

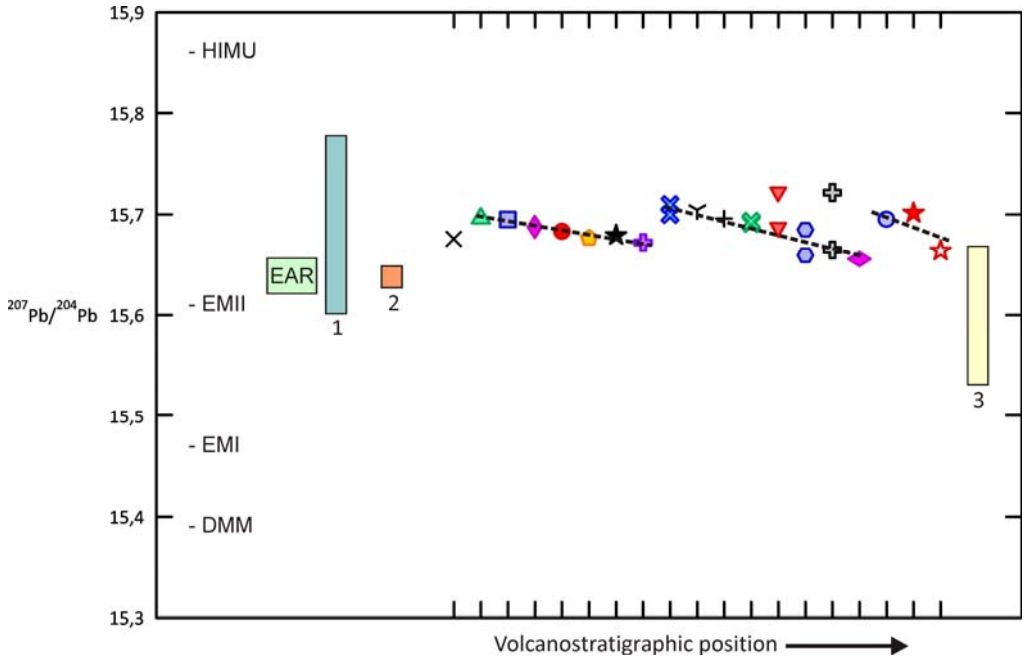

Figure 10.6: $^{207}Pb/^{204}Pb$ isotopic composition of the studied magmas in Sulcis compared to compositions of mantle, sediments (1) and other volcanic rocks in Sardinia (2: orogenic; 3 anorogenic). Data origin in Figure 9.7

contamination and/or incomplete magma mixing.

Three main trends are depicted by analysed rocks of the Sulcis area. The first trend has as end-members CM and CA units, the second one NU and PA, and the third one SP and CL. CM is the first ignimbrite to be erupted. NU and SP are two of the units with a higher volume and dispersion. CA and PA are also units with a large volume, and the product of very explosive eruptions as evidenced by its high fragmentation degree and scarce welding. Several hypotheses can be proposed to explain these trends. At the moment, only a first tentative simplified model is proposed here to explain the existence of these three trends. In the first place, the existence of a single magma chamber is considered, surrounded by wall rocks with a $^{207}Pb/^{204}Pb$ ratio higher than that of the incoming magmas. After the eruption of the andesitic sequence, CM represents a magma which resided for a longer time in the magma chamber, which was probably bigger, thus having more time to interact with wall rock and becoming more contaminated in Pb. The progressive arrival of new magmas into the chamber would progressively dilute this contamination, producing a descending trend. Eruption of CA unit would probably produce a large emptying of the chamber. After that, the evolution of a large volume of magma was needed for the production of NU unit. This large volume had to refill the existing magma chamber and probably expand it, thus needing a longer residence period which would explain the occurrence for a second time of a significant contamination like that seen in CM. This process would have occurred three times, one for each trend. $^{208}Pb/^{204}Pb$ ratios also depict these three trends, although less markedly. This is only a first model and further work (e.g. O isotope studies and accurate geochronology of each unit) needs to be done in order to support or rule out the several possible hypotheses that can be proposed to explain the observed lead isotopic ratios.

10.4 PARTICULARITIES

In the previous chapter section the magmatism in the Sulcis has been studied as a whole to obtain understanding on the general differentiation mechanisms that formed this suite. However, changes in original composition of each magma batch, as well as changes in cooling conditions, produced small differences in the crystallising mineral assemblages and in the final compositions of the studied magmas. In this section several of the particular cases generated by these differences will be addressed to obtain more information on the evolution of the studied magmas.

10.4.1 Feldspar crystallisation

Feldspars constitute the dominant phases in all the observed crystallising assemblages of the Sulcis. In the less evolved rocks plagioclase is the only feldspar present, while in the more

differentiated ones it is sanidine; rocks with intermediate compositions present a two feldspar assemblage containing simultaneously plagioclase and sanidine. Another observation is that most feldspar compositions appear in the feldspar ternary diagram along a dominant trend connecting the more K-rich sanidines with the more Ca-rich plagioclases (Fig. 10.7). Some exceptions exist, though, to this generic description of the feldspar behaviour in the Sulcis. For example PC and SP present a two feldspar assemblage which consists of anorthoclase and plagioclase instead of the sanidine plus plagioclase present in the rest of the units, and the more evolved rocks (peralkaline units plus PA and PM) present feldspar compositions which depart from the trend depicted by the other units in the feldspar ternary diagram. These and other issues will be addressed here.

Feldspar crystallisation occurs in a complex system. It consists of three essential components ($KAlSi_3O_8$, $NaAlSi_3O_8$, $CaAl_2Si_2O_8$), whose crystallisation is deeply influenced by an additional component, H_2O. The crystallisation of feldspars in rhyolites, trachytes and phonolites was discussed by Tuttle and Bowen (1958). Carmichael et al. (1974) used the experimental data of Bowen (1913, 1947), Bowen and Tuttle (1950) and Franco and Schairer (1951) to build a schematic diagram to illustrate the ternary feldspar system at high temperature and low pressure (Fig. 10.8). Three surfaces are represented: the liquidus, the solidus and the solvus. The curved parallel lines represent the liquidus surface, the stippled surface is the solidus, and the dome-shaped surface at the lower part is the solvus. The liquidus surfaces dipping down from the three

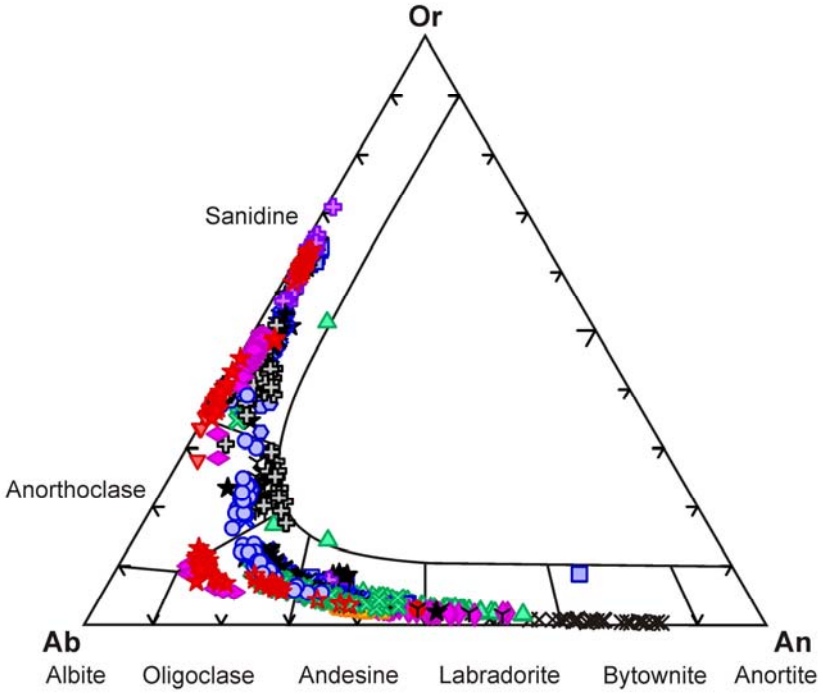

Figure 10.7: Feldspar compositions in the Sulcis magmatism

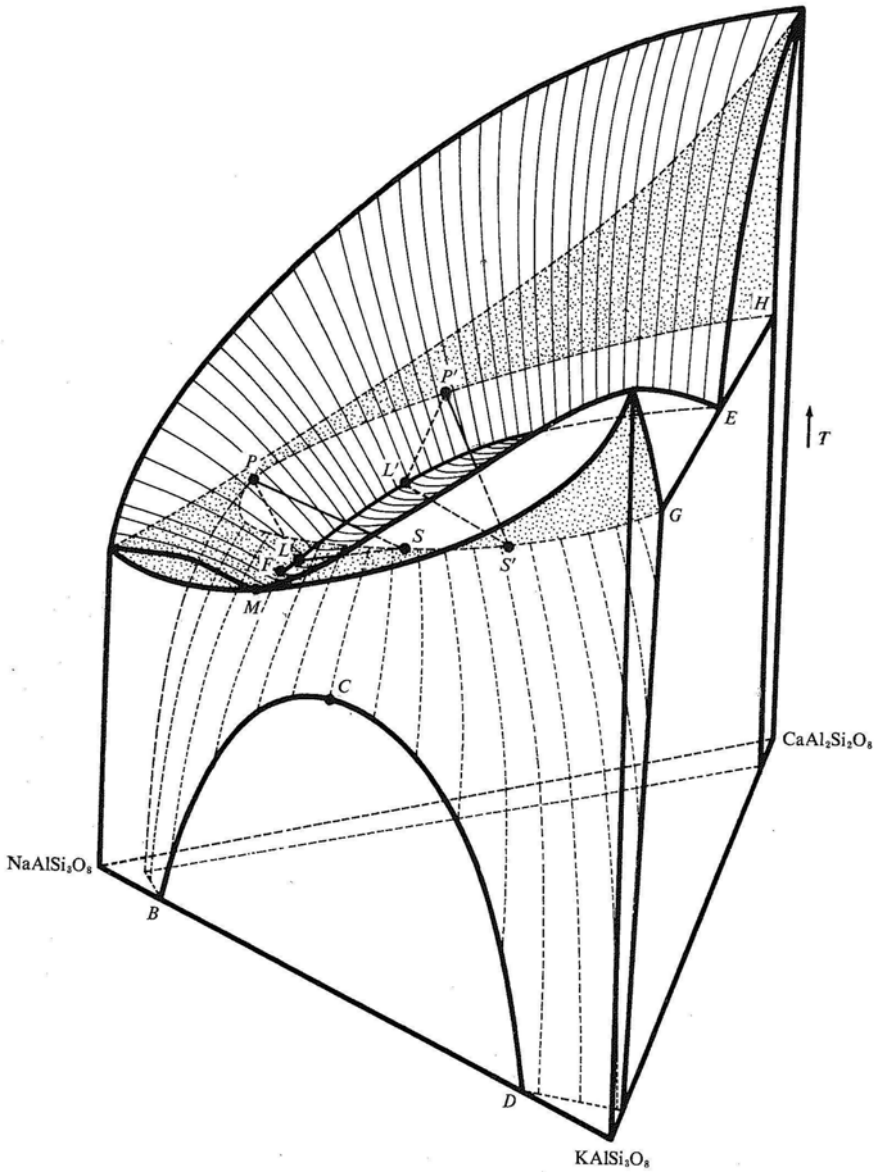

Figure 10.8: Schematic feldspar ternary system at high temperature and low pressure. Incongruent melting of sanidine is neglected. Extracted from Carmichael et al. (1974). Curved parallel lines show the liquidus surface, the stippled surface represents the solidus. The third dome-shaped surface is the solvus

components melting temperatures intersect at the liquidus field boundary (cotectic EF in this diagram). This cotectic separates the field in which plagioclase is the early crystallising phase from that in which sanidine is the first crystallising phase, and only intersects with the solvus at the eutectic E in the $CaAl_2Si_2O_8$-$KAlSi_3O_8$ system. From there it runs with falling temperature towards the alkali feldspar minimum M, which, however, does not reach, fading at F. This termination at F is produced by the complete solid solution that exists between alkali feldspars at high temperature. For liquids saturated in water at 4 KBar or more the cotectic extends towards the alkali feldspar binary part of the system, towards the alkali feldspar solvus, which it intersects at

C. The cotectic represents the liquid composition in equilibrium with two feldspars: plagioclase (or anorthoclase) and sanidine. Two hypothetical three-phase triangles (lines connecting the liquid and the two feldspars in equilibrium) are depicted at different temperatures. These triangles are parallel to the base of the prism. For liquids at the cotectic the crystallising feldspars compositions lay at the intersection between the solidus and solvus surfaces. Figure 10.9 shows the position of the solidus surface (and therefore the composition of the crystallising feldspars) at different temperatures. As the temperature decreases feldspar compositions move closer to the plagioclase and alkali feldspar sides of the system. The different positions of the feldspar compositions in the feldspar diagram of the Sulcis (Fig. 10.7) can be justified by this fact. The curves defined by the feldspars of each unit show trends which, the more evolved the unit, the closer the feldspar trend is to the sides of the diagram. The most evident cases are the PA and PM, which are two of the most evolved units, and therefore were at a lower temperature at the time of eruption. The case of peralkaline units is special because not only were they strongly evolved and therefore colder in respect to previous ones, but they were also formed from a magma which had an initially higher content in K_2O and Na_2O, and which subsequently underwent strong plagioclase fractionation thus reducing its CaO content to a minimum. As a result, peralkaline magmas only present sanidine with a very poor An content, lying by the alkali feldspar binary system in the ternary feldspar diagram.

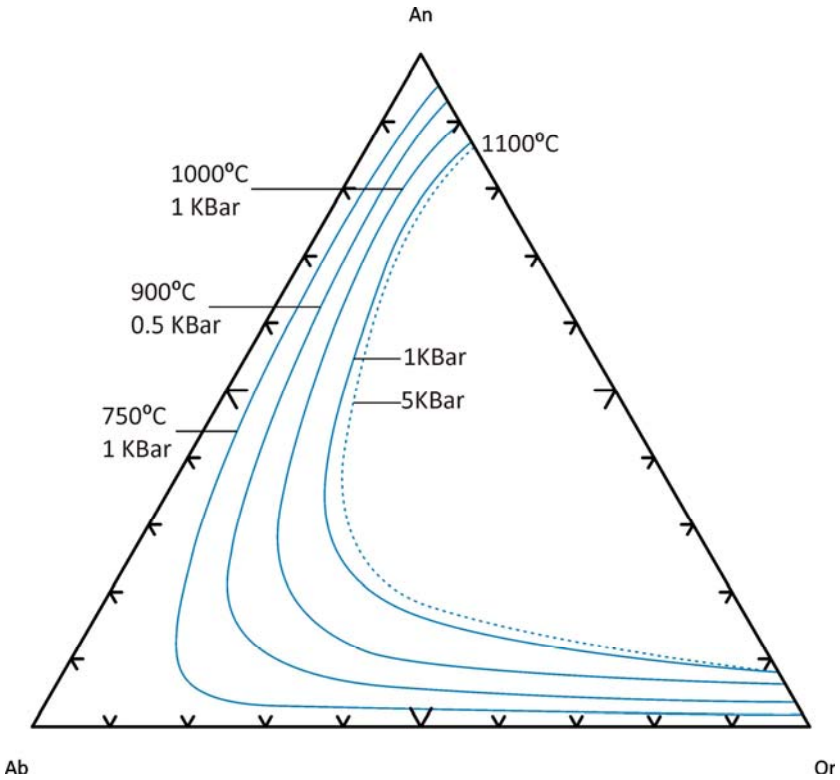

Figure 10.9: Position of the solidus surface at different temperatures in the feldspar ternary system. Modified from Deer et al. (1992)

The ternary system can be projected at the base of the prism to better represent the evolution of the crystallising feldspar composition (Fig. 10.10). This diagram depicts the approximate composition of the melt (field boundary, red line) co-existing in equilibrium with two feldspars (blue line). Triangles have been drawn connecting co-existing compositions at several evolution points. Melts with a composition right of the solidus curve and away from the cotectic will start crystallising either plagioclase or sanidine (depending on what side of the line they are at), changing their composition towards the cotectic. Once the field boundary is reached a second feldspar starts crystallising. At that point, two-feldspar crystallisation causes the melt to move along the field boundary. Feldspars in equilibrium with the melt progressively change their composition from the initial feldspars towards the K_s point, that is, to more albitic compositions. Crystallisation continues until no liquid remains. For example, a liquid with composition Y fractionates C' plagioclase until the cotectic is reached (at this point the liquid has composition C_L). This is a simplification because temperature decrease during crystallisation causes the solidus to vary, as has been previously seen, and thus plagioclase composition varies; it is not fixed at C', which only represents the plagioclase in equilibrium with C_L. This is also valid for the following examples. Then sanidine C starts to crystallize and the liquid composition starts moving along the field boundary until point B_L, where crystallisation is completed and feldspars in equilibrium have compositions B' and B. This pattern of feldspar crystallisation was the one followed by the studied magmas in the Sulcis presenting plagioclase or plagioclase plus sanidine assemblages, although equilibrium was not maintained during crystallisation as evidenced by textures such as plagioclase zoning and by the magma chemical variation shown by these units caused by crystal removal. The effects of fractionation are later discussed. Units presenting plagioclase as only feldspar represent magmas whose melt composition did not reach the cotectic (e.g. AND in Fig. 10.11), whereas two-feldspar units had a liquid moving along the field boundary at the time of eruption (e.g. NU in Fig. 10.11). However, feldspar crystallisation may be more complicated.

Crystallisation of a liquid in the field K_SK_LF may be illustrated using composition X. The first phase to crystallise is a plagioclase with composition G', and the liquid in equilibrium moves towards G_L. When this composition is reached sanidine starts to crystallise. The composition of the liquid changes along the cotectic to A_L, and feldspars in equilibrium change their compositions to A and A'. As the liquid composition moves towards A_L, once sanidine composition passes point F plagioclase starts to react with the liquid not only changing its composition, but also being reabsorbed. When composition A_L is reached all the plagioclase has been reabsorbed and the mixture consists of a liquid of composition A_L and an alkali feldspar of composition A. With further crystallisation the liquid composition leaves the cotectic moving towards the albite-orthoclase join

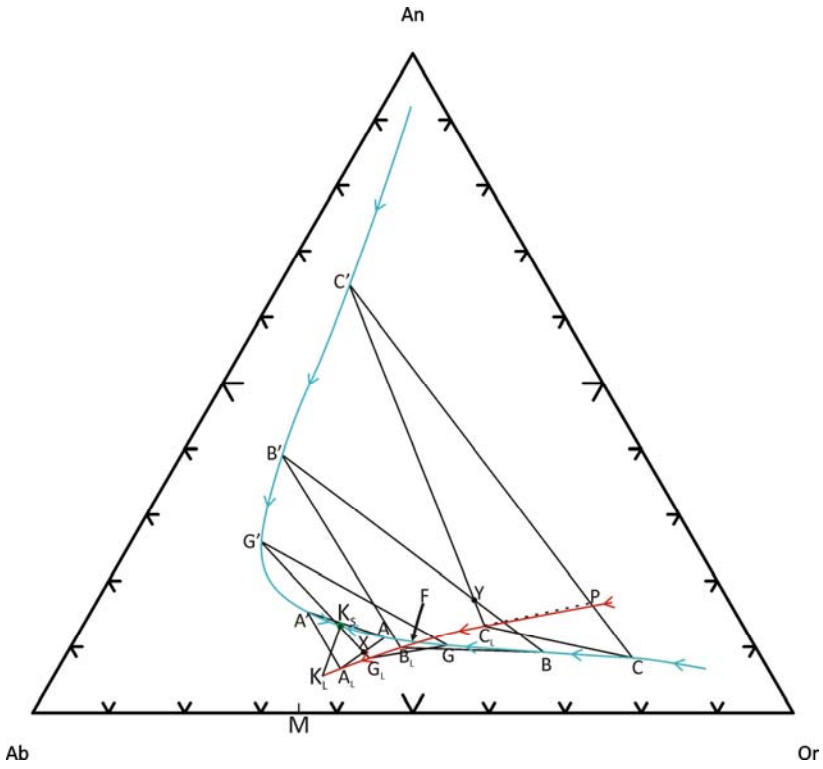

Figure 10.10: Ternary diagram of the feldspar system showing the approximate composition of liquids (red line) coexisting in equilibrium with two feldspars (compositions at the blue line) (after Tuttle and Bowen, 1958). Modified from Deer et al. (1963)

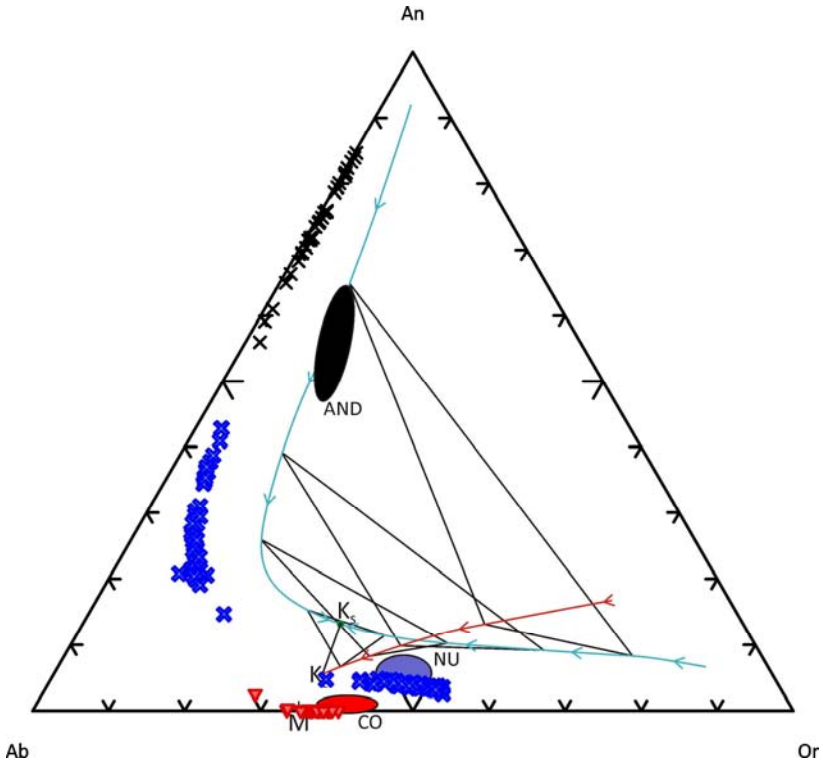

Figure 10.11: Feldspar ternary diagram equivalent to that in Fig. 10.10 showing the magma (solid areas) and feldspar compositions for AND, NU and CO units. Feldspar composition and field boundary lines are those of the original example, included here as a reference and hence do not representing the equivalent lines for the depicted units

(K_S) and the feldspar changes in composition towards X. Crystallisation is completed when alkali feldspar reaches composition X and no liquid remains. Therefore, for liquid compositions within the K_SK_LF field, crystallisation is characterised by initial crystallisation of plagioclase, followed later by alkali feldspar. With equilibrium crystallisation the plagioclase reacts with the liquid and is reabsorbed completely leaving an alkali feldspar and liquid, the crystallisation being completed when feldspar composition reaches the composition of the initial liquid. The probability of late crystallisation of a rhyolitic liquid producing formation of a single alkali feldspar is increased by crystal fractionation.

A liquid moving along the cotectic curve crystallizes two feldspars, and the proportion between them can be calculated using the lever rule. For example, for a liquid with composition C_L, the proportion between the two feldspars is given by C'P/PC, in which P is the intersection between the tangent to the cotectic at the liquidus composition and the line connecting both feldspar compositions. As the liquid descends the cotectic, point P moves toward the alkali feldspar composition until at point F it actually passes through it. Beyond this point the boundary between the fields of plagioclase and alkali feldspar is a reaction curve, with plagioclase reacting with the liquid to produce alkali feldspar. This reaction relation explains the common rimming of plagioclase by alkali feldspar (Deer et al., 1963; Rahman and McKenzie, 1969; Philpotts and Ague, 2009). As the liquid descends the field boundary curve still further, compositions of coexisting feldspars approach each other until, at K_S (the minimum at the ternary feldspar solvus) they become identical so only one feldspar crystallises, and the liquid has composition K_L. This situation can be more easily produced if equilibrium is not maintained and fractionation occurs. Fractionation causes liquids to move further along the cotectic curve than in equilibrium conditions, beyond the point where equilibrium crystallisation would end, so magmas which originally would remain in the normal cotectic zone may reach the reaction region between plagioclase and liquidus in the field boundary curve. In the Sulcis this situation, with the formation of albite-rich sanidine mantling plagioclase crystals, is clearly observed in MCR and PA units, in which sanidine is largely dominant and the scarce plagioclase crystals present sanidine mantles. Therefore these units would represent an incomplete transition towards single feldspar magmas. Sanidine mantles over plagioclase crystals can also be seen, although only occasionally, in NU and MZ units. In quickly chilled magmas such fractionation is usually effected by the zoning of plagioclase, which can be observed in all units in the Sulcis.

If fractionation is very effective it may produce extreme changes in magma and feldspar compositions. For example, for liquid Y, whose equilibrium crystallisation is completed at B_L, fractionation by zoning and/or crystal removal can cause the liquid to change beyond B_L towards

K_L, to leave the field boundary and to change in composition along a curved path to M, the Ab-Or system minimum, thus finally forming a single alkali feldspar during the late stages of crystallisation (Deer et al., 1963; Rahman and McKenzie, 1969). Most of the units in the Sulcis experienced fractionation, as evidenced by plagioclase zonation and by magma chemical evolution, but peralkaline units illustrate the extreme case explained here, because they represent magmas with a single feldspar (sanidine) whose compositions (both for magma and feldspars) are very close to M (e.g. CO in Fig. 10.9). High water pressure strongly reduces the liquidus temperature of the Ab-Or system so the end of the liquid boundary curve (K_L) can reach composition M. In this case fractionating magmas can reach this composition without liquids needing to depart from the field boundary.

Previous discussion allowed the explanation of feldspar compositions for most of the studied units. There are some units, though, whose feldspar assemblage is more complicated to explain, and which need further discussion.

The Serra di Paringianu unit has a whole rock geochemistry very similar to that of NU, as has been seen in the previous chapters of this study, and would be therefore expected to present a mineral assemblage equivalent to that of NU. However, instead of presenting a plagioclase plus sanidine assemblage like NU, it shows plagioclase and anorthoclase in an almost continuous trend (Fig. 10.12). There is yet another difference in the mineral assemblage: while NU may present pyroxenes as mafic minerals, SP may also present amphiboles. The presence of abundant water in the magma strongly reduces the liquidus temperature of the alkali feldspar system. This delays the crystallisation of sanidine, and causes plagioclase to crystallise to a larger extent than in dry melts (Deer et al., 1963; Carmichael et al., 1974). In the previous diagrams reduction in the stability field of sanidine would be marked by a displacement of the eutectic in the Or-An system towards the Or side, thus moving the field boundary line closer to the Ab-Or side of the ternary diagram. It is thought that SP had a higher water content which caused the precipitation of a single feldspar. This feldspar initially had a plagioclase composition, which evolved towards anorthoclase as the liquid progressively approximated a displaced cotectic line, which it didn't reach as evidenced by the absence of sanidine crystallisation. The higher water content in SP is supported by the occurrence of amphibole in the phenocryst assemblage. The absence of sanidine in MZ, although representing less extreme a case than SP, can also be attributed to the effect of a higher water content in the magma compared to other units. The presence of significant water pressure is evidenced in this unit by the occurrence of abundant biotite crystals.

The Punta dei Cannoni unit also presents an assemblage of plagioclase plus anorthoclase, but unlike in SP, these are not evenly distributed throughout the unit nor are they in equilibrium. PC

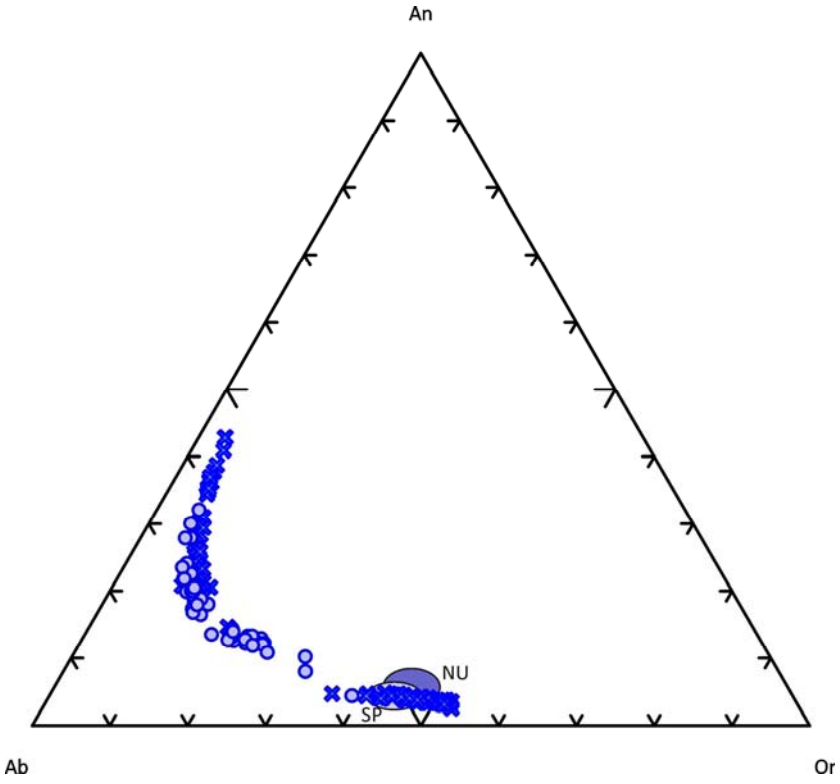

Figure 10.12: Whole rock and feldspar compositions for NU and SP units

presents two strongly different facies of different colour: brown and black. Brown facies are the most abundant and present dominant anorthoclase, with only scarce plagioclase crystals, both presenting signs of reabsorption. Altered mafics accompanying feldspars occur, which are thought to be pyroxenes by comparison with the black facies, in which these are preserved. Black facies only contain plagioclase as feldspar, together with the pyroxenes. In black facies glomerula interpreted as cumulate fragments are found formed by plagioclase and pyroxene with the same compositions as crystals in the groundmass. Both facies present a slightly different whole rock composition, the black one being a bit more primitive, containing more CaO. This is evidenced when projected in the feldspar ternary diagram (Fig. 10.13).

The feldspars found in each of the two facies are consistent with the observed whole rock compositions. The original liquid compositions were at an An content close to the inflexion zone of the feldspar solidus from plagioclase to alkali feldspar compositions, where small changes in the An content of the crystallising liquid may produce strong changes in the composition of the feldspars in equilibrium. Liquid of the black facies was a bit more rich in An, which caused the crystallisation of plagioclase, whereas the liquid of the brown facies produced anorthoclase. Since both liquids formed a single feldspar each, crystallisation occurred away from the cotectic line. The composition of both magmas is very similar and could be considered to be related by

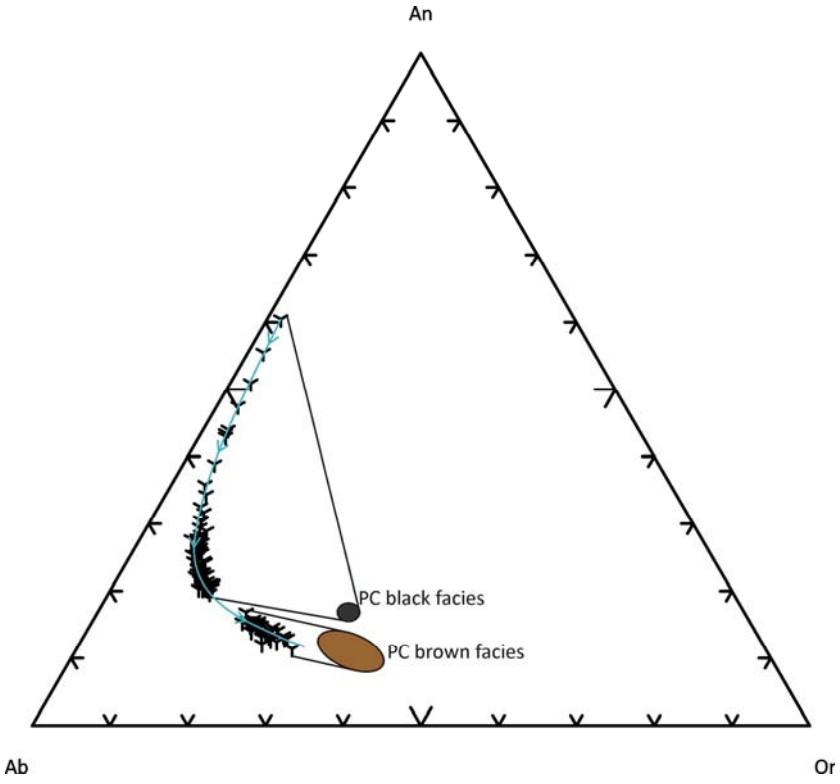

Figure 10.13: Whole rock (solid areas) and feldspar compositions in PC unit

fractional crystallisation; removal of plagioclase from the black liquid may produce a liquid like the brown one. The occurrence of the black level in the middle of the brown unit, and the presence of black pumices in the brown facies and of brown pumices in the black one evidence coexistence of the two magmas in the same magma chamber for some time. At the same time, sharp change in petrography and chemistry suggests magma mingling by input of the black magma into the magma chamber containing the brown one rather than the existence of a stratified chamber. Arrival of the black magma, more primitive and hotter, probably produced heating of the brown one, which may explain the widespread corrosion textures in its feldspars. The formation hypothesis for this unit is as follows: the magma batch that produced this unit stagnated at a deep magma chamber. From there, a portion reached a shallower and probably smaller chamber. Evolution in the shallow chamber progressed faster, producing the brown magma, which crystallised to a large extent as evidenced by its porphyricity (up to 50 vol %), which is one of the highest among the whole ignimbritic sequence. At some point there was a new input coming from the deeper chamber, which being deeper and probably bigger had undergone less cooling and differentiation, thus producing a more primitive and hotter magma, the black one. The brown magma was much colder and crystallised and therefore presented a higher viscosity, which avoided magma mixing, and even intense mingling (enclaves of the other magma, that is brown in black and vice versa, are restricted to a small thickness around the contact surface between the

two facies). The black magma probably produced one or several large blobs within the brown one. Brown magma was reheated, which caused destabilization of the pre-existing feldspars, which started to be reabsorbed. At the same time the black magma was cooled down, favouring rapid crystallisation. The cumulate textures observable within the black unit probably formed at this stage within the cooling black blobs, close to the interface between the two magmas. Reheating of the brown magma chamber may have been the trigger of the eruption which generated the PC unit. This eruption expelled mainly brown magma until at some point a black blob was also erupted forming the black level in the middle of the unit. The zone with presence of pumices/enclaves of the opposite magma within each facies may represent the interface zone between the two magmas in the chamber, where both underwent more mingling, or it may have been produced by the mixing of pyroclasts during transport. Plagioclase in the brown magma may represent either relict plagioclase from the early crystallisation of the brown magma, and/or be the result of a crystal exchange between the two magmas at the interface between the two magma bodies.

The Monte Crobu unit presents a sanidine plus plagioclase feldspar assemblage, which in the groundmass is dominated by sanidine. The black pumices found in some facies of this unit also present sanidine plus plagioclase, but in this case sanidine shows instability signs such as strong corrosion and embayments whereas plagioclase is in apparent stability. Sanidines in the black pumices present compositions similar to those in the groundmass, whereas plagioclases are slightly more rich in Or component. As has been previously said in this chapter, no analyses have been yet obtained of black pumices chemical composition and therefore little is known about it. Since feldspar composition in black pumices is very similar to that of feldspars in the rest of the unit a similar whole rock composition may be assumed, being a case similar to that of PC unit. The black pumices would represent a late input and mingling of slightly hotter magma. The higher Or content of plagioclase in the black pumices supports a higher temperature for this magma. The effect of magma input in this case was smaller than in PC unit and mingling was more effective. Sanidine instability in the black pumices could be regarded as being produced by the temperature change undergone by this magma on entering the cooler magma chamber, which produced a shift in the composition of the feldspar in equilibrium with the liquid at the new temperature.

There is a last particular case in the feldspars of the ignimbritic suite, the presence of more An-rich zones within the sanidine crystals of the MU units. This is discussed in the next section.

10.4.2 Monte Ulmus

Monte Ulmus unit presents a phenocryst assemblage formed almost exclusively by sanidine. Composition of this feldspar is very close to that of CO, consistently with its peralkaline character (Fig. 10.14). However, some crystals may present compositions richer in An component. These crystals, though, are not homogenously An-rich. The An-rich compositions occur as zones within the regular almost An-free sanidine crystals. This zoning does not have an optic expression in thin section and is only detected through chemical analysis of crystals (cryptic zoning). The zoned character of the An-rich portions rules out the possibility of the incorporation in the magma of An-rich sanidine xenocrysts. Instead, the presence of An-richer bands within the sanidine points at some kind of compositional heterogeneity in the magma, which produced a chemical zoning in sanidines. For example, a portion in the magma chamber richer in CaO could cause the precipitation of an An-richer band in the sanidines passing through it.

Occasionally, especially in the vitrophyre, scarce mm- to cm-sized yellowish lithic inclusions occur in the MU unit. Under detailed study these have shown to be limestone fragments metasomatised to garnet aggregates (research group, unpublished). Since metasomatism is a slow process, it is unlikely that it could have been produced on limestone fragments collected during ascent of magma on eruption, because the time from entrapment to cooling would have probably been too short. For example, in the Garrotxa Volcanic Field (NE Spain) hotter basaltic lavas may present marl xenoliths which present almost no signs of metamorphism. Therefore, this

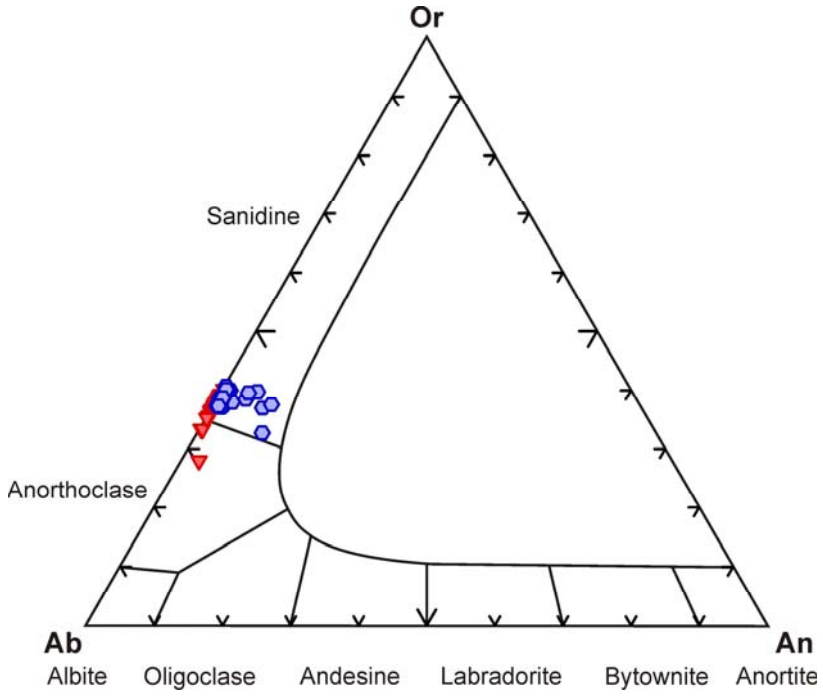

Figure 10.14: Composition of the feldspars in MU (blue) and CO (red) units

metasomatism probably occurred at the magma chamber during a somewhat longer time period by contact between a limestone body and the evolving magma. In the basement of the Sulcis area there are two big limestone bodies corresponding to Cambrian and Cretaceous rocks. It is possible that, during the differentiation of the MU magma, the magma chamber contacted one of these rock layers. Peralkaline liquids are the product of a long evolution of magmas, thus being at the lower end of the magmatic temperature range, with erupting temperatures typically in the range of 700-950°C (Scaillet and Macdonald, 2001). White et al. (2009) calculated temperatures lower than 700°C for pantellerites at Pantelleria. This temperature is insufficient to produce large dissociation of carbonates and incorporation into the magma at depth. Instead, reaction was probably more limited to element diffusion and exchange between the solid rock and the magma at the contact zone, and most likely only affected the region closer to the contact. At this contact zone limestones were metasomatised to a garnet assemblage, whereas the peralkaline magma got slightly enriched in sedimentary elements, one of them being calcium. Feldspars passing through these contaminated portions of the chamber would probably crystallise a band of An-richer sanidine. The contamination effect was very small and is barely detectable in whole rock geochemical data, MU presenting a CaO content equal to that of CO. Isotopes can provide valuable information about this matter because they are sensitive to contamination. As previously seen, lead isotopes mark some heterogeneity within the MU, which could be at least in part the result of this contamination by limestone assimilation. Sr isotopic data, though, are not capable of corroborating this hypothesis. Insufficient precision in the age correction of $^{87}Sr/^{86}Sr$ (due to the lack of precise age data for this unit and to the correction using $^{87}Rb/^{86}Sr$ values calculated from ICP-MS Rb/Sr measurements instead of direct isotope measurement) make these data unusable for this purpose.

The garnet-bearing lithics could represent portions of the chamber wall collected by the ascending magma during eruption, and/or small chunks incorporated previously into the magma, even in limestone form. The preferential occurrence of these inclusions in the vitrophyre does not translate into a higher CaO content in the whole rock data of vitrophyres. Several possibilities exist to explain this fact. In first place the apparently preferential occurrence of these particular lithic clasts in the vitrophyre could be related to a biased observation. These lithics present a light colour which strongly contrasts with the black colour of the vitrophyre, thus making them more easily detectable in this level than in other regions of the unit. The second possibility is that they really occur preferentially in the vitrophyre. This case leads to two possible interpretations (Fig. 10.15). It can be considered that the magma forming the vitrophyre was the one that in the magma chamber was closer to the contact with the limestone wall rock and therefore contained

more fragments of limestone detached from the wall. In this case, since lithic presence does not translate into a significant chemical modification, contamination necessarily needs to be considered as having a very small effect on magma chemistry. At the same time this interpretation requires this specific magma portion to be the first to be erupted. This is not difficult to explain if the limestone is considered to be located at the roof of the magma chamber (Fig. 10.15 A). The second possibility arises from considering the garnet lithic fragments as wall rock chunks collected during conduit opening and ascent of magma. The proportion of conduit lithic fragments is typically higher in the first lavas to be erupted due to conduit opening and erosion by the first ascending magma. Since the first magma to erupt in the studied ignimbrite is that which forms the vitrophyre, this would be expected to be enriched in these lithic fragments. This last hypothesis is also consistent with the lack of a significant chemical difference between vitrophyres and the rest of the unit, because the presence of garnet lithics would not be related to the position of magmas relative to the limestone in the magma chamber but to the order of eruption (Fig. 10.15 B). This hypothesis requires the conduit to be opened in the limestone magma chamber wall rock, which therefore would most probably be located at the roof.

Further work needs to be done to constrain the proposed hypotheses, including more garnet analysis, detailed study of its distribution within the unit, precise dating of MU, direct analysis of $^{87}Rb/^{86}Sr$ ratio, as well as determination of other useful isotopes as for example oxygen among other tasks.

Carloforte unit also presents two populations of sanidine: one with a composition like that of regular sanidines in CO or MU, which is found in the groundmass of the ignimbrite, and a second one of An-rich sanidines which is found in the black pumices. This An-rich population differs from that of MU in that crystals are homogeneously An-rich, having compositions equivalent to sanidines in less evolved and hotter magmas such as NU or MCR. This fact, added to the obvious instability of these crystals within the black magma, and to the chemical modifications they cause in it (e.g. Eu enrichment), are what allow the interpretation of this sanidine population as having been collected by the black magma from a sanidine cumulate deposit instead of having been precipitated directly from it. The origin of this cumulate, though, needs to be further investigated.

10.4.3 Zircon fractionation

In the discussion on the fractionating assemblage of the Sulcis magmas it has been shown that although several units present zircon crystals, fractionation of this mineral was not enough as to prevent Zr enrichment in magmas, which present progressively higher contents in this element with evolution (Fig. 10.4). Exceptions to this general trend are MLN, PA and PM units.

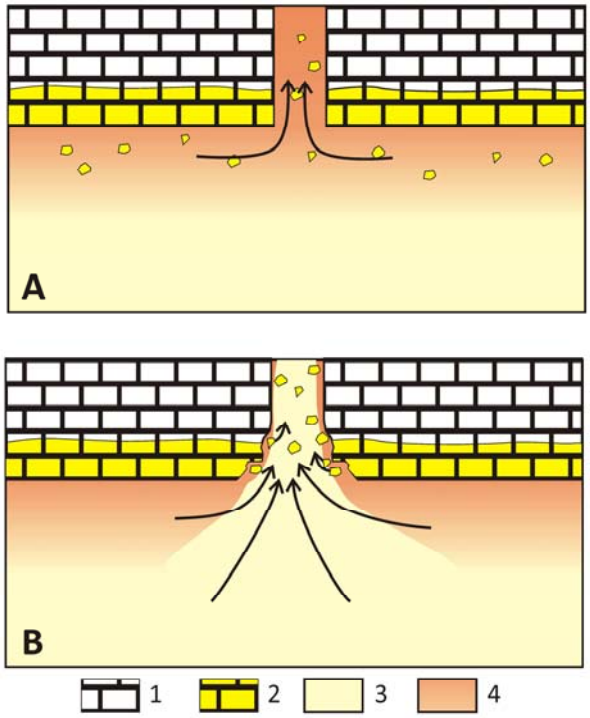

Figure 10.15: Schematic representation of the two possible hypotheses proposed to explain the preferential occurrence of garnet lithic fragments in the vitrophyre of the MU unit. 1) Carbonate wall rock; 2) Metasomatised wall-rock; 3) MU normal magma; 4) magma affected by diffusion from the wall rock

Watson and Harrison (1983) investigated the saturation of zircon in a variety of melts, studying the effect of temperature and melt composition. They found that zircon solubility increases with temperature and with a factor M, which is defined as the cation ratio (Na+K+2Ca)/(Al·Si). For example, their model predicts for a melt with M=1.3 (normal metaluminous granite) zircon solubilities that range in dissolved Zr concentration in the melt from 1330 ppm at 1020°C to only 100 ppm at 750°C. If the peralkaline units are not considered, the trend depicted by the rest of the units is consistent with a progressive Zr enrichment by insufficient zircon crystallisation and fractionation until at some point in the differentiation history of the magmas cooling finally causes a strong fractionation of this mineral. It is not a coincidence that the units impoverished in Zr are those with a higher evolution degree and hence formed from cooler magmas. In the case of the peralkaline units, though, cooling did not have the same effect than in the non-peralkaline magmas. Instead of presenting a strong depletion in Zr, peralkaline magmas become continuously richer in this element. This different behaviour of metaluminous and peralkaline magmas is well established (Dietrich, 1968; Collins et al., 1982; Linthout, 1984; Kogarko and Lazutkina, 1989). Higher solubility of zircon in the peralkaline magmas is interpreted to be due to the complexing of dissolved Zr^{4+} with the "free" alkalis not associated with Al in the melt (Watson, 1979). Another factor explaining this behaviour is the typical enrichment in F of peralkaline magmas; this element

is considered to reduce zircon stability in crustal settings (Conte and Dolfi, 2002). EMP and ICP-MS analysis on fluid inclusions in the comendites north of San Pietro revealed high F contents (Cioni and Gioncada, 2006).

10.4.4 Peralkaline magmas

In the Sulcis area the combined effect of an extensional setting producing transitional to mildly alkaline anorogenic magmas and the existence of magma chambers promoting its stagnation an extended differentiation caused the generation of peralkaline magmas, which formed the CO, MU and CF units. The first hypothesis proposed in this chapter for the origin of peralkaline magmas is that these may have originated from the evolution of magmas slightly more alkaline than those that formed units in the third trend in Figure 10.1, and whose primitive and intermediate terms were not sampled by any eruption and hence there are no evidences of them. This hypothesis originates from the observation of the trends depicted by peralkaline units in geochemistry diagrams such as the TAS (Fig. 10.1), the Nb vs. Rb (Fig. 10.3) or the Nb vs. Zr diagrams (previous Chapter); trends of peralkaline magmas appear invariably separated from trends marked by other units, in positions which could be expected to be occupied by more alkaline magmas. This hypothesis is also supported by the comparison of the Sulcis suite with other comendite-bearing magmatic suites in subduction-related environments. For example, Figure 10.16 depicts the area covered by the peralkaline suites of two subduction-related magmatisms in D'Entrecasteaux Islands (green) and Mexican Volcanic Belt (brown). As can be seen, the non-peralkaline magmas of the Sulcis area fall at the lower part and slightly below the trend of the Mexican Volcanic belt, while comenditic units fall well within it and can thus be considered to have been formed from evolution of similar magmas. Considering this hypothesis, in the Sulcis there would be no examples of the primitive compositions that later generated the peralkaline magmas, so these must be inferred using as reference other peralkaline suites around the world. The lack of primitive magmas in peralkaline suites is an extended problem, and in most places the basic and intermediate magmas only occur as enclaves in the more evolved ones, which are typically trachytic and rhyolitic (e.g. Smith, 1976; Souther and Hickson, 1984).

As seen in the previous chapter, over the past decades the study of peralkaline magmatism has shown that these magmas occur almost exclusively in mildly extensional settings and oceanic islands (Macdonald, 1974b; Mahood, 1984), being its presence in active subduction-related environments restricted to back-arc positions (Bowden, 1974). But for some exceptions (e.g. Martin, 1974), peralkaline magmas are always considered to be the product of extensive magma differentiation by crystal fractionation of mildly alkaline magma suites (Barberi et al., 1975;

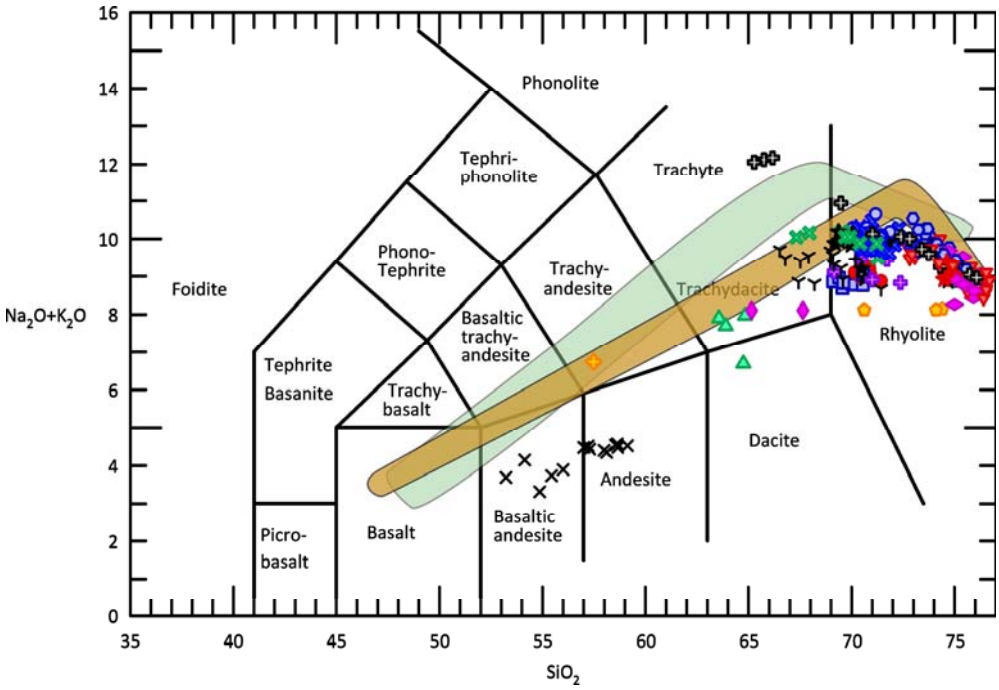

Figure 10.16: TAS diagram showing areas covered by two comenditic suites in D'Entrecasteaux Islands (green) (Smith, 1976; Smith et al., 1977) and Mexican Volcanic Belt (brown) (Nelson and Hegre, 1990)

Civetta et al., 1984). Regarding the most primitive terms of these suites, basaltic rocks associated with comendites are typically transitional and weakly alkaline, whereas basaltic rocks associated with pantellerites are characteristically more alkaline than those associated with comendites (Smith et al., 1977).

In extensional settings and ocean islands peralkaline magmas are regarded as the silicic end-members of an approximately silica-saturated olivine basalt-hawaiite-mugearite-(benmoreite)-trachyte-rhyolite lineage (MacDonald, 1974b). This association may be more or less closely related to more strongly undersaturated suites of basanitic and nephelinitic type (e.g. East African rifts) or to tholeiitic suites (e.g. Iceland). In ocean islands it is possible to find only the transitional basalt-trachyte series. In subduction areas the peralkaline rhyolites result from the evolution of a suite that contains transitional basalt, trachybasalt, trachyandesite, oversaturated trachyte and peralkaline rhyolite (Smith et al., 1977). Thus, the immediate parental magma of comendites and pantellerites is always a trachyte. In some locations peralkalinity is already reached in trachytic compositions (e.g. Socorro Island, Mexico (Bohrson and Reid, 1997), or Pantelleria (Civetta et al., 1998)).

The final stages of magma evolution previous to reaching peralkalinity from a trachyte are dominated by feldspar fractionation. Since the agpaitic index of sanidines (values between 0.95 and 1 in the Sulcis) is higher than that of crystallising magmas, transition to peralkalinity is

commonly accepted to be the result of plagioclase fractionation (plagioclase effect, Bowen, 1945). To reach peralkalinity plagioclase must crystallise and fractionate until magma surpasses the agpaitic index of sanidines, which is almost the same as saying until peralkalinity is reached. Crystallisation of plagioclase in trachytic magmas with such a high alkalinity and degree of evolution, which has left almost no CaO, is usually justified by the influence of fluids, especially water, which as seen previously in this chapter promotes crystallisation of plagioclase to a larger extent than in "dry" magmas. Once the agpaitic index of magmas surpasses that of sanidines, further crystallisation of this feldspar increases magma peralkalinity even when plagioclase stops forming. Alternative mechanisms for reaching peralkalinity have been proposed, such as partial melting of alkali gabbros (Scaillet and Macdonald, 2003) or of continental crust by halogen flux (Black et al., 1997), or that of Martin (1974), which suggests that peralkaline magmas might form at the top of more mafic magma chambers by preferential transport and accumulation of Si, Al and alkalis at this region.

Among the several areas bearing peralkaline suites to which the Sulcis one could be compared to obtain information, there is one that underwent a similar evolution, that in Dawson Strait in the D'Entrecasteaux Islands, south-eastern Papua. This area represents a particular case in which the subduction-related peralkaline suite is not located in back-arc positions, but in the arc itself (Smith, 1976). This position is anomalous, but study of the tectonic context revealed that at the time of emplacement of this suite that portion of the volcanic arc was no longer active, it was a deactivated subduction zone, as shown by the absence of a Benioff zone (Stolz et al., 1993). The andesitic island arc to which this suite belongs ranges in age from Miocene to Holocene and passes through the D'Entrecasteaux Islands and westward onto the Papuan mainland. Immediately to the east of D'Entrecasteaux Islands is located the Woodlark basin, a Quaternary spreading centre (Fig. 10.17). The currently accepted hypothesis is that the late Tertiary compressional regime in SE Papua is at present being replaced from the east by a tensional regime associated with sea-floor spreading in the Woodlark basin. At the D'Entrecasteaux Islands the occurrence of the peralkaline suite is a response to this change in the tectonic regime, with orogenic rocks no longer erupting in that portion of the arc. This peralkaline magmatism, though, overlaps in time with Quaternary subduction-related calc-alkaline volcanism in the same arc at the western D'Entrecasteaux Islands and the eastern Papuan mainland, where the shift to extensional regime has not yet arrived (Smith et al., 1977; Stolz et al., 1993). This situation is very similar to that proposed in the present work for the Sulcis area, for which it is suggested that the ignimbritic suite was a manifestation of a transition from orogenic to anorogenic magmatism by

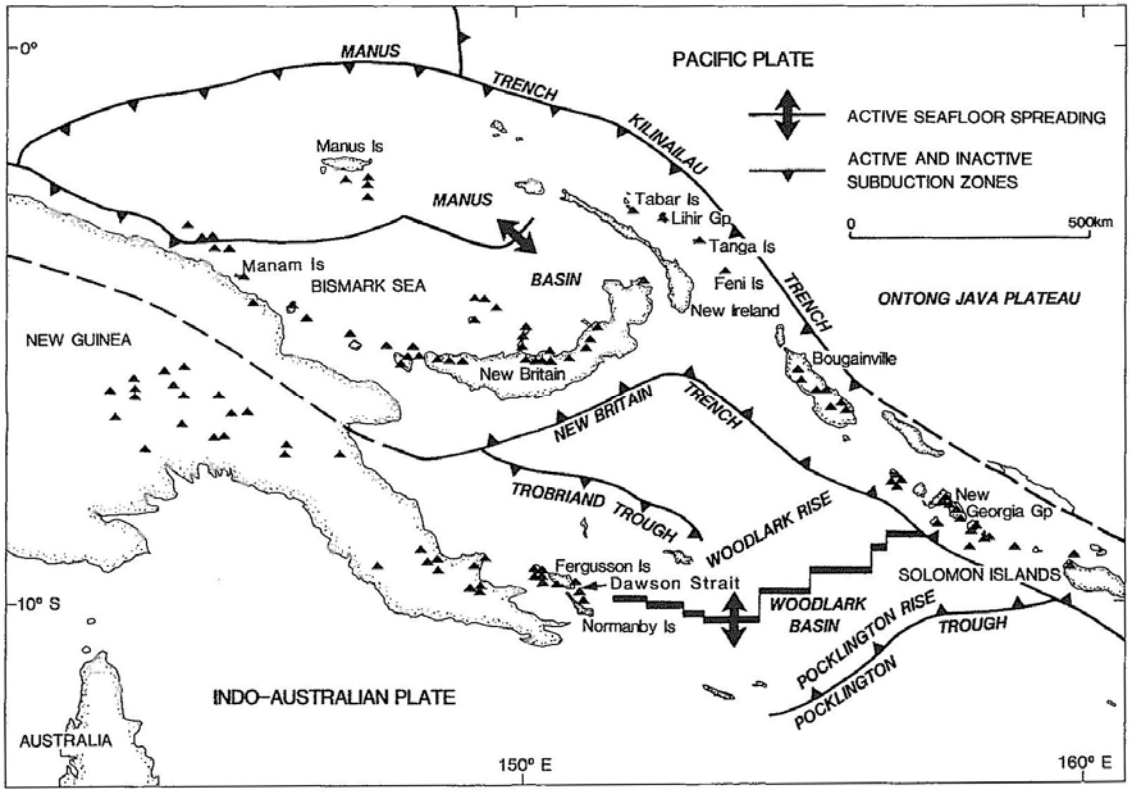

Figure 10.17: Map showing the main tectonic features of western Melanesia. Woodlark basin is propagating west toward the volcanic arc containing the comenditic suite of Dawson Strait, in the D'Entrecasteaux Islands. Figure extracted from Stolz et al. (1993)

end of subduction influence, being also a suite that coexisted with contemporaneous orogenic magmatism in other portions of the arc like in the D'Entrecasteaux Islands case.

The peralkaline association in the D'Entrecasteaux Islands presents associated basic and intermediate rocks, which have allowed the reconstruction the evolutionary path of the peralkaline magmas. These are considered to be the result of the evolution of an hypersthene-normative alkali basalt (transitional basalt) association, grading through benmoreite to oversaturated trachyte and peralkaline sodic rhyolite (Smith, 1976) (Fig. 10.16). Despite the similar tectonic origin of D'Entrecasteaxu Islands and Sulcis suites, the TAS diagram shows that the trends depicted by the two suites differ, so rocks in this suite cannot be used as reference for those which occurred in the Sulcis. Since D'entrecasteaux Islands suite cannot be used as reference, comparison with other peralkaline suites is needed.

Bowden (1974) described the phenocryst assemblage for comendites, which is fairly constant throughout the different tectonic environments, and typically consists of sodic-sanidine and quartz. Fayalite (Fa_{98-100}), hedenbergite-aegirine, arfvedsonite-riebeckite, and ferrohastingsite are only rarely recorded as microphenocrysts. Occasionally anorthoclase is recorded instead of sodic

sanidine, with aenigmatite as major phenocrysts in some comendites. Such an assemblage is said to be more characteristic of pantellerites than of comendites. The petrographic study of the peralkaline magmas in the Sulcis has revealed a mineral assemblage dominated by sanidine, with only minor quartz in most rocks, accessory opaque minerals and rare amphibole phenocrysts, with late crystallising amphiboles forming poikilitic laths and idiomorphic crystals in vesicles. This assemblage is consistent with that described by Bowden (1974), especially if the sporadic observation of aenigmatite, aegirine and fayalite in the Sulcis comendites described in literature is considered (Assorgia et al., 1990b; Morra et al., 1994; Cioni et al., 2001).

Regarding parental trachytes, those of Volcán las Navajas in the Mexico Volcanic Belt, which depict the trend in Figure 10.16 to which the studied comendites are closer to, show phenocrysts of alkali feldspar, ferrohedenbergite, and fayalitic olivine with a groundmass consisting of alkali feldspar laths with prisms of green ferrohedenbergite, iddingsitized olivine, Fe-Ti oxides, and small amounts of interstitial quartz (Nelson and Hegre, 1990). This assemblage strongly contrasts with that of the trachytes present in the Sulcis. This may be due to the higher agpaicity shown by these rocks, which differently from trachytes in the Sulcis, are close to and immediately above the peralkalinity limit. In Volcán las Navajas there is one trachyte that contrasts with the others because it is below peralkalinity and contains plagioclase, hornblende and biotite as phenocrysts, so it could be considered similar to a magma like that of MZ, which is the unit occurring immediately before comendites. In Pantelleria Island, Italy, where trachytes also reach peralkalinity, these are usually highly porphyritic (20-40 vol % phenocrysts) with abundant alkali feldspar, clinopyroxene, olivine, Ti-magnetite and ilmenite. The groundmass is almost exclusively glass, with sparse microlites of alkali feldspar, clinopyroxene, alkali-amphibole and Fe-Ti oxides (Civetta et al., 1998). In Mount Edziza complex (British Columbia, Canada) trachytes are not peralkaline, being nearly pure feldspar rock comprising sparse microphenocrysts of alkali feldspar in a trachytic groundmass of alkali feldspar laths, finely disseminated opaque oxides, minor interstitial sodic pyroxene and rarely sodic amphibole (Souther and Hickson, 1984). Given the initially low peralkalinity of the less evolved terms of CO and MU units, which present agpaitic index values close to 1, it is thought that trachytic parental magmas for the Sulcis comendites were probably below peralkalinity, having reached this in the rhyolitic field. Therefore, trachytic parental melts in the Sulcis probably presented an assemblage more similar to that of Mount Edziza than to that of Pantelleria or Volcán las Navajas.

Given the coincidence in whole rock geochemistry, petrography and mineral chemistry between Sulcis comendites and peralkaline magmas from other suites, it is assumed that the formation mechanism for the comendites in the Sulcis was the same as the one that formed comendites in

other areas; that is, by the evolution of a transitional to mildly alkaline magma suite from basaltic to trachytic compositions, and from there to peralkaline rhyolites by simple crystal fractionation. As previously explained, it is thought that the trachytic parental magmas for comendites presented a slightly higher alkalinity than those forming magmas in the third trend described in the TAS diagram (Fig. 10.1). In spite of this, the possibility of peralkaline magmas being formed by evolution of magmas similar to those forming the units in the third trend has been tested by using major element crystal fractionation numerical modelling, as was done by Morra et al. (1994), who genetically linked these two magmas. A more rigorous and systematic study is needed including major and trace elements modelling, but the first results obtained, which are thought to be significant, are given here as a first approach to the subject.

Average composition of NU unit has been used as parental magma because this unit was formed by one of the most alkaline magmas. The first modelling has consisted in calculating if plagioclase fractionation could generate a sufficient increase in alkalinity as to allow NU to reach peralkalinity. The result has been negative, even when mafic minerals were included in the fractionating assemblage. NU unit does not have enough CaO to produce sufficient plagioclase fractionation. This result rules out any possibility of NU being the parental magma of peralkaline units by simple crystal fractionation. A second possibility has been considered, in which reabsorption of a previously fractionated phase has been allowed.

The election of the reabsorbed phase has been done considering the major elements trends, in which peralkaline units show a marked enrichment in FeOt and depletion of Al_2O_3 relative to the other units. It has been considered previously in this chapter that this enrichment and depletion was caused by progressive feldspar fractionation, with quartz buffering the silica content of the magma. If it is considered that at least some part of these trends was caused by some phase reabsorption, the best candidate to match this effect is amphibole. Pyroxene assimilation would produce a strong enrichment in MgO, which is not observed, whereas biotite would produce it in TiO_2; amphibole is the only mineral containing the right element proportions, and moreover is the one that can be more easily destabilized, as evidenced by its preferential occurrence as an unstable phase. Its high FeOt and low Al_2O_3 can explain the observed trends. Regarding other released elements, fractionation of feldspars would capture most of them, while spinel would capture TiO_2. Spinel also retains FeOt, but it would not do it in enough quantity as to avoid its enrichment. Amphibole assimilation not only can explain the observed trends in major elements, but also has other advantageous effects when the objective is reaching peralkalinity. The agpaitic index of amphiboles is high (in the Sulcis it ranges from around 2 for the calcic amphiboles to up to 30 for the sodic ones), thus its reabsorption may produce a strong increase in alkalinity. In

addition, released CaO can favour further crystallisation of plagioclase, the agent traditionally considered responsible for alkalinity increase. In this sense amphibole reabsorption is optimal. This fact was also observed by Mungall and Martin (1995) when trying to model the generation of comendites from trachytic melts in Terceira, Azores. The authors saw that any attempt of using amphibole in the assemblage for mass-balance calculations invariably resulted in amphibole addition. Regarding petrographic evidences for this process having occurred, only scarce sodic-calcic amphibole phenocrysts can be found in some CO. These may show signs of instability and reabsorption, but this is a common feature of amphiboles, as seen in many other units in the Sulcis, and therefore cannot be taken as evidence for significant amphibole assimilation. Once the assimilated phase has been chosen, calculations have been done.

For this calculation average composition of MU unit has been chosen as objective composition because this unit represents one of the less evolved peralkaline magmas in the Sulcis. Calculation has been done using major elements and the Solver tool in Microsoft Excel. Optimization of the fractionating assemblage has been done by minimization of the sum of the squares of the relative differences (in %) between objective and calculated compositions for each element, and results have been only considered valid when the sum of the squares was below 1 for both absolute and relative differences. MnO and P_2O_5 have not been considered for optimization because their concentrations are very low in these magmas, hence analytical error having a stronger effect in these elements, which may distort the results when optimizing using relative differences. Obtained results are only preliminary and for guidance, but have shown that objective composition could be reached if assimilation of amphibole occurred. To give an approximate idea of the magnitude of the amphibole assimilation needed, a calculation has shown that NU could reach MU compositions by fractionation of 6.8 wt % plagioclase, 36.8 wt % sanidine, 1.2 wt % biotite, 8.9 wt % quartz, 1.7 wt % spinel (20 wt % TiO_2 and 80 wt % FeOt), and assimilation of 1.8 wt % amphibole. Feldspar compositions used are those of the sanidine and plagioclase found in the NU unit, and biotite is that of MZ. The amphibole composition used is that of the sodic-calcic phenocrysts occasionally found in CO, although similar results are obtained if a calcic amphibole like that found in the non-peralkaline units is used.

This hypothesis has several drawbacks. It requires the presence of amphibole as a fractionating phase, which has only been observed in some units. The presence of amphibole may be favoured by higher water pressure, which is not unlikely to have been present if it is taken into consideration that the last magma before comendites is that of MZ unit, which has abundant biotite. A second consideration relates to the location of the amphibole. Reaching rhyolitic compositions from primitive magmas requires a large amount of crystal fractionation, so the

amphibole should be expected to be present mainly as a cumulate phase, with only some phenocrysts being within the magma body. Location of the amphibole may facilitate or make difficult amphibole reabsorption and incorporation into the magma. If amphibole suspended in the magma is considered to be in enough amount, a simple variation in temperature (e.g. increase by income of a hotter magma into the magma chamber) or change in the water pressure conditions may produce amphibole destabilization and sufficient reabsorption (Scaillet and Evans, 1999; Scaillet and Macdonald, 2001). If the participation of amphibole in the cumulate is required, it is more difficult to think of a mechanism not only producing reabsorption, but also extracting the amphibole-rich melt from the cumulate area and homogenising it with the rest of the chamber. One of the main drawbacks is, though, the occurrence of peralkaline magmas over a range of time and magma inputs. The process of amphibole crystallisation and subsequent destabilization and reabsorption should have been repeated over time to keep generating peralkaline magmas. If such was the case it could be thought that cooling history of these magmas was such that this process automatically occurred as one more stage of their evolution. Evolved non-peralkaline magmas as those forming PA and PM would then represent either magmas with an initially different composition which underwent a different evolution path, or similar magmas for which the cooling conditions changed avoiding the same processes that generated peralkaline magmas to occur. The different location of peralkaline and PA and PM magmas in the trace element binary diagrams seems to rule out this second possibility. Finally, although numerical modelling using also trace elements is yet to be done, the marked trace element chemical differences presented by peralkaline magmas relative to the rest of the ignimbritic sequence seem to preclude the tested possible origin of peralkaline rocks by evolution of magmas as those forming units such as the NU. Taking into account this fact and the similarity of perakaline magmas in the Sulcis to other suites in which comendites evolved from more alkaline trachytic melts by simple fractional crystallisation, it is considered that this latter process is the most plausible one for explaining the formation of the studied comendites.

10.5 CONCLUSIONS

The analysis of data obtained on petrography, mineral chemistry and whole rock geochemistry has allowed the obtaining of information on the evolution of the Oligo-Miocene magmas of the Sulcis from their formation to its eruption to the surface.

In first place it has been seen that the Sulcis ignimbritic sequence was formed by the arrival, differentiation and eruption of several magma batches with slightly different initial compositions. In fact, all units but for LE and SE were formed from different magma batches.

Despite the different compositions of the several magmas, these followed a similar differentiation path dominated by crystal fractionation processes, assimilation having had a very small effect, only appreciable in Pb isotopes. In the more primitive magmas fractionating assemblage was dominated by pyroxenes, plagioclase and spinel, although amphibole and biotite may occasionally have significantly contributed to magma evolution. In more evolved magmas sanidine appeared in the fractionating assemblage, while pyroxene presence decreased. The most differentiated magmas presented a fractionating assemblage largely dominated by sanidine, with occurrence of quartz in the peralkaline magmas which buffered SiO_2 content. Apatite fractionation in the ignimbritic sequence occurred as evidenced by P_2O_5 content decrease. Zircon is found in several units although its fractionation was not enough to compensate the enrichment in Zr in the magmas caused by the fractionation of the other mineral phases until an advanced evolutionary stage was reached (PA and PM units). Peralkaline magmas represent an exception to this trend; in peralkaline melts increased zircon solubility prevented its crystallisation and removal, producing a continuous enrichment in Zr in these melts.

Peralkaline magmas are thought to have formed by evolution by simple crystal fractionation of magmas slightly more alkaline than those found in the Sulcis, and which were not sampled by any of the studied eruptions. The possibility of the more alkaline regular magmas in the Sulcis (NU unit) being the parental magmas of peralkaline ones has been tested using numerical modelling. Although further work is needed, it has been found that no relation by simple crystal fractionation is possible, and that the only way in which these two magmas could be related is by a mechanism of crystal fractionation plus assimilation of previously precipitated amphibole.

The study of feldspar petrography and mineral chemistry has shown that crystallisation conditions changed along the sequence, with variations induced by magma composition differences, magma mixing/mingling processes, assimilation of wall rock, or different water activity. Regular feldspar crystallisation involved the apparition of plagioclase as the first crystallising feldspar. As magmas evolution progressed, these reached a cotectic in the feldspar ternary system, simultaneously crystallising two feldspars (plagioclase and sanidine) whose compositions progressively converged towards the feldspar system minimum composition. Further magma evolution caused magmas to reach a reaction zone in which plagioclase was reabsorbed as it changed in composition. In the most extreme case, that of peralkaline magmas, these crystallised a single alkali feldspar (sanidine), and both the liquid and feldspar reached the minimum composition in the Ab-Or system. Magma mingling produced the occurrence of different feldspar populations in a single unit and the destabilization of these (PC, MC). Higher water pressure delayed the crystallisation of

sanidine (as in SP or MZ units). Finally, wall rock assimilation produced anomalous compositional zoning in sanidines in the MU unit.

CONCLUSIONS

During the complex recent evolution of the western Mediterranean, Sardinia played a central role, which was recorded by its tectonic evolution and volcanism during Oligo-Miocene and Plio-Pleistocene times. The Oligo-Miocene volcanism in Sardinia provides key information on the initial processes of this geological evolution, which implied the drift and rotation of the Corsica-Sardinia microplate from the European continental margin to its present position. In particular, the Sulcis corresponds to the crustal part of the Corsica-Sardinia block that underwent most displacement and extension during drifting and rotation of this microplate. In this area, a special volcanic suite was formed which began sharing the same calc-alkaline characteristics as the rest of the subduction-related volcanism throughout Sardinia but later migrated to different compositions, mildly alkaline, including the rarely occurring peralkaline volcanism. In spite of the marked differences of the Sulcis magmatism with respect to that in other regions of Sardinia and of its great interest and importance as a source of information for the correct interpretation of the recent geodynamic evolution of central and western Mediterranean and the volcanism associated with it, until this present research this sector could be regarded as probably the poorliest known Oligo-Miocene volcanic area in Sardinia from a geochemical, petrological and volcanological point of view. This special volcanic suite was considered to be only one more manifestation of the widespread subduction-generated orogenic volcanism of Sardinia. This study has, at least partially, solved this situation. A thorough and detailed study of the Sulcis Oligo-Miocene volcanic suite has been carried out which has allowed the revision of the available data on volcanostratigraphy and cartography, the characterization of the geochemistry, petrography and mineral chemistry of the several units present in this suite, and the obtaining of significant information on the petrogenesis of this suite and its geodynamic significance. Next, a summary of the main results and conclusions obtained in this work are exposed.

- The revision of the volcanostratigraphy of the Sulcis ignimbritic suite has resulted in the definition of a new unit, Carloforte, located between Monte Ulmus and Parigianu units. This unit, previously considered to be part of Monte Ulmus, crops out in San Pietro Island and the northern mainland and is characterized by bearing large highly porphyritic black pumices.
- The systematic sampling and analysis of the whole rock geochemistry of all the described ignimbritic units in the Sulcis has allowed the characterization of its chemistry and the development of a methodology for unit recognition based on whole rock geochemistry. Although this methodology has been developed for fresh samples, it has been observed that it also works for most of the available data from slightly altered rocks. Geochemistry-based unit recognition has been a fundamental tool for solving volcanostratigraphic and mapping doubts during the development of this research, and remains a powerful tool for future studies.
- Isotope and trace element data have revealed that the mantle beneath Sardinia presented in pre-Late Cretaceous times an EMI signature which was subsequently modified by the CAP event in Late Cretaceous and by subduction-released fluids from Oligocene to Miocene. The CAP event metasomatised the existing mantle by introducing a HIMU signature which produced the change in composition of the mantle from EMI to EAR-like. Metasomatism was not complete and left a diffusely stratified mantle with an upper part with an EMI signature and a lower more EAR-like region, both of them having an OIB mantle source-like composition. Subduction released into the mantle wedge hydrous fluids and partial melts carrying sediment and MORB isotope and trace element compositions, which introduced mostly into the more EAR-like mantle a subduction signature.
- Oligo-Miocene orogenic magmas, including the andesitic lower sequence in the Sulcis, were produced in the subduction-modified more EAR-like mantle portion by lowering of the melting temperature due to the input of subduction fluids.
- Magmas from the ignimbritic sequence in the Sulcis are interpreted to have had an origin different to that of the rest of the Oligo-Miocene magmatism in Sardinia. Unlike all the previous petrogenetic theories, which considered them as part of the regular orogenic magmatism, it is proposed that they represent a transition from orogenic to anorogenic magmatism. It is suggested that the transition was due to a change in the melting mechanism from fluid- to extension-controlled, related to the cessation in the subduction influence below the Sulcis. Despite the change in the melting mechanism, the magma source continued to be the subduction-modified more EAR-like mantle.

- As a consequence of the previous point, volcanics in Isola del Toro are reinterpreted to be a late occurrence of the same magmatism that generated the ignimbritic sequence in the Sulcis, and not an early manifestation of the Plio-Pleistocene anorogenic magmatism as previously proposed.
- The mechanism proposed to explain the contemporaneous occurrence of both orogenic and anorogenic magmatisms in Sardinia during the emplacement of the Sulcis ignimbritic suite is the formation of a slab break-off which started south of Sardinia and progressed northwards opening a slab window. A slab break-off not only explains the occurrence of anorogenic magmas, but also the strong slowdown in subduction and roll-back of the trench, which produced the 6 Ma-long pause in magmatic and tectonic activity between the end of the Corsica-Sardinia rotation and the opening of the southern Tyrrhenian basin.
- The ignimbritic sequence in the Sulcis was formed by the arrival and differentiation of several magma batches with slightly different initial compositions, apparently at least one for each unit except for Lenzu and Seruci units.
- Magma differentiation was dominated by crystal fractionation processes, which produced similar evolutionary trends, assimilation having a very small effect only appreciable in Pb isotopes. The fractionating assemblage in the more primitive magmas was dominated by pyroxenes, plagioclase and spinel, although amphibole and biotite may occasionally have significantly contributed to magma evolution. In more evolved magmas sanidine appeared in the fractionating assemblage, while pyroxene presence decreased. The most differentiated magmas presented a fractionating assemblage largely dominated by sanidine, with the occurrence of quartz in the peralkaline magmas which buffered SiO_2 content.
- Peralkaline magmas are interpreted to have formed through evolution by simple crystal fractionation of magmas slightly more alkaline than those found in the Sulcis, which were not sampled by any of the studied eruptions. The possibility of the more alkaline regular magmas in the Sulcis (NU unit) being the parental magmas of peralkaline ones has been tested using numerical modelling. Although further work is needed, it has been found that no relation by simple crystal fractionation is possible, and that the only way in which these two magmas could be related is by a mechanism of crystal fractionation plus assimilation of previously precipitated amphibole.
- The study of feldspar petrography and mineral chemistry has shown that feldspar crystallisation conditions changed along the sequence, with variations induced by magma composition differences, magma mixing/mingling processes, assimilation of wall rock, or

different water activity. Regular feldspar crystallisation involved the apparition of plagioclase as the first crystallising feldspar. As magmas evolution progressed, these reached a cotectic in the feldspar ternary system, simultaneously crystallising two feldspars (plagioclase and sanidine) whose compositions progressively converged toward the feldspar system minimum composition. Further magma evolution caused magmas to reach a reaction zone in which plagioclase was reabsorbed as it changed in composition. In the most extreme case, that of peralkaline magmas, these crystallised a single alkali feldspar (sanidine), and both the liquid and feldspar reached the minimum composition in the Ab-Or system. Magma mingling produced the occurrence of different feldspar populations in a single unit and the destabilization of these (PC, MC). Higher water pressure delayed the crystallisation of sanidine (as in SP or MZ units). Finally, wall rock assimilation produced compositional zoning in sanidines in the MU unit.

This study has provided significant information on the magma source, melting mechanisms and evolution of the magmas in the Sulcis and on its geodynamic implications. However, there is still a huge amount of information to be obtained from this volcanic suite which will require a lot of future work. One of the first necessary steps is to carry out the detailed dating of the ignimbritic sequence. This will allow us to constrain in time the processes involved in this area, and to correct more precisely isotope data, especially Sr. The dating of these materials was one of the initial objectives of this study, but time and economic constraints finally resulted in it being beyond the possibilities of it. Regarding petrogenesis, new data on isotopes not yet analysed, as oxygen, may proportionate valuable supplementary information which will help to support or withdraw the hypotheses proposed in this work, especially on assimilation processes. At the same time, more detailed numerical modelling on crystal fractionation processes, using both major and trace elements, may provide more constraints on the evolution of magmas, and especially on the origin of peralkaline magmas. Further investigation is also needed on the evolution of the magma chambers system beneath the Sulcis through a more detailed study of the petrography and volcanostratigraphy of the ignimbritic sequence, thermobarometric calculations being necessarily an important part of any work attempting to solve the problem. Finally, there is a field of study which hasn't been dealt with in this work but that is, however, of great importance: the study of the eruption and emplacement mechanisms of the ignimbritic sequence of the Sulcis, which will provide lots of information on the dynamics of large volume ignimbrites including eruption, transport, emplacement and post-emplacement evolution. A particularly interesting case is the study of the formation of the basal vitrophyres. Traditional textural observations will need to be

combined with new data sources, such as oxygen isotope ratios, which will probably reveal the origin of the water involved in the formation of these special levels. This is not intended to be a systematic revision of all the work that remains to be done in the Sulcis, but only an approximation to the future research that will be carried out in the area by the author of the present study and the host research group.

APPENDIXES

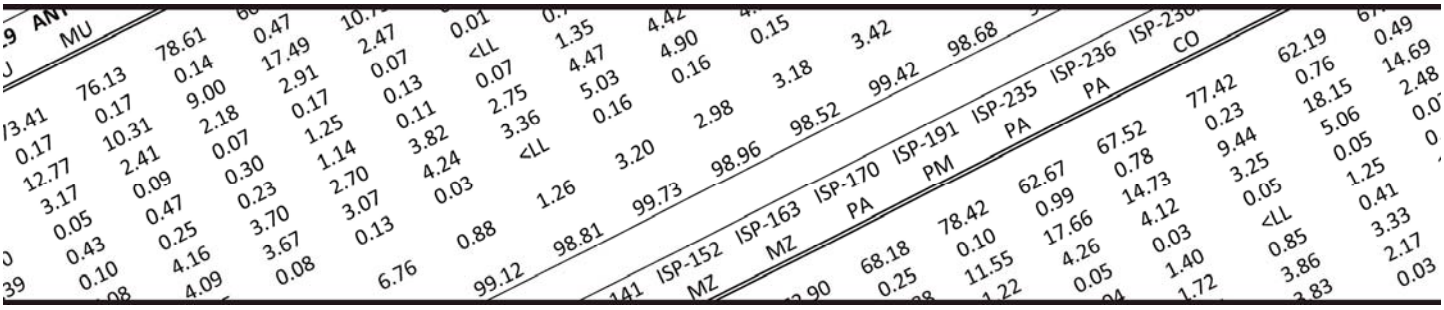
MU
ISP-152
ISP-163
ISP-170
ISP-191
ISP-235
ISP-236
CO
MZ
PA
PM
PA
PA

APPENDIX 1: REFERENCE CHART

REFERENCE CHART

Abbreviation and symbols		Phenocryst content (vol%) and assemblage		Short description
CL	☆	10	sa+pl+opq±zrn	Colonne/Punta Genniò: moderately welded cinerite
PM	★	<1	sa+ano+pl+opq+a.m. ±zrn	Punta Mingosa: moderately welded aphyric cinerite
SP	○	1-20	pl+ano+opq+px+amp	Serra di Paringianu: extremely welded and eutaxitic. Abundant extremely flattened light and dark grey pumices. Basal vitrophyre
PA	◆	<10	sa+pl+opq±bt±zrn	Paringianu: scarcely to moderately welded complex unit. Mostly cineritic. Low porphyricity and pumice content.
CF	✚	10-20	sa+opq+ano	Carloforte: strongly welded and eutaxitic with abundant sanidine-bearing black pumices. Also grey and white pumices.
MU	⬡	<3	sa+qz+opq+zrn +amp(v)	Monte Ulmus: stronlgy welded and eutaxitic aphyric unit with scarce pumices. Basal vitrophyre.
CO	▽	5-30 up to 50	sa+qz+amp+opq +amp(v)	Comendites: complex unit. Lava flows and variably welded ignimbrites with or without basal vitrophyre.
MZ	✖	3-20	pl+bt+opq	Matzaccara: variably welded. Presents bronze-coloured biotite.
MCR	+	5-20	sa+pl+opq±zrn	Montagna di Capo Rosso: lava flows and moderately welded lithic rich ignimbrites.
PC	Y	up to 50	ano+pl+opq+cpx+opx	Punta dei Cannoni: moderately to strongly welded, eutaxitic and porphyritic unit. Abundant big (several dm) pumices.
NU	✖	20-30	sa+pl+opq+cpx±amp(v)	Nuraxi: extremely welded and eutaxitic. Scarce extremely flattened grey pumices. Rheomorphic structures are abundant. Basal vitrophyre.
CA	✚	10	sa+pl+opq	Conca is Angius: slightly welded complex unit. Abundant pumices and accidental lithics. Degassing structures present.
MC	★	10-20	sa+pl+opq+amp(v)	Monte Crobu: moderately to extremely welded and eutaxitic. Abundant grey and occasionally black flattened pumices. Rheomorphic. Bas .Vit.
MLN	⬟	<5	pl+opq±bt	Monte la Noce: lava flows, cinerites and moderately to extremely welded ignimbrites with basal vitrophyre. Aphyric.
SE	●	10-20	pl+opq+a.m.±opx±cpx +amp(v)	Seruci: highly welded and eutaxitic with dm-sized pumices. Basal vitrophyre.
AC	♦	10-20	pl+bt+opq±amp	Acqua sa Canna: poorly welded, formed by several flows with pumice normal grading.
LE	■	10-20	pl+sa+opq+opx±zrn	Lenzu: strongly welded and eutaxitic. Abundant dm-sized big pumices. Basal vitrophyre.
CM	△	10-30	pl+cpx+opq±bt±amp	Corona Maria: scarcely to moderately welded and eutaxitic. Abundant pumices and lithic fragments. Basal vitrophyre.
AND	X		pl+opx+cpx+opq±ol	Andesites: lava flows and domes with associated breccias.

Mineral abbreviations; amp: amphibole; ano: anorthoclase; bt: biotite; cpx: clinopyroxene; ol: olivine; opq: opaque mineral; opx: orthopyroxene; pl: plagioclase; px: pyroxene; qz: quartz; sa: sanidine; zrn: zircon; a.m.: altered mafic; (v): vapour phase

Figure A.1.1: Reference chart for this Thesis

APPENDIX 2: EXTRAS FROM CHAPTER 4

A.2.1 ELECTRON MICROPROBE

Element	Standard
Si	Diopside
Al	Corundum
Ca	Wollastonite
Na	Albite
K	Orthoclase
Mg	Periclase
Fe	synthetic Fe_2O_3
Ti	Rutile
Ba	Barite
Rb	synthetic $RbTiPO_4$
Mn	Rhodonite
Cr	synthetic Cr_2O_3
Ni	synthetic NiO

Table A.2.1: Reference samples used for the calibration of the electron microprobe

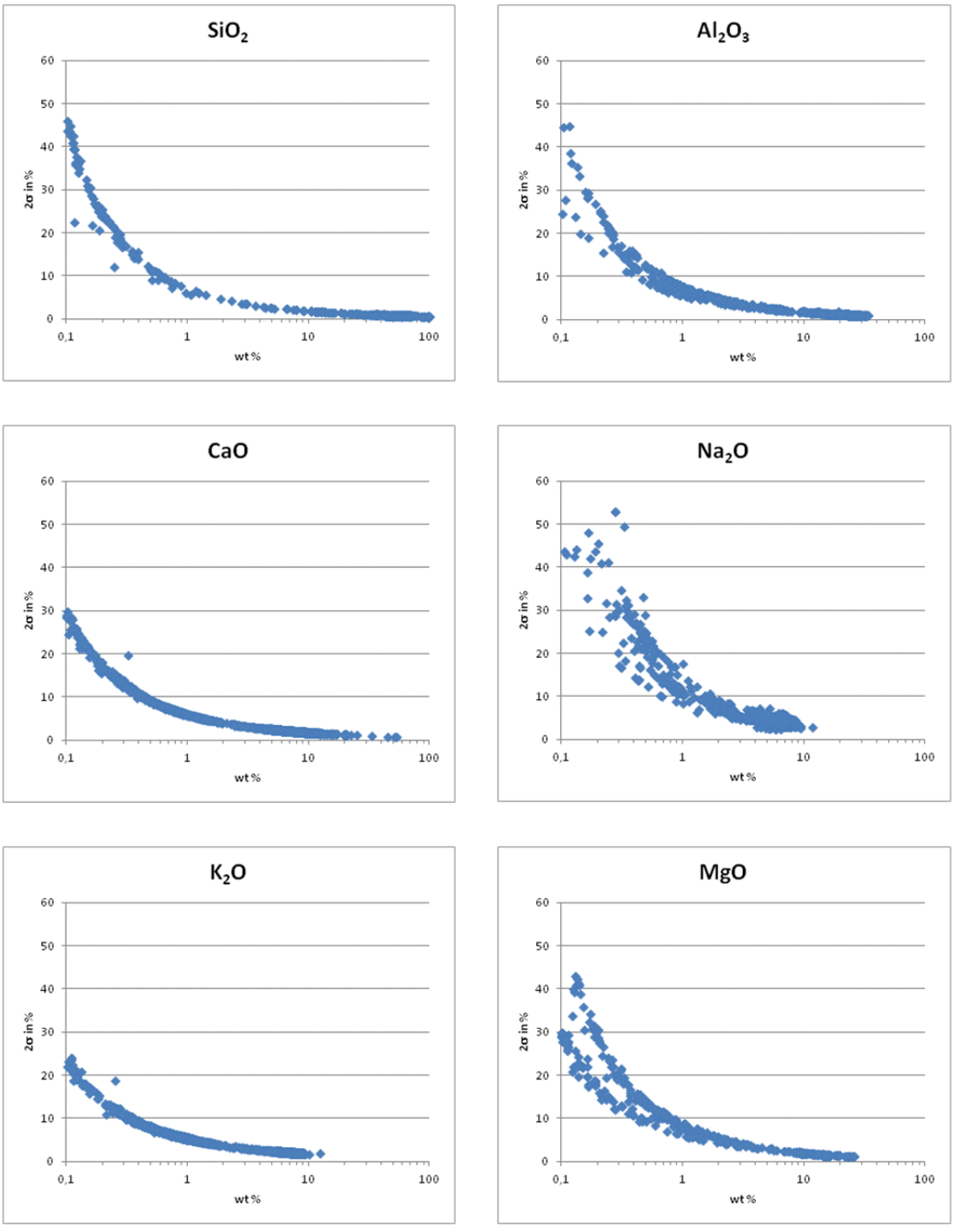

Figure A.2.1: Standard deviation (2σ) in microprobe analyses related to element concentration

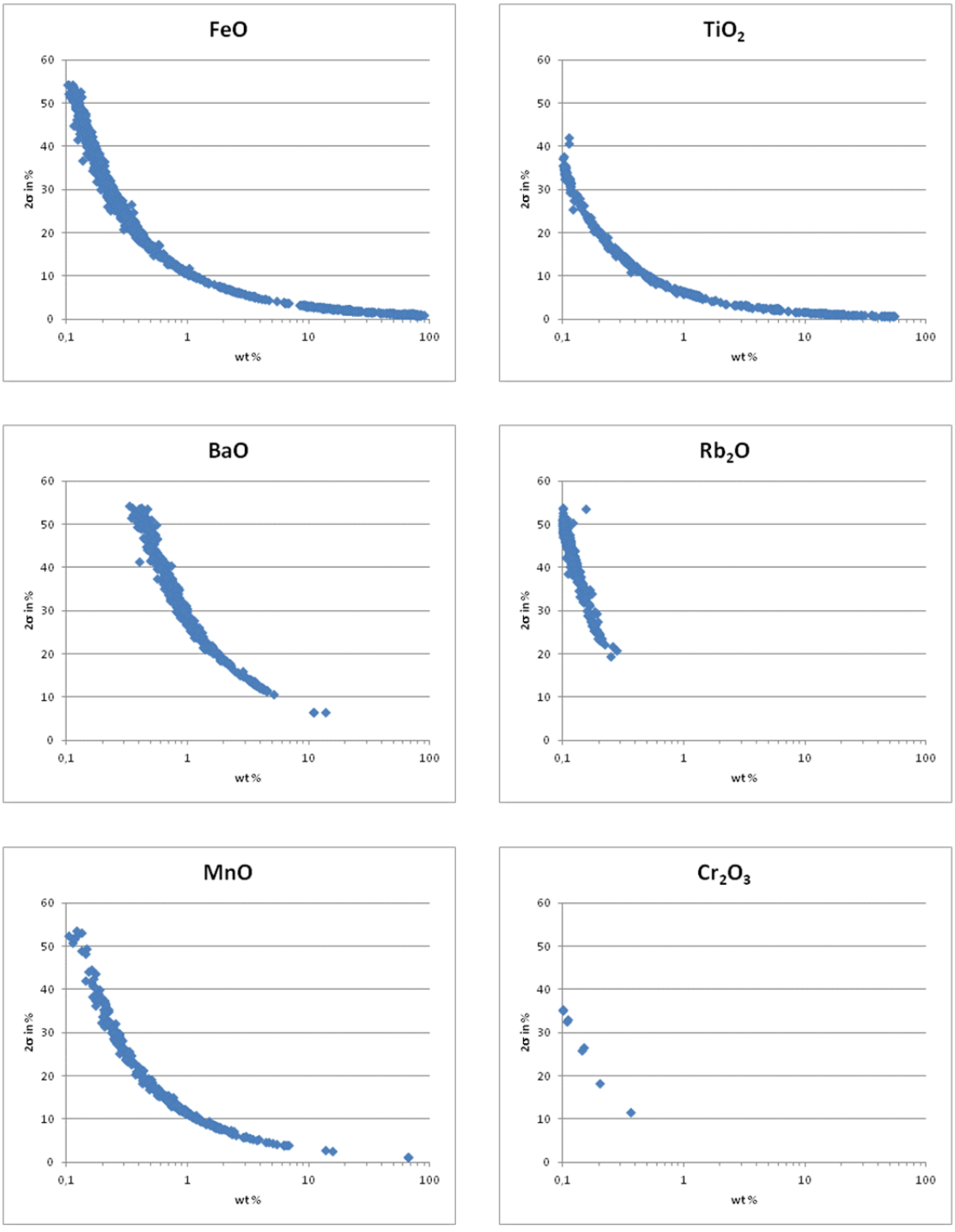

Figure A.2.1: (Continued) Standard deviation (2σ) in microprobe analyses related to element concentration

A.2.2 X-RAY FLUORESCENCE

Institution	Reference material	Institution	Reference material	Institution	Reference material
ANRT:	BX-N		GSD-5		BE-N
	DR-N		GSD-6		IF-G
	DT-N		GSD-7		MA-N
	FK-N		GSD-8		
	GL-O		GSD-9	MISC:	GV
	GS-N		GSD-10		MB
	UB-N		GSD-11		
			GSD-12	NIST:	NBS1645
BCS:	BCS375		GSR-1		NBS1C
	BCS376		GSR-2		NBS278
	BCS381		GSR-3		NBS688
	ECRM879-1		GSR-4		NBS88B
			GSR-5		NBS91
CCRMP:	SO-1		GSR-6		NBS97B
	SY-2		GSS-1		NBS98B
			GSS-2		
CRPG:	BR		GSS-3	NIM:	NIM-G
	GA		GSS-4		
	GH		GSS-5	NRC:	BCSS-1
	Mica-Fe		GSS-6		MESS-1
	Mica-Mg		GSS-7		
			GSS-8	USGS:	PCC-1
IGGE:	GSD-1				
	GSD-2	IWG-GIT	AC-E		
	GSD-3		AL-I		
	GSD-4		AN-G		

ANRT - National Working Group; Association Nationale de la Recherche Technique ANRT; Vandoeuvre, France
BCS - British Chemical Standards (BCS); Bureau of Analysed Samples (BAS); Middlebrou, Cleveland, England
CCRMP - Canada Center for Mineral and Energy Technology; Mines and Resources; Ottawa, Canada
CRPG - Centre de Recherches Pétrographiques et Géochimiques (CNRS); Vandoeuvre, France
IGGE - Institute of Geophysical and Geochemical Prospection; Ministry of Geology; Beijing, China
IWG-GIT - International Working Group; Analitical Standards of Minerals, Ores and Rocks; Vandoeuvre, France
MISC - Geological Research Laboratory; Sofia; Bulgaria
NIST - National Institute of Standards and Technology NIST (antic NBS); Gaithersburg, USA
NIM - SABS; Pretoria, South Africa
NRC - National Research Council; Institute for Environmental Chemistry; Ottawa, Canada
USGS - Branch of Geochemistry; Geological Survey; Denver Federal Center; Denver, USA

Table A.2.2: Reference samples used in the calibration of the Philips PW2400 sequential X-Ray spectrophotometer at the SCT-UB

	U	R	s	P	T	L	C	D	X	O	kV	mA	A	F+	F-
SiO_2	%	1.13 - 90.40	0.45	E	Rh	Kα	G	F	PE	1	40	70	109.2089	-	4.00
TiO_2	%	0.01 - 2.71	0.05	E	Rh	Kα	M	D	LIF200	1	40	70	86.1294	-	2.00
Al_2O_3	%	0.15 - 59.20	0.21	E	Rh	Kα	G	F	PE	1	40	70	145.1195	-	4.20
Fe_2O_3	%	0.07 - 25.65	0.31	E	Rh	Kα	M	D	LIF200	1	60	40	57.5133	-	2.00
MnO	%	0.01 - 0.35	0.01	E	Rh	Kα	M	D	LIF200	1	50	50	62.9680	2.00	2.00
MgO	%	0.12 - 43.51	0.13	E	Rh	Kα	G	F	PX1	1	40	75	22.3635	1.60	1.60
CaO	%	0.04 - 49.00	0.45	E	Rh	Kα	M	F	LIF200	1	40	70	113.0734	-	3.30
Na_2O	%	0.50 - 10.59	0.22	A	Rh	Kα	G	F	PX1	1	40	75	27.0102	1.80	1.80
K_2O	%	0.05 - 12.81	0.08	E	Rh	Kα	M	F	LIF200	1	40	70	136.6627	5.00	-
P_2O_5	%	0.01 - 15.70	0.01	E	Rh	Kα	G	F	GE	1	40	70	141.0351	3.20	-
Ba	ppm	40 - 2000	33	A	Rh	Kα	F	C	LIF220	1	60	40	15.6046	1.20	0.50
Ce	ppm	21 - 520	16	A	Rh	Kα	F	C	LIF220	1	60	50	14.4678	0.30	0.30
Co	ppm	5 - 112	6	A	Rh	Kα	F	D	LIF220	1	40	60	77.8942	1.00	0.50
Cu	ppm	4 - 1230	8	A	Rh	Kα	M	D	LIF200	1	60	50	45.0239	2.00	-
Ga	ppm	5 - 95	2	A	Rh	Kα	M	C	LIF200	1	60	50	38.9137	1.00	-
Mo	ppm	2 - 92	1	A	Rh	Kα	F	C	LIF220	1	60	40	28.9011	0.60	0.60
Nb	ppm	5 - 270	5	A	Rh	Kα	M	C	LIF220	1	40	30	30.4374	0.50	0.60
Ni	ppm	4 - 2380	9	A	Rh	Kα	M	D	LIF200	1	60	50	48.6632	1.00	1.00
Pb	ppm	3 - 928	8	A	Rh	Lß	F	C	LIF220	1	60	50	40.3786	0.80	0.80
Rb	ppm	10 - 3600	16	A	Rh	Kα	M	C	LIF220	1	60	50	37.9879	1.60	1.60
Sn	ppm	2 - 370	4	A	Rh	Kα	M	C	LIF200	1	60	40	14.0377	0.40	0.20
Sr	ppm	20 - 1370	11	A	Rh	Kα	M	C	LIF220	1	60	50	35.8550	0.70	0.70
Th	ppm	3 - 370	9	A	Rh	Lß	M	C	LIF220	1	60	50	31.1719	0.30	0.30
V	ppm	5 - 310	22	A	Rh	Kα	M	D	LIF220	1	40	75	123.1654	0.40	1.00
W	ppm	7 - 490	7	A	Rh	Lα	M	D	LIF200	1	60	50	430150	1.00	-
Y	ppm	7 - 180	2	A	Rh	Kα	M	C	LIF220	1	60	50	33.8976	0.90	0.90
Zn	ppm	10 - 1720	14	A	Rh	Kα	M	C	LIF200	1	60	50	41.7957	-	2.00
Zr	ppm	20 - 780	16	A	Rh	Kα	M	C	LIF220	1	60	50	32.0975	0.90	1.20

U: concentration units (in weight)
R: calibration limits (concentration range)
s: calibration sigma (*)
P: sample preparation (E: pearl, A: pressed pellets)
T: X-Ray tube(Rh anode)
L: spectral line used
C: collimator (G:thick/0.70mm, M: middle/0.30 mm, F: thin/0.15mm)
D: detector (F: flux, S: sealed, C: sparkling, D: duplex F+S)
X: dispersal crystal
O: optical order
kV: kilovolts
mA: milliamperes
A: ° goniometer angle (sen (2Θ))
F+: ° relative position of +background
F-: ° relative position of – background

(*) SIGMA(σ)
n = standards
k = regression coeficient
c.q.= chemical concentration
c.c.= calculated concentration

$$\sigma = \sqrt{\frac{\sum_n (c.q. - c.c.)^2}{n-k}}$$

Table A.2.3: Analytical conditions used in XRF analyses

Element	average concent.	σ	reference value	relative error (%)
major elements n=12, concentration in %				
SiO_2	51.17	0.14	50.96	0.42
TiO_2	1.38	0.02	1.44	-4.11
Al_2O_3	17.26	0.09	17.20	0.35
Fe_2O_3	11.68	0.19	11.41	2.33
MnO	0.17	0.00	0.18	-3.70
MgO	5.17	0.06	5.19	-0.43
CaO	9.67	0.09	9.79	-1.18
Na_2O	2.81	0.18	2.73	2.87
K_2O	0.77	0.01	0.78	-0.96
P_2O5	0.30	0.01	0.29	1.72
trace elements n=20, concentration in ppm				
Ba	235	12	245	-4.26
Ce	30.2	13.3	21.5	40.47
Co	30.9	1.2	34.3	-9.78
Cr	65.7	2.2	58.1	13.16
Cu	228	4	194	17.32
Ga	20.9	1.2	19.8	5.43
Mo	3.90	-	1.09	257.80
Nb	6.52	0.88	2.47	163.80
Ni	37.8	2.0	36.2	4.39
Pb	8.34	1.73	5.58	49.46
Rb	24.5	6.6	15.1	62.12
Sn	2.60	0.26	0.94	176.60
Sr	417	10	403	3.36
Th	6.56	2.74	1.27	416.82
V	279	4	372	-24.88
W	7.68	0.24	1.06 *	625.00
Y	27.1	2.1	26.9	0.69
Zn	100	2	100	0.20
Zr	107	3	98	9.76

Table A.2.4: XRF standard deviation calculated from n analyses of the sample JB-3 of the Geological Survey of Japan

A.2.3 INDUCTIVELY COUPLED PLASMA

Element	Wavelength (nm)	Calibration concentrations (μg/ml)				
		p0	p1	p2	p3	p4
Si	212/288	0	1	2	5	10
Ti	334.940	0	2.5	5	10	25
Al	308.215	0	10	25	50	100
Fe	259.939	0	10	25	50	100
Mn	257.610	0	0.2	0.5	1	2
Mg	279.077	0	10	25	50	100
Ca	317.933	0	20	50	100	200
Na	330.237	0	2	5	10	20
K	766.490	0	2	5	10	20
P	213.617	0	1	2.5	5	10
Ba	455.403	0	0.5	1.25	2.5	5
Sr	421.500	0	0.5	1.25	2.5	5
Zn	213.800	0	0.2	0.5	1	2

Table A.2.5: Concentrations of the calibration solutions for ICP-OES and peak wavelength

Element	JB-3				JR-3			
	average concent.	σ	reference value	relative error (%)	average concent.	σ	reference value	relative error (%)
SiO_2	52.90	2.02	50.96	3.81	-	-	-	-
TiO_2	1.40	0.02	1.44	-2.97	0.22	0.06	0.21	3.95
Al_2O_3	16.84	0.37	17.20	-2.11	11.11	3.90	11.90	-6.65
FeO_t	10.20	0.55	10.27	-0.63	4.33	0.99	4.21	2.91
MnO	0.18	0.00	0.18	-1.69	0.09	0.01	0.08	6.99
MgO	5.07	0.20	5.19	-2.22	0.05	0.00	0.05	4.23
CaO	9.71	0.21	9.79	-0.82	0.11	0.01	0.09	13.56
Na_2O	2.68	0.16	2.73	-1.65	7.97	0.91	4.69	69.91
K_2O	0.78	0.03	0.78	-0.59	4.26	1.87	4.29	-0.62
P_2O_5	0.29	0.02	0.29	-1.22	0.01	0.00	0.02	-42.32
Ba	234	7	245	-4.34	-	-	-	-
Sr	405	13	403	0.52	12.3	4.4	10.4	18.14
Zn	115	6	100	14.78	-	-	-	-

Table A.2.6: Precision and accuracy for ICP-OES measurements. JB-3 data are from Aulinas (2008), n=5; JR-3, this study, n=2

Element	Calibration concentration ng/ml				
	p0	p1	p2	p3	p4
As	0.0	1.0	2.0	5.0	10.0
Ba	0.0	1.0	2.0	5.0	10.0
Be	0.0	1.0	2.0	5.0	10.0
Bi	0.0	1.0	2.0	5.0	10.0
Ce	0.0	1.0	2.0	5.0	10.0
Co	0.0	1.0	2.0	5.0	10.0
Cr	0.0	1.0	2.0	5.0	10.0
Cs	0.0	1.0	2.0	5.0	10.0
Cu	0.0	1.0	2.0	5.0	10.0
Dy	0.0	1.0	2.0	5.0	10.0
Er	0.0	1.0	2.0	5.0	10.0
Eu	0.0	1.0	2.0	5.0	10.0
Ga	0.0	1.0	2.0	5.0	10.0
Gd	0.0	1.0	2.0	5.0	10.0
Ge	0.0	1.0	2.0	5.0	10.0
Hf	0.0	1.0	2.0	5.0	10.0
Ho	0.0	1.0	2.0	5.0	10.0
La	0.0	1.0	2.0	5.0	10.0
Li	0.0	1.0	2.0	5.0	10.0
Lu	0.0	1.0	2.0	5.0	10.0
Mo	0.0	1.0	2.0	5.0	10.0
Nb	0.0	1.0	2.0	5.0	10.0
Nd	0.0	1.0	2.0	5.0	10.0
Ni	0.0	2.5	5.0	10.0	25.0
Pb	0.0	1.0	2.0	5.0	10.0
Pr	0.0	1.0	2.0	5.0	10.0
Rb	0.0	1.0	2.0	5.0	10.0
Sc	0.0	1.0	2.0	5.0	10.0
Sm	0.0	1.0	2.0	5.0	10.0
Sn	0.0	1.0	2.0	5.0	10.0
Ta	0.0	1.0	2.0	5.0	10.0
Tb	0.0	1.0	2.0	5.0	10.0
Te	0.0	1.0	2.0	5.0	10.0
Th	0.0	1.0	2.0	5.0	10.0
Tl	0.0	1.0	2.0	5.0	10.0
Tm	0.0	1.0	2.0	5.0	10.0
U	0.0	1.0	2.0	5.0	10.0
W	0.0	1.0	2.0	5.0	10.0
Y	0.0	1.0	2.0	5.0	10.0
Yb	0.0	1.0	2.0	5.0	10.0
Zn	0.0	1.0	2.0	5.0	10.0
Zr	0.0	1.0	2.0	5.0	10.0

Table A.2.7: Concentrations of the calibration solutions for ICP-MS

Element	JB-3				JR-3			
	average concent.	σ	reference value	relative error (%)	average concent.	σ	reference value	relative error (%)
As	-	-	-	-	1.15	0.24	1.1*	4.55
Ba	-	-	-	-	63.8	3.3	65.8	-3.02
Be	-	-	-	-	7.59	0.37	7.6	-0.18
Bi	-	-	-	-	0.24	0.00	0.21*	12.12
Ce	21.5	0.8	21.5	-0.21	325	44	327	-0.64
Co	35.8	1.9	34.3	4.50	0.66	0.10	0.98	-32.29
Cr	56.7	1.8	58.1	-2.47	13.4	7.7	3.5	281.81
Cs	-	-	-	-	1.61	0.35	1	61.10
Cu	196	8	194	1.04	3.67	0.00	2.9	26.56
Dy	4.41	0.12	4.54	-2.80	12.0	0.2	21.5*	-44.36
Er	2.62	0.10	2.49	5.35	7.06	0.05	14*	-49.56
Eu	1.30	0.03	1.32	-1.33	0.35	0.02	0.53	-33.69
Ga	20.2	0.4	19.8	1.82	40.3	1.9	36.6	10.13
Gd	4.31	0.17	4.67	-7.80	18.1	0.4	19.7*	-8.11
Ge	-	-	-	-	2.72	0.27	-	-
Hf	2.72	0.17	2.67	1.75	18.4	0.4	40.3	-54.39
Ho	0.91	0.03	0.8	14.08	2.07	0.04	4.7*	-55.87
La	8.52	0.32	8.81	-3.29	170	14	179	-5.28
Li	-	-	-	-	115	13	120*	-3.95
Lu	0.37	0.01	0.39	-4.64	1.21	0.00	2.8	-56.95
Mo	1.22	0.14	1.09	12.05	0.74	0.16	0.49	50.44
Nb	1.49	0.96	2.47	-39.53	357	14	510	-29.98
Nd	15.4	0.5	15.6	-1.21	109	7	107	1.87
Ni	36.8	4.8	36.2	1.52	1.75	0.01	1.6*	9.58
Pb	5.66	0.33	5.58	1.45	38.6	0.1	32.8	17.74
Pr	3.13	0.14	3.11	0.72	32.4	1.3	33.1	-2.03
Rb	14.4	0.6	15.1	-4.52	436	38	453	-3.81
Sb	-	-	-	-	0.29	0.16	0.17*	69.82
Sc	35.0	4.1	33.8	3.55	0.72	0.12	0.5	43.79
Sm	4.09	0.13	4.27	-4.27	19.7	1.1	21.3	-7.40
Sn	3.11	3.71	0.94	230.76	18.3	0.7	17.4	5.22
Ta	0.16	0.05	0.15	4.54	49.8	30.0	36.8	35.30
Tb	0.74	0.02	0.73	1.32	2.15	0.03	4.29	-49.81
Te	-	-	-	-	0.31	0.04	-	-
Th	1.97	0.19	1.27	55.48	65.2	4.5	112	-41.77
Tl	-	-	-	-	0.54	0.04	0.93*	-42.13
Tm	0.38	0.02	0.42	-10.60	1.10	0.02	-	-
U	0.49	0.04	0.48	2.00	18.2	0.1	21.1	-13.88
V	-	-	-	-	0.30	1.12	4.2	-92.80
W	1.75	1.06	1.06*	64.67	5.11	3.04	7.8*	-34.47
Y	23.5	0.6	26.9	-12.53	54.4	3.4	166	-67.21
Yb	2.46	0.06	2.55	-3.49	7.98	0.20	20.3	-60.68
Zn	-	-	-	-	225	11	209	7.67
Zr	86.0	25.7	97.8	-12.09	518	18	1494	-65.33

Table A.2.8: Precision and accuracy for ICP-MS measurements. JB-3 data are from Aulinas (2008), n=5; JR-3, this study, n=2. *: values not certified

APPENDIX 3: LABORATORY PROTOCOLS

In this appendix the protocols for sample preparation for XRF and ICP analyses and LOI determination are presented.

A.3.1 PROTOCOL FOR THE DETERMINATION OF LOSS ON IGNITION (LOI) IN ROCKS BY MEANS OF CALCINATION

The method used for the determination of LOI is the following:

1. Ground samples and crucibles are placed in an oven at 90°C for at least 12 h to remove moisture.
2. Samples and crucibles are cooled to room temperature in a dessicator.
3. A crucible in weighted. The obtained value is 'A'.
4. 0.5 g of sample are introduced into the crucible and the whole is weighted. The obtained value is 'B'.
5. Steps 3 and 4 are repeated for each sample.
6. The crucibles with sample are introduced into a furnace at room temperature. The furnace is heated to 950°C and maintained at this temperature for at least 4 h. After calcination is complete the furnace is left to cool down to 100°C. The furnace used works under oxidizing environment.
7. Crucibles are removed from the furnace and placed into a dessicator to cool to room temperature.
8. The crucibles are weighted. The obtained value is 'C'.

To calculate the LOI the following formula is used:

$$LOI=[(C-A)/(B-A)]*100$$

The result is expressed in %, and reflects the content in structural volatiles of the analysed samples.

A.3.2 PROTOCOL FOR THE DETERMINATION OF MAJOR AND TRACE ELEMENTS BY MEANS OF XRF

Pearls and pressed pellets have been prepared for analysis following the SCT-UB preparation protocol.

Pearls

Pearls are used for the determination of major elements and are prepared as follows:

1. Ground samples are placed in an oven at 90°C for at least 12 h to remove moisture.
2. 0.3 g of sample are weighted in a pyrex glass.
3. Lithium tetraborate is added until the sample is diluted to 1/20 and thoroughly mixed with a glass rod.
4. The mixture is poured into a Pt crucible and between 5 and 10 ml of lithium iodide are added. Lithium iodide is used as tensioactive agent.
5. The mixture is fused at nearly 1250°C in a Perle'x 3 induction oven, which pours the melt into a Pt dish.
6. Steps 2 to 5 are repeated 3 times for each sample. The first pearl has a cleaning function; the other two are for analyses and duplicate.

Pressed pellets

Pressed pellets are used for the determination of trace elements and are prepared as follows:

1. Ground samples are placed in an oven at 90°C for at least 12 h to remove moisture.
2. 6 g of dry ground sample are mixed with 2 ml of Elvacite® diluted in acetone (20% solution) in an agate mortar until homogeneous powder is obtained.
3. The bottom of an Al capsule is filled with boric acid (powder) to save sample.
4. The mixture of sample and Elvacite® is placed over the boric acid in the Al capsule.
5. The filled capsule is then pressed at 200 kN for 1 minute

A.3.3 PROTOCOL FOR THE DETERMINATION OF TRACE ELEMENTS BY MEANS OF ICP

A whole rock total attack has been chosen for sample preparation. Samples have been prepared following an intern protocol of the research group:

1. Ground samples are placed in an oven at 90°C for at least 12 h to remove moisture.
2. 0.1 g of dry ground sample are weighted in a polytetrafluoroethylene (Teflon®) beaker.
3. 2.5 ml of HNO_3, 2.5 ml of $HClO_4$ and 5 ml of HF are added to the beaker.
4. The beaker is tightly closed and placed at 90°C for at least 12 hours.
5. The beaker is cooled to room temperature before opening, and then placed in a sand bath to evaporate its content until $HClO_4$ starts to evaporate (dense white smoke).
6. The beaker is removed from the bath and 5 ml of HF are added.
7. The beaker is closed and placed again at 90°C for 3 hours.
8. The beaker is cooled to room temperature. Then it is opened and the lid is washed with deionized water (milliQ Plus type (18.2 $M\Omega cm^{-1}$)) pouring the water into the beaker.

9. The beaker is placed again in a sand bath to evaporate to incipient dryness.
10. 1 ml HNO_3 is added, and beaker content is taken to incipient dryness once more; this step is done twice.
11. 1 ml HNO_3 and 2 ml deionized water are added and the beaker is heated in the sand bath until the pearl obtained by evaporation is dissolved
12. Attack solution is poured into a 100 ml volumetric flask which is afterwards filled with deionized water.
13. From each solution resulting from the total attack, two samples are prepared, one for ICP-MS and one for ICP-OES.

Beakers must be cleaned the day before the total attack. To carry out this cleaning, 3-5 ml of concentrated HNO_3 are poured into each beaker. The beakers are then tightly closed and placed in an oven at 90°C for about 12 h. Once cooled to room temperature, beakers must be rinsed first with distilled water and then with deionized water (milliQ Plus type (18.2 $M\Omega cm^{-1}$)).

APPENDIX 4: UNIT DISTRIBUTION

In this Appendix maps showing the outcropping areas of the studied units individually are provided. The first map contains town and landmark names to help following the descriptions given in Chapter 5 on the distribution of the different units. Next, one map per unit is provided, all of them sharing the same legend (Fig. A.4.1). Each unit is represented by the colour assigned to it in the legend of the reference chart in Appendix 1. Units below and above the represented unit are grouped and depicted in uniform colours (dark grey for the units below and light grey for the units above) to help visualize the stratigraphic position of the given unit.

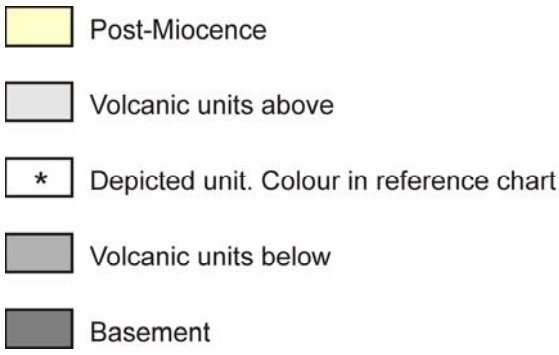

Figure A.4.1: Legend followed by maps in this Appendix

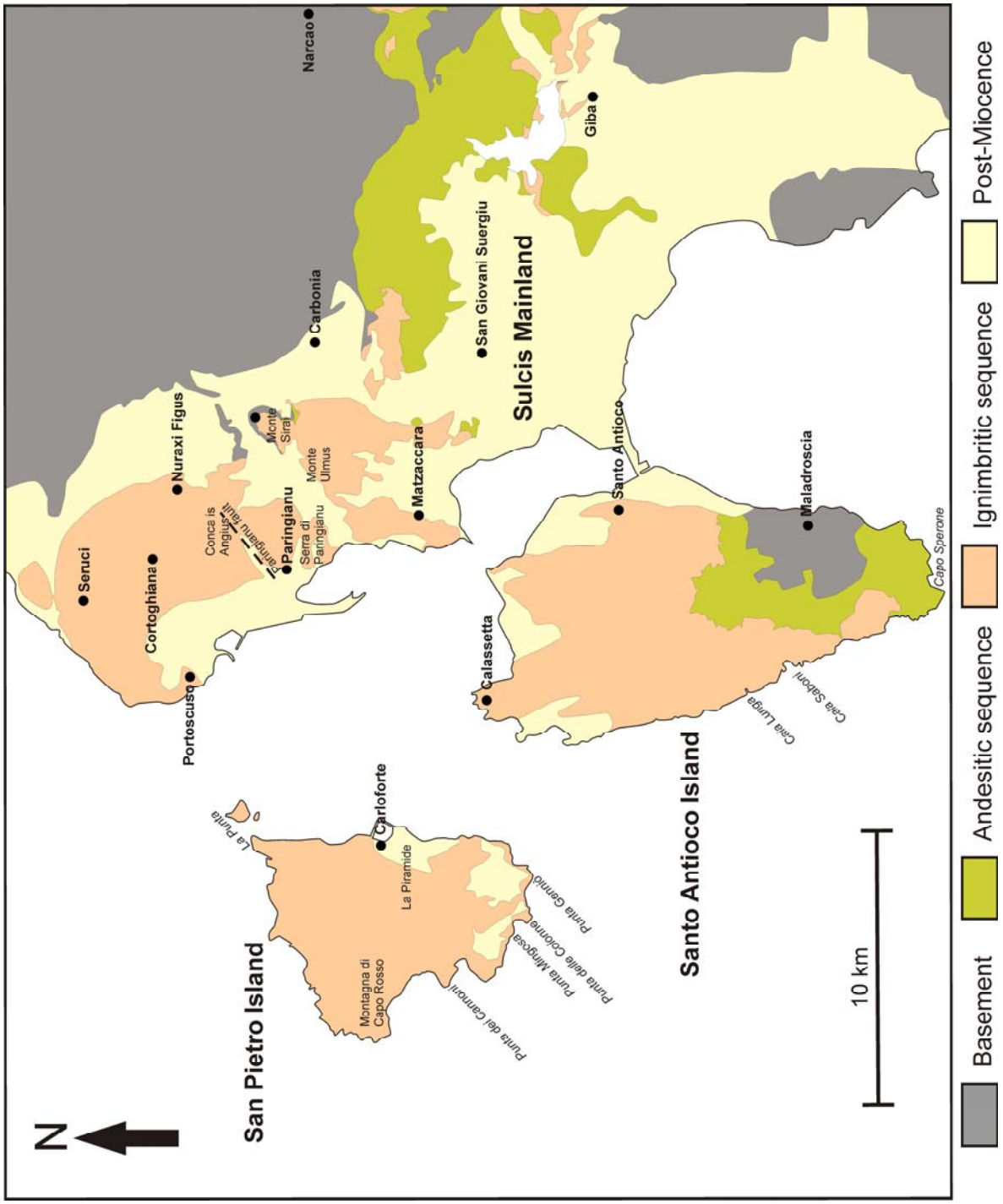

Figure A.4.2: Main towns and useful landmarks in the Sulcis area

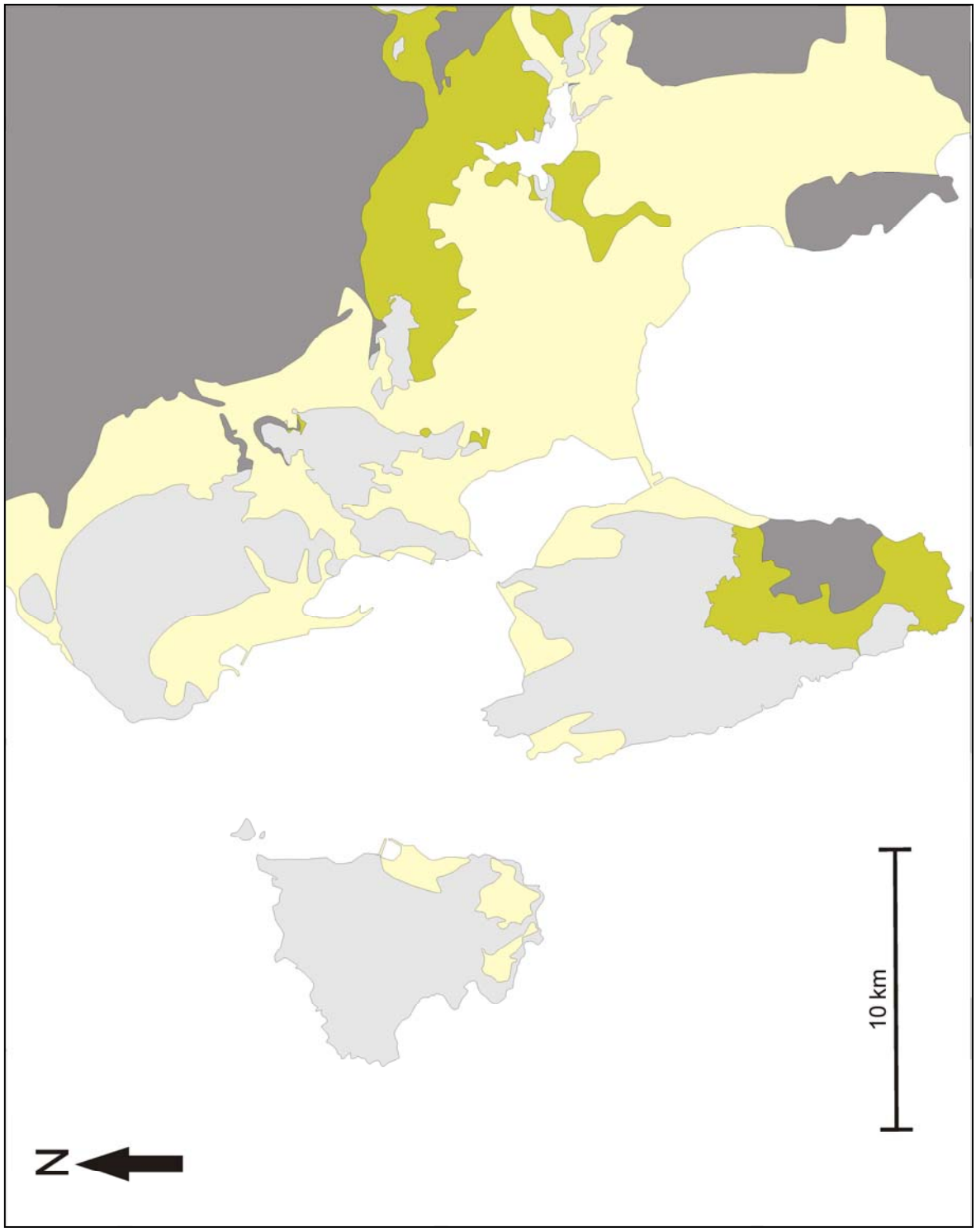

Figure A.4.3: Outcropping area of Andesites

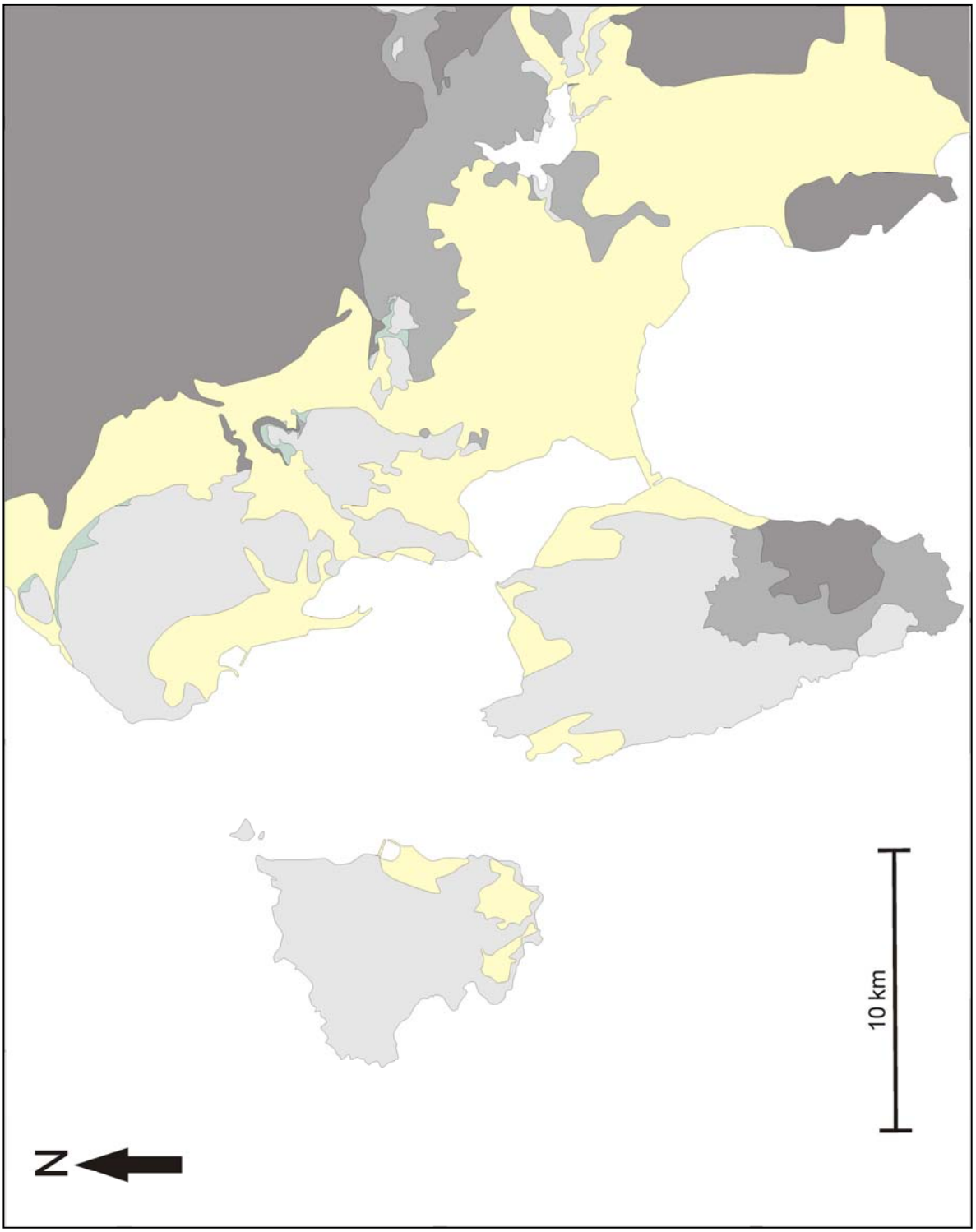

Figure A.4.4: Outcropping area of Corona Maria unit

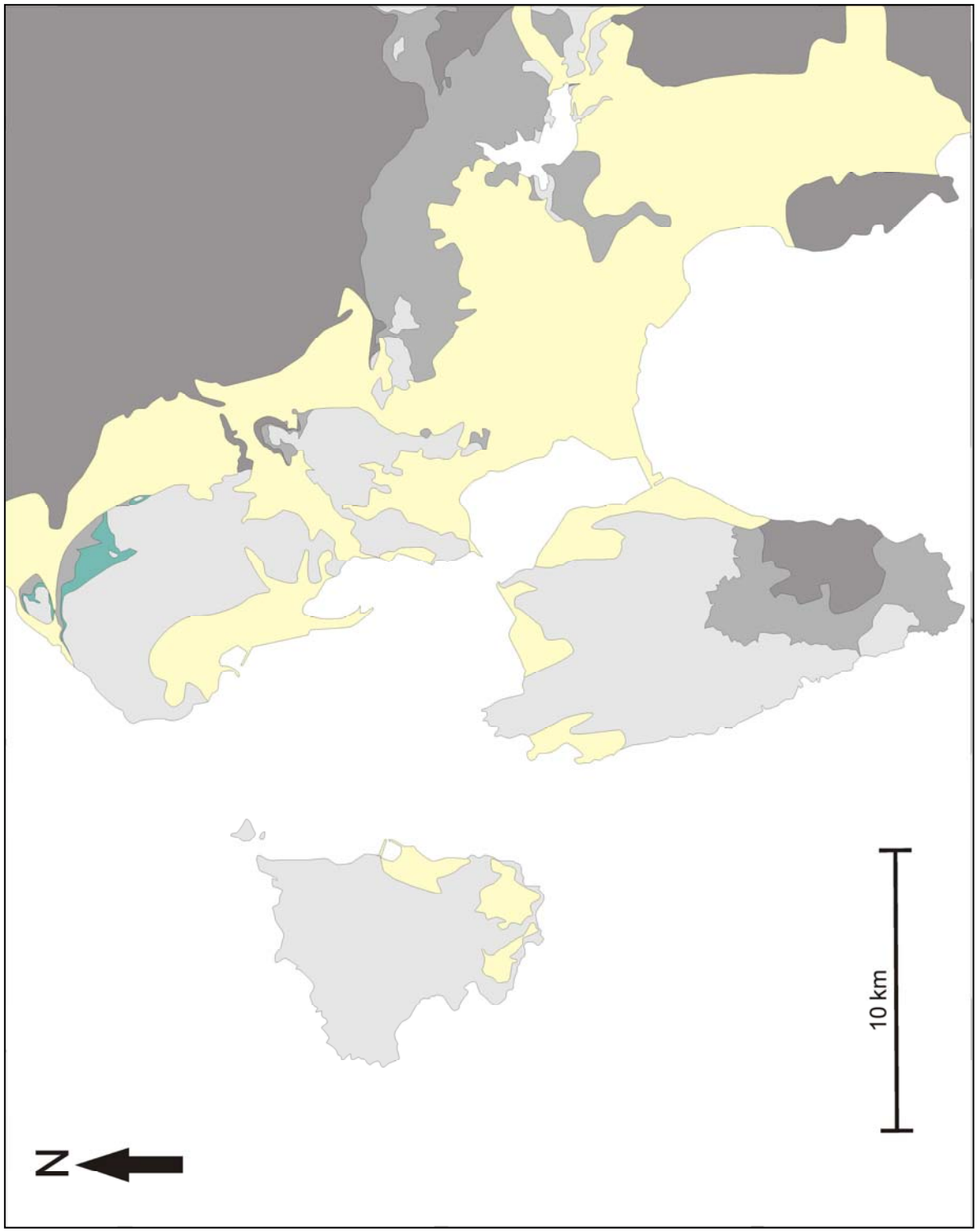

Figure A.4.5: Outcropping area of Lenzu unit

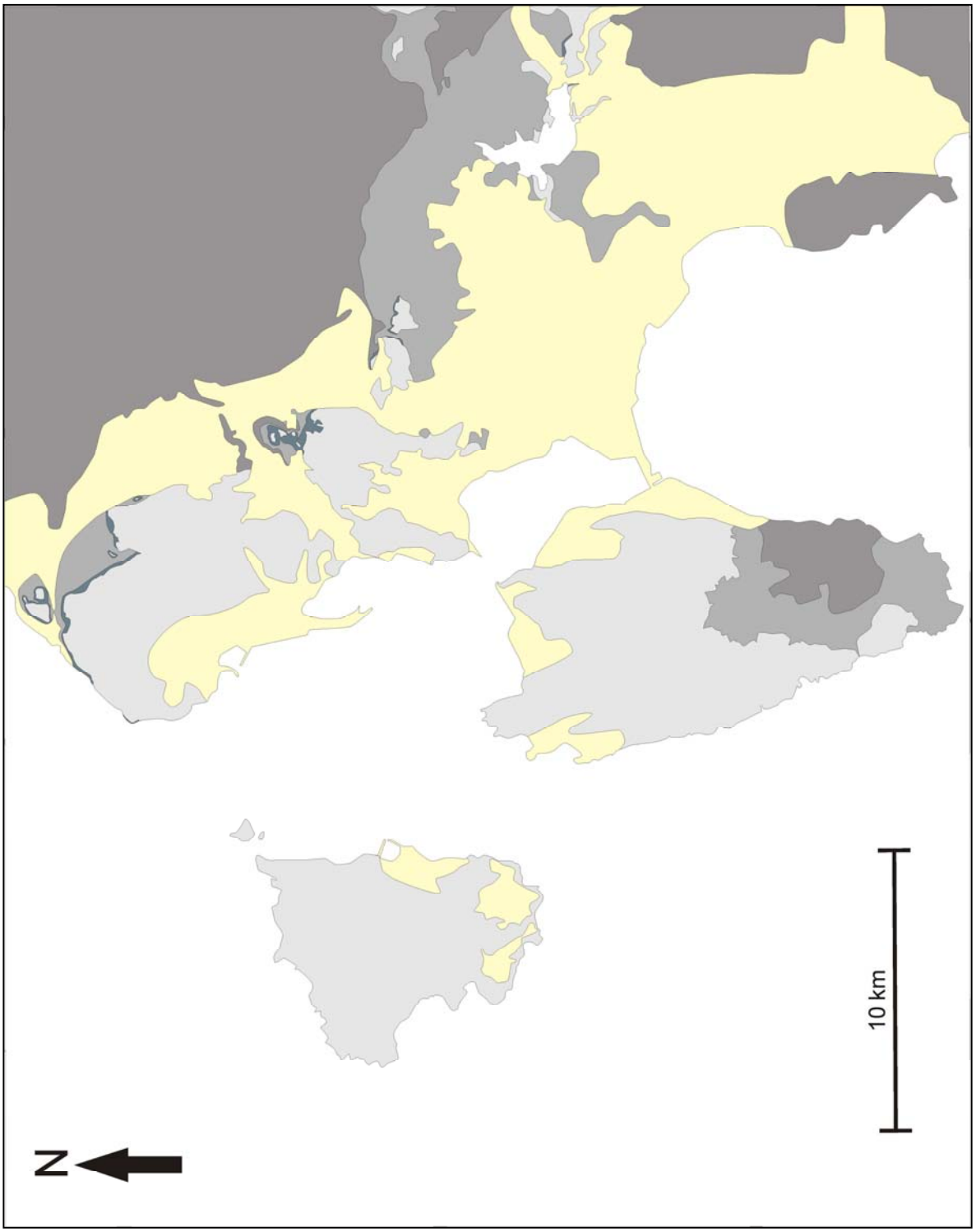

Figure A.4.6: Outcropping area of Acqua sa Canna unit

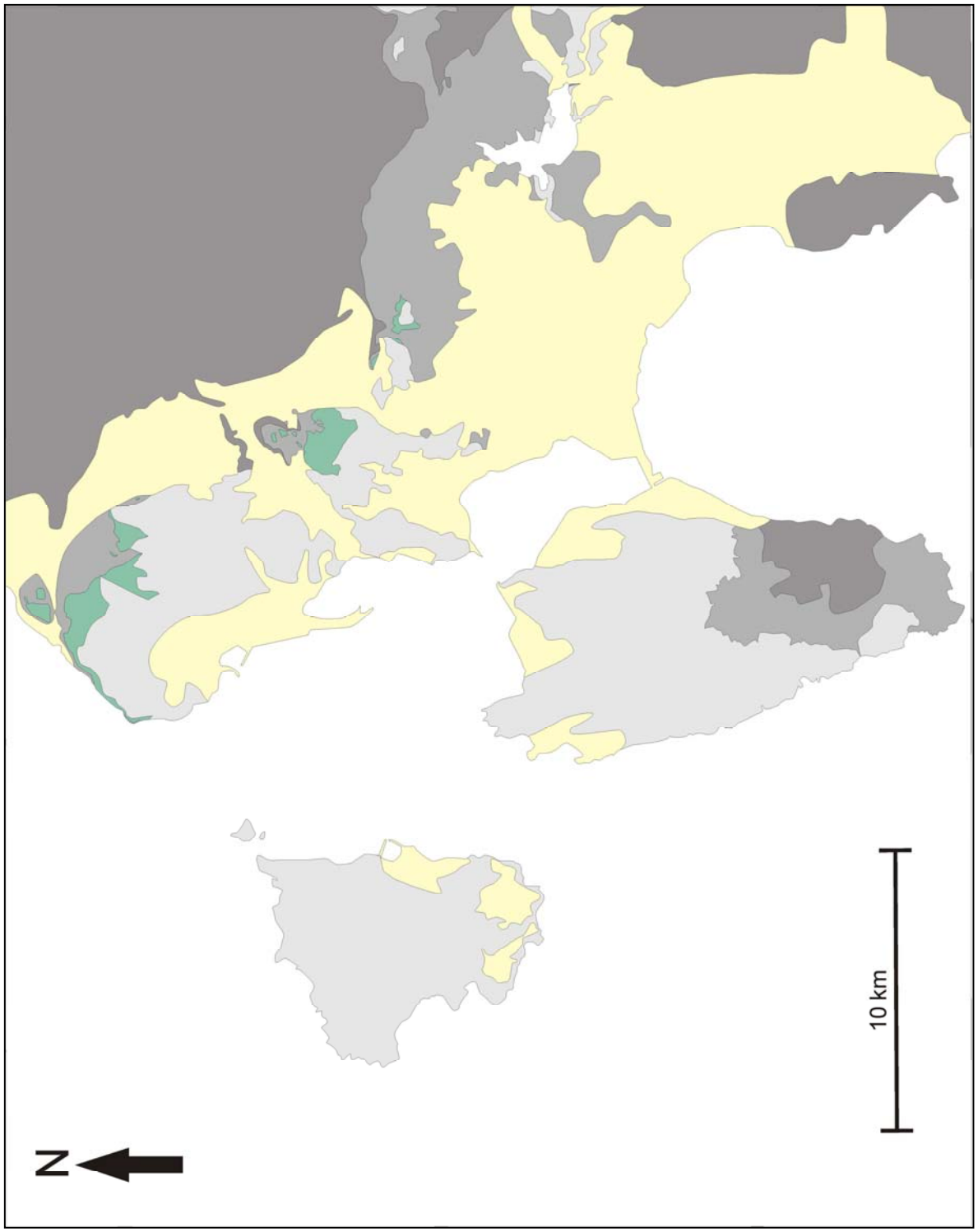

Figure A.4.7: Outcropping area of Seruci unit

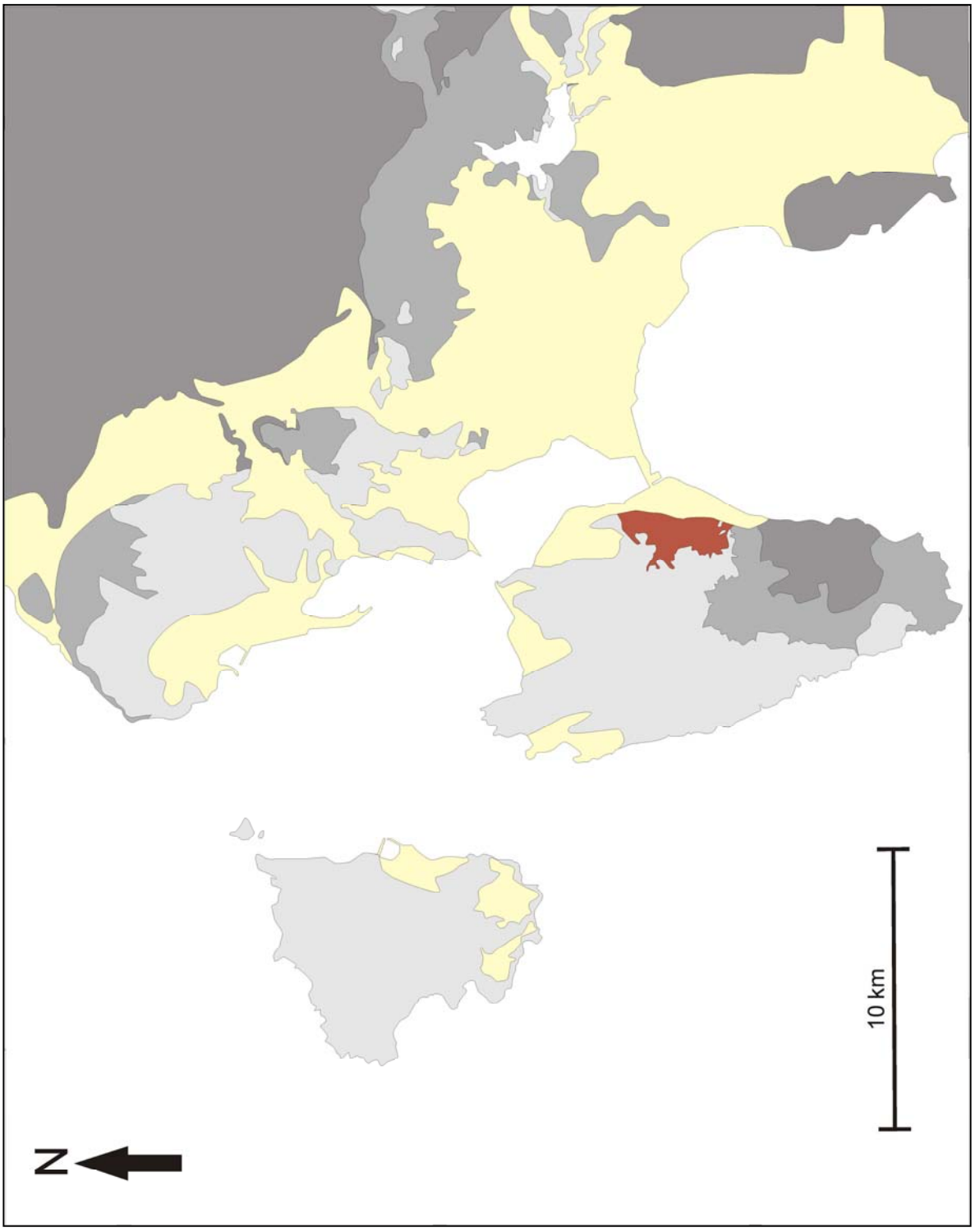

Figure A.4.8: Outcropping area of Monte la Noce unit

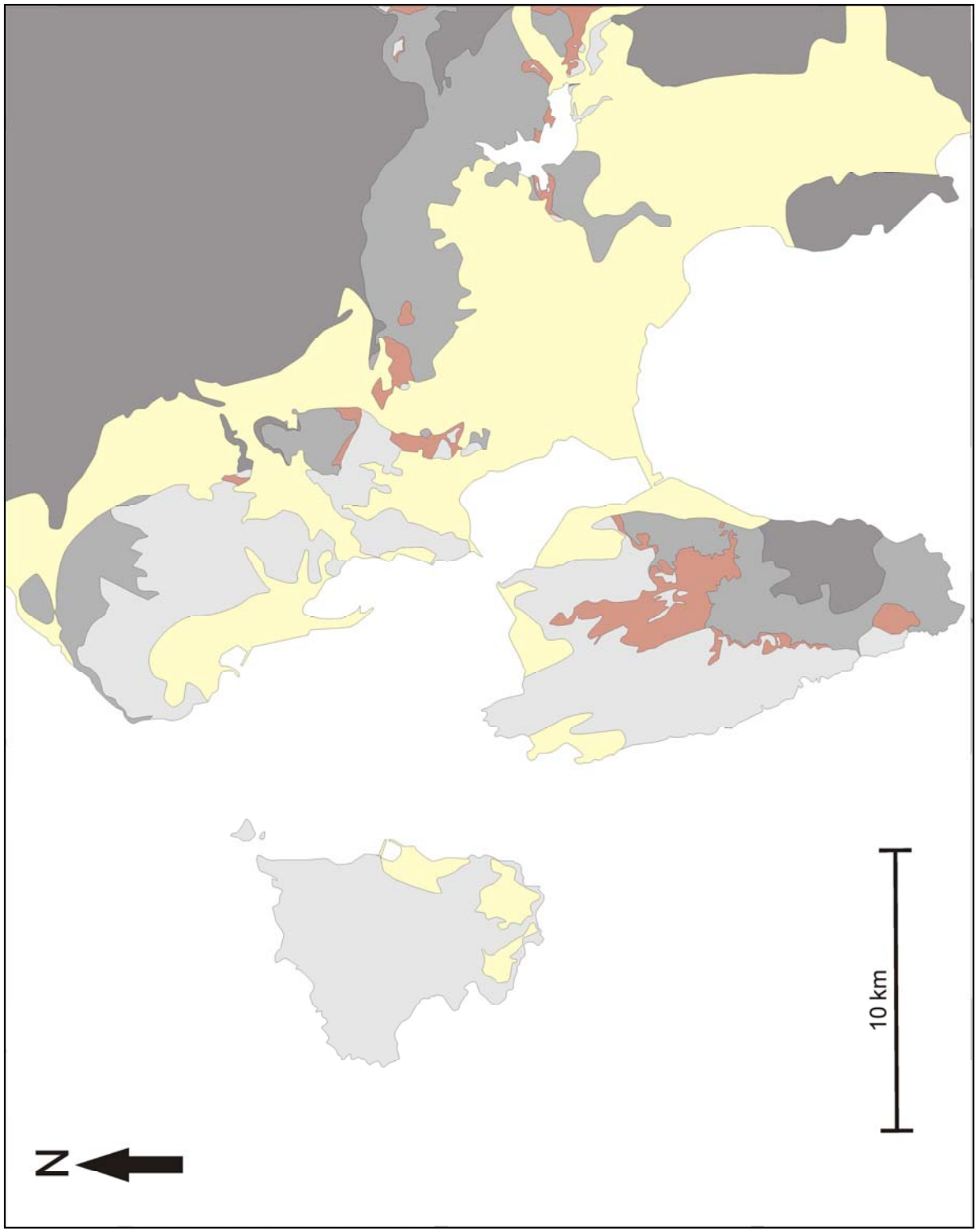

Figure A.4.9: Outcropping area of Monte Crobu unit

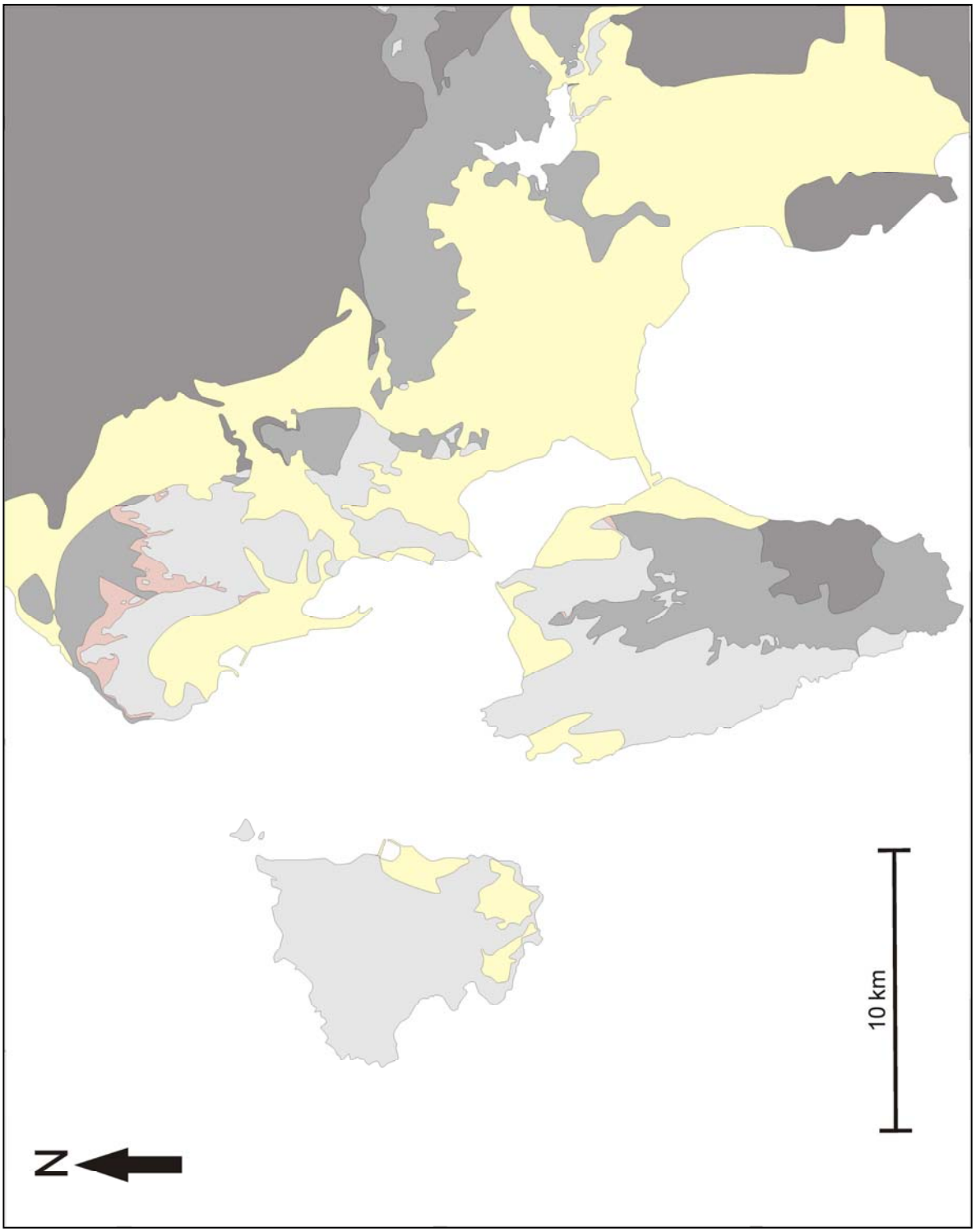

Figure A.4.10: Outcropping area of Conca is Angius unit

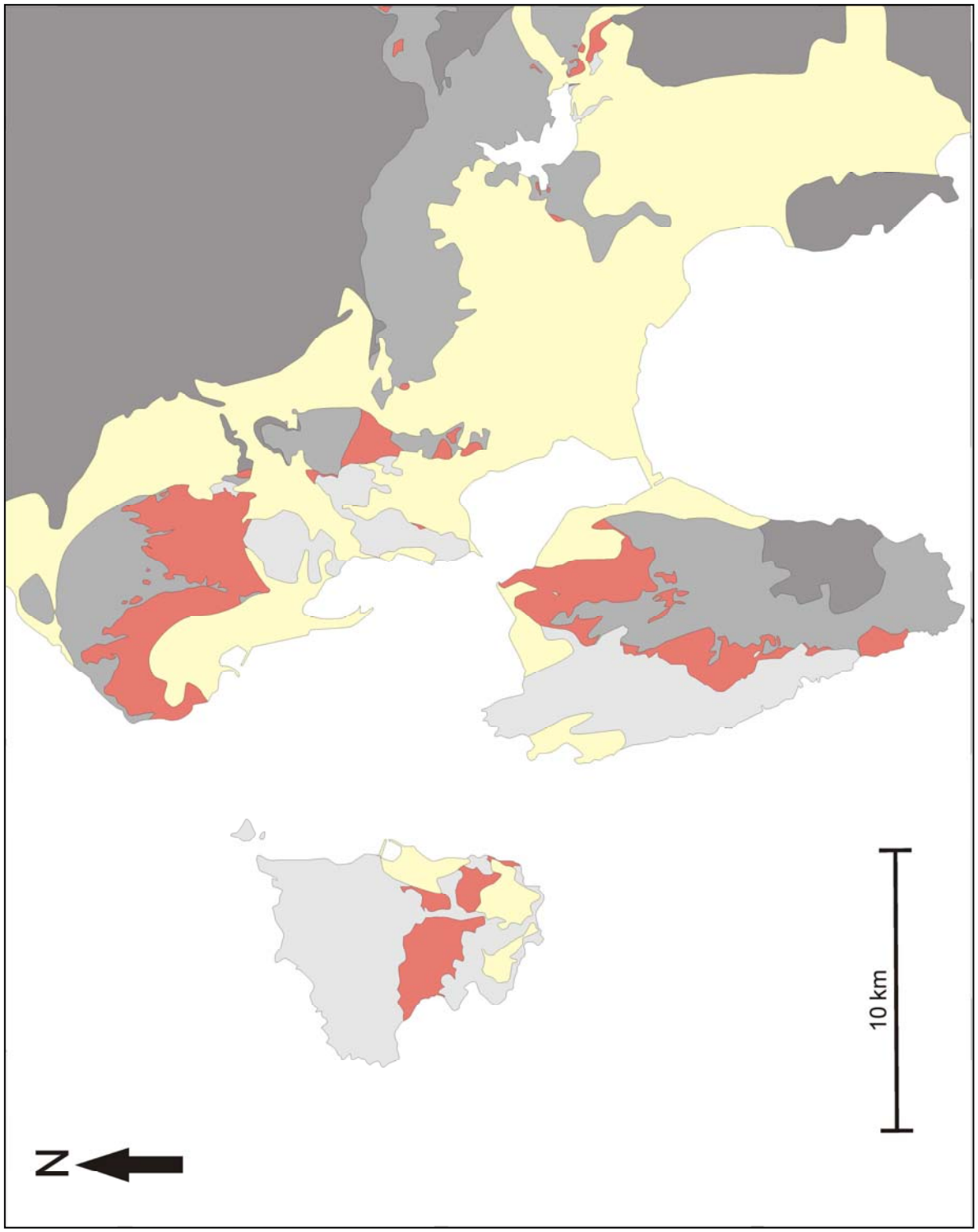

Figure A.4.11: Outcropping area of Nuraxi unit

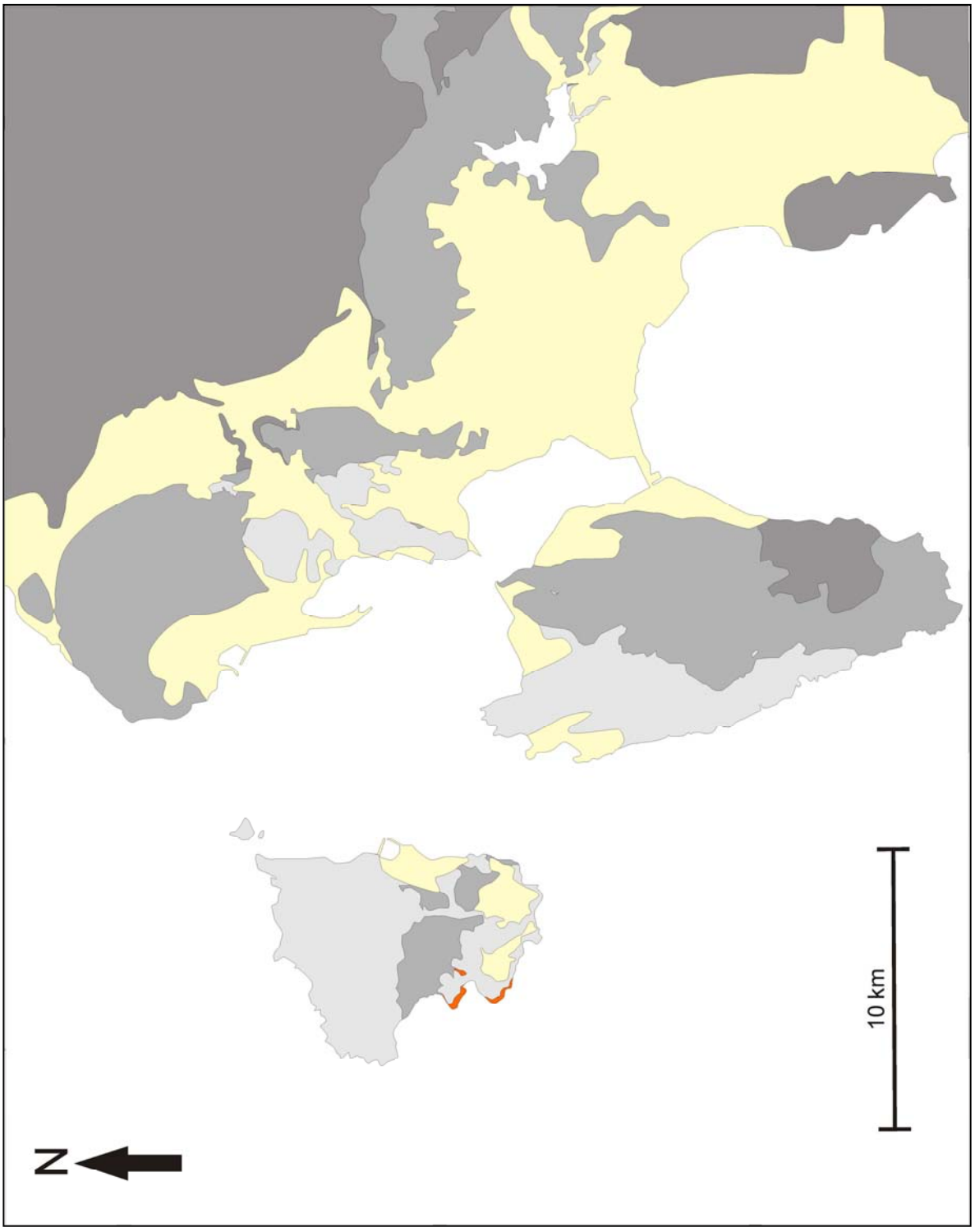

Figure A.4.12: Outcropping area of Punta dei Cannoni unit

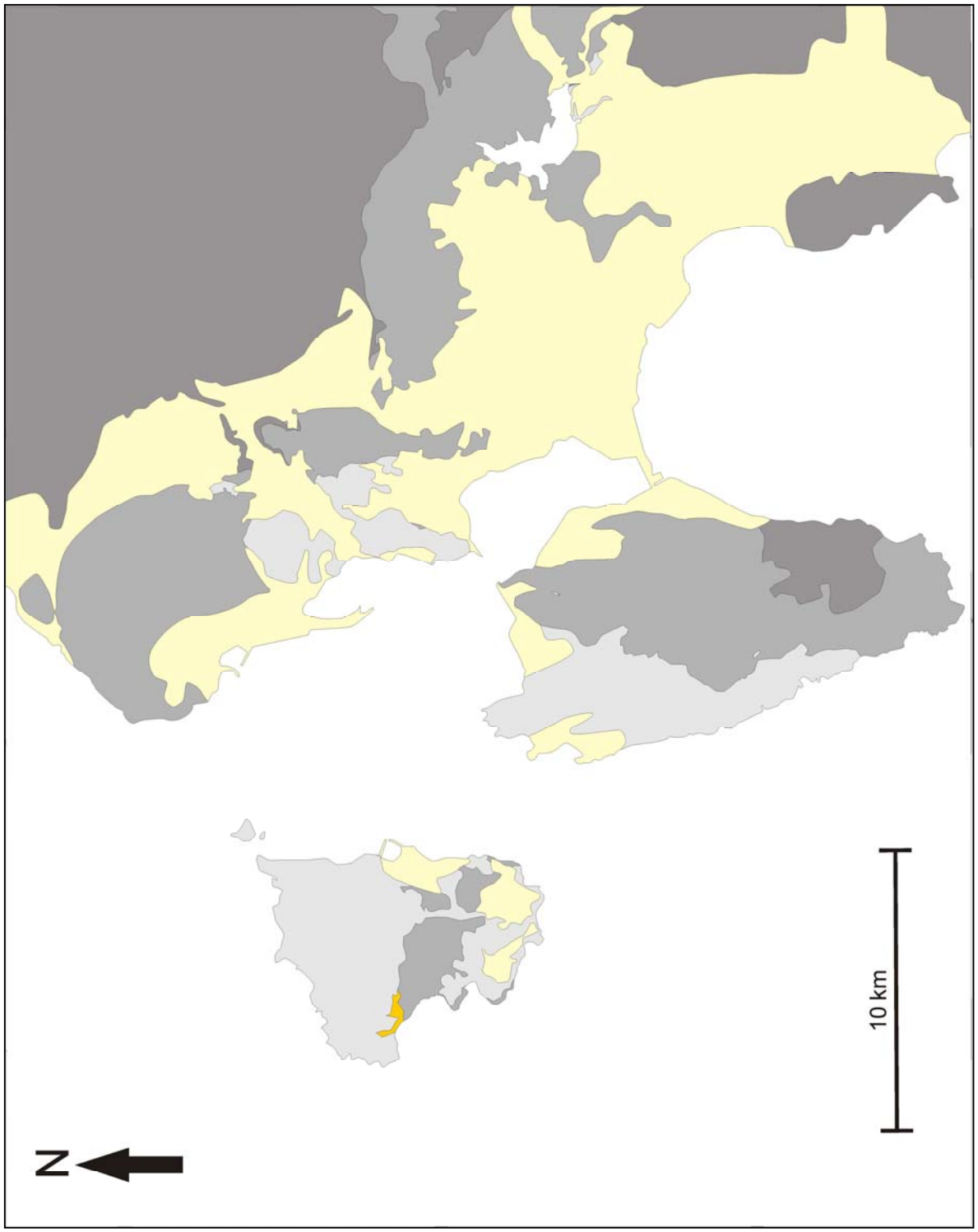

Figure A.4.13: Outcropping area of Montagna di Capo Rosso unit

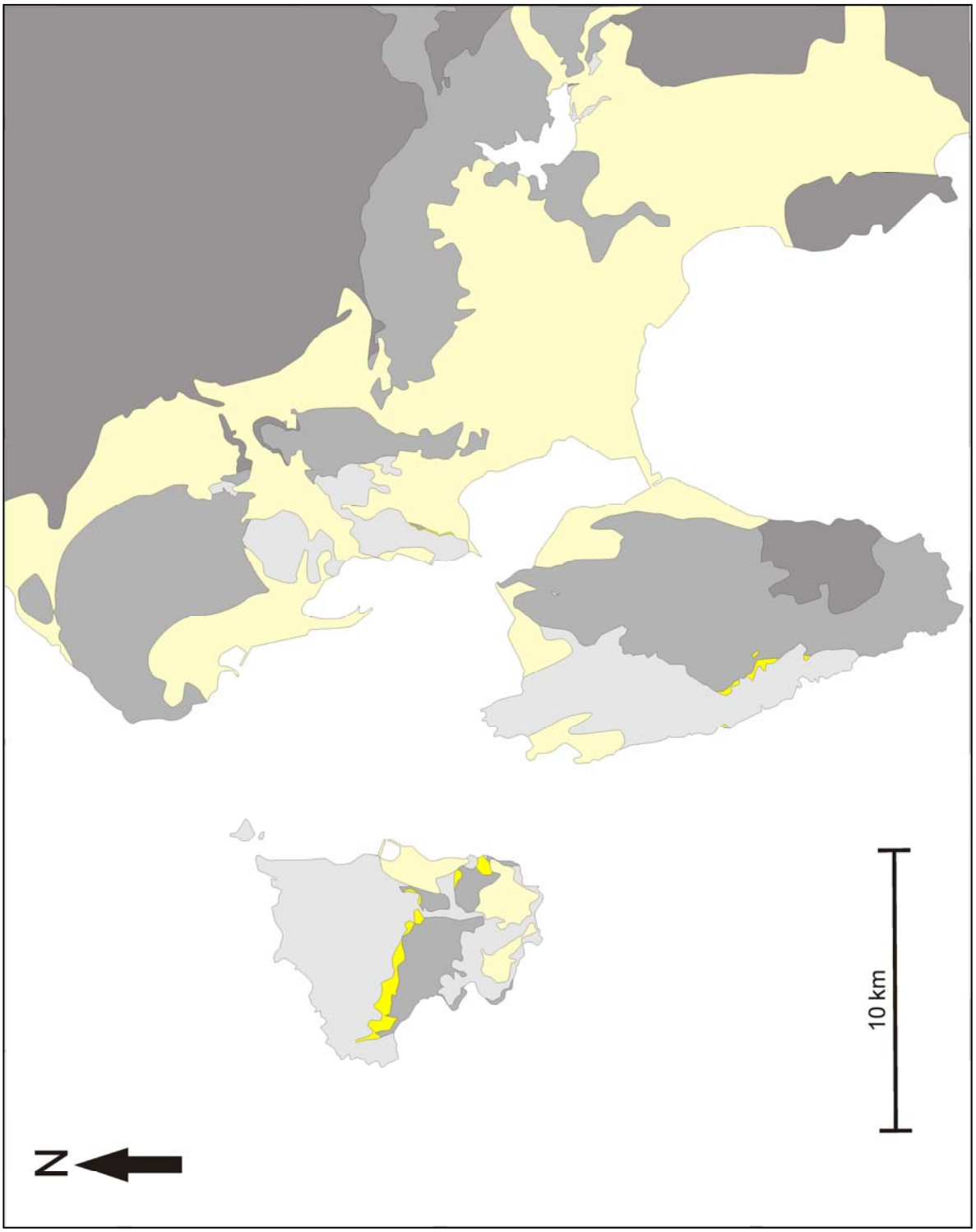

Figure A.4.14: Outcropping area of Matzaccara unit

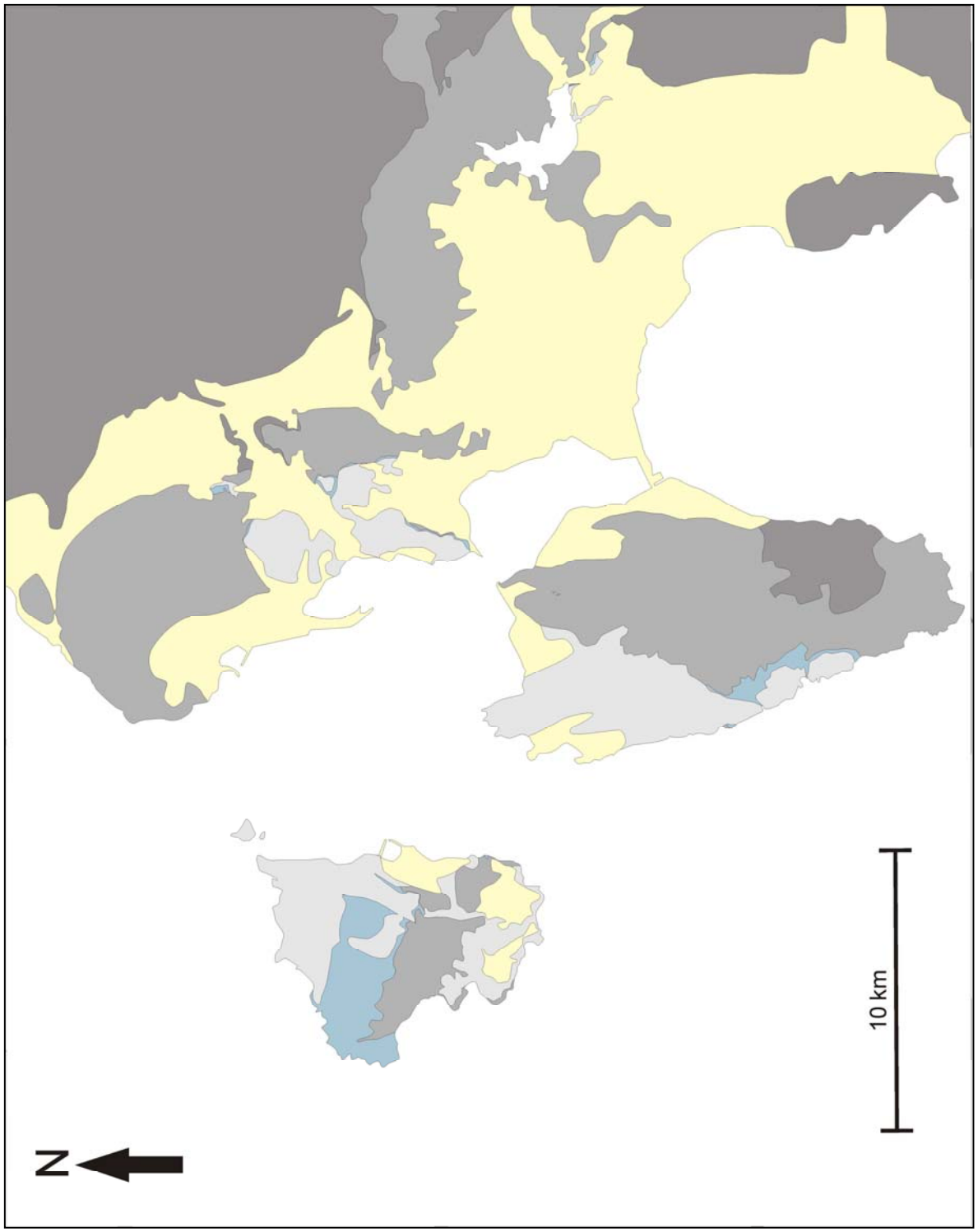

Figure A.4.15: Outcropping area of Comendites unit

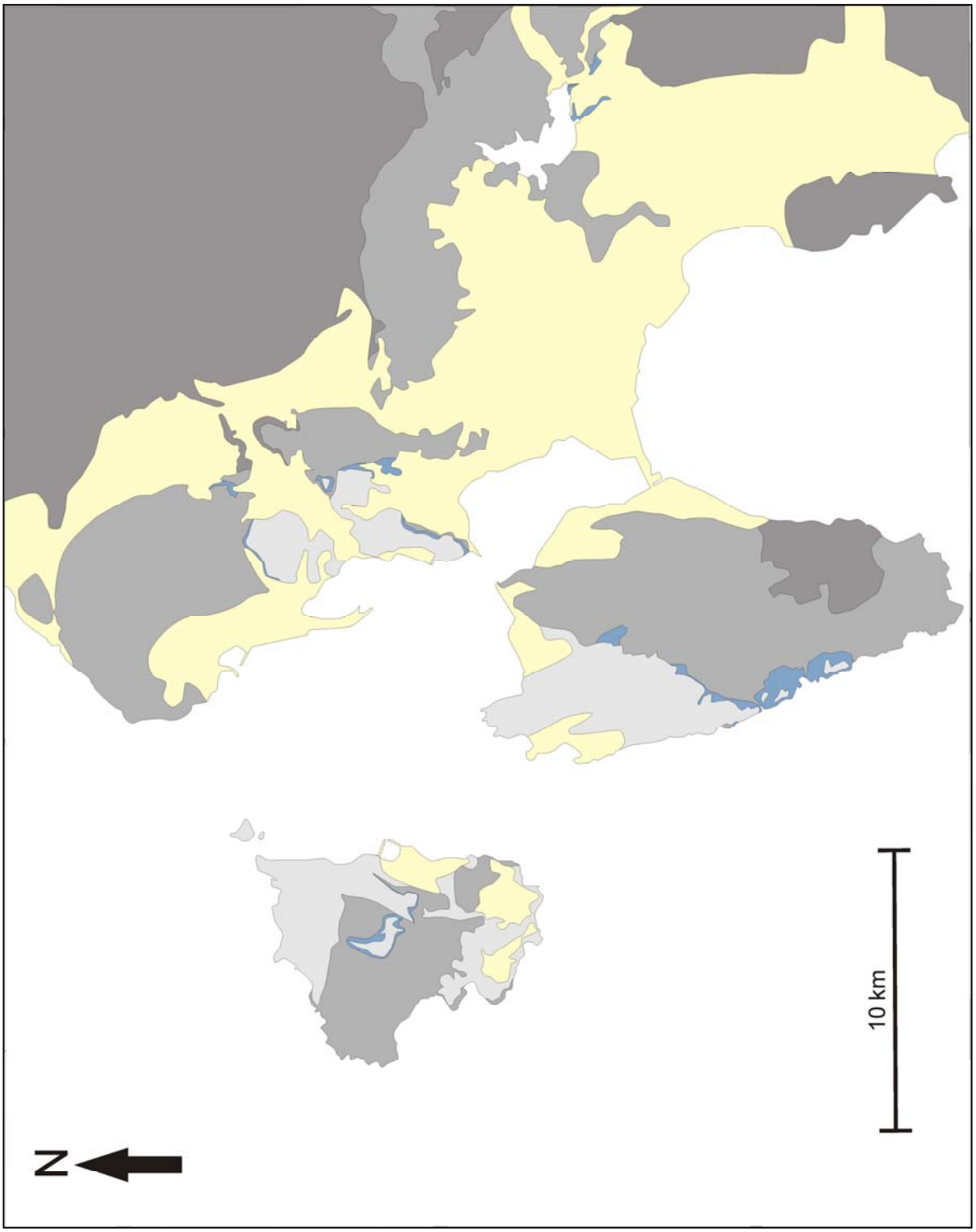

Figure A.4.16: Outcropping area of Monte Ulmus unit

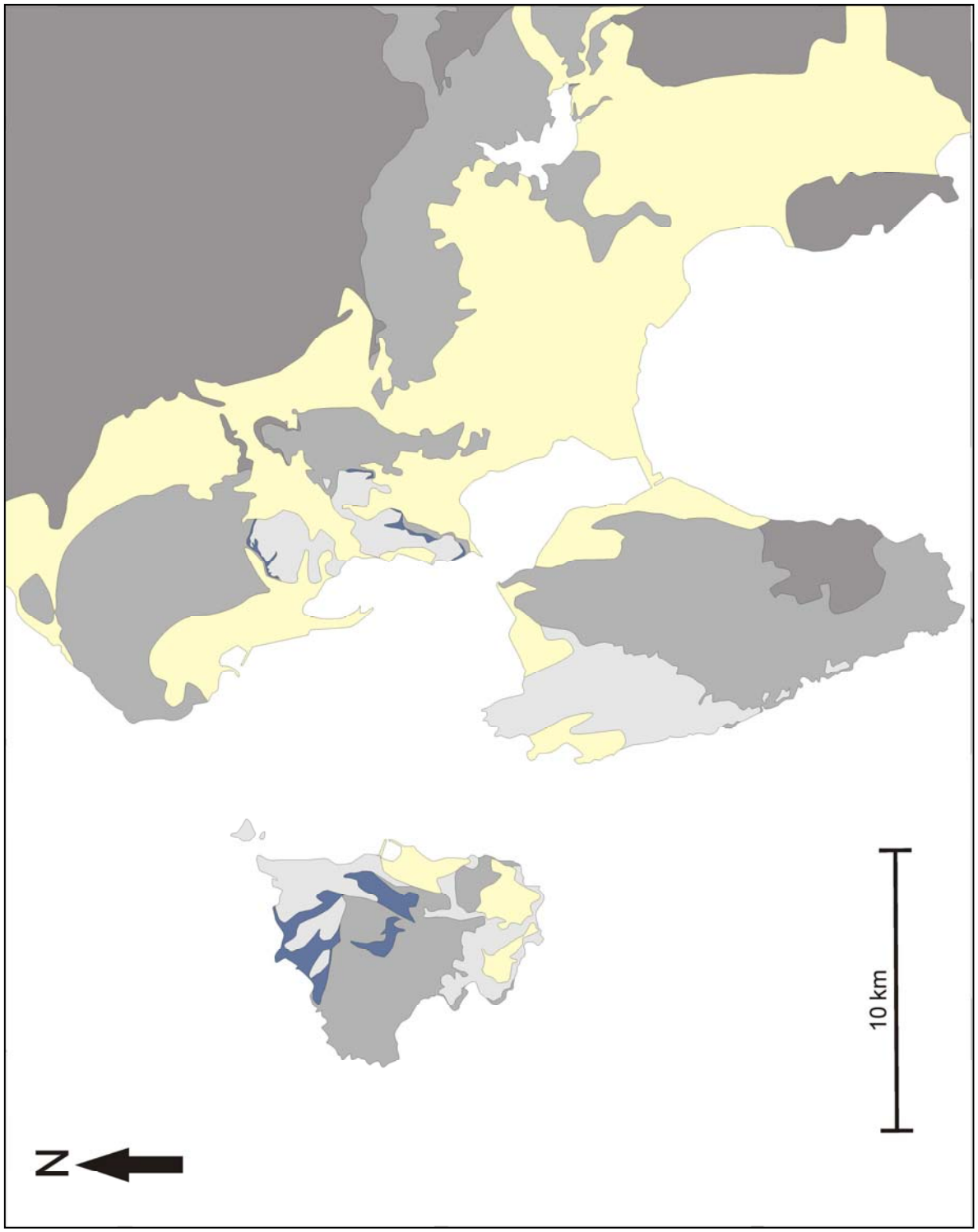

Figure A.4.17: Outcropping area of Carloforte unit

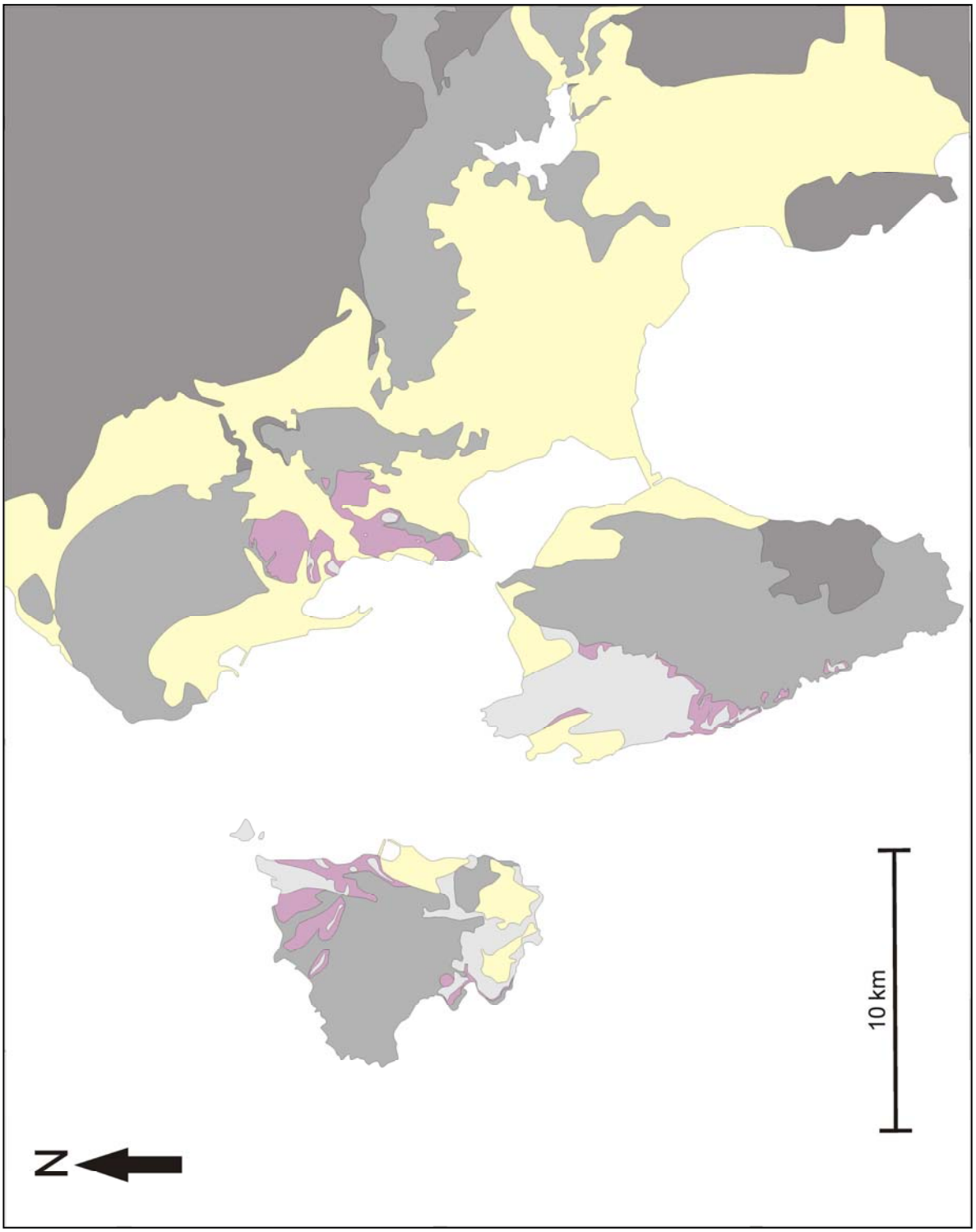

Figure A.4.18: Outcropping area of Paringianu unit

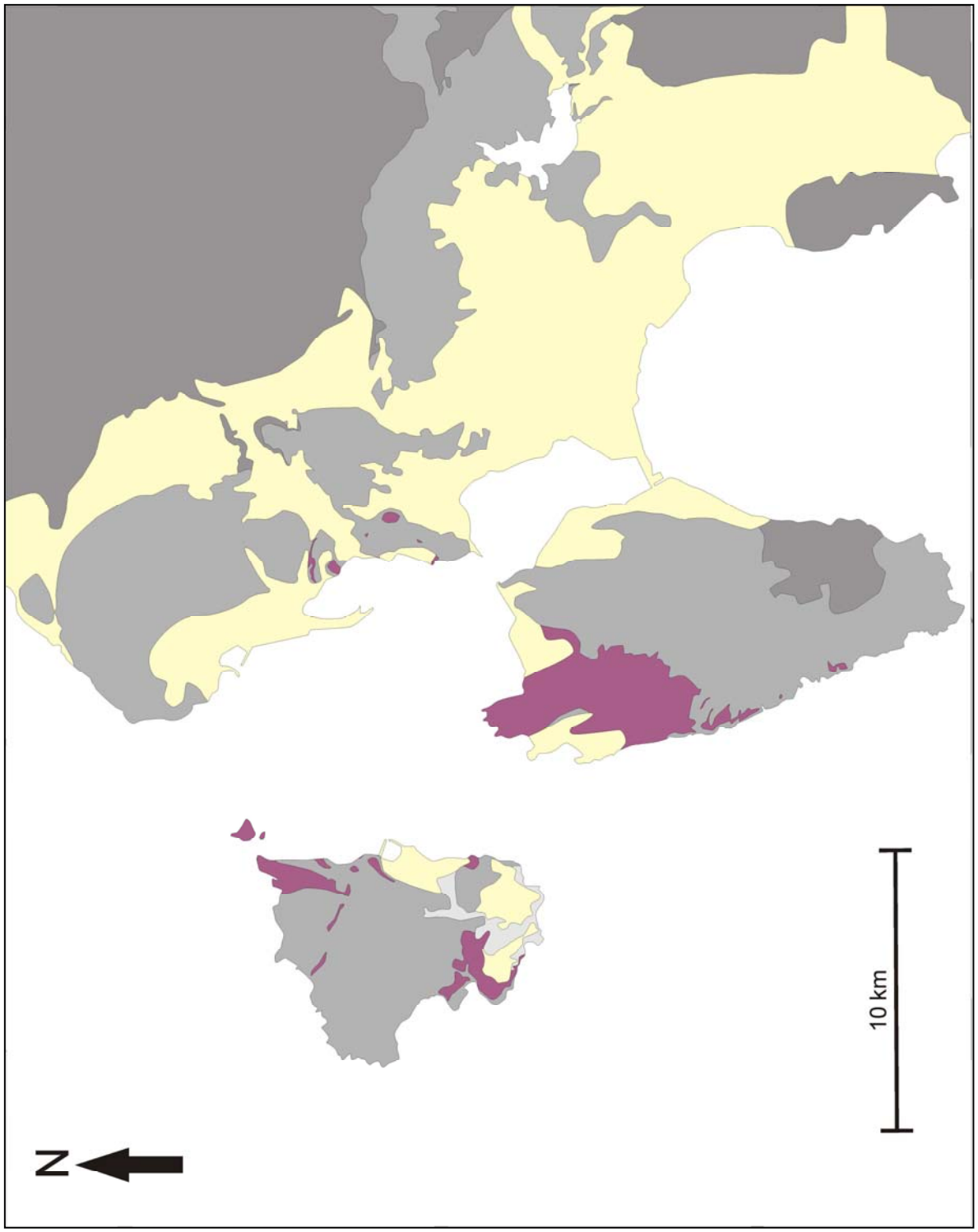

Figure A.4.19: Outcropping area of Serra di Paringianu unit

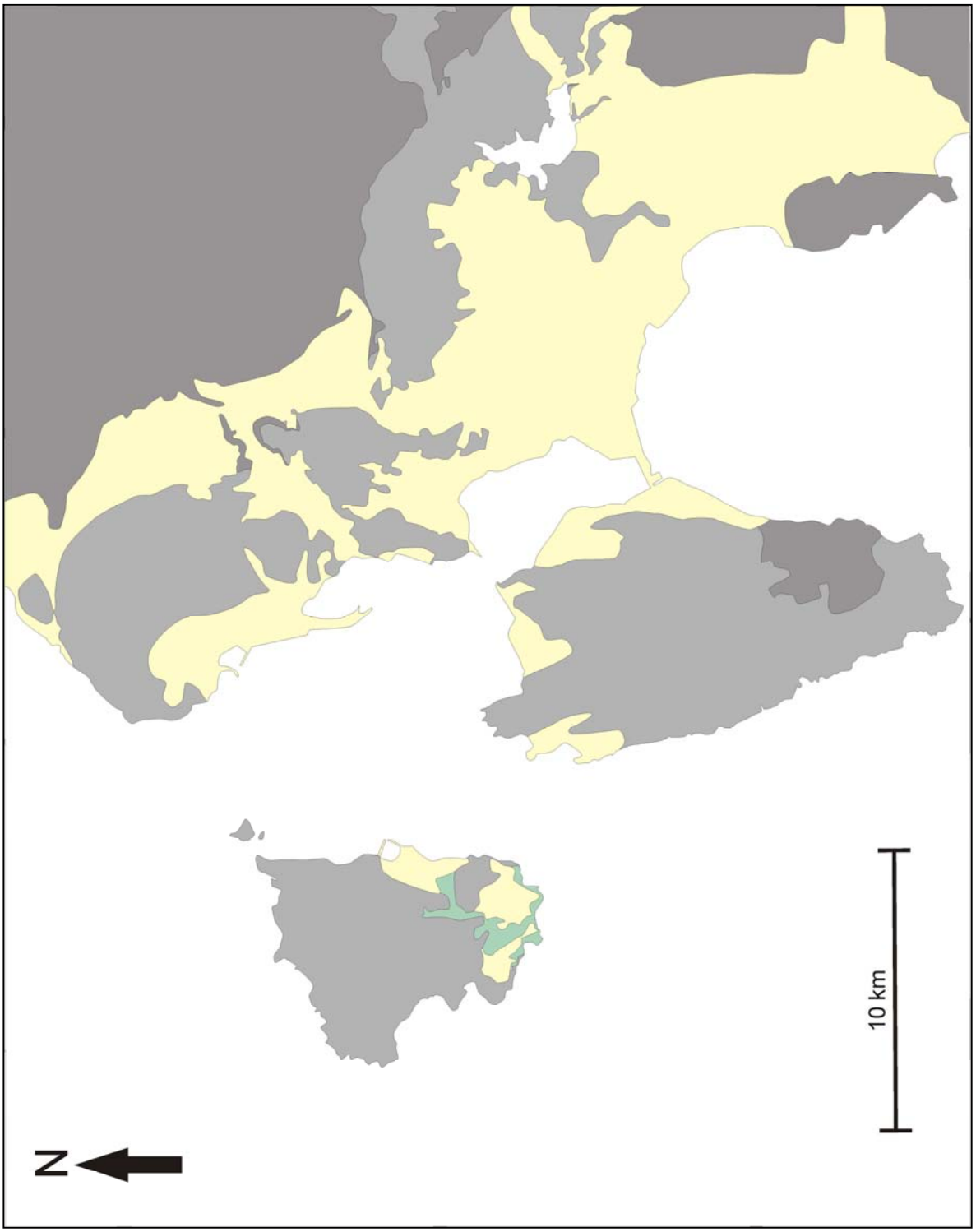

Figure A.4.20: Outcropping area of Punta Mingosa unit

APPENDIX 5: PREVIOUS PETROGENETIC MODELS FOR THE SULCIS OLIGO-MIOCENE MAGMATISM

In this appendix a summary of the two petrogenetic models previously available for the Sulcis Oligo-Miocene magmatic suite are presented, the one by Conte et al. (2010) on the origin of the andesitic suite in Santo Antioco, and the one by Morra et al. (1994).

A.5.1 ORIGIN OF THE ANDESITIC SEQUENCE ACCORDING TO CONTE ET AL. (2010)

The study by Conte et al. (2010) is focused on the origin of the high-alumina basalt-andesite rock association cropping out in southern Santo Antioco Island, which according to the authors represents the mafic end-member of the volcanism developed during the Oligo-Miocene in the Sulcis. In this suite basaltic andesites and andesites are the dominant rock types, while basalts and dacites are occasional.

According to geochemistry, the studied products classify as high-alumina (MgO vs. Al_2O_3 diagram by Kersting and Arculus, 1994) of medium-K calc-alkaline affinity (K_2O vs. SiO_2 diagram by Peccerillo and Taylor, 1976). Variation diagrams show broad correlations of major oxides with MgO (except for a wide scatter of Al_2O_3 and CaO), which are consistent with crystallisation and removal of the phenocryst phases (plagioclase, pyroxenes, Fe-Ti oxides, olivine). The scattering of Al_2O_3 and CaO implies at least different phase proportions and/or compositions during fractional crystallisation. Trace elements depict broad correlations with silica, despite considerable scattering. Rb, Ba, Zr and Y behave as incompatible, while V and Sr behave as compatible elements reflecting the removal of Fe-Ti oxides and plagioclase. Spider diagrams show depletion in HFSE with respect to LILE and LREE, as it's typical in arc magmas, being the pattern similar for the whole sequence. Thus, trace element patterns indicate that magmatic evolution was mostly controlled by fractional crystallisation, which is consistent with the major element variations. The

wide data point scatter implies that fractional crystallisation cannot account for all variations and that an additional process, such as crustal contamination, was likely to be involved in magma evolution. Assimilation is also suggested by the initial $^{87}Sr/^{86}Sr$ isotopic ratios (0.70698 to 0.70858±0.00001).

The crystallisation temperature of magmas was estimated using the two-pyroxene equilibrium geothermometer of Lindsley (1983) and the plagioclase-liquid geothermometer by Putirka (2008). Using Lindsley (1983) most temperatures fall in the 1000-1150°C, with a maximum of 1200°C. Using Putirka (2008) obtained temperatures are 1100-1165°C.

Water content in the system can be estimated using the plagioclase-melt equilibrium equation (Putirka, 2008). Calculations yield H_2O concentrations in the 2.3-3.9 wt % range. A similar range (2.0-4.1 wt%) is obtained with the Pichavant and Macdonald (2007) equation. In the study, the effect of PH_2O on crystallising plagioclase composition is addressed.

Petrogenetic inferences

The wide spectrum of low-MgO high-alumina rock types in Santo Antioco likely reflects extensive fractional crystallisation of a parental basaltic liquid, and changes in the fractionating mineral assemblages occurred in response to variable PH_2O conditions; this was coupled with crustal interaction to some extent.

It is suggested that a high-magnesia basalt (HMB) like the one in Montresta (Morra et al., 1997) may be the parental magma for the mafic suite in Santo Antioco. In orogenic arc-related magmatism HMB, which are representatives of the primitive mantle-derived magmas, are uncommon due to crustal thickness and low density, and to compressive settings preventing mafic magma ascent. In Sardinia HMB have only been found in the area of Montresta, where they have been invoked to be the parental magmas of the high-alumina basalts (HAB) in the same area (Morra et al., 1997). Magmas of similar composition are regarded as possible parental magmas for the Santo Antioco HAB rocks. Mass balance calculations following Stormer and Nicholls (1978) evidence that HAB compositions can be obtained from HMB after 45-50 wt % fractional crystallisation.

Regarding magma evolution, it has been proven that high H_2O concentration in high-alumina melts not only favours the early formation of spinel and the crystallisation of An-richer plagioclase, but also reduces the total proportion of plagioclase in the crystallizing assemblage, expands the stability field of olivine at the expense of other mafic phases such as pyroxene, and decreases the En-Fs contents of clinopyroxene in favour of CaTs (references in Conte et al., 2010). The observed geochemical differences among the least evolved rock types in Santo Antioco are

thus considered to be the result of different evolution paths from a common parental melt caused by changes in phenocrysts proportions and compositions determined by different H_2O concentrations in the melts and by the physical conditions controlling water exsolution from the system during magma ascent. The lack of typical disequilibrium textures in pyroxene crystals does not support additional low-pressure processes, such as mixing between compositionally different magmas.

At Santo Antioco the observed range of isotope data, the positive correlation of $^{87}Sr/^{86}Sr$ versus elements with crustal affinity (e.g. Si, Rb, Ba), as well as the wide scattering of trace elements strongly suggest contamination by crustal wall rocks.

A.5.2 PETROGENETIC HYPOTHESIS OF MORRA ET AL. (1994) FOR THE ORIGIN OF THE IGNIMBRITIC SEQUENCE

The study of Morra et al. (1994) focuses on the petrological aspects of the ignimbritic sequence of the Sulcis in an attempt to understand the origin of the peralkaline rocks, which in this area are associated to calc-alkaline rocks instead of transitional or alkaline rocks like in other settings.

Mineral assemblage, petrographic features, petrochemical data and stratigraphy are used to subdivide the upper sequence, which at this stage of research consisted in only 12 main units, into five major groups:

- G1: dacites. Contains CM, AC and MZ units
- G2: rhyodacites. Contains LE, SE, MC and CA units.
- G3: rhyolites “transitional” to peralkaline rhyolites. Contains only the NU unit.
- G4: comendites. Contains CO and MU units.
- G5: post-comenditic rhyolites “transitional” to peralkaline rhyolites. Contains PA and SP units.

The main chemical and petrographic characteristics of the groups can be seen in Figure 3.2 in Chapter 3.

Geothermometry and geobarometry

Several geothermometric and geobarometric calculations are done to provide useful constraints on the origin of the rocks. Temperatures obtained from single clinopyroxene and clinopyroxene/orthopyroxene solvus calibration consistently indicate decreasing magmatic temperatures from G1 to G3 from 1130°C to 1000°C. The calculated values for G1 are comparable to those obtained for the andesitic rocks of the lower sequence. Values calculated for plagioclase-

sanidine pairs in G3 are comparable to those obtained by pyroxene thermometry. These values refer to early crystallised phases and are considered liquidus temperatures. The temperature of 980°C obtained from Fe and Ti oxide pairs in comendites is in agreement with the above values for the upper sequence. Temperatures obtained for coexisting Fe-Ti oxide pairs in the groundmass of G2 and G5 should represent near solidus values and are well comparable to those obtained for late crystallised plagioclase-sanidine pairs in G2. Taking into account the magmatic temperatures, geobarometric indications give values of 7-6.5 Kbar, which may represent the depth of magma evolution.

Major and trace element distribution

When compared with Differentiation Index (DI), progressive depletion in Al_2O_3 and CaO, coupled with MgO, suggests that plagioclase and pyroxenes represent a significant proportion of any fractionate. On the other hand, K_2O shows a positive correlation with DI to the boundary with peralkaline units (G3), and then decreases in comendites (G4). This inversion suggests that alkali-feldspars are a possible fractionating phase in the final stage of the magmatic evolution. Na_2O increases from G1 to G4. FeOt decreases to G3 and then increases in G4. The Apgaitic Index (AI) increases with differentiation and crosses the peralkalinity limit at G3.

Regarding trace elements, a steady decrease in Sr through the whole sequence is evident. Instead, Ba shows a slight increase to G3 followed by a sharp decrease to G4. The Sr decrease requires extensive and continuous fractionation of plagioclase, whereas Ba increase requires that alkali feldspar become an important fractionating phase only in the late stage of magma evolution. The more incompatible trace elements (Zr, Nb, Rb and Y) are roughly constant in G1 and G2, and then increase progressively from G3 to G4. Eu negative anomaly indicates feldspar fractionation. G3 and G4 show the largest anomaly in response to the late alkali feldspar fractionation. Trace elements diagrams show a similar pattern for the whole sequence, characterised by LILE enrichment. They show an increasing negative spike for Ba and Sr from subalkaline to peralkaline rocks, accompanied by a strong increase in Zr and Nb content.

Crystal fractionation model

Mass-balance calculations following Stormer and Nicholls (1978) were made. G1 to G2 transition can be modelled by 12% fractionation of pl+opx+Ti-mag+cpx. G2 to G3 is explained by 17% crystallisation of pl+cpx+Ti-mag+afs. From G3 to G4 33% fractionation is required of an assemblage formed by 7% pl and 93% afs. Trace element variation due to the modelled fractionation was calculated and confirms the model. Discrepancies in the Zr, Nb and Y content are attributed to a possible role of volatiles complexes in peralkaline rocks.

Sr isotopic data

The virtually constant initial $^{87}Sr/^{86}Sr$ values (0.70745-0.70667) confirm that the upper sequence is genetically related. The values for the lower sequence are 0.70440-0.70711. The higher values for the andesites are comparable to those of the upper sequence, confirming that these rocks are residual products of a mafic, mantle-derived magma.

Discussion

A genetic link between the andesitic lower sequence and the acid upper sequence is established based on several factors; both sequences share a common mineral assemblage (pl+opx+cpx); in some dacites and rhyodacites there is occurrence of both cumulophyric inclusions of gabbronorites and rounded blobs of leucoandesitic composition. Moreover, petrochemical features and isotopic data do not preclude a common origin for the whole sequence.

Major and trace element chemistry confirmed the genetic relationship of the whole sequence. Together with isotope data it confirmed that the whole sequence from the Sulcis area is genetically related and that crystal/liquid fractionation was the dominant process in the evolution of the rocks from the upper sequence.

APPENDIX 6: COMPLEMENTARY WHOLE ROCK GEOCHEMICAL DATA

In the Tables of this Appendix own data from altered samples are presented.

Sample	ANT-28	ANT-29	ANT-32	ANT-33	ANT-34	ANT-51	ANT-87	VS-181	VS-182	VS-183	VS-184	VS-747	VS-748	VS-750	VS-770	VS-807	VS-809
Unit	MU	MU	MU	MU	PA	MU	CO	NU	NU	NU	NU	CO	CO	CO	MLN	MU	MU
SiO_2	70.19	73.41	76.13	78.61	60.47	76.50	82.12	66.95	66.41	65.75	65.77	81.45	78.18	79.56	67.84	78.50	63.93
TiO_2	0.17	0.17	0.17	0.14	0.47	0.16	0.15	0.67	0.65	0.53	0.74	0.16	0.19	0.19	0.24	0.14	0.16
Al_2O_3	12.17	12.77	10.31	9.00	17.49	10.73	8.09	14.72	14.86	14.73	14.83	6.56	8.05	8.29	15.29	9.65	10.90
Fe_2O_3	2.90	3.17	2.41	2.18	2.91	2.47	0.95	2.42	2.42	2.56	2.54	2.33	2.73	2.33	2.92	2.25	2.52
MnO	0.10	0.05	0.09	0.07	0.17	0.07	0.01	0.07	0.08	0.08	0.08	0.05	0.07	0.05	0.05	0.08	0.05
MgO	0.39	0.43	0.47	0.30	1.25	0.13	<LL	0.71	0.63	0.77	0.88	0.23	0.21	0.15	0.43	0.43	1.39
CaO	0.15	0.10	0.25	0.23	1.14	0.11	0.07	1.35	1.47	1.48	1.46	0.18	0.34	0.16	2.10	0.20	6.55
Na_2O	4.79	6.08	4.16	3.70	2.70	3.82	2.75	4.47	4.42	4.43	4.81	2.75	3.43	3.23	3.91	3.55	4.24
K_2O	5.19	5.06	4.09	3.67	3.07	4.24	3.36	5.03	4.90	4.86	4.77	2.75	3.36	3.25	3.52	3.86	4.43
P_2O_5	0.03	0.06	0.05	0.08	0.13	0.03	<LL	0.16	0.16	0.15	0.17	<LL	0.02	0.02	0.06	0.01	0.15
LOI	0.72	0.86	1.34	1.84	6.76	0.88	1.26	3.20	2.98	3.18	3.42	2.24	2.19	1.48	2.63	1.42	6.33
Total	96.80	102.16	99.47	99.82	96.56	99.12	98.81	99.73	98.96	98.52	99.42	98.68	98.74	98.69	98.97	100.07	100.64

Sample	ISP-43c	ISP-59	ISP-60	ISP-62	ISP-71	ISP-133	ISP-141	ISP-152	ISP-163	ISP-170	ISP-191	ISP-235	ISP-236	ISP-236bis	ISP-239	ISP-270
Unit	CO	MZ	MZ	MZ	CF	MCR	MZ	MZ	MZ	PA	PM	PA	PA	CO	PA	PA
SiO_2	73.58	77.98	80.80	75.57	77.65	68.65	71.14	75.70	72.90	68.18	78.42	62.67	67.52	77.42	62.19	67.89
TiO_2	0.27	0.34	0.32	0.50	0.18	0.58	0.64	0.46	0.72	0.25	0.10	0.99	0.78	0.23	0.76	0.49
Al_2O_3	10.43	10.42	9.23	11.11	11.61	14.75	13.41	11.75	12.08	14.88	11.55	17.66	14.73	9.44	18.15	14.69
Fe_2O_3	5.34	1.66	1.47	2.43	1.39	2.95	3.25	2.30	3.56	2.31	1.22	4.26	4.12	3.25	5.06	2.48
MnO	0.12	0.04	0.03	0.04	0.01	0.09	0.08	0.05	0.06	0.05	0.02	0.05	0.03	0.05	0.05	0.07
MgO	0.15	0.83	0.20	0.34	<LL	1.06	1.09	0.53	0.42	0.90	<LL	1.04	1.40	<LL	1.25	0.42
CaO	0.11	0.45	0.39	0.96	0.12	0.70	0.69	0.37	1.09	0.51	0.36	2.35	1.72	0.85	0.41	1.12
Na_2O	4.26	1.68	2.57	3.11	3.82	1.57	2.68	2.75	3.27	3.73	3.51	3.97	2.85	3.86	3.33	3.54
K_2O	4.83	4.79	3.84	4.45	4.52	8.23	4.76	4.38	4.63	4.32	4.34	2.44	1.92	3.83	2.17	5.27
P_2O_5	0.04	0.05	0.05	0.26	0.03	0.13	0.02	0.02	0.13	0.02	0.02	0.11	0.10	0.53	0.03	0.05
LOI	0.97	2.36	1.66	1.69	1.04	2.26	2.62	1.87	1.51	5.21	1.24	5.64	6.35	1.19	8.36	4.41
Total	100.09	100.58	100.55	100.43	100.49	100.95	100.36	100.15	100.35	100.35	100.86	101.16	101.48	100.63	101.75	100.41

Table A.6.1: Major element composition (in wt %) of altered samples of the Sulcis Oligo-Miocene volcanism. <LL: below the lower limit of the calibration range

Sample	ANT-28	ANT-29	ANT-32	ANT-33	ANT-34	ANT-51	ANT-87	VS-181	VS-182	VS-183	VS-184	VS-747	VS-748	VS-750	VS-770	VS-807	VS-809
Unit	MU	MU	MU	MU	PA	MU	CO	NU	NU	NU	NU	CO	CO	CO	MLN	MU	MU
As	-	17.3	4.43	-	-	-	-	-	-	-	-	-	-	4.77	-	-	-
Ba	73.8	11.4	84.9	45.7	548	<LL	<LL	1010	1030	1300	1020	<LL	<LL	73.7	916	<LL	<LL
Be	-	5.88	4.76	-	-	-	-	-	-	-	-	-	-	3.34	-	-	-
Bi	-	0.01	0.02	-	-	-	-	-	-	-	-	-	-	0.01	-	-	-
Ce	157	137	134	135	70.1	176	<LL	108	96.1	92.4	77.7	119	135	108	89.0	112	163
Co	21.0	17.8	15.2	20.1	54.0	38.2	47.6	72.9	48.7	60.9	40.0	57.4	59.7	63.3	23.5	10.4	<LL
Cr	49.3	19.3	20.0	52.6	26.4	<LL	<LL	26.2	28.9	31.5	28.3	<LL	<LL	7.63	<LL	<LL	<LL
Cs	-	2.96	2.54	-	-	-	-	-	-	-	-	-	-	2.68	-	-	-
Cu	<DL	2.56	2.79	<DL	<DL	<LL	<LL	<DL	<DL	<DL	<DL	<LL	<LL	2.25	<LL	<LL	6.20
Dy	-	15.1	12.5	-	-	-	-	-	-	-	-	-	-	9.03	-	-	-
Er	-	7.98	6.70	-	-	-	-	-	-	-	-	-	-	5.19	-	-	-
Eu	-	0.19	0.20	-	-	-	-	-	-	-	-	-	-	0.40	-	-	-
Ga	21.2	21.8	17.4	14.9	17.5	22.1	21.6	15.4	15.3	15.7	13.9	20.4	23.3	22.4	15.4	17.5	19.5
Gd	-	17.0	13.7	-	-	-	-	-	-	-	-	-	-	9.44	-	-	-
Ge	-	2.15	1.74	-	-	-	-	-	-	-	-	-	-	1.33	-	-	-
Hf	-	11.2	6.16	-	-	-	-	-	-	-	-	-	-	9.63	-	-	-
Ho	-	2.68	2.25	-	-	-	-	-	-	-	-	-	-	1.72	-	-	-
La	-	111	81.5	-	-	-	-	-	-	-	-	-	-	50.7	-	-	-
Li	-	30.6	41.5	-	-	-	-	-	-	-	-	-	-	16.7	-	-	-
Lu	-	1.11	0.89	-	-	-	-	-	-	-	-	-	-	0.77	-	-	-
Mo	2.60	2.43	1.09	0.20	3.30	<LL	<LL	5.00	5.00	4.90	4.90	<LL	<LL	1.24	<LL	<LL	<LL
Nb	78.8	82.7	62.2	54.7	39.0	78.6	55.0	38.5	36.5	36.3	33.5	67.1	76.8	57.5	19.9	69.9	77.6
Nd	-	91.7	68.1	-	-	-	-	-	-	-	-	-	-	47.7	-	-	-
Ni	<DL	1.36	1.91	<DL	<DL	<LL	<LL	<DL	<DL	<DL	<DL	<LL	<LL	1.70	<LL	<LL	<LL
Pb	21.4	19.8	15.2	19.7	45.7	20.0	8.70	27.5	26.5	22.7	23.9	24.1	20.2	13.2	24.4	17.6	25.8
Pr	-	25.2	18.7	-	-	-	-	-	-	-	-	-	-	12.7	-	-	-
Rb	195	201	153	197	97.6	189	145	165	157	153	139	119	145	112	138	165	188
Sb	-	0.78	0.48	-	-	-	-	-	-	-	-	-	-	0.45	-	-	-
Sc	-	4.12	3.52	-	-	-	-	-	-	-	-	-	-	2.29	-	-	-
Sm	-	17.4	13.2	-	-	-	-	-	-	-	-	-	-	9.49	-	-	-
Sn	4.20	5.20	3.20	3.10	2.40	3.60	3.20	3.70	3.90	3.10	2.40	6.60	7.00	4.80	3.70	7.90	7.70
Sr	23.5	5.18	14.6	24.6	83.7	<LL	<LL	96.2	104	109	103	<LL	42.5	14.8	195	20.1	70.1
Ta	-	5.17	3.29	-	-	-	-	-	-	-	-	-	-	6.70	-	-	-
Tb	-	2.57	2.11	-	-	-	-	-	-	-	-	-	-	1.49	-	-	-
Te	-	0.09	0.04	-	-	-	-	-	-	-	-	-	-	0.05	-	-	-
Th	24.6	22.3	19.5	17.4	24.0	15.7	3.20	18.3	18.9	20.1	18.5	8.40	9.10	8.50	13.4	13.7	15.0
Tl	-	0.57	0.36	-	-	-	-	-	-	-	-	-	-	0.18	-	-	-
Tm	-	1.10	0.92	-	-	-	-	-	-	-	-	-	-	0.75	-	-	-
U	-	4.28	2.98	-	-	-	-	-	-	-	-	-	-	5.50	-	-	-
V	20.5	15.0	15.7	14.2	22.5	11.0	7.60	22.0	23.8	24.1	24.9	10.5	10.8	11.2	12.9	8.10	9.20
W	169	105	138	155	176	397	464	546	363	357	267	302	288	320	150	125	70.6
Y	62.4	66.8	52.5	46.1	27.4	68.3	<LL	37.4	35.1	34.9	32.2	54.0	54.3	46.1	22.1	38.3	47.4
Yb	-	7.40	6.12	-	-	-	-	-	-	-	-	-	-	5.06	-	-	-
Zn	92.4	94.0	74.0	65.1	81.4	88.2	36.0	62.4	63.5	66.6	61.5	98.4	105	76.6	74.6	70.5	85.1
Zr	598	610	476	406	447	595	118	421	411	405	386	518	590	437	295	528	591

Table A.6.2: Trace element composition of altered volcanic rocks from the Sulcis. Concentrations in ug/g (ppm). <DL: below detection limit; <LL: below the lower limit of the calibration range; >UL: above the upper limit of the calibration range

Sample	ISP-43c	ISP-59	ISP-60	ISP-62	ISP-71	ISP-133	ISP-141	ISP-152	ISP-163	ISP-170	ISP-191	ISP-235	ISP-236	ISP-236bis	ISP-239	ISP-270
Unit	CO	MZ	MZ	MZ	CF	MCR	MZ	MZ	MZ	PA	PM	PA	PA	CO	PA	PA
As	-	-	-	-	8.27	-	6.66	2.95	-	-	-	-	-	-	-	-
Ba	<LL	596	554	683	34.5	943	867	676	960	121	41.9	648	597	108	1010	946
Be	-	-	-	-	4.86	-	1.78	2.31	-	-	-	-	-	-	-	-
Bi	-	-	-	-	0.01	-	0.01	0.00	-	-	-	-	-	-	-	-
Ce	323	86.6	67.2	77.5	158	119	81.9	87.1	146	86.3	90.3	89.4	83.4	173	100	100
Co	23.7	5.20	19.9	25.8	16.4	8.00	7.60	7.50	30.9	13.3	21.5	11.8	13.2	39.7	12.6	19.0
Cr	<LL	<LL	<LL	<LL	7.94	<LL	17.8	17.5	<LL	<LL	<LL	<LL	53.4	<LL	<LL	<LL
Cs	-	-	-	-	2.21	-	3.48	1.79	-	-	-	-	-	-	-	-
Cu	<LL	<LL	<LL	<LL	2.02	<LL	6.89	4.09	<LL	8.00	<LL	6.80	6.80	<LL	<LL	<LL
Dy	-	-	-	-	11.2	-	6.11	7.56	-	-	-	-	-	-	-	-
Er	-	-	-	-	5.72	-	3.21	3.74	-	-	-	-	-	-	-	-
Eu	-	-	-	-	0.54	-	1.57	1.74	-	-	-	-	-	-	-	-
Ga	25.0	14.5	12.0	13.4	24.4	17.0	14.1	12.0	14.9	15.8	15.2	18.8	15.5	20.5	21.9	16.1
Gd	-	-	-	-	13.0	-	7.06	9.26	-	-	-	-	-	-	-	-
Ge	-	-	-	-	1.67	-	1.08	0.93	-	-	-	-	-	-	-	-
Hf	-	-	-	-	2.44	-	2.44	1.60	-	-	-	-	-	-	-	-
Ho	-	-	-	-	1.99	-	1.09	1.34	-	-	-	-	-	-	-	-
La	-	-	-	-	79.5	-	44.8	54.9	-	-	-	-	-	-	-	-
Li	-	-	-	-	4.87	-	18.4	11.8	-	-	-	-	-	-	-	-
Lu	-	-	-	-	0.73	-	0.39	0.41	-	-	-	-	-	-	-	-
Mo	<LL	<LL	<LL	<LL	1.06	<LL	0.38	0.57	<LL	<LL	<LL	<LL	<LL	<LL	<LL	<LL
Nb	188	30.2	26.1	29.3	61.9	40.4	34.8	32.3	34.9	44.0	32.8	47.4	41.9	77.9	72.8	43.7
Nd	-	-	-	-	71.0	-	36.4	44.3	-	-	-	-	-	-	-	-
Ni	<LL	<LL	<LL	<LL	2.07	<LL	1.30	1.18	<LL	<LL	<LL	5.80	15.3	<LL	<LL	<LL
Pb	44.5	18.5	12.9	14.5	10.8	41.3	14.8	11.8	26.5	48.6	14.7	26.6	24.4	21.3	43.0	27.2
Pr	-	-	-	-	19.1	-	9.98	11.5	-	-	-	-	-	-	-	-
Rb	334	119	112	131	161	229	154	133	159	156	160	126	99.7	154	64.9	207
Sb	-	-	-	-	0.35	-	1.19	0.48	-	-	-	-	-	-	-	-
Sc	-	-	-	-	3.94	-	6.59	4.43	-	-	-	-	-	-	-	-
Sm	-	-	-	-	13.4	-	7.12	8.37	-	-	-	-	-	-	-	-
Sn	17.6	3.20	<LL	<LL	2.10	6.00	4.90	2.20	<LL	<LL	2.80	5.70	4.00	7.40	5.20	4.60
Sr	<LL	55.7	54.4	92.2	18.5	85.1	116	62.0	149	46.6	29.0	311	178	30.1	62.3	117
Ta	-	-	-	-	5.96	-	0.57	0.14	-	-	-	-	-	-	-	-
Tb	-	-	-	-	1.94	-	1.04	1.31	-	-	-	-	-	-	-	-
Te	-	-	-	-	0.01	-	0.17	0.07	-	-	-	-	-	-	-	-
Th	28.8	19.2	18.2	17.5	14.5	13.2	13.9	10.2	9.80	22.5	18.7	10.1	9.50	8.90	8.80	14.5
Tl	-	-	-	-	0.14	-	0.59	0.24	-	-	-	-	-	-	-	-
Tm	-	-	-	-	0.78	-	0.43	0.48	-	-	-	-	-	-	-	-
U	-	-	-	-	2.08	-	2.39	1.72	-	-	-	-	-	-	-	-
V	7.70	13.2	13.0	26.1	8.00	27.6	23.3	16.0	40.6	24.5	10.4	63.2	51.5	8.50	23.8	24.0
W	191	31.0	140	99.2	191	56.3	58.6	83.3	178	78.2	182	36.3	29.3	338	35.3	144
Y	>UL	33.5	24.2	33.1	71.2	37.9	35.6	44.5	62.7	28.9	26.0	23.9	33.6	68.6	40.9	52.9
Yb	-	-	-	-	4.98	-	2.68	2.88	-	-	-	-	-	-	-	-
Zn	271	64.0	27.5	35.5	32.4	93.5	47.3	33.9	47.8	173	43.7	127	133	93.6	184	71.3
Zr	>UL	323	283	322	621	445	364	336	333	247	227	380	340	614	504	440

Table A.6.2: (Continuation)

REFERENCES

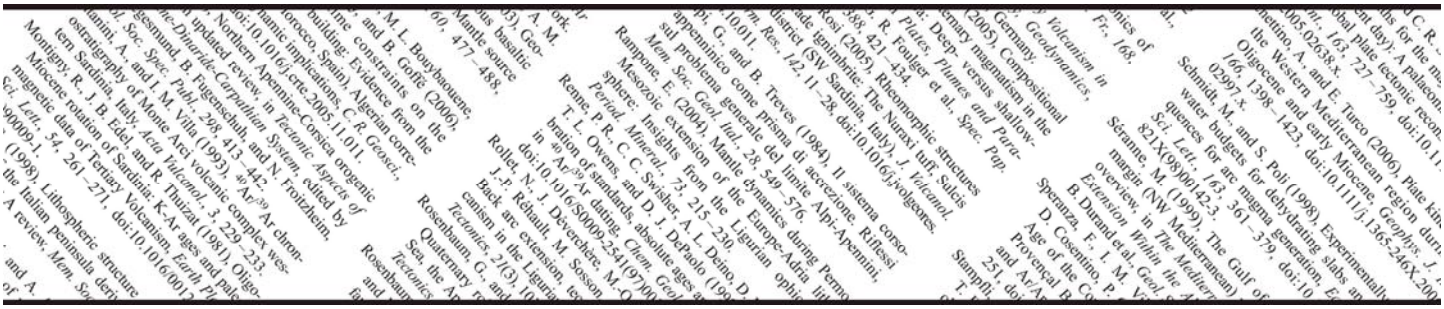

REFERENCES

Araña, V., F. Barberi, and R. Santacroce (1974), Some Data on the Comendite Type Area of S. Pietro and S. Antioco Islands, Sardinia, *Bulletin Volcanologique*, *38*, 725-736.

Argnani, A., and C. Savelli (1999), Cenozoic volcanism and tectonics in the southern Tyrrhenian sea: space-time distribution and geodynamic significance, *Journal of Geodynamics*, *27*(4-5), 409-432.

Armienti, P., and D. Gasperini (2007), Do we really need mantle components to define mantle composition?, *Journal of Petrology*, *48*(4), 693-709.

Armienti, P., and P. Longo (2011), Three-dimensional representation of geochemical data from a multidimensional compositional space, *International Journal of Geosciences*, 2, 231-239.

Assorgia, A., S. Barca, G. Onnis, F. A. G. Secchi, and C. Spano (1986a), Episodi sedimentari e vulcanici oligo-miocenici nel settore occidentale dell'Arcuentu e loro contesto geodinamico (Sardegna SW), *Memorie della Società Geologica Italiana*, *35*, 229-240.

Assorgia, A., P. Brotzu, R. Lonis, L. Morbidelli, M. Nicoletti, and G. Traversa (1986b), Carta geologica del complesso vulcanico calco-alcalino dell'Arcuentu (Sardegna centro-occidentale). 1:50,000. Editor: SELCA, Firenze.

Assorgia, A., A. Fadda, D. Gimeno Torrente, V. Morra, L. Ottelli, and F. A. Secchi (1990a), Risultati preliminari sullo studio delle successioni vulcaniche terziarie del Sulcis (Sardegna sud-occidentale), in *75º Congresso Nazionale della Società Geologica Italiana*, edited, Milano.

Assorgia, A., A. Fadda, D. Gimeno Torrente, V. Morra, L. Ottelli, and F. A. Secchi (1990b), Le successioni ignimbritiche terziarie del Sulcis (Sardegna sud-occidentale), *Memorie della Società Geologica Italiana*, *45*, 951-963.

Assorgia, A., A. Fadda, D. Gimeno, V. Morra, L. Ottelli, L. Pujolriu, and F. A. Secchi (1992a), Tectono-sedimentary evolution of the Upper Tertiary volcanic succession of Sulcis area (SW Sardinia, Italy), *Paleontologia i Evolució*, *24-25*, 307-320.

Assorgia, A., F. Cincotti, A. Fadda, D. Gimeno, V. Morra, L. Ottelli, and A. Secchi (1992b), Caratteri vulcanologici e petrografici delle successioni "ignimbritiche" terziarie del Sulcis (Sardegna sud-occidentale), Progetti Nazionali MURST 40%, Riunionie scientifica: Ignimbriti cenozoiche sarde, 9-12 June, Sardinia (Italy).

Assorgia, A., P. Brotzu, and E. Callegari (coord) (1992c), Carta geologica del distretto vulcanico del Sulcis. 1:50,000. Editor: SELCA, Firenze.

Assorgia, A., F. Cincotti, A. Fadda, D. Gimeno Torrente, V. Morra, L. Ottelli, and F. A. Secchi (1994), Il Complesso comenditico miocenico dell'entroterra Sulcitano (Sardegna sud-occidentale). Caratteri geologici, vulcanologici e petrochimici, *Memorie Descrittive della Carta Geologica d'Italia*, *49*, 347-362.

Assorgia, A., K. Balogh, L. Lecca, A. Ibba, A. Porcu, F. Secchi, and G. Tilocca (1995), Volcanological characters and structural context of Oligo-Miocene volcanic succesions from central Sardinia (Italy), in *Rapporti Alpi-Apennino (Peveragno CN), 1994*, edited by R. Polino and R. Sacchi, Accademia Nazionale delle Scienze, Roma, pp. 397-424.

Assorgia, A., S. Barca, and C. Spano (1997), A synthesis on the Cenozoic stratigraphic, tectonic and volcanic evolution in Sardinia (Italy), *Bollettino della Società Geologica Italiana*, *116*, 407-420.

Aulinas Juncà, M. (2008), The Plio-Quaternary volcanism (4 Ma to recent) in Gran Canaria (Canary Islands, Spain): mantle source and magma evolution, PhD Thesis, Universitat de Barcelona, Barcelona, 404 pp.

Barberi, F., G. Ferrara, R. Santacroce, M. Treuil, and J. Varet (1975), A transitional basalt-pantellerite sequence of fractional crystallisation, Boina Center (Afar Rift, Ethiopia), *Journal of Petrology*, *16*(1), 22-56.

Beccaluva, L., L. Civetta, G. Macciotta, and C. A. Ricci (1985), Geochronology in Sardinia: results and problems, *Rendiconti della Società Italiana di Mineralogia e Petrologia*, *40*, 57-72.

Beccaluva, L., P. Brotzu, G. Macciotta, L. Morbidelli, G. Serri, and G. Traversa (1989), Cainozoic tectono-magmatic evolution and inferred mantle sources in the Sardo-Tyrrhenian area, in *The lithosphere in Italy. Advances in Earth Sience Research*, edited by A. Boriani, M. Bonafede, G. B. Piccardo and G. B. Vai, Accademia Nazionale dei Lincei, Roma, pp. 229-248.

Beccaluva, L., G. Bianchini, M. Coltorti, W. T. Perkins, F. Siena, C. Vaccaro, and M. Wilson (2001), Multistage evolution of the European lithospheric mantle: new evidence from Sardinian peridotite xenoliths, *Contributions to Mineralogy and Petrology*, *142*(3), 284-297.

Bell, K., F. Castorina, G. Lavecchia, G. Rosatelli, and F. Stoppa (2004), Is there a mantle plume below Italy?, *EOS*, 85, 541-547.

Bellon, H. (1976), Séries magmatiques néogènes et quaternaires du pourtour méditerraneen occidental, comparées dans leur cadre géochronométrique; implications géodinamiques, PhD Thesis, University of Paris-Orsay, 367 pp..

Bellon, H., C. Coulon, and J. B. Edel (1977), Le déplacement de la Sardaigne. Synthèse des données géochronologiques, magmatiques et paleomagnétiques, *Bulletin de la Société Géologique de France*, *19*(4), 825-831.

Bertolio, S. (1985), Sulle comenditi, nuovo tipi di rioliti a aegirina (Nota preliminare), *Rendiconti della Reale Accademia dei Lincei*, *4*, 48-50.

Black, S., R. Macdonald, and M. R. Kelly (1997), Crustal origin for peralkaline rhyolites from Kenya: Evidence from U-series disequilibria and Th-isotopes, *Journal of Petrology*, *38*(2), 277-297.

Bobier, C., and C. Coulon (1970), Résultats préliminaires d'une étude paléomagnétique des formations volcaniques tertiaires et quaternaires du Logudoro (Sardegna septentrionale), *Comptes Rendus de l'Académie des Sciences*, *270*(11), 1434-1437.

Bohrson, W. A., and M. R. Reid (1997), Genesis of silicic peralkaline volcanic rocks in an ocean island setting by crustal melting and open-system processes: Socorro Island, Mexico, *Journal of Petrology*, *38*(9), 1137-1166.

Boni, M., L. Del Vecchio, and L. Lirer (1990), Considerazioni sul vulcanismo esplosivo Miocenico della Sardegna S-W, *Memorie della Società Geologica Italiana*, *45*, 989-1000.

Boryta, M., and K. C. Condie (1990), Geochemistry and origin of the Archaean Beit Bridge Complex, Limpopo Belt, South Africa, *Journal of the Geological Society*, *147*, 229-239.

Bowden, P. (1974), Oversaturated alkaline rocks: granites, pantellerites and comendites, in *The Alkaline Rocks*, edited by H. Sorensen, John Wiley and Sons, London, New York, Sydney, Toronto, pp. 109-123.

Bowen, N. L. (1913), The melting phenomena of the plagioclase feldspars, *American Journal of Science*, *35*, 577-599.

Bowen, N. L. (1945), Phase equilibria bearing on the origin and differentiation of alkaline rocks, *American Journal of Science*, *243A*, 75-89.

Bowen, N. L. (1947), Magmas, *Geological Society of America Bulletin*, *58*, 263-280.

Bowen, N. L., and O. F. Tuttle (1950), The system $NaAlSi_3O_8$-$KAlSi_3O_8$-H_2O, *Journal of Geology*, *58*, 489-511.

Branney, M. J., and P. Kokelaar (2002), *Pyroclastic density currents and the sedimentation of ignimbrites*, Geological Society, London, 143 pp..

Brotzu, P., E. Callegari, V. Morra, and R. Ruffini (1997a), The orogenic basalt-andesite suites from the Tertiary volcanic complex of Narcao, SW-Sardinia (Italy): petrology, geochemistry and Sr-isotope characteristics, *Periodico di Mineralogia*, *66*(1-2), 101-150.

Brotzu, P., R. Lonis, L. Melluso, L. Morbidelli, G. Traversa, and L. Franciosi (1997b), Petrology and evolution of calcalkaline magmas from the Arcuentu volcanic complex (SW Sardinia, Italy), *Periodico di Mineralogia*, *66*(1-2), 151-184.

Burrus, J. (1989), Review of geodynamic models for extensional basins; the paradox of stretching in the Gulf of Lions (northwest Mediterranean), *Bulletin de la Société Géologique de France*, *5*(2), 377-392.

Cadoux, A., J. Blichert-Toft, D. L. Pinti, and F. Albarede (2007), A unique lower mantle source for Southern Italy volcanics, *Earth and Planetary Science Letters*, *259*(3-4), 227-238.

Carmichael, I. S. E., F. J. Turner, and J. Verhoogen (1974), *Igneous petrology*, McGraw-Hill, 739 pp..

Carmignani, L., R. Carosi, A. Dipisa, M. Gattiglio, G. Musumeci, G. Oggiano, and P. C. Pertusati (1994), The Hercynian chain in Sardinia (Italy), Geodinamica Acta, 7(1), 31-47.

Carr, M.J. (2005), Igpet for Windows Petrology Software, Terra Softa Inc., Somerset (New Jersey).

Casula, G., A. Cherchi, L. Montadert, M. Murru, and E. Sarria (2001), The Cenozoic graben system of Sardinia (Italy): geodynamic evolution from new seismic and field data, *Marine and Petroleum Geology*, *18*(7), 863-888.

Cebria, J. M., and M. Wilson (1995), Cenozoic mafic magmatism in Western/Central Europe: a common European asthenospheric reservoir, *Terra Nova*, *7*(abstract Suppl.), 162.

Chamot-Rooke, N., J.-M. Gaulier, and F. Jestin (1999), Constraints on Moho depth and crustal thickness in the Liguro-Provençal basin from a 3D gravity inversion: geodynamic implications, in *The Mediterranean basins: tertiary extension within the Alpine orogen*, edited by B. Durand, L. Jolivet, F. Horváth and M. Séranne, Geological Society, London, pp. 37-61.

Chayes, F., and E. G. Zies (1964), Notes on some Mediterranean comendite and pantellerite specimens, *Annual Report of the Geophysical Laboratory*, Yearbook 63, Carnegie Institution Washington, 186-193.

Cherchi, A., and L. Montadert (1982), Oligo-Miocene rift of Sardinia and the early history of Western Mediterranean Basin, *Nature*, *298*(5876), 736-739.

Cincotti, F., A. Assorgia, A. Fadda, M. Farns, D. Gimeno, V. Morra, L. Ottelli, R. Rizzo, and F. A. Secchi (1992), Il Complesso Ignimbritico di Acqua Sa Canna (Sulcis, Sardegna SO), Progetti Nazionali MURST 40%, Riunionie scientifica: Ignimbriti cenozoiche sarde, 9-12 June, Sardinia (Italy).

Cioni, R., and A. Funedda (2005), Structural geology of crystal-rich, silicic lava flows: A case study from San Pietro Island (Sardinia, Italy), *Geological Society of America Special Paper*, *396*, 1-14.

Cioni, R., and A. Gioncada (2006), Evoluzione della fase fluida in una camera magmatica peralcalina: un essempio dall'Isola di San Pietro (Sardegna, Italia), presented at 85º Congresso SIMP, 27-30 September, Fluminimaggiore (Italy).

Cioni, R., R. Clocchiatti, G. M. Dipaola, R. Santacroce, and S. Tonarini (1982), Miocene calc-alkaline heritage in the Pliocene post-collisional volcanism of Monte Arci (Sardinia, Italy), *Journal of Volcanology and Geothermal Research*, *14*(1-2), 133-167.

Cioni, R., L. Salaro, and L. Pioli (2001), The Cenozoic volcanism of San Pietro Island (Sardinia, Italy), *Rendiconti del Seminario della Facoltà di Scienze dell'Università di Cagliari*, *71*(2), 149-163.

Civetta, L., Y. Cornette, G. Crisci, P. Y. Gillot, G. Orsi, and C. S. Requejo (1984), Geology, geochronology and chemical evolution of the island of Pantelleria, *Geological Magazine*, *121*(6), 541-562.

Civetta, L., M. D'Antonio, G. Orsi, and G. R. Tilton (1998), The geochemistry of volcanic rocks from Pantelleria island, Sicily channel: Petrogenesis and characteristics of the mantle source region, *Journal of Petrology*, *39*(8), 1453-1491.

Class, C., D. M. Miller, S. L. Goldstein, and C. H. Langmuir (2000), Distinguishing melt and fluid subduction components in Umnak Volcanics, Aleutian Arc, *Geochemistry Geophysics Geosystems*, *1*(1), 1999GC000010.

Collins, W. J., S. D. Beams, A. J. R. White, and B. W. Chappell (1982), Nature and origin of A-type granites with particular reference to Southeastern Australia, *Contributions to Mineralogy and Petrology*, *80*(2), 189-200.

Condie, K. C., M. Wilks, D. M. Rosen, and V. L. Zlobin (1991), Geochemistry of metasediments from the Precambrian Hapschan series, eastern Anabar Shield, Siberia, *Precambrian Research*, *50*(1-2), 37-47.

Conte, A. M. (1997), Petrology and geochemistry of Tertiary calcalkaline magmatic rocks from the Sarroch district (Sardinia, Italy), *Periodico di Mineralogia*, *66*(1-2), 63-100.

Conte, A. M., and D. Dolfi (2002), Petrological and geochemical characteristics of Plio-Pleistocene Volcanics from Ponza Island (Tyrrhenian Sea, Italy), *Mineralogy and Petrology*, *74*(1), 75-94.

Conte, A. M., D. M. Palladino, C. Perinelli, and E. Argenti (2010), Petrogenesis of the High-Alumina Basalt-Andesite suite from Sant'Antioco Island, SW Sardinia, Italy, *Periodico di Mineralogia*, *79*(1), 27-55.

Coulon, C. (1977), Le volcanisme calco-alcalin cénozoïque de Sardaigne (Italie). Petrographie, géochimie et génèse des laves andesitiques et des ignimbrites. Signification géodynamique, PhD Thesis, University of Aix-Marseille III, 288 pp..

Coulon, C., L. Baque, and C. Dupuy (1973), Les andésites cénozoïques et les laves associées en Sardaigne Nord-Occidentale (Provinces du Logudoro et du Bosano) - Caractères minéralogiques et chimiques, *Contributions to Mineralogy and Petrology*, *42*(2), 125-139.

Coulon, C., A. Demant, and C. Bobier (1974), Contribution du paléomagnétisme à l'étude des séries volcaniques cénozoïques et quaternaires de Sardaigne nord-occidentale. Le problème de la dérive de la Sardaigne, *Tectonophysics*, *22*(1-2), 59-82.

Coulon, C., J. Dostal, and C. Dupuy (1978), Petrology and geochemistry of the ignimbrites and associated lava domes from NW Sardinia, *Contributions to Mineralogy and Petrology*, *68*(1), 89-98.

Cravatte, J., P. Dufaure, M. Prine, and S. Ronaix (1974), Les forages du Golfe du Lion. Stratigraphie, sédimentologie, *Compagnie française des pétroles: Notes et Mémoires*, *11*, 215-274.

De Jong, K. A., M. Manzoni, and J. D. A. Zijderve (1969), Paleomagnetism of the Alghero trachyandesites, *Nature*, *224*(5214), 67-69.

De Jong, K. A., M. Manzoni, T. Stavenga, F. Van Dijk, R. Van Der Voo, and J. D. A. Zijderve (1973), Paleomagnetic evidence for rotation of Sardinia during Early Miocene, *Nature*, *243*(5405), 281-283.

Deer, W. A., R. A. Howie, and J. Zussman (1963), *Rock-forming minerals. Volume 4: Framework silicates*, Longman Group Limited, London, 435 pp..

Deer, W. A., R. A. Howie, and J. Zussman (1992), *An introduction to the rock-forming minerals*, 2nd ed., Longman Scientific and Technical, Hong Kong, 696 pp..

Del Veccio, L. (1989), Consideracioni sul vulcanismo esplosivo miocenico della Sardegna SW. PhD Thesis, Università degli Studi di Napoli Federico II, Napoli.

Deriu, M. (1962), Stratigrafia, cronologia e caratteri petrochimici delle vulcaniti "oligoceniche" in Sardegna, *Memorie della Società Geologica Italiana*, *3*, 675-706.

Dietrich, R. V. (1968), Behaviour of zirconium in certain artificial magmas under diverse P-T conditions, *Lithos*, *1*, 20-25.

Dostal, J., C. Coulon, and C. Dupuy (1982), Cainozoic andesitic rocks of Sardinia (Italy), in *Andesites*, edited by R. S. Thorpe, John Wiley & sons, London, pp. 353-370.

Downes, H., M. F. Thirlwall, and S. C. Trayhorn (2001), Miocene subduction-related magmatism in southern Sardinia: Sr-Nd- and oxygen isotopic evidence for mantle source enrichment, *Journal of Volcanology and Geothermal Research*, *106*(1-2), 1-21.

Duggen, S., M. Portnyagin, J. Baker, D. Ulfbeck, K. Hoernle, D. Garbe-Schonberg, and N. Grassineau (2007), Drastic shift in lava geochemistry in the volcanic-front to rear-arc region of the Southern Kamchatkan subduction zone: Evidence for the transition from slab surface dehydration to sediment melting, *Geochimica Et Cosmochimica Acta*, *71*(2), 452-480.

Edel, J. B. (1979), Paleomagnetic study of the Tertiary volcanics in Sardinia, *Journal of Geophysics-Zeitschrift Fur Geophysik*, *45*(3), 259-280.

Edel, J. B., and A. Lörtscher (1977), Paléomagnétisme du volcanisme tertiaire de Sardaigne. Noveaux résultats et synthèse, *Bulletin de la Société Géologique de France*, *19*(4), 815-824.

Edel, J. B., D. Dubois, R. Marchant, J. Hernandez, and M. Cosca (2001), La rotation miocène inférieur du bloc corso-sarde. Nouvelles contraintes paléomagnétiques sur la fin du mouvement, *Bulletin de la Société Géologique de France*, *172*(3), 275-283.

Egger, A., M. Demartin, J. Ansorge, E. Banda, and M. Maistrello (1988), The gross structure of the crust under Corsica and Sardinia, *Tectonophysics*, *150*(3), 363-389.

Ellam, R. M., C. J. Hawkesworth, M. A. Menzies, and N. W. Rogers (1989), The volcanism of southern Italy: role of subduction and the relationship between potassic and sodic alkaline magmatism, *Journal of Geophysical Research-Solid Earth and Planets*, 94(B4), 4589-4601.

Faccenna, C., F. Speranza, F. D. Caracciolo, M. Mattei, and G. Oggiano (2002), Extensional tectonics on Sardinia (Italy): insights into the arc back-arc transitional regime, *Tectonophysics*, *356*(4), 213-232.

Fedele, L., M. Lustrino, L. Melluso, V. Morra, and F. D'Amelio (2007), The Pliocene Montiferro, volcanic complex (central-western Sardinia, Italy): geochemical observations and petrological implications, *Periodico di Mineralogia*, *76*, 101-136.

Franciosi, L., M. Lustrino, L. Melluso, V. Morra, and M. D'Antonio (2003), Geochemical characteristics and mantle sources of the Oligo-Miocene primitive basalts from Sardinia: The role of subduction components, *Ofioliti*, *28*(2), 105-114.

Franco, R. R., and J. F. Schairer (1951), Liquidus temperatures in mixtures of the feldspars of soda, potash and lime, *Journal of Geology*, *59*, 259-267.

Garbarino, C., and L. Maccioni (1968), Contributo alla conoscenza delle vulcaniti dell'isola di S.Pietro (Sardegna sud-occidentale). Nota I.- Le commenditi, *Periodico di Mineralogia*, *37*(3), 895-1018.

Garbarino, C., and L. Maccioni (1969), Contributo alla conoscenza delle vulcaniti dell'isola di S.Pietro (Sardegna sud-occidentale). Nota II.- Le commenditi filoniane, *Periodico di Mineralogia*, *39*, 1-19.

Garbarino, C., and L. Maccioni (1970a), Contributo alla conoscenza delle vulcaniti dell'isola di S.Pietro (Sardegna sud-occidentale). Nota III.- Le rioliti di base (tau4 di Taricco), *Periodico di Mineralogia*, *39*, 33-102.

Garbarino, C., and L. Maccioni (1970b), Contributo alla conoscenza delle vulcaniti dell'Isola di S. Pietro (Sardegna sud-occidentale). Nota IV: sopra una particolare facies riolitica pre-τ_4(r-g), *Periodico di Mineralogia*, *39*, 103-124.

Garbarino, C., L. Maccioni, and I. Salvadori (1985), Carta geopetrografica dell'Isola di S. Pietro (Sardegna). Scala 1:25.000. SELCA, Firenze.

Garbarino, C., L. Lirer, L. Maccioni, and I. Salvadori (1990), Carta vulcanologica dell'Isola di San Pietro (Sardegna). 1:25,000. Editor: SELCA, Firenze.

Garbarino, C., S. Naitza, R. Rizzo, S. Tocco, S. Barca, A. Farci, A. Forci, and R. Serri (2005), New evidence of Pre-Hercynian volcanics from Southern Sulcis (Southwestern Sardinia), *Bollettino della Società Geologica Italiana*, *124*(1), 69-85.

Gasperini, D., J. Blichert-Toft, D. Bosch, A. Del Moro, P. Macera, P. Telouk, and F. Albarede (2000), Evidence from Sardinian basalt geochemistry for recycling of plume heads into the Earth's mantle, *Nature*, *408*(6813), 701-704.

Gattacceca, J., A. Deino, R. Rizzo, D. S. Jones, B. Henry, B. Beaudoin, and F. Vadeboin (2007), Miocene rotation of Sardinia: New paleomagnetic and geochronological constraints and geodynamic implications, *Earth and Planetary Science Letters*, *258*(3-4), 359-377.

Gennesseaux, M. G., and D. J. Stanley (1983), *Neogene to recent displacement and contact of Sardinian and Tunisian margins, Central Mediterranean*, 21 pp., Washington.

Gimeno, D., A. Assorgia, N. Díaz, and C. Segura (1996), Vitrófiros basales en flujos piroclásticos de composición riolítica: el caso de la unidad de Nuraxi (Sulcis, SE de la isla de Cerdeña, Italia), *Geogaceta*, *20*(3), 564-568.

Gimeno, D., N. Diaz, M. Garcia-Valles, and S. Martinez-Manent (2002), Genesis of bottom vitrophyre facies in rhyolitic pyroclastic flows: a case study of syneruptive glass welding (Nuraxi unit, Sulcis, SW Sardinia, Italy), paper presented at 4th International Conference on Glasses in Geoscience, Environmental Sciences and Archeometry, 29-31 August, Lyon (France).

Gimeno, D., N. Diaz, M. Garcia-Valles, and S. Martinez-Manent (2003), Genesis of bottom vitrophyre facies in rhyolitic pyroclastic flows: a case study of syneruptive glass welding (Nuraxi unit, Sulcis, SW Sardinia, Italy), *Journal of Non-Crystalline Solids*, *323*(1-3), 91-96.

Gorini, C., A. Lemarrec, and A. Mauffret (1993), Contribution to the structural and sedimentary history of the Gulf of Lions (western Mediterranean), from ECORS profiles, industrial seismic profiles and well data, *Bulletin de la Société Géologique de France*, *164*(3), 353-363.

Gromet, L. P., R. F. Dymek, L. A. Haskin, and R. L. Korotev (1984), The North-American shale composite: its compilation, major and trace element characteristics, *Geochimica Et Cosmochimica Acta*, *48*(12), 2469-2482.

Guarino, V., L. Fedele, L. Franciosi, R. Lonis, M. Lustrino, M. Marrazzo, L. Melluso, V. Morra, I. Rocco, and F. Ronga (2011), Mineral compositions and magmatic evolution of the calcalkaline rocks of northwestern Sardinia, Italy, *Periodico di Mineralogia*, *80*(3), 517-545.

Guerrera, F., M. Mattioli, F. Serrano, M. Tramontana, and G. Raffaelli (2004), Stratigraphy of the miocene syn-rift volcano-sedimentary succession in a sector of the central-southern Sardinia Trough (Italy), *Geologica Carpathica*, *55*(1), 51-63.

Hanan, B. B., and D. W. Graham (1996), Lead and helium isotope evidence from oceanic basalts for a common deep source of mantle plumes, *Science*, *272*(5264), 991-995.

Harangi, S., H. Downes, and I. Seghedi (2006), Tertiary-Quaternary subduction processes and related magmatism in the Alpine-Mediterranean region, in *European lithosphere dynamics*, edited by D. G. Gee and R. A. Stephenson, Geological Society, London, pp. 167-190.

Harangi, S., H. Downes, M. Thirlwall, and K. Gmeling (2007), Geochemistry, petrogenesis and geodynamic relationships of miocene calc-alkaline volcanic rocks in the western carpathian arc, eastern central Europe, *Journal of Petrology*, *48*(12), 2261-2287.

Hart, S. R., E. H. Hauri, L. A. Oschmann, and J. A. Whitehead (1992), Mantle plumes and entrainment - Isotopic evidence, *Science*, *256*(5056), 517-520.

Hawkesworth, C. J., J. M. Hergt, R. M. Ellam, and F. McDermott (1991), Element fluxes associated with subduction related magmatism, *Philosophical Transactions of the Royal Society of London Series a-Mathematical Physical and Engineering Sciences*, *335*(1638), 393-405.

Hoernle, K., Y. S. Zhang, and D. Graham (1995), Seismic and geochemical evidence for large-scale mantle upwelling beneath the eastern Atlantic and western and central Europe, *Nature*, *374*(6517), 34-39.

Hofmann, A. W. (1988), Chemical differentiation of the Earth: The relationship between mantle, continental crust and oceanic crust, *Earth and Planetary Science Letters*, *90*(3), 297-314.

Houghton, B. F., S. D. Weaver, C. J. N. Wilson, and M. A. Lanphere (1992), Evolution of a Quaternary peralkaline volcano: Mayor Island, New Zealand, *Journal of Volcanology and Geothermal Research*, *51*(3), 217-236.

Irvine, T. N., and W. R. A. Baragar (1971), Guide to chemical classification of common volcanic rocks, *Canadian Journal of Earth Sciences*, *8*(5), 523-548.

Johnsen, A. (1912), Zur petrographie der Insel S. Pietro und S. Antioco (Sardinien), *Zentralblatt für Mineralogie, Geologie, und Paläontologie*.

Kastens, K., et al. (1988), ODP Leg-107 in the Tyrrhenian sea: insights into passive margin and mack-arc evolution, *Geological Society of America Bulletin*, *100*(7), 1140-1156.

Kersting, A. B., and R. J. Arculus (1994), Klyuchevskoy Volcano, Kamchatka, Russia: The role of high-flux recharged, tapped and fractionated magma chamber(s) in the genesis of High-Al_2O_3 from High-MgO basalt, *Journal of Petrology*, *35*(1), 1-41.

Kiminami, K., and T. Imaoka (2006), Occurrence and petrography of volcaniclastic rocks in the Tertiary Shimanto Supergroup along the east coast of the Hata Peninsula, southwestern Shikoku, Southwest Japan, and its significance, *Journal of the Geological Society of Japan*, *112*(2), 107-121.

Kogarko, L. N., and L. N. Lazutkina (1989), Zirconium in silicate liquids and magmas, *Geochemistry International*, *4*, 47-57.

Kuno, H. (1966), Lateral variation of basalt magma types across continental margins and island arcs, *Bulletin Volcanologique*, *29*, 195-222.

La Marmora, A. (1957), *Voyage en Sardaigne. Troissième partie: description géologique et paleontologique*, Ed. Bertrand, Paris, 650 pp..

Le Bas, M. J., R. W. Le Maitre, A. Streckeisen, and B. Zanettin (1986), A chemical classification of volcanic rocks based on the Total Alkali-Silica diagram, *Journal of Petrology*, *27*(3), 745-750.

Le Maitre, R. W. (editor) (1989), *Classification of igneous rocks and glossary of terms. Recommendation of the International Union of Geological Sciences. Subcomission on the Systematics of Igneous Rocks*, Blackwell Scientific Publications, Oxford, London, 193 pp..

Le Maitre, R. W. (editor) (2002), *Igneous Rocks: A Classification and Glossary of Terms. Recommendations of the International Union of Geological Sciences Subcommission on the Systematics of Igneous Rocks*, Cambridge University Press, Cambridge, 236 pp..

Leake, B. E., et al. (1997), Nomenclature of amphiboles: Report of the subcommittee on amphiboles of the International Mineralogical Association, Commission on New Minerals and Mineral Names, *Canadian Mineralogist*, *35*, 219-246.

Leat, P. T., S. E. Jackson, R. S. Thorpe, and C. J. Stillman (1986), Geochemistry of bimodal basalt subalkaline peralkaline rhyolite provinces within the Southern British Caledonides, *Journal of the Geological Society*, *143*, 259-273.

Lecca, L., R. Lonis, S. Luxoro, E. Melis, F. Secchi, and P. Brotzu (1997), Oligo-Miocene volcanic sequences and rifting stages in Sardinia: a review, *Periodico di Mineralogia*, *66*(1-2), 7-61.

Lindsley, D. H. (1983), Pyroxene thermometry, *American Mineralogist*, *68*(5-6), 477-493.

Linthout, K. (1984), Alkali-zirconosilicates in peralkaline rocks, *Contributions to Mineralogy and Petrology*, *86*(2), 155-158.

Lofgren, G. (1971), Experimentally produced devitrification textures in natural rhyolitic glass, *Geological Society of America Bulletin*, *82*(1), 111-124.

Lonis, R., V. Morra, M. Lustrino, L. Melluso, and F. Secchi (1997), Plagioclase textures, mineralogy and petrology of Tertiary orogenic volcanic rocks from Sindia (central Sardinia), *Periodico di Mineralogia*, *66*(1-2), 185-210.

Lustrino, M. (2000), Petrogenesis of tholeiitic volcanic rocks from central-southern Sardinia, *Mineralogica et Petrographica Acta*, *43*, 49-64.

Lustrino, M. (2005), How the delamination and detachment of lower crust can influence basaltic magmatism, *Earth-Science Reviews*, *72*(1-2), 21-38.

Lustrino, M., and M. Wilson (2007), The circum-Mediterranean anorogenic Cenozoic igneous province, *Earth-Science Reviews*, *81*(1-2), 1-65.

Lustrino, M., L. Melluso, V. Morra, and F. Secchi (1996), Petrology of Plio-Quaternary volcanic rocks from central Sardinia, *Periodico di Mineralogia*, *65*, 275-287.

Lustrino, M., L. Melluso, and V. Morra (1999), Origin of glass and its relationships with phlogopite in mantle xenoliths from central Sardinia (Italy), *Periodico di Mineralogia*, *68*(1), 13-42.

Lustrino, M., L. Melluso, and V. Morra (2000), The role of lower continental crust and lithospheric mantle in the genesis of Plio-Pleistocene volcanic rocks from Sardinia (Italy), *Earth and Planetary Science Letters*, *180*(3-4), 259-270.

Lustrino, M., L. Melluso, and V. Morra (2002), The transition from alkaline to tholeiitic magmas: a case study from the Orosei-Dorgali Pliocene volcanic district (NE Sardinia, Italy), *Lithos*, *63*(1-2), 83-113.

Lustrino, M., V. Morra, M. Meelluso, P. Brotzu, F. D'Amelio, L. Fedele, F. Franciosi, R. Lonis, and A. M. Petteruti Liebercknecht (2004), The Cenozoic igneous activity of Sardinia, *Periodico di Mineralogia*, *73*, 105-134.

Lustrino, M., V. Morra, L. Fedele, and M. Serracino (2007a), The transition between 'orogenic' and 'anorogenic' magmatism in the western Mediterranean area: the Middle Miocene volcanic rocks of Isola del Toro (SW Sardinia, Italy), *Terra Nova*, *19*(2), 148-159.

Lustrino, M., L. Melluso, and V. Morra (2007b), The geochemical peculiarity of "Plio-Quaternary" volcanic rocks of Sardinia in the circum-Mediterranean Cenozoic Igneous Province, in *Cenozoic volcanism in the Mediterranean area*, edited by L. Beccaluva, G. Bianchini and M. Wilson, Geological Society of America Special Paper, 418, pp. 277-301.

Lustrino, M., V. Morra, L. Fedele, and L. Franciosi (2009), Beginning of the Apennine subduction system in central western Mediterranean: Constraints from Cenozoic "orogenic'' magmatic activity of Sardinia, Italy, *Tectonics*, *28*, 23.

Lustrino, M., S. Duggen, and C. L. Rosenberg (2011), The Central-Western Mediterranean: Anomalous igneous activity in an anomalous collisional tectonic setting, *Earth-Science Reviews*, *104*(1-3), 1-40.

Maccioni, L. (1969), Ialoclastiti e pillow-lave nel Miocene della Marmilla, *Rendiconti del Seminario della Facoltà di Scienze dell'Università di Cagliari*, *39*, 207-220.

Maccioni, L. (1974), Nuovi rinvenimenti di lave a cuscino nel Miocene della Marmilla (Sardegna centro-occidentale), *Rendiconti del Seminario della Facoltà di Scienze dell'Università di Cagliari*, *43*, 277-282.

Maccioni, L., M. Marchi, and A. Assorgia (1990), Carta geopetrografica dell'Isola di Santo Antioco (Sardegna). 1:25,000. Editor: SELCA, Firenze.

MacDonald, G. A. (1968), Composition and origin of Hawaiian lavas, in *Studies in volcanology: a memoir in honour of Howel Williams*, edited by R. R. Coats, R. L. Hay and C. A. Anderson, Geological Society of America Memoirs, 116, pp. 477-522.

Macdonald, R. (1974a), Nomenclature and Petrochemistry of the Peralkaline Oversaturated Extrusive Rocks, *Bulletin Volcanologique*, *38*(3), 498-516.

Macdonald, R. (1974b), Tectonic settings and magma associations, *Bulletin Volcanologique*, *38*(3), 575-593.

Mahood, G. A. (1984), Pyroclastic rocks and calderas associated with strongly peralkaline magmatism, *Journal of Geophysical Research*, *89*(NB10), 8540-8552.

Manzoni, M. (1974), Un'interpretazione dei dati paleomagnetici del Terziario della Sardegna ed alcuni nuovi risultati, *Rendiconti del Seminario della Facoltà di Scienze dell'Università di Cagliari*, *43*, 283-295.

Manzoni, M. (1975), Paleomagnetic data from Tertiary volcanism of the Campidano and associated grabens, Sardinia, *Earth and Planetary Science Letters*, *27*, 275-282.

Martin, R. F. (1974), Role of water in pantellerite melts, *Bulletin Volcanologique*, *38*, 666-679.

Mattioli, M., F. Guerrera, M. Tramontana, G. Raffaelli, and M. D'Atri (2000), High-Mg Tertiary basalts in Southern Sardinia (Italy), *Earth and Planetary Science Letters*, *179*(1), 1-7.

Middlemost, E. A. K. (1989), Iron oxidation ratios, norms and the classification of volcanic rocks, *Chemical Geology*, *77*(1), 19-26.

Montanini, A., and S. Meli (1992), Mineralogy and petrology of the mafic inclusion-bearing trachytes from Mt. Arci volcanic massif (Western Sardinia), *Neues Jahrbuch Fur Mineralogie-Abhandlungen*, *164*(2-3), 139-168.

Montanini, A., M. Barbieri, and F. Castorina (1994), The role of fractional crystallisation, crustal melting and magma mixing in the petrogenesis of rhyolites and mafic inclusion-bearing dacites from the Monte Arci volcanic complex (Sardinia, Italy), *Journal of Volcanology and Geothermal Research*, *61*(1-2), 95-120.

Montigny, R., J. B. Edel, and R. Thuizat (1981), Oligo-Miocene rotation of Sardinia - K-Ar ages and paleomagnetic data of Tertiary volcanics, *Earth and Planetary Science Letters*, *54*(2), 261-271.

Morimoto, N. (chairman) (1989), Nomenclature of Pyroxenes, *Canadian Mineralogist*, *27*, 143-156.

Morra, V., F. A. Secchi, and A. Assorgia (1994), Petrogenetic significance of peralkaline rocks from Cenozoic calc-alkaline volcanism from Sardinia, Italy, *Chemical Geology*, *118*(1-4), 109-142.

Morra, V., F. A. G. Secchi, L. Melluso, and L. Franciosi (1997), High-Mg subduction-related tertiary basalts in Sardinia, Italy, *Lithos*, *40*(1), 69-91.

Mundula, F., R. Cioni, and R. Rizzo (2009), A simplified scheme for the description of textural features in Welded Ignimbrites: the example of San Pietro Island (Sardinia, Italy), *Bollettino della Società Geologica Italiana*, *128*(3), 615-627.

Mungall, J. E., and R. F. Martin (1995), Petrogenesis of basalt-comendite and basalt-pantellerite suites, Terceira, Azores, and some implications for the origin of ocean-island rhyolites, *Contributions to Mineralogy and Petrology*, *119*(1), 43-55.

Nairn, A. E. M., and M. Westphal (1968), Possible implications of the paleomagnetic study of late Paleozoic igneous rocks of northwestern Corsica, *Palaeogeography Palaeoclimatology Palaeoecology*, *5*(2), 179-204.

Nelson, S. A., and J. A. Hegre (1990), Volcán Las Navajas, a Plio-Pleistocene trachyte/peralkaline rhyolite volcano in the northwestern Mexican volcanic belt, *Bulletin of Volcanology*, *52*(3), 186-204.

Noble, D. C. (1968), Systematic variation of major elements in comendite and pantellerite glasses, *Earth and Planetary Science Letters*, *4*, 167-172.

Noble, D. C. (1970), Loss of sodium from crystallized comendite welded tuffs of Miocene Grouse Canyon member of the Belted Range Tuff, Nevada, *Geological Society of America Bulletin*, *81*(9), 2677-2687.

Noble, D. C., and J. Haffty (1969), Minor-element and revised major-element contents of some Mediterranean pantellerites and comendites, *Journal of Petrology*, *10*(3), 502-509.

Novarese, V., and G. Pullè (1920), Carta Geologico-Mineraria dell'Iglesiente, sheet 232: Nebida. 1:25,000. Editor: Istituto Geografico de Agostini, Novara.

Novarese, V., and G. Pullè (1926), Carta Geologico-Mineraria dell'Iglesiente, sheet 232: Portoscuso. 1:25,000. Editor: L. Salomone, Roma.

Novarese, V., M. Taricco, and G. Pullé (1933), Carta Geologica d'Italia, sheets 232 and 232bis: Isola di San Pietro and Capo Sperone. 1:100,000. Editor: L. Salomone, Roma.

Othman, D. B., W. M. White, and J. Patchett (1989), The geochemistry of marine sediments, island arc magma genesis, and crust-mantle recycling, *Earth and Planetary Science Letters*, *94*(1-2), 1-2121.

Panza, G. F., A. Peccerillo, A. Aoudia, and B. Farina (2007), Geophysical and petrological modelling of the structure and composition of the crust and upper mantle in complex geodynamic settings: The Tyrrhenian Sea and surroundings, *Earth-Science Reviews*, *80*(1-2), 1-46.

Parfitt, E. A., and L. Wilson (2008), *Fundamentals of physical volcanology*, Blackwell, Malden, Oxford, Carlton, 230 pp..

Pasci, S., L. Pioli, G. Pisanu, M. Rosi, V. Sale, E. Benvenuti, and M. Laurenzi (2001), Tettonica e vulcanismo miocenici nel Sulcis (Sardegna SW), Presentation at Geoitalia, III FIST Meeting, 5-8 September, Chieti (Italy).

Pasci, S., and P. Orrù (coord) (unpublished), Carta Geologica d'Italia, sheet 564 of the 1:50.000 map of the Istituto Geografico Militare: Carbonia. 1:50,000. Editor: APAT– Dipartamento Difesa del Suolo – Servizio Geologico d'Italia. Consulted at http://www.isprambiente.gov.it/MEDIA/carg/564_CARBONIA/Foglio.html on March 16th, 2012.

Peccerillo, A., and S. R. Taylor (1976), Geochemistry of Eocene calc-alkaline volcanic rocks from Kastamonu area, northern Turkey, *Contributions to Mineralogy and Petrology*, *58*(1), 63-81.

Pecorini, G., and A. Pomesano Cherchi (1969), Ricerche geologiche e biostratigraphiche sul Campidano meridionale (Sardegna), *Memorie della Società Geologica Italiana*, *8*, 421-451.

Philpotts, A. R., and J. J. Ague (2009), *Principles of igneous and metamorphic petrology*, 2nd ed., Cambridge University Press, 667 pp..

Pichavant, M., and R. Macdonald (2007), Crystallization of primitive basaltic magmas at crustal pressures and genesis of the calc-alkaline igneous suite: experimental evidence from St Vincent, Lesser Antilles arc, *Contributions to Mineralogy and Petrology*, *154*(5), 535-558.

Pioli, L. (2003), High-grade ignimbrites from the Sulcis volcanic district (SW Sardinia, Italy): the example of Nuraxi tuff, PhD Thesis, Università di Pisa, Pisa, 157 pp..

Pioli, L., and M. Rosi (2005), Rheomorphic structures in a high-grade ignimbrite: The Nuraxi tuff, Sulcis volcanic district (SW Sardinia, Italy), *Journal of Volcanology and Geothermal Research*, *142*(1-2), 11-28.

Pioli, L., R. Lanza, M. Ort, and M. Rosi (2008), Magnetic fabric, welding texture and strain fabric in the Nuraxi Tuff, Sardinia, Italy, *Bulletin of Volcanology*, *70*(9), 1123-1137.

Piromallo, C., D. Gasperini, P. Macera, and C. Faccenna (2008), A late Cretaceous contamination episode of the European-Mediterranean mantle, *Earth and Planetary Science Letters*, *268*(1-2), 15-27.

Plank, T., and C. H. Langmuir (1998), The chemical composition of subducting sediment and its consequences for the crust and mantle, *Chemical Geology*, *145*(3-4), 325-394.

Porcu, A. (1972), Geologia della media valle del Tirso (Sardegna centrale), *Bollettino della Società Sarda di Scienze Naturali*, *10*, 1-24.

Putirka, K. A. (2008), Thermometers and barometers for volcanic systems, in *Minerals, inclusions and volcanic processes*, edited by K. A. Putirka and F. J. Tepley, The Mineralogical Society of America, 69, Washington D.C, pp. 61-120.

Rahman, S., and W. S. MacKenzie (1969), The crystallisation of ternary feldspars: a study from natural rocks, *American Journal of Science*, *267*, 391-406.

Ramon Sala, L. (2009), Estudi de la successió piroclàstica miocena de l'oest de l'illa de Sant'Antioco al sector de Cala Saboni-Sa Corona de su Crobu, Minor thesis, Universitat de Barcelona, Barcelona, 52 pp..

Regelous, M., J. A. Gamble, and S. P. Turner (2010), Mechanism and timing of Pb transport from subducted oceanic crust and sediment to the mantle source of arc lavas, *Chemical Geology*, *273*(1-2), 46-54.

Rodríguez López, A. (2009), Cartografia i anàlisi geoquímic al Sud-oest de l'illa de Sant'Antioco, Minor thesis, Universitat de Barcelona, Barcelona, 47 pp..

Rollet, N., J. Deverchere, M. O. Beslier, P. Guennoc, J. P. Rehault, M. Sosson, and C. Truffert (2002), Back arc extension, tectonic inheritance, and volcanism in the Ligurian Sea, Western Mediterranean, *Tectonics*, *21*(3), 26.

Rosselló Espuny, Z. (2005), Estudi vulcanoestratigràfic, petrològic i geoquímic d'una unitat piroclàstica miocènica situada a l'Isola di San Pietro, SW de Sardenya (Itàlia), Minor thesis, Universitat de Barcelona, Barcelona, 57 pp..

Rutter, M. J. (1987), Evidence for crustal assimilation by turbulently convecting, mafic alkaline magmas: geochemistry of mantle xenolith-bearing lavas from northern Sardinia, *Journal of Volcanology and Geothermal Research*, *32*(4), 343-354.

Sartori, R. (1990), The main results of ODP Leg 107 in the frame of Neogene to recent geology of peri-Tyrrhenian areas, *Proceedings of the Ocean Drilling Program Scientific Results*, *107*(715-730).

Sartori, R., and O. L. S. Staff (1989), Drillings of ODP Leg 107 in the Tyrrhenian sea: tentative basin evolution compared to deformations in the surrounding chains, in *The lithosphere in Italy. Advances in Earth science research*, edited by A. Boriani, M. Bonafede, G. B. Piccardo and G. B. Vai, Accademia Nazionale dei Lincei, Roma, pp. 139-156.

Sau, A., L. Lecca, R. Lonis, F. Secchi, and M. L. Fercia (2005), The second stage of the Sardinian Rift: volcanism and evolution of Ardara-Chilivani and Bonorva sub-basins (Northern Sardinia), *Bollettino della Società Geologica Italiana*, *124*(1), 3-20.

Savelli, C. (1975), Datazioni preliminari col metodo K-Ar di vulcaniti della Sardegna sud-occidentale, *Rendiconti della Società Italiana di Mineralogia e Petrologia*, *31*, 191-198.

Savelli, C., L. Beccaluva, M. Deriu, G. Macciotta, and L. Maccioni (1979), K-Ar geochronology and evolution of the Tertiary calc-alkalic volcanism of Sardinia (Italy), *Journal of Volcanology and Geothermal Research*, *5*(3-4), 257-269.

Scaillet, B., and B. W. Evans (1999), The 15 June 1991 eruption of Mount Pinatubo. I. Phase equilibria and pre-eruption P-T-fO_2-fH_2O conditions of the dacite magma, *Journal of Petrology*, *40*(3), 381-411.

Scaillet, B., and R. MacDonald (2001), Phase relations of peralkaline silicic magmas and petrogenetic implications, *Journal of Petrology*, *42*(4), 825-845.

Scaillet, B., and R. Macdonald (2003), Experimental constraints on the relationships between peralkaline rhyolites of the Kenya rift valley, *Journal of Petrology*, *44*(10), 1867-1894.

Schettino, A., and E. Turco (2006), Plate kinematics of the Western Mediterranean region during the Oligocene and Early Miocene, *Geophysical Journal International*, *166*(3), 1398-1423.

Schmidt, M. W., and S. Poli (2003), Generation of mobile components during subduction of ocean crust, in *Treatise on geochemistry. Volume 3: The crust*, edited by H. D. Holland and K. K. Turekian, Elsevier, Oxford, pp. 567-591.

Séranne, M. (1999), The Gulf of Lion continental margin (NW Mediterranean) revisited by IBS: an overview, in *The Mediterranean Basins: Tertiary extension within the Alpine orogen*, edited by B. Durand, L. Mascle, L. Jolivet, F. Horváth and M. Séranne, The Geological Society, London, pp. 21-53.

Serri, G. (1990), Neogene-Quaternary magmatism of the Tyrrhenian region: characterization of the magma sources and geodynamic implications, *Memorie della Società Geologica Italiana*, *41*, 219-242.

Smith, I. E. M. (1976), Peralkaline rhyolites from the D'Entrecasteaux Islands, Papua New Guinea, in *Volcanism in Australasia*, edited by R. W. Johnson, Elsevier, Amsterdam, pp. 275-285.

Smith, I. E. M., B. W. Chappell, G. K. Ward, and R. S. Freeman (1977), Peralkaline rhyolites associated with andesitic arcs of southwest Pacific, *Earth and Planetary Science Letters*, *37*(2), 230-236.

Smith, R. K., R. L. Tremallo, and G. E. Lofgren (2001), Growth of megaspherulites in a rhyolitic vitrophyre, *American Mineralogist*, *86*(5-6), 589-600.

Souther, J. G., and C. J. Hickson (1984), Crystal fractionation of the basalt comendite series of Mount Edziza volcanic complex, British Columbia: major and trace elements, *Journal of Volcanology and Geothermal Research*, *21*(1-2), 79-106.

Sowerbutts, A. A., and J. R. Underhill (1998), Sedimentary response to intra-arc extension: controls on Oligo-Miocene deposition, Sarcidano sub-basin, Sardinia, *Journal of the Geological Society*, *155*, 491-508.

Speranza, F., I. M. Villa, L. Sagnotti, F. Florindo, D. Cosentino, P. Cipollari, and M. Mattei (2002), Age of the Corsica-Sardinia rotation and Liguro-Provencal Basin spreading: new paleornagnetic and Ar/Ar evidence, *Tectonophysics*, *347*(4), 231-251.

Stolz, A. J., G. R. Davies, A. J. Crawford, and I. E. M. Smith (1993), Sr, Nd and Pb isotopic compositions of calc-alkaline and peralkaline silicic volcanics from the D'Entrecasteaux Islands, Papua New Guinea, and their tectonic significance, *Mineralogy and Petrology*, *47*(2-4), 103-126.

Stormer, J. C., and J. Nicholls (1978), XLFRAC - program for the interactive testing of magmatic differentiation models, *Computers & Geosciences*, *4*(2), 143-159.

Stracke, A., A. W. Hofmann, and S. R. Hart (2005), FOZO, HIMU, and the rest of the mantle zoo, *Geochemistry Geophysics Geosystems*, *6*.

Streck, M. J., and A. L. Grunder (1995), Crystallisation and welding variations in a widespread ignimbrite sheet - The Rattlesnake tuff, eastern Oregon, USA, *Bulletin of Volcanology*, *57*(3), 151-169.

Streckeisen, A. (1978), Classification and nomenclature of volcanic rocks, lamprophyres, carbonatites and melilitic rocks, *Neues Jahrbuch für Mineralogie*, *136*, 169-206.

Sulpizio, R., and P. Dellino (2008), Sedimentology, depositional mechanisms and pulsating behaviour of pyroclastic density currents, in *Caldera Volcanism. Analysis, modelling and response*, edited by J. Gottsmann and J. Martí, Elsevier, Amsterdam, pp. 57-96.

Sun, S. S., and W. F. McDonough (1989), Chemical and isotopic systematics of oceanic basalts; implications for mantle composition and processes, in *Magmatism in the ocean basins*, edited by A. D. Saunders and M. J. Norry, Geological Society of London, London, pp. 313-435.

Taricco, M. (1932), Carta Geologico-Mineraria dell'Iglesiente, sheet 233: Barbusi. 1:25,000. Editor: L. Salomone, Roma.

Taricco, M. (1934), Geologia del Foglio dell'Isola di S. Pietro y Capo Sperone (Sardegna), *Bollettino del Reale Ufficio Geologico d'Italia*, *59*(2), 75 pp.

Taylor, S. R., and S. M. McLennan (1981), The composition and evolution of the continental crust: rare earh element evidence from sedimentary rocks, *Philosophical Transactions of the Royal Society of London Series a-Mathematical Physical and Engineering Sciences*, *301*(1461), 381-399.

Todt, W., R. Cliff, A. Hanser, and A. Hofmann (1996), Evaluation of a ^{202}Pb-^{205}Pb double spike for high-precision lead isotope analysis, *Geophysical Monograph Series*, *95*, 429-437.

Tommasini, S., G. Poli, and A. N. Halliday (1995), The role of sediment subduction and crustal growth in Hercynian plutonism - isotopic and trace-element evidence from the Sardinia-Corsica batholith, *Journal of Petrology*, *36*(5), 1305-1332.

Tuttle, O. F., and N. L. Bowen (1958), *Origin of granite in the light of experimental studies in the system $NaAlSi_3O_8$-$KAlSi_3O_8$-SiO_2-H_2O*, Geological Society of America Memoirs, 74, 153 pp..

Vidal-Solano, J. R., F. A. Paz-Moreno, A. Demant, and M. López-Martínez (2007), Ignimbritas hiperalcalinas del Mioceno medio en Sonora Central: revaluación de la estratigrafía y significado del volcanismo terciario, *Revista Mexicana de Ciencias Geológicas*, *24*(1), 47-67.

Vigliotti, L., and V. E. Langenheim (1995), When did Sardinia stop rotating - new paleomagnetic results, *Terra Nova*, *7*(4), 424-435.

Walker, G. P. L., R. F. Heming, and C. J. N. Wilson (1980), Low-aspect ratio ignimbrites, *Nature*, *283*(5744), 286-287.

Watson, E. B. (1979), Zircon saturation in felsic liquids: experimental results and applications to trace element geochemistry, *Contributions to Mineralogy and Petrology*, *70*(4), 407-419.

Watson, E. B., and T. M. Harrison (1983), Zircon saturation revisited: temperature and composition effects in a variety of crustal magma types, *Earth and Planetary Science Letters*, *64*(2), 295-304.

Westphal, M., J. Orsini, and P. Vellutini (1976), Le microcontinent Corso-Sarde, sa position initiale: donnés paléomagnétiques et raccords géologiques, *Tectonophysics*, *30*(1-2), 141-157.

Wezel, F. C. (1985), Structural features and basin tectonics of the Tyrrhenian sea, in *Geological evolution of the Mediterranean basin*, edited by D. J. Stanley and F. C. Wezel, Springer-Verlag, New York, pp. 153-194.

Wezel, F. C., D. Savelli, M. Bellagamba, M. Tramontana, and R. Bartole (1981), Plio-Quaternary depositional style of sedimentary basins along insular Tyrrhenian margins, in *Sedimentary basins of Mediterranean margins*, edited by F. C. Wezel, Tecnoprint, pp. 239-269.

White, J. C., D. F. Parker, and M. Ren (2009), The origin of trachyte and pantellerite from Pantelleria, Italy: Insights from major element, trace element, and thermodynamic modelling, *Journal of Volcanology and Geothermal Research*, *179*(1-2), 33-55.

Wilson, C. J. N. (1993), Ignimbritas y calderas: perspectivas históricas, ideas actuales y desarrollos futuros, in *La volcanología actual*, edited by J. Martí and V. Araña, Consejo Superior de Investigaciones Científicas, Madrid, pp. 197-275.

Wilson, M., and H. Downes (1991), Tertiary-Quaternary extension-related alkaline magmatism in western and central Europe, *Journal of Petrology*, *32*(4), 811-849.

Zanettin, B. (1984), Proposed new chemical classification of volcanic rocks, *Episodes*, *7*(4), 19-20.

Zeck, H. P. (1999), Alpine plate kinematics in the western Mediterranean: a westward-directed subduction regime followed by slab roll-back and slab detachment, in *The Mediterranean basins: Tertiary extension within the Alpine Orogen*, edited by B. Durand, L. Jolivet, F. Horváth and M. Séranne, Geological Society, London, pp. 109-120.